Petrogenesis of late cenozoic collision volcanism in western Anatolia, Turkey

Aldanmaz, Ercan

Petrogenesis of Late Cenozoic Collision Volcanism in Western Anatolia, Turkey

by

Ercan Aldanmaz

A thesis submitted in partial fulfilment of the requirements for the degree of Doctor of Philosophy

Department of Geological Sciences

University of Durham

September 1998

Declaration

I declare that this thesis, which I submit for the degree of Doctor of Philosophy at the University of Durham, is my own work and not substantially the same as any which has previously been submitted at this or another university.

Ercan Aldanmaz

University of Durham

September 1998

ABSTRACT

Petrogenesis of Late Cenozoic Collision Volcanism in Western Anatolia, Turkey

Western Anatolia exhibits a record of almost all stages of a collision event and its related magmatic processes. Following an Eocene continent-arc collision, Western Anatolia region experienced a complete cycle of thickening and orogenic collapse. The early stage of collision-related volcanism, which was most evident during the Early Miocene (<21 Ma), produced a considerable volume of lavas and pyroclastic deposits covering a broad compositional range from basaltic andesites to rhyolites. The volcanic activity continued into the Middle Miocene with a gradual change in eruptive style and rock compositions. The Middle Miocene activity, formed in relation to localised extensional basins and was dominated by lava flows and dykes of basalts to andesites composition. Both the Early-Middle Miocene rocks have calc-alkaline and shoshonitic character. The late stage volcanism, from 11.0 to 8.3 Ma, was marked by alkali basalts and basanites erupted along the localised extensional zones.

The Early-Middle Miocene volcanic rocks exhibit enrichment in LILE and LREE relative to the HFSE (characterised by negative Nb and Ta anomalies) and are characterised by high $^{87}Sr/^{86}Sr$ and low $^{143}Nd/^{144}Nd$ ($-\varepsilon_{Nd}$) ratios. These characteristics indicate a mantle lithospheric source region carrying a subduction component inherited from a pre-collision subduction event. Perturbation of this subduction-metasomatised lithosphere by delamination of the thermal boundary layer is the likely mechanism for the initiation of the post-collision magmatism.

Trace elements systematics suggest that the Early-Middle Miocene series underwent a hydrous crystallisation (dominated by pargasitic amphibole) in deep crustal magma chambers. Subsequent crystallisation in shallower magma chambers follows two different trends: (1) anhydrous (pyroxene + plagioclase-dominated; and (2) hydrous (edenitic amphibole + plagioclase + pyroxene dominated).

Trace element and isotope modelling shows that the Early-Middle Miocene rocks have been affected by assimilation combined with fractional crystallisation processes, and that the effects of assimilation decrease gradually from the Early Miocene into the Middle Miocene. This indicates a progressive crustal thinning related to the extensional tectonics that prevailed from the latest Early Miocene onwards.

In contrast to the Early-Middle Miocene rocks, the Late Miocene alkaline rocks are characterised by low $^{87}Sr/^{86}Sr$ and high $^{143}Nd/^{144}Nd$ ($+\varepsilon_{Nd}$) ratios and have OIB-type like trace element patterns characterised by enrichment in LILE, HFSE and L-MREE, and a slight depletion in HREE, relative to the N-MORB compositions. REE inversion modelling indicates that these rocks formed by partial melting (with degrees of ~2 to ~10%) of a spinel + garnet lherzolite source. Trace element and isotopic systematics are consistent with decompression melting of an enriched mantle asthenospheric source.

Acknowledgements

First, my deepest thanks to my supervisor, Dr. Julian A. Pearce, for his helpful comments, criticisms and patience. Needles to say, this work would never have been finished without his constant help and encouragement. He painstakingly went through each chapter and offered many invaluable suggestions.

I would like to express my gratitude to the University of Kocaeli, Turkey, and to the Turkish Higher Educational Council for their financial support during the past four years.

The original idea of this project stems from Prof. Yücel Yilmaz who first aroused my interest in the magmatic evolution of Western Anatolia. I would like to express my personal gratitude to him.

I would like to thank Dr. Mehmet Keskin for his invaluable help and advise during the initial stage of this project.

Particular thanks must go to Ron Hardy for his help and encouragement during the sample preparation and XRF analyses; and to Dr. Chris Ottley for his help and advise on ICP-MS analyses.

I would like to thank Drs. Peter Hill, Stuart Kearns and Simon Burgess at the Electron Probe Unit of Edinburg University for their help and advise on Electron Probe analyses.

I would like to express my appreciation to Prof. John Mitchell at Newcastle University for carrying out radiometric dating; and to Dr. Matthew Thirlwall, Gery Ingram and Dr. Robin Gill at Royal Holloway, University of London, for their help and advise on radiogenic isotope analyses.

The list of people from the department in Durham, who I would like to thank, is quite long. It starts with the staff: Prof. Maurice Tucker, Prof. Bob Thompson, Dr. Gill Foulger, Dr. Grenvile Holland, Dr. Graeme Pearson, D. Stevenson, G. Ruth, Gerry, Alan, R. Lambert, Julie, Karen, Carol, Claire, D. Asbury, D. Schofield; the fellow geochemists: Nurdane, Affonso, Teresa, Vicky, Robin, Andy, Gordon, Sarah(s), Kate; the postgraduate friends: Roberto, Tobby, Alun, Wayne, Jonny, Ziad, Simon, Gail, Ismail, Caroline, Ian, Matt.

Final thanks go to my parents for their continual moral support during the course of this study.

CONTENTS

Chapter 1: INTRODUCTION	Page
1.1. Geological Setting and Distribution of Volcanism	2
1.1.1. Tectonic Setting	2
1.1.2. Distribution of the Volcanism	6
1.2. Previous Studies of Western Anatolian Volcanism	8
1.3. Objectives of This Thesis	14
1.4. Description of The Thesis	16
Chapter 2: GEOLOGY AND VOLCANO-STRATIGRAPHY OF WESTERN ANATOLIA	
Introduction	18
2.1. The Ezine-Gulpinar-Ayvacik Area (EGA)	20
2.1.1. The Basement Rocks	22
2.1.2. The Ezine-Ayvacik Section	26
2.1.2.1. The Kestanbol Pluton	26
2.1.2.2. The Kiziltepe (Volcanic) Unit	27
2.1.2.3. The Cinarkoy Pyroclastic Deposits	27
2.1.2.4. The Cakmak Tuff	27
2.1.2.5. The Ezine (Volcanic) Unit	28
2.1.2.6. The Dededag (Volcanic) Unit	28
2.1.2.7. The Ultrapotassic Lamproite Dykes	29
2.1.2.8. The Tastepe Volcanics	29
2.1.2.9. The Ezine Volcanics	30
2.1.2.10. The Ayvacik Volcanics	31
2.1.3. The Assos-Babakale-Gulpinar Section	32
2.1.3.1. The Babakale (Volcanic) Unit	32
2.1.3.2. The Bademli (Volcanic) Unit	35
2.1.3.3. The Koyunevi Ignimbrite	36
2.1.3.4. The Suruce Andesite	37
2.1.3.5. The Bergas Ignimbrite	38
2.1.3.6. The Bakacak (Volcanic) Unit	44
2.1.3.7. The Behram Andesite	44
2.1.3.8. The Balabanli Ignimbrite	46
2.1.3.9. The Kovacli Dyke Swarms	54
2.2. The Dikili-Ayvalik-Bergama (DAB) Area	55
2.2.1. The Basement Rocks	55

2.2.2. The Ayvalik-Kozak Section 60
2.2.2.1. The Kozak Pluton 60
2.2.2.2. The Maden Island Pluton 61
2.2.2.3. The Kucukkoy (Volcano-sedimentary) Unit 61
2.2.2.4. The Ballica (Volcanic) Unit 61
2.2.2.5. The Alibey Dyke Swarms 62
2.2.2.6. The Ulubey (Volcanic) Unit 62
2.2.2.7. The Akcapinar (Volcanic) Unit 63
2.2.2.8. The Seytansofrasi Ignimbrite 64
2.2.2.9. The Besiktepe Dacite 65
2.2.2.10. The Odaburnu Dke Swarms 65
2.2.3. The Dikili-Bergama-Foca Section 66
2.2.3.1. The Kiratli (Volcanic) Unit 66
2.2.3.2. The Madra River Dyke Swarms 66
2.2.3.3. The Salihler Volcanics 69
2.2.3.4. The Kabakum Dacite 69
2.2.3.5. The Mt. Seyret (Volcanic) Unit 71
2.2.3.6. The Karagol (Volcanic) Unit 72
2.2.3.7. The Kalarga Andesite 72
2.2.3.8. The Foca (Volcanic) Unit 75
2.2.3.9. The Foca Dyke Swarms 77
2.2.3.10. The Egrigol Andesite 77
2.2.3.11. The Nebiler Volcanics 79
2.3. Summary 80

Chapter 3: MAJOR AND TRACE ELEMENT GEOCHEMISTRY

Introduction 82
3.1. Major Element Characteristics of the Volcanic Rocks 82
3.1.1. Classification of the Volcanic Rocks Using Major Element Geochemistry 82
3.1.2. Harker Diagrams for Major Elements 87
3.2. Trace Element Characteristics of The Volcanic Rocks 90
3.2.1. Trace Element Variations of The Volcanic Rocks 90
3.2.2. Rare Earth Element Patterns 94
3.2.3. Multi-Element Patterns 98
3.2.4. Trace Element Ratios 102
3.3. Chapter 3 Summary 105

Chapter 4: PETROGRAPHY

Introduction 106
4.1. Volcanic Rocks From The Ezine-Gulpinar-Ayvacik (EGA) Area 106
4.1.1. Highly Porphyritic Acid-Intermediate Lavas (Early Miocene) 106
4.1.2. Pyroclastic Rocks (Ignimbrites) (Early Miocene) 112
4.1.3. Weakly to Moderately Porphyritic Dyke Swarms (Early Miocene) 118
4.1.4. Aphyric to Weakly Porphyritic Mafic Alkaline Lavas (Late Miocene) 121
4.2. Volcanic Rocks From The Dikili-Ayvalik-Bergama (DAB) Area 126
4.2.1. Highly Porphyritic Acid-Intermediate Lavas (Early Miocene) 126
4.2.2. Aphyric to Slightly Porphyritic Intermediate Lavas (Middle Miocene) 128
4.2.3. Aphyric to Moderately Porphyritic Basaltic Lavas (Middle Miocene) 130
4.3. Interpretation and Summary of the Petrography 134

Chapter 5: MINERAL CHEMISTRY

Introduction 137
5.1. Classification of the Minerals 137
5.1.1. Olivine 137
5.1.2. Pyroxene 140
5.1.3. Plagioclase Feldspar 145
5.1.4. Amphibole 147
5.1.5. Biotite-Phlogopite 147
5.1.6. Oxide Minerals 150
5.2. Estimation of Magmatic Intensive Parameters 152
5.2.1. Temperatures and Oxygen Fugacities 152
5.2.1.1. Pyroxene geothermometer 152
5.2.1.2. Amphibole-Plagioclase geothermometer 155
5.2.1.3. Fe-Ti Oxide geothermometer 157
5.2.2. Pressure Estimates 159
5.2.2.1. Clinopyroxene geobarometer 159
5.2.2.2. Al-in-hornblende geobarometer 161
5.3. Chapter 5 Summary 164

Chapter 6: ISOTOPE SYSTEMATICS AND PETROGENESIS

Introduction 166

6.1. Nd-Sr Isotope Characteristics of The Volcanic Rocks 166
6.2. Petrogenesis of The Volcanic Rocks 171
6.2.1. Petrogenesis of the Calc-alkaline and Shoshonitic Volcanic Rocks (Eraly-Middle Miocene) 171
6.2.1.1. Crystallisation history of the volcanic rocks 172
6.2.1.2. Assimilation combined with fractional crystallisation (AFC) 178
6.2.1.2.1. Evidence for assimilation and/or mixing: Overwiev 178
6.2.1.2.2. Estimation of the end-member compositions and bulk partition coefficients 180
6.2.1.2. AFC Plots 181
6.2.1.3. Model for magma generation 186
6.2.1.4. Mantle melting in response to post-collisional tectonics 191
6.2.1. Petrogenesis of the Alkaline Volcanic Rocks (Late Miocene) 197
6.2.2.1. Fractional crystallisation 197
6.2.2.2. The source mineralogy 200
6.2.2.3. Partial melting processes 202
6.2.2.3.1. Overwiev 202
6.2.2.3.2. Modelling mantle melting 204
6.2.2.4. Constraints on the degree of partial melting and the initial mantle composition 207
6.2.2.5. The source characteristics 217
6.2.2.6. Mantle melting and magma generation in response to lithospheric extension 223
6.3. Chapter 6 Summary 224

Chapter 7: CONCLUSIONS

Introduction 227
7.1. Volcano-stratigraphy 227
7.2. Structural Evolution 228
7.3. Magmatic Evolution 229

REFERENCES 232

APPENDIX 261
A. ANALYTICAL GEOCHEMISTRY 261
B. GEOCHEMICAL DATA SET
XRF DATA 265
ICP-MS DATA 279

C. ACCURACY AND PRECISION OF THE DATA

CHAPTER ONE

INTRODUCTION

In recent years, magmatism generated in continental collision settings has attracted significant attention. It is widely accepted that a large proportion of volcanic and plutonic bodies in collision settings may be genetically related to collisional tectonic processes during the formation of mountain belts. However, there has also been increasing recognition of the complexity of the genesis and evolution of collision zone magmatism. The widely accepted general view is that three main stages of tectonic processes are involved in collision settings: (1) a subduction period marked by subduction magmatism and high-P, low-T metamorphism; (2) a major compression period which is marked by large thrusts and syn-collision magmatism; and (3) a late-collision period which is marked by extension, transtension and transpression tectonics and post-collision magmatism. Magmatism in collision settings may be a consequence of various mechanisms, including crustal thickening, strike-slip movement related to continental escape and late-stage lithospheric thinning either by localised extension and lithospheric stretching or orogenic collapse and/or lithospheric delamination. In this context, magma can be generated by: (1) mantle and crustal melting by subduction of continental crust; (2) decompression melting of mantle by localised lithospheric extension: and (3) mantle or crustal melting by internal heat generated by mantle-derived magma injections or asthenospheric upwelling resulted by lithospheric delamination (Pearce et al, 1994).

In this study, an attempt has been made to evaluate the nature and characteristics of the volcanism of Western Anatolia (Turkey) and the relationship between collisional tectonics and magma generation. Western Anatolia has been chosen because this region exhibits a record of almost all stages of a collision event and its related magmatic processes. Attention has been focused on the petrogenetic evolution of Western Anatolian volcanism and its relationship to the regional tectonic evolution.

1.1. Geological Setting and The Distribution of Volcanism

1.1.1. Tectonic Setting

Much of the geological and tectonic history of Turkey is linked to Tethyan evolution. Şengör and Yılmaz (1981) suggested that Turkey was situated on the northernmost part of the Gondwanaland during the Permian. After the Middle Triassic, the northern margin of Gondwanaland began to rift away from the main continent to form a continental fragment known as the Cimmerian continent. This in turn caused the formation of a southern branch of the ocean known as Neotethys between the Cimmerian continent and Gondwanaland. Further rifting and fragmentation of the Cimmerian continent itself also took place during the Early Jurassic to form a northern branch of Neotethys and the Anatolite-Tauride platform between the two branches of the Neotethys (Şengör and Yılmaz, 1981; Şengör et al., 1984). The Palaeotethys Ocean was eliminated by a subduction event during the Late Palaeozoic-Early Mesozoic. The direction of subduction of Palaeotethys is, however, still debated. Some authors (e.g. Şengör et al., 1980, 1984; Okay et al., 1991) proposed a southward direction for the subduction of Palaeotethys that can explain northward-vergent structures in NW Anatolia. Others (e.g. Adamia et al., 1981; Robertson and Dixon 1984) put forward a northward-dipping subduction model which can fit with the broad picture of an active Eurasian margin and a passive Gondwanan margin, extending from the Eastern Mediterranean to the Himalayas. However, Pickett and Robertson (1996) have recently suggested that elements of both northward and southward subduction are involved in closure of the Palaeotethys Ocean in NW Anatolia. In their model, the Cimmerian continent collided with Eurasia during the Middle Jurassic, causing regional uplift and the terminal closure of the Palaeotethys Ocean. This was followed by northward-dipping subduction from the Late Cretaceous to the Paleocene which formed the Pontide volcanic arc and led to the closure of Neotethys.

The north-dipping subduction episode ended when the Anatolide-Tauride platform collided with the Pontide arc along the Izmir-Ankara suture zone (Fig. 1.1). The timing of this collision is poorly constrained. Şengör et al. (1979) and Şengör and Yılmaz (1981) proposed a Late Palaeocene - Early Eocene collision age. Harris et al. (1994) have also recently discussed that the obduction of the ophiolite fragments along the collision zone indicate that the time of collision was certainly earlier than Middle Eocene (50 Ma) and probably later than the Upper Cretaceous (Turonian). However, arc

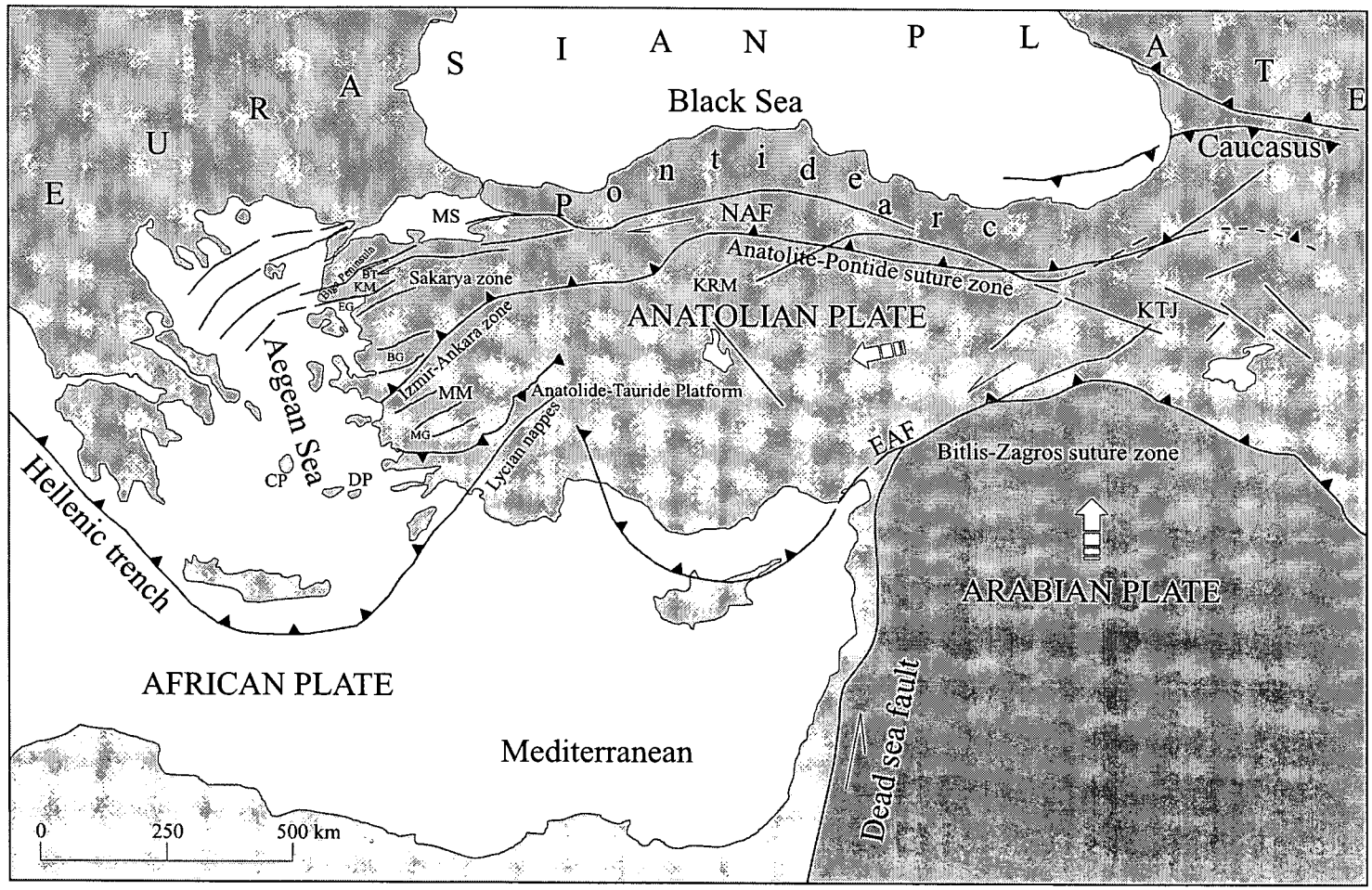

Figure 1.1. *Tectonic setting of Eastern Mediterranean. NAF = North Anatolian Fault; EAF = East Anatolian Fault; KTJ = Karliova Triple Junction; MS = Marmara Sea; KRM = Kirsehir Massif; KM = Kazdag Massif; MM = Menders Massif; CP = Cyclades Province; DP = Dodecanese Province; BT = Bayramic Trough; EG = Edremit Graben; BG = Bergama Graben; MG = Menderes Graben.*

magmatism along the Pontide zone continued into the Middle Eocene (Şengör and Yılmaz, 1981). This may indicate a Middle Eocene age for the collision. This collision caused large-scale intra-crustal deformation and thickening together with the burial of the Menderes metamorphic Massif beneath the Lycian nappe piles.

Further to the east, collision between the Arabian and the Anatolian plates started along the Bitlis-Zagros suture zone during the Middle to early-Late Miocene (Şengör and Yılmaz, 1981; Şengör et al., 1985; Pearce et al., 1990) (Fig. 1.1). This caused uplift of the eastern part of Anatolia to form a plateau and also led to the tectonic escape of the Anatolian plate by right-lateral strike-slip along the North Anatolian Fault (NAF) and left-lateral strike-slip along the East Anatolian Fault (EAF). Although estimates of the onset of the NAF give variable ages from Late Miocene to Pliocene (13 - 4 Ma) (Ketin, 1969; Barka and Hancock, 1984; Şengör et al., 1985), Barka and Kadinsky-Cade (1988) used stratigraphic correlations in the basins related to strike-slip movements of NAF to suggest that the North Anatolian Fault initiated during the Late Miocene.

Towards Western Anatolia, the NAF splays into three main branches: (1) a northern branch which lies mostly offshore, beneath the Marmara Sea; (2) a middle branch which lies south to the Marmara Sea and extends from Çan to Ezine through the Bayramiç trough; and (3) a southern branch which extends through the Edremit Graben (Fig. 1.1). The total relative displacement of the northern branch of NAF has been reported as approximately 40 km in the Marmara Sea (Barka and Kadinsky-Cade, 1988) and northeastern Aegean Sea (Le Pichon et al., 1984). The estimated displacement on the middle and southern branches is ~40 – 45 km (Westaway, 1994). The effect of the major, dextral, E-W trending strike-slip activity in Northwestern Anatolia was that the movement of the Anatolian plate relative to the Pontides changed from westwards to southwestwards. This generated small pull-apart basins related to NE-SW trending strike-slip faulting in the north (in the Biga Peninsula and Edremit Graben) and E-W trending normal faults with significant strike-slip movements linked to graben formation in the south (south of the Edremit Bay).

Since the Late Miocene-Pliocene, Western Anatolia has experienced extensive crustal extension and lithospheric thinning, leading to the formation of E-W trending, low angle, listric normal faults with strike-slip components on their hanging-wall blocks (Angelier et al., 1981; King and Vita Finzi, 1982; Eyidoğan and Jackson, 1985; Şengör

et al., 1985). The cause of this extension is still debated. Mechanisms that may contribute include: (1) gravitational collapse and spreading of thickened and unstable lithosphere (Dewey, 1988; Seyitoğlu and Scott, 1996); (2) subduction beneath the Aegean and Anatolian plates along the Hellenic trench (Le Pichon and Angelier, 1979; 1981; Meulenkamp et al., 1988); and (3) counterclockwise rotation of the Anatolian plate (Westaway, 1994; Reilinger et al., 1997).

The geological and seismological analyses of Zanchi and Angelier (1993) show that the Quaternary stress regime of Western Anatolia was dominantly extensional and associated with approximately NNE - SSW and NE - SW trending normal faults. Although strike-slip mechanisms are subordinate in the area between the Menderes Massif and Edremit Graben, there is an increase of strike-slip faulting from south to north, towards the Edremit Graben (the southern branch of the North Anatolian Fault system). Crustal thicknesses and extension rates of the Aegean area cannot be calculated accurately because of a lack of gravity and seismic data. However, it has been reported that the average crustal thicknesses are approximately 40 km on the Anatolian plate, 30-35 km on the coastal region of Western Anatolia and 25 km beneath the central and southern Aegean Sea (Makris and Stobbe, 1979; 1984a, b; Meissner et al., 1987; Mindevallı and Mitchell, 1989). A southward extensional strain rate across much of the Western Anatolia has been modelled by Jackson (1992) as $>2 \times 10^{-15}$ s^{-1}. Similarly, Paton (1992) calculated from the topography that the stretching factor β (the ratio of initial to final lithospheric thickness) gives a maximum value of approximately 2 in the central Aegean and 1.2 - 1.5 in Western Turkey.

Although most of the extension is considered to have taken place during the Late Miocene-Pliocene and, particularly, Quaternary Periods, there is no clear consensus about the timing of the initiation of the extension in Western Anatolia and Aegean. Şengör and Yılmaz (1981), Şengör (1982) and Şengör et al. (1985) proposed that extensional tectonics started to be effective in the Late Miocene, following N-S compression and crustal shortening. Hayward (1984) also proposed a Late Miocene age for the timing of the final emplacement of the Lycian nappes and hence the end of the compressional tectonic regime. Controversially, Kaya (1981) reported Early Miocene, graben-fill sequences in the Gördes and Foça areas that may indicate that subsidence started during the Early Miocene, although Şengör et al. (1985) interpreted these basins as palaeotectonic structures which have been resurrected by neotectonic episodes.

Similarly, Seyitoğlu and Scott (1992, 1995) have recently used sporomorph assemblages in the sedimentary basins (Benda and Meulenkamp, 1979) to propose that extensional tectonics initiated in the Latest Oligocene-Early Miocene (~20-24 Ma). This is supported by the radiometric dating of syntectonic granitoids in the Menderes Massif (Hetzel et al., 1995). However, these controversies may be a result of the complex tectonic patterns of Western Anatolia which include both compressional and extensional regimes and localised extension and basin formation during the compressional episodes.

1.1.2. Distribution of The Volcanism

Extensive volcanic activity has characterised the Aegean area since the Late Eocene. Volcanic products cover a large area from the Hellenic subduction zone through Western Anatolia and the Aegean islands into Thrace (Fig. 1.2). Volcanism in the area may be divided into two groups according to their relationship to regional tectonic activity: (1) Late Eocene-Recent volcanism related to collision between the Anatolide-Tauride platform and Pontides and to subsequent orogenic collapse; and (2) Late Miocene-Recent volcanism related to northward-dipping subduction of the African plate beneath the Eurasian plate along the Hellenic trench (Fig. 1.2). The products of the subduction-related volcanism are distributed along the southern Aegean arc, from the Cyclades through the Dodecanese provinces (Samos, Patmos and Kos islands) to SW Anatolia (the Bodrum Peninsula) and have been dated as 12 Ma to Recent (~3 Ka) (Keller, 1982; Schliestedt et al., 1987; Wyers and Barton, 1987; Robert et al., 1992). The products of the Late Eocene-Recent, collision-related volcanism, however, occupy a wide area in the northern part of the Aegean Sea and Western Anatolia. The collision-related volcanism of Western Anatolia is the subject of this thesis and termed as "The Western Anatolian, Late Cenozoic Volcanic Province".

The Western Anatolian, Late Cenozoic Volcanic Province is one of the few modern examples of volcanism associated with continental crust which has been thickened and subsequently thinned by orogenic processes. The volcanic rocks in Western Anatolia are observed in a large area from the Menderes Massif in the south to Thrace in the north (Fig. 1.2). The oldest radiometric ages (K-Ar) on the Western Anatolian collision-related volcanism are 37.3 ± 0.9, 31.4 ± 0.4 and 30.4 ± 0.7 Ma (Ercan and Satır, 1994; Ercan et al., 1995). Thus, the volcanic activity is believed to have started in the Late Eocene-Early Oligocene, following the collision between the

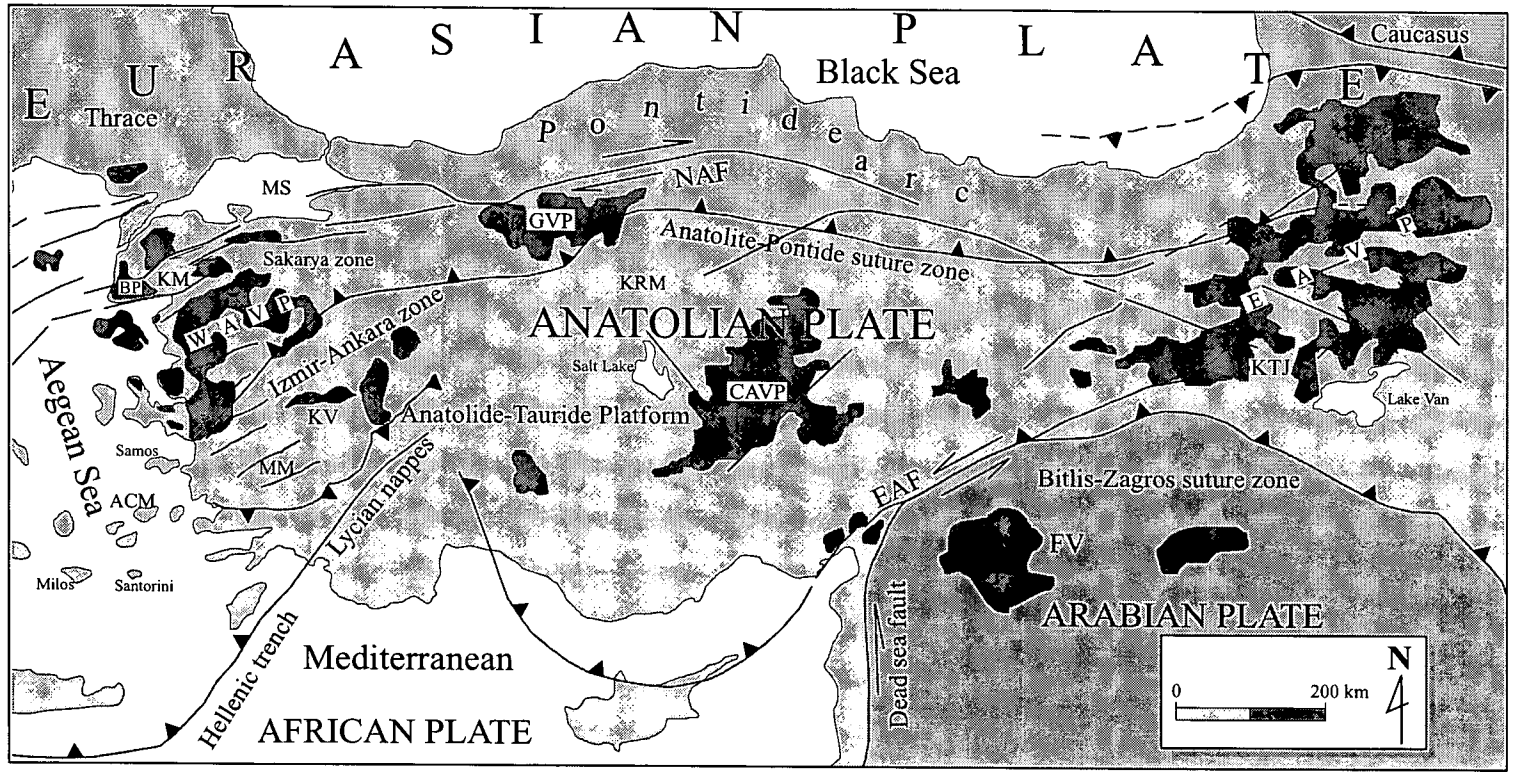

Figure 1.2. *Distribution of the Tertiary volcanic provinces of Turkey and the Aegean. FV = Foreland Volcanism; EAVP = East Anatolian Volcanic Province; CAVP = Central Anatolian Volcanic Province; GVP = Galatia Volcanic Province; WAVP = West Anatolian Volcanic Province ACM = Attic-Cycladic Massif; MM = Menderes Massif; KM = Kazdag Massif; KRM = Kirsehir Massif; MS = Marmara Sea; NAF = North Anatolian Fault; EAF = East Anatolian Fault; KTJ = Karliova Triple Junction; KV = Kula Volcanic Area; BP = Biga Peninsula.*

Anatolide-Tauride Block and the Pontides. The volcanic products of Late Eocene-Early Oligocene ages, however, occupy only small areas of the Northern and eastern part of the Biga Peninsula (Ercan et al., 1995). In the area studied, most of the volcanic rocks are of Early to Late Miocene age. The youngest known radiometric ages on the Western Anatolian volcanism are 1.67 ± 0.22, 1.10 ± 0.03, 0.13 ± 0.09 and 0.025 ± 0.006 Ma (Borsi et al., 1972; Ercan et al., 1984; Richardson-Bunbury, 1996). These are the dates reported for the alkaline basic volcanics from the Kula area (outside the area studied in this thesis).

The volcanic products show a considerable compositional variability in time and space. Three major stages of volcanic activity may be distinguished on the basis of the compositional variations. The Early stage of volcanic activity (Late Oligocene-Early Miocene) is represented by acid-intermediate rock types. These are pyroclastic fall and flow deposits accompanied by mostly porphyritic lava flows, domes and dykes. The Middle stage (Middle-Late Miocene) volcanic activity gave dominantly basic-intermediate rock types. Common volcanic products were lava flows, domes and dykes. Pyroclastic eruptions were absent in this stage. The Late stage activity (Late Miocene-Recent) is, however, represented by locally-developed small lava flows of basic and ultrabasic rock types.

1.2. Previous Studies of Western Anatolian Volcanism

The first study on the Western Anatolian volcanics was carried out by Washington (1893; 1900) who used wet chemical analyses on the Kula basalts to suggest an alkaline character and the term "Kulaite" for the hornblende-bearing basaltic rocks in the Kula area (Fig. 1.2).

Borsi et al. (1972) discussed the general petrological characteristics and the geochronological relationships of the Eastern Aegean and Western Anatolian volcanics. They described a Lower-Middle Miocene (21.5 to 16.2 Ma) calc-alkaline volcanism associated with minor acid and basic products, mainly of Late Miocene age (11.9-9.7 Ma). They proposed two principal models for the origin of the calc-alkaline, andesitic volcanics based on their geochemical data: (1) andesitic liquids are derived from high-Al basaltic magma by fractional crystallisation or assimilation of crustal materials; and (2) andesites are primary liquids derived by melting of the lower crust or the upper

mantle material. On the basis of their isotope data, they also argued that the rhyolitic volcanic rocks were derived by partial melting of the upper crust.

Krushensky (1976) carried out research on the Neogene, calc-alkaline extrusive and intrusive rocks of the Karalar-Yesiller area (east of Edremit Bay), NW Anatolia. On the basis of petrological, geochemical data and radiometric ages, he suggested that the intrusive and extrusive rocks are comagmatic and that the parent magma is probably derived from partial melting of subducted oceanic crust and accompanying oceanic sediments.

Fytikas et al. (1976) argued that the magmatism in the Aegean area and Western Anatolia could be divided into two groups, each of which is related to different subduction processes. These are: (1) Tertiary magmatism, which is related to subduction in the northern Aegean; and (2) Recent calc-alkaline magmatism, which is related to the Hellenic subduction zone in the southern Aegean. Fytikas et al. (1984) further classified the Tertiary-Quaternary volcanics in the area into three distinct groups: (1) an Oligo-Miocene volcanic phase (North Aegean Tertiary activity); (2) a Pliocene-Quaternary volcanic phase (South Aegean active arc) and (3) an Upper Miocene to Quaternary scattered volcanic activity. They argued that the volcanic activity started in the northernmost part of the North Aegean area mostly with calc-alkaline, intermediate and acid volcanic products. The volcanism shifted successively southward becoming progressively enriched in potassium. They interpreted this evolution as being related to a subduction zone which moved gradually south as a result of slab steeping and extension of the overlying crust and increase in the dip of the Benioff zone under the Eurasian plate, resulting from a reduction in the plate convergence rate after continental collision.

Ercan (1979; 1982) reported some major element geochemical data for the Cenozoic volcanic rocks from Western Anatolia, Thrace and Aegean islands. Ercan et al. (1984) further reported and interpreted some major-trace element, isotopic and radiometric age data on the Cenozoic volcanics of Western Anatolia. They identified calc-alkaline and alkaline volcanics with K-Ar ages between 37.3 and 21.7 Ma and between 7.55 Ma and 25.0 Ka respectively. On the basis of their isotope data, they proposed a crustal and an upper mantle origin for calc-alkaline and alkaline volcanics respectively. Ercan and Satir (1994) and Ercan et al. (1995) dated the Tertiary volcanics of the Biga Peninsula, NW Anatolia and classified the volcanics into four groups: (1) an Eocene volcanism (commenced about 37.3 Ma ago), which consists generally of

pyroclastics and lavas of dacite and andesite compositions; (2) an Oligocene volcanism (34.3 to 23.6 Ma), which consists of andesitic, dacitic, trachy-andesitic and rhyodacitic lavas; (3) an Early-Middle Miocene volcanism (22.3 to 15.3 Ma) which is characterised by lava, tuff and ash flows of dacitic, rhyodacitic, andesitic and trachy-andesitic composition; and (4) a Late Miocene alkaline volcanism (11.0 to 8.4 Ma) which consists of alkali olivine basalts.

Pe-Piper (1980) studied on the Miocene volcanics of the Lesbos Island (west of Edremit Bay) in the NE Aegean and showed that thick Miocene volcanics of the Island have calc-alkaline and shoshonitic character. A main phase of shoshonitic volcanism was dominant and followed by minor calc-alkaline volcanism. Pe-Piper (1980) argued that the shoshonites show two distinct differentiation trends on the basis of the major element data. One trend, characteristics of the earlier shoshonites, resulted from fractional crystallisation of anhydrous phases. The second trend, characteristics of later shoshonites, resulted from fractional crystallisation of amphibole and biotite. A further study was carried out on the Cenozoic high-K volcanic rocks of the Lesbos Island by Pe-Piper and Piper (1992). They pointed out that shoshonitic and calc-alkaline volcanic rocks alternate in the Miocene volcanic sequence of the Island. According to their geochemical and radiometric data, volcanism on the Island started 21.5 Ma ago with a calc-alkaline character. Following a 3 Ma hiatus, the main shoshonitic phase took place from 17.7 to 16.9 Ma and was followed by minor late calc-alkaline phase.

The study of Pe-Piper and Piper (1989) concentrated on the Late Cenozoic extensional volcanic rocks of the Aegean area and Western Anatolia. They described the Late Cenozoic volcanics of the Aegean area as back-arc volcanism formed behind the southern Aegean arc. They used the geochemical and radiometric data to classify the magmatic rocks into five groups: (1) calc-alkaline rocks of the Voras-Kamena-Vourla area which are characterised by LIL element enrichment and Nb depletion; (2) shoshonitic rocks of the Volos-Atalanti area and the Voras Mountains which are characterised by greater LIL element enrichment than the calc-alkaline rocks and by greater fractionation of HREE; (3) potassic, trachytic rocks of the Cos, Bodrum, Patmos, Urla and Doirani-Stratonion areas; (4) sodic mafic rocks of the Psathoura, Kalogeri, Samos, Urla, Foça and Chios areas and (5) continental alkaline rocks of the Kula area.

Gülen et al. (1986) used Sr-Nd-Pb isotope systematics and the existence of the hydrous mineral assemblages (e.g. kaersutite and phlogopite) in the alkaline rocks from

the Kula area to suggest that the alkaline magma was generated from a mixture of components from a mantle which has had a time-integrated depletion in Rb/Sr, Nd/Sm and Pb/U and a mantle which had undergone a recent metasomatism event.

Gülen (1990) studied the isotopic characterisation of Aegean magmatism and the geodynamic evolution of the Aegean subduction. He argued that the least contaminated, Quaternary Kula alkali basalts and the Miocene granitoids within the Attic-Cycladic-Menderes Massif, represent Sr, Nd and Pb isotopic compositions for the Aegean mantle and crust respectively. On the basis of isotopic data, he suggested that the Aegean volcanics and granitoids can be interpreted in terms of four end-member components, namely the upper crust, the lower crust, the sub-continental mantle and the asthenosphere. He considered that the Oligo-Miocene magmatism in the area was related to the subduction of the Aegean slab. He argued that the Aegean magmatism throughout the Oligocene-Recent period could be explained by more than one subduction event.

Yılmaz (1989; 1990) suggested that the Post-Oligocene volcanism in Western Turkey had a strong tectonic control. He argued that, following the continental collision during the Late Cretaceous-Early Eocene, Western Anatolia was affected by a north-south compressional tectonic event and crustal thickening processes until the Middle Miocene. Hence, young calc-alkaline volcanic activity began and produced andesites, latites and dacites as a result of continental underthrusting and crustal melting. He argued that a mechanism similar to the MASH (melting, assimilation, storage and homogenisation) hypothesis of Hildreth and Moorbath (1988) was effective during the formation of the hybrid andesitic magma. According to his observations, hybrid andesitic magmatism lasted until the end of the compressional tectonic regime and extended until the initial stage of the extensional regime (Late Miocene). He also suggested that, during the Middle Miocene, the north-south compressional regime was replaced by a north-south extensional regime and that the basic alkaline magmatism was related to this extension during the more advanced stage of rifting in the Pliocene and Quaternary. He used the Ti contents of the rocks to divide the alkaline magmatism into two subgroups (low-Ti and high-Ti), and related these varieties to a heterogeneous source region which had, in part, been metasomatised prior to rifting.

Güleç (1991) used the Sr and Nd isotope geochemistry of the Western Anatolian Tertiary-Quaternary volcanic rocks to suggest that crust-mantle interaction was an

important factor in the magma genesis. She argued that the volcanics were derived from variable mixtures of melts generated from two different mantle sources: (1) the calc-alkaline volcanics were generated from the continental lithospheric or shallow asthenospheric mantle and contaminated with upper crustal materials; and (2) the alkaline volcanics were derived from relatively deep, isotopically depleted mantle regions and contaminated with lower crustal materials. She identified two possible crustal components: an upper crustal material with radiogenic Sr and non-radiogenic Nd; and a lower crustal material with non-radiogenic Sr and non-radiogenic Nd. She also argued that the relative involvement of mantle and crustal components is time-dependent with a general decrease in a crustal component by a factor of about five from Tertiary to Quaternary, consistent with a change in tectonic regime from compressional to extensional.

Seyitoğlu and Scott (1992) argued that the Late Cenozoic volcanism occurred in relation to an extensional tectonic regime in the north-eastern Aegean and that activity began in north-eastern Greece during the Early Oligocene, and in north-western Turkey during the Late Oligocene-Early Miocene. They proposed that the volcanic activity was initially characterised by acid-intermediate, calc-alkaline volcanic products; however, from the Late Miocene onwards, basic-intermediate, alkaline products became dominant. They used stratigraphic correlation between volcanic and sedimentary units in extensional basins to suggest that N-S extensional tectonic regime in Western Turkey began in the Latest Oligocene-Early Miocene. Thus, they proposed that the transition of the regional tectonic pattern from compressional to extensional and the transition of volcanic character from acid-intermediate, calc-alkaline to basic-intermediate, alkaline are not simultaneous and related events.

Seyitoğlu et al. (1997) examined the magmatism in the Uşak-Selendi-Emet area (Western Anatolia) which evolved from potassic character in the Miocene to sodic in the Quaternary. They reported some new K-Ar ages and major and trace element analyses and suggested that the characteristics of volcanism changed from dominantly calc-alkaline and siliceous in the Early Miocene to largely alkaline and mafic in the Middle Miocene. They argued that all the Miocene volcanism formed in an extensional regime, and that the change in magma characteristics reflects a decreasing amount of contamination from the crustal components with time as a result of extensional tectonics. They used the high levels of incompatible elements and the variations in

element ratios (Nb/Y, Ti/Y and Th/Nb) to suggest a lithospheric mantle source heterogeneously enriched by two processes: (1) subduction enrichment producing high Th/Nb but low Nb/Y and Ti/Y; and (2) enrichment by small degree melts of depleted upper mantle producing low Th/Nb but high Nb/Y and Ti/Y. They considered that both of these enrichment processes contributed to Middle Miocene, high-K (or ultrapotassic) volcanics. To produce the calc-alkaline magma, they proposed a decompression-melting model to initiate the melting of the mantle lithosphere, resulting from lithospheric extension. They also argued that the lower K_2O/Na_2O ratios of Pliocene-Quaternary Kula lavas with respect to those of Miocene lavas and their high levels of incompatible elements relative to OIB indicate that these lavas have been derived from the melting of an anhydrous asthenospheric source as a result of the continued extension, and that they were contaminated by mantle lithosphere material during their ascent to the crust.

Paton (1992) studied the relationship between extension and volcanism in Western Turkey, the Aegean Sea and central Greece. He suggested that extension in the area began about 12 Ma ago, but has been most effective and rapid in the last 5 Ma. He classified the volcanism into two groups: (1) an arc volcanism associated with subduction along the Hellenic trench; and (2) an extension-related volcanism, which is younger than 12 Ma and characterised by higher Nb and Ti concentrations than the rocks of the arc volcanism. He argued that asthenospheric melting should not produce the extension-related mafic volcanics, as the amount of extension in the area is too small (maximum β ~2) to generate asthenospheric melting. He used REE modelling of the extensional volcanics to suggest that the source composition for all the extensional volcanics is a depleted lithospheric mantle that has been further depleted by the removal of an arc tholeiite, and then re-enriched by a small amount (~3-5 %) of a small degree melt from the asthenosphere.

Richardson-Bunbury (1992) used the relationship between sedimentation, eruption and erosion to suggest that the timing of the volcanism is closely related to the start of extension in the Kula area. She also used the REE to propose that the melts are derived from an amphibole-bearing, enriched lithospheric mantle source as a result of decompression melting that underwent to form the basalts. She reported Ar-Ar ages in the Kula area between 1.67 ± 0.22 Ma and 0.13 ± 0.09 Ma.

McKenzie and O'Nions (1995) used REE data to propose that the extension-related basic volcanics of Western Anatolia and Aegean area were derived from melts

generated within continental lithosphere. They argued that the concentrations of moderately incompatible elements, such as Nd and Pr, in the volcanic rocks are greater than can be generated by a single-stage melting process from either the primitive mantle or MORB source. Thus, they suggested that the melts must be generated from a source that had previously been enriched and that the most likely source for such melt generation is continental lithosphere that had previously been enriched by the addition of a small melt fraction with high concentrations of incompatible elements, water and carbonates that may reduce the melting point.

1.3. Objectives of this thesis

As described above, Western Anatolia has been the subject of numerous studies in recent years. The common belief is that the Late Cenozoic magmatic activity of the area is strongly controlled by regional tectonic evolution. Thus, recent attempts have been made to relate magma composition and regional tectonic activity. However, the mechanisms associated with the Late Cenozoic tectonic evolution and related magmatic processes are still debated. Some authors (e.g. Yılmaz, 1989, 1991; Savaşçın, 1990) have suggested that a N-S compressional regime was replaced by a N-S extension during the Middle-Late Miocene and that these two different tectonic patterns are represented by dominantly acid-intermediate calc-alkaline and basic alkaline magmatic assemblages respectively. Güleç (1991) used Sr-Nd isotopes on volcanic rocks from a variety of locations to propose that the Early-Middle Miocene volcanics were generated from a shallow mantle and modified by extensive crustal contamination, and that the Late Miocene-Quaternary volcanics were generated by upwelling of an isotopically-depleted deeper mantle source and are extension-related. Others (e.g. Seyitoğlu and Scott, 1992, Seyitoğlu et al.,1997), however, propose that the N-S extension started in the Latest Oligocene-Early Miocene and hence that even the volcanism which has been active since the Latest Oligocene-Early Miocene may have been generated in an extensional tectonic regime.

In this work, volcanic rocks from the Western Anatolian, Late Cenozoic Volcanic Province have been studied to examine the spatial and temporal variations in magma type and chemical characteristics across the collision zone. Research has been focused on some key areas in the coastal section of Western Anatolia (Fig. 1.3).

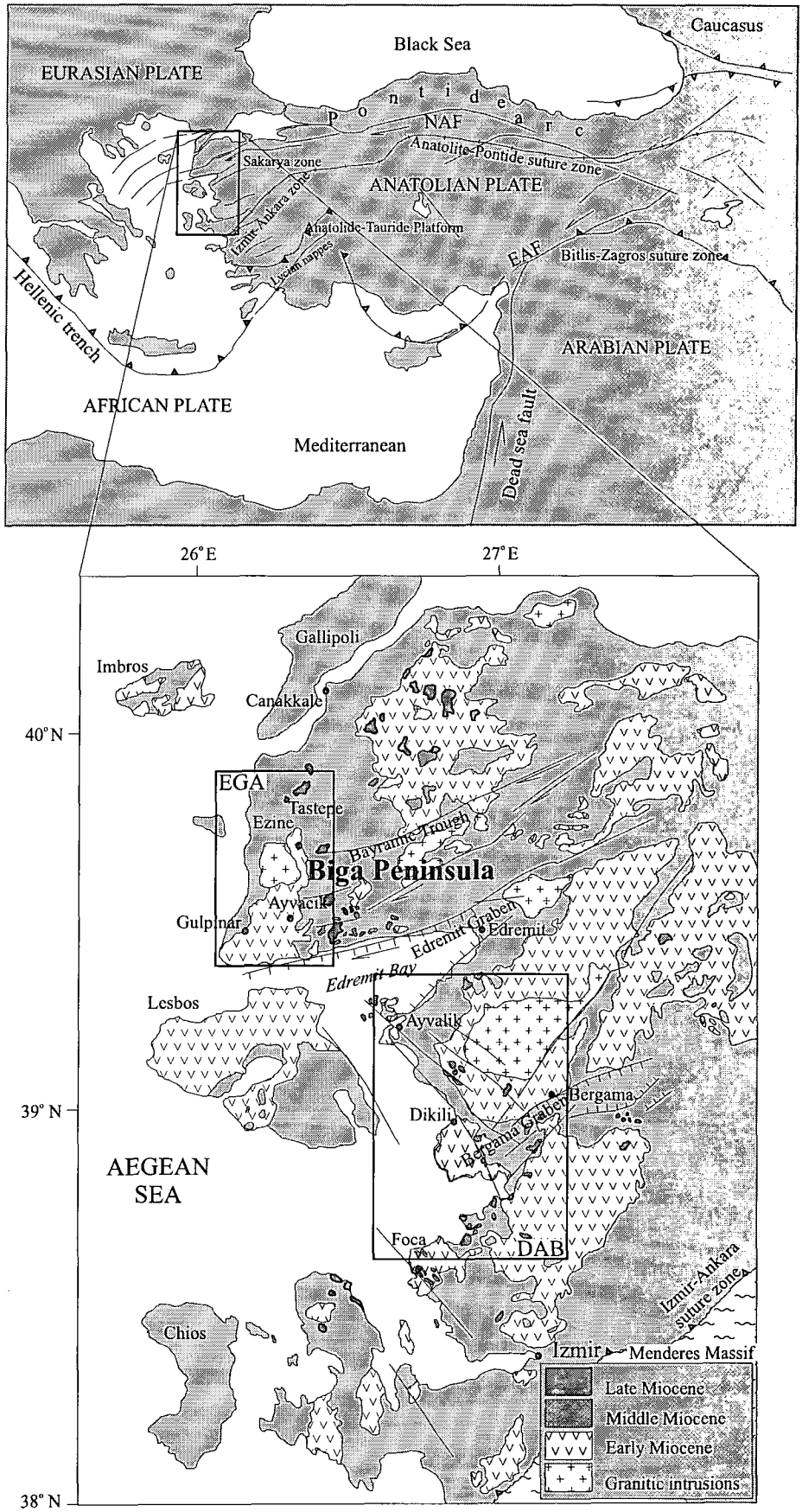

Figure 1.3. *Map of Western Anatolia showing the location of the "Western Anatolian Late Cenozoic Volcanic Province" and the distribution of the vol canic products.*

The major objectives of this thesis are: (1) to document the type and the distribution of volcanic rocks across the collision zone and so to describe the volcanic evolution of the collision zone; (2) to document the spatial and temporal variations in the geochemical characteristics of the magmas to investigate any relationship between the regional tectonic patterns and the mechanisms that may have generated magma; (3) to investigate the type and extent of lithosphere involvement during the processes of subduction, continental collision and late stage crustal stretching, transpression-transtension; (4) to define the compositional variations of the mantle source in time and space; and (5) to achieve major implications for our understanding of how magmas are generated and evolved in continental collision environments.

1.4. Description of the thesis

This thesis consists of seven chapters:

Chapter 2 describes the general geological and the volcano-stratigraphic characteristics of the Western Anatolian, Late Cenozoic Volcanic Province, including the distribution and the type of the volcanic products, eruptive types and spatial-temporal variations.

Chapter 3 documents the major and trace element geochemical characteristics of the volcanic rocks of Western Anatolia and classifies them on the basis of their element concentrations.

Chapter 4 presents the petrographic characteristics of the volcanic rocks. This chapter mainly describes textural and mineral compositional properties of the rock groups from the Western Anatolian Late Cenozoic Volcanic Province using the microscopic observations.

Chapter 5 documents the mineral chemical characteristics of the volcanic rocks. This chapter is in two parts: (1) chemical compositions of minerals (olivine, pyroxenes, feldspars, amphibole, biotite-phlogopite, magnetite and ilmenite) and compositional variations of minerals throughout the magmatic evolution; and (2) calculations and estimations of the magmatic, intensive parameters including pressure-temperature-oxygen fugacity.

Chapter 6 consists of three parts. The first part describes the Nd-Sr isotopic characteristics of the volcanic rocks and presents the preliminary observations that may be useful to interpret the petrogenesis of the rocks. The second part discusses the

possible magmatic processes and develops a petrogenetic model for the magma genesis of the volcanic rocks related to collisional tectonics and crustal thickening events. The third part discusses the petrogenetic model for the magma genesis of the lavas related to lithospheric extensional processes.

Chapter 7 summarises the overall conclusions documented in the previous Chapters.

CHAPTER TWO

GEOLOGY AND VOLCANO-STRATIGRAPHY OF WESTERN ANATOLIA

Introduction

This chapter describes the general geological and the volcano-stratigraphic characteristics of the Western Anatolian, Late Cenozoic Volcanic Province. It incorporates the field observations obtained from the fieldwork carried out in an area of approximately 3500 km^2. The area studied is located in the coastal region of Western Anatolia, between the cities of Çanakkale in the north and Izmir in the south (Fig. 2.1). The fieldwork has been undertaken in two key areas, each of which comprise a number of sub-areas characterised by specific geological and volcanological characteristics. These are: (1) the Ezine-Gulpinar-Ayvacik (EGA) area which is located in the southwest of the Biga Peninsula; and (2) the Dikili-Ayvalik-Bergama (DAB) area which is located further south, between the cities of Izmir and Edremit (Fig. 2.1).

Two, 2-month field seasons have been carried out in Western Anatolia. During the fieldwork, some key areas in both the EGA and the DAB areas have been mapped. In order to establish the relationship between the volcanic units and define the lateral and vertical variations in the volcanic succession, a number of representative sections through the volcanic sequences have been logged. The volcanic facies criteria described by Cas and Wright (1988) have been used to describe the volcanics and distinguish the volcanic formations from one another. These main criteria are eruptive styles, depositional properties, petrographic characteristics and general physical properties of the volcanic products. A total of 350 volcanic rock samples have been collected systematically through the sections for further petrographic studies and geochemical analyses.

Construction of the volcano-stratigraphic sections and mapping in Western Anatolia was difficult not only because of the complexities of the stratigraphic relationships of the volcanic rocks in general but also due to the lack of basic geological

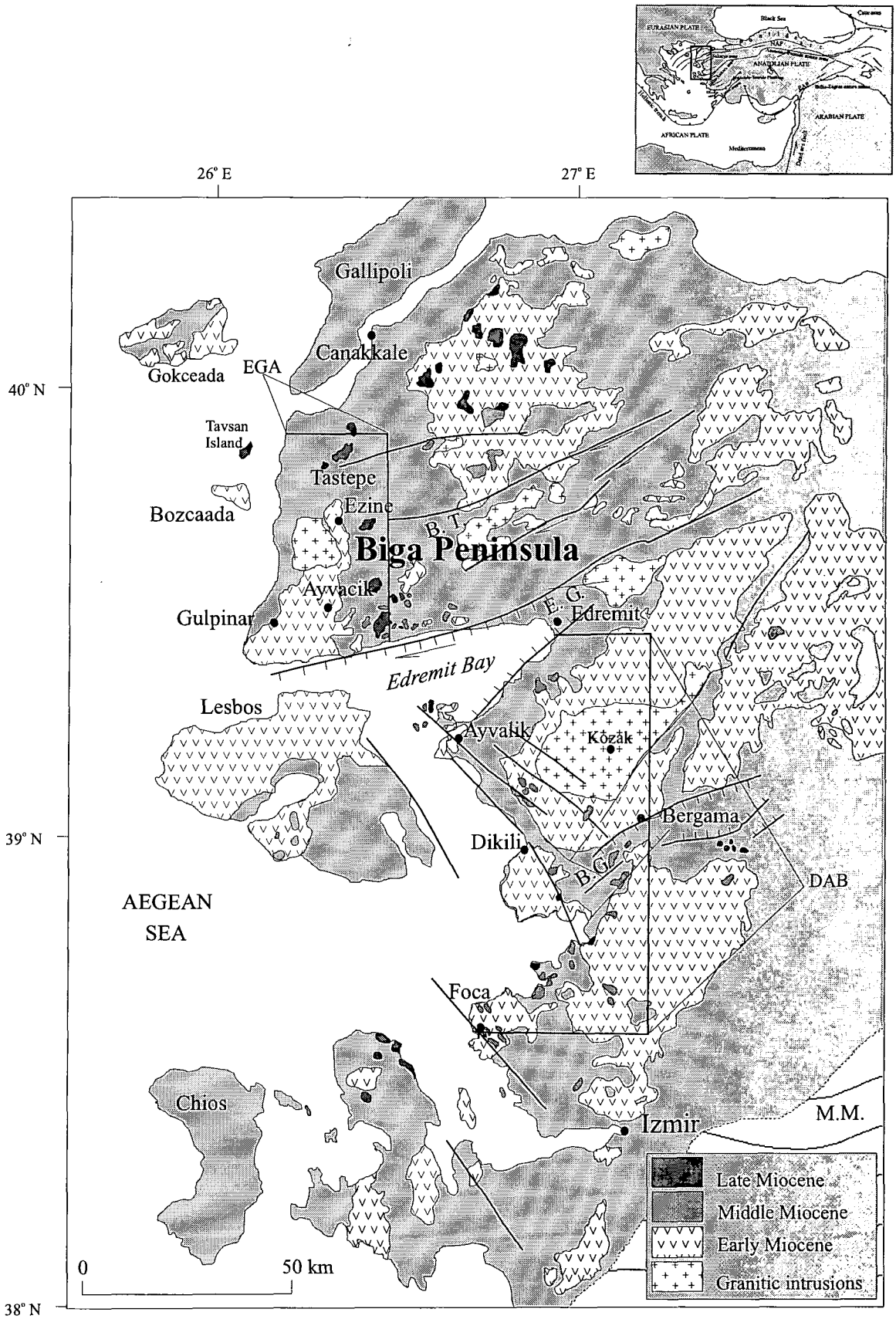

Figure 2.1. *Map of Western Anatolia showing the distribution of the volcanic products and the location of the areas studied. EGA = Ezine-Gulpinar-Ayvacik area; DAB = Dikili-Ayvalik-Bergama area; B.G. = Bergama Graben; E.G. = Edremit Graben; B.T. = Bayramic Trough; M.M. = Menderes Massif.*

information on the stratigraphy of the Western Anatolian volcanic rocks. This study is the first attempt of its kind to differentiate and map volcanic formations in detail in the area. Thus, most of the formation names used here are the names assigned in this study except for those of the basement rocks, plutonic bodies and a few volcanic formations that have previously been named by other workers. The main criteria used to name the volcanic formations are the type localities, rock compositions (given by the observable modal mineralogy here) and general depositional characteristics (for the pyroclastic deposits). The lava units with unique composition and eruptive style, for instance, have been named by their locality and rock type (e.g. The Behram Andesite), whereas the term "Unit" has been used with locality names to term the lava units with multiple composition (e.g. The Dededag Unit). Pyroclastic deposits have been termed by their locality and depositional type (e.g. The Cakmak Tuff or The Bergas Ignimbrite).

In the following section, the geological and volcanological characteristics of the Ezine-Gulpinar-Ayvacik (EGA) and the Dikili-Ayvalik-Bergama (DAB) areas will be introduced.

Table 2.1. *Whole-rock K-Ar ages for selected volcanic rocks from Western Anatolia.*

Sample name	Area	Locality and formation name	Rock Type (TAS classification)	SiO_2 (wt %)	K_2O (wt %)	radiogenic ^{40}Ar ($mm^3\ g^{-1x10-3}$)	Atm. cont. (%)	Age (Ma ± 1σ)
EA270	EGA	Ayvacik (Ayvacik volcanics)	Basanite	41.81	1.43	0.385 ± 0.080	54.1	8.32 ± 0.19
EA418	EGA	Ayvacik (Kovacli dyke swarms)	Basaltic TraAndesite	56.24	2.48	1.662 ± 0.022	35.8	19.7 ± 0.30
EA37	EGA	Assos (Behram andesite)	Trachyandesite	61.67	3.53	3.330 ± 0.060	19.7	20.3 ± 0.60
EA77	EGA	Ayvacik (Koyunevi Ignimbrite)	Rhyolite	73.43	5.04	3.330 ± 0.080	78.9	20.7 ± 0.50
EA67	EGA	Ezine (Kiziltepe Unit)	Trachyandesite	59.96	4.77	3.090 ± 0.040	19.7	21.3 ± 0.30
EA143	DAB	Dikili (Nebiler volcanics)	Basaltic andesite	52.69	2.33	1.312 ± 0.028	41.6	15.2 ± 0.40
EA314	DAB	Bergama (Egrigol andesite)	Andesite	60.32	2.67	1.116 ± 0.021	36.5	15.5 ± 0.30
EA151	DAB	Ayvalik (Akcapinar Unit)	Trachyandesite	60.95	3.42	2.188 ± 0.032	32.9	19.7 ± 0.30
EA278	DAB	Ayvalik (Ballica Unit)	Trachyandesite	59.40	3.27	2.220 ± 0.050	66.9	20.9 ± 0.50

2. 1. The Ezine-Gulpinar-Ayvacik (EGA) Area

The Ezine-Gulpinar-Ayvacik (EGA) area is located in the south-westernmost part of the Biga Peninsula (Fig. 2.1). Tectonically, the area is characterised by E-W and NE-SW trending fault systems. Some of the faults have right-lateral strike-slip patterns and were formed related to the North Anatolian Fault (e.g. the Bayramic Trough), whilst

Table 2.2. *Published radiometric ages for the volcanic rocks from Western Anatolia and the Aegean.*

Locality	(Corresponding) Unit Name	Rock Type	SiO_2 (wt %)	Age (Ma)	Analytical Method	Data Source
Late Miocene-Recent						
Kula (Divlit)	Kula basalt	Alkali basalt	46.36	0.025 ± 0.006	K-Ar	2
Kula (Elekci)	Kula basalt	Alkali basalt	47.13	0.03 ± 0.005	K-Ar	2
Kula (Burgaz)	Kula basalt	Alkali basalt		0.13 ± 0.09	Ar-Ar	1
Kula	Kula basalt	Alkali basalt		1.10 ± 0.03	K-Ar	5
Kula (Burgaz)	Kula basalt	Alkali basalt		1.67 ± 0.22	Ar-Ar	1
Kula (Burgaz)	Kula basalt	Alkali basalt	46.10	7.55 ± 0.11	K-Ar	2
Ezine	Ezine volcanics	Alkali basalt		7.10 ± 2.3	Ar-Ar	3
Ayvacik	Ayvacik volcanics	Basanite	41.44	8.40 ± 0.3	K-Ar	4
Ezine	Ezine volcanics	Alkali basalt	46.38	9.70 ± 0.33	K-Ar	5
Ezine	Ezine volcanics	Alkali basalt	46.39	9.90 ± 0.6	K-Ar	4
Tavsan Island		Alkali basalt	45.00	9.50 ± 0.3	K-Ar	4
Prosa Island		Alkali basalt	45.14	10.1 ± 0.2	K-Ar	4
N of Ezine	Tastepe volcanics	Alkali basalt	47.17	11.0 ± 0.4	K-Ar	4
Izmir (Urla)		Hawaiite		11.3 ± 0.4	K-Ar	5
Izmir (Urla)		Alkali trachyte		11.9 ± 0.4	K-Ar	5
Middle Miocene						
Selendi		Trachyandesite	57.42	14.9 ± 0.3	K-Ar	8
Lesbos Island		Basaltic andesite	52.94	15.5 ± 0.5	K-Ar	5
Usak		Trachyandesite	57.67	15.5 ± 0.4	K-Ar	8
Chios Island		Basaltic andesite	55.92	15.9 ± 0.8	K-Ar	7
Lesbos Island		Trachyandesite		16.5 ± 0.6	K-Ar	6
Izmir (Karaburun)		Trachyandesite		16.6 ± 0.5	K-Ar	5
Early Miocene						
Selendi		Trachyandesite	59.75	16.8 ± 0.7	K-Ar	8
Lesbos Island		Rhyolitic ignimbrit	68.46	16.9 ± 0.6	K-Ar	5
Bergama Graben	Kalarga andesite	Andesite	61.13	17.3 ± 0.6	K-Ar	5
Bergama Graben	Kalarga andesite	Andesite	62.44	17.6 ± 0.6	K-Ar	5
Dikili	Karagol Lavas	Trachyandesite	61.37	17.7 ± 0.6	K-Ar	5
Usak		Rhyolite	71.80	17.6 ± 0.1	K-Ar	8
Lesbos Island		Trachyandesite	62.18	18.0 ± 0.6	K-Ar	5
Izmir (Karaburun)		Trachyandesite		18.2 ± 0.5	K-Ar	5
Izmir (Karaburun)		Trachyandesite		19.2 ± 0.6	K-Ar	5
Gulpinar	Babakale Unit	Trachyandesite	57.82	19.5 ± 0.6	K-Ar	5
Bozcaada		Trachyandesite	58.92	19.6 ± 0.4	K-Ar	4
Selendi		Rhyolite		20.3 ± 0.6	K-Ar	8
Izmir (Karaburun)		Trachyandesite		21.3 ± 0.7	K-Ar	5
Ayvacik	Dededag Unit	Trachyandesite	62.93	21.5 ± 0.7	K-Ar	5
Lesbos Island		Trachyandesite		21.5 ± 0.6	K-Ar	6
Edremit		Trachyandesite	57.58	21.9 ± 0.6	K-Ar	4
Oligocene						
E of Edremit		Andesite		23.6 ± 0.6	K-Ar	9
Can				27.6 ± 0.6	K-Ar	4
Gokceada		Trachyandesite	61.05	30.4 ± 0.7	K-Ar	4
Ayvalik		Trachyandesite	57.32	31.4 ± 0.4	K-Ar	2
Gokceada		Trachyandesite	57.9	34.3 ± 1.2	K-Ar	4
Late Eocene						
Biga		Dacite	63.57	37.3 ± 0.9	K-Ar	4

Data source: (1) Richardson Bunbury, 1996; (2) Ercan et al.,1984; (3) Paton, 1992; (4) Ercan et al., 1995; (5) Borsi et al., 1972; (6) Pe-Piper, 1980; (7) Bellon et al., 1979; (8) Seyitoglu et al., 1997; (9) Krushensky, 1976.

others are normal faults formed in a relation to the N-S extension and the opening of the Aegean (e.g. the Edremit Graben).

In the EGA area, the Cenozoic igneous activity started with pluton emplacement (the Kestanbol Pluton) which has been dated as 28 Ma (Bingöl et al., 1982). The volcanic activity followed the emplacement of the pluton after an about 6-Ma hiatus.

The oldest dates obtained for the volcanic rocks are 21.3 ± 0.3 Ma (in this study; Table 2.1) and 21.5 ± 0.7 Ma (Ercan et al., 1982; 1995). The volcanic products cover well over 1200 km^2 area with a thickness reaching over 900m. They are represented by lava flows, domes and pyroclastic fall and flow deposits. Abundant dyke swarms cut the volcanic successions in some places. The Early stage of volcanic activity (the Early Miocene) commenced with lava flows and continued with lava and pyroclastic successions. This stage of activity was restricted in the short interval of time from 21.3 ± 0.3 Ma to 20.3 ± 0.6 Ma and was followed by the injection of abundant dyke swarms which have been dated as 19.7 ± 0.3 (Table 2.1). Middle Miocene activity is absent in the EGA area.

A new stage of volcanic activity began in the Late Miocene and produced locally developed, small lava flows of basic and ultrabasic compositions. The available radiometric data indicate that the Late Miocene volcanism continued during the period from 11.0 ± 0.4 Ma (Ercan et al., 1995) to 8.32 ± 0.19 Ma (Table 2.1).

In the following sections, characteristics of the lithological formations of the EGA area will be presented as two different sub-areas each of which represents a unique volcano-stratigraphic sequence. These are: (1) the Ezine-Ayvacik section (in the north); and (2) the Assos-Babakale-Gulpinar section (in the south). Although there is a close similarity between the Early Miocene volcanic products from the two sections in terms of the compositions and age of the rocks, the physical properties of the products are remarkably different from one another. The volcanic succession in the former consists dominantly of lava flows with minor debris (lahar) and ash flow deposits, whilst the volcanic rocks form a large ignimbrite deposits with much lesser amount (volumetrically) of lava flows in the later. The two sections are separated from one another by the Tuzla fault system which obscures the stratigraphic relationships between the rock formations from these two sections (Fig. 2.2).

2. 1. 1. The Basement Rocks

The basement of the volcanic sequences in the EGA area is represented by two different formations: (1) a metamorphic basement unit known as the Kazdag Massif; and (2) a Palaeo-Tethyan subduction-accretionary complex known as the Karakaya Complex.

The metamorphic rocks of the Kazdag Massif are observed in the southern and southeastern part of the Biga Peninsula. The Massif has a total structural thickness

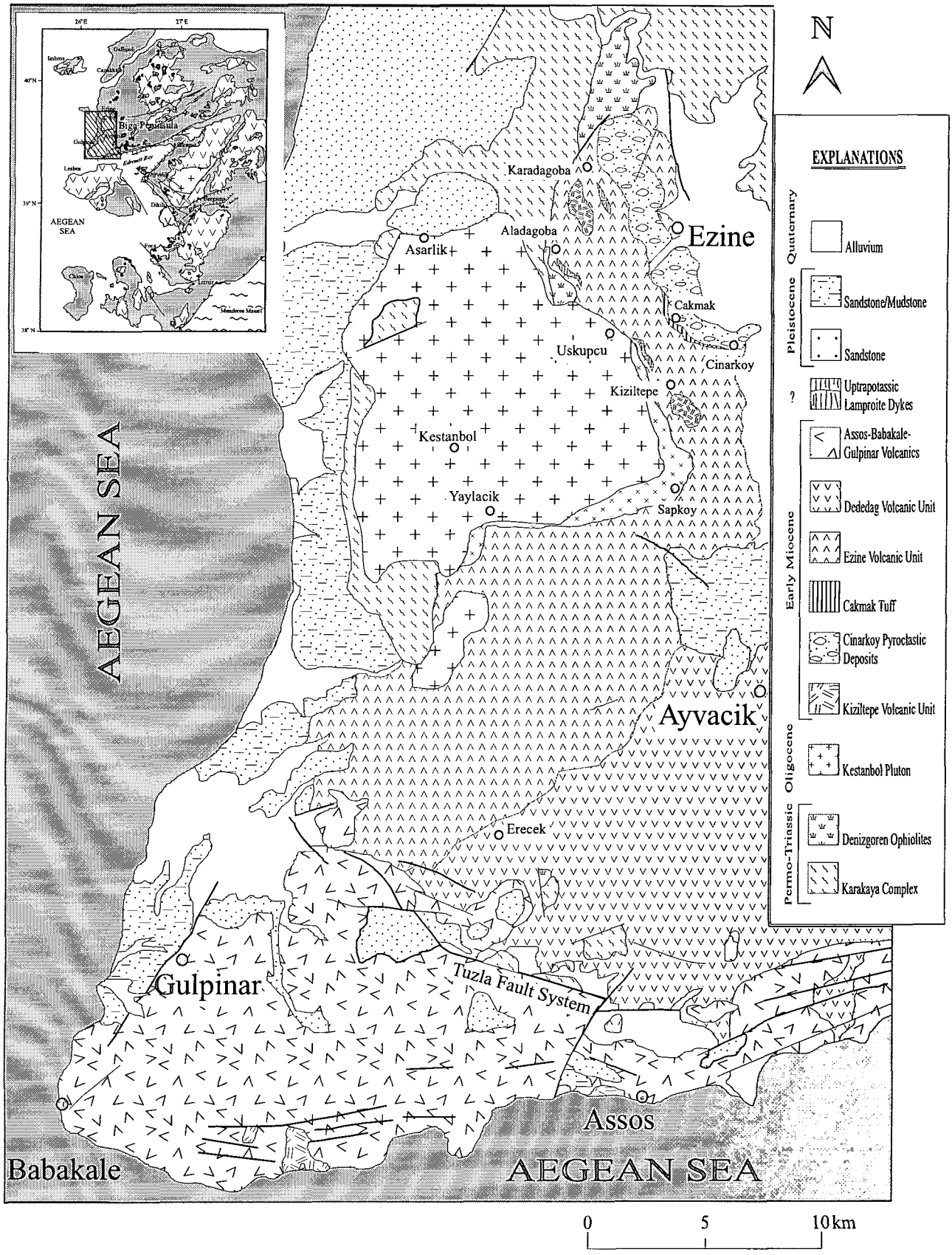

Figure 2.2. *Simplified geological map of the SW part of the Biga Peninsula (modified from Karacik and Yilmaz, 1995)*

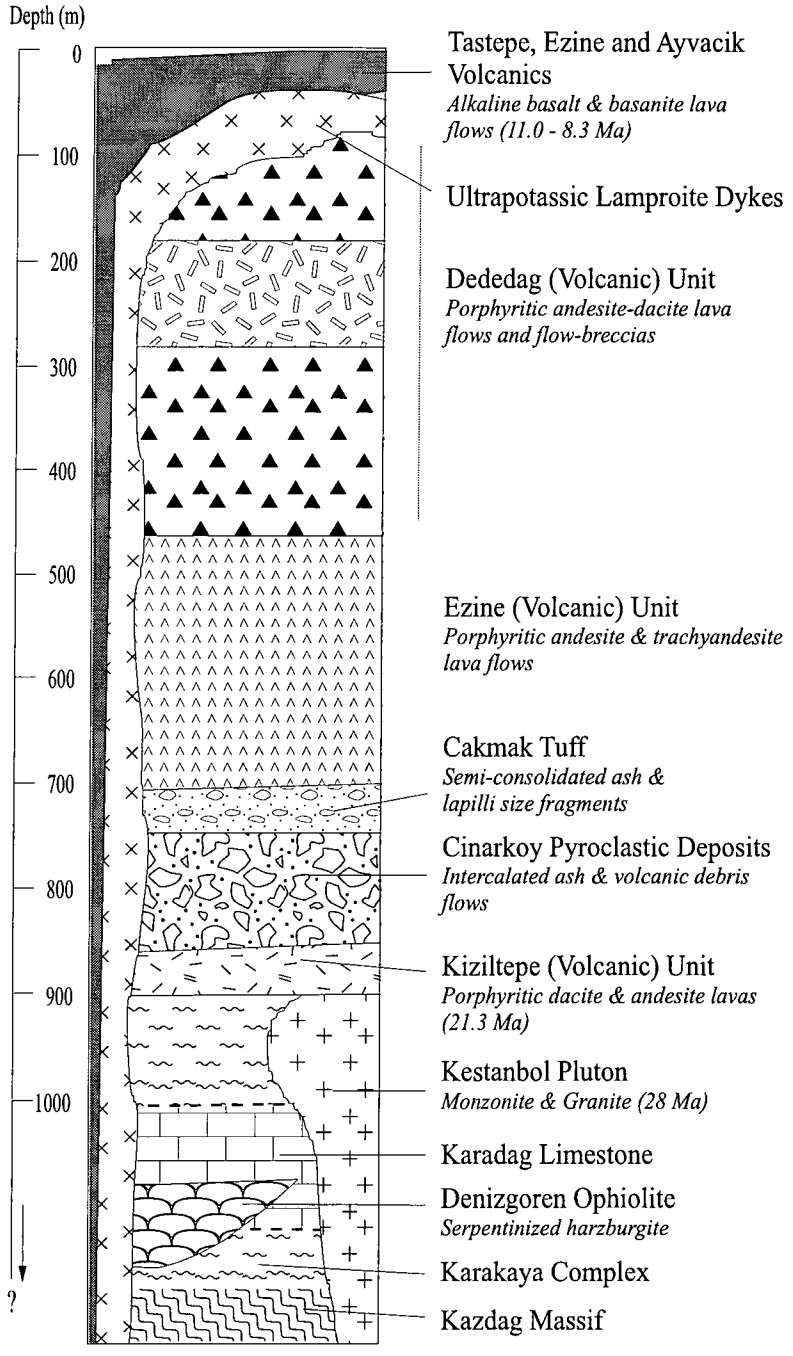

Figure 2.3. *Schematic generalised stratigraphic column illustrates the volcano-stratigraphy of the Ezine-Ayvacik section*

of over 10 km (Bingöl, 1969; Okay et al., 1991) and is composed mainly of quartzo-feldspathic micashist and gneiss intercalated with marble and amphibolite. According to Okay et al. (1991), the core of the Massif includes meta-ophiolite assemblages of meta-gabbro, meta-harzburgite, plagiogranite and amphibolite. These metamorphic assemblages have a faulted contact with an Upper Cretaceous Neotethyan mélange and are intruded by Oligo-Miocene granitoids. Okay et al. (1991) and Pickett (1994) interpreted the Massif as a metamorphic core complex that was exhumed along normal faults, detachments and extensional mylonite zones during the Miocene. Bingöl (1971) used radiometric dating on the Kazdag gneisses to suggest a pre-Late Triassic age for the protoliths of these rocks. More recently, however, Okay et al. (1996) used $^{207}Pb/^{206}Pb$ dating to obtain Upper-Middle Carboniferous ages (292 ± 8 Ma and 323 ± 14 Ma) of single zircon crystals separated from a cordierite-gneiss and a quartzo-feldspathic gneiss. They interpreted these dates as representing the high-grade metamorphism and migmatization ages of the rocks of the Kazdag Massif.

The metamorphic rock assemblages of the Karakaya Complex are abundant in the Biga Peninsula and the Edremit area. The Complex is composed mainly of low-grade meta-sedimentary and meta-volcanic rocks and a succession of clastic deposits. Okay et al. (1991) described the Karakaya Complex as intra-oceanic fore-arc deposits and divided them into three different units, namely the Nilüfer, Ortaoba and Çal Units. The Nilüfer Unit is best observed in the southern part of the Biga Peninsula and Edremit area. It contains green spilitic basalts, volcaniclastic debris flow deposits, ignimbrites, volcanogenic sedimentary rocks and recrystallised limestone. Kaya and Mostler (1992) dated the Nilüfer Unit as Middle Triassic using conodonts. The Nilüfer Unit is tectonically overlain by the clastic rocks of the Ortaoba Unit which is composed mainly of disrupted basalt, siliceous mudstone, grey chert and sandstone. These rock assemblages are tectonically overlain by debris flows, disrupted fragments of Upper Permian carbonate platform sequences and basal clastic rocks of the Çal Unit (Okay et al., 1991; Pickett and Robertson, 1996).

The rocks of the Karakaya Complex have been, in general, deformed extensively and affected by greenschist facies metamorphism leading to the formation of spilitised basalts. Pickett and Robertson (1996) used the existence of MORB-type basic rocks overlain by pelagic sediments to suggest that the Karakaya Complex was originally formed in a wide oceanic basin.

The metamorphic rocks of the Karakaya Complex are accompanied by serpentinized harzburgite (the Denizgören ophiolite of Okay et al., 1991). These ophiolitic assemblages form large thrust sheets with approximately SSW-NNE orientation from Ezine to Çanakkale and tectonically overlie the Permian platform carbonate sequences (the Karadag Unit of Okay et al., 1991) and the other metamorphic lithologies of the Karakaya Complex. Pickett (1994) proposed that the geochemical characteristics of NW Anatolian ophiolites are similar to those from supra-subduction-type ophiolites of the Eastern Mediterranean such as Troodos and Oman ophiolites.

2. 1. 2. The Ezine-Ayvacik Section

2. 1. 2. 1. The Kestanbol Pluton

A plutonic body known as the Kestanbol Granite (Karacik and Yilmaz, 1995) intruded the basement units of the Ezine-Gulpinar-Ayvacik area. Its outcrops are common over a large area (approximately 260 km^2 of total outcrops) to the southwest of the town of Ezine, between the villages of Asarlik to the northeast, Yaylacik to the south and Kestanbol to the southwest (Fig. 2.2). Bingöl et al. (1982) reported a K-Ar age of 28 Ma for the pluton. The rock types forming the pluton are dominantly quartz-monzonite, monzonite and granite in composition. They are made up of oligoclase (An_{36-45}), alkali-feldspar, quartz, biotite, hornblende, augite and minor amounts of apatite, sphene, magnetite and zircon. Textures vary between inequigranular and porphyritic, with grain sizes of about 1 to 5mm, although some K-feldspar megacrysts may reach 10-12mm. Towards the edge of the pluton, fine-grained rock types with the dominant textures of micro-granular porphyritic to granophyric are observed. Extensive aplite and aplogranite dykes and quartz veins have cut the pluton. Pegmatitic dykes have also been found in some areas. The wall rocks are represented by the metamorphic assemblages of Karakaya Complex, Karadag Unit (carbonate sequences) and serpentinized harzburgite of the Denizgören ophiolite. Contact metamorphism has been identified around the pluton leading the formation of hornblende-hornfels and pyroxene-hornfels facies rocks. Contact metamorphism has produced the assemblages of garnet, diopsite, epidote, tremolite, actinolite, wollastonite and chlorite along the contact between the Kestanbol Pluton and the dolomitic rocks of the Karadag Unit. Along the southwest margin of the Pluton, gneissic texture has been developed.

2. 1. 2. 2. The Kiziltepe (Volcanic) Unit

The Kiziltepe Unit crops out to the southwest of Ezine, in the vicinity of the villages of Kiziltepe, Uskupcu, Karadagoba and Çinarköy (Fig. 2.2). It is composed of porphyritic dacite and andesite and covers an area of about 10-15 km^2. It overlies unconformably the metamorphic assemblages and ophiolitic rocks of the basement units. The volcanic rocks of this Unit also cover the contact between the basement rocks and the monzonites and granites of the Kestanbol pluton along the southeastern border of this intrusive body. The Unit consists mainly of massive lava flows, displaying variable shades of pink, grey and purple. The total thickness of the Unit varies between 60 and 100m. The rocks are composed mainly of plagioclase, K-feldspar, augite, biotite and minor amounts of sphene, zircon and magnetite. Some dacite samples also contain phenocrysts of quartz. In the area between Çinarköy and Kiziltepe villages, the lavas of this volcanic Unit have effectively been altered, leading the formation of iron oxides on joints and flow surfaces of the lavas.

An andesite sample from the lavas of this Unit gave a K-Ar age of 21.3 ± 0.3 Ma (Table 2.1).

2. 1. 2. 3. The Çinarköy Pyroclastic Deposits

Pyroclastic flow deposits crop out over a large area to the south of Ezine, in the vicinity of Çinarköy village and to the west of Ezine, in the vicinity of Karadag village. They consist mainly of intercalated unconsolidated or semi-consolidated ash flow and volcanic debris flow deposits. Ash layers have variable thickness up to 2-3m, whereas the thickness of the deposits as a whole, varies from few meters to 60m. The deposits are internally structureless, unsorted to poorly sorted and matrix-supported. The matrix is made up of grey, pink, orange and brown-coloured, sand-size volcanic materials and includes volcanic clasts of pebble-size to 0.5-1m in diameter. The clasts are andesitic and dacitic in composition and mostly exhibit porphyritic textures.

2. 1. 2. 4. The Çakmak Tuff

The Çakmak tuff layer overlies the Çinarköy pyroclastic deposits between Ezine and Ayvacik towns. It is mainly composed of semi-consolidated fine ash and lapilli size pyroclastic fragments. Its best exposure has been observed to the east of Çakmak village where it crops out over a small area of about 2-3 km^2. The tuff layer mantles the topography and its thickness varies from 1m to 15m. Pumice is the most common

detrital material comprising approximately 80% of the total. Lithic fragments of andesites and dacites are common at the base of the layer and decrease upwards. In some localities, it consists of alternations of fine-ash and sandstone beds, which are entirely made up of volcanic rock fragments. The Çakmak tuff layer is wedged out to the southeast, between the Çinarköy pyroclastic deposits and the Ezine Unit.

2. 1. 2. 5. The Ezine (Volcanic) Unit

The Ezine Unit overlies the Çinarköy pyroclastic deposits and the Çakmak tuff layer over a wide area between Ezine and Ayvacik and in some localities to the west of Ayvacik (Fig. 2.2). It is entirely made up of massive porphyritic lava flows. The rocks are mainly andesitic and trachy-andesitic in composition and are light grey, beige-yellowish in colour. In some localities, the alteration of augite phenocrysts causes a change in colour to reddish and purple. The maximum thickness has been estimated as approximately 300m, although the thickness of the lavas varies from one locality to another depending mostly on degrees of resistance of the rocks to erosion which is controlled mainly by degree of alteration.

The rocks are composed mainly of plagioclase, K-feldspar, augite and biotite. Most samples also contain magnetite, apatite, zircon and ilmenite. The groundmass is made up of microcrysts of plagioclase and, rarely, augite set in a partly glassy matrix.

To the west of Ayvacik, lava flows have extensively been affected by weathering and alteration. Iron oxide and copper salts are common on joints and flow surfaces. Secondary albite, calcite, sericite and chlorite were formed mainly as a consequence of sericitic alteration. In some areas, alteration also formed economic mineral deposits such as clay minerals of kaolinite-montmorillonite (to the southwest of Ezine) and Cu-Zn mineralisation (to the west of Ayvacik).

2. 1. 2. 6. The Dededag (Volcanic) Unit

The Dededag volcanic Unit crops out in a large area around the town of Ayvacik. In the area studied, the total extent of the Unit is approximately 300 km^2. It consists mainly of porphyritic andesite and dacite lava flows and flow-breccias. The lavas form massive layers almost constant texture and colour. In some places, the lavas

were emplaced as cryptodomes[1] indicating that near-surface intrusions caused the formations of the lavas.

The rocks are mainly composed of phenocrysts of plagioclase, augite, K-feldspar, biotite, magnetite and minor zircon and apatite in a groundmass containing microcrysts of plagioclase, minor augite and a cryptocrystalline matrix.

In the Dededag Unit, flow-breccias (fragmental rocks) are as abundant as the porphyritic, massive lava flows with which they appear in lateral continuity. The flow-breccias show compositional and textural similarities to the lava flows. In some parts, they have striated and/or gouged margins that may indicate that they have been formed by autobrecciation during the movement of the highly viscous lavas.

In some places (e.g. Erecek village), volcaniclastic sediments are intercalated with the lava and breccia flows of the Dededag Unit. The sediments are mostly lacustrine sandstones and have a maximum thickness of about 15m.

2. 1. 2. 7. The Ultrapotassic Lamproite Dykes

Locally developed, minor, isolated lamproite dykes have been observed in a few localities around the town of Ezine (Fig. 2.2). To the south of Ezine, between Kiziltepe and Uskupcu villages, a small (with a total extent of only 0.5 km^2), NW-SE trending dyke is found near the contact zone between the Ezine Unit and the peripheral micro-granitic zone of the Kestanbol Pluton. Further northwest, to the north of Aladagoba village, a few small (with a total extent of <0.3 km^2) lamproite dykes cut the lavas of the Ezine Unit. The lamproites are hard, compact, fresh looking, aphyric or microporphyritic rocks with a characteristic black colour. They are mostly absarokite in composition and contain microcrysts of augite, olivine, plagioclase, Ti-phlogopite, magnetite and ilmenite.

2. 1. 2. 8. The Tastepe Volcanics

The name "Tastepe Volcanics" was first used by Ertürk et al. (1990) for the basic volcanic rocks that crop out in an area of about 7.5 - 8 km^2 between the city of Çanakkale in the north and the town of Ezine in the south (Fig. 2.1). The best exposure is observed in the east of Tastepe village in a cutting on the main Çanakkale to Ezine road. The products of the Tastepe Volcanics are also abundant in the northeast of

[1] A dome-like uplift of the surface rocks as described by Cas and Wright (1988).

Tastepe. They consist mainly of small, isolated lava flows, with a total thickness of about 50-60m. The rocks are fine-grained, aphyric and/or olivine-phyric basalts. They are composed mainly of plagioclase, diopside, olivine, ilmenite and magnetite.

The lavas in most places lie on the ophiolitic rocks of the basement lithologies (the Denizgören ophiolite). To the northeast of Tastepe, the lavas have been found overlying young sedimentary rocks which made up of limestone (lacustrine sediments) interbedded with poorly consolidated sandstone. Towards the east and southeast of Tastepe village, a number of SW-NE trending faults have been observed cutting the lavas. The fault zones are characterised by abundant brecciated, serpentinized harzburgite of the Denizgören ophiolites.

Ercan and Satir (1994) and Ercan et al. (1995) reported whole-rock, K-Ar age of 11.0 ± 0.4 Ma for the rocks of the Tastepe Volcanics (Table 2.2). This is the oldest known age for the Late Miocene volcanic rocks in the EGA area.

2. 1. 2. 9. The Ezine Volcanics

The rocks of the Ezine Volcanics crop out around the town of Ezine. They are represented by small, isolated lava flows in the vicinity of Kizilkoy, Araplar and Akköy villages. The lavas have a total aerial extent of approximately 6.5 - 7 km^2. The average thickness is about 5-10m, but towards the southeast of Ezine, the maximum thickness was observed as 30-40m. The rocks are compositionally rather similar to the basalts of the Tastepe Volcanics. They are mainly fine-grained, olivine-phyric basalts. More basic rock types such as basanites are also found, particularly in the vicinity of Akköy village (North of Ezine). The rocks are composed mainly of microcrysts of plagioclase, diopside, olivine, ilmenite and magnetite set in a black, glassy matrix.

The lavas lie on the southern side of the Bayramic trough, which extends in a NE-SW direction along the middle branch of the North Anatolian Fault (NAF). Interpretation of the tectonic processes and understanding the fault geometries and their relationships with lava formations are difficult because of the complex tectonic history of the area. Although the area has widely been affected by normal faulting linked to the opening processes of the Aegean, tectonic and seismological analyses (e.g. Barka and Kadinsky-Cade, 1988; Zanchi and Angelier, 1993) have shown that the strike-slip activity related to the NAF is predominant in this part of Western Anatolia. Existence of

both normal and strike-slip fault patterns further emphasises that the distribution of the lavas is influenced by both of the processes mentioned above.

K-Ar ages of 9.7 ± 0.4 Ma and 9.9 ± 0.6 Ma have been reported for the Ezine volcanics by Borsi et al. (1972) and Ercan et al. (1995) respectively. Paton (1992) also obtained a date of 7.1 ± 2.3 Ma by Ar-Ar laser ablation for the basalts from the same area (Table 2.2).

2. 1. 2. 10. The Ayvacik Volcanics

They are exposed in two different localities around the town of Ayvacik. These are Karayiv hill, which is located to the northeast of Ayvacik, and Ahmetce village, which is located to the southeast of Avyacik. On Karayiv hill, where the lavas are best exposed, they cover an area of approximately 3-4 km^2 with a total volume of about 0.2 km^3.

Plate 2.1. *Columnar jointed basalts of the Ayvacik Volcanics.*

The volcanic products consist mainly of small, isolated lava flows. The rocks are composed almost entirely of fine-grained, aphyric and/or weakly porphyritic basanites.

The microcrysts are plagioclase, diopside, olivine, ilmenite and magnetite in a black glassy groundmass. The rocks have a hard, compact appearance and are black in colour. Columnar jointing is abundant (Plate 2.1). The joint spacing is generally about 30-35 cm and the joint surfaces are vertical and sub-vertical.

In the Ahmetce area, the Ayvacik Volcanics are represented by small, isolated lavas. They were formed along N-E trending fault boundaries related to the opening processes of the Edremit Bay. The lavas are generally poorly exposed with a total estimated volume of approximately 0.02 km^3. They have similar composition and petrographic properties to those that crop out on Karayiv hill.

A basanite sample from Karayiv, which is considered to be the youngest volcanic product of the Ayvacik volcanics according to the field observations, has been analysed using the K-Ar method, as 8.32 ± 0.19 Ma (Table 2.1). This is the youngest known age for the Late Miocene volcanic rocks in the EGA area. Ercan et al. (1995) also reported K-Ar age of 8.40 ± 0.30 Ma for the basic rocks from Karayiv area (Table 2.2).

2. 1. 3. The Assos-Babakale-Gulpinar Section

The distribution and the stratigraphic position of the lithological formations of the Assos-Babakale-Gulpinar section are shown in Figures 2.4 and 2.5 respectively. The following paragraphs describe the formations in order of their position in the volcano-stratigraphic succession, from bottom to top.

2. 1. 3. 1. The Babakale (Volcanic) Unit

The Babakale Unit consists mainly of lavas and volcanogenic debris-flows. The Unit was first named by Karacik and Yilmaz (1995) as the "Babakale lava-lahar association". Volcanic products of the Unit crop out to the east of Babakale, along the coastal line of the south-westernmost part of the Peninsula (Fig. 2.4). The maximum thickness of the Unit has been measured as approximately 150-200m. Lavas are mainly porphyritic andesites and dacites. They contain phenocrysts of plagioclase, augite, K-feldspar, biotite and magnetite.

Debris-flows contain clasts which are between 10 mm and 25 cm in diameter. They are mostly sub-angular to sub-rounded (Plate 2.2). All clasts have volcanic origin

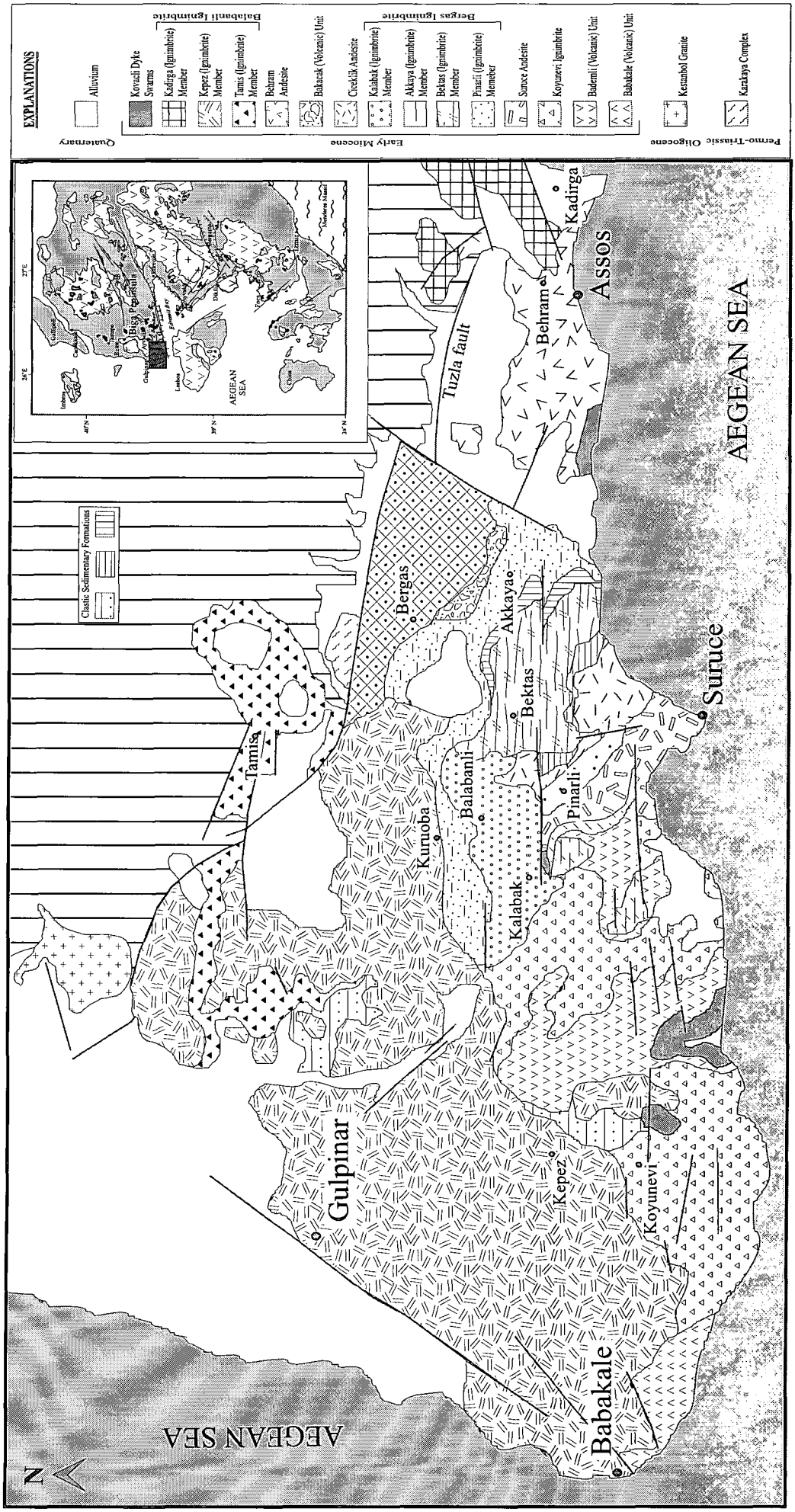

Figure 2.4. Geological map of the Assos-Babakale-Gulpinar Section (modified from Karacik and Yilmaz, 1995)

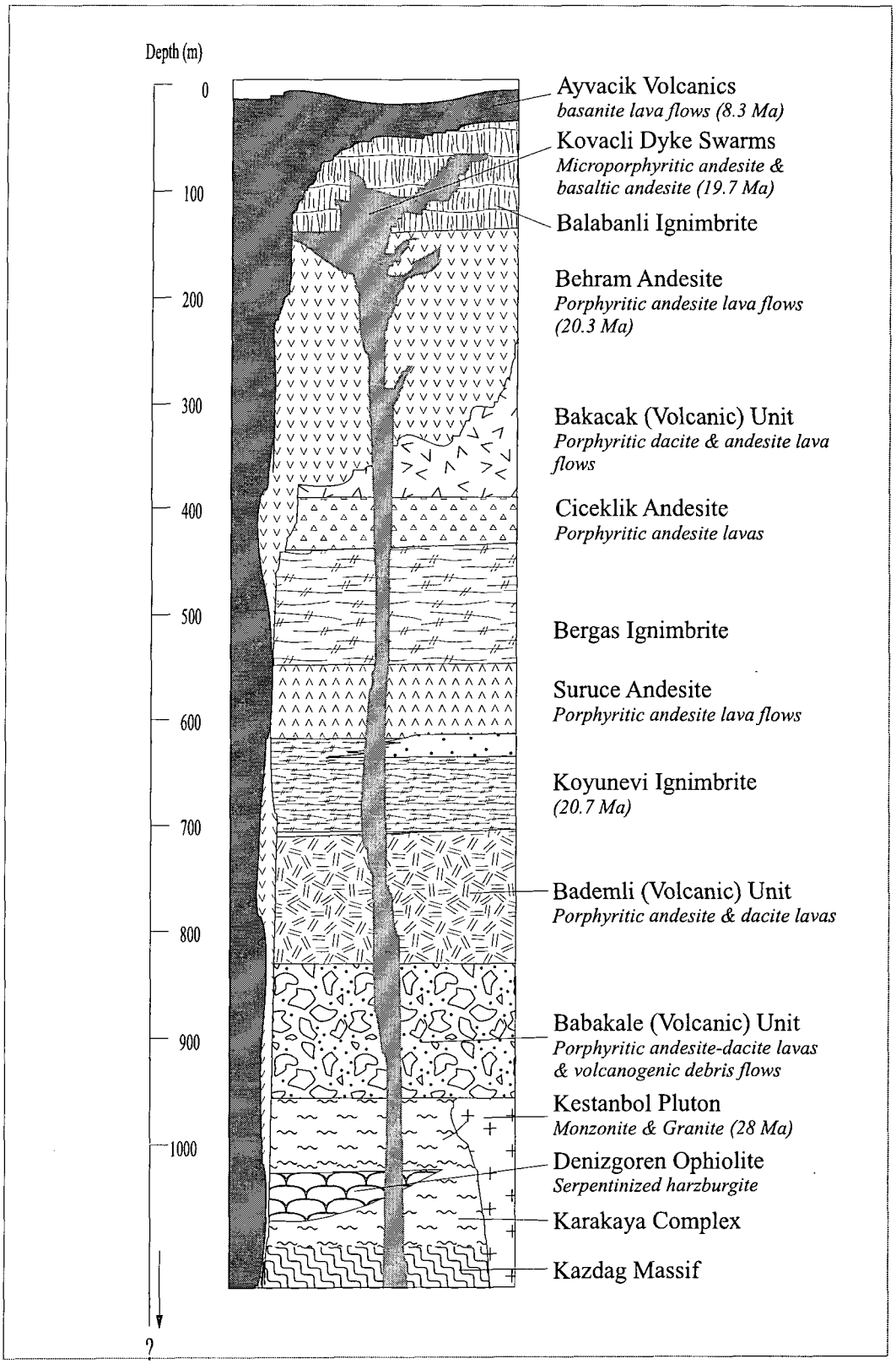

Figure 2.5. *Schematic generalised stratigraphic column illustrates the volcano-stratigraphy of the Assos-Babakale-Gulpinar section.*

and display compositional characteristics similar to the lava flows. In some places, extensive weathering and alteration formed Fe oxide and secondary clay mineralisation, particularly around the outer zone of the clasts.

Plate 2.2. *Debris flow deposits of the Babakale volcanic Unit.*

The Babakale Unit is stratigraphically the oldest in the Assos-Babakale-Gulpinar section. In most localities, it is cut by extensive dyke systems (the Kovacli Dyke Swarms). The Unit is overlain by the Kepez Ignimbrites towards the north and by the Koyunevi Ignimbrite to the east.

2. 1. 3. 2. The Bademli (Volcanic) Unit

The Bademli Unit crops out to the east of Kepez and to the south of Bademli village with a total aerial extent of 20 km^2. It is composed mainly of massive lava flows of porphyritic andesites and dacites. The total thickness of the lavas has been estimated about 150-200m. Plagioclase is the most abundant phenocryst and is accompanied by K-feldspar (sanidine), augite and biotite. Unlike all other volcanic products in the Ezine-Gulpinar-Ayvacik area, some rocks of this unit also contain amphibole xenocrysts. They are mostly pargasitic and ferroan-pargasitic hornblende and surrounded by opaque outer zone.

Plate 2.3. *Basaltic and basaltic-andesitic feeder dykes cut the massive lava flows of the Bademli Unit with NNW-SSE and NNE-SSW orientations.*

In the coastal part of the region, the lavas of the Bademli Unit are cut by a number of E-W trending, listric normal faults that are related to the opening of the Edremit Bay (Graben). A number of dyke swarms (the Kovacli Dyke Swarms) also cuts the massive lavas (Plate 2.3).

2. 1. 3. 3. The Koyunevi Ignimbrite

The Koyunevi Ignimbrite crops out over a large area along the Tuzla stream valley and in the south-westernmost part of the Biga Penisula, along the coast (Fig. 2.4). The total thickness of the ignimbrite is about 30-35m. It consists of several cooling parts. The lower part is characterised by a thin (approximately 1m) ground surge deposit which mantles the topography. The ground surge is followed by pumice fallout deposit which consists of fibrous pumice clasts. In most localities, pumice clasts are porphyritic and contain phenocrysts of zoned plagioclase, biotite, quartz and oxides. Clasts are also strongly flattened in some localities. Pumice fallout deposits are followed by a flattened tuff layer with a thickness of about 2m. The tuff layer contains abundant pumice as well as lithic fragments of mainly dacite and andesite.

The upper part of the ignimbrite is a conspicuous pinkish-reddish, welded layer defining flat structural surfaces on top of the pyroclastic sequence (Plate 2.4). It overlies the flattened tuff layer and consists mainly of three different zones: (1) a slightly welded zone (2-3 m-thick) which is characterised by glass shards, lithic fragments of dacites and andesites and crystals of biotite, plagioclase, quartz, oxides and K-feldspar; (2) a welded zone which has a thickness of approximately 5-10m and includes flattened pumice fragments, small fiamme and lithics; (3) a sillar zone, which is characterised by abundant vapour phase crystallisation of K-feldspar, tridymite and cristobalite resulting from the percolation of hot gases through the pyroclastics during cooling. The sillar zone is the extremly welded portion of the ignimbrite and has a thickness of about 20m and regular columnar jointing.

Plate 2.4. *Welded zone of the Koyunevi Ignimbrite forming flat structural surface on top of the pyroclastic sequence.*

The field evidence show that the Koyunevi ignimbrite is stratigraphically the oldest ignimbrite formation among the pyroclastic deposits erupted in the Assos-Tuzla-Gulpinar area. A sample from this ignimbrite has been analysed, using K-Ar method, as 20.7 ± 0.3 Ma (Table 2.1).

2. 1. 3. 4. The Suruce Andesite

The lavas of the Suruce Andesite crop out around Cape Suruce (Fig. 2.4) and overlie the pyroclastic assemblages of the Koyunevi Ignimbrite. The lavas have a total thickness of about 50m and extend over an area of 10 km^2. The rocks are hard, compact porphyritic andesites, generally variable shades of grey and beige. The phenocryst phase consists mainly of plagioclase, hypersthene, augite, K-feldspar, biotite and magnetite.

The lava flows are extensively cut by E-W trending listric normal faults and locally intercalated with thin layers (<5-10m) of volcanogenic lacustrine sandstone. Towards the north and the northeast from the coast, the lavas are overlain by the pyroclastics of the Bergas Ignimbrite. The Suruce Andesite is a good stratigraphic marker horizon between the Koyunevi and Bergas Ignimbrites.

2. 1. 3. 5. The Bergas Ignimbrite

The Bergas Ignimbrite is exposed over an area of approximately 55-60 km^2 around the villages of Bergas, Pinarli, Bektas, Akkaya and Kalabak (Fig. 2.4). It is named after its best outcrops in the vicinity of Bergas village. The Ignimbrite is exposed as a succession of prominent, partly cliff-forming ignimbrite sheets, which are laterally continuous and of near-constant thickness. Individual sheets range in thickness from 15 to 40m. Four successive sheets may be distinguished and as they represent progressive deposition within the ignimbrite formation may be designated as members. These are: (1) the Pinarli member; (2) the Bektas member; (3) the Akkaya member; and (4) the Kalabak member. Each member has a characteristic texture and most may be further subdivided into sub-units on the basis of depositional types, degree of welding and devitrification. Some members are also separated from one another by clastic sedimentary rock formations.

The Pinarli member crops out to the southeast of Pinarli village (Fig. 2.4). It is approximately 35m thick and consists of a succession of three different parts (Fig. 2.6a). The lower part begins with a rhyolitic basal pumice fall deposit which exhibits internal stratification resulting from fluctuations in grain size and lithic content. The lithic concentration decreases upwards. The basal pumice fall deposits are overlain by an internally-layered pumice deposit that includes locally-developed ash beds. The ash layers are generally graded and partly intercalated with pumice falls. Pumice clasts exhibit a strongly fibrous texture and include phenocrysts of plagioclase, biotite and quartz. A layer of pumice tuff with a thickness of about 0.5-1m overlies the fallout

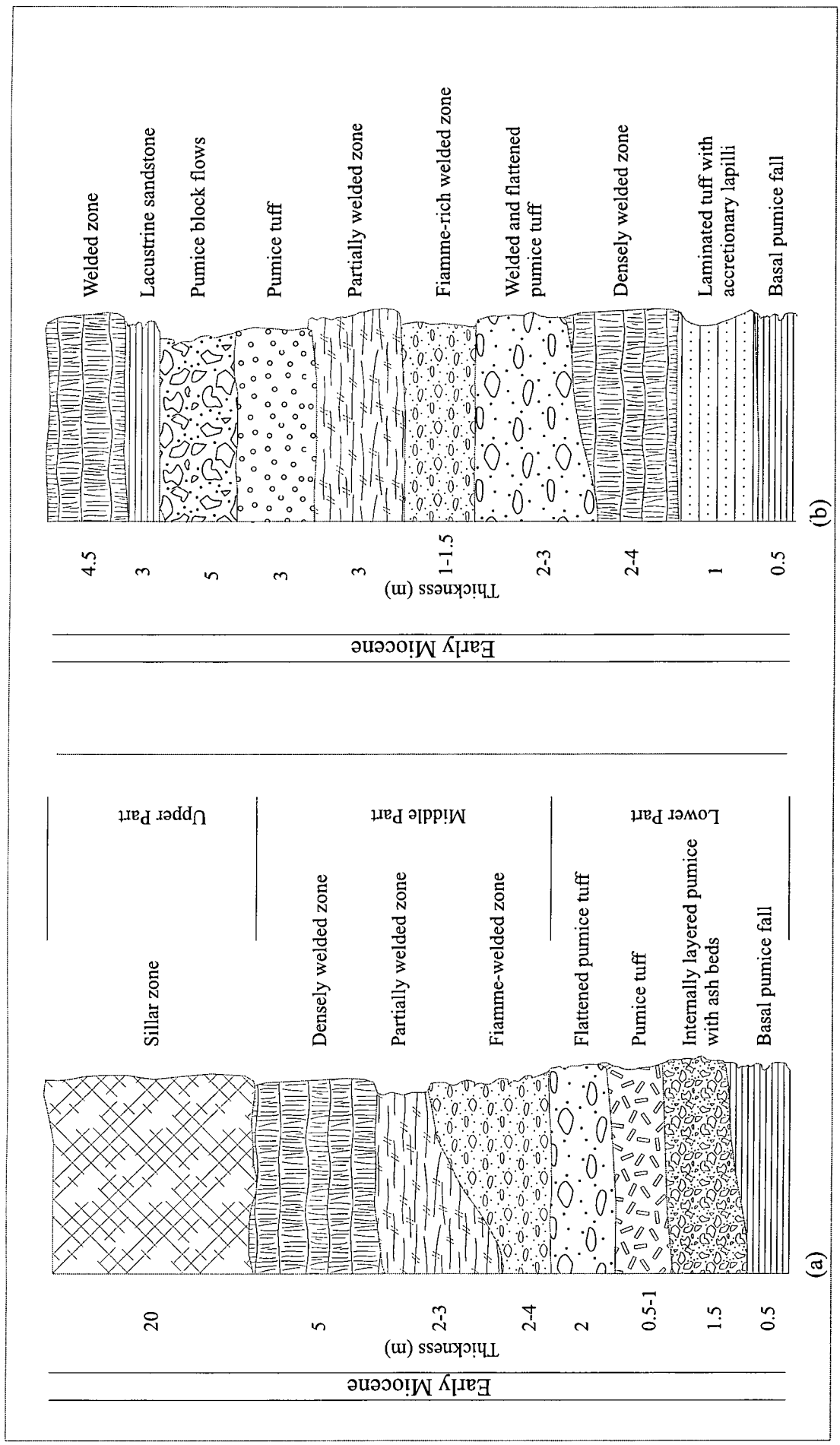

Figure 2.6. *Representative sections illustrare the stratigraphy of the (a) Pinarli and (b) Bektas members.*

deposits. Pumice tuffs pass upwards into flattened pumice tuffs.

The middle part is represented by welded ignimbrites. The base of this part is characterised by a remarkably high proportion of glassy fiamme that exhibit a strong flattening and rheomorphic structures with parallel lineations (Plate 2.5). The fiamme-rich zone is overlain by partially welded and welded ignimbrites. The welded zone is approximately 10m thick and contains a considerable amount of lithics of mostly andesitic-dacitic and rarely metamorphic rock fragments.

Plate 2.5. *The glassy fiamme-rich part of the Pinarli member exhibits rheomorphic structures.*

The upper part is a relatively thick (approximately 20-m) layer of a sillar zone. It consists mainly of densely welded and devitrified tuffs and is characterised by abundant sub-solidus crystallisation of K-feldspar. The Pinarli member is overlain by volcanogenic lacustrine sandstones (7-10-m thick) which separate the Pinarli member from the Bektas member.

The Bektas member crops out to the south of Bektas village, over an area of approximately 13-15 km^2 (Fig. 2.4). The base of the member is characterised by an extensive basal pumice fall layer with a low content of phenocrysts (K-feldspar, plagioclase, biotite, quartz, oxides) and lithics (volcanic rock fragments). In most places, the fallout basement layer is overlain by a set of laminated, fine-grained layers with

plane-parallel or low-angle cross bedding and abundant accretionary lapilli. This 1.5-m thick fall deposit is followed by a welded zone, which includes four different zones, each of which is characterised by different degree of welding (Fig. 2.6b). From bottom to top, they are: (1) a densely welded zone that is characterised by a dark, glassy-looking, reddish-brown vitrophyre with poorly-developed columnar jointing; (2) a welded and flattened pumice tuff with abundant microlites of K-feldspar, plagioclase, biotite and quartz; (3) a 1-1.5 m-thick fiamme-rich zone; and (4) a partially welded zone that includes abundant andesitic and dacitic rock fragments.

The top (~15m thick) of the Bektas member consists of several flows, with inverse grading of pumice in each. The size of the pumice clasts varies from 10 to 25 cm. The pumice clasts are strongly banded and contain two types of matrices: (1) a clear, colourless matrix; and (2) a dark, grey matrix with abundant microlites of plagioclase, biotite and oxides. The sharp contacts between the clear and grey matrices may be attributed to mingling of different magmas to form hybrid compositions (Anderson, 1976; Sparks and Marshall, 1986). The concentration of the lithic clasts increases from bottom to top.

The Akkaya member is exposed around Akkaya, SW of Kuruoba and north of Bektas village (Fig. 2.4). The base of the member is represented by locally-developed base surge deposits (Fig. 2.7a) consisting of alternating, internally-bedded, particulate ash and pumice and fine-ash beds. To the north of Bektas village, the deposits show cross-stratification with minor sand-wave bedding. The bedding changes gradually up into plane parallel and/or low-angle cross-stratification. In some localities, fine-grained ash beds enclose abundant accretionary lapilli. The surge deposits are overlain by pumice tuff layers with a maximum thickness of about 5m. They contain a high proportion of predominantly tuffaceous, lithic clasts at the base of the layer. Throughout the layer, the abundance of the clasts decreases with height, but their size remains constant, suggesting a decreasing supply rather than a decreasing eruption intensity.

A welded zone overlies the pumice tuffs in most localities. This zone is a 10 m-thick zone of generally massive, lithic-bearing ignimbrites with occasional well-sorted tuff layers near the top.

The uppermost part of the Akkaya member consists mainly of approximately 20 m-thick pumice flow with depositional and textural characteristics similar to those from the upper part of the Bektas member.

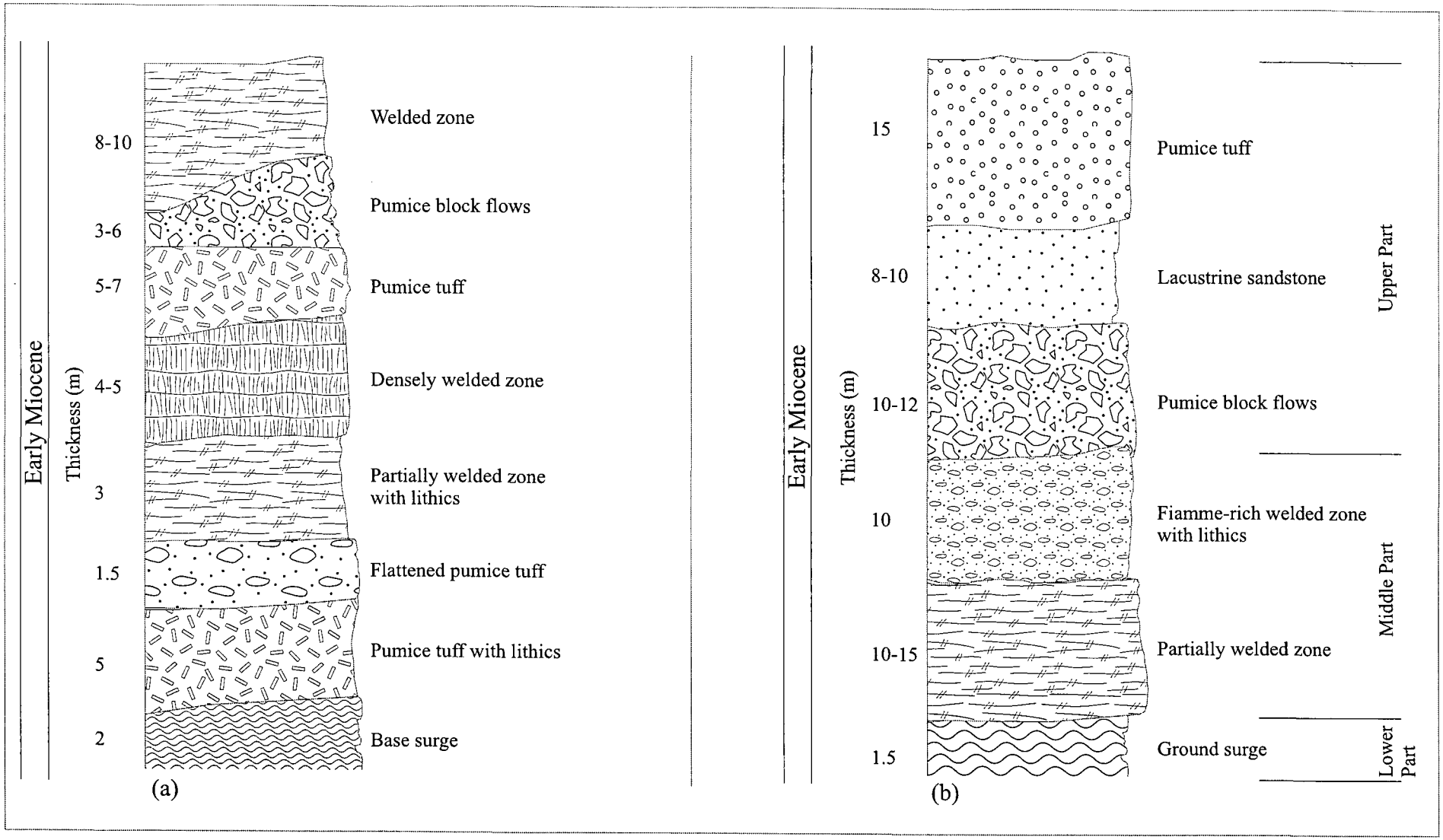

Figure 2.7. *Representative sections illustrare the stratigraphy of the (a) Akkaya and (b) Kalabak members.*

The Akkaya member is cut by a number of E-W and SE-NW trending fault systems near the coast, south of the Bektas village. These fault systems appear to be responsible for the general tilting of the basal layers of the ignimbrite to the north. This member is overlain by a 5-7 m-thick sedimentary unit, which consists mainly of lacustrine volcanogenic sandstones.

The Kalabak member is best exposed around Kalabak village and to the south of Balabanli village. It overlies the Akkaya member and, in some localities, the Bektas member. It has a total thickness of about 50m and consists of three different parts each of which represents a different depositional type (Fig. 2.7b).

The lower part is characterised by ground surge deposits. They are mostly stratified and cross-stratified deposits and up to 1.5m total thickness. They are composed of alternating coarse and fine-grained laminae that are typically inclined at low angles (up to 10^{o}) and commonly form large wavelength, sand-wave structures. The presence of stratification and cross-stratification may indicate that the deposits are pyroclastic surges that formed by deposition directly from dilute turbulent flows.

The middle part is represented by a welded zone that consists of partially welded and welded ignimbrites containing abundant homogeneously distributed lithic fragments. There are two types of lithic fragments: xenoliths; and cognate lithics (juvenile magmatic fragments). The xenoliths originate mainly from the metamorphic basement unit (the Karakaya Complex) and the serpentinized harzburgites of the Denizgören ophiolites. The cognate lithics are mainly of porphyritic rock fragments of rhyolite, dacite and andesite. Rheomorphic structures are common around the lithic fragments.

The main volume of the upper part is characterised by distinctive pumice flows with flattened, elongate vesicles, sub-rectangular shapes and milk-white glass. Pumice clasts generally show inverse grading and local concentrations of lithic clasts. The latter consist mainly of lavas with compositions from rhyolite to andesite. Locally, these pumice flows are intercalated with volcaniclastic sandstones and thin (<10m) lava flows.

2. 1. 3. 5. The Ciceklik Andesite

The Ciceklik Andesite overlies the pyroclastic assemblages of the Kalabak member. It is composed of several lava flows and crops out to the south of Bektas

village with an aerial extent of approximately 5 km^2 (Fig. 2.4). The maximum total thickness of the lavas is about 20m. The rocks are mainly porphyritic andesites and characterised by their hard, compact appearance and dark grey, black colour. They contain phenocrysts of plagioclase, augite, K-feldspar, biotite and minor hypersthene.

2. 1. 3. 6. The Bakacak (Volcanic) Unit

The lava flows of the Bakacak Unit crop out to the west of Behram village over an area of approximately 4-5 km^2. The total maximum thickness of the lavas is about 15-20m. The rocks are mostly porphyritic dacites, though rocks of andesitic composition are also present. The microcrystalline matrix includes phenocrysts of plagioclase, augite, sanidine biotite and quartz with minor zircon, apatite and magnetite. The rocks have extensively been altered along the joints and flow surfaces to form a pale green appearance. In some places, the original mineral phases have been replaced by calcite, sericite, kaolinite and quartz.

2. 1. 3. 7. The Behram Andesite

The Behram lavas comprises olivine- and orthopyroxene-bearing andesites which form several isolated lava flows. The lavas crop out in an area of approximately 12 km^2, near Behram (Assos) village, along the coast (Fig. 2.4.). The thickness of the lavas varies widely, with a maximum (estimated as 250m) in the region of Behram castle (Plate. 2.6). In the Behram castle, well-formed columnar and blocky jointed lava lobes are found. Further south, towards the coast, the lava lobes are surrounded by irregular layers of scoriaceous and blocky lavas. These are interpreted to be autobrecciated lavas (Plate. 2.7) formed by continuous movement and expansion of the viscous, congealed lava as described by Sigurdsun, (1981); and Cas and Wright, (1988).

The rocks of the Behram Andesite are porphyritic, grey and beige. They contain phenocrysts of plagioclase, hypersthene, olivine, augite, sanidine, biotite and magnetite.

To the southwest of Behram village, the lavas are cut by several NW-SE trending normal faults. To the west and the north of Behram village, the lavas are overlain by young sediments deposited in the Tuzla stream valley which obscure the stratigraphic relationships between the lavas of the Behram Andesite and the older volcanic formations. However, to the east of Behram castle, at the eastern end of the outcrop, the stratigraphic relationship between the Behram lavas and the Balabanli

Plate 2.6. *Columnar jointed andesitic front of the Behram Andesite.*

Plate 2.7. *Autobrecciated lavas of the Behram Andesite.*

Ignimbrite can be observed asa sharp and planar contact. In this locality, the Behram lavas are overlain by the Kadirga member of the Balabanli Ignimbrite.

A sample from the Behram Andesite has been dated as 20.3 ± 0.6 Ma using the K-Ar method (Table 2.1).

2. 1. 3. 8. The Balabanli Ignimbrite

The Balabanli Ignimbrite occupies a large area in the southwest part of the Biga peninsula with a total aerial extent of >200 km^2. Its best exposures are around the localities of Tamis, Kepez, Balabanli and Kadirga (Fig. 2.4). Although the Balabanli ignimbrite forms a single stratigraphic level on the basis of its position in the volcano-stratigraphic succession, it consists of several ignimbrite sheets, each of which is characterised by specific depositional properties. Characteristics of the ignimbrites vary from one locality to another. Thus, the Balabanli Ignimbrite has been divided into three different ignimbrite members: (1) the Tamis member; (2) the Kepez member; and (3) the Kadirga member.

The Tamis member is best observed to the north of the Tuzla stream valley, around the village of Tamis (Fig. 2.4). It covers an area of about 35-40 km^2 with a total thickness of approximately 45-50m (Fig. 2.8a). The base of the member is characterised by a basal pumice fall layer, a moderately low content of phenocrysts and a white, yellow colour. A pumice tuff layer with a thickness of 1-1.5m mantles the pumice fall deposits. Pumice clasts in this layer typically have a strongly fibrous texture and a milk-white colour. Towards the top of the sequence, the pumice tuff passes gradually into flattened tuffs. Here, pumice clasts characteristically contain tabular bubbles and translucent pearly glasses. Pumice tuffs are overlain in many places by a welded layer (~1.5-m thick) which consists mainly of densely flattened, fiamme-rich tuffs, the amount of the fiamme decreasing towards the top.

The welded lower layer is overlain by pumice flows, which are made up of pumice tuff, pumice block flows and flattened pumice tuffs from the bottom towards the top of the succession respectively. The total thickness of this pumice-rich layer is about 7-7.5m. The pumice clasts are mostly porphyritic and contain approximately 10-15 volume % phenocrysts, which in order of decreasing abundance consist of euhedral-subhedral plagioclase, biotite, K-feldspar, augite and titano-magnetite.

Further towards the top of the succession, a welded upper layer with an average

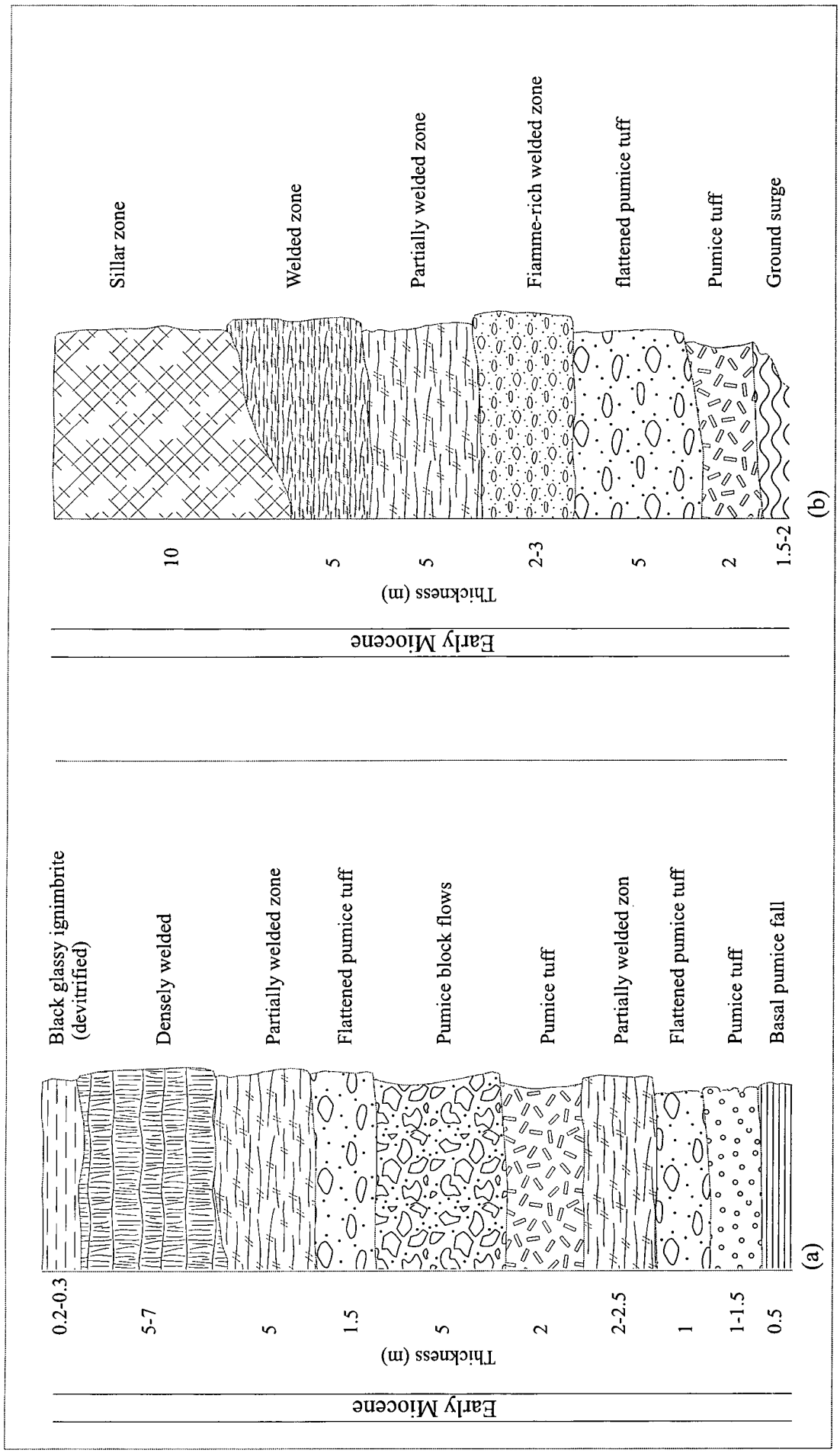

Figure 2.8. *Representative sections illustrares the stratigraphy of the (a) Tamis and (b) Kadirga members.*

Plate 2.8. *The welded upper part of the Tamis member overlaying pumice flows.*

Plate 2.9. *Large glassy, elongated fiamme in the welded upper part of the Tamis member.*

total thickness of about 10m overlies the pumice unit (Plate 2.8). The welded zone begins with a slightly welded zone and passes gradually upward into a densely welded zone. The densely-welded zone is a typical pinkish-yellow ignimbrite characterised by abundant large (up to 10-15 cm), black fiamme (Plate 2.9) with some phenocryst-rich layers. A thin (20-30 cm) layer of black, glassy ignimbrite mantles the welded zone.

The Kepez member is the most abundant ignimbrite deposit in the area. It is exposed in the south-westernmost part of the Biga Peninsula, between the villages of Tamis to the northeast, Babakale to the southwest and Gulpinar to the northwest (Fig. 2.4). It has a total aerial extent of about 175-180 km^2 and is best exposed in the Kepez area. The member is cut by two faults. The northern end of the outcrop is bounded by the NW-SE trending Tuzla fault which forms the Tuzla stream valley, whereas the northwestern end is bounded by the SW-NE trending Gulpinar fault. Although the thickness of the Kepez member varies from one locality to another, the average thickness has been estimated as about 80-90m.

The Kepez member consists of three different cooling parts (lower, middle and upper in Fig. 2.9), with intervening volcaniclastic sediments of continuous and lenticular bodies. Each layer has a characteristic textural variation and can be further subdivided into zones on the basis of varying degrees of welding and devitrification.

The base of the lower part is characterised by ground surge deposits with a thickness of about 0.5m. They consist mainly of alternating, internally-bedded ash and pumice and fine ash beds. A pumice tuff about 4-6m thick covers the surge deposits. The pumice tuff begins with a plinian fallout and passes gradually into flattened pumice tuff (Plate 2.10). The pumice clasts are milk-white and yellowish colour, and include phenocrysts of plagioclase, biotite, K-feldspar, magnetite and minor amount of augite. Some exhibit fibrous textures which form thin elongate vesicles. Clastic sedimentary rocks overlie the lower part of the Kepez member. They are mainly lacustrine volcanogenic sandstones and have a total thickness of about 1.5-2m (Plate 2.11).

The middle part, which overlies the clastic sediments, consists mainly of welded ignimbrites. The base of it is represented by a 1-1.5 m-thick fiamme-rich zone which characteristically shows a eutaxitic texture with planar foliation and regular alignment of glassy fiamme. The fiamme-rich zone is followed by a densely welded zone which has an average thickness of 1.5m. The rocks of this zone are hard, compact, glassy, dark red and partly brown ignimbrites. They can easily be recognised in the field with their high

Plate 2.10. *Pumice tuffs of the Kepez member overlain by flattened pumice layers.*

degrees of resistance to erosion which build up continuous layers and red colours resulted from oxidation. The densely-welded zone passes gradually up into a 3-4m thick, partially-welded zone which is composed of crystal-rich rhyolites and dacites. In some parts lithic clasts are also abundant. The ignimbrites in the partially-welded zone exhibit rheomorphic structures and flow banding surrounding the crystals and lithic fragments. K-feldspar is the most abundant phenocryst and is accompanied by plagioclase, biotite and magnetite. Some also contain clinopyroxene and quartz phenocrysts. The welded zone is partly overlain by lava-like ignimbrites in some areas. They are characterised by their high (>60% vol.) proportions of phenocrysts and lava-like flow structures. The phenocryst phases are the same as those of the partially welded ignimbrites.

The upper part of the Kepez member overlies volcaniclastic, shallow lacustrine sediments and consists mainly of variable proportions of pumice block flows and welded ignimbrites with a total thickness of about 65-70m. The pumice blocks are present at the base of the upper part. They are mostly vesiculated, porphyritic, white-grey pumices and contain phenocrysts of plagioclase, K-feldspar, biotite, quartz and titano-magnetite. The matrix glass in the grey pumices is generally colourless, but

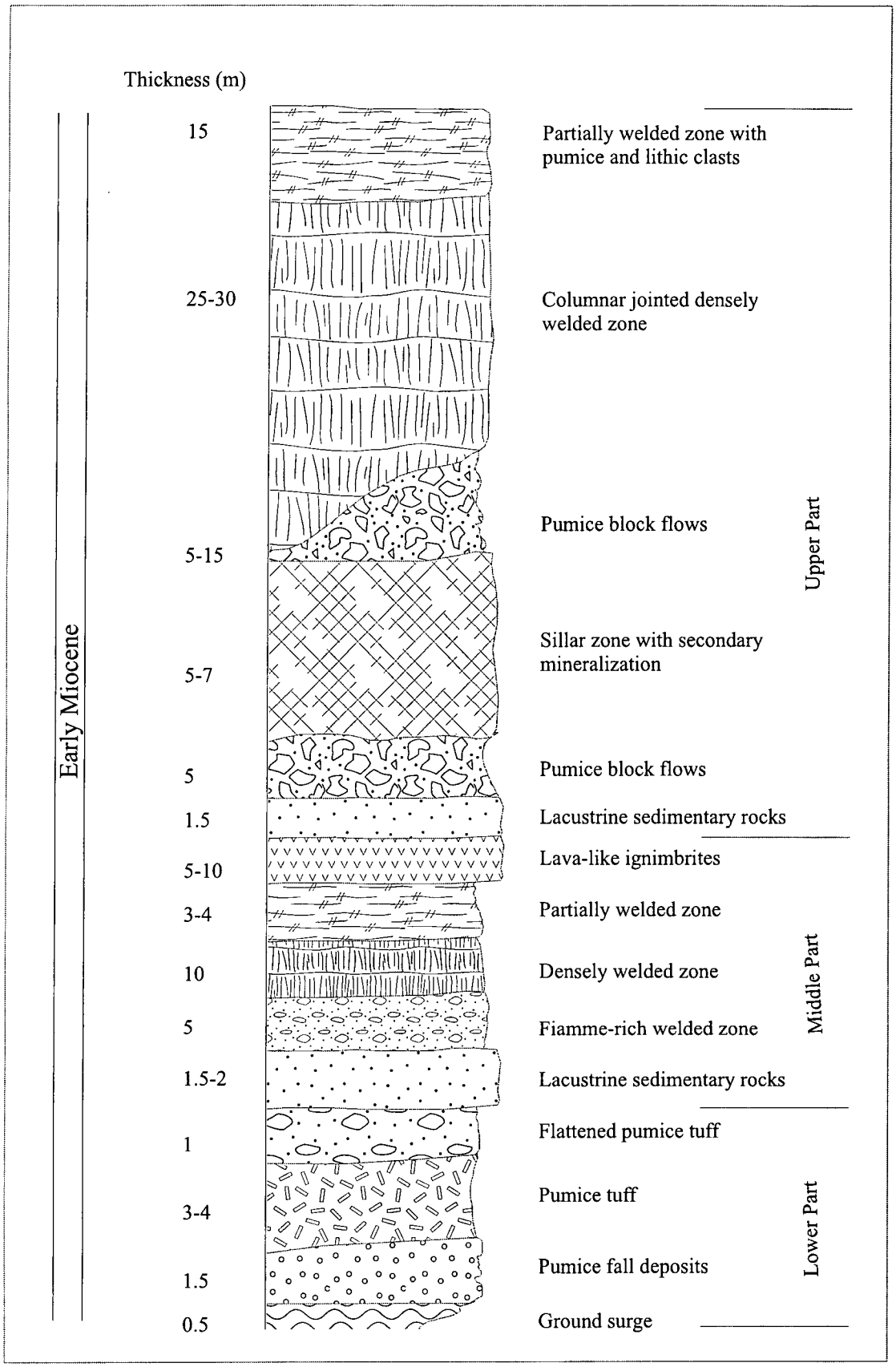

Figure 2.9. *Representative section illustrates the stratigraphy of the Kepez member.*

Plate 2.11. *Lacustrine clastic sediments overlaying flattened pumice tuffs of the Kepez member.*

contains abundant microlites of magnetite and titano-magnetite which give the glass its grey colour. In some places, vapour-phase crystallisation results in the formation of quartz, tridymite, K-feldspar and zeolite as infills of pumices cavities and pore spaces of the matrix. These crystallisation events form a 5-7m thick sillar zone. In most localities, the pumice blocks are flattened and banded at the base. However, the degree of flattening decreases upwards.

Further upwards, a widespread welded zone mantles the pumice blocks. The bottom 25-30m of this welded zone is massive strongly welded, high grade, and brick-red ignimbrites, outcropping as cliff-forming sheets with well-formed columnar jointing (Plate 2.12). It contains abundant proportions of fiamme and glass shards which generally exhibit compactional flattening. Rheomorphic structures are well-developed in places. This may be due to secondary mass flowage leading to form a lineation parallel to the plane of fiamme. The glassy matrix is partly devitrified to form radiating fibrous crystallites of quartz, K-feldspar and cristobalite as spherules and orbs. A basal layer of partially-welded zone (10-15 m-thick) which is a good stratigraphic marker horizon overlies the densely-welded zone.

Plate 2.12. *Columnar jointed densely-welded layers of the Kepez member.*

A number of feeder-dykes filled with ignimbritic material was observed along the coast near Babakale village. This may indicate that the ignimbrites formed mostly by fissure eruptions.

The Kadirga member crops out further east, near Kadirga village (Fig. 2.4) with a total thickness of approximately 30-35m and an aerial extent of 20-25 km^2. It is cut by the SW-NE oriented Tuzla fault system in several places to the north of the Kadirga village. Although the Kadirga member appears to be a single outcrop isolated from the other ignimbrites, its position in the volcanostratigraphic succession and depositional characteristics show remarkable similarities to those of the Tamis and the Kepez members.

A 2-3 m-thick of ground surge deposit characterises the base of the member. The depositional properties of this ground surge deposit resemble to the surge deposits of the Kepez member. The surge deposits are overlain by a thin layer (2m of maximum thickness) of pumice tuffs which pass gradually up into flattened pumice blocks. High proportions of large fiamme were observed in most localities overlying the pumice tuffs and blocks. In some localities, a welded zone overlies the pumice blocks with an absence of fiamme-rich layers. The welded zone shows a remarkable similarity to those

of the Tamis member and consists mainly of interbedded partially welded ignimbrites and welded zones. Unlike the Tamis and the Kepez members, however, the densely welded ignimbrites are absent in the Kadirga member. The top of the Kadirga member is represented by an approximately 8-10 m-thick sillar zone characterised by vapour phase crystallisation.

2. 1. 3. 9. The Kovacli Dyke Swarms

A widespread dyke system occupies large areas, particularly in the southernmost part of the Peninsula, along the northern coast of the Edremit Bay. They typically have NNW-SSE and NNE-SSW directions. The dykes are mainly fresh, hard, compact, grey to black microporphyritic andesites and basaltic andesites. They consist mainly of microcrysts of plagioclase, augite and hypersthene with subordinate olivine, magnetite and ilmenite set in a microlitic groundmass. A basaltic andesite sample from the dyke swarms gave a K-Ar age of 19.7 ± 0.3 Ma (Table 2.1).

2. 2. The Dikili-Ayvalik-Bergama (DAB) Area

The Dikili-Ayvalik-Bergama (DAB) area is located to the south of Edremit Bay, between the city of Izmir to the south and the town of Edremit to the north (Fig. 2.1). Recent tectonic activity in the area, related to the structural system of the Aegean region, led to the formation of NW-SE and NE-SW oriented fault systems. A number of E-W and NW-SE trending graben (e.g. the Edremit and Bergama Graben) (Plate 2.13) have been formed in relation to these fault systems.

The oldest known age for the Cenozoic igneous activity in the DAB area is 37.6 ± 3.3 Ma. This is the age reported by Bingöl et al. (1982) for the emplacement of the plutonic body known as the Kozak Pluton, although the reported ages for the pluton vary significantly from 13 to 37 Ma (Ataman, 1975; Bingöl et al., 1982). Ercan et al. (1985) and Krushensky (1976) also reported K-Ar dates of 31.4 ± 0.4 Ma (near Ayvalik) and 23.6 ± 0.6 Ma (east of Edremit; outside the area studied) respectively for the minor pre-Miocene volcanism.

In this study, the oldest date obtained for the volcanic rocks of the DAB area is 20.9 ± 0.5 Ma (Table 2.1). The eruptive products of the Miocene volcanism cover an area of >1500 km^2 along the coastal section of Dikili, Ayvalik and Foca as well as inland between Ayvalik and Bergama (Fig. 2.10). They are mainly lava flows, domes and pyroclastic fall and flow deposits. The Early Miocene volcanism began with lava and pyroclastic successions and lasted until the latest Early Miocene (17.3 ± 0.6 Ma; Borsi et al., 1972).

The volcanic activity continued into the Middle Miocene with a gradual change in eruptive style and rock compositions. The Middle Miocene activity mostly produced lava flows and dyke swarms of basic-intermediate compositions. Pyroclastic eruptive products are totally absent in this period. The Middle Miocene volcanism continued from 16.6 ± 0.6 Ma (Borsi et al., 1972) to 15.2 ± 0.4 Ma (Table 2.1).

The volcano-stratigraphy of the Dikili-Ayvalik-Bergama area will be described in the following paragraphs as two different sub-areas: (1) the Ayvalik-Kozak section; and (2) the Dikili-Bergama-Foca section. The volcanic units of each sub-areas are illustrated using schematic column sections (Fig. 2.12 and 2.14 respectively).

2. 2. 1. The Basement Rocks

In the Dikili-Ayvalik-Bergama (DAB) area, the basement is represented by two

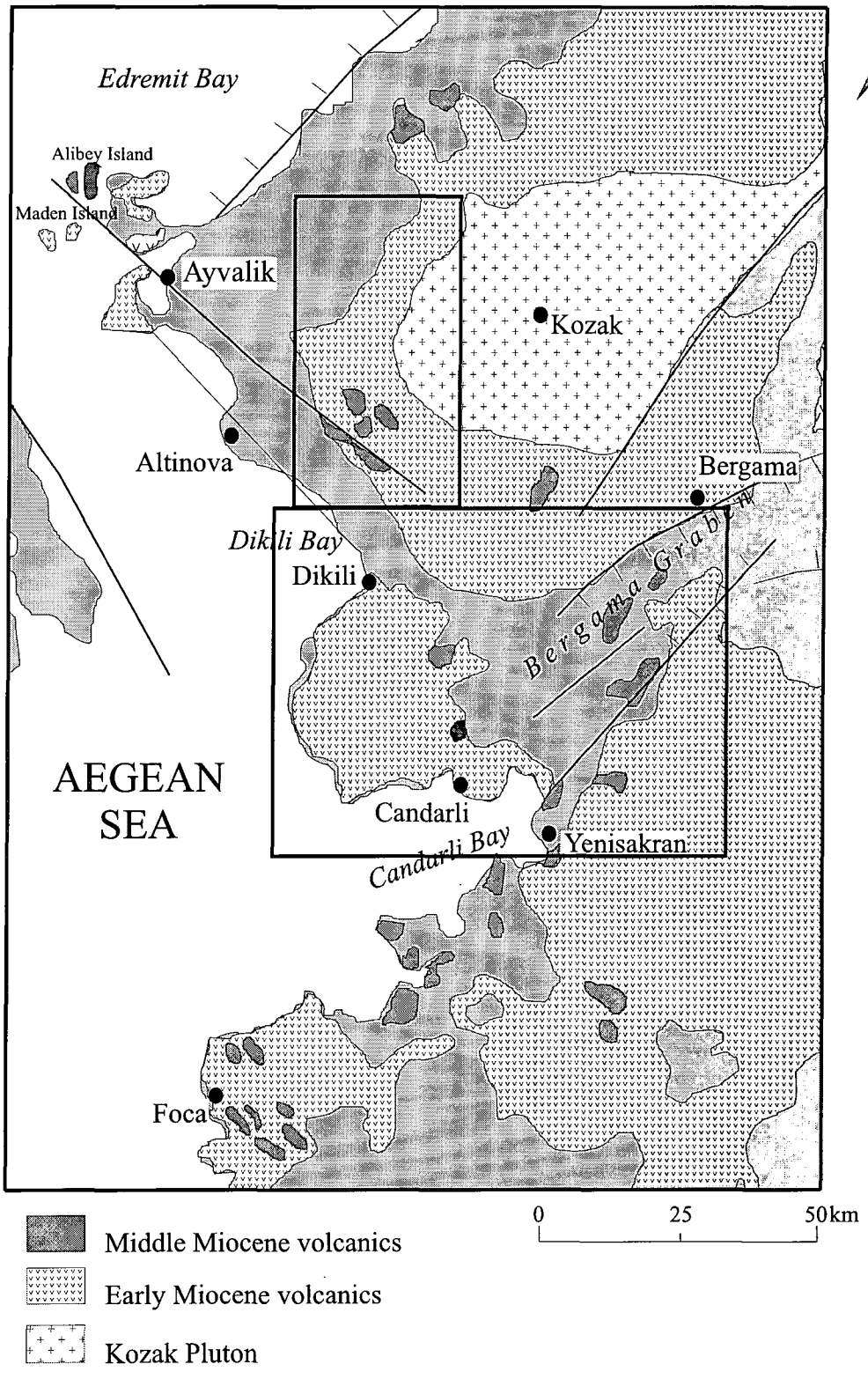

Figure 2.10. *Simplified geological map of the Ayvalik-Dikili-Bergama area showing the distribution of the volcanics and the areas that have been mapped (rectangles). For the location of this area in Western Anatolia, see Figure 2.1.*

different formations. In the northern part of the area, between Edremit and Bergama towns, the dominant basement lithologies are the metamorphic rocks of the Karakaya Complex that have been described in Section 2.1.1. Further south, the metamorphic basement known as the Menderes Massif occupies a large area. This crystalline Massif is a large (~ 200 x 300 km) structural dome that is identified as the eastern continuation of the Aegean domain (Attic-Cycladic Crystalline Complex) (Dürr et al., 1978). It is elongated in a SW-NE direction along the Izmir-Ankara suture zone (Sengör et al., 1984) (Fig. 2.1).

Plate 2.13. *A view of the Bergama Graben from the south of the town of Bergama.*

The rocks of the Massif have been subdivided into two structural divisions: (1) a core complex; and (2) an overlying cover series (Verge, 1993; Hetzel et al., 1995). The core complex is represented mainly by granitic augen gneisses, high-grade schists and metavolcanic rocks. The augen gneisses are the most abundant lithologies in the core division and exhibit porphyritic textures, characterised by large megacrysts of alkali feldspar and plagioclase within a fine-to medium-grained matrix of quartz, muscovite and biotite. Bozkurt et al. (1995) proposed that the augen gneisses were former granitic plutons intruded into high-amphibolite – greenschist metamorphics of garnetiferous pelitic and psammitic gneisses, garnet ortho-amphibolites and dolomitic marbles. The

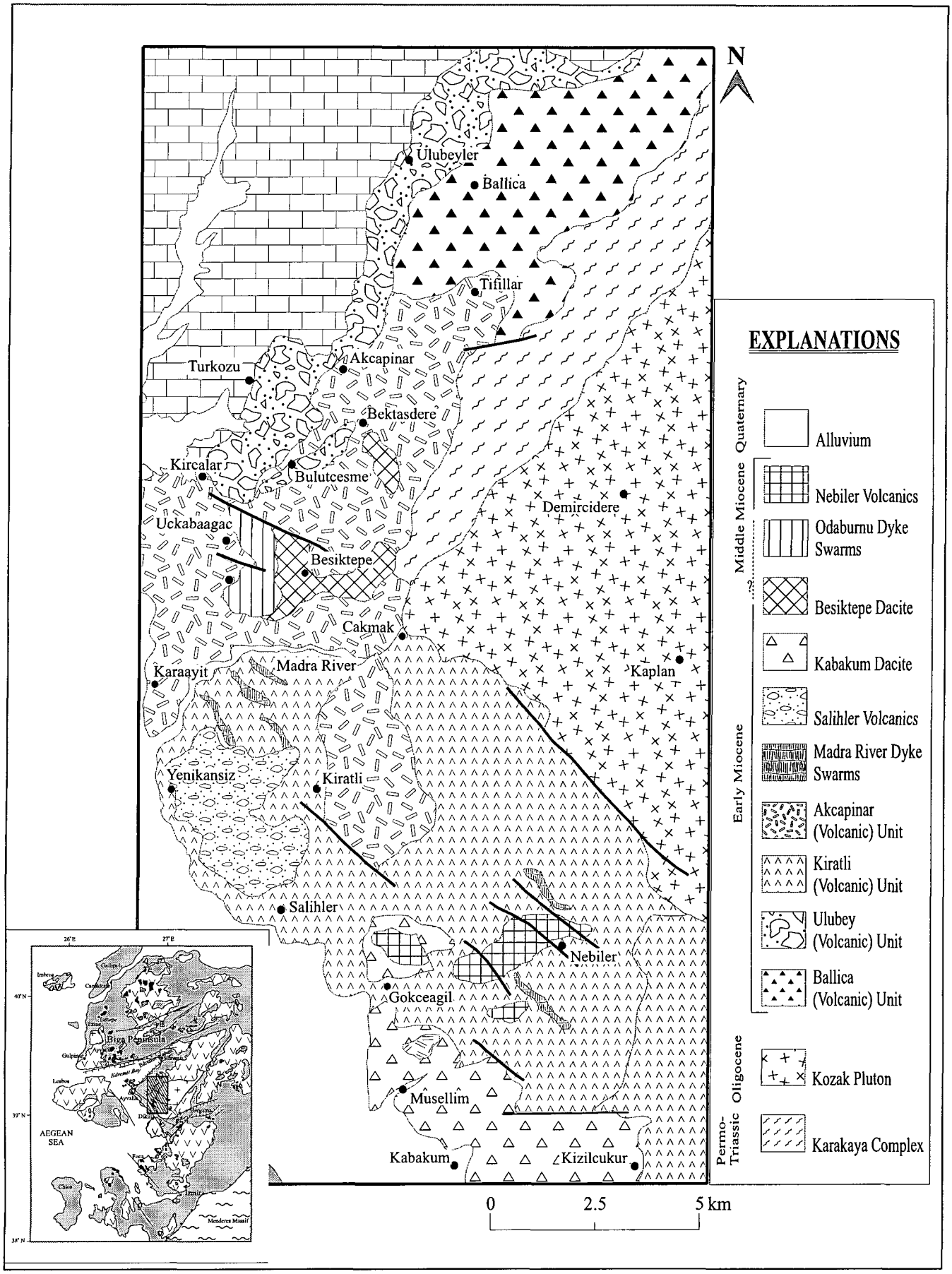

Figure 2.11. *Geological map of the east of Ayvalik Peninsula.*

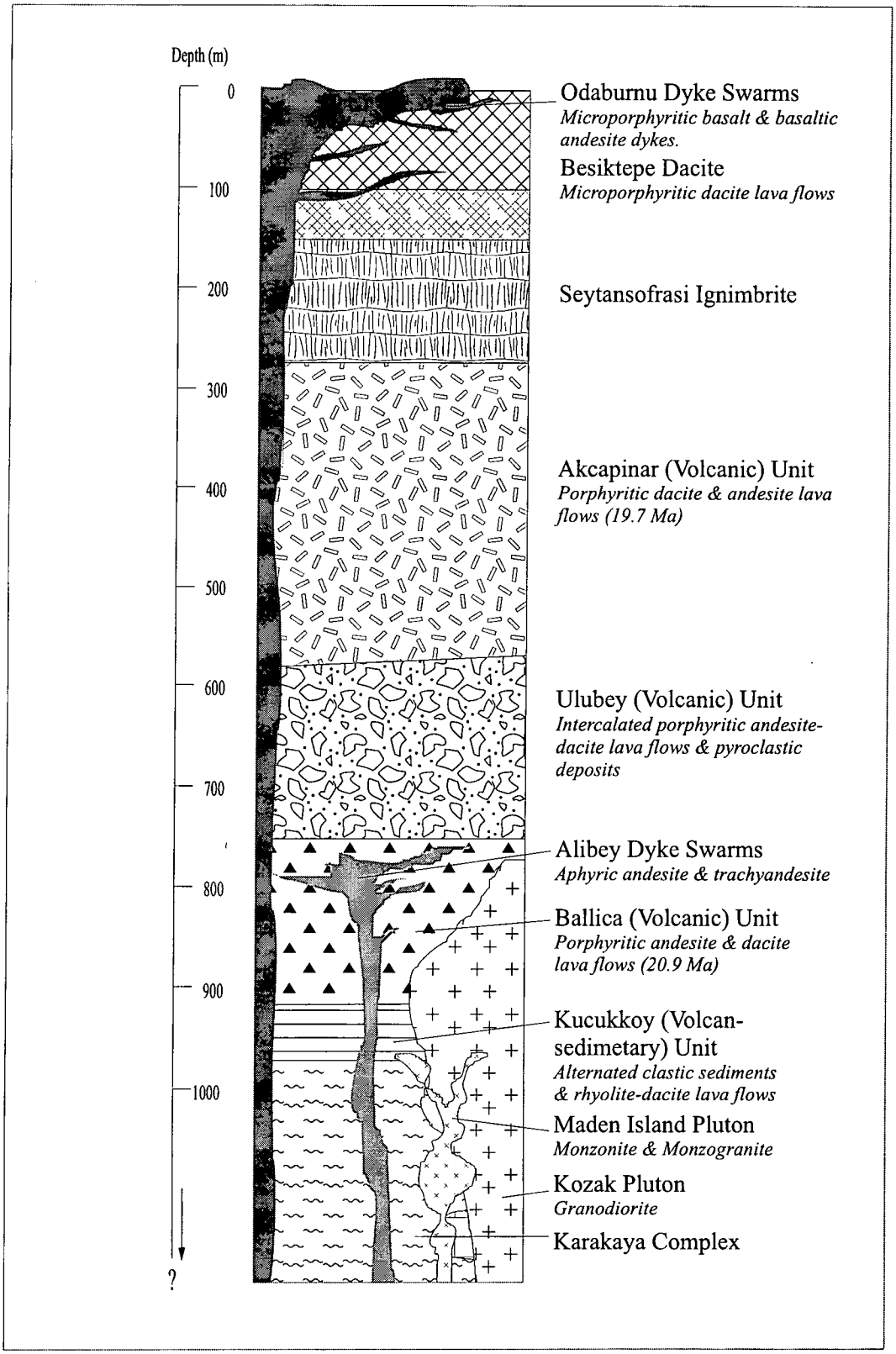

Figure 2.12. *Schematic generalised stratigraphic section illustrates the volcano-stratigraphy of the Ayvalik-Kozak section.*

cover series consists of metasedimentary rocks of low-grade schists, phyllites, quartzites and marbles (Dora et al., 1990). Mica-schist is the most abundant rock type in the cover series and consists mainly of quartz, muscovite, biotite, chlorite, plagioclase and minor garnet (Hetzel et al., 1995). Reischman et al. (1991) reported zircon dating for the augen gneisses as Late Proterozoic to Early Palaeozoic which corresponds to the early metamorphism of the Massif at upper amphibolite facies conditions. Following the collision between the Anatolide-Tauride Block and the Pontides, the Massif underwent Barrovian metamorphism that has been attributed to its burial beneath the Lycian nappes during the Late Paleocene-Early Eocene (Sengör et al., 1984; Satir and Friedrichsen, 1986).

The central part of the Massif contains syntectonic granitoid intrusions that have andalusite and sillimanite in their contact aureoles (Whitney and Dilek, 1998). Similar Miocene granitoid intrusions are found in the Cycladic Islands of the Aegean (Lister et al., 1984; Altherr et al., 1988; Lee and Lister, 1992) and the Central Anatolian Crystalline Complexes (e.g. the Niğde and Kirşehir Massifs; Koçak and Leake, 1996; Whitney and Dilek, 1998).

2. 2. 2. The Ayvalik-Kozak Section

2. 2. 2. 1. The Kozak Pluton

In the Dikili-Ayvalik-Bergama (DAB) area, the Kozak Pluton is the oldest known magmatic body. The pluton intruded the basement metamorphic rocks and occupies a large area of about 290-300 km^2 (Figs. 2.10; 2.11). It was first named by Bingöl et al. (1982) as Kozak Pluton after its best exposure around the town of Kozak. The rocks are dominantly granodiorite in composition and display inequigranular and porphyritic textures with medium to coarse grains of minerals. They contain plagioclase (An_{32-40}), amphibole, K-feldspar, augite, biotite and quartz. Sphene, zircon, magnetite and apatite are the accessory minerals. Amphibole is the most abundant mafic phase and has the compositions of edenite and ferroan pargasitic hornblende. Blocky jointing and spheroidal weathering are common in places. In some localities, aplite, aplogranite and granodiorite porphyry dykes cut the pluton. Hornblende-hornfels and pyroxene-hornfels facies contact metamorphism has produced the assemblages of epidote, tremolite, actinolite, wollastonite and rare garnet along the northwestern margin of the pluton (the contact zone between the Kozak pluton and basement metamorphic rocks).

The timing of emplacement of the pluton is poorly constrained. Ataman (1975) obtained Rb/Sr ages of 13, 16 and 23 Ma from the granodiorites of the Kozak pluton. Bingöl et al. (1982), however, reported K/Ar ages of 20.3 ± 0.3 and 24.6 ± 1.5 Ma obtained from biotite separates and 37.6 ± 3.3 and 24.2 ± 1.1 Ma obtained from orthoclase separates.

2. 2. 2. 2. The Maden Island Pluton

A small plutonic intrusion crops out on Maden Island, to the west of the town of Ayvalik (Fig. 2.10). The remaining portion of the plutonic body occupies a small area of only a few km^2. The dominant rock types forming the pluton are monzonites and monzogranites. The rocks are generally inequigranular and medium- to coarse-grained. They contain a high proportion of feldspar which significantly exceeds the quartz content and confirms its monzonitic affinity. Plagioclase is represented by oligoclase and andesine (An_{19-38}) and is accompanied by large, fresh orthoclase megacrysts. The mafic mineral phase is represented by clinopyroxene (augite) and orthopyroxene (mostly hypersthene). Minor amphibole is also present in some rocks accompanying apatite and oxides (magnetite and ilmenite). The Maden Island Pluton has not been yet studied in detail and therefore no geochronological age has been obtained so far. However, stratigraphic relations indicate that the rock formations of the pluton are partly overlain by the Kucukkoy volcano-sedimentary Unit. Thus, the pluton is considered to be older than the overlying volcanic rocks.

2. 2. 2. 3. The Kucukkoy (Volcano-Sedimentary) Unit

The Kucukkoy volcano-sedimentary Unit consists mainly of alternating clastic sedimentary rocks and lava flows. It is best observed to the southwest of Ayvalik and on Alibey Island (Fig. 2.10). The total thickness of the Unit has been estimated as about 75-80m. The sediments are mostly volcanogenic sandstones which make up 10-15 m-thick layers. The volcanics are generally made up of rhyolitic and dacitic lava flows. The rocks have been extensively affected by alteration and weathering. Towards the top of the Unit, hard, compact, strongly silicified lavas are abundant. In some places, the rocks of this Unit are cut by the Alibey dyke swarms.

2. 2. 2. 4. The Ballica (Volcanic) Unit

The Ballica volcanic Unit crops out to the east of Ayvalik, around the villages of

Ballica, Haciveliler and Kumgedigi (Fig. 2.11). It is made up of massive lava flows with a maximum total thickness of about 250m. The rocks are mostly andesite and dacite. They are locally jointed, grey to black, porphyritic lavas with fine-grained groundmass. The phenocrysts are primarily of plagioclase, hornblende, augite and titano-magnetite. Most dacites also contain quartz and rare sanidine phenocrysts.

The mineral composition, texture and colour of the lava flows differ little laterally or vertically throughout the logged sections. The lavas usually do not show any oxidised zones at the top of flows. Thus, it is generally difficult to recognise individual lava flows within the Unit. In some places, however, lava flows include platy-jointing (related to flow banding) which has been developed parallel to the basal surface as a result of intensive shear between the channel walls and the coherent central part of lava. Close to the base, the distance between these joints is in the order of centimetres or even millimetres. The joint spacing increases upwards and, after a certain limit, it disappears where the lava turns into a massive body. In the field, the platy-jointing is one of the criteria which has been used to differentiate individual lava flows one from another.

An andesite sample from the lavas has been dated as 20.9 ± 0.5 Ma using the K-Ar method (Table 2.1).

2. 2. 2. 5. The Alibey Dyke Swarms

An aphyric dyke system is located particularly in the coastal section of Ayvalik and on Alibey Island. The rocks of this dyke system crop out in only a small area of 2-3 km^2. They are hard, fresh, compact, black- grey- and beige-coloured andesites and trachy-andesites. They consist mainly of plagioclase, hypersthene, K-feldspar, augite and subordinate olivine. Unlike most other volcanic rocks of the Dikili-Ayvalik-Bergama area, the rocks of the Alibey Dyke Swarms contain hypersthene, but no amphibole. Their mineral compositions are rather closely similar to the Behram Andesite of the Ezine-Gulpinar-Ayvacik area, although they display aphyric textures, unlike the Behram Andesite. They also contain some xenoliths of monzonitic composition that indicates that the dykes may have been generated from the same source as the monzonites of the Maden Island Pluton.

2. 2. 2. 6. The Ulubey (Volcanic) Unit

The Ulubey Unit consists of intercalated lava flows and pyroclastic deposits. It

crops out in an area of about 25 km^2, between Ayvalik and Kozak towns, around the villages of Ulubeyler, Bektasdere, Türközu and Kircalar (Fig. 2.11). The maximum total thickness of the Unit has been estimated as approximately 250m. Although thin lava flows (<10m) have been observed within the volcaniclastics, the Unit is dominantly made up of pyroclastic deposits. The lavas are mostly porphyritic andesites, dacites and rarely rhyolites and contain phenocrysts of plagioclase, hornblende, K-feldspar, biotite, augite and quartz. Accessory minerals of magnetite, apatite and zircon are also observed in some rocks. The matrix is made up of microcrysts of plagioclase set in a glassy groundmass. In some places, the lavas have been strongly affected by alteration leading to the formation of oxides and copper salts on flow surfaces.

The pyroclastic deposits are mainly lithic ash-flow tuffs but also include breccia, lapilli tuff and fine-ash. The tuffs are of mostly rhyodacitic to rhyolitic in composition. The breccias are abundant and form massive layers. They are interbedded with the lavas and contain clasts of andesites, dacites and rhyodacites. The clasts are mostly angular, poorly sorted and their sizes vary between 1 and 30 cm. They are surrounded by a matrix that was previously glass displaying fluidal textures and collapsed vesicles.

Lapilli and fine-ash flows alternate with breccias and lavas. The best exposures of the lapilli and ash flows are observed to the west of the Karayit and Bektasdere villages. They form several different layers, each of which has thickness of about 10-15m and is separated by lavas and/or breccias. In the lower part of the Unit, they are represented by relatively coarse-grained, poorly stratified lapilli tuffs and they pass gradually up into well-bedded fine-tuffs. The lapilli tuffs are crystal-rich and include lithic clasts of andesite - dacite and metamorphic fragments from the basement rocks. The tuffs comprise euhedral-subhedral quartz, plagioclase, hornblende and K-feldspar as well as abundant pumice and glass shards that have mostly been chloritised and silicified.

The lapilli tuff grades into the overlying bedded fine-grained tuffs in which the bedding is accentuated by thin, graded parallel laminae. The thickness of the fine-grained tuffs varies from centimetre- to metre-scale and may reach up to 10m in some localities.

2. 2. 2. 7. The Akcapinar (Volcanic) Unit

This volcanic unit, composed mainly of porphyritic dacite and andesite, occupies

a large area to the east of Ayvalik and south of Edremit, between the villages of Akcapinar, Tifillar, Karaayit and Cakmak (Fig. 2.11). In general, the Unit forms massive lava flows with a maximum thickness of approximately 350m, although a few lava domes have been observed in some localities. The lavas overlie the metamorphic basement rocks in the east and the Ballica volcanic Unit in the north. The rocks exhibit a variety of shades of grey and beige and contain phenocrysts of plagioclase, augite, amphibole (edenite and edenitic hornblende), biotite and quartz. Accessory phases are represented by zircon, apatite and magnetite. The groundmass is mostly glassy and includes microlites of plagioclase and hornblende.

In some localities, between Ayvalik and Dikili, porphyritic dyke swarms cut the lavas of the Akcapinar Unit. The prevalent directions of the dykes are approximately NNE-SSW and NNW-SSE, consistent with the regional tectonic trends and fault directions. The dykes are porphyritic andesites and dacites with the same mineral compositions as the rocks of the Akcapinar lavas. An andesite sample from the Akcapinar Unit has been dated as 19.7 ± 0.3 Ma using the K-Ar method (Table 2.1).

2. 2. 2. 8. The Seytansofrasi Ignimbrite

An ignimbrite sheet crops out in an area of about 10 km^2, to the southwest of Ayvalik. The best exposure of the ignimbrite is around Seytansofrasi and on a few small islands, near Ayvalik. The total thickness is approximately 75-80m. It forms a succession of massive, cliff-forming sheets which shows lateral continuity along the SW coast of Ayvalik. The base of the sequence is characterised by lithic-rich pumice tuff. Lithics are mostly andesitic, dacitic and rhyolitic fragments. Metamorphic xenoliths from the basement rocks are also abundant in some places. A layer of flattened pumice tuff overlies the lithic-rich pumices. The pumice clasts are characterised by a high proportion of phenocrysts of mainly plagioclase, K-feldspar, biotite, quartz and titano-magnetite.

Welded ignimbrites make up more than half of the total thickness. The base of the welded zone is represented by densely-welded ignimbrites, which display distinctive pink and reddish coloration and strong eutaxitic texture. They exhibit well-developed columnar jointing (Plate 2.14). Towards the top, welded ignimbrites are characterised by varying proportions of lithic clasts, crystals and obsidian-like lenticles set in a devitrified glass shard matrix. Lithic clasts are represented by volcanic rocks (mostly

dacites). The phenocrysts are mainly plagioclase, K-feldspar, biotite and magnetite.

Plate 2.14. *Columnar jointed densely-welded layers of the Seytansofrasi Ignimbrite*

2. 2. 2. 9. The Besiktepe Dacite

The lavas of the Besiktepe Dacite with a total thickness of about 50-60m crops out to the east of Ayvalik, between Besiktepe and Uckabaagac villages (Fig. 2.11). The rocks are mostly microporphyritic/porphyritic dacites and exhibit pale grey to black colours. The phenocryst phase consists primarily of plagioclase, hornblende, quartz and biotite with minor K-feldspar, augite and magnetite. The lavas are mostly homogenous in terms of texture and composition. They overlie the lavas of the Akcapinar Unit over an area of approximately 5-6 km^2.

2. 2. 2. 10. The Odaburnu Dyke Swarms

This dyke system cuts the lavas of the Akcapinar Unit with a prevalent direction of NW-SE. The dykes have a total aerial extent of only 2-2.5 km^2 and crop out on the northern side of the Madra River valley, around the villages of Odaburnu and Uckabaagac (Fig. 2.11). The rocks are predominantly microporphyritic basalts and basaltic andesites. Plagioclase is the most abundant phenocryst and is accompanied by

augite, olivine and titano-magnetite. Some basaltic andesites also contain minor K-feldspar and biotite set in a fresh matrix.

2. 2. 3. The Dikili-Bergama-Foca Section

2. 2. 3. 1. The Kiratli (Volcanic) Unit

The Kiratli Unit crops out over a large area (~70-80 km^2) to the SE of Ayvacik and west of Bergama, between the villages of Kiratli to the north, Ovacik to the east and Islamlar to the southwest (Fig. 2.11; 2.13). It is made up of intercalated lava flows and silicified ash tuff and is cut by minor dyke swarms. The total maximum thickness has been estimated approximately 250m, although the thickness of the Unit varies considerably from a few tens of meters to over hundred of meters. A large portion of the Unit is made up of massive lava flows. The rocks are predominantly porphyritic andesites and dacites. They show a great similarity in appearance and phenocryst composition to the lavas of the Akcapinar Unit. They are, however, distinguished by their higher volume of phenocrysts. The phenocrysts are plagioclase, amphibole (edenitic hornblende) and biotite with subordinate augite and quartz. Small zircon and apatite crystals form inclusions in biotite. Some rocks also include minor sanidine.

The lavas are interlayered with thick layers of ash flows in some localities (Plate 2.15). They are mostly crystal-rich and include abundant plagioclase, hornblende, quartz and biotite. Some ash flows have widely been affected by alteration to silicified and partly oxidised. The altered layers have distinctive pinkish to reddish colours and usually form good stratigraphic marker horizons. In some places, NW-SE dyke swarms cut the lava-tuff intercalation. The dykes are mostly aphyric andesites/dacites and only locally developed as a few small outcrops. In some localities (e.g. west of Bergama), the lavas are cut by silicified rocks forming large epithermal gold deposits.

2. 2. 3. 2. The Madra River Dyke Swarms

This dyke system cuts the volcanic rocks of the Kiratli Unit to the SE of Ayvalik, along the Madra River (Fig. 2.11). The dykes are only locally developed over a small area of approximately 8-10 km^2 and are oriented in a NW-SE direction, consistent with the regional tectonic trends and fault orientations. The rocks are completely porphyritic and display light-grey and beige colours. They are mostly andesites and rarely dacites. Phenocrysts are plagioclase, biotite and augite with minor amount of K-feldspar, magnetite and zircon. The more acid rocks also contain quartz phenocrysts.

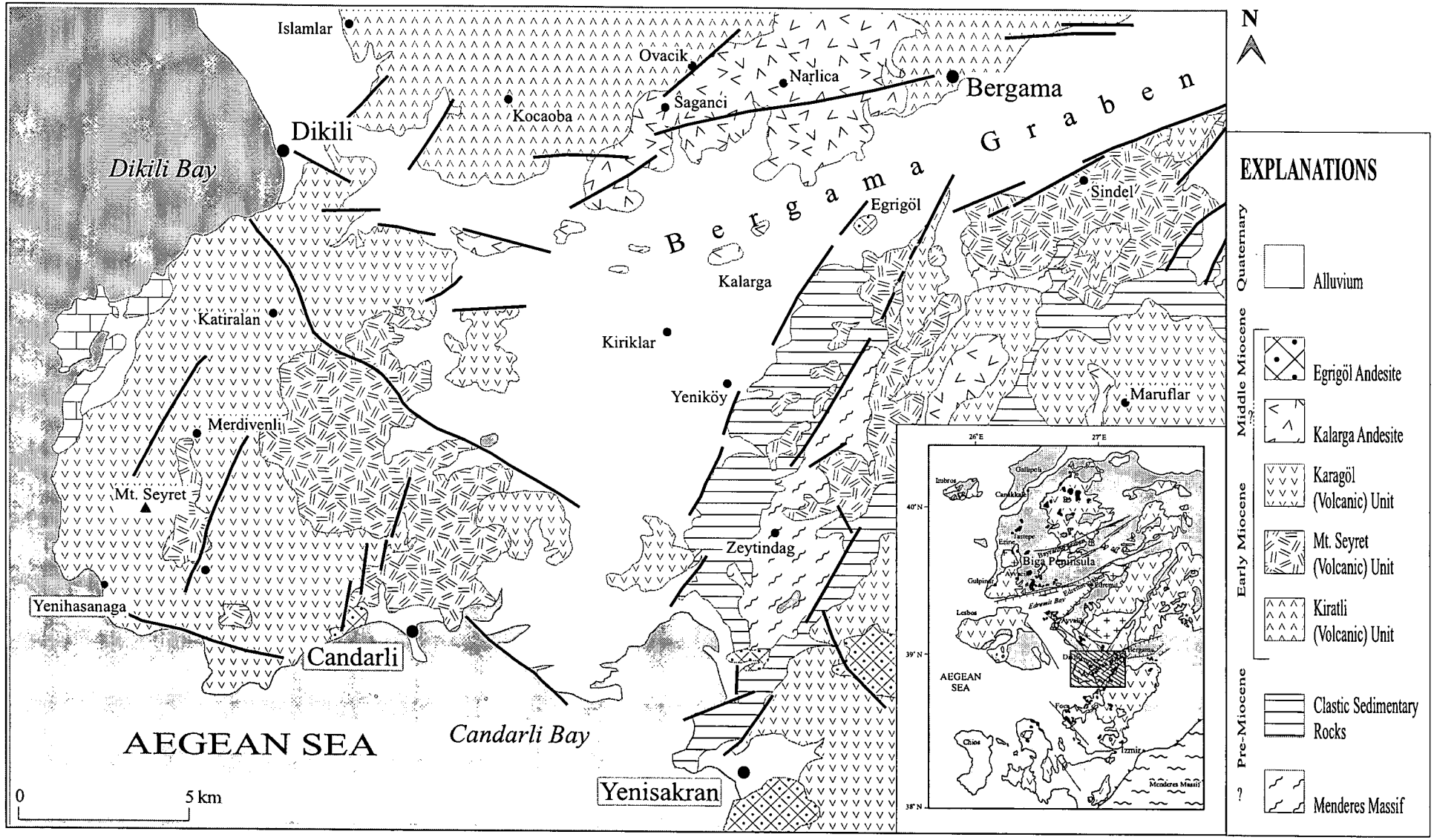

Figure 2.13. *Simplified geological map of the Dikili-Bergama-Candarli area.*

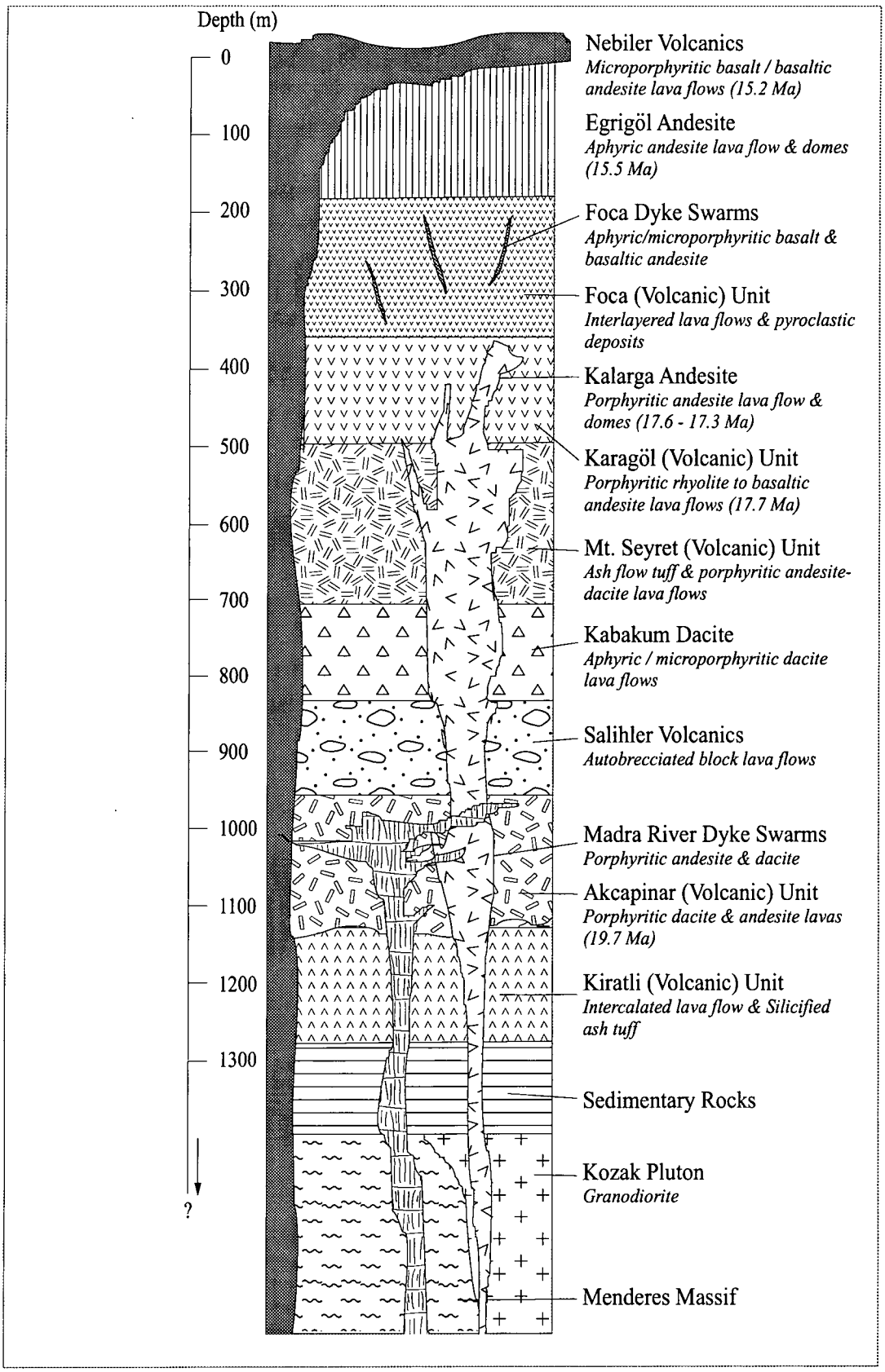

Figure 2.14. *Schematic generalised stratigraphic column illustrating the volcano-stratigraphy of the Dikili-Bergama-Foca section.*

Plate 2.15. *Massive lava layers of the Kiratli Unit overlie ash flow deposits of the same Unit.*

2. 2. 3. 3. The Salihler Volcanics

The Salihler Volcanics crop out to the east of Altinova, around the villages of Salihler and Yenikansiz and occupy an area of approximately 10-15 km^2 (Figs. 2.10; 2.11). They are composed mainly of autobrecciated block lava flows. Although the lava flows are fairly irregular and the thicknesses vary from one locality to another, the maximum thickness of the lavas has been estimated about 150m. The blocks are mostly angular or sub-rounded and their sizes vary between 5 and 60 cm. Most have striated with partly gouged margins indicating a high viscosity before they were extruded. The lavas are compositionally homogenous and show no significant lateral or vertical variation. They are porphyritic andesites and are characterised by a high proportion of phenocrysts. The phenocrysts are plagioclase, hornblende, biotite and minor sanidine. Accessory minerals are apatite, zircon and magnetite. In most places, the rocks are extensively altered to form sericite, calcite and chlorite.

2. 2. 3. 4. The Kabakum Dacite

The Kabakum Dacite consists of aphyric and/or microporphyritic basal lava

flows and overlies the Kiratli Unit (Plate. 2.16). The lavas crop out to the southeast of Altinova, between the villages of Kabakum to the south, Gokceagil to the north and Kizilcukur to the east (Figs. 2.10; 2.11). They extend over an area of about 20-25 km^2 with a total thickness of over 150m. The rocks are almost completely dacite in composition and grey to black in colour. They are mostly homogenous lavas and show almost no mineral compositional difference between the separate lava flows throughout the sequence. The individual lava flows can generally, however, be distinguished by their altered and oxidised flow surfaces.

Plate 2.16. *Lava flows of the Kabakum Dacite forming a basal layer on top of the Kiratli Unit.*

The rocks contain phenocrysts of plagioclase, quartz, biotite and hornblende with minor sanidine and augite embedded in a glassy matrix. In some localities, there are hard, compact, black vitreous lava layers, characteristically displaying vitrophyric textures. Towards the top, highly vesicular lava flows are abundant. Alteration affected the rocks extensively, forming secondary sericite, calcite, chlorite and Fe-oxides.

Abundant fault systems with approximate NW-SE trend cut the lava flows, particularly to the northwest of Kabakum village. To the north of Gokceagil village, the lavas are overlain by Nebiler Volcanics. Young sediments also cover the Kabakum

dacites along the coast.

2. 2. 3. 5. The Mt. Seyret (Volcanic) Unit

The Mt. Seyret Unit consists mainly of pyroclastic deposits with minor lava flows. It crops out around the villages of Katiralan and Merdivenli, near Mt. Seyret and the village of Sindel, to the south of Bergama, with an aerial extent of >70 km^2 (Fig. 2.13). The lava flows interspersed with the pyroclastic deposits are mostly porphyritic andesite and dacite. The pyroclastics are consolidated and semi-consolidated crystal ash flow tuffs. They are mostly intermediate- to coarse-grained, crystal-rich, well-sorted, and form beds with a variable thickness from 2 to 50m. The dominant crystal size is

Plate 2.17. *Consolidated and semi-consolidated pumice ash flows of the Mt. Seyret Unit including abundant rounded and sub-rounded andesitic and dacitic blocks.*

about 1 cm. The tuffs are rhyolitic in composition and contain abundant fresh, euhedral/subhedral, often zoned and fragmented plagioclase accompanied with biotite, hornblende and sanidine. Quartz crystals are concentrated in some parts but are sparse and isolated. Some augite, apatite and zircon in biotite crystals, and magnetite are present in lesser amounts. The clasts are abundant in all parts of the succession. They

are mostly andesites and dacites and have similar mineral compositional and petrographic characteristics to the interlayered lava flows. Clast sizes vary from a few mm to 50-60 cm. In some places, rounded and sub-rounded, andesitic and dacitic blocks are common (Plate 2.17).

In the upper part of the Unit, massive, coarse-grained, heterolithic, clast- to matrix-supported debris flow deposits are abundant. In some places, they are intercalated with volcaniclastic sandstones and tuffs. Lithic clasts in the debris flow deposits range in composition from andesite to rhyolite and are petrographically indistinguishable from the lava flows.

2. 2. 3. 6. The Karagöl (Volcanic) Unit

Abundant acid-intedmediate lavas crop out in the Dikili area and to the northeast of Yenisakran (Fig. 2.13). The products of this period are mostly lava flows and domes. Andesites and dacites are the dominant rock types, although lesser amounts of basaltic andesites and rhyolites are found in some places. The best exposures of the lavas are around the Karagöl Caldera Lake, which is located on the summit of one of the most important eruptive centres of this area known as Mt. Seyret (Plate 2.18). The lavas are all porphyritic and contain phenocrysts of plagioclase, hornblende, sanidine, biotite and augite. Quartz is found in dacites and rhyolites. Most samples also contain zircon, magnetite and apatite. The most silicic rhyolites contain a trace amount of sphene phenocrysts.

The outcrops of the Karagöl Unit are mostly located at the intersection of two major fault systems. One of these fault systems is oriented in a NE-SW direction and forms the Bergama Graben. It cuts the volcanic rocks outcropping in the area between Bergama and Dikili. Another fault system extends from Ayvalik through Dikili to Candarli Bay (Fig. 2.13) with a NW-SE orientation.

In some localities, clastic sedimentary rocks are interbedded within the lavas indicating the lava flows have been formed by several eruptive phases. Borsi et al. (1972) reported a K-Ar age of 17.7 ± 0.6 Ma for the lava flows from the Mt. Seyret (Table 2.2).

2. 2. 3. 7. The Kalarga Andesite

The Kalarga Andesite crops out between the towns of Dikili to the west and Bergama to the east. It consists of lava domes and flows and its best exposures are

Plate 2.18. *A view of the Karagöl Caldera Lake located on the summit of the Mt. Seyret.*

located around Kalarga hill (SW of Bergama), and the villages of Saganci and Narlica. To the southwest of Bergama, it forms a few isolated lava domes on the Bergama Graben floor (Plate 2.19). On Kalarga hill, the lavas display folded structures characterised by massive lavas in the center, but with a concentrically jointed and autobrecciated outer zone (Plate 2.20). This may indicate that the lavas were highly viscous when extruded.

The rocks are porphyritic andesites and characterised by their high proportions of phenocrysts. Plagioclase is the most abundant phenocryst and is accompanied by euhedral/subhedral amphibole (mostly edenite and ferroan pargasitic hornblende) and less abundant biotite. Augite and minor sanidine also form in phenocryst phases. Zircon and apatite form inclusions in biotite phenocrysts and are accompanied by accessory magnetite.

Almost all the outcrops of the Kalarga Andesite are found along the Bergama Graben. Exposure of these lava domes on the Graben floor may indicate a relationship with the extensional tectonics that formed the Graben. Borsi et al. (1972) reported K-Ar ages of 17.6 ± 0.6 and 17.3 ± 0.6 Ma for the andesites from the lava domes (Table 2.2).

Plate 2.19. *Porphyritic lavas of the Kalarga Andesite forming isolated lava domes on the Bergama Graben floor.*

Plate 2.20. *Folded lavas of the Kalarga Andesite forming concentric jointed and autobrecciated outer zone.*

2. 2. 3. 8. The Foca (Volcanic) Unit

The Foca Unit consists mainly of interlayered acid-intermediate lava flows and pyroclastic deposits. The total maximum thickness of this lava-pyroclastic succession has been estimated as about 350m. The base of the Unit is represented by a tuff layer. The tuffs are mostly semi-consolidated and include abundant crystals of plagioclase, K-feldspar and biotite. They pass upwards into a fine-grained, consolidated, white tuff. Massive lava flows overlie the tuffs in most places (Plate 2.21). They are mostly porphyritic and show a compositional range from rhyolite to andesite. The thickness of

Plate 2.21. *Massive lava flows overlie the crystal-rich tuffs of the Foca volcanic Unit.*

the massive lavas varies between 30 and 70m. Further upwards, altered, silicified tuff layers alternate with the massive lavas. The thickness of the tuffs may reach 50-60m. Abundant white perlite and dark-green to black obsidian is present in some parts of the Unit (Plate 2.22).

The uppermost part of the succession is represented by a 30-40m thick, welded ignimbrite layer. It is made up of densely-welded, crystal- and fiamme-rich ignimbrites displaying columnar jointing in some places. It forms a basal layer on top of the Foca Unit (Plate 2.23).

Plate 2.22. *White perlite and dark-green obsidian deposits included in the tuffs of the Foca Unit*

Plate 2.23. *Densely-welded ignimbrites forming a basal layer on top of the volcanic succession of the Foca Unit*

2. 2. 3. 9. The Foca Dyke Swarms

A dyke system with a prevalent direction of NW-SE cuts the rocks of the Foca volcanic Unit. The rocks are fine-grained, aphyric to microporphyritic basalts and basaltic andesites. They are composed mainly of plagioclase, diopsite and forsteritic olivine. Ilmenite and magnetite are also found in some rocks. In some localities, the fresh, hard, black basalts are accompanied by highly vesiculated scoria flows. They also have basaltic compositions and include abundant, calcite-filled cavities and vesicules.

Foca dyke swarms formed along the NW-SE oriented normal faults, indicating a relationship with local extensional tectonics. Savaşçin (1975) reported a K-Ar age of 16.5 Ma for the Foca dykes.

2. 2. 3. 10. The Egrigöl Andesite

The Egrigöl Andesite crops out over an area of about 15-20 km^2 to the south of the town of Yenisakran and to the southwest of Bergama (Fig. 2.13). It forms massive lava flows and domes around Yenisakran and lava domes in Egrigöl hill, near Bergama. The rocks are fresh, grey to black aphyric andesites with a fine grained, partly glassy groundmass. The maximum thickness of the lavas has been estimated as 250m. The lavas have well-developed columnar jointing. On Egrigöl hill, the joint surfaces are vertical in orientation, producing regular polygonal columns (Plate 2.24). Further southwest, near Yenisakran, however, columnar jointing displays a two-tiered arrangement. The bottom of the lavas consist of well-formed, thick, vertical columns normal to the base of the flows whereas the top is characterised by an entablature layer forming thinner, irregular, sub-vertical and sometimes horizontal columns (Plate 2.25).

The rocks contain microphenocrysts of plagioclase, clinopyroxene (mostly diopsite and augite) and minor olivine, although the phenocryst contents are always <5%. Amphibole (edenitic and pargasitic hornblende) is found in some samples together with accessory magnetite and ilmenite. Unlike most of the volcanic rocks in the Dikili-Bergama-Foca section, minor orthopyroxene (hypersthene) is present in some rocks. Although the mineral assemblages of the rocks indicate that they are basaltic in composition, the whole rock chemical analyses give mostly andesitic compositions (see also Chapter 3).

The lavas lie mostly on the small localised extensional basins bounded by NE-SW oriented fault systems. To the southwest of Bergama, lavas emplaced at the bottom of the Graben forming isolated lava domes on the Bergama Graben floor (Plate 2.26).

Plate 2.24. *Vertical oriented, well-developed, regular polygonal columns of the Egrigol Andesite.*

Plate 2.25. *The Upper layer of the Egrigol Andesite forming thin, sub-vertical and horizontal polygonal jointing.*

Plate 2.26. *Isolated lava domes of the Egrigol Andesite formed on the Bergama Graben floor.*

This may indicate a close relationship between the emplacement of the lavas and the localised extensional movements. An andesite sample from Egrigöl, southwest of Bergama, gave K-Ar age of 15.5 ± 0.5 Ma (Table 2.1).

2. 2. 3. 11. The Nebiler Volcanics

The Nebiler Volcanics crop out to the southeast of the town of Altinova, around the villages of Nebiler and Gokceagil and to the southwest of Dikili (Fig. 2.11). The volcanic products consist mainly of lava flows with a maximum thickness of about 50m. The lavas are locally developed with a total aerial extent of about 15 km^2. The rocks are predominantly fresh, grey to black basalts, basaltic andesites and basaltic trachy-andesites. They are mostly microporphyritic, though some aphyric samples are also present. Mineral phases are clinopyroxene (mostly diopsite and augite), microcrystalline plagioclase and forsteritic olivine. Minor phases include Fe-Ti oxides (magnetite and ilmenite) together with phlogopite and Ti-rich biotite.

The lavas are distributed along the NW-SE oriented faults which are related to the local extensional movements that produce hot spring activity in the area. The lavas

overlie the andesite and dacite lavas of the Kiratli Unit. A basalt sample from the Nebiler area, near Dikili, gave a K-Ar age of 15.2 ± 0.4 Ma (Table 2.1).

2. 3. Summary

The Late Cenozoic igneous activity, both in the Ezine-Gulpinar-Ayvacik (EGA) and Dikili-Ayvalik-Bergama (DAB) areas started with pre-Miocene pluton emplacements (e.g. the Kestanbol and the Kozak plutons). The field observations, volcanological characteristics and radiometric data show that major volcanic activity took place both in the EGA and DAB areas during the Early Miocene. It produced a considerable volume of pyroclastics and lavas of intermediate-acid composition. 21.3 ± 0.3 Ma is the oldest K-Ar age obtained for the Early Miocene volcanic rocks of the EGA area. The early stage of activity began with lava flows and continued with lava and pyroclastic successions. The lavas, in general, andesitic to rhyolitic in composition and are characterised by their high proportions of phenocryst contents. The pyroclastics generally form large ignimbrite deposits and accompanied by minor debris (lahar) and ash flow deposits. Compositionally, the pyroclastics are rhyolitic and dacitic. Abundant dyke swarms cut the lava-pyroclastic successions in most places. Radiometric (K-Ar) analyses performed during the course of this study give ages of 21.3 ± 0.3, 20.9 ± 0.5, 20.7 ± 0.3, 20.5 ± 0.3, 20.3 ± 0.6 and 19.7 ± 0.3 Ma for the Early Miocene rocks. Clastic sedimentary deposits within the lava-pyroclastic successions indicate that the volcanic rocks formed by several eruptive phases.

Although the rock types and volcanological characteristics of the Early Miocene volcanics from the both areas (EGA and DAB) are similar to one another, they show some differences in mineral composition. Amphibole is the main hydrous phase for the lavas from the DAB and none of the samples contains orthopyroxene. On the other hand, orthopyroxene is one of the most common phenocrysts and amphibole is absent in the lavas from the EGA area.

In the EGA area, 19.7 Ma is the youngest date for the Early Miocene volcanism and Middle Miocene volcanism is absent. In the DAB area, however, volcanic activity continued into the Middle Miocene with a gradual change in eruptive style and rock compositions. The Middle Miocene activity is marked by lava flows, domes and dykes of basic-intermediate compositions. Pyroclastic eruptive products are absent in this period. The Middle Miocene lavas erupted along the major normal faults related to

graben tectonics, indicating a relationship between volcanism and an extensional tectonics. Radiometric data show that the Middle Miocene volcanism lasted until 15.2 ± 0.4 Ma.

A new stage of volcanic activity in the EGA area began in the Late Miocene and produced locally-developed small lava flows of basic and ultrabasic compositions. The Late Miocene activity continued from 11.0 ± 0.4 to 8.3 ± 0.19 Ma. The distribution of the Late Miocene lavas along the strike-slip fault zones (the middle and southern branches of the North Anatolian Fault) indicate a close relationship with the strike-slip activity and localised extension in the area.

CHAPTER THREE

MAJOR AND TRACE ELEMENT GEOCHEMISTRY

Introduction

In this chapter, the major and trace element geochemical characteristics of whole-rock samples from the Western Anatolian, Late Cenozoic Volcanic Province will be presented. Geochemical data used in this chapter were obtained by two different analytical techniques: (1) the concentrations of major element oxides and selected trace elements (Sc, Cr, V, Ni, Co, Zn, Ga, Rb, Sr, Y, Zr, Nb, Ba, La, Ce, Nd, Pb, Th and U) were determined using X-ray Fluorescence (XRF) spectrometer on a total of 219 samples; and (2) a subset of 56 whole-rock samples was analysed using Inductively Coupled Plasma Mass spectrometry (ICP-MS) for Cs, Hf, Ta and Rare Earth Elements (REE) from La to Lu in addition to all the elements previously analysed by XRF. Both XRF and ICP-MS analyses were performed at the University of Durham. The sample preparation methods-analytical procedures and the full data set are described in Appendix A and B respectively. Estimates of precision and accuracy calculated using replicate analyses on International Reference Materials (IRM) are presented in Appendix C.

The chapter is subdivided into two main parts: (1) classification of the volcanic rocks from Western Anatolia on the basis of major element oxides, and assessment of the major element variations throughout the volcano-stratigraphic successions; (2) trace element characteristics of the volcanic rocks presented as (a) log-normal trace element plots; (b) multi-element patterns (MORB- and chondrite-normalised diagrams); and (c) element ratio plots.

3.1. Major Element Characteristics of the Volcanic Rocks

3.1.1 Classification of The Volcanic Rocks Using Major Element Geochemistry

The volcanic rocks of Western Anatolia have been classified here on the basis of their total alkalis and silica contents using the total alkalis (K_2O+ Na_2O) versus SiO_2 (TAS) classification diagram of Le Bas et al. (1986) (Fig 3.1 and 3.2). The alkaline and

subalkaline fields defined by Irvine and Baragar (1971) have also been plotted onto this diagram. The volcanic rocks have been plotted onto the diagram as 7 different data groups according to their age, locality, position on the volcano-stratigraphic succession, eruptive properties and/or petrographic characteristics (e.g. aphyric or porphyritic). Each group corresponds to either a particular stratigraphic age which may include several volcanic units or to a rock formation (e.g. a dyke swarm). These groups are presented in Table 3.1, together with their corresponding formation names used in Chapter 2. The rocks from the EGA (Ezine-Gulpinar-Ayvacik) area have been plotted as four different groups: (1) Early Miocene, (highly porphyritic) lavas; (2) Early Miocene crystal- and clast-free ignimbrites (plotted as Early Miocene Ignimbrites); (3) Early Miocene dykes (Kovacli Dyke Swarms); and (4) Late Miocene basaltic lavas. The volcanic rocks of the DAB (Dikili-Ayvalik-Bergama) area have been plotted as three different groups: (1) Early Miocene (highly porphyritic) lavas; (2) Middle Miocene intermediate rocks; and (3) Middle Miocene basaltic rocks.

Table 3.1. *The volcanic rock groups from the Western Anatolian, Late Cenozoic Volcanic Province.*

Area	Groups	Age (Ma)		Formation names
EGA	Late Miocene basaltic lavas	8.3		*Ayvacik Volcanics*
				Ezine Volcanics
		11.0		*Tastepe Volcanics*
	Early Miocene dykes	19.7		*Kovacli Dyke Swarms*
	Early Miocene (crystal-free) ignimbrites			*Balabanli Ignimbrite*
				Bergas Ignimbrite
				Koyunevi Ignimbrite
	Early Miocene (highly porphyritic) lavas	20.3		*Behram Andesite*
				Bakacak Unit
				Ciceklik Andesite
				Suruce Andesite
				Bademli Unit
				Babakale Unit
				Dededag Unit
				Ezine Unit
		21.3		*Kiziltepe Unit*
DAB	Middle Miocene basic rocks	15.2		*Nebiler Volcanics*
				Foca Dyke Swarms
	Middle Miocene intermediate rocks	15.5		*Egrigol Andesite*
				Odaburnu Dyke Swarms
	Early Miocene (highly porphyritic) lavas			*Kalarga Andesite*
		17.7		*Karagol Unit*
				Mt. Seyret Unit
		19.7		*Akcapinar Unit*
				Kiratli Unit
				Ulubey Unit
		20.3		*Ballica Unit*

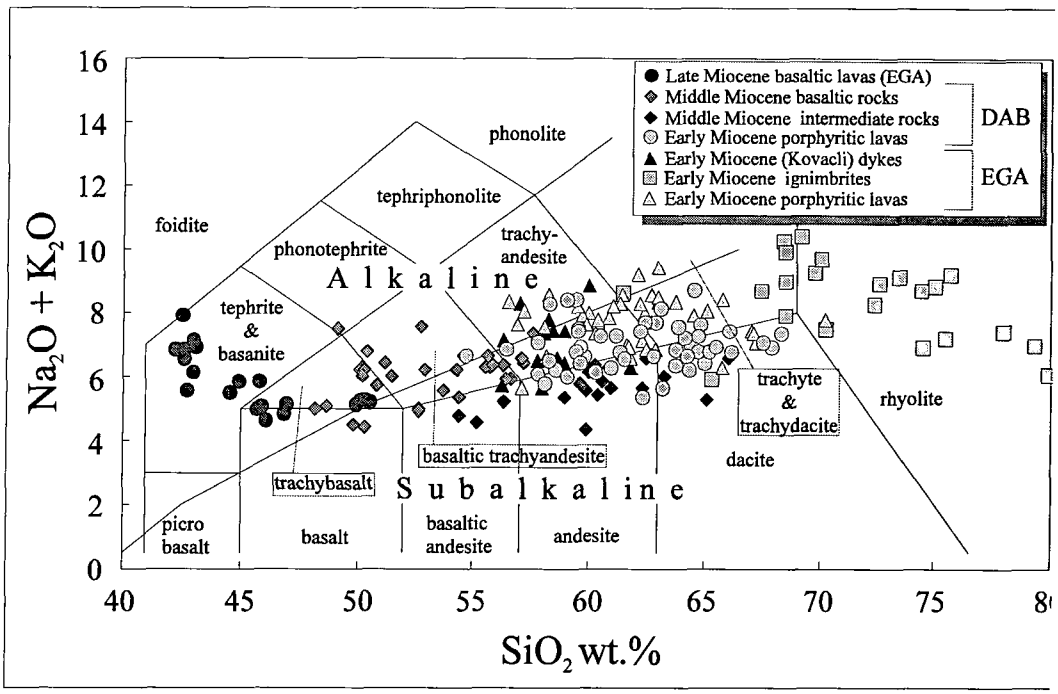

Figure 3.1. *Western Anatolian volcanic rocks plotted on the total alkalis versus silica diagram of Le Bas et al. (1986). The alkaline and subalkaline fields are from Irvine and Baragar (1971).*

Almost all the Early Miocene rocks from the EGA area fall in the subalkaline field and show a compositional trend from trachyandesite to trachydacite and rhyolite. The Early Miocene, porphyritic lavas fall mostly within the trachyandesite and trachydacite compositional fields with silica contents ranging from 56 to 70 wt.% SiO_2, whereas the crystal-free ignimbrites plot mostly in the rhyolite field with silica contents between 65 and 80 wt.% SiO_2 (Fig. 3.1 and 3.2a). The total alkalis contents of the crystal-free ignimbrites show a strong negative correlation with SiO_2 content. The Early Miocene dykes are, however, restricted to the trachyandesite field having a lower silica content (from 55 to 63 wt.% SiO_2) than the other Early Miocene rocks from the EGA area (Fig. 3.2a).

The Early Miocene rocks from the DAB area also plot in the subalkaline field and classify as trachyandesite, trachydacite and dacite with silica contents ranging from 55 to 68 wt.% (Fig. 3.2b). The Early Miocene rocks from both the EGA and DAB areas are compositionally similar to one another and are characterised by high silica contents. Overall, their silica contents range from 55 to 80 wt.% SiO_2 and true basalts and basaltic andesites (<55 SiO_2 wt.%) are rare or absent.

The Middle Miocene rocks from the DAB area range from trachybasalt to dacite

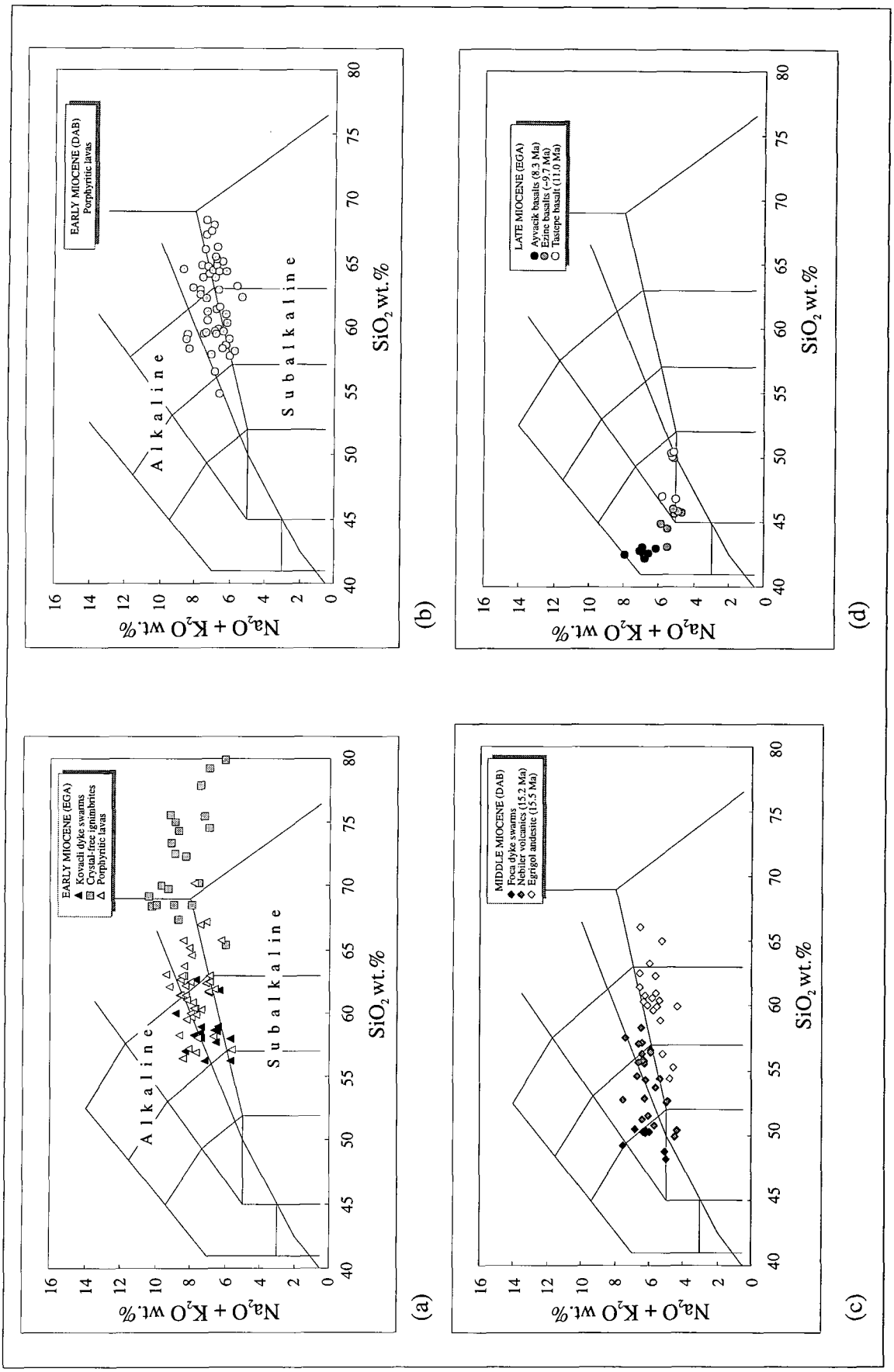

Figure 3.2. *Classification of the volcanic rocks from the Western Anatolian, Late Cenozoic Volcanic Province using the classification diagrams of Le Bas et al. (1986).*

with silica contents ranging from 48 to 57 wt.% SiO_2 for the basic suite and from 54 to 66 wt.% SiO_2 for the intermediate suite (Fig. 3.1). Although few samples show alkaline character and plot in the trachybasalt and basaltic trachyandesite fields, most are subalkaline and classify as basalt, basaltic trachyandesite, basaltic andesite, trachyandesite and andesite. A few samples also plot in the dacite field.

A more detailed classification for the Middle Miocene rocks is given in Figure 3.2c where they are plotted as three different subgroups on the basis of age and locality as mentioned in Chapter 2. These are: (1) the Foca Dyke Swarms; (2) the Egrigöl Andesite; and (3) the Nebiler Volcanics. The Foca Dykes, which are the most basic rocks of Middle Miocene age, plot in the alkaline field and classify as trachybasalt, whereas the Nebiler samples follow a trend from basalt through basaltic trachyandesite to trachyandesite. The rocks of the Egrigöl Andesite are characterised by lower total alkalis for a given silica content relative to the other Middle Miocene rocks and plot mostly in the andesite field.

All Late Miocene lavas from the EGA area plot in the alkaline field and also classify as basanite (with >10% olivine), basalt and trachybasalt. They have silica contents ranging from 42 to 50 wt.% SiO_2. The TAS diagram also reveals a significant negative correlation between SiO_2 and total alkalis content for this group (Fig. 3.1). The rocks from the Tastepe, Ezine and Ayvacik Volcanics have been defined as individual groups in Figure 3.2d to illustrate the compositional differences and evolution of the volcanics through time. The Tastepe Volcanics, which are the oldest known rocks of the Late Miocene alkaline group (11.0 Ma), plot mostly in the trachybasalt field, spanning the alkaline and subalkaline fields. Some of the rocks are, however, strongly alkaline. The samples from the Ezine Volcanics (8.4 to ~9.7 Ma) plot in the basalt, trachybasalt and basanite fields. The rocks of the Ayvacik Volcanics (8.3 Ma) are the most basic of the Late Miocene alkaline suite and plot in the basanite field (Fig. 3.2d).

The subalkaline rocks (Early-Middle Miocene age) from both the EGA and DAB areas have been plotted onto the SiO_2 versus K_2O classification diagram of Peccerillo and Taylor (1976) (Fig. 3.3). The potassic nature of virtually all the Early-Middle Miocene rocks is demonstrated by this plot in which most of the data follow either shoshonitic or high-K calc-alkaline trends. The Early Miocene rocks from both the EGA and the DAB areas fall within the high-K andesite, banakite, high-K dacite and rhyolite fields. The Middle Miocene rocks from the DAB area, however, plot in two distinct

fields. The intermediate rocks follow a high-K calc-alkaline trend and display a range from high-K basaltic andesite to high-K dacite, whereas the more basic rocks are characterised by their higher potassium content with respect to the intermediate rocks and fall within the absarokite and shoshonite fields.

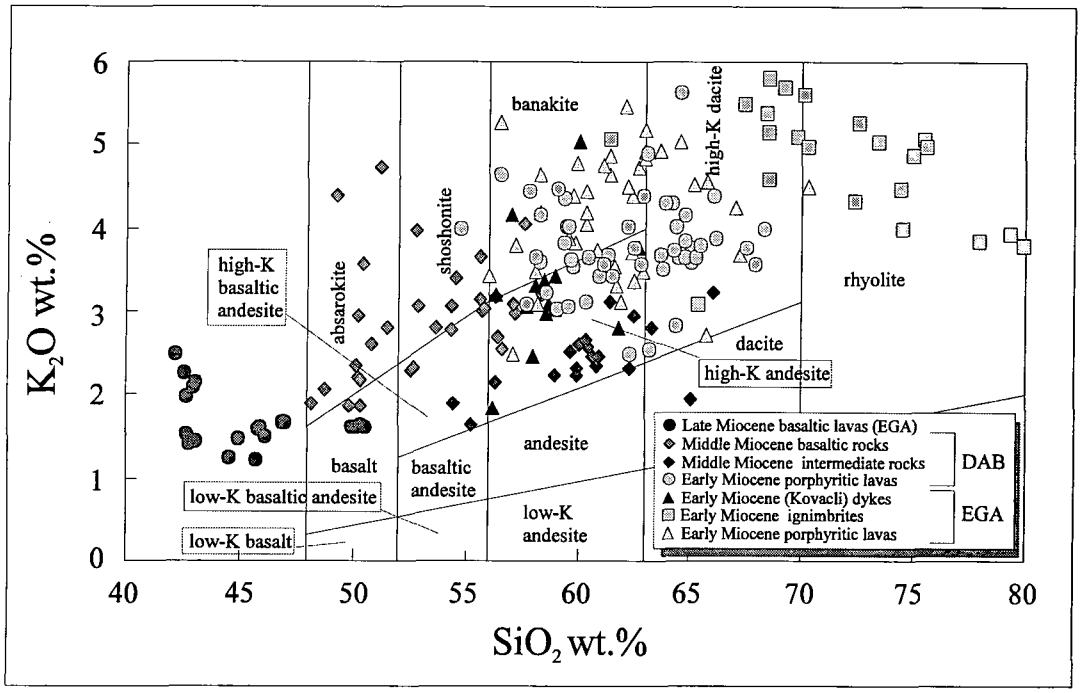

Figure 3.3. *Western Anatolian volcanic rocks plotted on the K_2O versus silica classification diagram of Peccerillo and Taylor (1976).*

The terms absarokite and shoshonite were first used to describe rocks from the Absaroka volcanic field of Montana and Wyoming (Iddings, 1895). The terms have been used in several ways to describe potassic, basic and intermediate volcanic rocks. Absarokite describes the volcanic rocks with abundant phenocrysts of olivine and augite but no feldspar. Shoshonites and banakites were also defined as possessing less olivine and augite but more feldspar. Gary et al. (1972) proposed the term shoshonite for volcanic rocks containing leucite in the groundmass. Morrison (1980) used the shoshonite nomenclature for volcanic rocks that were relatively oxidised, silica-saturated and characterised by high contents of large ion lithophile elements (LILE). However, the chemical definition of Peccerillo and Taylor (1976) is used here (Fig. 3.3).

3.1.2 Harker diagrams of major elements

Harker diagrams of major elements plotted against silica are shown in Figure

3.4. Of these, the TiO_2 plot is particularly distinctive. The TiO_2 concentrations of all the volcanic rocks from Western Anatolia decrease with increasing silica contents. The Late Miocene alkaline basalt and basanites, however, have distinctively high TiO_2 contents ranging from 2.5 to 3.1 wt.%, whereas the TiO_2 concentration of the most basic of the Middle Miocene rocks only reaches 1.2 wt.%. The Early Miocene porphyritic lavas and the dykes from the EGA area also have slightly higher TiO_2 concentrations with respect to the Early Miocene rocks from the DAB area at a given silica value.

As with the TiO_2 concentrations, the alkaline basalts and basanites of the Late Miocene suite have distinctly low Al_2O_3 (<15 wt.%) contents. The Al_2O_3 concentrations for these lavas increase with increasing silica. For the basic-intermediate and acid rocks of the Early-Middle Miocene as a whole, there is an inflection in the Al_2O_3 against silica diagram. This probably reflects a change in the extent of plagioclase crystallisation. Basic-intermediate rocks of the Middle Miocene suite are non-porphyritic (e.g. the Egrigöl Andesite) or weakly to moderately porphyritic (e.g. the Foca Dykes and the Nebiler Volcanics), containing microlites and small phenocrysts of plagioclase. They follow a trend of increasing Al_2O_3 with increasing silica. They have probably been fractionated in deep-crustal levels where plagioclase is unstable and the role of plagioclase in determining differentiation trends is limited. On the other hand, most highly porphyritic rocks of Early Miocene age describe a trend of decreasing Al_2O_3 with increasing silica. This may be attributed to fractionation of plagioclase-dominated mineral assemblages, most probably in long-lived, shallow level magma chambers. The highly porphyritic nature of the rocks and high abundances of plagioclase phenocrysts may also support this idea.

The volcanic rocks, as a whole, exhibit a negative correlation between Fe_2O_3-SiO_2 (Fe_2O_3 is taken here as total Fe_2O_3) and also between MnO-SiO_2. The alkaline group follows a separate trend on the Fe_2O_3 versus silica diagram having higher Fe_2O_3 contents than the other rock groups. The Early Miocene, porphyritic lavas and dykes from the EGA area also have slightly lower MnO concentrations relative to the Early Miocene rocks from the DAB area at a given silica value.

The MgO concentrations of the Late Miocene alkaline suite generally increase with increasing silica except for few samples. On the other hand, the majority of the Middle Miocene and almost all the Early Miocene rocks from both the EGA and the DAB areas exhibit a negative correlation between MgO and silica. MgO concentrations

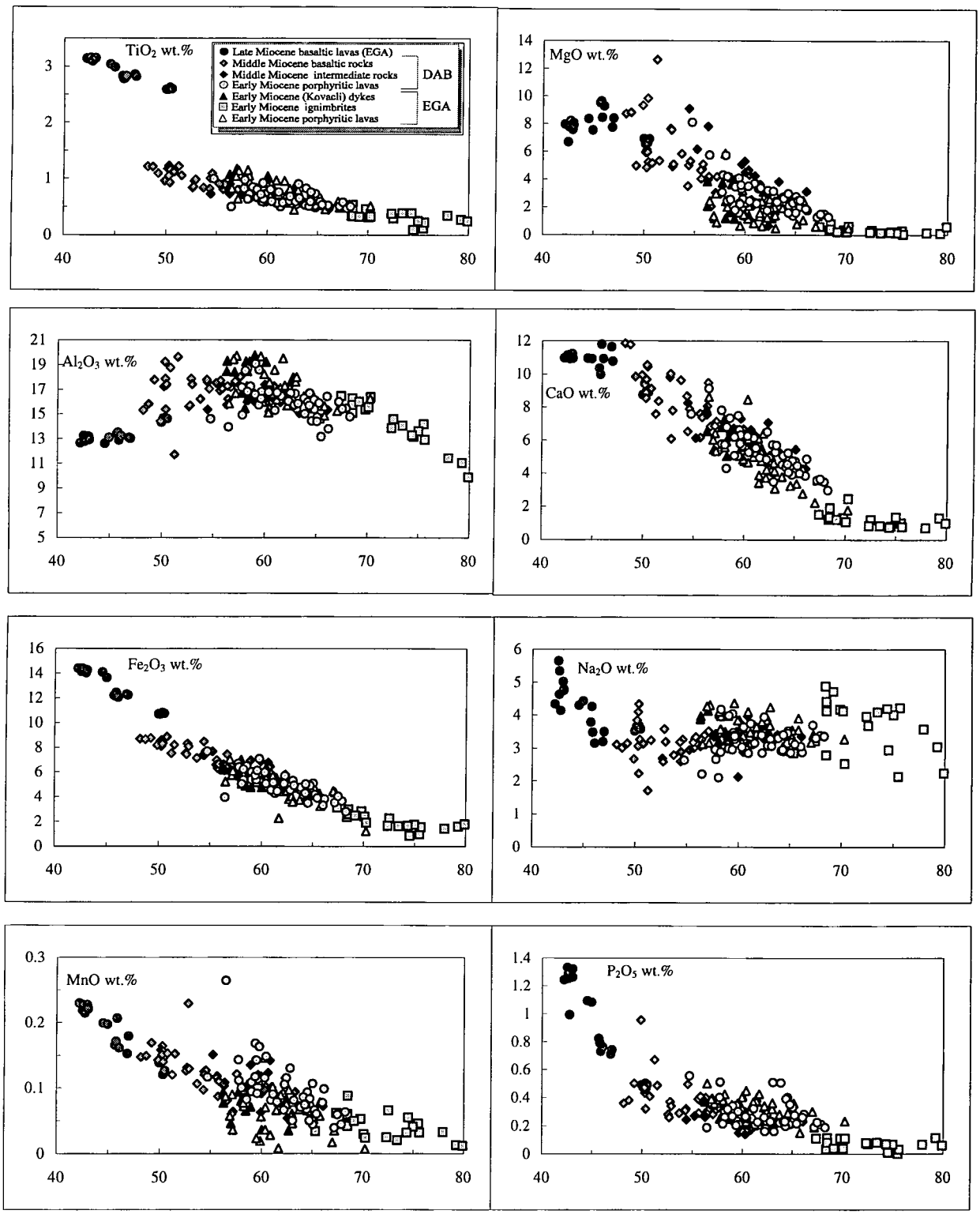

Figure 3.4. *Harker diagrams of the volcanics rocks from Western Anatolia.*

for some samples from the Middle Miocene basic group, however, increase with silica. This may be due to forsteritic olivine accumulation as some of these rocks contain abundant olivine xenocrysts. The Middle Miocene intermediate rocks are generally characterised by higher MgO concentrations than the Early Miocene rocks at a given silica value.

CaO concentrations are roughly constant for most of the Late Miocene alkaline rocks. On the other hand, CaO shows a rapid decrease with silica for almost all the Early-Middle Miocene rocks except for the crystal-free ignimbrites of the EGA area which are characterised by constant CaO concentrations with increasing silica values.

P_2O_5 abundances steadily decrease for the Late Miocene alkaline rocks from 1.33 wt.% at 42 SiO_2 wt.% to 0.49 wt.% at 50 wt.% SiO_2 forming a good negative trend between phosphorous and silica. The basic and intermediate rocks of the Middle Miocene suite together with the Early Miocene porphyritic lavas have P_2O_5 values that decrease with silica forming a negative correlation. P_2O_5 concentrations of the crystal-free ignimbrites, however, stay constant with increasing silica values over a considerable range from 65 wt.% SiO_2 to 80 wt.% SiO_2.

3.2. Trace Element Characteristics of the Volcanic Rocks

3.2.1 Trace Element Variations of The Volcanic Rocks

Trace element concentrations are plotted on log-normal diagrams against silica in Figure 3.5 to demonstrate the compositional differences between the different volcanic rock groups. The transition metals Sc, Ni, Cr, Co, V, Cu and Zn show negative correlations with silica for the Early-Middle Miocene calc-alkaline and shoshonitic rocks from both the EGA and the DAB areas (Fig. 3.5). On the other hand, Sc, Co, V and Cu concentrations of the Late Miocene basic alkaline lavas stay broadly constant with increasing silica values. Cr and Ni for the same lavas increase steadily and Zn concentrations decrease with increasing SiO_2.

The incompatible trace elements, Sr, Rb, Y, Zr, Nb, Ba, La, Ce, Nd and Th, show a negative correlation with SiO_2 for all the Late Miocene basic alkaline suite. Fractional crystallisation from a basic magma would be expected to create a positive correlation between silica and incompatible elements. Thus, the negative correlation observed in Figure 3.5 may best be explained by a decrease in the degree of partial melting towards the top of the sequence of the alkaline lavas (partial melting processes

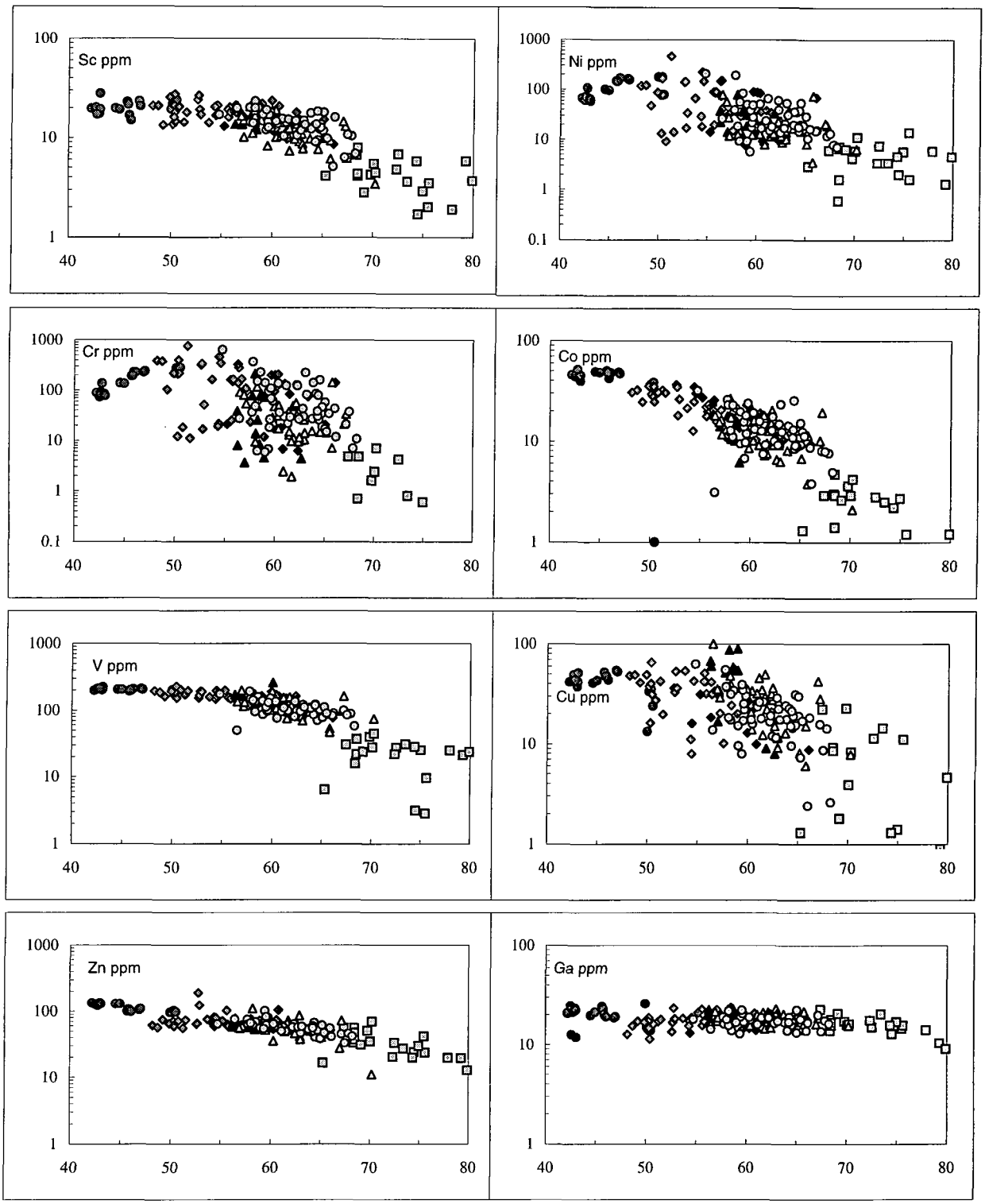

Figure 3.5. Log-normal plots showing trace element behaviour of the volcanic rocks from Western Anatolia.

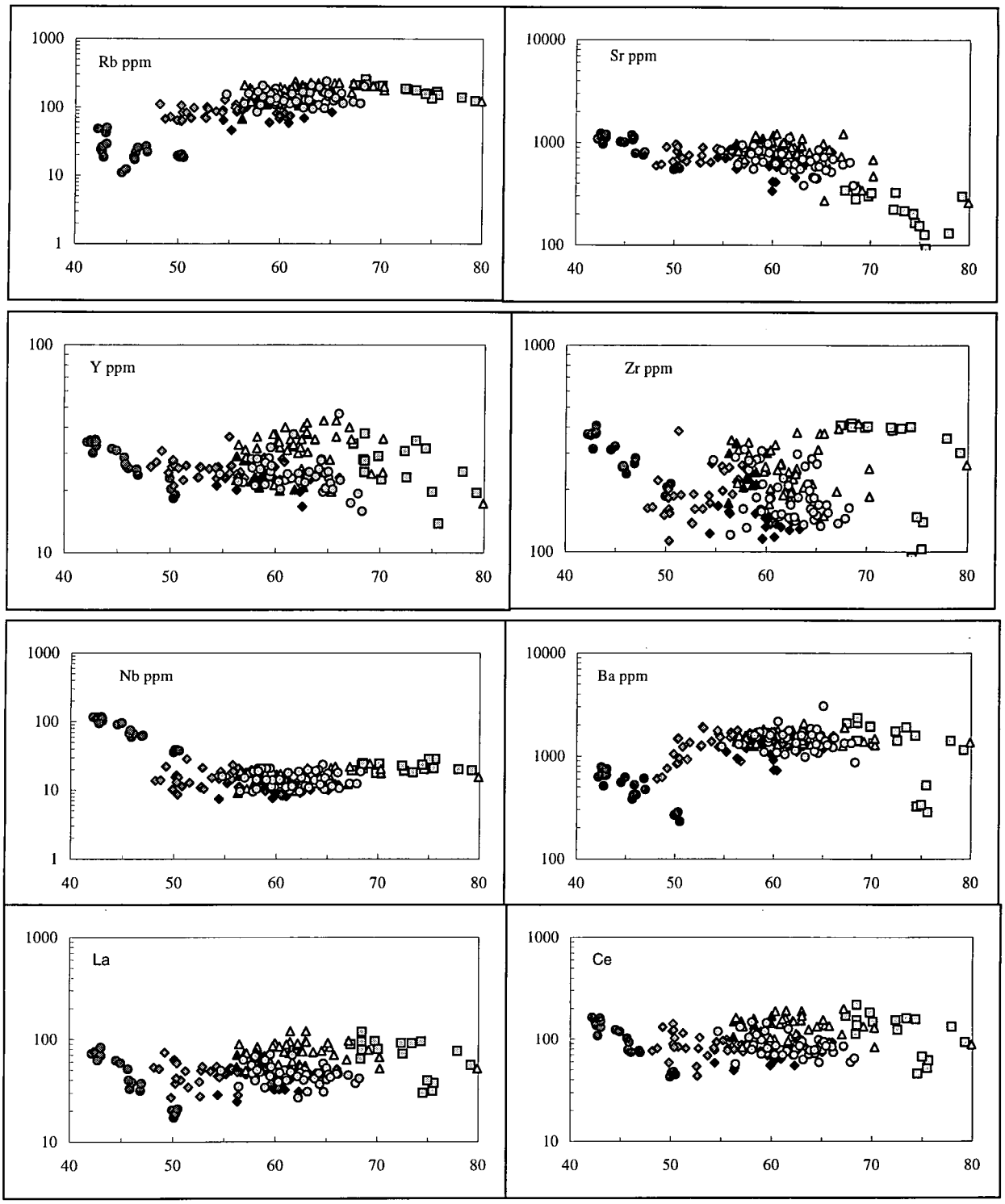

Figure 3.5. (Continued)

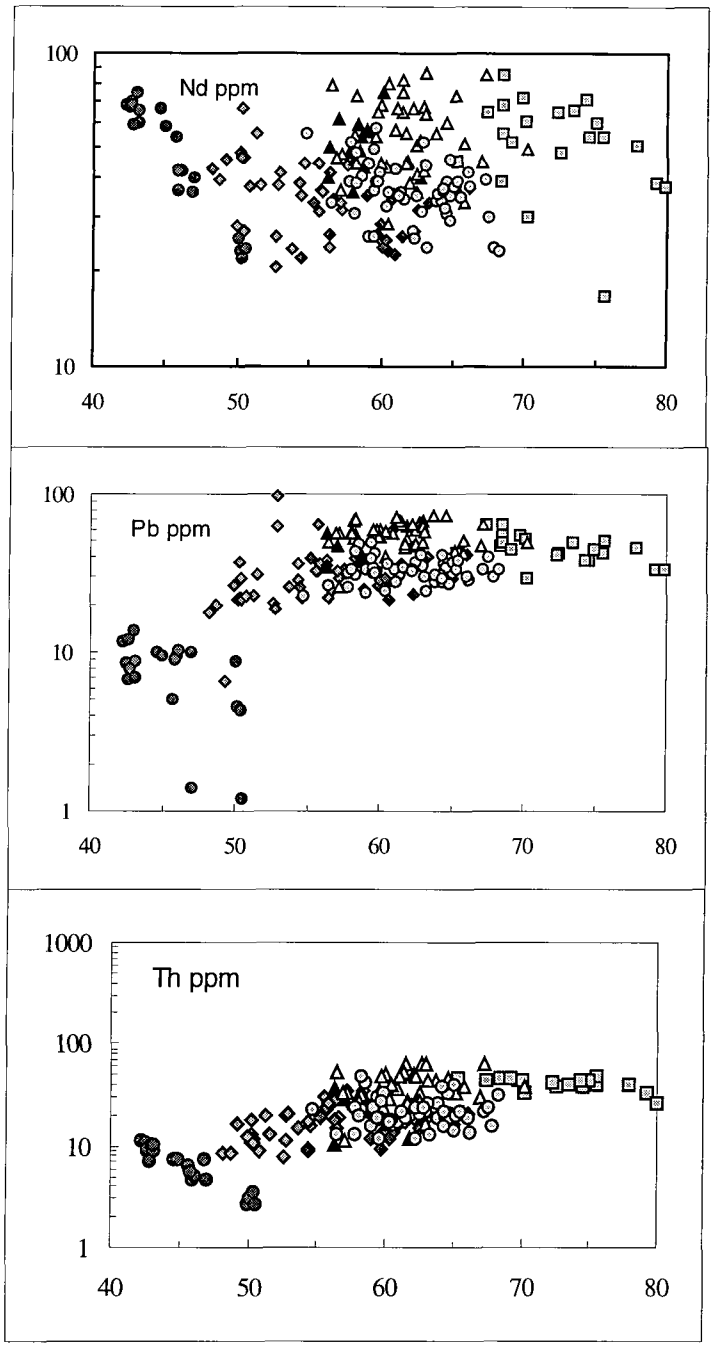

Figure 3.5. *(Continued)*

are discussed further in Chapter 6).

On the log-normal, incompatible trace element diagrams, the Early Miocene rocks from the EGA area are, in general, enriched in La, Ce, Nd and Pb at a given silica value with respect to the Early-Middle Miocene rocks from the DAB area (Fig. 3.5). The Middle Miocene basic-intermediate rocks have lower Y, Zr and Rb at a given silica content than the Early Miocene rocks from both the EGA and the DAB areas. Ba concentrations of the Middle Miocene rocks in general exhibit a strong positive correlation with silica, whereas Ba values of the Early Miocene rocks from both areas

stay almost constant with increasing silica content from 54 wt.% SiO_2 to 80 wt.% SiO_2.

Th and Rb concentrations, in general, exhibit a good positive correlation with silica for most Early-Middle Miocene rocks except for the crystal-free ignimbrites for which Th stays constant and Rb decreases with increasing in silica.

3.2.2 Rare Earth Element (REE) Patterns

The rare earth element (REE) data used in this study were obtained from ICP-MS (Inductively Coupled Plasma-Mass Spectrometry) analyses and the REE concentrations of the rocks have been normalised to the chondritic (C1) abundances proposed by Boynton (1984). Chondrite-normalised ratios of $(La/Eu^*)_N$ and $(Eu^*/Yb)_N$ have been taken as the LREE/MREE and MREE/HREE ratios respectively. Eu* has been taken as extrapolated Eu calculated using normalised concentrations of Sm, Eu and Gd (the geometric mean; Taylor and McLennan, 1985).

The chondrite-normalised REE patterns for representative samples of acid, intermediate and basic rocks from both the EGA and DAB areas are shown in Figure. 3.6 (a-e). Samples have been plotted in order of increasing SiO_2 contents. The Early Miocene, calc-alkaline and shoshonitic rocks from the EGA area in general show L-MREE enriched patterns with LREE/MREE $(La/Eu^*)_N$ ratios of about 5.5-8.2 for the intermediate porphyritic lavas, 6.5-7.8 for the intermediate dykes, 8.1-9.1 for the crystal-free acid rocks (ignimbrites) and MREE/HREE $(Eu^*/Yb)_N$ ratios of 2.6-5.2 for the porphyritic lavas, 3.0-3.4 for the dykes and 2.5-2.8 for the ignimbrites (Fig. 3.7). Although all the Early Miocene calc-alkaline and shoshonitic samples from the EGA area have similar REE patterns, the crystal-free acid ignimbrites (e.g. EA33a) have higher LREE/MREE ratios and negative Eu anomalies. The intermediate rocks of the Kovacli Dyke Swarms from the EGA area have Eu/Eu* ratios of 0.79-0.89 and show only small Eu anomalies, whereas acid rocks have larger negative Eu anomalies with Eu/Eu* ratios of 0.62-0.73 (Fig. 3.8). Intermediate, porphyritic lavas from the EGA area also show small Eu anomalies with Eu/Eu* ratios ranging between 0.76 and 0.93.

The Early and Middle Miocene basic-intermediate, calc-alkaline and shoshonitic rocks of the DAB area have similar REE profiles. The Early Miocene porphyritic lavas of intermediate compositions have LREE/MREE $(La/Eu^*)_N$ ratios of 4.9-7.7 and MREE/HREE $(Eu^*/Yb)_N$ ratios of 1.8-2.9. The Middle Miocene rocks from the same

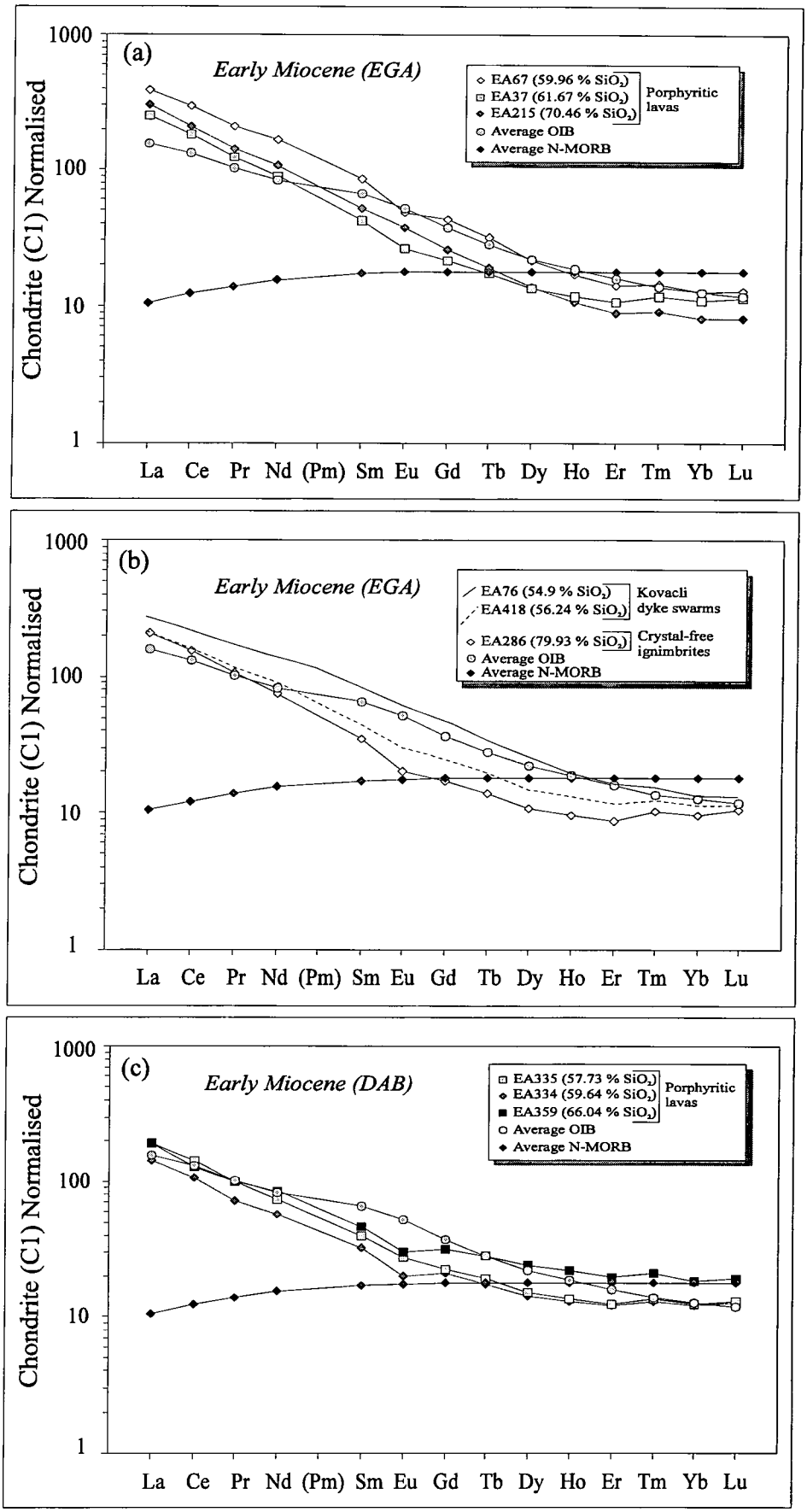

Figure 3.6. *Chondrite (C1) normalised REE plots for the volcanic rocks from Western Anatolia. Chondrite normalising values are taken from Boynton (1984) and average N-MORB and OIB values are taken from Sun and McDonough (1989).*

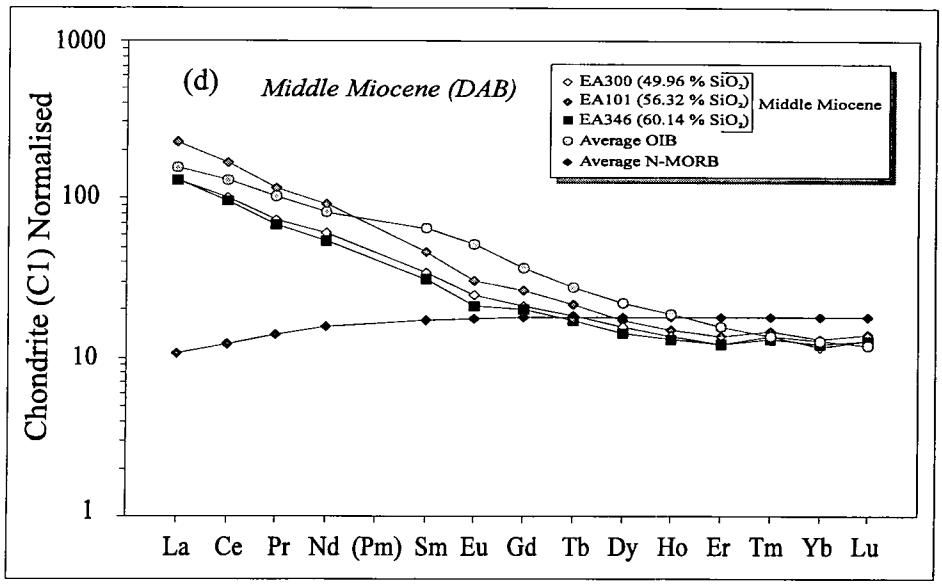

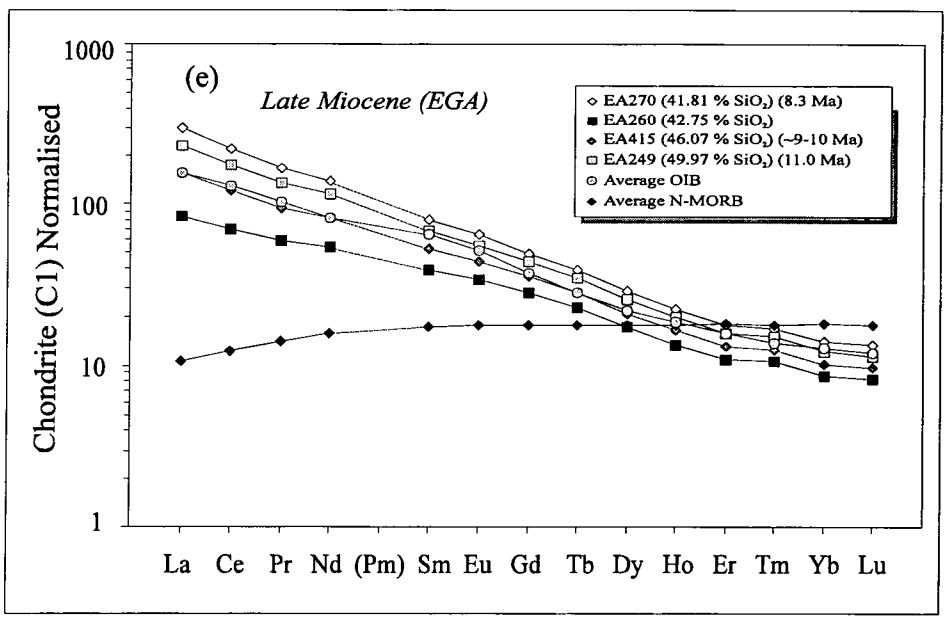

Figure 3.6. *(Continued)*

area have LREE/MREE $(La/Eu^*)_N$ ratios of 4.9 - 6.8 at intermediate compositions, 4.2 - 7.5 at basic compositions and MREE/HREE $(Eu^*/Yb)_N$ ratios of 1.9-2.8 at intermediate compositions, 2.1-4.3 at basic compositions. Eu/Eu* ratios range from 0.76 to 0.97 for the Early Miocene porphyritic lavas of intermediate compositions. The Middle Miocene rocks also have Eu/Eu* ratios ranging from 0.77 to 0.93 at intermediate compositions and from 0.76 to 0.83 at basic compositions. Eu anomalies for almost all calc-alkaline and shoshonitic rocks from the DAB area are generally small (Fig. 3.8).

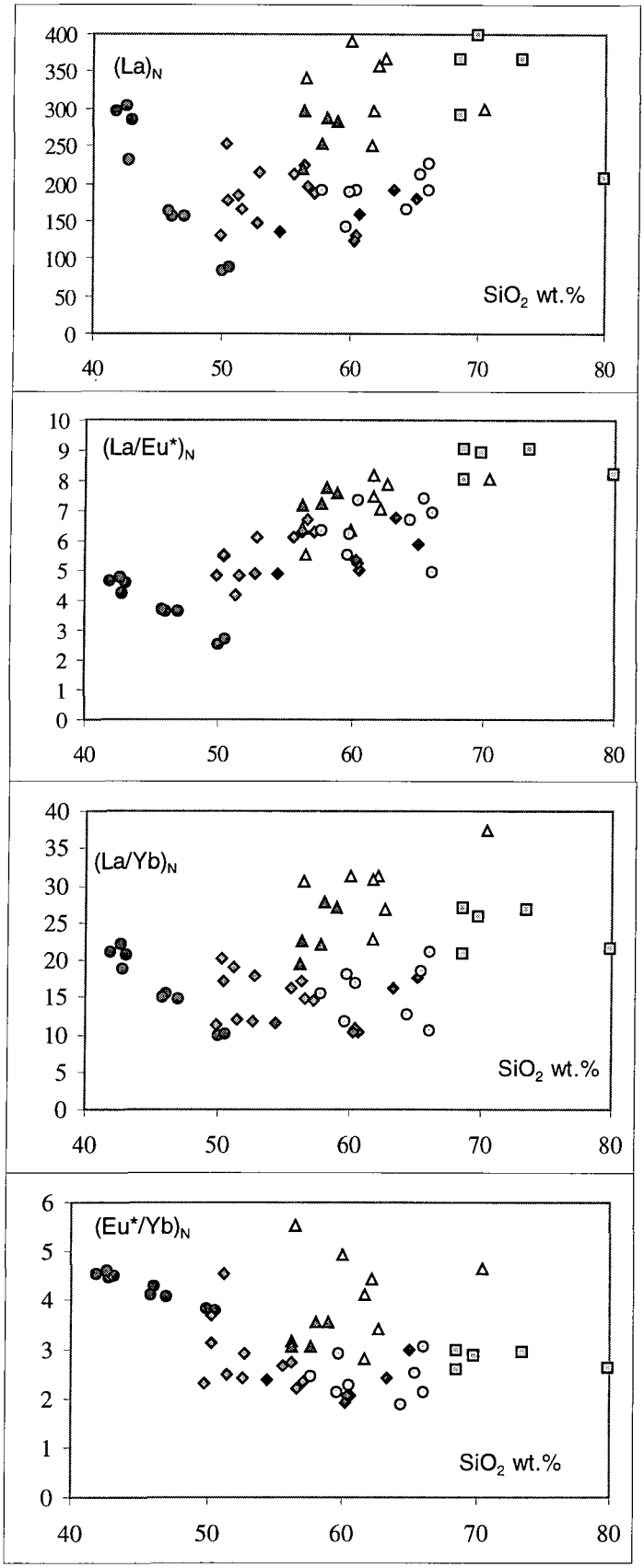

Figure 3.7. *REE variations for the volcanic rocks from Western Anatolia. See Fig. 3.4 for the symbols.*

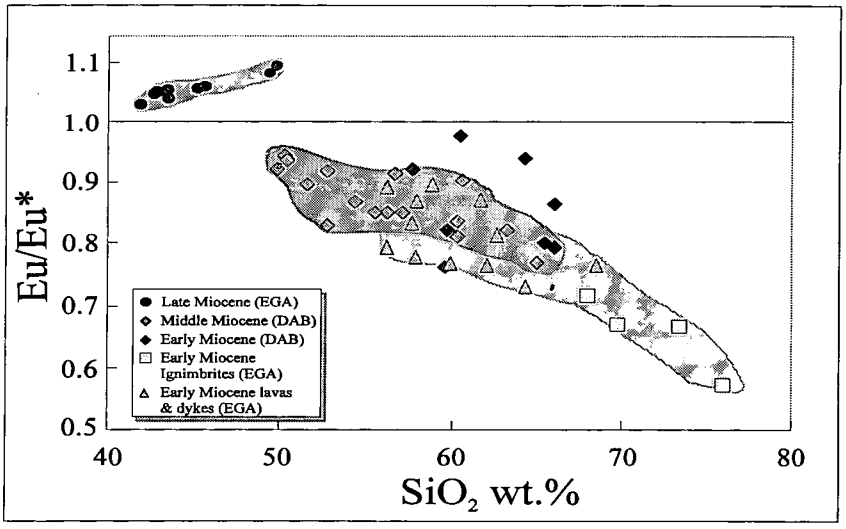

Figure 3.8. *Variable Eu anomalies (Eu/Eu*) for the volcanic rocks from Western Anatolia.*

LREE concentrations of the Early Miocene rocks differ significantly between the EGA and DAB areas. The plot of La against silica demonstrates that the rocks from the EGA area have higher La abundances than the rocks from the DAB area at a given silica content (Fig. 3.7). LREE/MREE (La/Eu*) and LREE/HREE (La/Yb) plots also highlight the relative enrichment in LREE for the Early Miocene rocks of the EGA area as a whole with respect to the rocks from the DAB area.

REE concentrations of samples representative of the whole compositional range of the Late Miocene, mafic alkaline lavas from the EGA area are shown in Figures. 3.6e and 3.7. All alkali basalts and basanites of this group have almost straight chondrite-normalised REE patterns with LREE/MREE $(La/Eu^*)_N$ ratios of 2.5 - 4.8 and MREE/HREE $(Eu^*/Yb)_N$ ratios of 3.6 - 4.3. The samples show sub-parallel patterns and absolute REE concentrations that decrease with increasing SiO_2 content. Although most of the rocks have slightly greater LREE/HREE ratios than average OIB (except for the Tastepe Volcanics; EA249), they show OIB-like REE element patterns. These alkaline lavas have Eu/Eu* ratios of around 1.0, indicating no significant Eu anomalies (Fig. 3.8). Eu/Eu* ratios slightly increase with increasing SiO_2 contents of the rocks. Strong negative correlations between REE concentrations and silica values may indicate a possible decrease in the degree of partial melting for the Late Miocene, mafic alkaline rocks through time as the silica contents of the rocks decrease with time. This possibility is examined in detail in Section 6.2.2.

3.2.3 Multi-Element Patterns

N-type MORB normalised trace element concentrations of representative rocks from the West Anatolian, Late Cenozoic Volcanic Province have been plotted on incompatible multielement diagrams in Figure 3.9(a-f) to demonstrate some of the petrogenetic variations in space and time. The rocks have been plotted as the 7 different groups defined previously. Normalised, average OIB values have also been plotted on each diagram for comparison. Normalisation values (N-MORB) and average trace element abundances of OIB used for the diagrams are from Sun and McDonough (1989).

As can be seen from Figure 3.9(a-c), the Early Miocene, calc-alkaline and shoshonitic rocks from the EGA and DAB areas have similar multielement profiles. These patterns are all characterised by significant enrichment in all the large ion lithophile elements (LILE), Rb, Ba, Th, U, Pb, K and the light rare earth elements (LREE), La, Ce, Pr, Nd, relative to the high field strength elements (HFSE) Ta, Nb, Ti, Zr, Hf, Y and heavy rare earth elements (HREE). Ta, Nb, Zr and Hf are, however, themselves slightly enriched, and HREE are slightly depleted (except for sample EA359 which contains abundant amphibole phenocrysts) with respect to N-type MORB.

Almost all the Early Miocene volcanic rocks exhibit similar N-MORB normalised patterns. Average enriched abundances, as a whole, range considerably from 100 to 500 times N-MORB normalising values for Cs – U and 5 to 40 times for LREE. The Middle Miocene, basic-intermediate rocks of the DAB area also have similar patterns to those of the Early Miocene rocks (Fig. 3.9d). The abundances of the HFSE of Ta, Nb, P, Zr, Hf and Ti are, however, slightly higher than those of the Early Miocene rocks at similar silica contents (Fig. 3.9e).

The Early-Middle Miocene volcanic rocks from both the EGA and DAB areas are characterised by trace element patterns with significant negative Nb and Ta anomalies. These are similar to those from subduction-related (active) continental margins, where the preferred explanation is now a metasomatism of a mantle source by a subduction component selectively enriched in LILE. Basic and intermediate magmas generated from a mantle source enriched by a subduction component (e.g. aqueous fluids and/or sedimentary component) show enrichment in large ion lithophile elements (LILE) because these elements are highly mobile. They can be transported by aqueous fluids from the subduction zone to the mantle wedge (Pearce, 1983). However, records of the

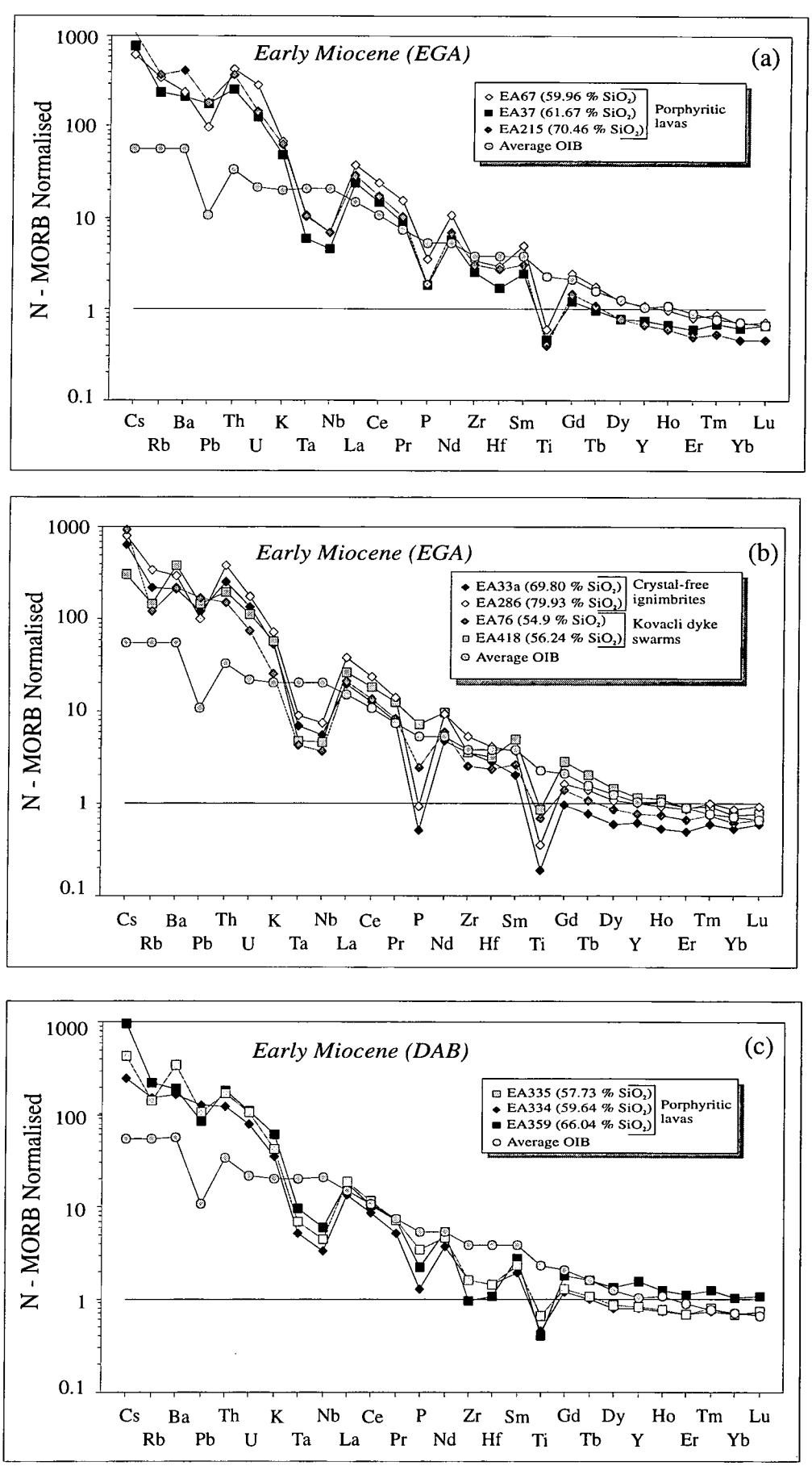

Figure 3.9. *N-MORB normalised patterns for the volcanic rocks from Western Anatolia. N-MORB normalising and average OIB values are taken from Sun and McDonough (1989).*

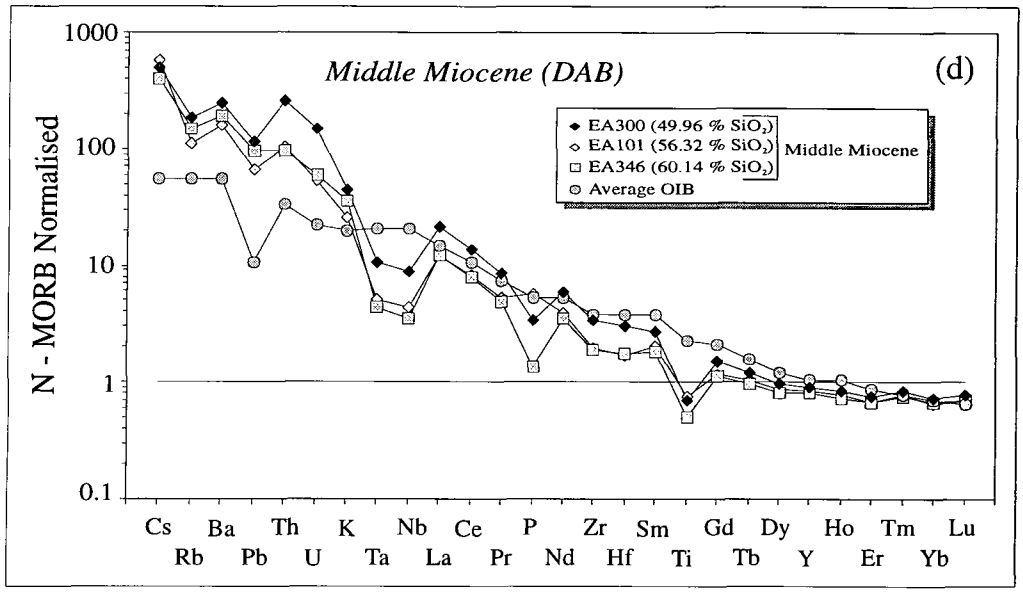

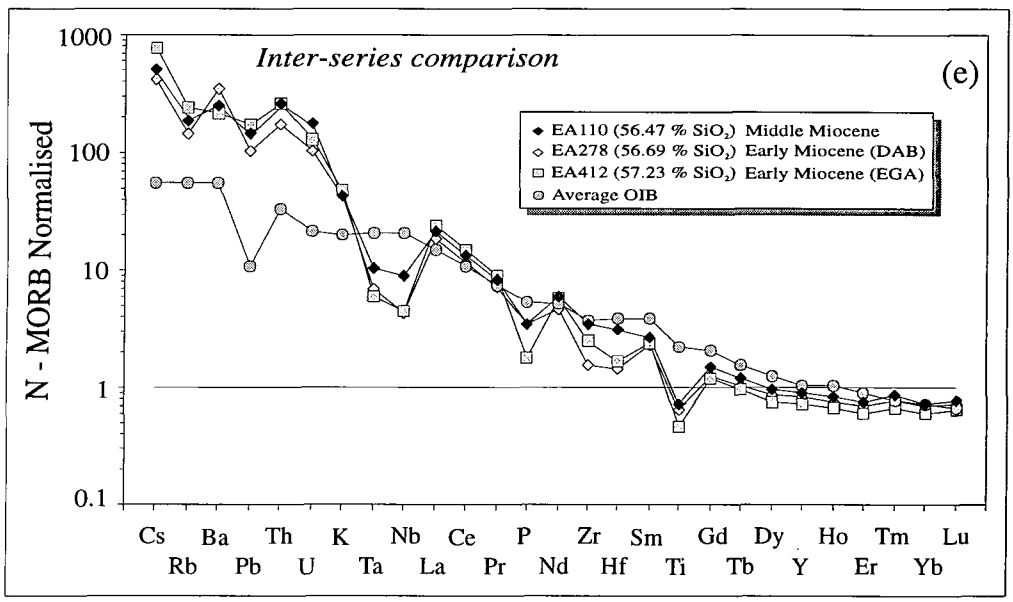

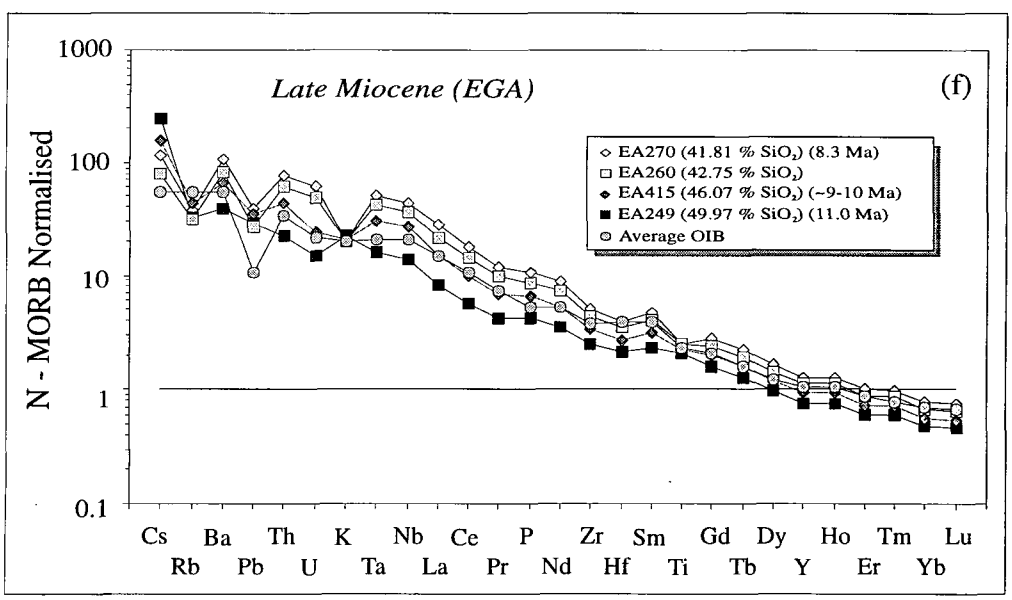

Figure 3.9. *(continued)*

tectonic evolution of the area indicate that the Late Cenozoic volcanism of Western Anatolia formed in a collision setting following the Late Cretaceous-Middle Eocene north-dipping, subduction beneath the Pontides which ended in a collision between the Anatolide-Tauride platform and the Pontides (see also Chapter 1 for details). For collision-related (post-collisional) calc-alkaline and shoshonitic magmas, the possible options to explain enrichment in LILE and LREE relative to Ta and Nb are: (1) a subduction component from earlier subduction events; or (2) crustal contamination through AFC (assimilation and fractional crystallisation) and/or MASH (melting, assimilation, storage and homogenisation) processes.

Representative patterns from the Late Miocene mafic alkaline lavas of the EGA area have also been plotted in Figure 3.9f. All are enriched in LILE, HFSE and L-MREE, and slightly depleted in HREE relative to the N-MORB normalising values. Average enriched abundances range from 20-100 times N-MORB values for LILE, 20-60 times N-MORB for Ta and Nb and 3-30 times N-MORB values for the LREE. Incompatible element concentrations correlate with both silica contents and age. Almost all incompatible element concentrations of the rocks increase with decreasing SiO_2 contents towards the top of the sequence of the alkaline suite. In general, their patterns are parallel to that of an average OIB. Unlike the Early-Middle Miocene volcanic rocks, none of the alkali basalt or basanite samples of the Late Miocene age show negative Ta or Nb anomalies. This may indicate that the Late Miocene alkaline volcanic rocks have not been derived from the same source as the earlier calc-alkaline and shoshonitic rocks. The source region for the alkaline basalts and basanites carries no subduction component and the lavas have not been affected by crustal contamination. High abundances of both LILE and HFSE for the alkaline rocks with respect to N-MORB may, however, be explained by several mechanisms: (1) melting of a lithospheric mantle source enriched by a small volume melt fraction derived from the asthenosphere; (2) melting of a lithospheric mantle which has previously been depleted in LILE and LREE by extraction of earlier calc-alkaline and shoshonitic magmas and lost its subduction component; or (3) small degrees of partial melting of an asthenospheric mantle source (e.g. Depleted MORB Mantle). These options are discussed in detail in Section 6.2.2.

3.2.3 Trace Element Ratios

Representative basic and intermediate samples from the West Anatolian, Late

Cenozoic Volcanic Province have been plotted on the Th/Yb versus Ta/Yb diagram proposed by Pearce (1983) (Fig. 3.10). Plots of these ratios are almost independent of fractional crystallisation and/or partial melting (with pyroxenes and feldspars as the dominant- crystallisation or residual phases), and highlight source variations and crustal assimilation. Basaltic magmas derived from the mantle asthenosphere (e.g.,Depleted MORB Mantle; DMM), plume asthenosphere or mantle lithosphere enriched by small-degree melts from the asthenosphere all lie within or close to a diagonal mantle array defined by constant Th/Ta ratios. Source region metasomatism by subduction processes, however, results an enrichment of Th with respect to Ta and hence in Th/Yb ratios higher than Ta/Yb, as subduction components in general carry Th but not Ta or Yb. Crustal contamination may also increase Th/Yb ratios relative to Ta/Yb ratios because of higher abundances of Th relative to Ta in the crustal rocks (except for granulite facies crust, which has low Th contents; Pearce, 1983).

Figure. 3.10 shows that all Early and Middle Miocene volcanic rocks from both the EGA and the DAB areas are shifted to high Th/Yb ratios relative to the mantle array. Although the effects of crustal contamination on magma compositions are difficult to distinguish from those of metasomatism by subduction processes, the significantly high Th/Yb ratio for the most basic sample (49.82 wt.% SiO_2) of the Early-Middle Miocene rocks is unlikely to be explained solely by crustal contamination. Furthermore, because basic and intermediate volcanic rocks are shifted equally from the mantle array forming a sub-parallel trend to that array, source region metasomatism by an earlier subduction component is a more likely explanation than crustal contamination for this shift. However, there is likely also to be further crustal contamination as the degree of displacement in Figure 3.10 correlates with the silica content for most of the rocks (Fig. 3.11).

The Early Miocene rocks of the EGA area are characterised by higher Th/Yb ratios than the rocks of the DAB area, indicating either a greater subduction component in the source region or further crustal assimilation of a metasomatised-mantle derived magma for the rocks from the EGA area. Note that three different groups (Early Miocene EGA and Early-Middle Miocene DAB) all form trends parallel to the mantle array. This can reflect a variety of processes from fractional crystallisation (rocks up to 63 wt.% SiO_2 are plotted), partial melting and crustal assimilation-fractional crystallisation (AFC) acting on a magma derived from mantle containing a subduction

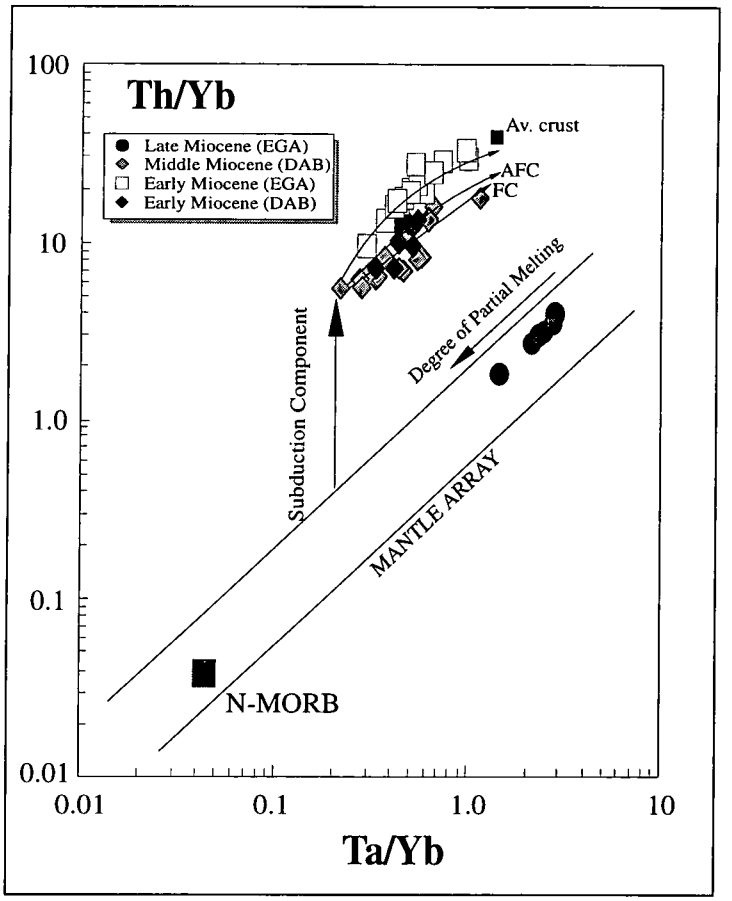

Figure 3.10. *Th/Yb versus Ta/Yb diagram (after Pearce, 1983) for basic and intermediate (<63 % SiO_2) volcanic rocks from Western Anatolia. The Late Miocene alkaline lavas follow the mantle array, indicating no subduction enrichment or significant crustal contamination signatures, whereas the Early and Middle Miocene calc - alkaline and shoshonitic rocks exhibit a consistent displacement from the mantle array indicating subduction-related metasomatism. Possible subduction component and AFC / FC vectors are indicated. The average crust composition represents the metamorphic basement rocks.*

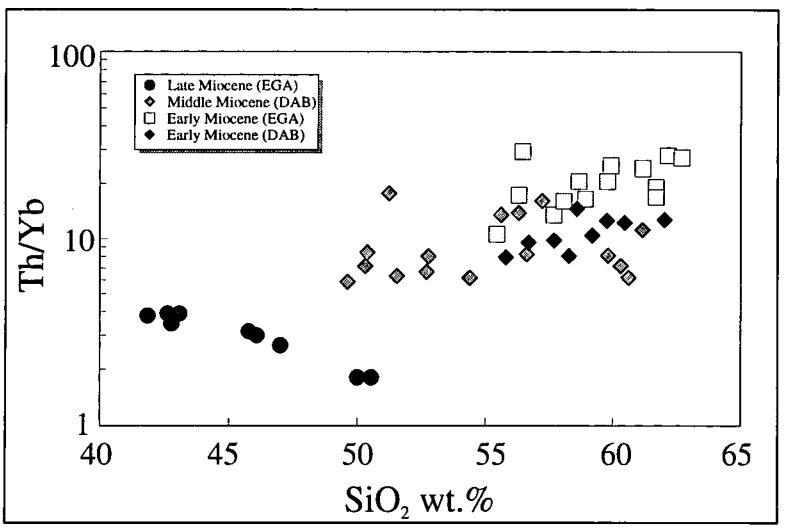

Figure 3.11. *Diagram showing the variations in the ratio of Th/Yb with changing silica for the volcanic rocks from Western Anatolia.*

component.

The Late Miocene mafic alkaline lavas of the EGA area plot on the MORB-OIB mantle trend, confirming the interpretation from the trace element patterns (e.g. N-MORB normalised patterns) that the mantle source had no subduction component and that the resulting magma was not affected by any significant crustal contamination. High ratios of both Ta/Yb and Th/Yb relative to N-MORB suggest that the magma has been generated either by melting of an enriched mantle or by small degree partial melting of a garnet-bearing mantle source, or by a combination of both processes.

3.2. Chapter 3 Summary

The volcanic products of the Western Anatolian, Late Cenozoic Volcanic Province can be distinguished into two main groups on the basis of their major and trace element characteristics. These are: (1) the Early-Middle Miocene, calc-alkaline and shoshonitic group; and (2) the Late Miocene alkaline group.

The calc-alkaline and shoshonitic rocks of Early Miocene age are generally acid-intermediate (55-80 wt.% SiO_2), changing progressively to basic-intermediate (48-62 wt.% SiO_2) into the Middle Miocene.

The calc-alkaline and shoshonitic rocks have characteristic enrichments in LILE and LREE relative to the HFSE (characterised by negative Ta and Nb anomalies). Trace element ratio plots have shown that this feature can most likely be explained by a subduction component in a mantle source region, though crustal contamination processes may also have contributed.

The Late Miocene, alkaline rocks are mostly classified as basalts and basanites with their low silica contents ranging between 42 and 50 wt.% SiO_2. They are sodic alkaline ($[Na_2O-2]>K_2O$) and are characterised by high TiO_2 (2.5-3.1 wt.%) and low Al_2O_3 (12-15 wt.%) contents.

Trace element characteristics show that the alkaline rocks have been generated from a mantle source that carries no subduction component and that the alkaline magma has not been greatly affected by crustal contamination processes. The most likely source for the alkaline magma may be either a mantle lithosphere with significant enrichment of a small volume melt fraction from the asthenosphere, or a small degree of partial melting of asthenospheric mantle (e.g. Depleted MORB Mantle).

CHAPTER FOUR

PETROGRAPHY

Introduction

This Chapter describes the petrographic characteristics of the volcanic rock groups from the Western Anatolian, Late Cenozoic volcanic province and discusses some of the genetic implications of phenocryst assemblages and textural features. The volcanic rock formations from both the Ezine-Gulpinar-Ayvacik (EGA) and Dikili-Ayvalik-Bergama (DAB) areas have been divided into different groups according to their main textural and compositional properties and age as described in Chapters 2 and 3.

4.1. Volcanic rocks from the Ezine-Gulpinar-Ayvacik (EGA) Area

4.1.1. Highly Porphyritic Acid-Intermediate Lavas (Early Miocene)

The calc-alkaline and shoshonitic rocks of the Early Miocene porphyritic lavas from the Ezine-Gulpinar-Ayvacik area are generally hypersthene- or quartz-normative andesites and dacites. Most of the rocks in this suite are highly porphyritic, with modal proportions of total phenocrysts ranging from 20 to 60% by volume. The rocks generally include both macrophenocrysts (>0.5mm) and microphenocrysts (from 0.05 to 0.5mm in diameter). The most common phenocryst phases are plagioclase, clinopyroxene, orthopyroxene, alkali feldspar, biotite and magnetite. Minor apatite and zircon accompany them in most of the lavas. Quartz and olivine are present in only few andesitic and dacitic lavas, and then only rarely. Amphibole is rare or absent and present in only one of the lava Units of Early Miocene age (The Bademli Unit).

Plagioclase is the dominant phenocryst phase and is present in almost all the volcanic rocks of the porphyritic lavas. Its modal abundances vary between 30 and 65% of the total phenocrysts. The crystals are generally euhedral or subhedral and their sizes range from <0.05mm (microcryst) to 4mm (macrophenocryst). They usually display complex oscillatory normal zoning and sometimes reverse zoning. Compositionally they are andesine and labradorite. Core and rim compositions are An_{37-60} and An_{35-66}

respectively. Most phenocrysts include small needles of euhedral **apatite** as inclusions. In some andesite samples, rounded phenocrysts characterised by irregular rounded edges are common and are accompanied by multiply-intercepted re-entrants characterised by spongy cores or dusty core and zones (sieve texture). These characteristics may be attributed to resorption (or reaction) resulting from magma mixing. In some cases, however, resorbed centers are mantled by fresh, non-resorbed rims indicating an interior melting followed by overgrowth of equilibrium plagioclase resulting from the subsequent quenching (Cox et al., 1979) (Plate 4.1,2,3). The sieve-textured phenocrysts contain abundant glass inclusions.

Clinopyroxene is present as phenocrysts in all andesites and dacites. Its modal abundance varies from <5% to 25%. In general, clinopyroxene phenocrysts become much less abundant in the lavas with increasing SiO_2 contents. They are mostly subhedral-euhedral, although some rounded anhedral and partially resorbed crystals are present. They are compositionally augite and diopside and most phenocrysts exhibit oscillatory-normal and/or sector zoning. Core and rim compositions are Wo_{42-45} En_{46-44} Fs_{12-11} and Wo_{43-41} En_{41-39} Fs_{14-11} respectively.

Most samples contain **orthopyroxene** as phenocrysts. Their modal abundances range between <5% and 25%, similar to the abundances of clinopyroxene. The ratio of augite to hypersthene is, however, greater in more felsic rocks, and some dacites and rhyodacites include no orthopyroxene phenocrysts. They usually form euhedral crystals with grain sizes between 0.02 and 0.5mm (Plate 4.4). They are generally unzoned or slightly zoned with Mg-rich cores, and compositionally, they are hypersthene (En_{62} - En_{68}). Most phenocrysts are optically homogenous and are characterised by pale pink colours and slight pleocroism under the microscope (Plane Polarized Light). Some are rimmed by, or aggregated with, augite and diopside.

The fourth most abundant phenocryst phase is **biotite**. Almost all lavas contain biotite phenocrysts. They are mostly subhedral-euhedral with grain sizes ranging from <0.03mm to 1mm. Apatite needles, small zircon and magnetite crystals and plagioclase laths are common inclusions in biotite phenocrysts. In some samples, biotite phenocrysts are always subhedral and resorbed, and they are often surrounded by thick granular breakdown corona of pyroxene, opaque oxides and plagioclase. These features may indicate that biotites were not in equilibrium with the host liquid.

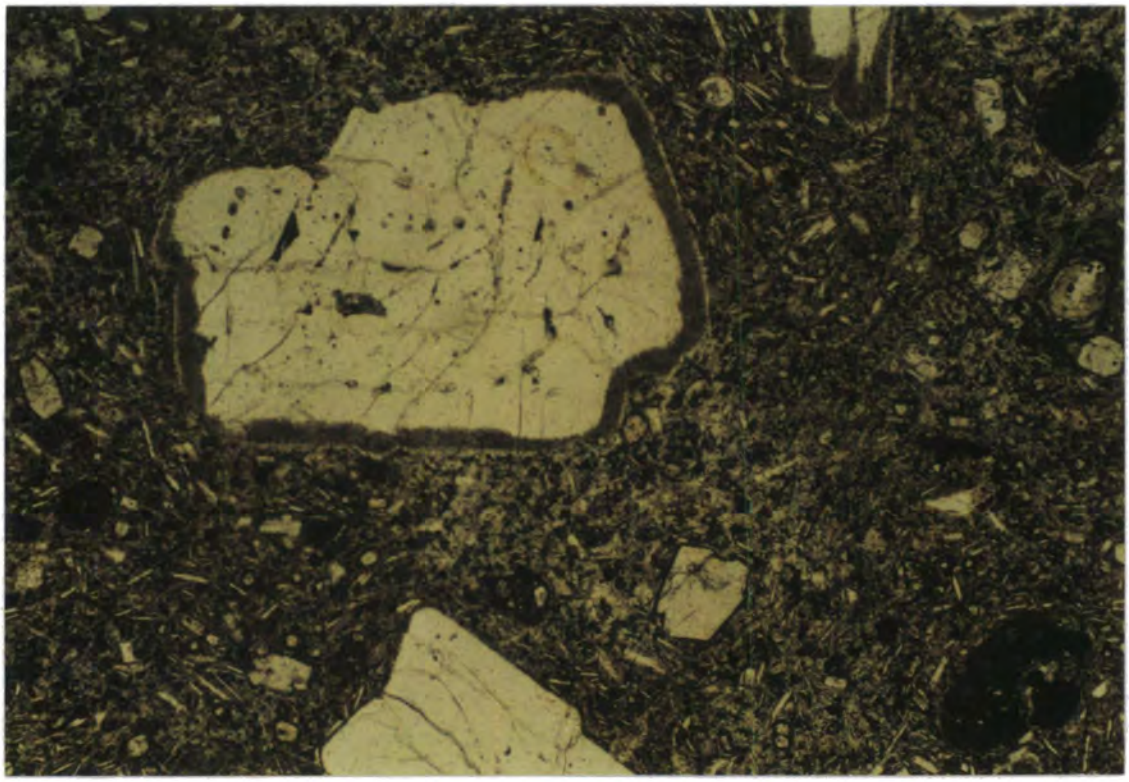

Plate 4.1. *Large, intermediate plagioclase set in a partially crystalline groundmass. The plagioclase is surrounded by a dark, dusty reaction rim. Field of view 3x1.9mm, shown in plane polarized light (PPL).*

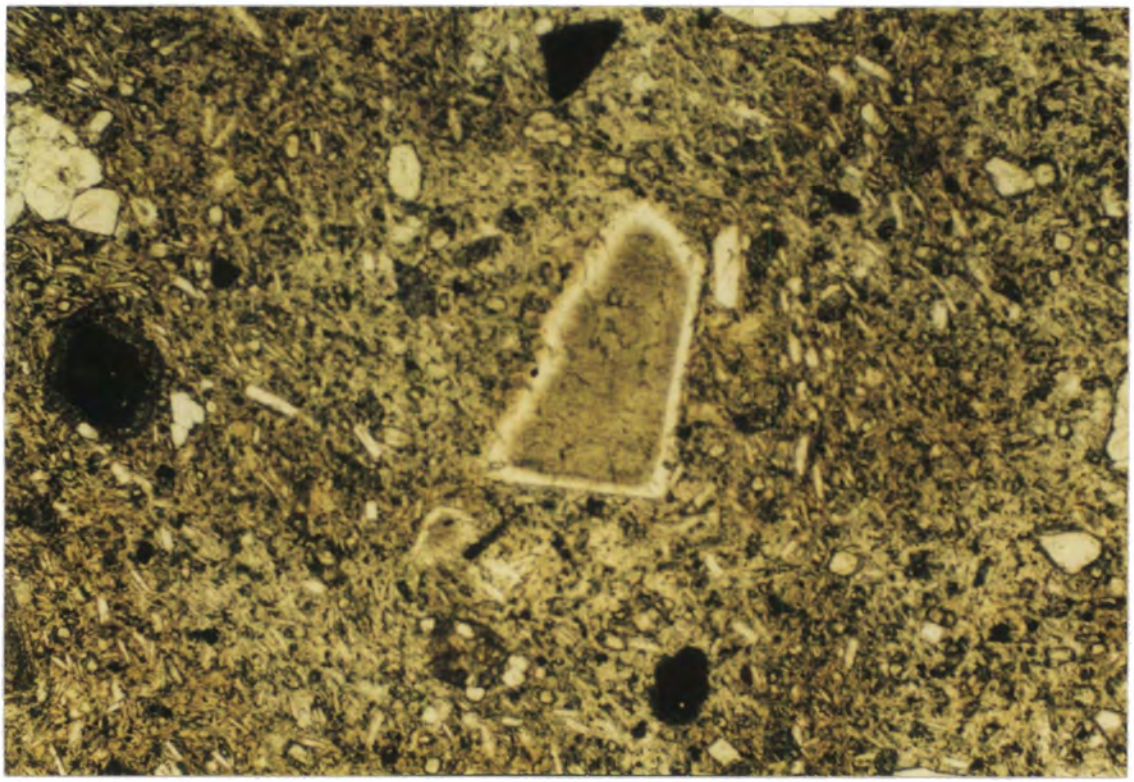

Plate 4.2. *Intermediate plagioclase with a resorbed core surrounded by a fresh, equilibrium rim. Field of view 3x1.9mm, PPL*

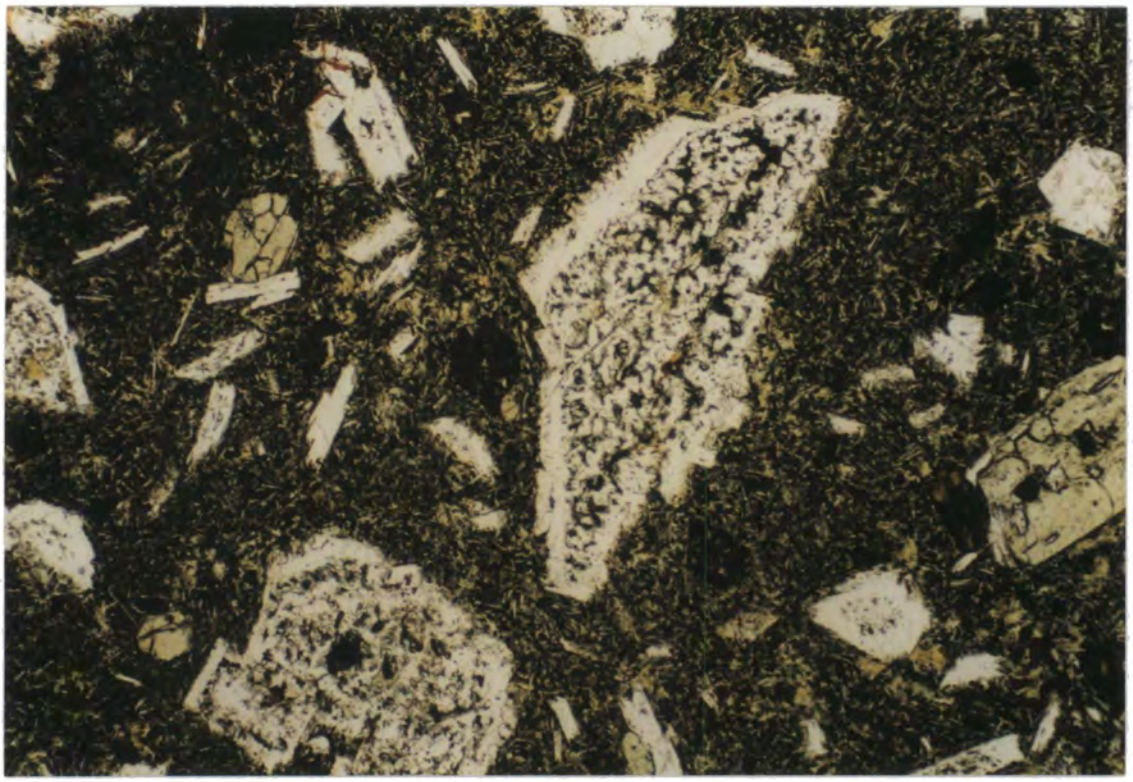

Plate 4.3. *A sieve-textured plagioclase shows extensive internal melting followed by overgrowth of equilibrium rim. 3x1.9mm, PPL*

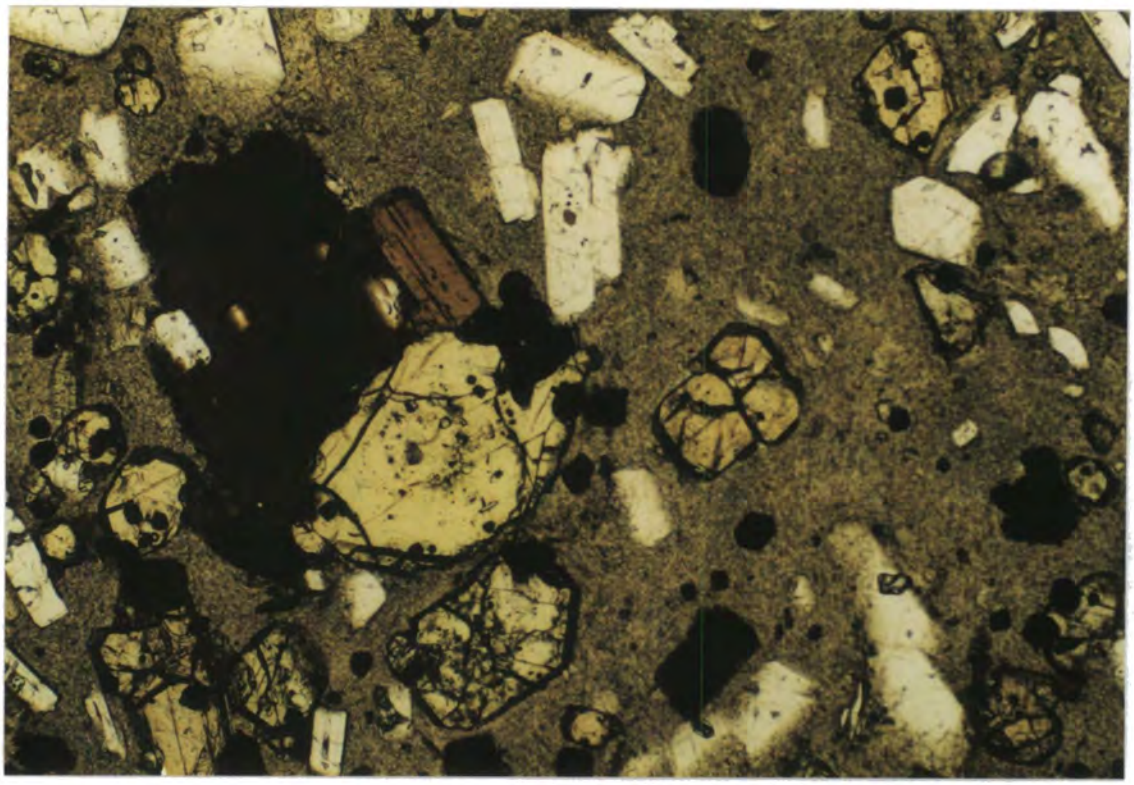

Plate 4.4. *A trachyandesite containing euhedral orthopyroxene with plagioclase, clinopyroxene, magnetite and biotite phenocrysts set in a glassy matrix. 3x1.9mm, PPL*

Olivine is rare and present as a phenocryst phase only in the least siliceous (57-62 % SiO_2) andesites-trachyandesites. It generally occurs as subhedral crystals 0.1-0.5mm across and as larger (up to 1mm), equant crystals with euhedral outline. Most crystals have been altered along crystal margins to form serpentine.

Amphibole is characteristically absent in the lavas of this suite and it is found as phenocryst in only one lava Unit (the Bademli Unit). It mostly forms euhedral and subhedral crystals ranging from 0.05-0.5mm in size. Almost all phenocrysts are surrounded by opaque rim that may indicate that they were not in equilibrium with the host liquid (Plate 4.5). Some are completely altered to form opaque granules. They are, however, still recognisable by the euhedral shapes of their basal sections (amphibole pseudomorphs) (Plate 4.6).

Alkali feldspar is present as phenocrysts in some andesites and dacite lavas. The phenocrysts are generally large (up to 4mm) and represented by sanidine. Alkali feldspar is, however, more abundant in the groundmass of most of the rocks in this group. **Magnetite**, with or without ilmenite, is present as phenocrysts and in the groundmass in most rocks. In most cases, magnetite is present as inclusions in pyroxene phenocrysts. Trace amounts of **sphene** are also found in some rocks.

Groundmass is generally glassy and may include plagioclase microlites. In some cases, alkali feldspar, clinopyroxene and magnetite microcrysts accompany plagioclase laths. The crystallinity (the ratio of total microlites to glass) of the groundmasses is highly variable ranging from <5% to 60%. Texturally, the groundmasses vary between intersertal and intergranular depending on the degree of crystallinity. Some samples also show trachytic textures (pilotaxitic or hyalopilitic) characterised by a subparallel arrangement of plagioclase microlites. In addition to the main textural types, most of the andesite and some dacite samples are glomeroporphyritic as they contain up to 5% coarse-grained polycrystalline aggregates, or crystal-clots (Plate 4.7). The aggregates are generally 2 to 4mm across but may be up to 6mm. Most commonly, the aggregates consist of euhedral plagioclase and magnetite complexly intergrown with euhedral or subhedral clinopyroxene and orthopyroxene. Some samples also include olivine glomerocrysts with plagioclase and clinopyroxene. Plagioclase glomerocrysts are often more calcic than the average composition of isolated plagioclase phenocrysts. They range from An_{48-67}.

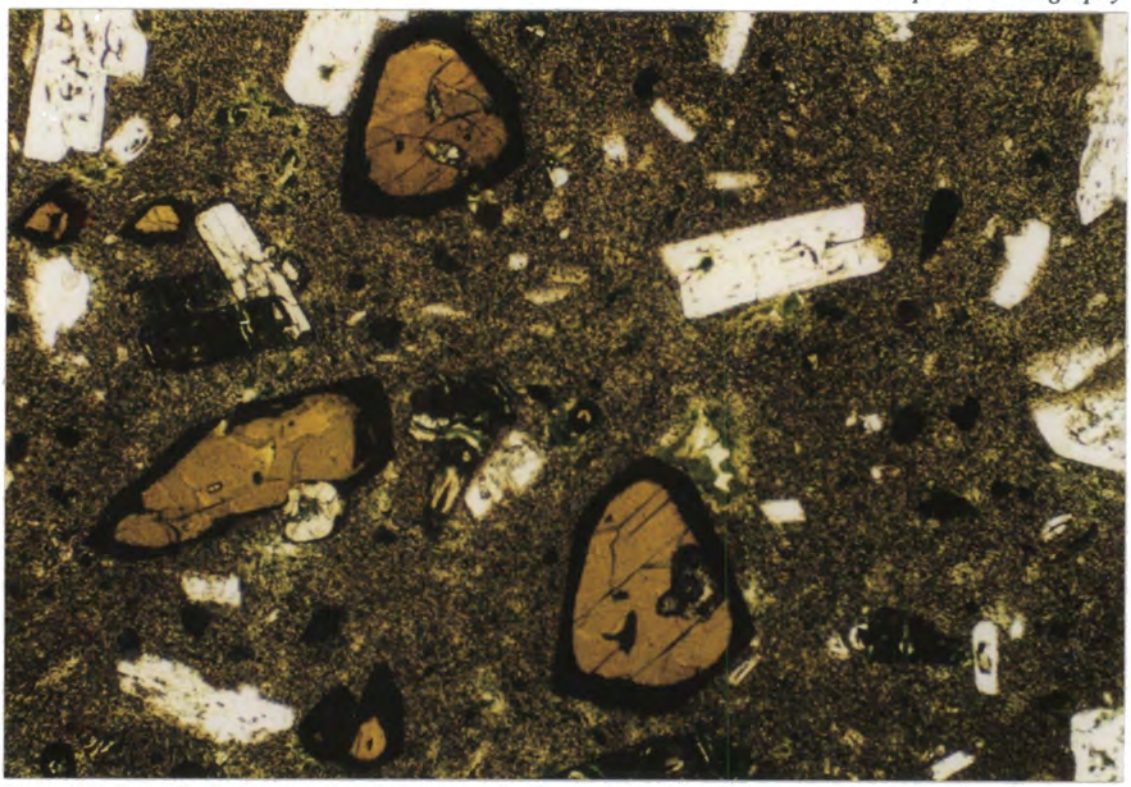

Plate 4.5. *Amphibole phenocrysts are surrounded by opaque rims. This may suggest that the phenocrysts are not in equilibrium with the host liquid. 3x1.9, PPL*

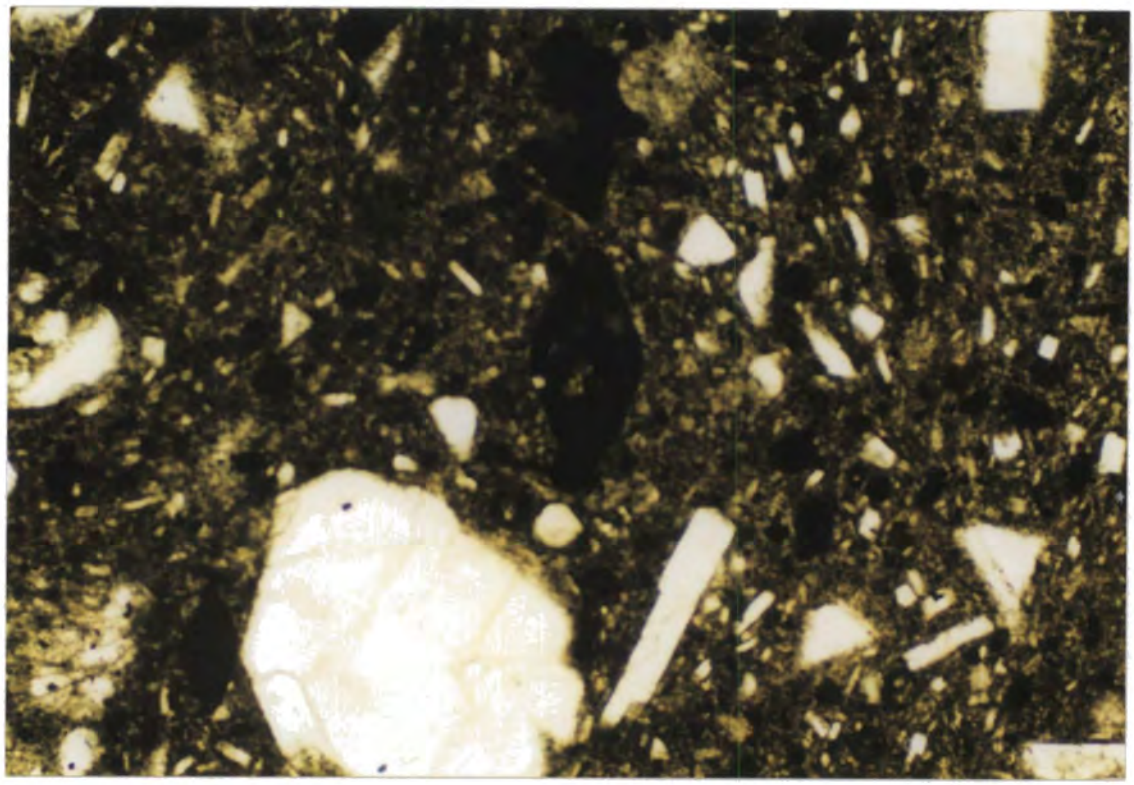

Plate 4.6. *Amphibole pseudomorphs are represented by opaque granules in an altered trachyandesite. 3x1.9, PPL*

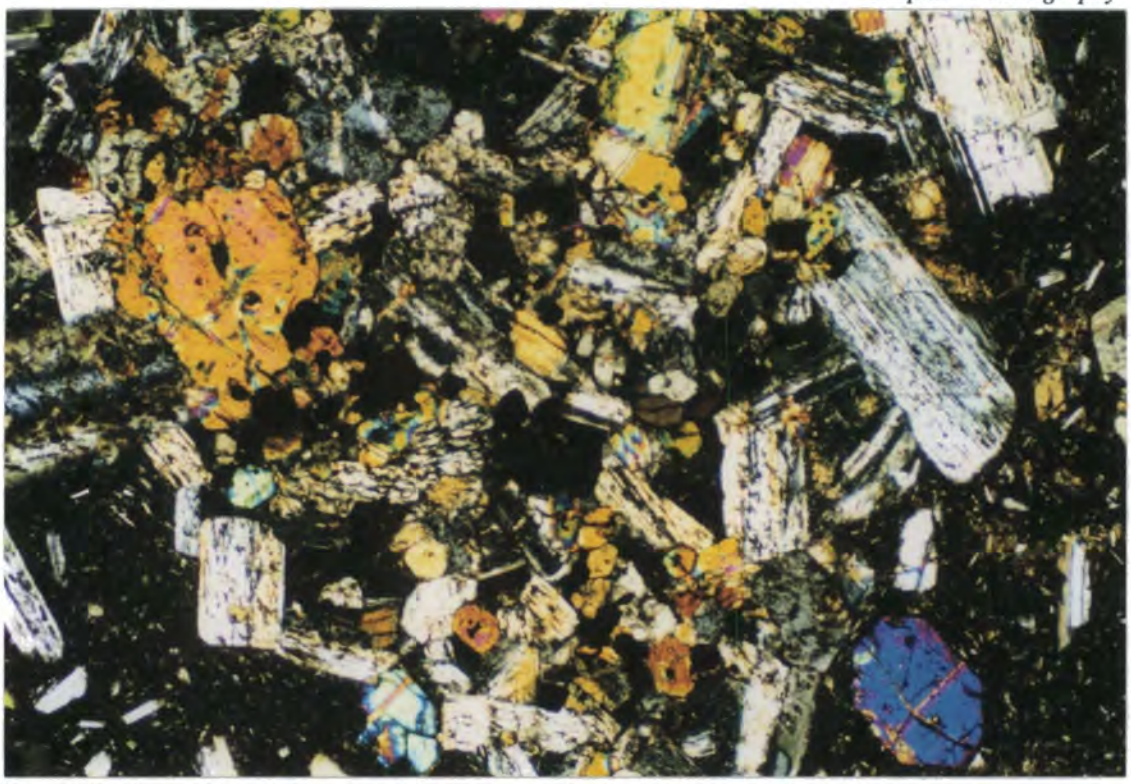

Plate 4.7. *A trachyandesite containing glomerophyric aggregates of plagioclase, orthopyroxene, clinopyroxene and magnetite. 6x3.7mm, Crossed Polars (XP)*

4.1.2. Pyroclastic Rocks (Ignimbrites) (Early Miocene)

Crystal-rich, lava-like ignimbrites contain phenocrysts and microphenocrysts of plagioclase, biotite, K-feldspar, quartz, clinopyroxene, orthopyroxene and magnetite. These are set in a red-brown glass (Plate 4.8). Plagioclase phenocrysts exhibit complex zoning and are represented mainly by oligoclase and andesine with core and rim compositions of An_{28-40} and An_{23-37} respectively. Biotite is the second most abundant phenocryst forming prismatic, subhedral crystals ranging from 0.05 to 2mm in size. Most contain trace amounts of zircon and magnetite inclusions. K-feldspar is represented mainly by sanidine. It mostly forms small crystals (<0.5mm) and has compositions of Ab_{47-29} Or_{48-68} An_{5-3}. Clinopyroxene is present as phenocrysts and microphenocrysts and represented by augite. Hypersthene and quartz also accompany the other mineral assemblages in the phenocryst phase. Olivine and amphibole are absent in the crystal-rich ignimbrites. Glass compositions are generally rhyolitic (72-74% SiO_2).

Small (mm- to cm-sized) lithic fragments comprising varying proportions of plagioclase, clinopyroxene, orthopyroxene, olivine and magnetite occur in most samples (Plate 4.9). They are predominantly medium- to fine-grained andesites, and rarely basaltic andesites. Most samples are largely oxidised. The mineral assemblages of the

volcanic fragments in the pyroclastic rocks are similar to those of the intermediate lavas in the area.

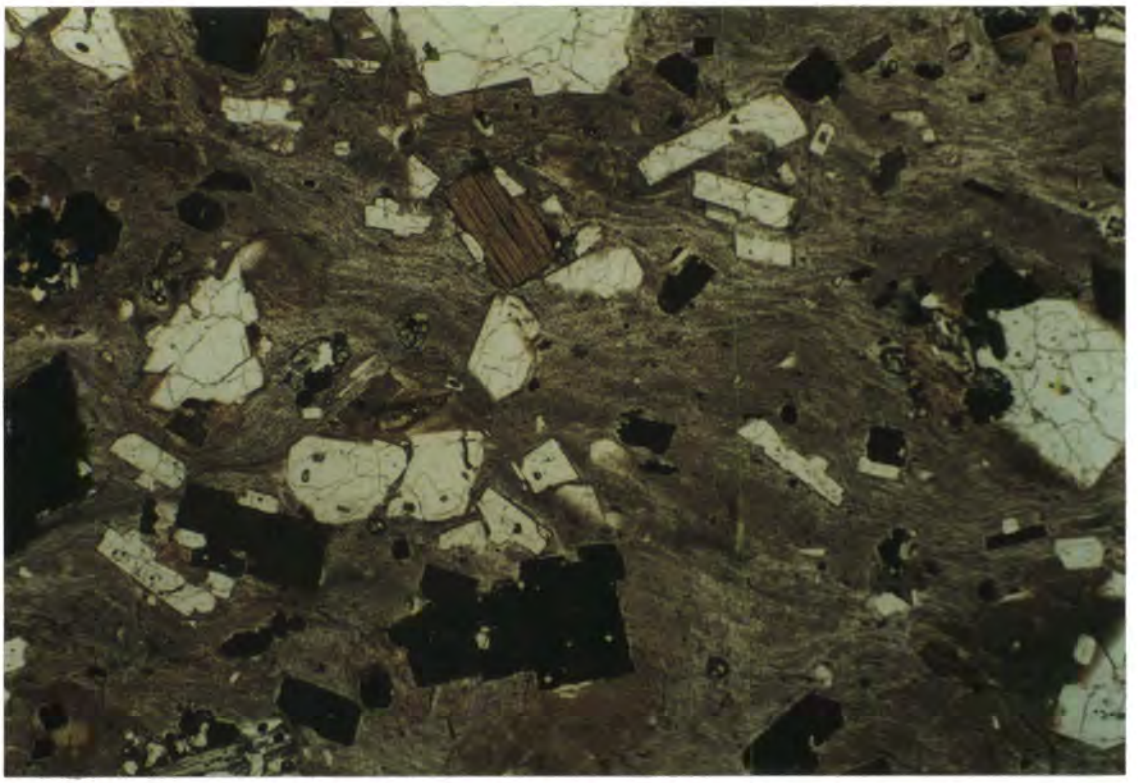

Plate 4.8. *A crystal-rich ignimbrite containing phenocrysts of plagioclase, biotite, sanidine, magnetite and minor clinopyroxene set in a eutaxitic-textured glassy groundmass. 3x1.9mm, PPL*

Pumice fragments and glass shards are found in most ignimbrites. They are generally flattened (Plate 4.10) and some are homogenised by extreme welding (Plate 4.11). Most ignimbrites exhibit layering which is due to alternating poikilomosaic layers (Shelley, 1993) and felcitic layers. The poikilomosaic layers comprise altered pumiceous material that often exhibits a whispy structure interpreted to be collapsed or sheared-out vesicles from extremely attenuated fiamme. Individual layers generally show considerable variation in thickness along their length in response to deformation around rigid lithic fragments and phenocrysts. The layers usually exhibit elongate or lens-shaped snowflake texture subparallel to the fiamme. Felsitic layers are lighter in colour than the poikilomosaic layers and were originally fragmental ash layers while the poikilomosaic layers are interpreted as intact pumiceous pyroclasts.

In the welded ignimbrites, devitrification processes during cooling of the tuff layers led to the formation of different crystallisation zones such as the vapour phase zone, pervasively devitrified phase zone, spherulite zone and lithophysae zone. These crystallisation phases generally occur successively throughout the welded zones of the

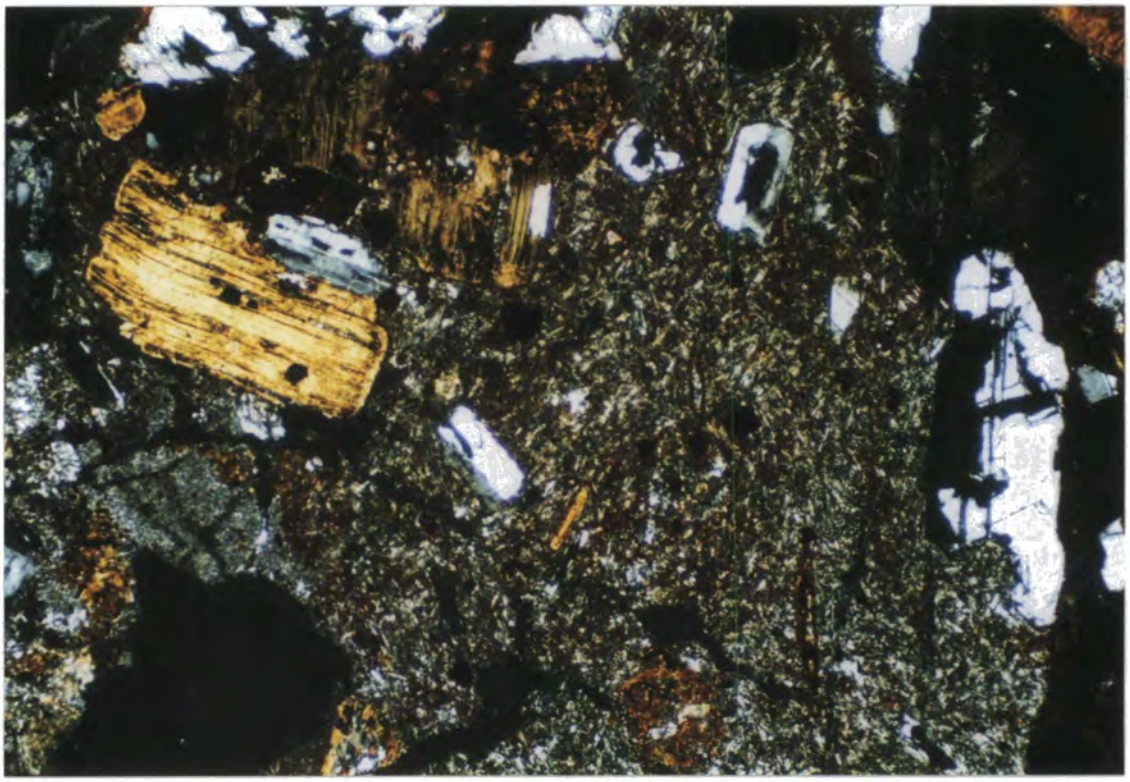

Plate 4.9. *A large volcanic fragment set in a glassy ignimbrite. The fragment is andesitic in composition and partly oxidised. 3x1.9mm, PPL*

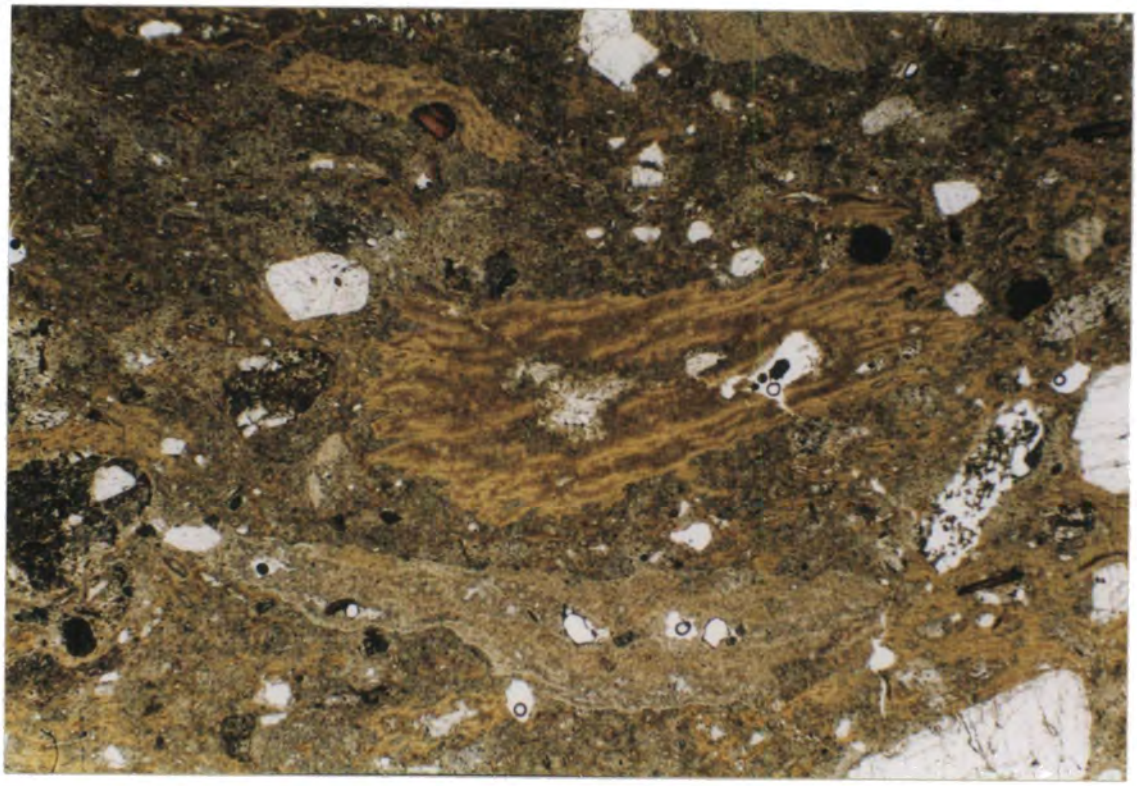

Plate 4.10. *A partially welded glassy rhyolite tuff containing flattened pumice fragments and crystals of plagioclase, alkali feldspar and quartz embedded in a glassy groundmass. 3x1.9mm, PPL*

ignimbrite sequences, and transitions between the phases are mainly gradational.

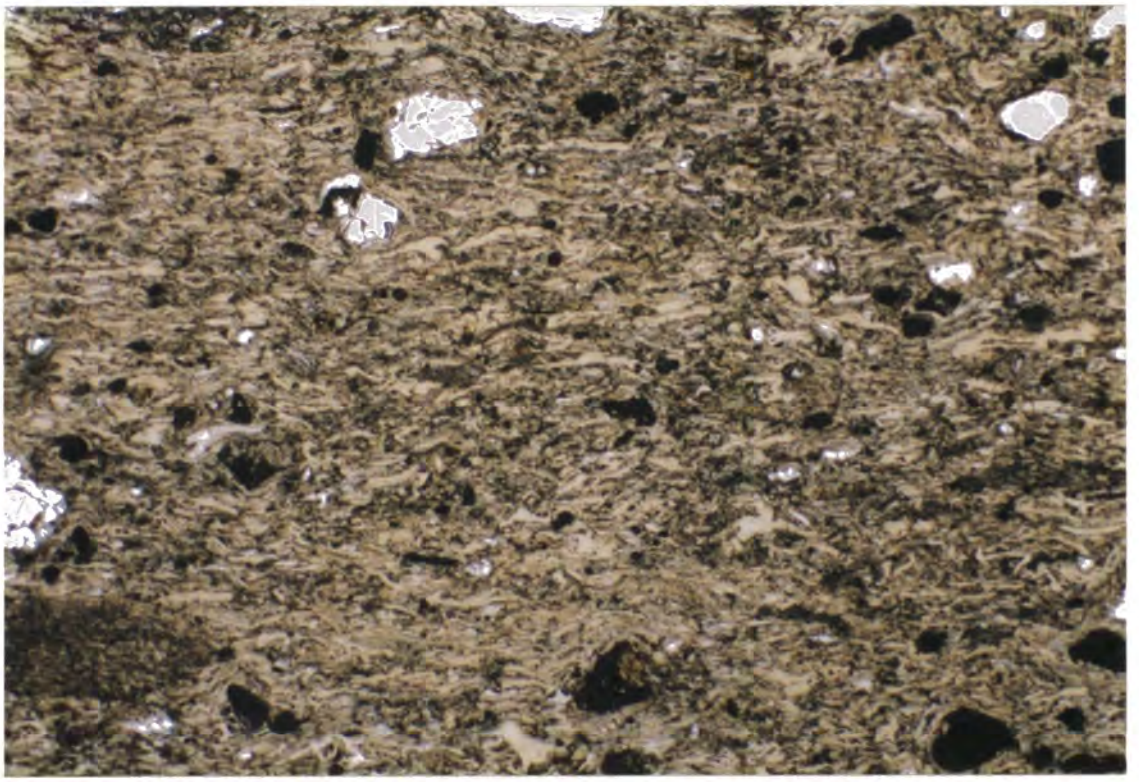

Plate 4.11. *A welded crystal tuff containing abundant glass shards that are flattened and partially homogenized. 3x1.9mm, PPL*

The vapour phase zone, which may be described as a sillar zone, is developed in most of the welded and partially welded ignimbrites. These zones comprise mainly porous devitrified tuff with mineral precipitation from vapour crystallisation. The sizes of these minerals range from cryptocrystalline to microcrystalline. In the cryptocrystalline vapour phase zones, most glassy material crystallised, but the vitroclastic texture is partly preserved. In many cases, devitrification crystals are not recognisable in hand specimens. The very fine-grained, axiolitic structure of shards is revealed under the microscope. The silica phase is mostly cristobalite. In the microcrystalline subzones, the axiolitic structures are, however, coarser grained with crystal sizes ranging between 0.05 and 1mm; the largest crystals occur along vesicle walls (Plate 4.12). The silica phase in the microcrystalline subzones is mostly tridymite with minor cristobalite.

Pervasively devitrified zones are mostly developed in tuffs that are densely welded with fiammés. They are generally characterised by good retention of flattened glass shard structures in thin section. The sizes of devitrification crystals are similar to

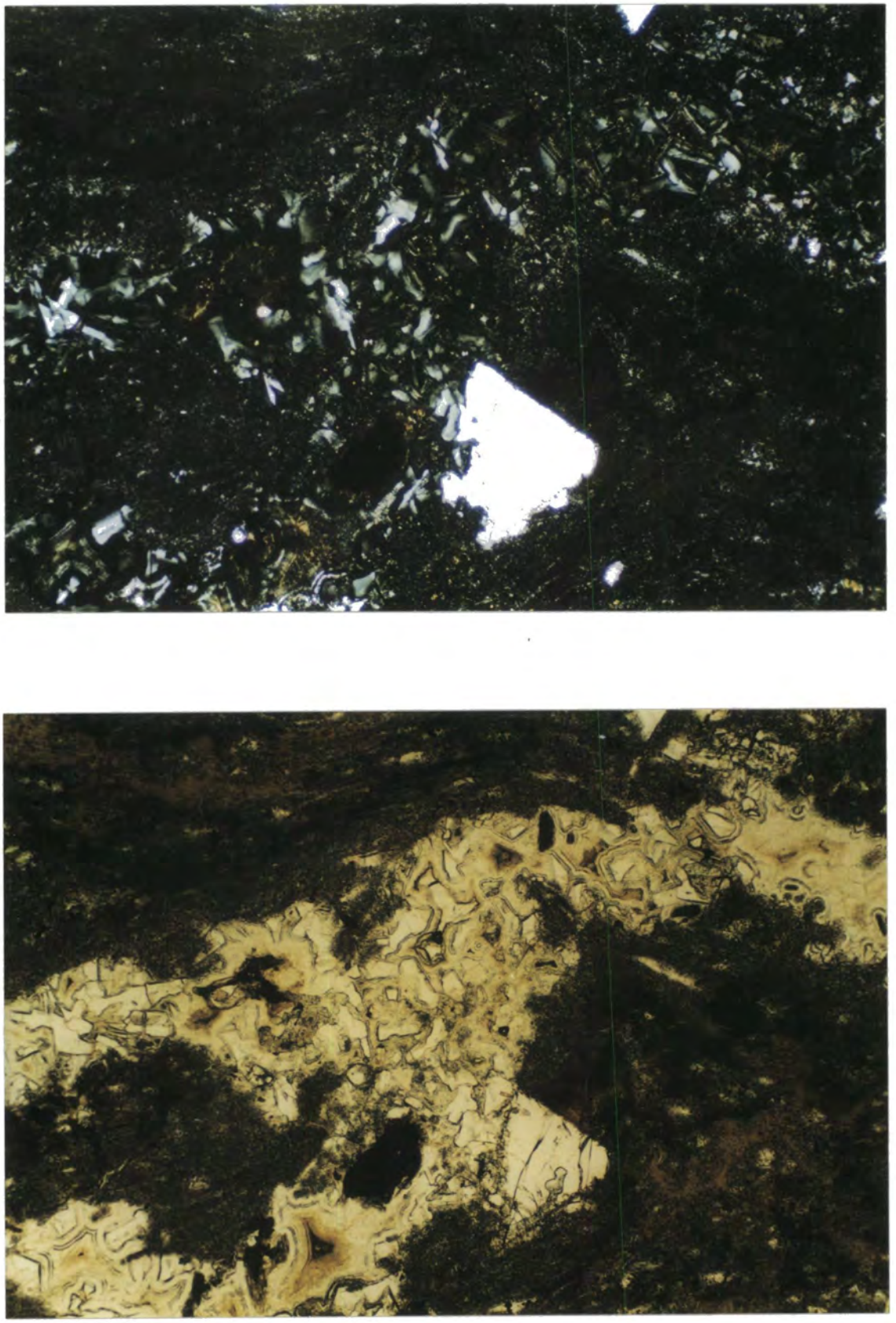

Plate 4.12. *Microcrystalline vapour phase crystallisation products of tridymite and cristobalite formed along the vesicle walls. 1.3x0.77mm, XP and PPL*

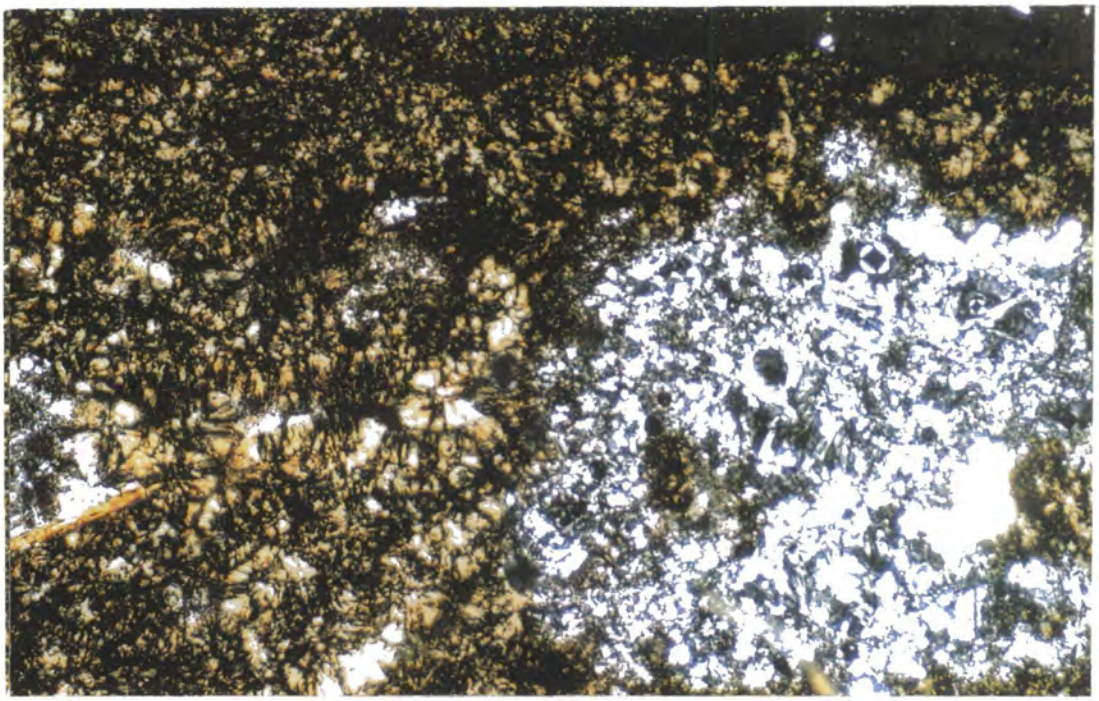

Plate 4.13. *Radiate-fibrous divitrification spherulites set in a devitrified glassy ignimbrite. 3x1.9mm, PPL*

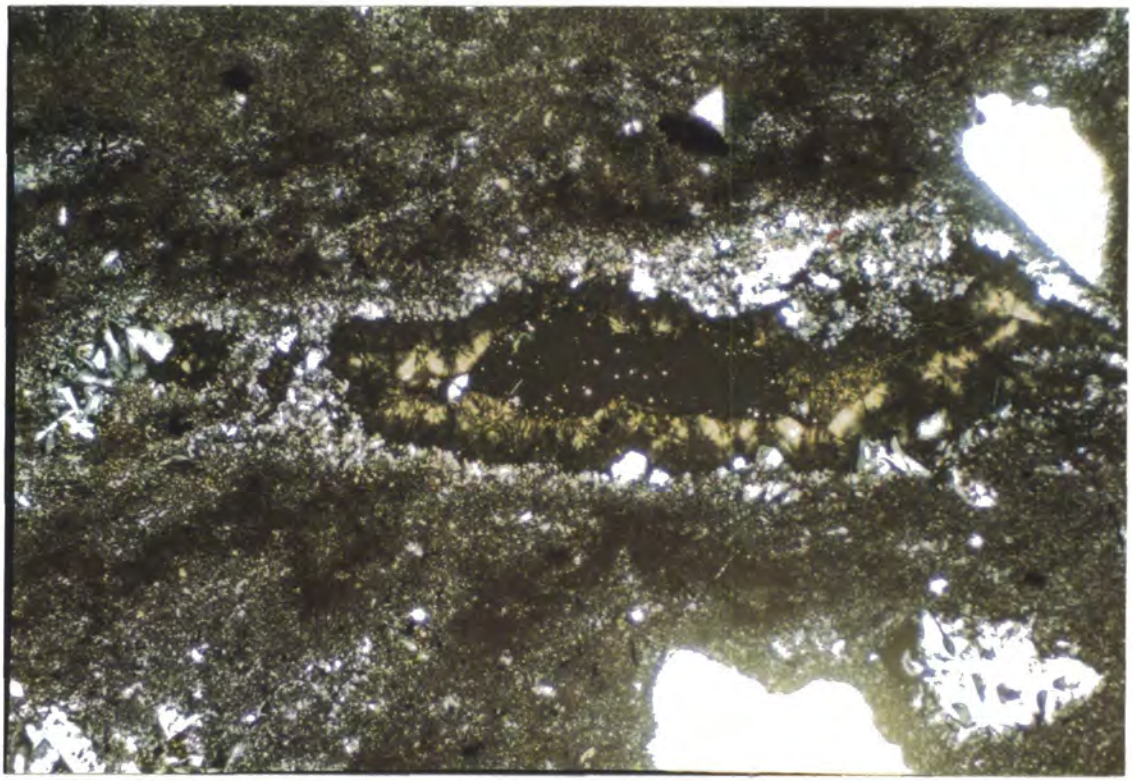

Plate 4.14. *Silica phase crystallisation products and spherulites formed in the gas cavities of a devitrified ignimbrite. 3x1.9mm, XP*

Plate 4.14. *Continued (PPL)*

those of the microcrystalline vapour phase. The spherulite zone develops almost exclusively in most of strongly welded vitric tuff layers. Spherulites range from 0.3 to 1mm (Plate 4.13). Glass shards and lenticular fiammes are not visible in the spherulite zones, suggesting that most were totally homogenised by welding. The lithophysae are developed in the devitrified matrix as spherical shapes (Plate 4.14). They may range from solid to completely hollow with a crystallisation rind lining the walls. The silica phase is mainly tridymite and cristobalite. The generation of hollow lithophaysae may be related to the release of volatiles as suggested by Ross and Smith (1980).

4.1.3 Weakly to Moderately Porphyritic Dyke Swarms (Early Miocene)

The rocks in this suite are of silica saturated, hypersthene-normative andesites and trachyandesites. The crystallinities of the rocks vary considerably from <10% to about 45%. Phenocrysts are mainly plagioclase, orthopyroxene and clinopyroxene with subordinate olivine and magnetite. Hydrous minerals (amphibole and biotite) are absent in these rocks.

In most of the rocks, **plagioclase** accounts for approximately 40-45% of the total phenocrysts. It usually forms prismatic crystals with grain sizes range between 0.2 and 3mm. Lamellar twinning is common and most of the phenocrysts exhibit complex

zoning (normal and/or reverse zoning): core and rim compositions are An_{54-62} and An_{48-66} respectively. Most phenocrysts have been resorbed along their crystal margins. Some crystal centres have also been resorbed to form sieve texture (Plate 4.15). Resorption characteristics may be attributed either to thermal disequilibrium and mixing of magmas with different compositions (Cox et al., 1979) or to rapid, isothermal decompression accompanied by magma mixing processes in magma chambers (Nelson and Montana, 1992). Despite the fairly high K_2O whole rock contents, there are no alkali feldspar phenocrysts.

Orthopyroxene is an abundant phenocryst (~ 20-25% of total phenocrysts) and is represented mainly by bronzite and hypersthene. It is typically homogenous, but rare zoned examples show a core to rim variation of Wo_{3-2} En_{75-69} Fs_{22-27} and Wo_{3-4} En_{69-67} Fs_{27-29} which span the entire range of orthopyroxene variation. Most of the orthopyroxene phenocrysts range between 0.02 and 0.5mm in size, although some may reach up to 1mm. They are mostly euhedral and subhedral and occur either as individual phenocrysts or, occasionally, in glomerocrysts and radiating crystals with clinopyroxene and/or plagioclase. Most have body colours of pale-pink or pale green and are slightly pleochroic under the microscope. Small apatite needles and opaque magnetite crystals are common inclusions in most of the orthopyroxene phenocrysts.

The relative abundance of **clinopyroxene** is about 20-25% of phenocrysts. The sizes of the crystals are variable ranging between 0.01 and 0.1mm. They mostly form oscillatory-zoned crystals, but no systematic compositional variation has been observed between the zones. The phenocrysts are generally augite and diopsite in composition. Observed core and rim compositions are Wo_{42-38} En_{46-44} Fs_{12-18} and Wo_{40-41} En_{51-44} Fs_{8-16} respectively. Some samples show abundant evidence of disequilibrium crystallisation, with coexisting skeletal, resorbed large phenocrysts and smaller euhedral crystals. Some clinopyroxenes also have alteration rims suggesting that a reaction has taken place with the host matrix.

Olivine is rare or absent in this suite and, when present, does not exceed 2% of the total phenocrysts. It generally forms small, euhedral-subhedral crystals which are mostly altered to serpentine and iddingsite (Plate 4.15). In addition to the phenocrysts described above, minor amounts of **magnetite**, **ilmenite** and **apatite** are also present in the phenocryst phase of the rocks of this suite. They form small euhedral crystals with grain sizes ranging from 0.02 to 0.3mm. Some are present as inclusions in the other

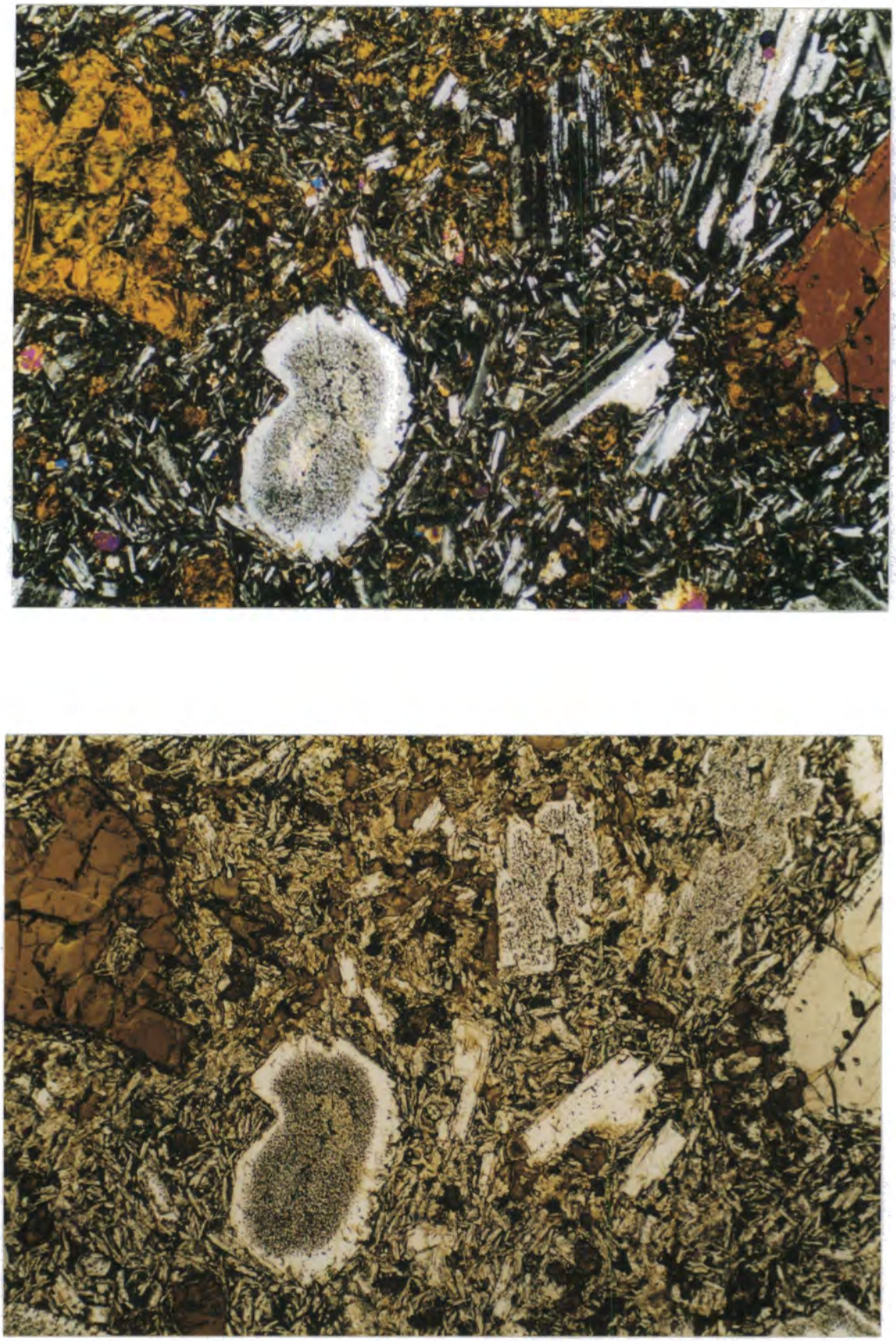

Plate 4.15. *Resorbed plagioclase and altered olivine phenocrysts set in a microcrystalline groundmass. Olivines are altered to iddingsite. 3x1.9mm, XP and PPL*

phenocrysts.

The **groundmasses** are generally fine-to medium-grained and consist mainly of microcrystalline plagioclase laths and, more rarely, anhedral clinopyroxene and magnetite set in a brown glass. The abundance of crystallinity of the groundmass ranges between 30 and 60%. Groundmass plagioclase compositions are rather similar to those of phenocrysts, ranging between labradorite and bytownite (An_{57-65}). The groundmass is usually intersertal and intergranular. Some rocks also have a hyalophitic groundmass with abundant fresh, brown glass.

4.1.4 Aphyric to Weakly Porphyritic Mafic Alkaline Lavas (Late Miocene)

The Tastepe, Ezine and Ayvacik Volcanics are alkali basalts and basanites, ranging from strongly alkaline, silica undersaturated, nepheline-normative to mildly alkaline, silica saturated hypersthene-normative rock types, with corresponding mineralogy. They consist mainly of olivine, clinopyroxene and plagioclase phenocrysts in a microcrystalline to glassy groundmass. Phenocryst contents are variable, generally ranging from <3% (aphyric) to 20% (weakly porphyritic), although the majority of the rocks are aphyric. The degree of crystallinity decreases gradually in time from the Tastepe volcanics towards the Ayvacik volcanics.

In the weakly porphyritic rocks, **clinopyroxene** generally forms subhedral phenocrysts with grain sizes from 0.1 to 1.5mm (mostly <0.5mm). They are mostly fresh and display simple twinning and strain banding in some cases. They are all either diopside or augite with core and rim compositions of Wo_{47-43} En_{44-46} Fs_{9-11} and Wo_{50-45} En_{40-44} Fs_{10-13} respectively. In some samples, clinopyroxene phenocrysts display glomerophyric textures, forming spherulite shapes with clustered pyroxene crystals radiating outwards from an early formed olivine crystal (Plate 4.16). In some samples from the Ayvacik Volcanics, clinopyroxene microphenocrysts are intergrown with **nepheline**.

The **olivine** phenocrysts are commonly subhedral and range from 0.1 to 1mm in size. Their abundances range between 40 and 70% of total phenocrysts. They are mostly fresh but are sometimes altered to serpentine, chlorite and reddish-brown iddingsite minerals along cracks and around the crystal margins (Plate 4.16). Some crystals display skeletal (quench texture) forms indicating rapid cooling. No significant compositional

zoning has been observed in the olivine phenocrysts; core and rim compositions are Fo_{75-86} and Fo_{71-83} respectively.

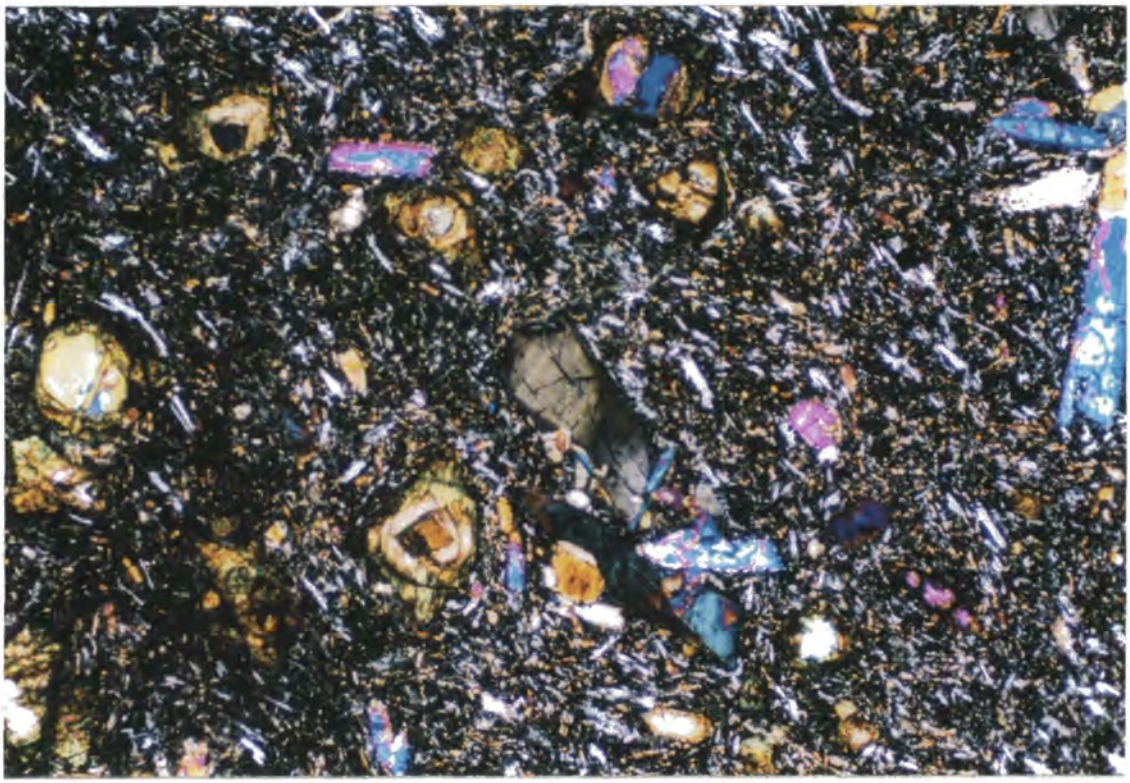

Plate 4.16. *Alkali olivine basalt, containing small altered olivine and zoned clinopyroxene phenocrysts. Pyroxenes form spherulite shape glomerocrysts. 3x1.9mm, XP*

Plagioclase occurs as a phenocryst phase in only the least basic rocks of the Tastepe Volcanics. Average plagioclase phenocryst content has been accounted <5%. It, when presents, generally forms prismatic, tabular crystals with grain sizes ranging between 0.2 and 0.5mm. Lamellar twinning is typical for most of the phenocrysts and none of the plagioclases show compositional zoning. Their compositions range between labradorite and bytownite (An_{68-95}).

Ilmenite and magnetite are common phases in the groundmass and as microphenocrysts. In most samples, ilmenite is more abundant than magnetite. Typically, oxide phases form euhedral and subhedral microcrysts that range in size from ~0.3 to 0.05mm. Modal proportions of the oxides range from about 5 to 15% by volume of phenocrysts.

The **groundmass** in the rocks consists of: plagioclase microlites of mainly andesine – labradorite and rarely bytownite; clinopyroxene as subhedral and, more

Plate 4.17. *Alkali olivine basalt characterised by intergranular groundmass texture with abundant plagioclase microlites and interstitial clinopyroxenes. 3x1.9mm, XP*

Plate 4.18. *Felty textured aphyric alkaline basalt. Plagioclase microlites characteristically show parallel alignment. 3x1.9mm, XP*

Plate 4.19. *Olivine microphenocrysts set in an intergranular groundmass that consists of plagioclase laths and interstitial clinopyroxenes. 3x1.9mm, XP*

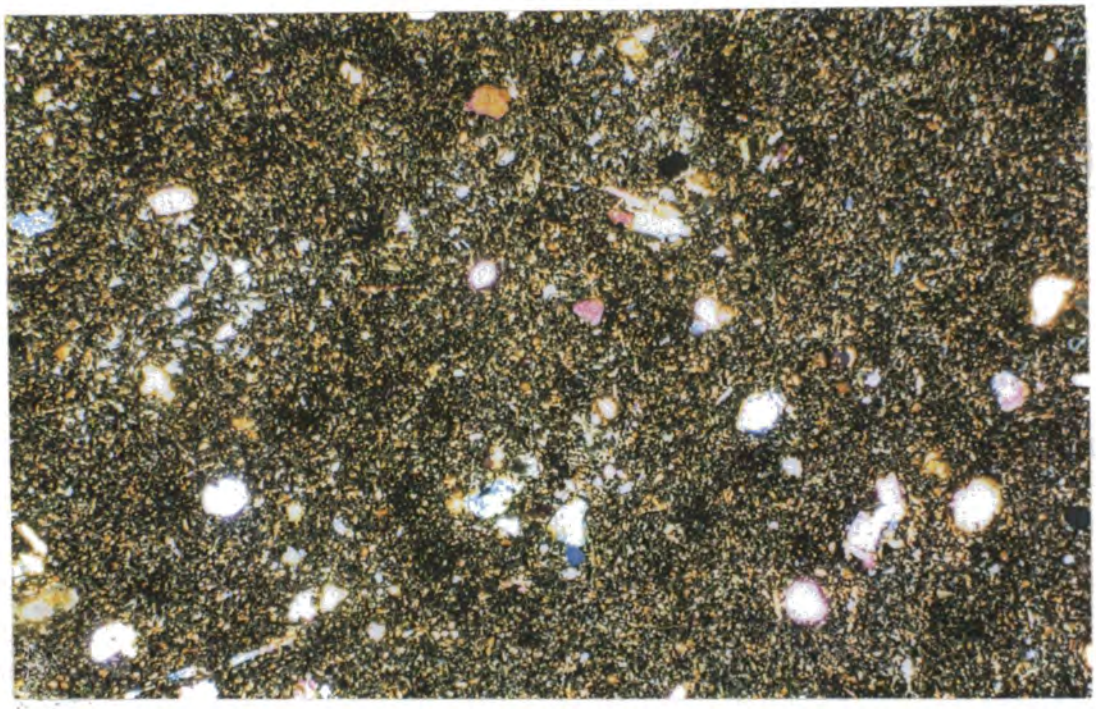

Plate 4.20. *A basanite with olivine microphenocrysts set in a very fine-grained groundmass. 3x1.9mm, XP*

Plate 4.21. *Prismatic crystals of clinopyroxene set in a fine-grained groundmass. 1.3x0.77mm, XP*

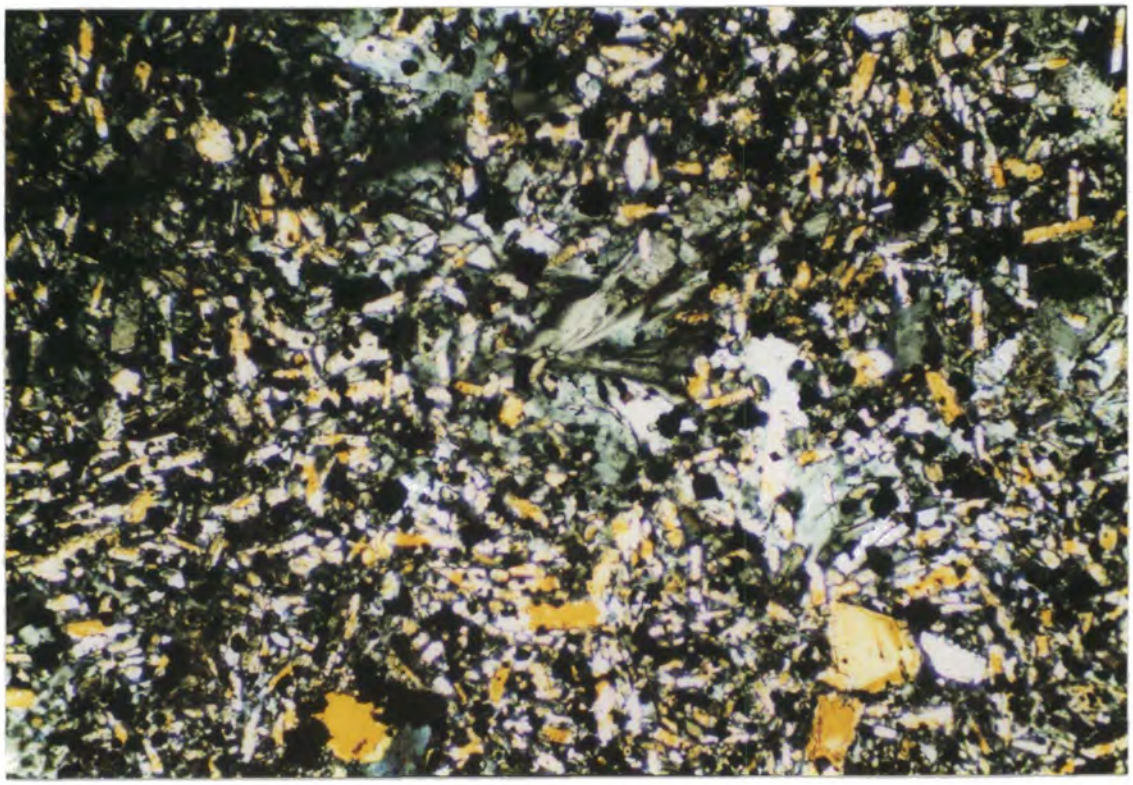

Plate 4.22. *Curved quench crystals of plagioclase aggregates in a basanite sample. 1.3x0.77mm, XP*

commonly, anhedral yellow/brown grains or laths of augite and diopside; abundant subhedral/euhedral magnetite and needles of ilmenite; glass and alteration products of mostly calcite and chlorite. Small subhedral to anhedral olivine crystals also occur in the groundmass. The size of the grains varies from microcrystalline (~0.3mm) to cryptocrystalline. The groundmass textures show a considerable variation; most are intersertal and intergranular, characterised by glassy material or pyroxene microcrysts filling spaces between plagioclase laths (Plate 4.17), and an ophitic/subophitic texture with plagioclase laths embedded in clinopyroxene crystals. Pilotaxitic and felty textures are also seen in some aphyric samples characterised by randomly-aligned plagioclase microlites. (Plate 4.18). Most of the rocks from the Ayvacik volcanics are characterised by their very fine-grained, black, partly glassy matrix (Plate 4.19, 20). Some also exhibit quench textures with skeletal, swallowtail and parallel-elongated olivine, small prismatic crystals of clinopyroxene with hollow terminations, and sheaf-like, curved, acicular quench crystals of plagioclase in a fine-grained groundmass (Plate 4. 21, 22).

4.2 Volcanic rocks from the Dikili-Ayvalik-Bergama (DAB) area

4.2.1 Highly Porphyritic, Acid-intermediate Lavas (Early Miocene)

The Early Miocene, porphyritic lavas of the Dikili-Ayvalik-Bergama area are represented by hypersthene- or quartz normative andesites and dacites. The rocks are generally highly porphyritic with modal abundances of total phenocrysts varying between 15 and 65% by volume. The most abundant phenocrysts are plagioclase, amphibole, clinopyroxene, biotite, alkali feldspar and magnetite. Subordinate quartz and olivine also occur in the least siliceous and the most siliceous rock types respectively, whereas orthopyroxene is rare or absent.

Plagioclase occurs in all lavas and makes up 35 to 60% by volume of phenocrysts. The sizes of crystals vary from microcrystalline (<0.05) to large macrophenocrysts (up to 5mm). They characteristically exhibit oscillatory-normal and oscillatory-reverse zoning (Plate 4.23). In general, there is a similarity between the zoning in the mantles of large phenocrysts and the complete zoning patterns of the smaller, euhedral phenocrysts. Core and rim compositions are An_{33-74} and An_{31-57} respectively. Some andesites contain plagioclase grains that are coarsely embayed or finely sieved. They display sieve-textured cores (penetrative resorption features in core). Resorption surfaces exhibit variable morphologies, from smooth to irregular. Cores of

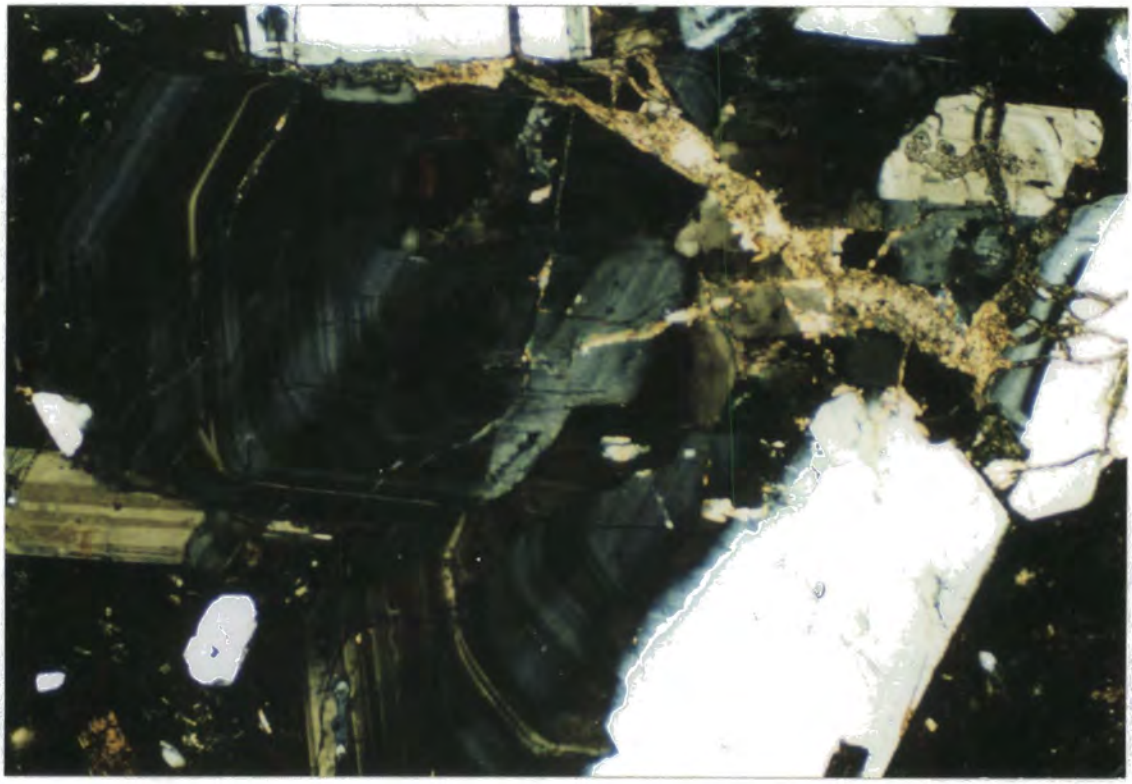

Plate 4.23. *Large oscillatory zoned plagioclase in an andesite sample. 3x1.9, XP*

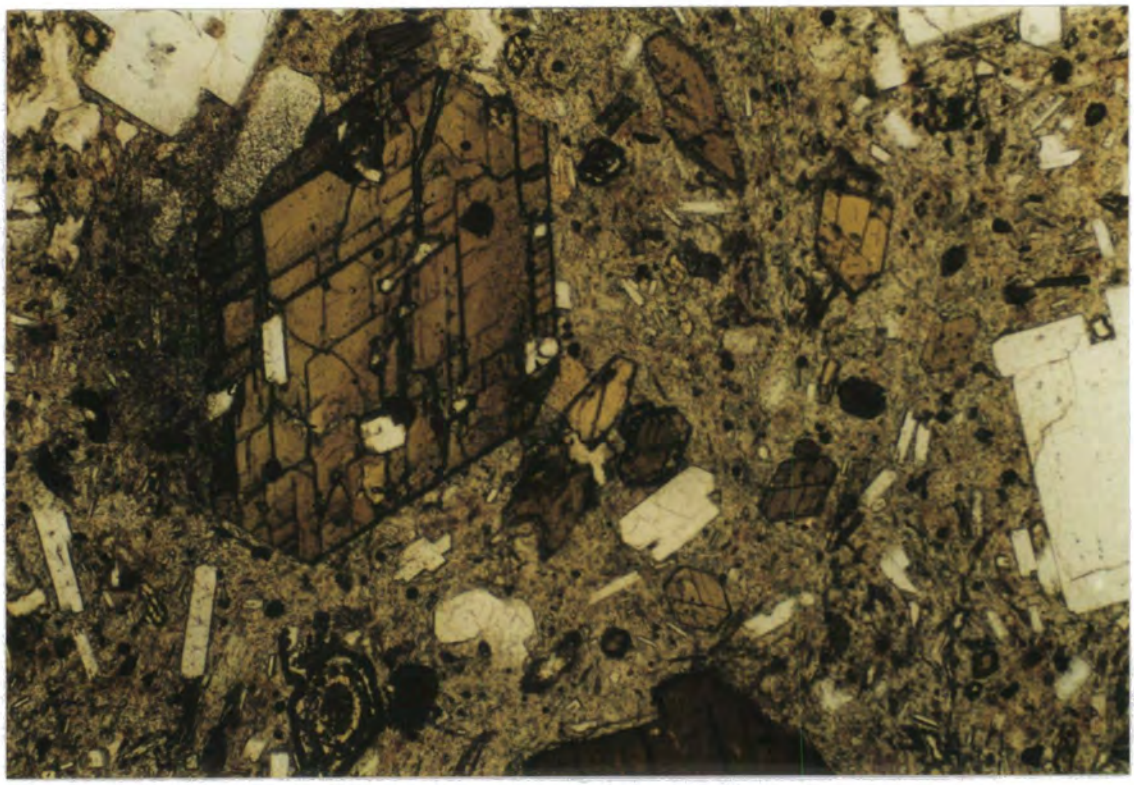

Plate 4.24. *Euhedral amphibole phenocrysts set in a mostly glassy groundmass. 3x1.9mm, PPL*

these grains may be either similar to or more calcic than unsieved grains. The textural and zoning characteristics may result from magma mixing, as discussed by Dungan and Rhodes (1978) and Tsuchiyama (1985) or, from rapid adiabatic decompression during magma ascent as discussed by Nelson and Montana (1992).

Amphibole is the second most common phenocryst phase in most andesite and dacite samples. It mostly forms euhedral and subhedral individual crystals (Plate 4.24) as well as glomerocrysts with plagioclase, magnetite and more rarely clinopyroxene (Plate 4.25). The sizes of phenocrysts are generally between 0.02 and 2mm. They are mostly hornblende in composition. Some contain magnetite and small plagioclase laths as inclusions. In most of the samples, the hornblende phenocrysts are remarkably free of reaction rims indicating no oxidation or disequilibrium with the host liquid, although crystals surrounded by a fine-grained reaction rim of opacite are found in some samples.

Clinopyroxene occurs in most andesitic and some dacitic samples. It makes up between <5% and 15% by volume of total phenocrysts. The sizes of crystals are usually 0.05-0.5mm but some may reach up to 1mm in length. Most display oscillatory-normal or reverse zoning and cluster to form glomerocrysts with magnetite and plagioclase (Plate 4.26). They are generally augite and diopside with core and rim compositions of Wo_{40-43} En_{45-47} Fs_{15-10} and Wo_{42-46} En_{45-42} Fs_{13-12} respectively.

Biotite is primarily a subhedral-euhedral phenocryst phase in most andesites and dacites; exceptions include some less siliceous (57-60% SiO_2) andesite samples. Most of the phenocrysts contain apatite, zircon, magnetite and small plagioclase crystals as inclusions. **Alkali feldspar** joins the other phenocryst mineral assemblages in some lava Units. They are mostly subhedral crystals and represented mainly by sanidine and anorthoclase.

The groundmass is highly variable, ranging from glassy or cryptocrystalline to microcrystalline. The crystallinity of the groundmasses generally decreases with silica content of the rocks. Microcrystalline plagioclase laths are common in the groundmasses of most rocks and are accompanied by microcrysts of clinopyroxene, magnetite and rarely amphibole. Groundmass textures are rather similar to those of highly porphyritic lavas of the EGA area, varying between intersertal and intergranular. Trachytic textures are also found in some rocks.

4.2.2 Aphyric to Slightly Porphyritic Intermediate Lavas (Middle Miocene)

The Egrigöl andesites are characteristically very fine-grained (<0.15mm), fresh,

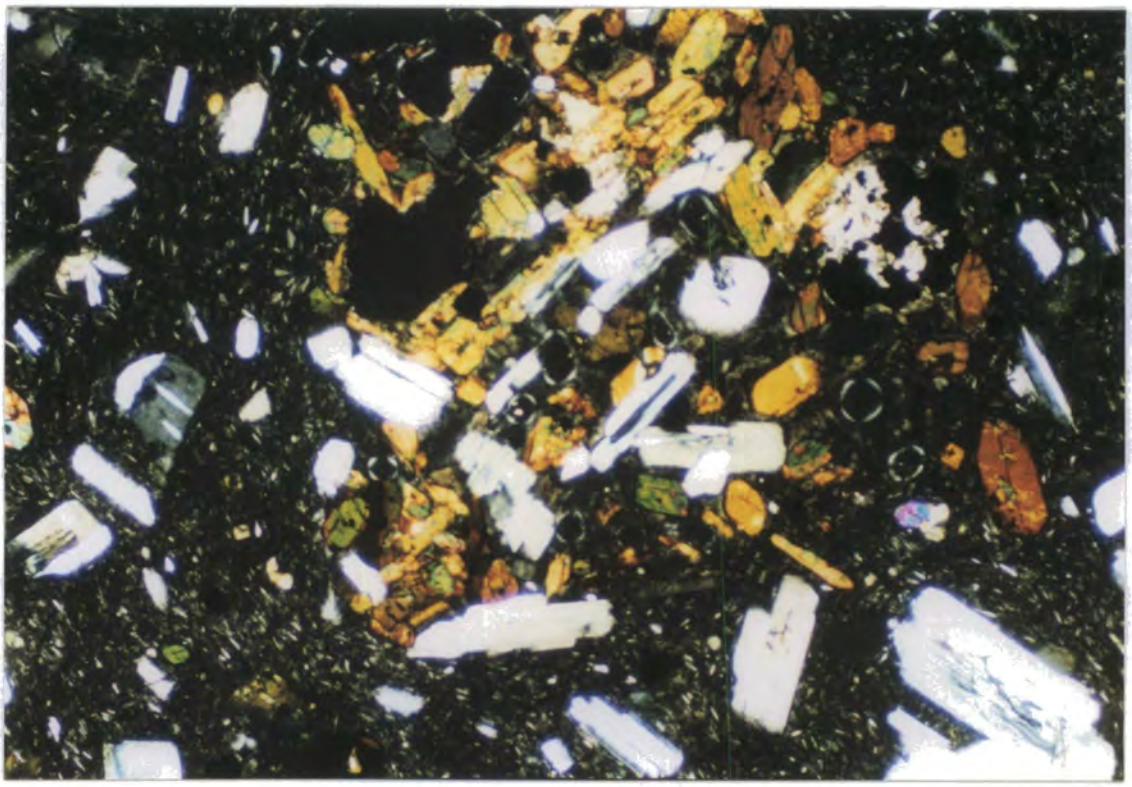

Plate 4.25. *Large glomerophyric aggregates of amphibole, magnetite and plagioclase. 3x1.9mm, XP*

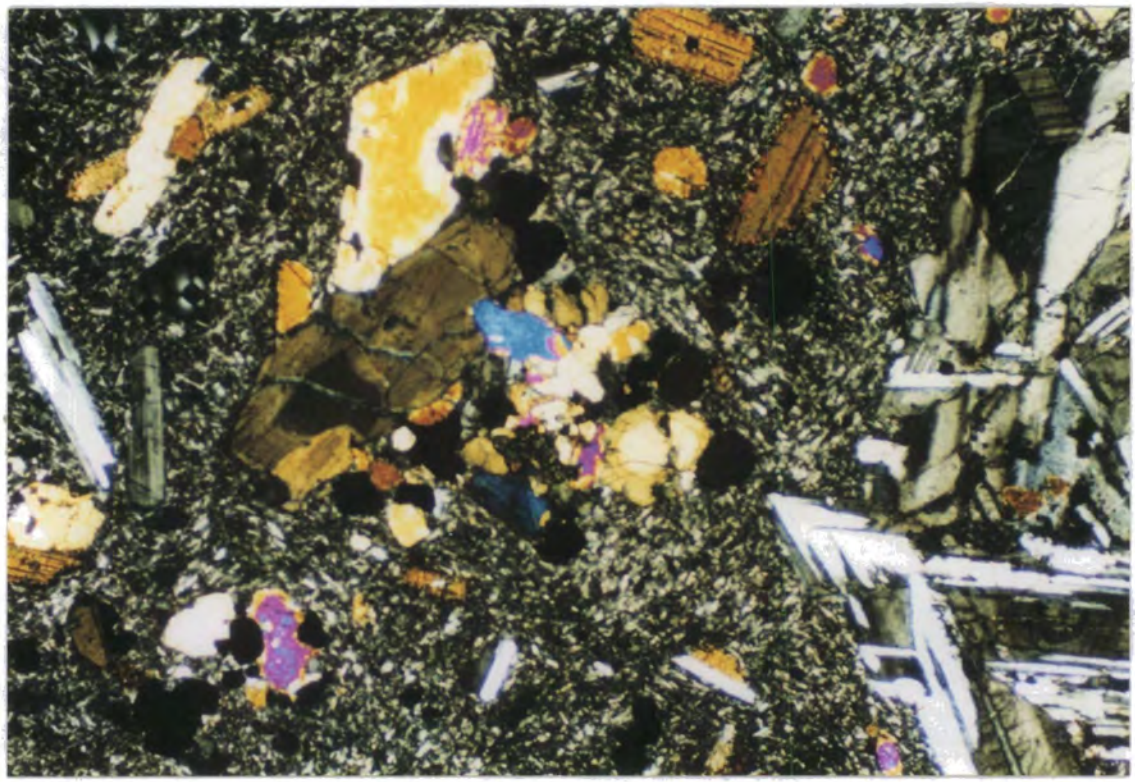

Plate 4.26. *Glomerocrysts of zoned pyroxene and plagioclase set in a microlitic groundmass. 3x1.9mm, XP.*

mostly aphyric rocks. Although some minor porphyritic rocks are found, their total phenocryst contents are always <10% by volume. In these weakly porphyritic andesites, **clinopyroxene** is the most abundant phenocryst, forming small (0.1-0.5mm), subhedral crystals. Most clinopyroxenes exhibit oscillatory zoning with a composition of Wo_{46-40} En_{46-51} Fs_{8-9}. Clinopyroxene is accompanied by relatively lesser amounts of plagioclase and olivine as phenocryst phases. **Plagioclase** forms predominantly small (<5mm) tabular crystals and displays normal zoning. They are all labradorite and bytownite with core and rim compositions of An_{63-75} and An_{64-77} respectively. **Olivine** phenocrysts (Fo_{73-86}) are also generally <0.5mm in diameter, euhedral or subhedral, partly altered to serpentine. Subordinate **orthopyroxene** is also present in the phenocryst phase of some, though not all, the slightly porphyritic samples. It is generally hypersthene in composition and forms euhedral-subhedral in shape.

The **groundmass** always contains a brown glass, invariably with minute colourless blebs that are taken to be a silicate melt. Plagioclase forms abundant small (fine-grained to cryptocrystalline) microlites in the groundmass. The plagioclase laths are often flow-aligned and are accompanied commonly by clinopyroxene to form trachytic and felty textures. Hyalopilitic examples are also present with glassy material between the plagioclase microlites.

4.2.3 Aphyric to Moderately Porphyritic Basaltic Lavas (Middle Miocene)

The Nebiler Volcanics are of silica-saturated, hypersthene normative, absarokites, shoshonites and banakites. They range widely from very fine-grained glassy rock types to very much coarser-grained, holocrystalline types. The vast majority of the rocks are moderately porphyritic with 10-30% of phenocrysts, although some completely aphyric samples are also present. The phenocrysts are mainly clinopyroxene, olivine, plagioclase and subordinate phlogopite and Fe-Ti oxides (magnetite and ilmenite).

Clinopyroxene is phenocryst in almost all of the porphyritic rocks of this suite. It varies from 15-65% of the total phenocrysts. It forms prismatic, often twinned, subhedral and euhedral crystals and frequently clusters to form glomerocrysts with olivine and, rarely, plagioclase. Phenocryst sizes are generally between 0.01-1mm, but may reach up to 3mm in some samples. They characteristically show oscillatory and sector zoning (Plate 4.27). They are generally diopside and diopsidic augite. Some are

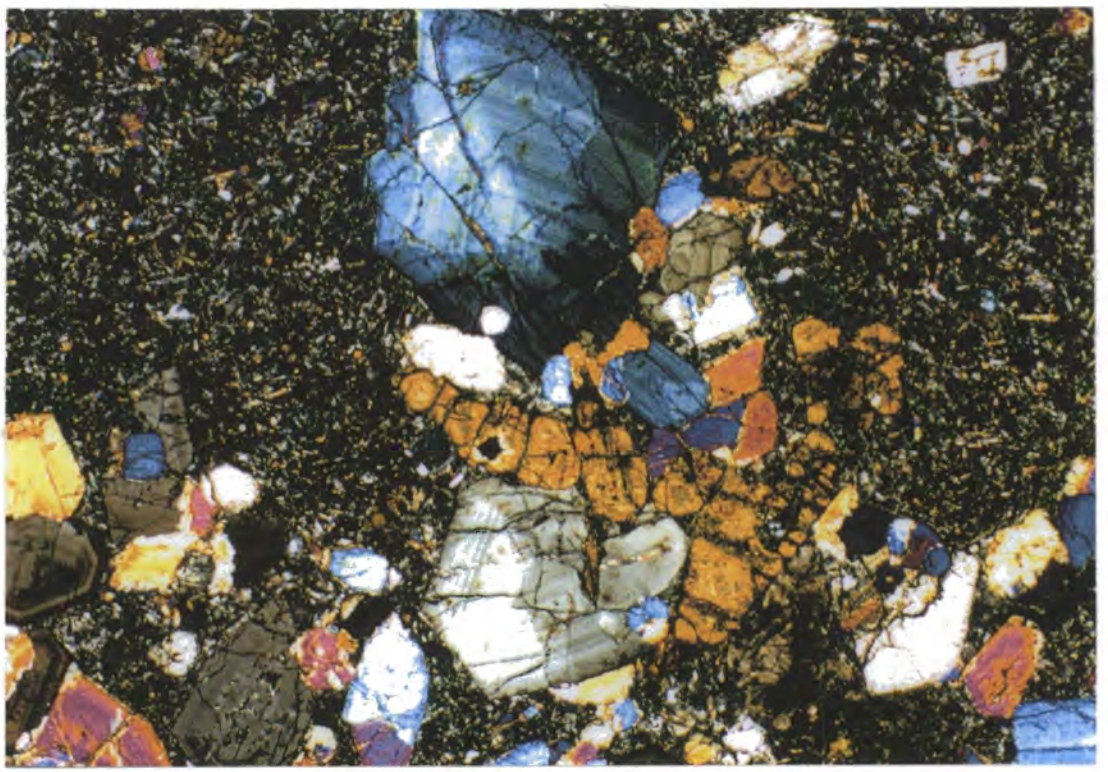

Plate 4.27. *Oscillatory zoned phenocrysts of clinopyroxenes forming glomerocrysts with olivine crystals that are largely altered to iddingsite. 3x1.9mm, XP*

characterised by colourless diopside cores and pale greenish augite overgrowths with well-developed oscillatory zoning near the rims. The observed core and rim compositions are Wo_{48-42} En_{44-51} Fs_{8-7} and Wo_{49-45} En_{4-40} Fs_{9-15} respectively. In some of the basaltic andesite samples, large (~3mm) augite phenocrysts have been resorbed and the interiors of crystals have been pervaded by calcite (Plate 4.28) and, more rarely, opaque oxides arranged in trains parallel to the oscillatory zones. These characteristics may have been resulted from extensive internal melting followed by overgrowth of the phenocrysts and reflect a thermal and/or compositional disequilibrium during crystallisation in the magma chambers (Cox et al., 1979).

Olivine is the characteristic phenocryst of most of the rocks. The abundance of olivine phenocrysts is highly variable: the absarokites contain abundant olivine phenocrysts (30 and 65% of the total phenocryst), whereas the shoshonites contain lesser amounts of olivine (~ 5-20% of the total phenocryst). They mostly form euhedral-subhedral crystals and their sizes vary considerably ranging between 0.01 and 1.5mm, but mostly less than 0.5mm in diameter. In most samples, olivines are zoned fresh crystals although, in some shoshonitic samples, they have been replaced by green

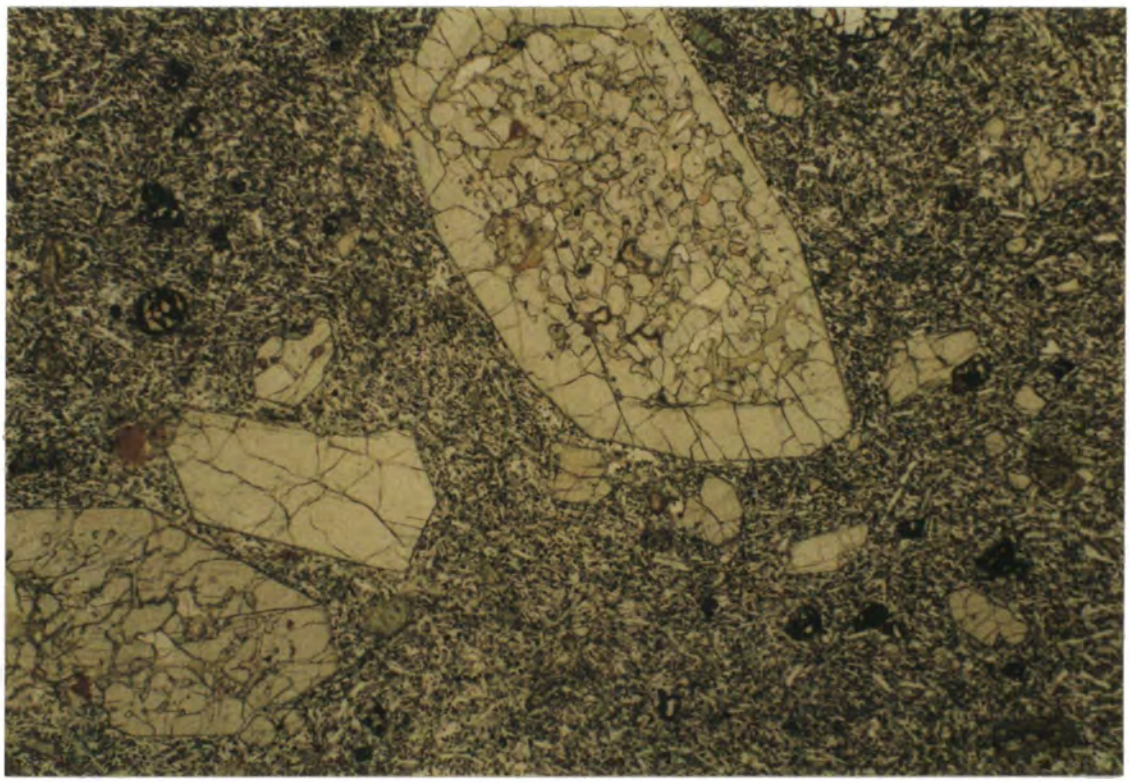

Plate 4.28. *A zoned clinopyroxene phenocryst shows extensive internal resorption. 3x1.9mm, XP and PPL*

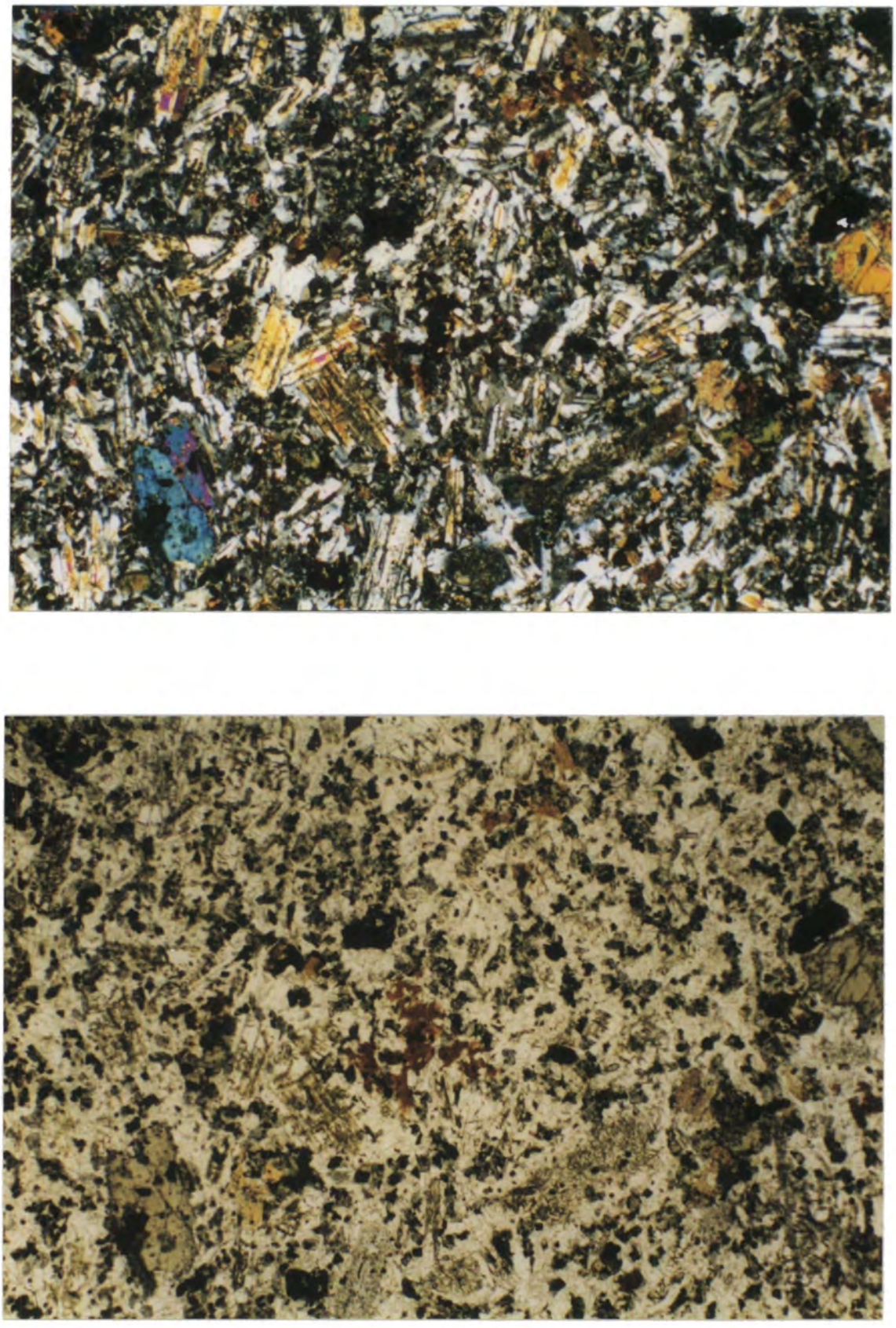

Plate 4.29. *Poikilitic phlogopite crystals set in a coarse-grained matrix of sanidine, diopsite and magnetite-ilmenite. 3x1.9mm, XP and PPL*

serpentine and red-brown iddingsite. Core and rim compositions are Fo_{74-91} Fo_{73-86} respectively. In most cases, olivine forms the core to glomerocrysts of predominantly clinopyroxene.

Plagioclase phenocrysts are notably rare or absent in the absarokites (48-52% SiO_2) but present in most of the shoshonites and andesites with abundances ranging from 5-30% of the total phenocrysts. They are generally prismatic crystals with grain sizes of 0.3-1mm in length. Although some unzoned plagioclase phenocrysts are found, they predominantly exhibit oscillatory zoning in the shoshonites and normal zoning in the andesites. A large compositional difference can be observed between the zones: the observed core and rim compositions are An_{30-85} and An_{30-65} respectively.

Phlogopite is found in some absarokites representing the only hydrous phase. It is often present as a late, poikilitic phase. Although phlogopite is found an essential phenocryst in some samples (~20% of the total phenocrysts), and some crystals may reach up to 1mm length in the phenocryst phase, they are in general minor and restricted to the groundmass.

The **groundmass** consists of microcrystalline plagioclase laths with subordinate interstitial clinopyroxene, magnetite-ilmenite and olivine microlites. Glass is rare and present only in few samples. The sizes of groundmass plagioclase range from very fine- to medium-grained. The most common groundmass textures vary between intergranular and intersertal depending on whether the material between the plagioclase laths are crystalline (mostly clinopyroxene) or glassy. Some also show pilotaxitic texture characterized by randomly oriented plagioclase microlites around the glomerocrysts and/or phenocrysts.

For most of the phlogopite-bearing rocks, the groundmass is a significant feature with a considerable amount of alkali feldspar (mostly sanidine), accompanied by phlogopite, plagioclase, augite and magnetite-ilmenite (Plate 4.29). The textural relationship of most of the phlogopites may imply the presence of a late volatile- and K-rich fluid. Such a fluid may also be responsible for the existence of alkali feldspar of variable compositions in the groundmass.

4.3. Interpretation and Summary of the Petrography

General petrographic features (e.g. the degree of crystallinity and average phenocryst abundances) of the volcanic rocks from Western Anatolia is summarised in

Table 4.1. Summary of the petrographic characteristics of the volcanic rocks from Western Anatolia.

Area	Volcanic Rock Group	Age	Whole-rock	Average	Abundances of Phenocrysts (%)						
			SiO_2 (wt.%)	Phenocrysts (%)	*plagioclase*	*olivine*	*c/pyroxene*	*o/pyroxene*	*amphibole*	*biotite*	*phlogopite*	*oxides*
EGA	Alkaline Mafic Lavas	Late Miocene	42 - 50	<3 - 20	<5	45 - 55	40 - 55					5 - 15
	Porphyritic Dyke Swarms	Early Miocene	55 - 61	<10 - 45	40 - 45	<2	20 - 25	20 - 25				<15
	Crystal-rich Ignimbrites	Early Miocene	65 - 80	15 - 50	35 - 60		<5 - 15	<5 - 15		20 - 55		<5
	Highly Porphyritic Lavas	Early Miocene	56 - 70	20 - 60	30 - 65	<2	<5 - 25	<5 - 25	<5	15 - 35		<5
DAB	Basic Lavas	Middle Miocene	48 - 57	<3 - 10	<5 - 30	30 - 65	15 - 65				0 - 20	5 - 10
	Intermediate Lavas	Middle Miocene	54 - 66	<10 - 30	30 - 40	10 - 25	35 - 50	<10	<2			5 - 10
	Highly Porphyritic Lavas	Early Miocene	55 - 68	15 - 65	35 - 60		<5 - 15		30 - 45	15 - 25		<5

Table 4.1. Compositional and textural characteristics of the rocks have shown that the most important petrographic features of the Early Miocene, acid-intermediate rocks are their high proportions of phenocrysts (up to 65%) and complex compositional zoning of phenocrysts (especially plagioclases and some pyroxenes).

Complex compositional zoning of crystals is mostly attributed to magma mixing processes (e.g. Kuno, 1936 and 1950; Dungan and Rhodes, 1978; Tsuchiyama, 1985; Nixon and Pearce, 1987). For plagioclase, normal compositional zoning that is characterised by more calcic core compositions relative to rim compositions can be explained by increasing degree of crystallinity within a sample. However, reversed zoning that is accompanied by normal zoning in crystals within the same rock can most likely be explained by magma mixing (or crustal contamination). In mixing systems, a more sodic crystal, derived from the felsic magma component, will tend to be resorbed as it is reheated by the more mafic magma component. This may give rise a subsequent crystallisation of more calcic plagioclase at the outer zones of phenocrysts. If calcic crystals of the mafic component happen to be present at the time of mixing, they will not be resorbed and will retain good crystal shape and mostly enclosed by further growth zones. Overgrowths of these mixing plagioclase crystals are mostly dusty and dendritic plagioclase resulting from quenching of relatively calcic plagioclase melt of the mafic component. In some cases, nucleation of plagioclase dendrites may form a dendritic core of a crystal that has an overgrowth of later formed non-dendritic plagioclase rim. In some other cases, repetitive injection of the mafic magma into a relatively less mafic magma chamber may form oscillatory zoned phenocrysts which are marked by multiple resorption cycles producing resorbed and sieve-textured crystals, although, as previously mentioned, Nelson and Montana (1992) argue that forming of sieve-textured plagioclase may be attributed to rapid magmatic decompression rather than mixing.

Most plagioclase phenocrysts of the highly porphyritic, Early Miocene acid-intermediate rocks from both the EGA and DAB areas display most of the textural

features described above. These mineralogical and textural characteristics of plagioclase phenocrysts may indicate that lavas in these suites have experienced extensive, open-system differentiation. Highly porphyritic nature of most of these lavas may further suggest that the open-system modification might be operational in shallow magma chambers (crystallisation depths are discussed further in Chapter 5).

It is evident from the low proportion of phenocrysts contents (<3-30%) of the Middle Miocene basic-intermediate rocks that the degree of crystallinity decreases gradually in time from the Early Miocene to the Middle Miocene. Unlike the Early Miocene rocks, aphyric or weakly porphyritic nature of the rocks of Middle Miocene age may indicate that the magma has not experienced long-lived, shallow magma chamber processes. This may possibly reflect a rapid ascent of the magmas through the continental crust as a consequence of progressive crustal thinning related to extensional tectonics.

The Late Miocene, mafic alkaline rocks contain phenocryst phases of olivine, clinopyroxene, ilmenite and magnetite with subordinate plagioclase and nepheline. Phenocryst contents are generally low (<3 – 20%) and most samples exhibit quench textures.

CHAPTER FIVE

MINERAL CHEMISTRY

Introduction

This chapter presents the mineral chemical characteristics of the volcanic rocks from the Western Anatolian, Late Cenozoic volcanic province. It is subdivided into two main parts. The first part defines the compositions of the mineral assemblages from different volcanic formations throughout the volcano-stratigraphic sequence and discuses the crystallisation conditions of the minerals. The second part presents the estimates of magmatic intensive parameters, including crystallisation temperatures (T), pressures (P) and oxygen fugacities (fO_2).

Analytical data used in this chapter were obtained using the facilities of the Electron Microprobe Unit of Edinburgh University. Details of the analyses and the full electron-probe dataset are given in Appendix A and B respectively.

5.1. Classification of the Minerals

5.1.1. Olivine

Olivine occurs in some form in all basanites and alkali basalts of Late Miocene age (the Tastepe, Ezine and Ayvacik Volcanics) and most calc-alkaline and shoshonitic basic-intermediate rocks of Middle Miocene age (the Foca Dyke Swarms, the Nebiler Volcanics, the Egrigöl Andesite and the Odaburnu Dyke Swarms). It is, however, a scarce phenocryst phase in the acid-intermediate rocks of Early Miocene age, although the rocks of the Kovacli Dyke Swarms and the Behram Andesite contain serpentinized olivine phenocrysts.

Olivine phenocrysts and microphenocrysts in general show a range of compositions from Fo_{91} to Fo_{67} (Fig. 5.1). Mg concentrations of the olivines show only a small variation within the olivine-bearing rocks. The most Mg-rich (forsteritic) olivines are found in the Middle Miocene shoshonites and absarokites of the Nebiler Volcanics (e.g. sample EA350) while the most Fe-rich (fayalitic) are from the Middle Miocene aphyric or slightly porphyritic intermediate rocks of the Egrigöl Andesite (e.g.

sample EA313) and the Odaburnu Dyke Swarms. Most of the phenocrysts are normally zoned within a range of 5-15 mole % Fo. However, extreme core to rim zonations (Fo_{89} to Fo_{67}) are also observed in some samples (e.g. EA309 of the Foca Dyke Swarms).

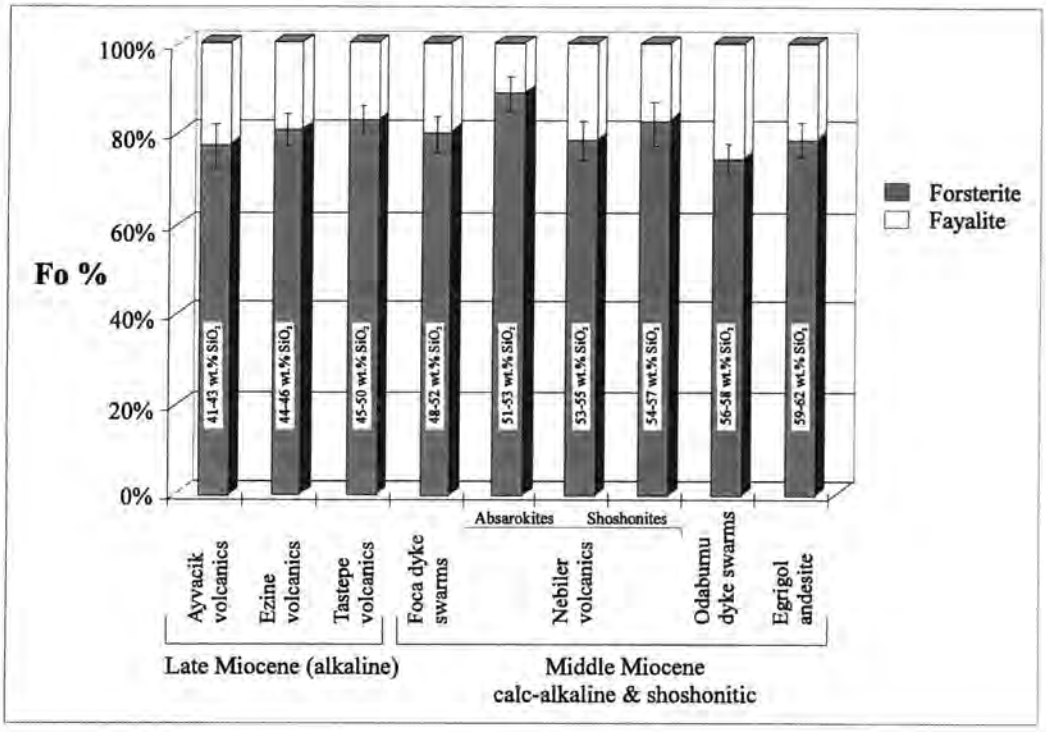

Figure 5.1. *Distribution of average composition of olivine phenocrysts and microphenocrysts from the different formations of the Late Cenozoic West Anatolian volcanic province.*

Figure 5.2 illustrates the variation in the forsterite content (Fo) of olivines with changing silica concentration (SiO_2) of host whole-rocks. The forsterite contents of the olivines from the Middle Miocene calc-alkaline and shoshonitic basic-intermediate rocks generally decrease with increasing silica content which can be explained by fractional crystallisation. The exception is one of the basalt samples which includes abundant xenocrysts with extreme compositional zoning. The forsterite content of the olivines from the Late Miocene alkali basalts and basanites increases with increasing silica content of the host rock.

The experimental work of Roder and Emslie (1970) on olivine-liquid equilibria in basaltic systems shows that the exchange coefficient (K_D) relating the distribution of Fe and Mg between olivine and liquid should be 0.3 (±0.03) if equilibrium has been attained. Using the method of Roder and Emslie (1970), the Mg/Fe ratios of the liquid with which the olivine compositions would have been in equilibrium were calculated

and compared with the Mg/Fe ratio of the bulk rock, to assess whether the olivines were in equilibrium with the host rock. To avoid the effects of phenocrysts, calculations were applied only to aphyric or <10% phyric samples assuming that they represent liquid compositions.

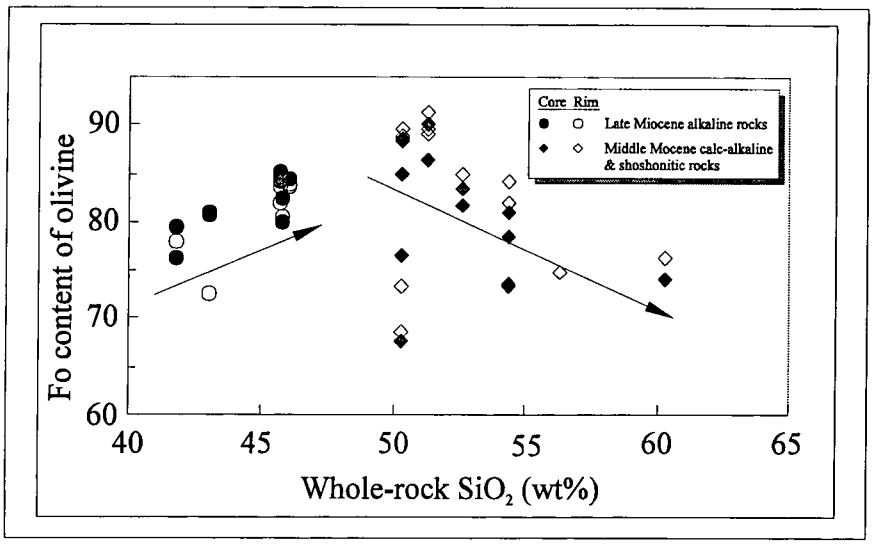

Figure 5.2. *Olivine compositions plotted against silica content (SiO_2 wt%) of their host whole-rock.*

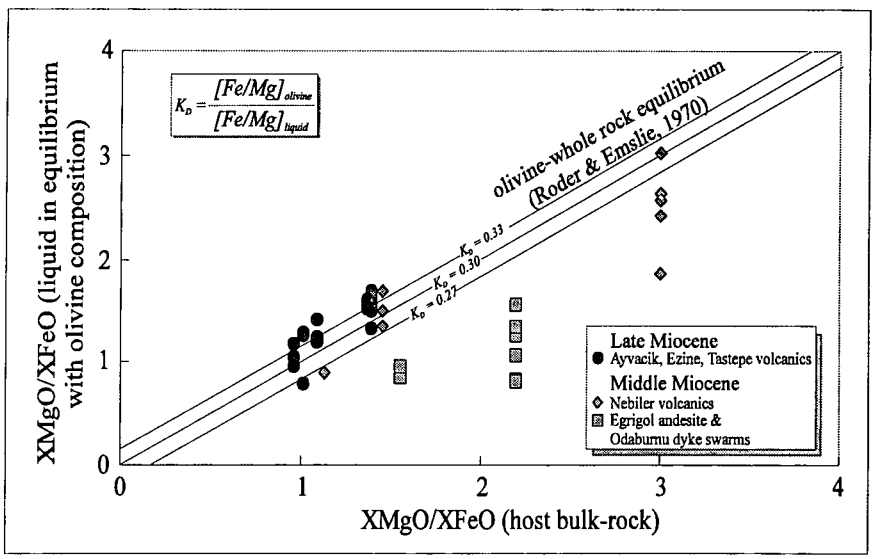

Figure 5.3. *Equilibrium XMgO/XFeO ratio of liquid calculated from olivine compositions plotted against XMgO/XFeO ratio of host bulk-rock. X is the mole fraction of the oxide. Lines represent equilibrium between minerals and bulk rock compositions. Equilibrium* $^{Fe/Mg}K_{Dmin/liq}$ *values are from Roeder and Emslie, (1970).*

Figure 5.3 illustrates that most of the olivines from the alkaline basalts and basanites of the Late Miocene lavas are within the equilibrium range. Among the calc-alkaline and shoshonitic rocks of the Middle Miocene age, some olivines are within the equilibrium range, but the majority is not. In particular, olivines from the intermediate rocks (e.g. the Egrigöl Andesite) are too Fe-rich to have crystallised from a liquid compositionally similar to their host rocks. This may be explained either by mixing of magmas with different compositions or by the existence of olivine xenocrysts.

5.1.2. Pyroxene

Clinopyroxene is one of the most abundant mineral phases in the non-acidic alkaline, calc-alkaline and shoshonitic volcanic rocks. Orthopyroxene is found in most of the calc-alkaline and shoshonitic rocks from the Ezine-Gulpinar-Ayvacik (EGA) area, while it is a rare or scarce phenocryst phase in the rocks from the Dikili-Ayvalik-Bergama (DAB) area.

Pyroxene end-members were calculated using the computer program PX (Gómez, 1990) and plotted on the diopside (Di: $CaMgSi_2O_6$) - hedenbergite (Hd: $CaMgSi_2O_6$) - enstatite (En: $Mg_2Si_2O_6$) – ferrosilite (Fs: $Fe_2Si_2O_6$) classification quadrilateral (Fig. 5.4). Clinopyroxenes in general plot into the diopside, salite, endiopside and augite fields, whilst the orthopyroxenes plot mostly into the bronzite and hypersthene fields.

It is apparent from Figure 5.5 that clinopyroxenes and orthopyroxenes from most of the Early-Middle Miocene, calc-alkaline and shoshonitic rocks have both reverse and normal zoning. Reverse zoning of phenocrysts may be explained by a number of processes including: (1) decompression during magma ascent (Ewart et al., 1975; Kontak et al., 1984); (2) more oxidising conditions during the later stages of crystallisation (Luhr and Carmichael, 1980; Grunder and Mahood, 1988); or (3) magma mixing (Nixon, 1988). Clinopyroxenes from the Late Miocene, alkaline rocks mostly show normal zoning, though the compositional difference between cores and rims are generally small.

In Figure 5.6, minor elements in pyroxenes are plotted against the Fs (Ferrosilite = $Fe_2Si_2O_6$) contents. TiO_2 generally shows a positive correlation with Fs content of clinopyroxenes (Fig. 5.6a). Distinctively high TiO_2 concentrations of the clinopyroxenes

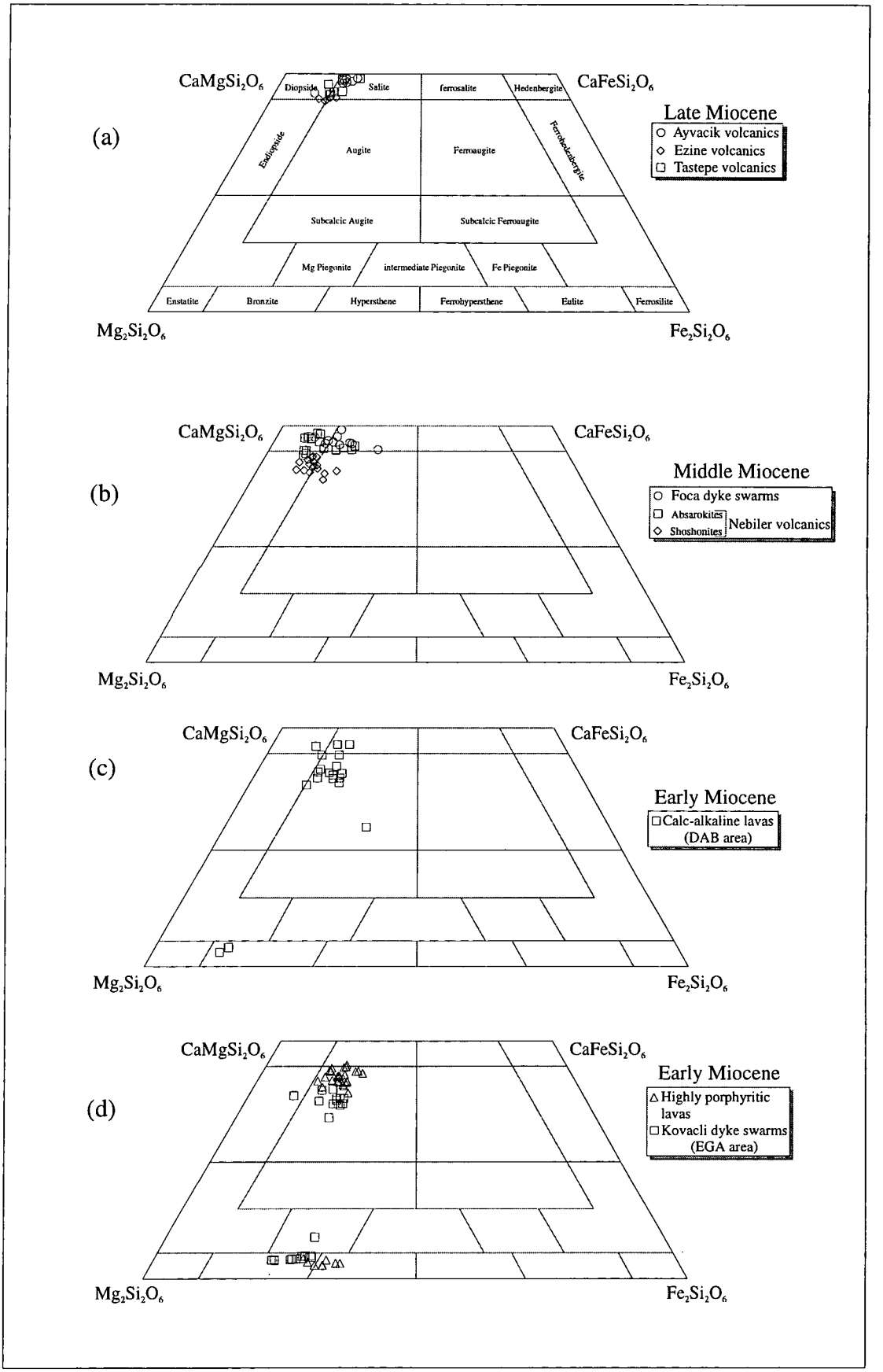

Figure 5.4. *Compositions of pyroxene pheno- and microphenocrysts from the volcanic rocks of Western Anatolia.*

of the Late Miocene alkaline rocks (the Ayvacik, Ezine and Tastepe Volcanics) relative to the Early-Middle Miocene, calc-alkaline and shoshonitic rocks are consistent with the TiO_2 contents of the whole rocks (previously given in Chapter 3). This may be attributed to the high concentrations of TiO_2 in the alkaline magma.

Notably, clinopyroxenes of the acid-intermediate rocks of the DAB area including the highly porphyritic rocks, the Egrigöl Andesite and the Odaburnu Dyke Swarms are in general enriched in MnO at a given Fs content relative to those of the more basic Middle Miocene rocks of the Foca Dyke Swarms and the Nebiler Volcanics (Fig. 5.6b). A similar relationship is observed between pyroxenes of the Early Miocene rocks from the EGA area as both clinopyroxenes and orthopyroxenes of the highly porphyritic lavas are more enriched in MnO than those of the Kovacli Dyke Swarms (Fig. 5.6c). Since Mn^{2+} can substitute for Fe^{2+}, not only in pyroxene, but also in olivine and/or Fe-Ti oxides, this may be explained by olivine crystallisation (with or without Fe-Ti oxides) prior to pyroxene crystallisation for the later-formed volcanic rocks from the two areas. This is also supported by the existence of abundant olivine phenocrysts in the Foca Dyke Swarms and the Nebiler volcanics of the DAB area and the Kovacli Dyke Swarms of the EGA area.

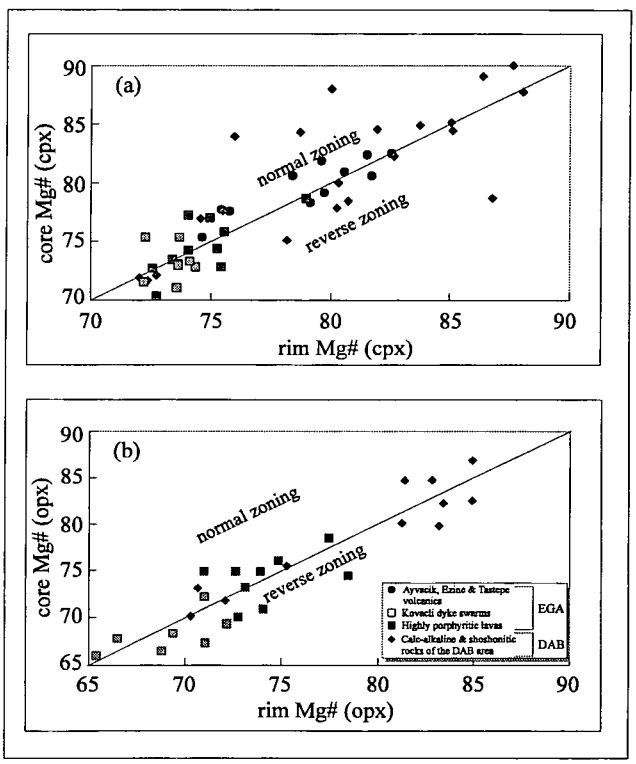

Figure 5.5. *Molar Mg-number (Mg# = 100Mg/[Mg+Fe^{2+}]) of (a) clinopyroxene and (b) orthopyroxene cores and rims.*

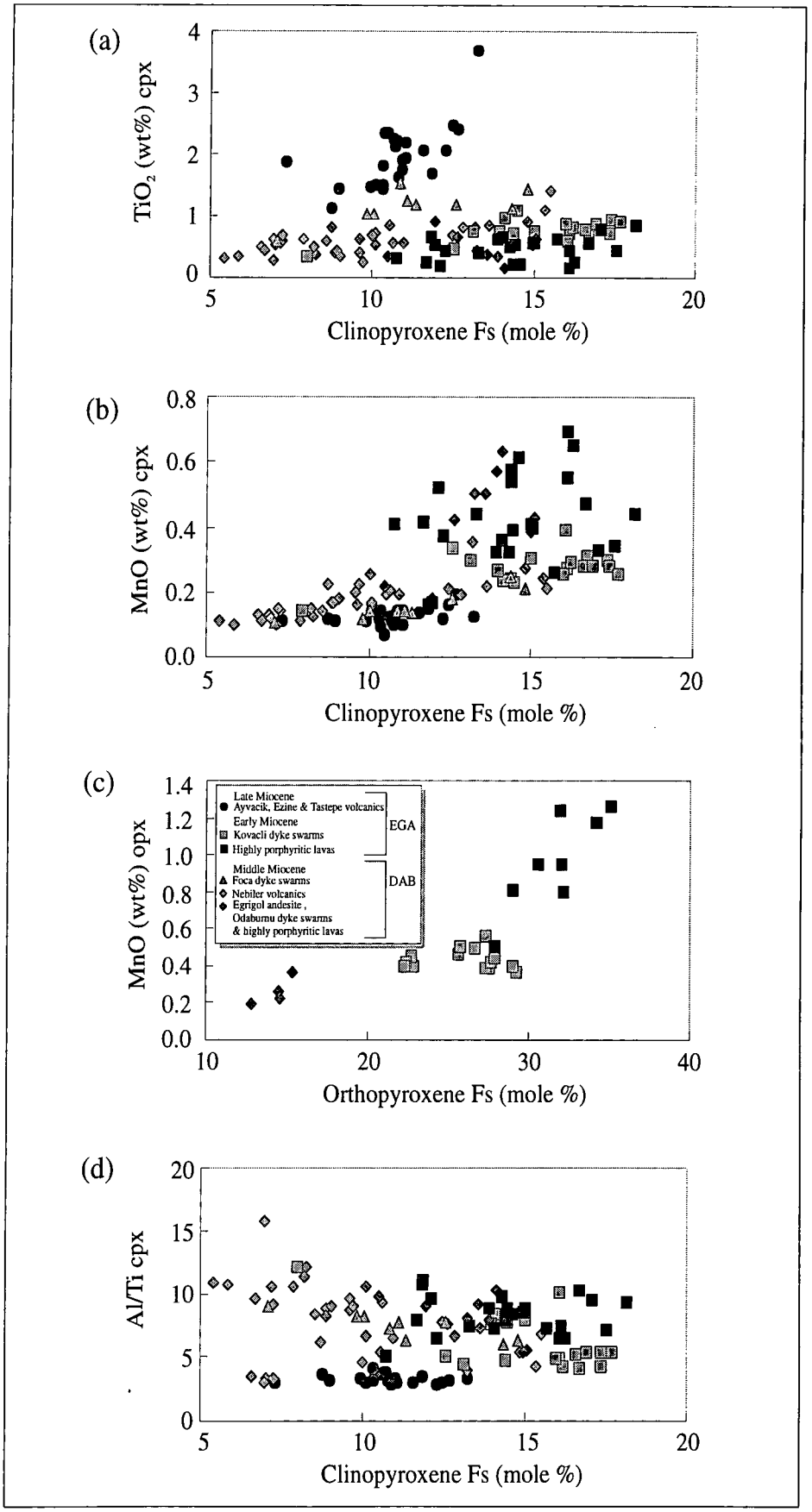

Figure 5.6. *Minor element variations in pyroxene shown by plots of (a) TiO_2 content of clinopyroxene, MnO contents of (b) clinopyroxene and (c) orthopyroxene and (d) Al/Ti molar ratio of clinopyroxene against the molar percentage of ferrosilite (Fs) in pyroxene.*

The Al/Ti ratios in the clinopyroxenes of most of the calc-alkaline and shoshonitic rocks increase with decreasing Fs contents from the Early Miocene acid-intermediate rocks towards the Middle Miocene basic-intermediate rocks (Fig. 5.6d). This may reflect the greater rate of depletion of Al tied up in plagioclase relative to Ti in ilmenite or titano-magnetite in a plagioclase-dominated fractionation for the Early Miocene rocks. Supporting this is the absence of ilmenite in the Early Miocene rocks. Elevated ratios of Al/Ti in the clinopyroxenes of the Middle Miocene rocks of the Nebiler Volcanics coincide with the appearance of ilmenite which has extremely low Al/Ti ratios requiring removal of only a small amount of ilmenite to cause rapid depletion of Ti, and thus increase Al/Ti ratios even in liquids fractionating plagioclase.

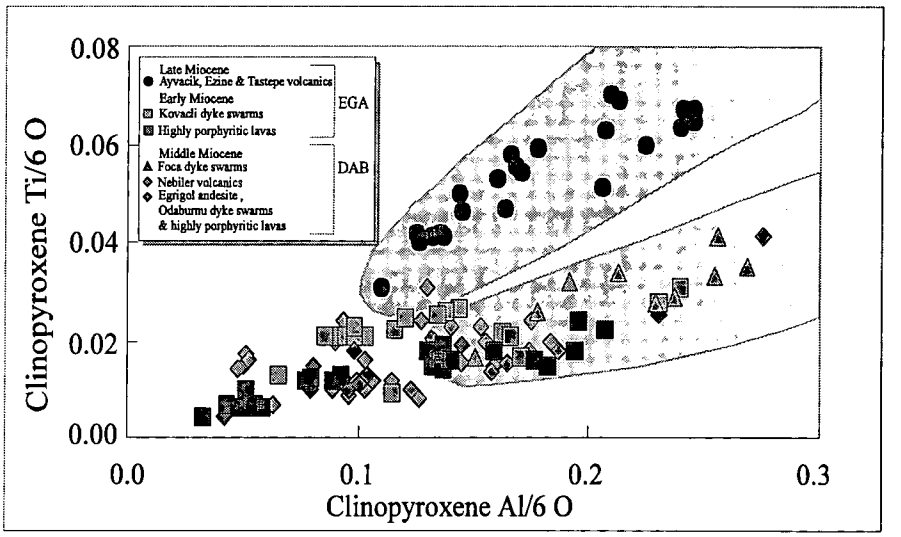

Figure 5.7. *Ti versus Al (per 6 oxygens) for clinopyroxenes showing compositional differences between the volcanic rocks.*

Experimental and petrological studies have demonstrated that partitioning of minor elements such as Ti and Al into pyroxene is strongly growth-rate dependent, although equilibrium partitioning of Ca, Mg and Fe may not be seriously affected by cooling rates (Grove and Bence, 1977; Gamble and Taylor, 1980). In particular, high cooling rates favour crystallisation of pyroxene with elevated Ti and Al contents (Fig. 5.7). The existence of the Ti- and Al-rich microphenocrysts particularly in some of the alkaline basalt and basanites of the Late Miocene suite and basalts from the Foca dyke swarms therefore probably reflect more elevated cooling rates. Their aphyric or weakly porphyritic nature also supports this idea.

5.1.3. Plagioclase Feldspar

Most plagioclase phenocrysts show some degrees of compositional zoning. Zoning may be normal, reverse, and oscillatory or a complex combination of these three types. Thus, plagioclase analyses of at least two points, one near the rim, the other in the centre, were conducted. The compositional range of Western Anatolian Late Cenozoic volcanic suite as a whole is summarised in Figure 5.8. The majority of plagioclase feldspars lie within the andesine, labradorite and bytownite fields, although two analyses plot in the oligoclase field.

Compositions of plagioclases generally correlate with the silica contents of the host rocks (Fig. 5.9). The most An-rich plagioclases are found in the Middle Miocene basic rocks of the DAB area (The Foca dyke swarms and the Nebiler volcanics) while the most Ab-rich are from the Early Miocene acid porphyritic lavas. The phenocrysts are mostly within the range of 5-25 mole % An unit, although extreme core to rim zoning (up to 45 mole % An unit) is observed in some phenocrysts.

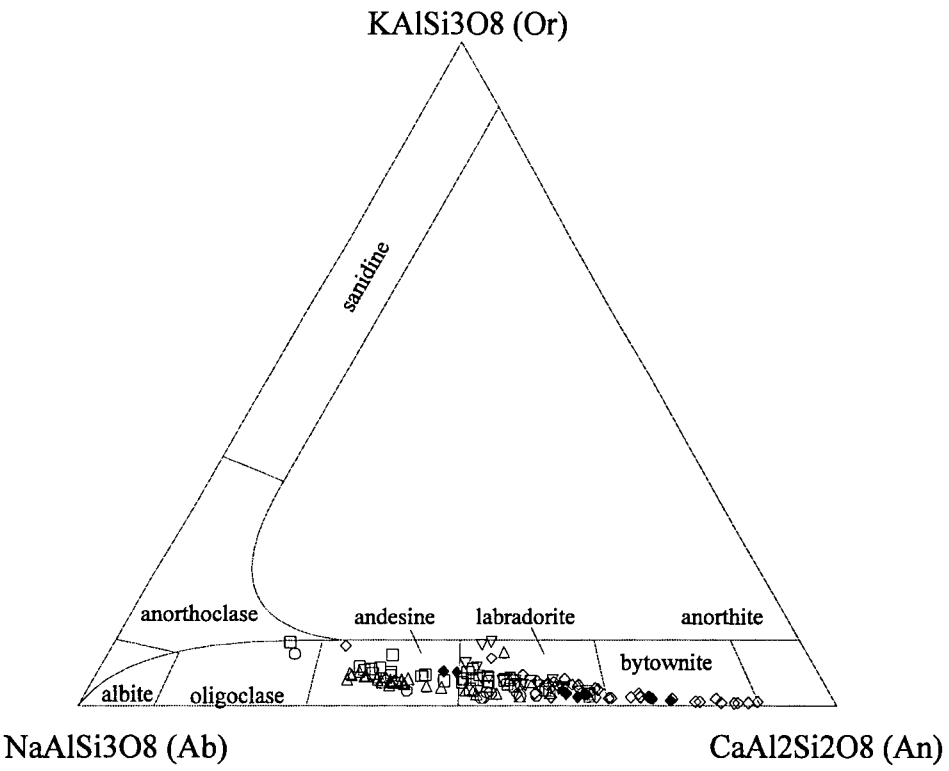

Figure 5.8. *Ternary projection of plagioclase compositions from the Western Anatolian volcanic rocks.*

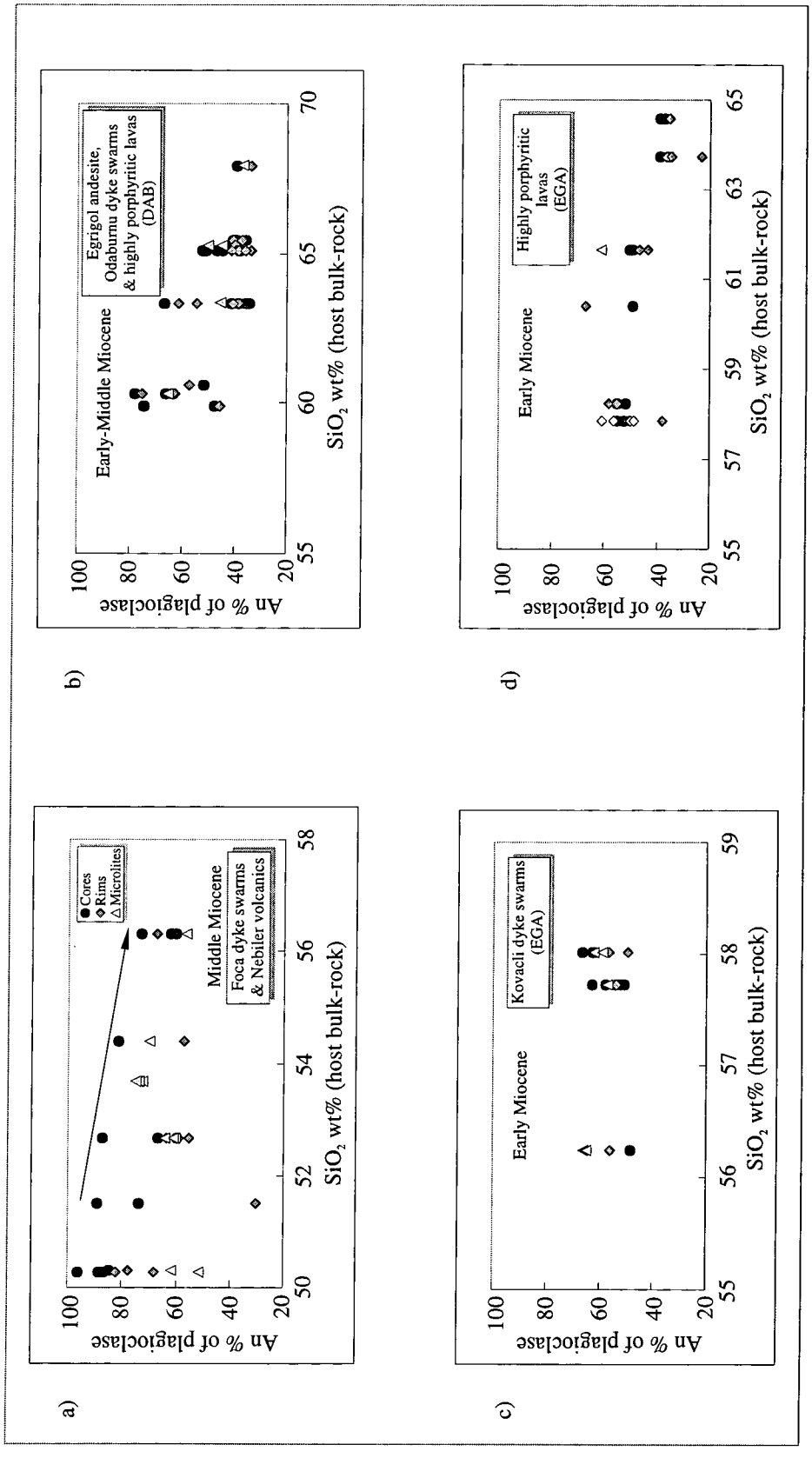

Figure. 5.9. *Anorthite contents of plagioclase core rim and groundmass microlites plotted against SiO_2 content of their host bulk-rock.*

5.1.4. Amphibole

Amphibole is an abundant mineral phase in most of the Early Miocene acid-intermediate rocks from the DAB area. Some intermediate rocks of the Middle Miocene age from the DAB area (e.g. the Egrigöl Andesite) and of Early Miocene age from the EGA area (e.g. the Bademli Unit) also include a minor amount of amphibole phenocrysts and xenocrysts in some forms.

All the analysed amphibole phenocrysts from the Western Anatolian volcanic rocks have $(Ca + Na)_{M4}>1.34$ and $(Na)_{M4}<0.67$, and thus are calcic amphiboles according to the classification scheme of Leake (1978). In Figure 5.10, the data have been plotted on the classification diagram of Hawthorne (1981). Two distinct compositional ranges can be identified: (1) edenites; and (2) pargasites. Amphibole phenocrysts and microphenocrysts from the Early Miocene, highly porphyritic acid-intermediate lavas of the DAB area predominantly classify as edenite and partly edenitic hornblende, though some of the data points fall into the pargasitic hornblende and ferroan pargasite fields. Amphiboles from the Middle Miocene Egrigöl Andesite of the DAB area and the highly porphyritic lavas of the EGA area mostly classify as pargasite or ferroan pargasite and are characterised by their low silica contents (<6.5 Si mole %).

The plots of Al^{IV} against (Na + K) cations in the A site of amphibole phenocrysts also reveal two distinct compositional trends (Fig. 5.11). The experimental studies of Helz (1973) demonstrated that amphibole compositions, in general, exhibit correlated increases in Al^{IV} and $(Na + K)_A$ with increasing crystallisation temperatures. The significant compositional difference between the two trends can therefore be attributed to different crystallisation temperatures (P-T conditions for amphiboles are discussed further in Section 5.2). The co-existence of both edenitic and pargasitic amphibole in some samples (e.g. the Kalarga Andesite) may further indicate that they are the composite products of more than one petrogenetic step.

5.1.5. Biotite-Phlogopite

Biotite occurs as phenocrysts in only the highly porphyritic acid-intermediate rocks (Early Miocene) from both the EGA and DAB areas. Some absarokites and shoshonites of the Nebiler Volcanics include phlogopite as phenocryst and groundmass phases, as previously mentioned in Chapter 4. In Figure 5.12, Ti, Al contents and Mg/Fe ratios of biotite and phlogopite phenocrysts are plotted against the silica contents of their

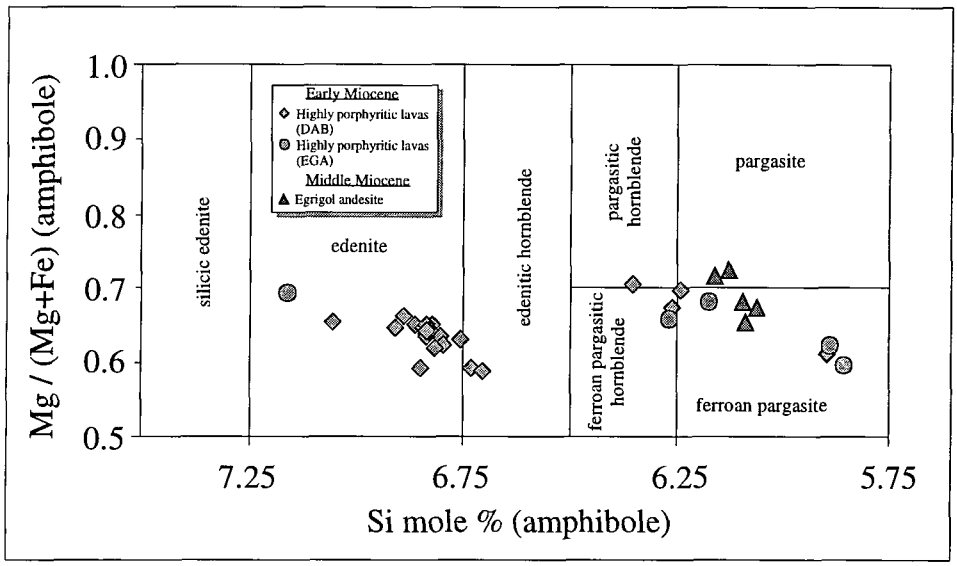

Figure 5.10. *Amphibole phenocrysts plotted on the classification diagram of Hawthorne (1981).*

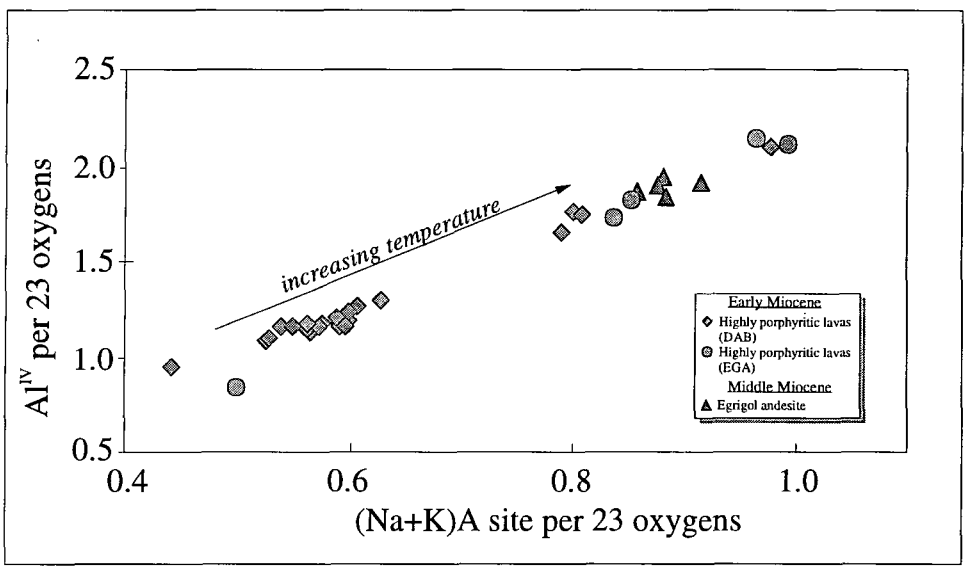

Figure 5.11. *Al^{IV} versus $(Na+K)_A$ site occupancy for amphibole phenocrysts.*

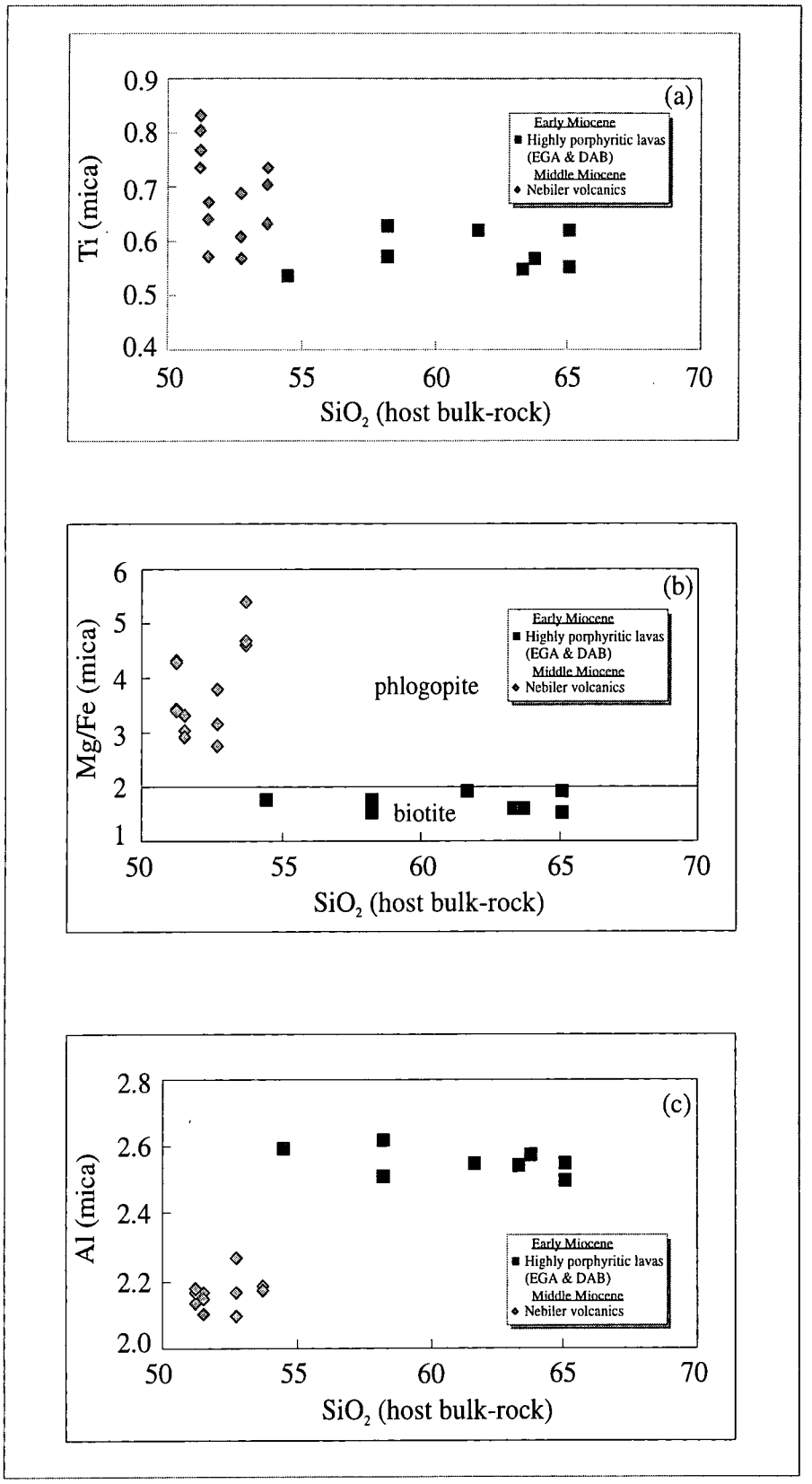

Figure 5.12. *(a) Ti content, (b) Mg/Fe ratio and (c) Al content of biotite and phlogopite phenocrysts plotted against silica content of the host bulk-rock.*

whole rocks. The compositions of the biotite phenocrysts do not show any significant variations among different volcanic rock groups and within individual lava flows. They have constant Mg/Fe ratios (<2) and Al contents (>2.5 mole %). Phlogopite phenocrysts characteristically have higher Mg/Fe ratios (>2.5) and lower Al contents (<2.3 mole %) than biotites. Ti contents are high for all the phlogopites.

5.1.6. Oxide minerals

A magnetite-rich (Fe_3O_4 – Fe_2TiO_4) phase is found in most of the rocks from Western Anatolian volcanic suites, the exception being the crystal-free ignimbrites. Magnetite (or titano-magnetite) occurs in the groundmass and as microphenocrysts. Ilmenite is less abundant and is found only in the alkaline basalts and basanites of Tastepe, Ezine and Ayvacik Volcanics (Late Miocene) and some basic-intermediate members of the Nebiler Volcanics (Middle Miocene). Figure 5.13 highlights the compositional variations of the oxide phases on the basis of their FeO, TiO_2 and Fe_2O_3 contents. It should be noted that the Fe^{3+} in the oxide minerals is estimated from the difference between Ti and Fe plus other divalent cations. Compositions of titano-magnetite lie close to the binary solid solution series of magnetite-ulvospinel.

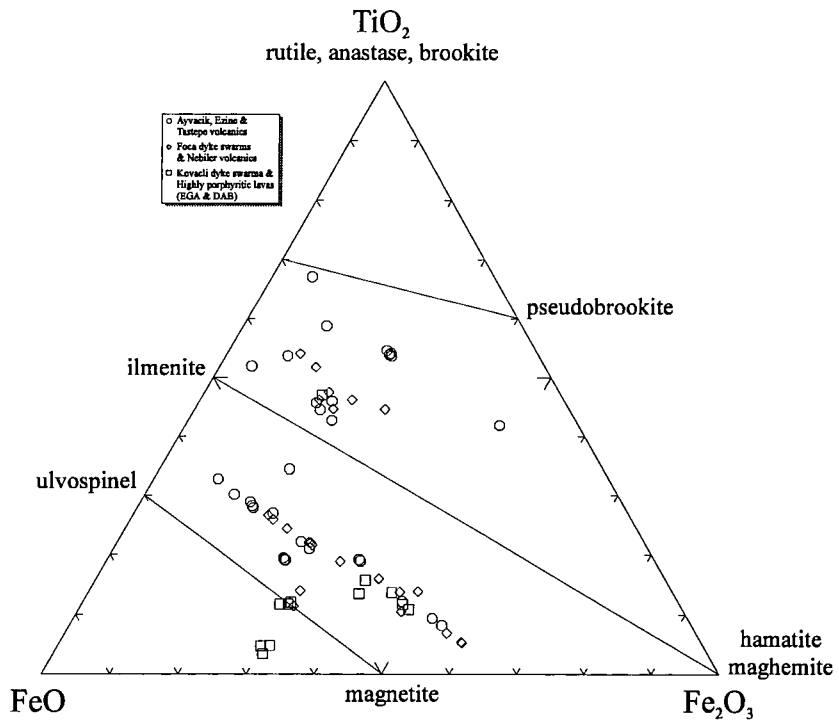

Figure 5.13. *Triangular diagram for the Fe-Ti oxides in the Fe-Ti-O systems.*

The TiO_2 concentrations of both titano-magnetites and ilmenites are plotted against the silica content of the host rock in Figure 5.14. Titano-magnetite and ilmenite from the basalts and basanites of the alkaline lavas (the Ayvacik, Ezine and Tastepe Volcanics) generally have the highest TiO_2 contents, consistent with the high TiO_2 contents of their whole-rocks (see Chapter 3). The average mole fraction of Fe_2TiO_4 (ulvospinel) in titano-magnetites from the alkaline rocks is also generally higher than that of the other rocks (calc-alkaline and shoshonitic), which reflects the higher Ti content of the alkaline lavas.

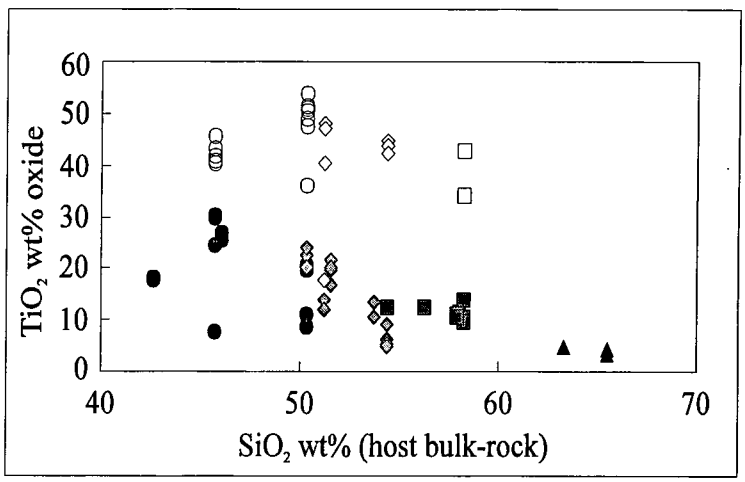

Figure 5.14. *TiO_2 concentration of titanomagnetite and ilmenite grains plotted against silica content of host bulk-rock. Closed symbols represent titanomagnetites and open symbols represent ilmenites (see Fig. 5.13 for the symbols).*

Bacon and Hirschmann (1988) used Mg/Mn partitioning between coexisting Fe-Ti oxides to examine whether the coexisting oxide phases are in equilibrium. According to their experiments, a plot of $\log[Mg/Mn]_{magnetite}$ against $\log[Mg/Mn]_{ilmenite}$ should yield a straight line if the oxide phases are in equilibrium. They conducted their experiments over a temperature range of 600 to 1100°C. They also argue that the effect of oxygen fugacity (fO_2) on the partitioning of the Mg/Mn ratios between coexisting oxide phases is insignificant. The test is, however, only applicable to fresh volcanic rocks and may not be accurate enough for oxidised or exsolved oxide minerals. Coexisting titano-magnetite and ilmenite grains in the volcanic rocks from the Western Anatolian suites are variable in composition, although a dominant population is usually present. Most titano-magnetite - ilmenite pairs from the alkaline basalts, basanites and calc-alkaline basalts and basaltic andesites have Mg/Mn atomic ratios consistent with equilibrium partitioning as defined empirically by Bacon and Hirschmann (1988). This implies that

they are coexisting phases in equilibrium (Fig. 5.15). Deviation of some of the analyses above the best-fit equilibrium line in Figure 5.15, especially at lower Mg/Mn ratios, may suggest a temperature and/or compositional dependence on partitioning in the oxide minerals, which is consistent with experimental studies of Bacon and Hirschmann (1988).

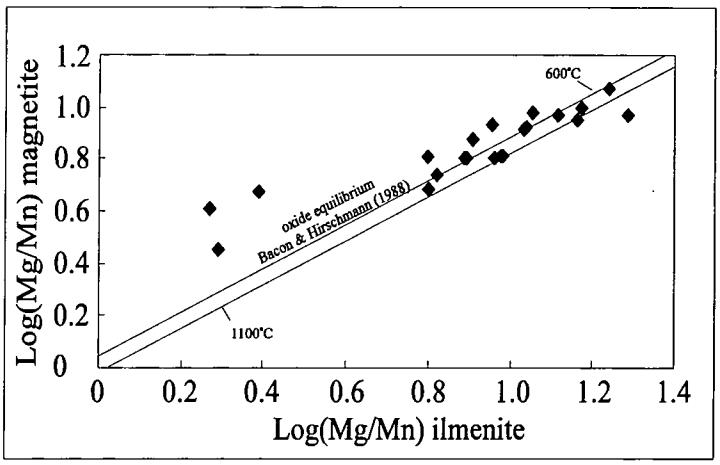

Figure 5.15. *Atomic Mg/Mn ratios of titanomagnetite and ilmenite grains. Line represents equilibrium between two oxide phases determined by Bacon and Hirschmann (1988).*

5.2. Estimation of Magmatic Intensive Parameters

5.2.1. Temperatures and Oxygen Fugacities

5.2.1.1. Pyroxene geothermometry

In recent years, a number of researchers have attempted to define a relationship between crystallisation temperature and crystal chemical composition of pyroxenes (Boyd, 1969 and 1973; Saxena and Nehru, 1975; Wells, 1977; Saxena, 1976; Mercier, 1976; Kretz, 1982; Lindsley and Andersen, 1983; Lindsley, 1983). Most of the studies on pyroxene thermometry are established on the basis of the theory that the Ca content of Ca-rich pyroxene (augite-diopsite) decreases with increasing temperature, whereas that of Ca-poor pyroxene (orthopyroxene) increases. Kretz (1982) used the temperature-dependence of Ca contents and Mg/Fe^{2+} ratios of pyroxenes determined by transfer and exchange reactions respectively to produce empirical temperature indicators applicable to natural metamorphic and igneous pyroxene minerals. He also estimated the uncertainty in this method to be ±60°C. Lindsley and Anderson (1983) and Lindsley (1983) produced one of the most successful and commonly used pyroxene geothermometers. They used experimentally-determined Ca-Mg-Fe pyroxene phase

relations over pressure range of 1atm to 15 kbar and combined them with calculated phase equilibria for the diopside-enstatite and hedenbergite-ferrosilite joins to propose a graphical two-pyroxene thermometer applicable to natural systems. Their geothermometer is mainly based on Ca partitioning between coexisting Ca-rich (augite-diopsite) and Ca-poor (orthopyroxene) pyroxenes and involves plotting the pyroxene end-member compositions onto the pyroxene quadrilateral and using experimentally-determined temperature contours to estimate the temperature. The uncertainty in this method, due to the calculation and location of the isotherms was estimated as ±20-30°C by Lindsley and Anderson (1983). The total error in this two-pyroxene geothermometry, including the errors in the analyses of the pyroxenes, is approximately ±50°C according to same authors.

Electron microprobe data of pyroxenes from the Western Anatolian volcanic rocks were used to calculate the Wo-En-Fs end-members according to the projection scheme of Lindsley and Anderson (1983). The ratio of Fe^{2+} to Fe^{3+} for these calculations was estimated using the PX program of Gómez (1990). Compositions of coexisting clinopyroxene and orthopyroxene with less than 10% nonquadrilateral components were used to estimate the temperatures. Figure 5.16 shows data plotted on the Di-En-Hd-Fs quadrilateral of Linsley (1983) which is calibrated for 1atm and contoured at 100°C intervals. The use of low-pressure (1atm) diagram for pyroxene phenocrysts is appropriate only if the host magmas resided and fractionated in shallow magma chambers. However, estimated pyroxene temperatures would be negligibly different at 5kbar, as there is only a slight difference between the contours of the diagrams calibrated for 1atm and 5kbar.

Unfortunately, orthopyroxene does not coexist with clinopyroxene in most of the rocks. Thus, the use of the two-pyroxene geothermometer was restricted to the Early Miocene rocks of the EGA area (the highly porphyritic lavas and the Kovacli Dyke Swarms) and some Middle Miocene lavas of the DAB area (the Egrigöl Andesite). Within the volcanic rocks from the EGA area, pyroxenes from the porphyritic lavas have lower crystallisation temperatures than those from the Kovacli Dyke Swarms. Temperature estimates for the former range between 750 and 980°C while the estimates for the later range between 850 and 1170°C. Pyroxenes from the Middle Miocene intermediate rocks (the Egrigöl Andesite) yield high crystallisation temperatures ranging between 1000 and 1120°C. Distribution of the pyroxene temperature estimates is also

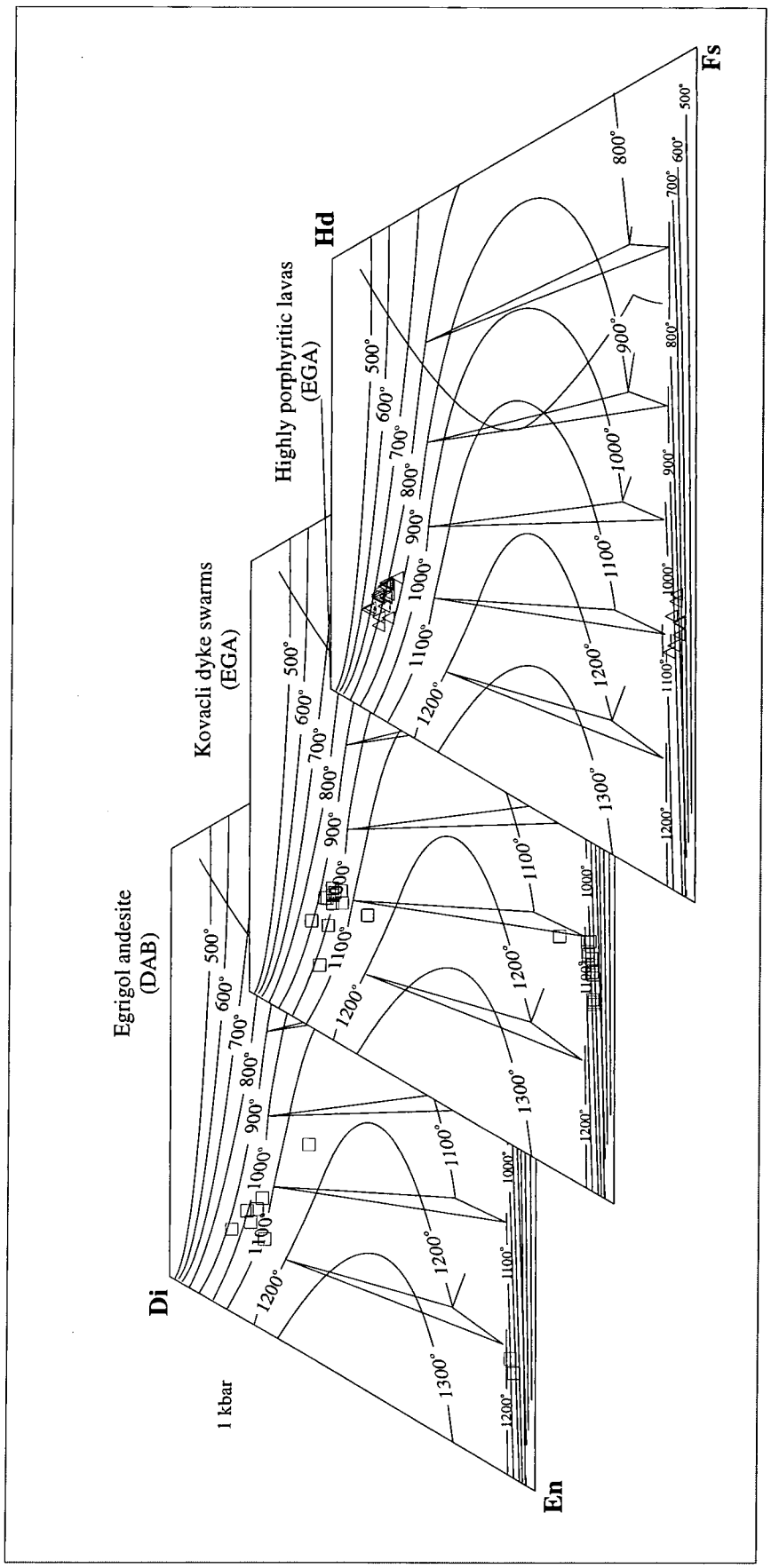

Figure 5.16. *Diagrams showing the liquidus temperatures of pyroxenes which are plotted on the Di-En-Hd-Fs quadrilateral of Lindsley (1983) that is calibrated to 1 kbar pressure and contoured at 100°C intervals.*

listed in Table 5.1.

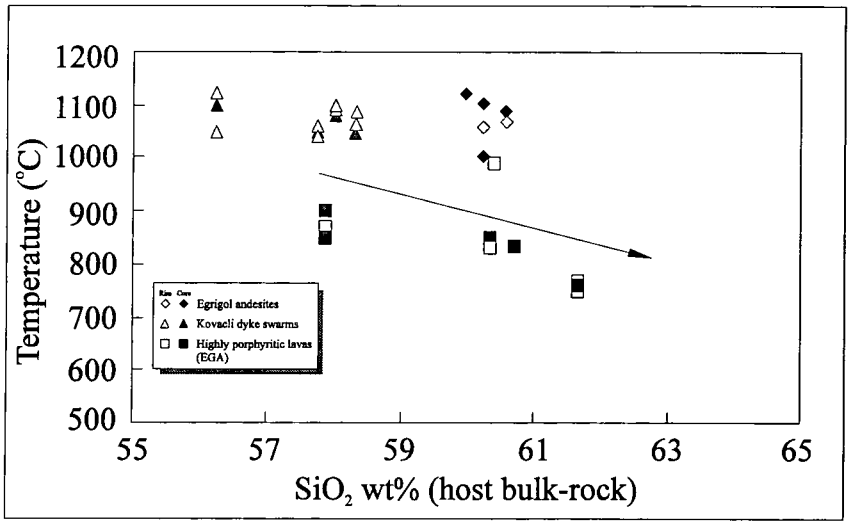

Figure 5.17. *Pyroxene temperature estimates of different volcanic suites of Western Anatolia plotted against silica content of host bulk-rock. Closed and open symbols represent temperatures obtained from pyroxene core and rim compositions respectively.*

In Figure 5.17, the available pyroxene temperature estimates are plotted against silica content of their host rocks. Pyroxene temperature estimates of most of the highly porphyritic Early Miocene acid-intermediate rocks from the EGA area display a negative correlation with their host rock silica contents indicating that acidity of the melt has a significant influence on the pyroxene temperatures. On the other hand, the temperature estimates of the pyroxenes from the Kovacli Dyke Swarms stay mostly constant with increase in their host rock silica contents. Notably, phenocryst cores in most samples of the highly porphyritic Early Miocene lavas yield higher temperatures than their rims. In the Kovacli Dyke Swarms, however, clinopyroxene phenocrysts are reversely zoned and their Ca-poor rims yield temperature estimates 5-50°C higher than their core compositions. This feature may suggest that, throughout the formation of these rocks, the magma chambers were periodically heated, probably through recharge of hotter magma to their bases.

5.2.1.2. Amphibole-plagioclase geothermometer

A number of recent experimental studies have focused on amphibole minerals (e.g. Plyusnina, 1982; Hammarstrom and Zen, 1986; 1992; Hollister et al., 1987; Blundy and Holland, 1990; Schmidt, 1992) because it is generally considered that amphiboles are a good potential indicator of pressure and temperature for many igneous and

metamorphic suites. Holland and Richardson (1979) and Graham and Powell (1984) used amphibole stability to calculate crystallisation temperatures in metamorphic rocks. Nabelek and Lindsley (1985) proposed an empirical calibration of a hornblende-plagioclase thermometer. Subsequently, Blundy and Holland (1990) used their experimental data on amphiboles together with published data to develop an empirical hornblende-plagioclase thermometer. Their model is mainly based on the Al^{iv} content of amphibole and the albite (Ab) content of coexisting plagioclase in silica-saturated systems. This model has been criticised for its over-simplicity (Hammarstrom and Zen, 1992; Poli and Schmidt, 1992). More recently, however, Holland and Blundy (1994) improved their previous thermometer and formulated two new amphibole-plagioclase thermometers for the following reactions:

a) *edenite + 4quartz = tremolite + albite*

b) *edenite + albite = richterite + anorthite*

These thermometers are pressure-dependent and the temperature uncertainty is given as ±20-30°C by the authors, although the uncertainty may increase for iron-rich amphiboles with different oxidation states from those used for the calibrant dataset. According to Holland and Blundy (1994), the thermometers can be applied to natural systems in the temperature range of 400-1000°C and the pressure range of 1-15 kbar over a broad compositional range.

In this study, electron microprobe data of amphibole and plagioclase phenocrysts from the Western Anatolian volcanic rocks are used to estimate temperatures using the equations of Holland and Blundy (1994). Since amphibole does not occur in most of the volcanic rocks from the EGA area (with one exception) and any of the basic rocks from the DAB area, application of Holland and Blundy's (1994) method was restricted to amphibole-bearing porphyritic acid-intermediate rocks from the DAB area. For these calculations, core compositions of amphibole and plagioclase phenocrysts were selected assuming that they are coexisting phases. Pressures for the mineral assemblages used in the temperature calculations are estimated using Schmidt's (1992) Al-in-hornblende geobarometer (see Section 5.2.2.2 for details).

The results obtained from the amphibole-plagioclase thermometer are illustrated in Figure 5.18. The temperatures estimated from the amphibole phenocrysts in the highly porphyritic lavas (the Bademli Unit; sample EA273 and EA231) of the EGA area range between 860 and 980°C, which is slightly higher than the range of the

temperatures obtained from the pyroxene geothermometry (Table 5.1). The temperature estimates from the amphibole phenocrysts of the Early Miocene acid-intermediate porphyritic rocks from the DAB area (the Ballica volcanic Unit, the Akcapinar volcanic Unit, Karagol volcanic Unit, the Mt. Seyret volcanic Unit and the Kalarga Andesite in Table 5.1) range between 790 and 970°C. The estimates obtained from the rocks of the DAB area are generally lower (<900°C) than those obtained from the rocks of the EGA area.

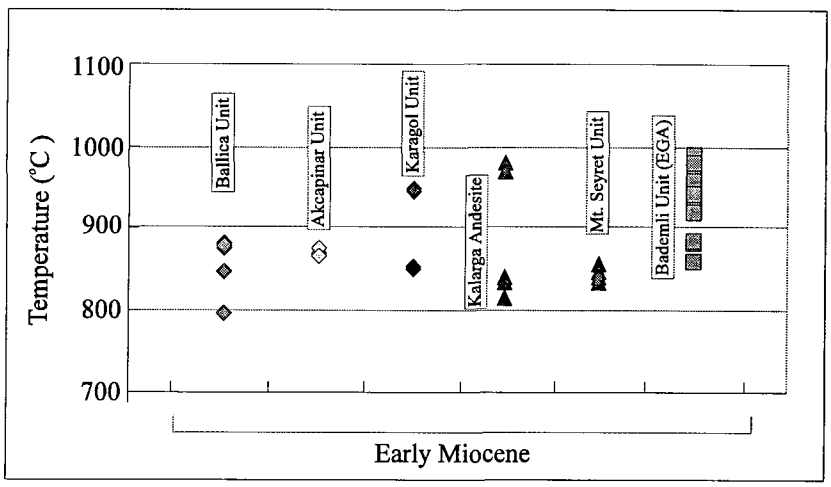

Figure 5.18. *Temperatures of crystallisation estimated using amphibole-plagioclase geothermometer of Holland and Blundy, (1994). .*

5.2.1.3. Fe-Ti oxide thermometry and oxygen fugacities

The thermodynamic significance of the compositional variations of coexisting Fe-Ti oxides was first realized by Buddington et al. (1955) and Buddington (1956). Subsequently, Buddington and Lindsley (1964) experimentally calibrated the following equilibria in the system FeO-Fe_2O_3-TiO_2 and developed a graphical Fe-Ti oxide geothermometer / oxygen barometer.

$$Fe_2O_3 + Fe_2TiO_4 = FeTiO_3 + Fe_3O_4$$

$$6FeTiO_3 + 2Fe_3O_4 = 6Fe_2TiO_4 + O_2$$

They used the first reaction to determine temperature and the second reaction to determine fO_2 because the reactions are independent of fO_2 and temperature respectively. In recent years, a number of additional attempts have been made to improve and simplify the use of the Fe-Ti oxide geothermometer and oxygen barometer (Powell and Powell, 1977; Andersen and Lindsley, 1979, 1981, 1988; Ghiorso and Carmichael, 1981; Ghiorso and Sack, 1991; Lindsley and Spencer, 1982; Lindsley et al., 1990; Stormer, 1983; Stormer and Whitney, 1985). Among these, that of Lindsley et al.

(1990), which couples the projection algorithm of Lindsley and Spencer (1982) with thermodynamic analysis of the Fe-Mg-Ti oxides calibrated by Andersen (1988), is probably the most successful and commonly used method.

In this study, temperatures and oxygen fugacities (fO_2) at the time of crystallisation were estimated using the equilibria between two solid solutions (ilmenite and titano-magnetite). Only samples that were likely to have preserved equilibrium conditions, as previously determined from Mg and Mn partitioning (Fig. 5.15), were used to calculate temperatures. Unfortunately, as mentioned in Section 5.1.6, ilmenite does not coexist with titano-magnetite in most of the rocks from the Western Anatolian volcanic suites, preventing utilisation of the "two-phases method" to estimate temperature and fO_2. Temperature and fO_2 estimation using Fe-Ti oxides was therefore restricted to the alkaline basalts and basanites of the Tastepe, Ezine and Ayvacik Volcanics together with a few samples from the Nebiler Volcanics and the Kovacli Dyke Swarms.

Figure 5.19 shows the temperatures and fO_2 values estimated using a routine in the QUILF program developed by Andersen (1992) based on the model of Andersen (1988). Although some of the results obtained have large uncertainties (>50°C) due to

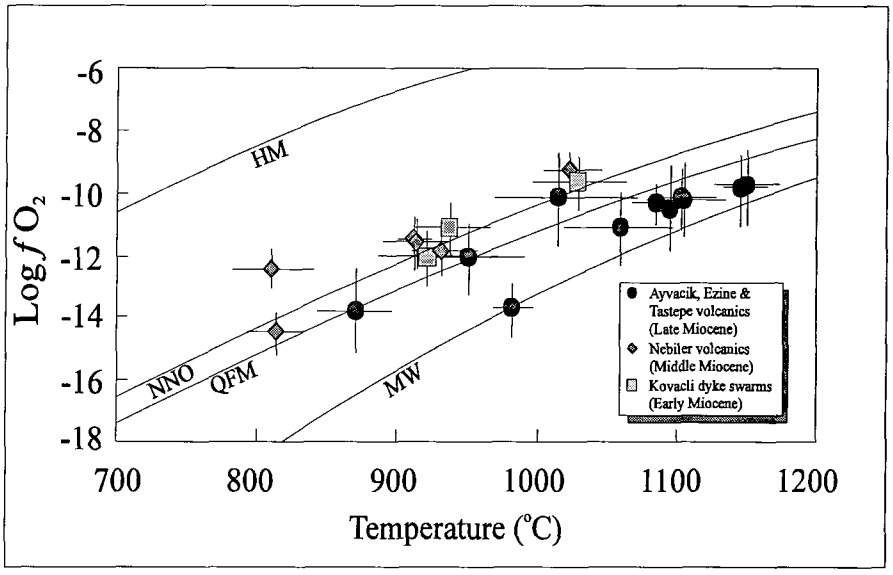

Figure 5.19. *Values of temperature and oxygen fugacity calculated from the composition of coexisting cubic (titanomagnetite) and rhombohedral (ilmenite) oxides. Curves define solid oxygen buffers corresponding to hematite-magnetite (HM, Myers and Eugster 1983), quartz-fayalite-magnetite (QFM, Berman 1988), magnetite-wüstite (MW, Myers and Eugster 1983) and nickel-nickel oxide (NNO, Huebner and Sato 1970). Error bars relate to the variation in oxide composition within the individual samples.*

significant quantities of minor elements (Al, Mg etc.) and to a high variation of oxide compositions within samples, only temperature estimates with uncertainties <50°C are plotted in Figure 5.19. The majority of Fe-Ti oxide pairs in the alkaline basalts and basanites yield temperatures that range from 870 to 1150°C. The temperature estimates lie between 800 and 1040°C for samples of the Nebiler Volcanics (e.g. EA350 and EA348) and between 910 and 1070°C for the Kovacli Dyke Swarms. Temperatures of the intermediate rocks of the Kovacli Dyke Swarms lie within the range of the temperatures obtained from the two-pyroxene geothermometer (850-1170°C; Table 5.1), although the number of coexisting oxide pairs is very limited for a precise comparison. The oxygen fugacities of the alkaline basalt and basanite samples are mostly slightly below the curve of the synthetic quartz-fayalite-magnetite (QFM) buffer of Berman (1988), although a few data points plot onto QFM buffer. On the other hand, the oxygen fugacities obtained from the basic-intermediate rocks of the Nebiler Volcanics and Kovacli Dykes Swarms fall just above the QFM buffer curve.

5.2.2. Pressure Estimates

5.2.2.1. Clinopyroxene geobarometer

Providing quantitative information about pressures at the time of crystallisation has a great importance in petrology because it can be used to estimate the depth of mineral crystallisation and hence the location of magma reservoirs. A number of workers have attempted to extract thermodynamic information from the chemical compositions of clinopyroxenes in basaltic systems, comparing the compositions of natural minerals with those of minerals synthesised at known pressure-temperature conditions (e.g. Green and Hibberson, 1970; Knutson and Green, 1975). It is, however, a difficult task to establish a general relationship between the pressure of crystallisation and the chemical composition of pyroxenes because of the great variance of magmatic systems. In recent years, some workers have attempted to relate the pressure effects to the structural parameters of natural clinopyroxenes using the sensitivity of cell and site volumes to crystallisation pressures, instead of using the chemical components (Dal Negro et al., 1989a,b; Bertolo et al., 1994; Salviulo, 1997). Most of these methods require crystal structural data that can be obtained from crystal chemical study of pyroxenes based on single-crystal X-ray diffraction (XRD).

Nimis (1995) combined experimental chemical and structural data to produce a

crystal-structure simulation that makes it possible to calculate the structural parameters of clinopyroxene from a known chemical composition without requiring direct X-ray diffraction (XRD) analyses. The empirical clinopyroxene geobarometer constructed by Nimis (1995) is mainly based on the relationship between cell volume (Vc) and M1-site volume (VM1). According to the author, the clinopyroxene geobarometer is applicable only to natural mega- or phenocrysts crystallised from melts of basaltic composition ($[Mg / (Mg + Fe^{2+})]_{cpx}$ = 0.7-0.9) excluding high-alumina basalts (Al_2O_3>18). The error in the calculation is also given by the same author to be within ± 2kbar in the range 0-24kbar. For this crystal-structure modelling, calculation of the distribution of Mg and Fe^{+2} between M1 and M2 sites has critical importance because calculations of the structural parameters or pressures directly from the chemical data are too sensitive to the site occupancies. Thus, this method should be used with caution.

The electron microprobe data of clinopyroxene phenocrysts from the Western Anatolian volcanic rocks were used to estimate the pressure of crystallisation according to the clinopyroxene geobarometer of Nimis (1995). Representative clinopyroxene analyses were selected according to the above restrictions on the use of this method. The results are presented in Figure 5.20 and Table 5.1.

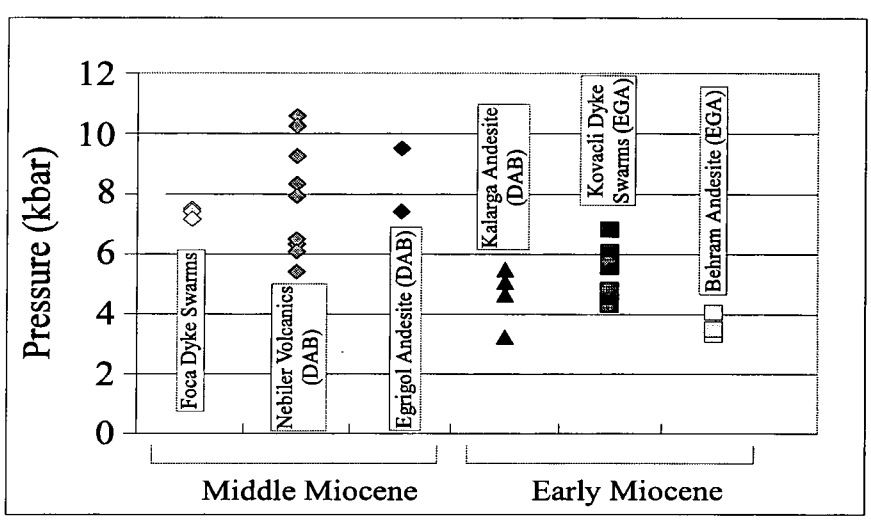

Figure 5.20. *Pressures estimated using clinopyroxene geobarometer of Nimis, 1995.*

Pressure estimates of clinopyroxenes from the Middle Miocene basic-intermediate rocks of the Foca Dyke Swarms, the Nebiler Volcanics and the Egrigöl Andesite are between 5.0 and 11.0kbar, but the majority is >7.0kbar. Pressure estimates of clinopyroxenes from the Early Miocene intermediate volcanic rocks including the

highly porphyritic rocks from both the EGA and DAB areas and Kovacli Dyke Swarms range between 3.0-7.0kbar and are generally lower than those obtained from Middle Miocene basic-intermediate rocks. Within the Early Miocene volcanic rocks from the EGA area, a remarkable difference can be observed between the pressure estimates of clinopyroxenes from the highly porphyritic lavas and those from the Kovacli Dyke Swarms. Clinopyroxenes from the highly porphyritic lavas (e.g. the Behram Andesite) yield pressure estimates in the range of 3.0-4.5kbar while the clinopyroxene pressure estimates from the Kovacli Dyke Swarms give a range of 4.0 to 7.0kbar.

5.2.2.2. Al-in-hornblende geobarometer

An empirical formulation of the Al-in-hornblende barometer was first produced by Hammarstrom and Zen (1986). This barometer is mainly based on pressures determined in adjacent aureole rocks. Subsequently, Hollister at al. (1987) calibrated the Al-in-hornblende barometer with a larger dataset to improve the method. Johnson and Rutherford (1989) and Thomas and Earnst (1990) have attempted to calibrate the barometer experimentally for the assemblage of quartz + alkali feldspar + plagioclase + hornblende + biotite + Fe-Ti oxides + titanite + melt + fluid. More recently, Schmidt (1992) used an experimental calibration conducted at near H_2O saturated solidus temperatures to produce a barometer.

All the proposed Al-in-hornblende barometers mentioned above use the linear increase in Al^{tot} content of magmatic hornblende with pressure and are given by following equations.

$P(\pm 3kbar) = -3.92 + 5.03Al^{tot}$ $r^2 = 0.80$ (Hammarstrome and Zen, 1986)

$P(\pm 1kbar) = -4.76 + 5.64Al^{tot}$ $r^2 = 0.97$ (Hollister et al. 1987)

$P(\pm 0.5kbar) = -3.46 + 4.23Al^{tot}$ $r^2 = 0.99$ (Johnson and Rutherford, 1989)

$P(\pm 0.6kbar) = -3.01 + 4.76Al^{tot}$ $r^2 = 0.99$ (Schmidt, 1992)

The electron microprobe data of amphibole phenocrysts from the Early-Middle Miocene intermediate rocks are used to estimate crystallisation pressures by applying the Schmidt (1992) Al-in-hornblende barometer. The results are illustrated in Figure 5.21 and Table 5.1. Amphibole phenocrysts of the samples from most of the highly porphyritic lavas of the DAB area (the Ballica volcanic Unit, the Akcapinar volcanic Unit and the Mt.Seyret volcanic Unit) generally yield similar pressure between 3.2 and

Table 5.1. Estmates of the magmatic intensive parameters for the volcanic rocks from Western Anatolia.

Area	EZINE - GULPINAR - AYVACIK (EGA)															
Age	Late Miocene					Early Miocene										
Formation name	*Ayvacik Volcanics*		*Ezine Volc.*	*Tastepe Volcanics*		*Kovacli Dyke Swarms*			*Behram Andesite*		*Ciceklik Andesite*		*Bademli Unit*		*Bakacak Unit*	
	Alkaline lavas					*Dykes*			*Highly porphyritic lavas*							
Sample no	*EA82b*	*EA270*	*EA415*	*EA252*	*EA256*	*EA45*	*EA412*	*EA418*	*EA37*	*EA275*	*EA78*	*EA73*	*EA273*	*EA231*	*EA62*	*EA67*
Rock type	Basanite	Basanite	Alk. Basalt	Alk. Basalt	Alk. Basalt	TracAnd	TracAnd	BasTraAnd	TracAnd	TracAnd	TracAnd	TracAnd	TracAnd	TracAnd	TracAnd	TracDacite
Range of Temperature (°C) (Two pyroxene thermometer) (Lindsley, 1983)						970-975 *[970]*	1080-1170 *[1100]*	830-920 *[910]*	750-930 *[865]*	810 - 970 *[880]*	950 - 980 *[965]*	765 - 810 *[785]*	760 - 935 *[850]*	840 - 910 *[870]*	750 - 890 *[870]*	790 - 810 *[800]*
Range of Temperature (°C) (Amphibole-Plagioclase therm.) (Holland & Blundy, 1994)													860 - 980 *[930]*	880 - 910 *[895]*		
Range of Temperature (°C) (Fe-Ti oxide thermometer) (Andersen, 1988)	870 - 1095 *[980]*	960 - 1058 *[1010]*	1100 - 1150 *1125]*	950 - 1145 *[1050]*	1104 - 1150 *1120]*			920 - 1050 *[960]*								
Range of Pressure (kbar) (Clinopyroxene geobarometer) (Nimis, 1995)						4.1 - 5.2 *[4.6]*		4.5 -7.0 *[5.2]*	3.0 - 4.5 *[4.0]*							
Range of Pressure (kbar) Al-in-hornblende barometer) (Schmidt, 1992)													6.4 - 9.1	3.1 - 6.2		
Oxygen fugacities (-Log fO2) (Andersen, 1988)	14.8 - 10.5	14.8 - 11.1	10.7 - 10.2	12.8 - 10.8	10.6 - 10.2			12.0 - 11.1								

Table 5.1. (Continued)

Area	DIKILI - AYVALIK - BERGAMA (DAB)											
Age	Middle Miocene							Early Miocene				
Formation name	*Foca Dyke Swa.*	*Nebiler Volcanics*					*Odaburnu Dyke Sw.*	*Egrigol Andesite*	*Kalarga Andesite*	*Akcapinar Unit*	*Ballica Unit*	*Karagol Unit*	*Mt. Seyret Unit*
		Lava flows					*Dykes*	*Lava flo/Do.*	*Highly porphyritic lavas*				
Sample no	*EA409*	*EA109*	*EA143*	*EA348*	*EA350*	*EA134*	*EA101*	*EA313*	*EA316*	*EA147*	*EA99*	*EA364*	*EA326*
Rock type	TracBasalt	BasTraAnd	BasAnd	BasAnd	BasTraAnd	BasTraAnd	BasTraAnd	Andesite	Dacite	Dacite	TracAnd.	TracAnd.	TracDacite
Range of Temperature (°C) (Two pyroxene thermometer) (Lindsley, 1983)								1000 - 1120 *[1095]*					
Range of Temperature (°C) (Amphibole-Plagioclase therm.) (Holland & Blundy, 1994)									810 - 970 *[930]*	850 - 880 *[865]*	790 - 880 *[830]*	850 - 950 *[900]*	830 - 860 *[850]*
Range of Temperature (°C) (Fe-Ti oxide thermometer) (Andersen, 1988)				830 - 930 *[880]*	870 - 1040 *[920]*								
Range of Pressure (kbar) (Clinopyroxene geobarometer) (Nimis, 1995)	7.4 -7.5 *[7.4]*		5.3 - 7.9 *[6.5]*			6.5 - 10.1 *[8.0]*	8.2 - 10.2 *[9.0]*	7.4 - 9.5 *[8.1]*	3.0 - 5.5 *[4.0]*				
Range of Pressure (kbar) Al-in-hornblende barometer) (Schmidt, 1992)								7.2 - 8.1 *[7.5]*	3.3 - 7.4	3.3 - 3.7 *[3.5]*	3.2 - 4.0 *[3.3]*	2.1 - 8.6	3.0 - 3.8 *[3.4]*
Oxygen fugacities (-Log fO2)				14.8 - 11.1	13.0 - 9.8								

4.0kbar. On the other hand, amphiboles of the Karagöl volcanic Unit and the Kalarga Andesite from the same area yield two different pressure estimates: one ranges between 2.1 and 3.8kbar (edenites) and the other ranges between 6.0 and 8.6kbar (pargasites-ferroan pargasites). This may be explained by more than one phase of amphibole crystallisation in magma chambers at different depths. The pressure estimates for the edenites from the Kalarga Andesite are between 3.0 and 3.8, which lies within the range of the pressure estimates obtained from the same samples using the pyroxene geobarometer (3.0 - 5.5kbar). Amphiboles from the Early Miocene, Bademli volcanic Unit of the EGA area also yield two different pressure estimates, namely 3.2 to 3.4kbar and 6.5 to 9.1kbar respectively. Pargasitic (or ferroan pargasitic) amphibole xenocrysts from the Middle Miocene, Egrigöl Andesite of the DAB area also yield high pressures of 7.2 - 8.1kbar.

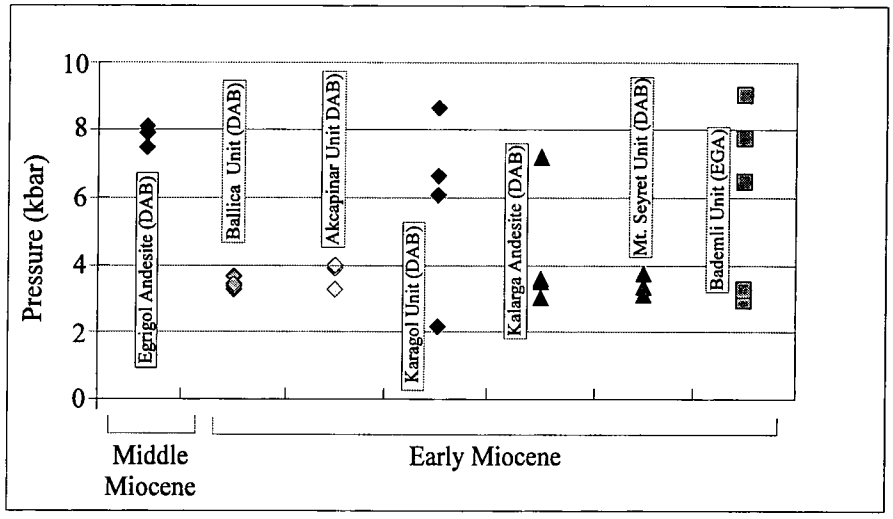

Figure 5.21. *Pressures estimated using Al-in-hornblende barometer of Schmidt, 1992.*

5.3. Chapter 5 Summary

Phenocryst phases (pyroxene and plagioclase) from most of the Early-Middle Miocene rocks show complex (normal and reverse) compositional zoning which may indicate a strong influence of mixing or crustal assimilation processes in their genesis.

The existence of hydrous mineral phases (e.g. phlogopite) and high fO_2 for the basic rocks of the Middle Miocene age may imply crystallisation from melts with high-H_2O contents.

A number of geothermometers, including two-pyroxene thermometer (Lindsley, 1983), amphibole-plagioclase thermometer (Holland and Blundy, 1994) and Fe-Ti oxide

thermometer (Lindsley et al., 1990) have been used to estimate the temperatures of crystallisation of the Western Anatolian volcanic rocks. Within the Early Miocene volcanic rocks, the highest temperatures of crystallisation have been obtained from the rocks of the Kovacli Dyke Swarms from the EGA area (850-1170°C) using the two-pyroxene and Fe-Ti oxide geothermometers. For the porphyritic lavas from the same area, the two-pyroxene geothermometry gave temperatures of crystallisation ranging between 750 and 980°C, but mostly >900°C. The temperatures of the porphyritic lavas from the DAB area have been estimated using the amphibole-plagioclase thermometer. The temperatures range between 790 and 970°C, but they are mostly <900°C.

For the Middle Miocene suites, the two-pyroxene and Fe-Ti oxide thermometers have been applied to estimate the temperatures of crystallisation for the intermediate and the basic rocks respectively. The temperatures range between 1000 and 1120°C and between 830 and 1040°C for the intermediate and basic rocks respectively. The temperature estimates obtained from the Middle Miocene rocks are generally higher than those obtained from the Early Miocene rocks.

For the Late Miocene, basic alkaline lavas the temperatures of crystallisation have been estimated using the Fe-Ti oxide geothermometer. They range between 870 and 1150°C, but are mostly >1050°C.

The pressures of crystallisation for the volcanic rocks have been estimated using the clinopyroxene geobarometer (Nimis, 1995) and the Al-in-hornblende barometer (Schmidt, 1992). For the Early Miocene rocks from both the EGA and the DAB areas, two distinct ranges of pressure have been obtained: one range between 2.1 and 4.0kbar and the other range between 6.0 and 9.1kbar. The significant difference between the two ranges has been attributed to more than one phase of crystallisation at different depths.

The pressure estimates for the Middle Miocene rocks are between 5 and 11kbar, but are mostly >7kbar.

For the Late Miocene alkaline rocks, the lack of hydrous mineral phases and Fe-Ti oxide equilibria indicate that the fO_2 was low and the magma was probably dry.

CHAPTER SIX

ISOTOPE SYSTEMATICS AND PETROGENESIS

Introduction

This Chapter is divided into two parts. The first part presents the Sr-Nd isotope characteristics of the volcanic rocks from Western Anatolia. The second part uses combinations of the major-trace element and isotopic data to describe the petrogenesis of the rocks and to establish a model for the genesis of the volcanic rocks. The petrogenetic modelling presented here is mainly based on the framework of assimilation and fractional crystallisation and melt modelling.

The isotope data used in this chapter were obtained on 9 whole-rock samples using the VG 354 5-collector thermal ionisation mass spectrometer of the London University radiogenic isotope facility at Royal Holloway College. The samples are representative of composition and age. Details of the sample preparation methods and analytical procedures are given in Appendix A.

6.1. Nd-Sr isotope characteristics of the volcanic rocks

The Nd and Sr isotopic ratios for the chosen samples are reported in Table 6.1. Notably, all the analysed calc-alkaline and shoshonitic rocks of the Early Miocene volcanic suites of the EGA area, and the Early-Middle Miocene volcanic suites from the DAB area, give a range of high $^{87}Sr/^{86}Sr$ ratios (0.707517 - 0.708681) and low $^{143}Nd/^{144}Nd$ ratios (0.512318 - 0.512460) (ε_{Nd} = -3.64 to -6.50). In contrast, the Late Miocene alkaline lavas of the EGA area are characterised by low $^{87}Sr/^{86}Sr$ ratios (0.703108 - 0.703253) and high $^{143}Nd/^{144}Nd$ ratios (0.512929 - 0.512978) (ε_{Nd} = +5.49 to +6.51).

Ercan et al. (1984) and Güleç (1991) also obtained isotope data from the volcanic rocks of Western Anatolia. Some of their samples were the Early-Middle Miocene, calc-alkaline and shoshonitic volcanic rocks collected from one part of the area studied in this thesis (the Dikili-Ayvalik-Bergama area) and the isotopes analysed are mainly Sr (Ercan et al., 1984) and Sr-Nd (Güleç, 1991). The data are reported in

Table 6.1. Nd-Sr isotope compositions for the volcanic rocks from Western Anatolia.

Sample	Locality and unit name	Rock Type	Age (Ma)	SiO_2 (wt %)	Rb (ppm)	Sr (ppm)	$(^{87}Sr/^{86}Sr)m$	$(^{87}Sr/^{86}Sr)i$	Sm (ppm)	Nd (ppm)	$^{143}Nd/^{144}Nd$	ε_{Nd}
EA270	Ayvacik (Ayvacik Volc.)	Basanite	8.3	41.81	21.3	1077.4	0.703108 ± 11	0.703101	12.40	65.62	0.512978 ± 5	6.51
EA249	Civler (Tastepe Volc.)	Alk. Basalt	11.0	49.97	17.9	505.9	0.703253 ± 12	0.703239	6.01	25.36	0.512929 ± 4	5.49
EA399	Dikili (Nebiler Volc.)	Tra.Basalt	15.2	49.82	62.8	797.0	0.707568 ± 10	0.707517	9.43	52.40	0.512460± 4	-3.64
EA348	Foca (Foca Dyke)	Basaltic And.	15.5	54.40	63.3	714.6	0.708147 ± 09	0.708091	5.35	28.84	0.512395 ± 5	-4.96
EA314	Bergama (Egrigol And.)	Tra.Andesite	15.5	60.32	108.4	441.1	0.708681 ± 29	0.708528	4.51	24.31	0.512372 ± 5	-5.40
EA101	Dikili (Odaburnu Dyke.)	Basaltic And.	16.0	56.32	103.9	907.8	0.707885 ± 29	0.707812	7.24	42.81	0.512398 ± 4	-5.00
EA147	Ayvalik (Akcapinar Unit)	Dacite	19.0	65.08	88.6	849.8	0.708505 ± 11	0.708421	6.19	35.96	0.512318 ± 4	-6.50
EA418	Ayvacik (Kovacli Dyke)	Basaltic And.	20.1	56.24	68.3	944.8	0.708351 ± 10	0.708290	7.06	43.49	0.512336 ± 4	-6.10
EA37	Assos (Behram And.)	Tra.Andesite	20.3	61.67	132.9	760.9	0.708601 ± 12	0.708456	6.48	42.10	0.512324 ± 5	-6.36

Table 6.2. Published Nd-Sr isotope compositions for the volcanic rocks from Western Anatolia.

Locality and (corresponding) unit name	Rock Type	Age ~(Ma)	SiO_2 (wt %)	Rb (ppm)	Sr (ppm)	$(^{87}Sr/^{86}Sr)i$	Sm (ppm)	Nd (ppm)	$^{143}Nd/^{144}Nd$	ε_{Nd}	Data source
Kula (Kula Basalts)	Basanite	< 1	45.48	27.0	1585.0	0.703534 ± 22	10.62	61.45	0.512851 ± 16	4.42	1
Kula (Kula Basalts)	Phonotephrite	< 1	46.10	64.0	1146.0	0.703334 ± 30	7.30	40.29	0.512921 ± 12	5.50	1
Kula (Kula Basalts)	Phonotephrite	< 1	46.31	72.0	1136.0	0.703229 ± 14	8.41	47.38	0.512936± 14	5.80	1
Kula (Kula Basalts)	Phonotephrite	< 1	47.20	76.0	912.0	0.703153 ± 26	6.62	35.54	0.512998 ± 16	6.80	1
Kula (Kula Basalts)	Phonotephrite	< 1	47.53	78.0	1016.0	0.703128 ± 30	7.09	39.62	0.512449 ± 18	6.10	1
Kula (Kula Basalts)	Phonotephrite	< 1	47.76	81.0	913.0	0.703240 ± 36	6.92	37.17	0.512998 ± 18	7.00	1
Kula (Kula Basalts)	Phonotephrite	< 1	48.43	58.0	953.0	0.703311 ± 22	7.01	38.19	0.512933 ± 18	5.70	1
Kula (Kula Basalts)	Basanite	7.5	46.10	79.0	946.0	0.703420					2
Kula (Kula Basalts)	Phonotephrite	0.03	47.13	78.0	868.0	0.702990					2
Kula (Kula Basalts)	Phonotephrite	0.02	46.36	80.0	961.0	0.703150					2
Bergama (Egrigol And.)	Andesite	15.0	60.40	80.0	700.0	0.707695 ± 32	4.89	26.95	0.512430 ± 20	-4.10	1
Bergama (Kalarga And.)	Andesite	17.0	62.13	136.00	636.0	0.708139 ± 32	8.44	50.29	0.512393 ± 12	-4.80	1
Bergama (Kalarga And.)	Andesite	17.0	61.12	181.00	557.0	0.707741 ± 24	7.99	44.92	0.512514 ± 24	-4.40	1
Bergama	Rhyolite		74.11	262.0	267.0	0.709139 ± 24	3.70	23.54	0.512362 ± 14	-6.40	1
Dikili (Karagol Vol.)	Dacite	20.0	64.22	205.0	482.0	0.707150					2
Bergama (Egrigol And.)	Andesite	15.0	57.88	106.0	423.0	0.708520					2
Ayvalik	Andesite	20.0	57.32	125.0	551.0	0.708360					2
Ayvalik (Seytansof. Ignim.)	Rhyolite	20	70.4	196.00	335.0	0.708320					2

Data source : (1) Gulec, 1991; (2) Ercan et al., 1985

Table 6.2 for comparison. The published data from the Quaternary, mafic alkaline lavas of the Kula area are also listed in Table 6.2. Although the Kula area is SE of the area studied (see Chapter 2 for details) and the Kula volcanism is not the subject of this thesis, they are comparable with the Late Miocene mafic alkaline lavas of the EGA area. This is because there is a close similarity between the mafic volcanic rocks of Kula and those of the Late Miocene mafic alkaline suite of the EGA area in terms of major and trace element compositions (Innocenti et al., 1982; Ercan et al., 1984; Güleç, 1991; Richardson-Bunbury, 1992).

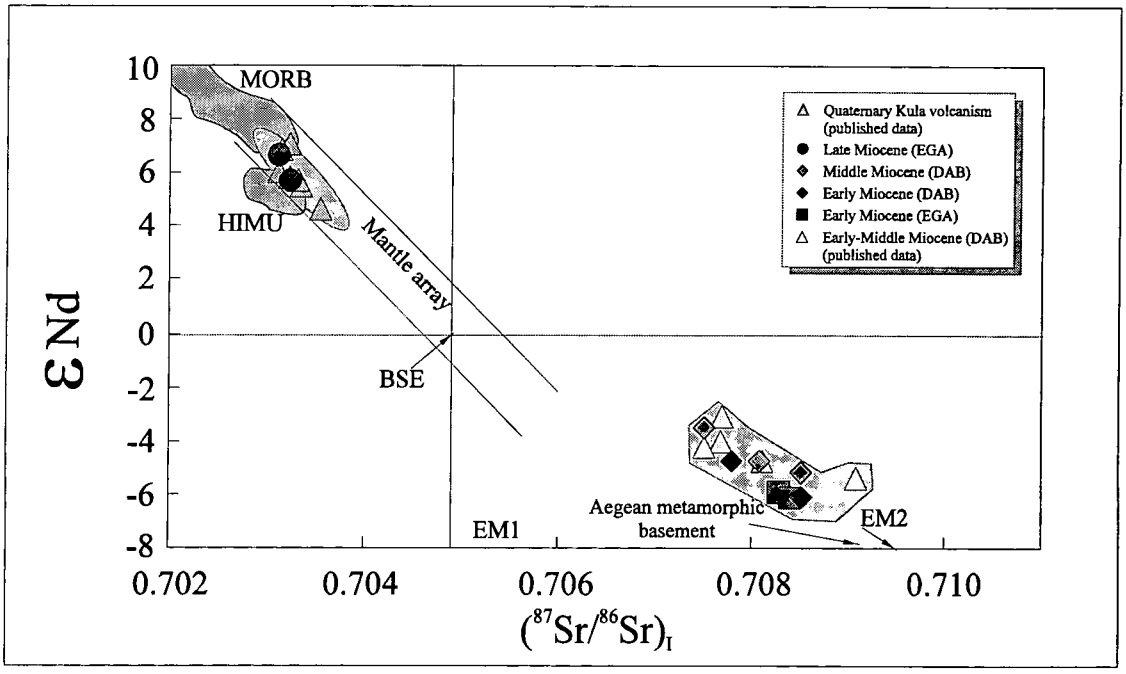

Figure 6.1. *The Nd-Sr isotope covariation shows that the Late Miocene alkaline rocks of Ayvacik and Tastepe Volcanics, together with the Quaternary alkaline rocks of Kula (Western Anatolia) plot in the mantle array, extending from MORB-OIB (HIMU)-like compositions towards Bulk Earth. The Early-Middle Miocene calc-alkaline and shoshonitic rocks plot in the enriched quadrant. MORB and HIMU compositions are from Zindler and Hart (1986), BSE (Bulk Silicate Earth) and enriched mantle compositions (E1 and E2) are from Hart et al. (1992). The Aegean basement rocks are from Briqueu et al. (1986).*

In Figure 6.1, the isotope data from Table 6.1, together with the published data from the volcanic rocks of the DAB area and the alkaline lavas of Kula, have been plotted on diagram of ε_{Nd} against $(^{87}Sr/^{86}Sr)_I$ (Sr initial ratio). Also plotted for comparison are the MORB and HIMU fields (Zindler and Hart, 1986), Bulk Silicate Earth, enriched mantle end-members (EM1 and EM2) (Hart et al., 1992) and metamorphic basement rocks from the Aegean area (Briqueu et al., 1986). Volcanic rocks from Western Anatolia as a whole show a curvilinear trend on a ε_{Nd} versus

$(^{87}Sr/^{86}Sr)_I$ diagram. The Late Miocene alkaline lavas of the EGA area (the Ayvacik and Tastepe Volcanics in Table 6.1) and the Quaternary lavas of the Kula area plot within the mantle array and extend from MORB-like compositions towards Bulk Earth. The Early Miocene volcanic rocks from the EGA area (the Behram Andesite and the Kovacli Dyke Swarms in Table 6.1) and the Early-Middle Miocene volcanic rocks from the DAB area (the Foca Dyke Swarms, the Nebiler Volcanics, the Egrigöl Andesite, the Odaburnu Dyke Swarms and the Akcapinar Unit in Table 6.1), together with the published data from the same area, are, however, displaced from the mantle array with higher $^{87}Sr/^{86}Sr$ initial ratios and lower ε_{Nd} values. All samples in this group are displaced into the enriched quadrant relative to Bulk Earth and show a linear trend extending towards the compositions of the metamorphic basement rocks (Briqueu et al., 1987). Samples from the Early Miocene volcanic suites of the EGA and DAB areas may, however, be distinguished by their slightly lower ε_{Nd} values with respect to the Middle Miocene volcanic rocks of the DAB area at given $^{87}Sr/^{86}Sr$ ratios.

In Figure 6.2, the initial $^{87}Sr/^{86}Sr$ ratios have been plotted against the SiO_2 and the Rb contents of the volcanic rocks respectively to carry out a preliminary evaluation into the role of assimilation and fractional crystallisation (AFC) processes in their magma genesis. Both diagrams show two distinct trends. The Late Miocene mafic alkaline rocks of the EGA area together with the Quaternary alkaline rocks of Kula show fairly constant $^{87}Sr/^{86}Sr$ initial ratios with an increase in SiO_2 content from 41.81 to 49.97 wt.% and an increase in Rb content from 17.8 to 80.0 ppm. This can be explained either by a variable degree of partial melting and/or by a variable fractional crystallisation of an isotopically homogeneous source. In both cases, however, contamination from continental crust can be ruled out for these mafic alkaline rocks.

The calc-alkaline and shoshonitic rocks of the Early Miocene suites from the EGA area and of the Early-Middle Miocene suites from the DAB area are, however, characterised by high and slightly variable $^{87}Sr/^{86}Sr$ initial ratios. Figure 6.2 shows that the most primitive sample (49.82 wt.% SiO_2) of these Early-Middle Miocene rocks has a $^{87}Sr/^{86}Sr$ initial ratio as high as 0.707517 indicating derivation from a source that had been modified by earlier additions of material having high Rb/Sr and/or Sr isotope ratio, most probably a subduction-modified mantle source. The rocks from all the Early-Middle Miocene suites follow a low angle, linear trend in which $^{87}Sr/^{86}Sr$ ratios only increase slightly (from 0.7075 to 0.7091) for a significant increase in SiO_2 (from 49.82

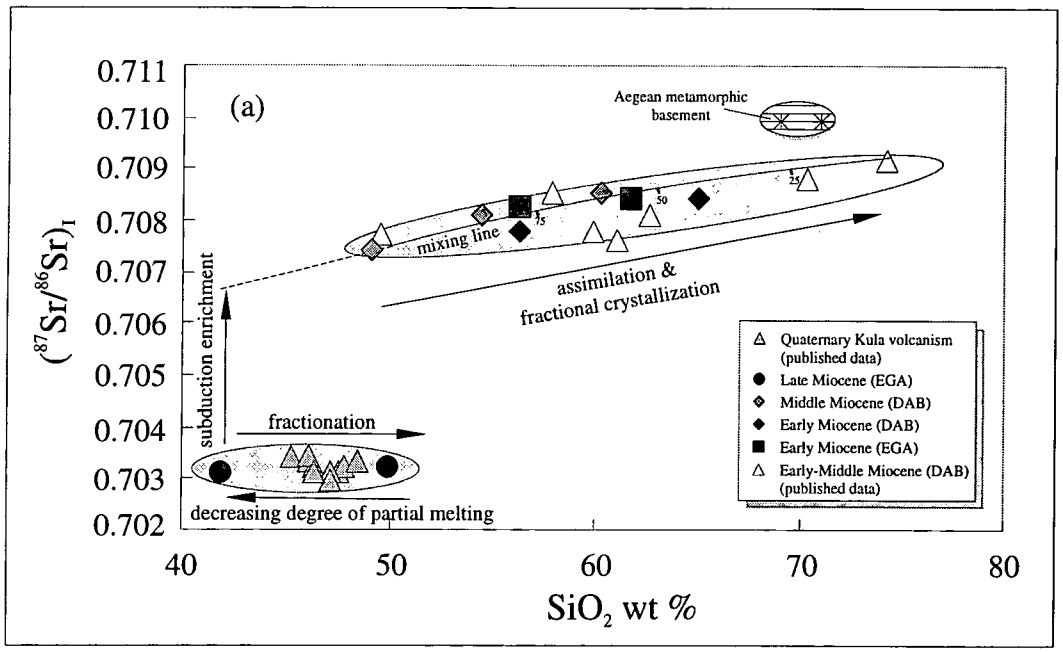

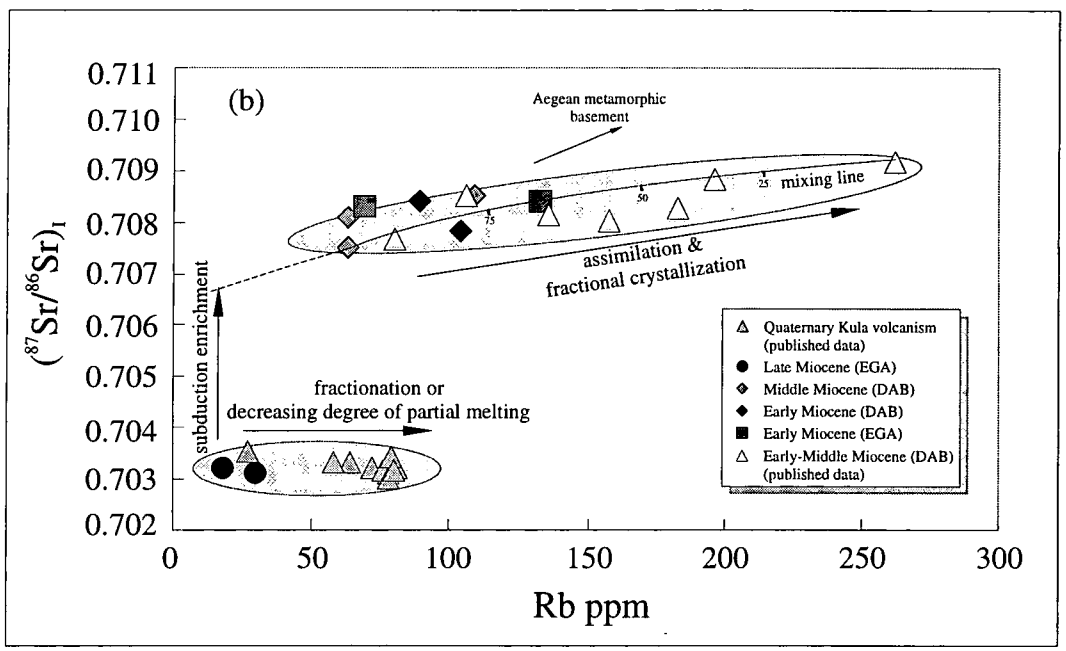

Figure 6.2. *Plots of Sr initial isotope ratios against (a) silica and (b) Rb contents highlighting subduction metasomatism and assimilation-fractional crystallisation (AFC) processes for the volcanic rocks from Western Anatolia.*

to 75.08 wt.%) and in Rb (from 63.2 to 262.1 ppm) contents. These increases indicate that the line between the most basic and the most acidic members of these volcanic rocks represents an AFC trend. Extrapolation of this trend to low SiO_2 gives a mantle with extremely high $^{87}Sr/^{86}Sr$ initial ratio. Extrapolation to high SiO_2 gives a possible contaminant end-member. Note that the flat trend results because the mantle and the crustal end-members have similar and high $^{87}Sr/^{86}Sr$ initial ratios. Plots in Figure 6.2 may also suggest that all the calc-alkaline and shoshonitic rocks were generated from similar sources and that the compositional differences between the Early- and Middle-Miocene rocks (from both the EGA and DAB areas) are mainly controlled by AFC processes.

In accordance with the behaviour of trace elements, as previously described in Chapter 3, isotopic ratios of the volcanic rocks from Western Anatolia also support the hypothesis that the alkaline and calc-alkaline/shoshonitic volcanic rocks are unlikely to have generated from a single source. Two different sources can therefore be considered for the Western Anatolian volcanic rocks: (1) a subduction modified, radiogenic mantle source characterised by high $^{87}Sr/^{86}Sr$ but low $^{143}Nd/^{144}Nd$ ratios (for the Early - Middle Miocene, calc-alkaline and shoshonitic volcanic rocks); and (2) an isotopically homogeneous and possibly OIB-type mantle source characterised by low $^{87}Sr/^{86}Sr$ but high $^{143}Nd/^{144}Nd$ ratios (for the Late Miocene (and Quaternary) alkaline volcanic rocks).

6.2. Petrogenesis of The Volcanic Rocks

This section aims to identify the petrogenetic processes that produced the magma(s) and affected the primary magma compositions. The preliminary observations obtained from the major-trace element and isotopic characteristics of the volcanic rocks from Western Anatolia have shown that the petrogenetic processes (e.g. the source region characteristics and assimilation-fractional crystallisation) which produced the Early-Middle Miocene calc-alkaline-shoshonitic volcanic rocks differ from those which affected the nature of the Late Miocene alkaline volcanic rocks. The petrogenesis of these rocks will therefore be investigated in two separate parts.

6.2.1 Petrogenesis of The Calc-alkaline and Shoshonitic Volcanic Rocks (Early-Middle Miocene)

6.2.1.1 Crystallisation history of the volcanic rocks

The observed mineral phases in the volcanic rocks represent the fractionating mineral assemblages: (1) plagioclase, clinopyroxene, orthopyroxene, olivine, Ti-magnetite and biotite with minor ilmenite for the Early Miocene rocks from the EGA area; (2) plagioclase, clinopyroxene, amphibole, Ti-magnetite and biotite for the Early Miocene rocks from the DAB area; and (3) clinopyroxene, olivine, plagioclase, Ti-magnetite and ilmenite for the Middle Miocene rocks.

Quantitative modelling of fractional crystallisation has been carried out to evaluate the variations in trace element concentrations. Theoretical fractionation trends for the crystallisation of a particular mineral or relevant mineral assemblages from the magma are drawn and compared with observed trends. The Rayleigh equation used to calculate the theoretical fractionation vectors is:

$C_L / C_0 = F^{(D-1)}$ where

C_L: weight concentration of a trace element in the liquid
C_0: the weight concentration of a trace element in the parental liquid
F: the fraction of melt remaining
D: bulk distribution coefficient of the fractionation assemblage during crystal fractionation.

The mineral/melt partition coefficients of trace elements used here for the modelling (e.g. olivine, clinopyroxene, plagioclase, hornblende, biotite, orthopyroxene and garnet in basic-intermediate-acid compositions) have been taken from a compilation of Keskin (1994; unpublished Ph.D. Thesis) (Table 6.3).

For fractional crystallisation modelling, Th and Rb are used as fractionation indexes because they are highly incompatible, resulting in a good positive correlations with silica contents for all rocks except the crystal-free ignimbrites from the EGA area for which Rb contents decrease and Th contents stay mostly constant with increasing silica (Section 3.2.1). In Figure 6.3, Y concentrations are plotted against Th, together with calculated fractionation vectors to examine possible crystallisation phases for the calc-alkaline and shoshonitic volcanic rocks. The data were plotted as three different series. These are: (1) the Early Miocene rocks from the EGA area (note that the rocks from the porphyritic lavas and the Kovacli Dyke Swarms do not exhibit discrete patterns and therefore were plotted together; and that the crystal-free ignimbrites are excluded for the reason mentioned above); (2) the Early Miocene rocks from the DAB area; and

Table 6.3. Partition coefficients used for fractional crystallisation modelling (partition coefficient values are from Keskin, 1994)

	Cs	Rb	Ba	Th	U	Ta	Nb	La	Ce	Sr	Nd	Zr	Hf	Sm	Eu	Gd	Tb	Dy	Y	Ho	Er	Tm	Yb	Lu
PLAGIOCLASE																								
Basic	0.023	0.05	0.23	0.004	0.018	0.018	0.01	0.12	0.1	1.2	0.12	0.01	0.015	0.085	0.3	0.08	0.035	0.08	0.03		0.07		0.045	0.03
Intermediate	0.045	0.13	0.5	0.015	0.04	0.025	0.025	0.23	0.18	2.6	0.17	0.03	0.04	0.15	0.95	0.13	0.07	0.1	0.06	0.15	0.1	0.2	0.07	0.05
Acid	0.095	0.3	0.9	0.04	0.1	0.04	0.06	0.43	0.3	6	0.25	0.1	0.1	0.2	3	0.2	0.15	0.13	0.15		0.18		0.1	0.075
SANIDINE																								
Basic		0.1	0.04			0.007			0.008	0.3		0.1			0.3		0.1						0.001	
Intermediate		0.18	0.5	0.008		0.009			0.017	0.9		0.15	0.02	0.01	1								0.003	0.002
Acid		0.25	6	0.015	0.025	0.013		0.05	0.035	3	0.04	0.25	0.025	0.02	6.5		0.015						0.008	0.006
AMPHIBOLE																								
Basic		0.1	0.45	0.05	0.08	0.25	0.3	0.2	0.35	0.45	0.65	0.4	0.5	0.85	0.8	0.95	1.2	1.3	1.1	1	0.9	0.9	0.8	0.8
Intermediate		0.13	0.5	0.1	0.16	0.6	1	0.5	0.7	0.6	1.7	0.5	0.75	2.3	2	2.7	3.4	3.3	3	3	3	2.8	2.5	2
Acid		0.15	0.6	0.2	0.3	1.5	3.5	1.5	1.7	0.8	4	0.65	1.3	6	5	7.5	8	9	9	10	8.5	8.5	7	6
BIOTITE																								
Basic	1	2.5	4.5	0.075	0.1	0.4	0.45	0.035	0.03	0.08	0.04		0.14	0.03	0.04	0.03	0.03	0.035	0.2		0.03		0.04	0.03
Intermediate	1.6	3.2	6	0.15	0.15	0.7	1.4	0.15	0.16	0.15	0.2	0.15	0.25	0.17	0.15	0.7	0.55	0.65	0.8		0.4		0.45	0.45
Acid	2.5	4.5	7.5	0.35	0.3	1.3	3.5	0.5	0.75	0.25	0.9	0.5	0.45	0.6	0.6	0.7	0.55	0.65	0.8		0.4		0.45	0.45
CLINOPYROXENE																								
Basic	0.003	0.035	0.05	0.03	0.02	0.06	0.04	0.15	0.15	0.06	0.4	0.1	0.2	0.4	0.6	0.7	0.9	0.7	0.55	0.6	0.7		0.6	0.6
Intermediate	0.03	0.06	0.15	0.1	0.07	0.15	0.2	0.4	0.4	0.09	1	0.25	0.3	1.2	1.4	1.5	2	1.5	1.2	1.5	1.5	0.8	1.3	1.5
Acid	0.35	0.1	0.4	0.35	0.2	0.35	0.8	1.2	1	0.15	2.5	0.6	0.5	3	3	3	4	3.5	2.5	3.2	2.6		2.5	3
ORTHOPYROXENE																								
Basic		0.003	0.002	0.13	0.035	0.15	0.15	0.025	0.01	0.007	0.02	0.03	0.055	0.03	0.02	0.06	0.07	0.1	0.2	0.15	0.2	0.1	0.2	0.2
Intermediate	0.15	0.025	0.01	0.15	0.07	0.25	0.2	0.2	0.1	0.03	0.3	0.09	0.1	0.3	0.15	0.25	0.4	0.4	0.45	0.5	0.3	0.4	0.5	0.5
Acid	0.5	0.2	0.2	0.16	0.15	0.5	0.7	1.5	1.5	0.7	2.5	0.25	0.2	2.5	0.9	1.2	2	1.5	1	2	0.6	1.5	1.5	1.5
OLIVINE																								
Basic	0.0004	0.002	0.002	0.04	0.045	0.04	0.01	0.04	0.01	0.002	0.01	0.01	0.03	0.01	0.01		0.04	0.015	0.01				0.025	0.15
Intermediate	0.0004	0.035	0.01	0.1	0.1	0.1	0.01	0.15	0.06	0.02	0.06	0.01	0.06	0.05	0.06		0.1	0.07	0.01				0.15	0.35
Acid				0.3	0.2	0.25	0.01	0.6	0.4		0.4	0.01	0.15	0.2	0.3		0.25	0.35	0.01				0.7	0.8
GARNET																								
Basic		0.001	0.001				0.1	0.03	0.03	0.002		0.3	0.3	0.5	0.35	2.4	1.3		2	3		1	5.5	10
Intermediate		0.005	0.006				0.1	0.1	0.15	0.008		0.6	1	1.2	0.9	5	4	15	12	10		3.5	17	25
Acid		0.02	0.02				0.1	0.4	0.7	0.05	0.7	1.3	4	3	2	12	15	30	35	35		10	50	60

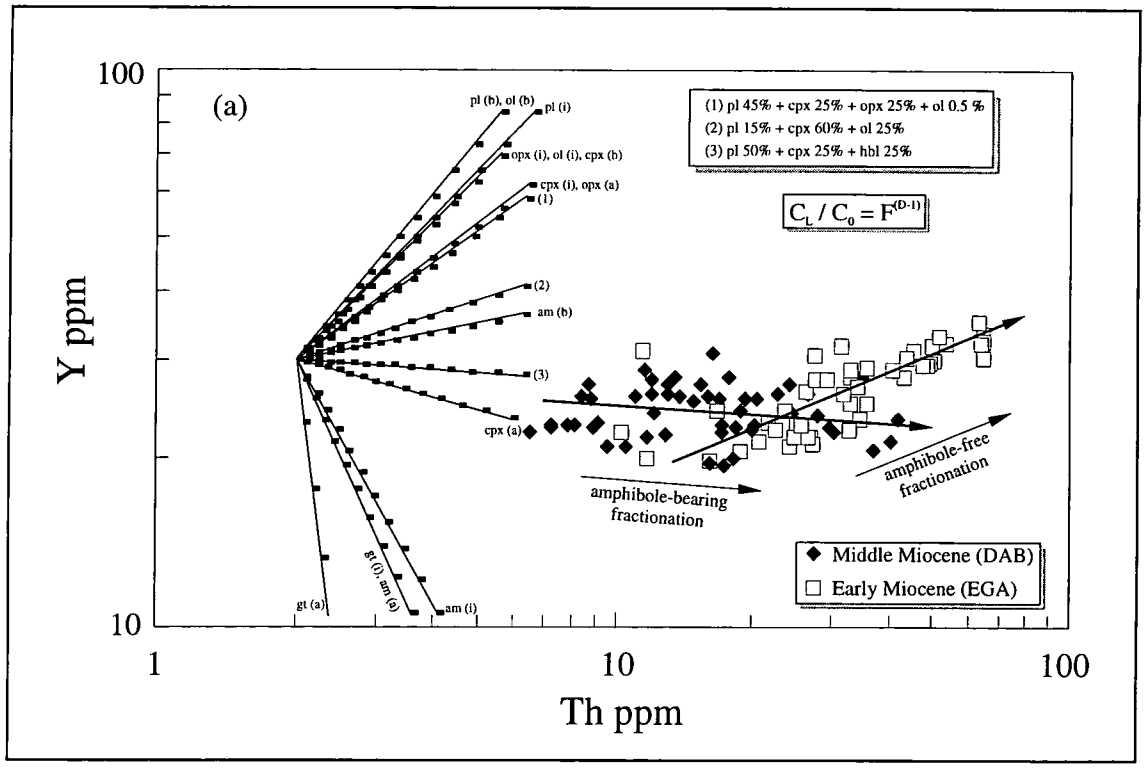

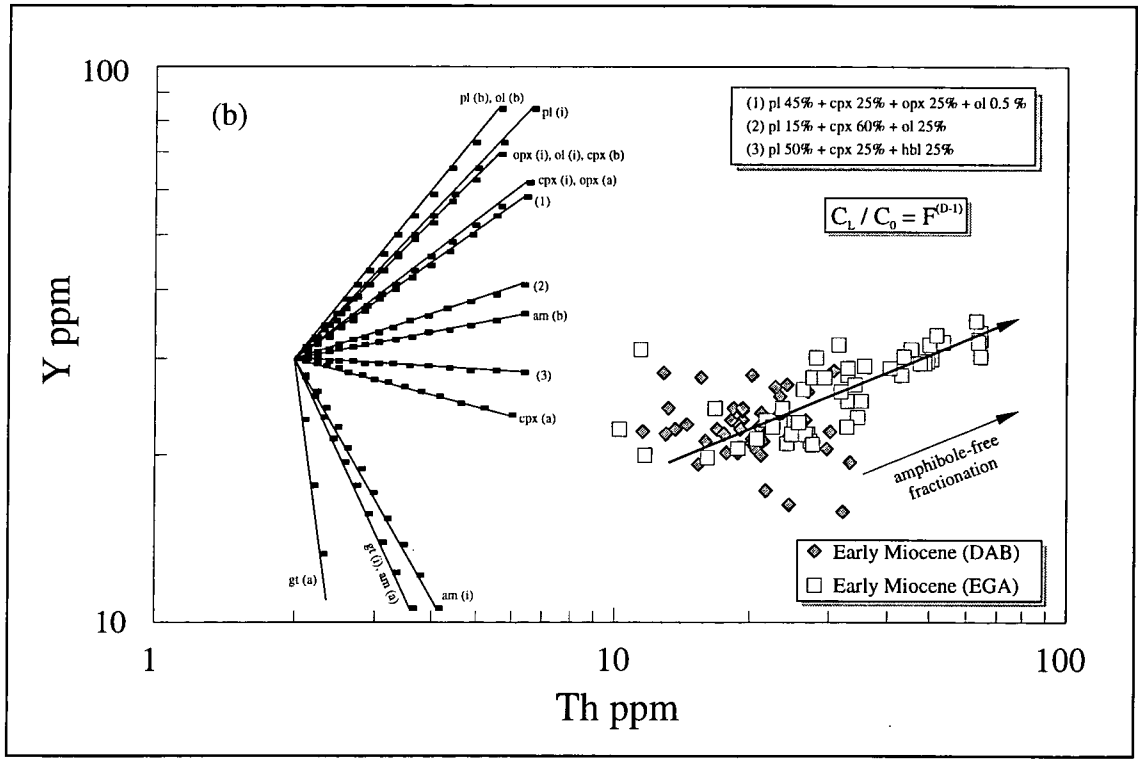

Figure 6.3. *Y against Th log-log diagram showing theoretical Rayleigh fractionation vectors modelled for crystallisation of individual mineral phases and also phase assemblages. Phase combinations ar e presented in the inset. Thick marks on each vector correspond to 5% crystallisation intervals.*
Key to abbreviations: am: amphibole, ol: olivine, cpx: clinopyroxene, opx: orthopyroxene, pl: plagioclase, bi: biotite, gt: garnet, b: basic, i: intermediate, a: acid.

(3) the Middle Miocene rocks from the DAB area. The rocks from the DAB area were plotted in two different diagrams in order to avoid overlap between the data points of the Early and Middle Miocene rocks, but the rocks from the EGA area were plotted in both diagrams for comparison.

It can be seen that the data points generally follow two distinct trends. The Y content of the Early Miocene volcanic rocks from the EGA area exhibit a good positive correlation with Th content which can be explained by plagioclase, orthopyroxene, clinopyroxene and olivine crystallisation according to the theoretical Rayleigh vectors. The theoretical vector calculated using the average mineral assemblage of the Early Miocene volcanic rocks of the EGA area ($plg_{[45\%]}$ + $opx_{[25\%]}$ + $cpx_{[25\%]}$ + $olv_{[5\%]}$) (shown as vector 1 in Fig. 6.3) is also consistent with the observed fractionation trend.

In accordance with observed phenocryst assemblages, fractional crystallisation modelling also indicates an amphibole-free fractionation for the volcanic rocks from the EGA area. However, this does not completely rule out early amphibole crystallisation, as amphibole phenocrysts might have been resorbed. Supporting this is the existence of a minor amount of resorbed amphibole phenocrysts in some of the rocks in this area.

The Y contents of the Middle Miocene basic-intermediate rocks from the DAB area, on the other hand, slightly decrease or stay constant with increasing Th contents (Fig. 6.3a). As mentioned in Chapter 4, the observed phenocryst assemblage for these rocks is predominantly clinopyroxene, olivine and plagioclase. However, the theoretical vector calculated using the average mineral assemblage of these rocks ($cpx_{[60\%]}$ + $plg_{[15\%]}$ + $olv_{[25\%]}$) (shown as vector 2 in Fig. 6.3) is not consistent with the observed fractionation trend. This results because, even domination of clinopyroxene (a mineral with the highest distribution coefficient for Y ($^{cpx\text{-}liq}Kd_Y \approx 0.55$) after garnet ($^{gt\text{-}liq}Kd_Y \approx 2.0$) and amphibole ($^{amp\text{-}liq}Kd_Y \approx 1.1$) at basic compositions) cannot create a negative trend between Y and Th. An Y retaining phase is therefore needed to explain the fractionation history of these rocks. Although garnet fractionation could explain Y depletion, there is no petrographic evidence for garnet fractionation in any of the volcanic rocks from Western Anatolia. Thus, amphibole fractionation is the most likely Y-retaining phase for the Middle Miocene basic-intermediate rocks. Although most of the rocks of Middle Miocene age do not contain amphibole phenocrysts or microphenocrysts (which occur in the Egrigöl Andesite only), earlier amphibole fractionation is evident from the significant amount of amphibole in the phenocryst

phases of the Early Miocene volcanic rocks from the same (DAB) area. The Early Miocene volcanic rocks from the DAB area themselves, however, show no clear trend on an Y versus Th log-log diagram. This may be explained by their highly porphyritic nature and variable content of amphibole phenocrysts (Fig. 6.3b). However, most of them still have lower Y concentrations relative to the rocks from the EGA area.

Similar fractional crystallisation modelling has been carried out for the middle rare earth element (MREE) of Sm which is an effective indicator of amphibole fractionation (Fig 6.4). Since Sm has high distribution coefficients for amphibole ($^{amp\text{-}liq}Kd_{Sm} \approx 0.85\text{-}6.0$), its concentration in the melt is strongly controlled by amphibole fractionation. The trends are consistent with the earlier modelling (Y v Th) and support the hypothesis that the contrast in trace element behaviour between the volcanic rocks from the EGA and DAB areas reflects two different fractionation assemblages.

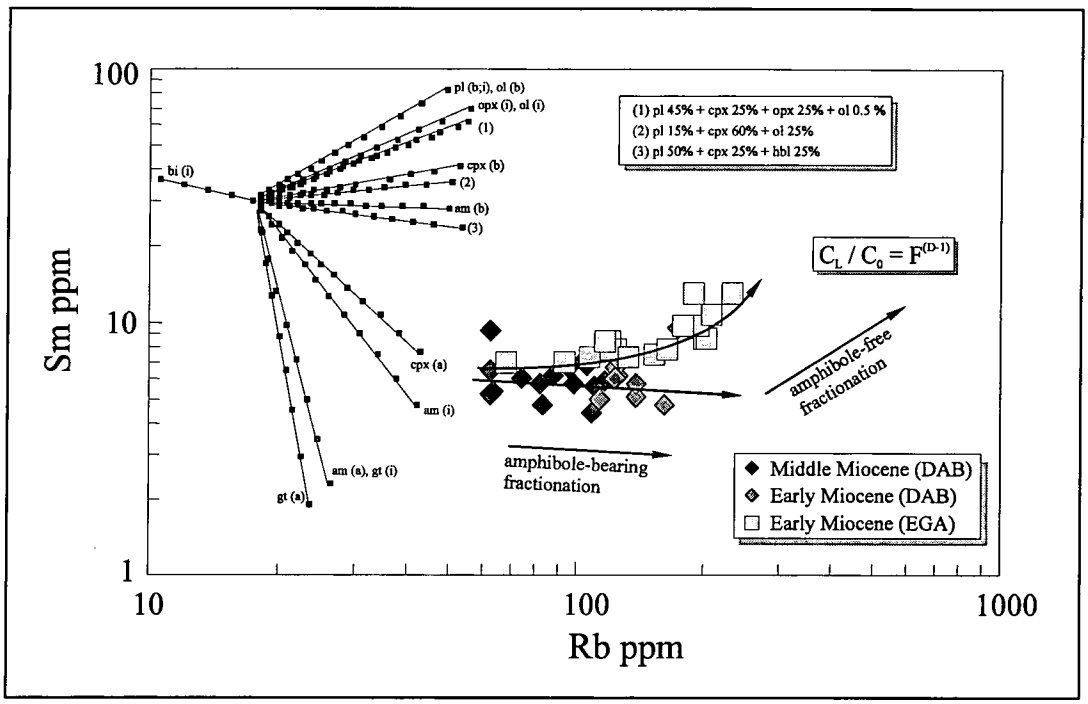

Figure 6.4. *Log-Log diagram of Sm against Rb showing the contrast in REE behavior between the volcanic rocks from the EGA and DAB areas.*

As previously mentioned, the Rb content of most crystal-free ignimbrites, unlike that of the other volcanic rocks, decreases with increasing silica. In order to evaluate the extent to which fractionation phase or phases control trace element distribution, Sr was plotted against Rb on the log-log variation diagram on which theoretical Rayleigh fractionation vectors were modelled for the removal of individual minerals (Fig. 6.5). It can be seen that the both Sr and Rb concentrations decrease with fractionation

(monitored by the silica contents of the rocks), which should imply plagioclase- and biotite-dominated fractional crystallisation for these high-silica pyroclastic rocks. The rocks themselves are mostly crystal-free and show no indication of which crystal assemblages were effective in their genesis. However most of the ignimbrites, which are cogenetic with the crystal-free ignimbrites, have variable proportions of plagioclase, K-feldspar and biotite phenocrysts that can account for the observed fractionation trend in Figure 6.5. The trend on Figure 6.5 also emphasises that the fractional crystallisation was more effective than crustal assimilation in the genesis of the ignimbrites. This is equally evident from the negative correlation between the Rb (and Th) and the silica contents.

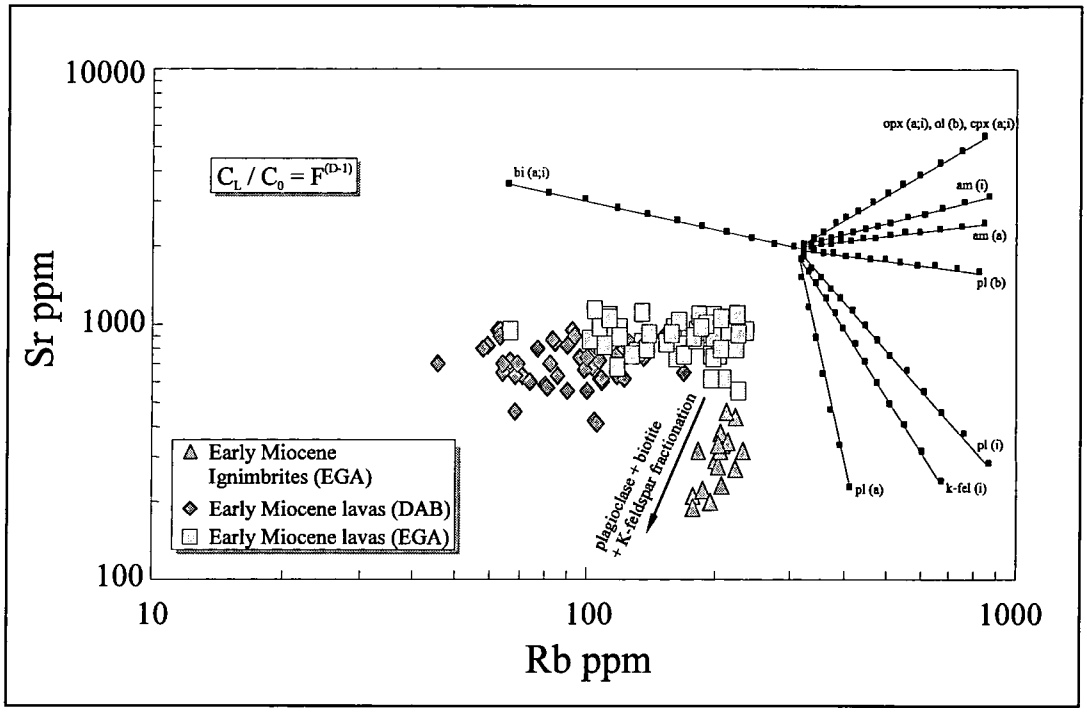

Figure 6.5. *Log-Log diagram of Sr against Rb highlights the possible fractionation trend of the crystal-free ignimbrites from the EGA area.*

Figure 6.6 shows that most calc-alkaline and shoshonitic volcanic rocks of the Early-Middle Miocene age, as mentioned in Section 3.2.2, have Eu/Eu* ratios less than 1.0 (ranging between 0.97-0.56). The presence of negative Eu anomalies should generally result from plagioclase fractionation. This is because Eu (present in the divalent state) is compatible in plagioclase (particularly in acid and intermediate compositions; $^{plg\text{-}liq}Kd_{Eu}$ = 1.0-6.5), in contrast to the trivalent REE which are incompatible. Alternatively, mixing of mafic magmas with components formed by

crustal melting with a plagioclase-rich residue can create a negative Eu anomaly. For the calc-alkaline and shoshonitic rocks of Western Anatolia, these alternatives are illustrated in Figure 6.6 where Eu anomalies were plotted against silica contents. Figure 6.6 shows that the Eu anomalies for most of the calc-alkaline and shoshonitic rocks are related to increasing silica content. The theoretically-calculated, plagioclase fractionation-dominated AFC line and the bulk mixing line between the most mafic rock (with 49.82 wt.% SiO_2) and the most acidic rock (with 79.9 wt.% SiO_2) follow similar trends and do not provide a definitive answer to whether they reflect plagioclase fractionation or crustal contamination. However, taking into account the fact that most of the rocks contain substantial amount of plagioclase phenocrysts, it can be argued that the Eu anomalies are mostly reflections of plagioclase fractionation, although crustal contamination may contribute. The observed negative correlation between the Eu anomalies and the silica contents of the ignimbrites also reveals a greater fractional crystallisation effect than contamination.

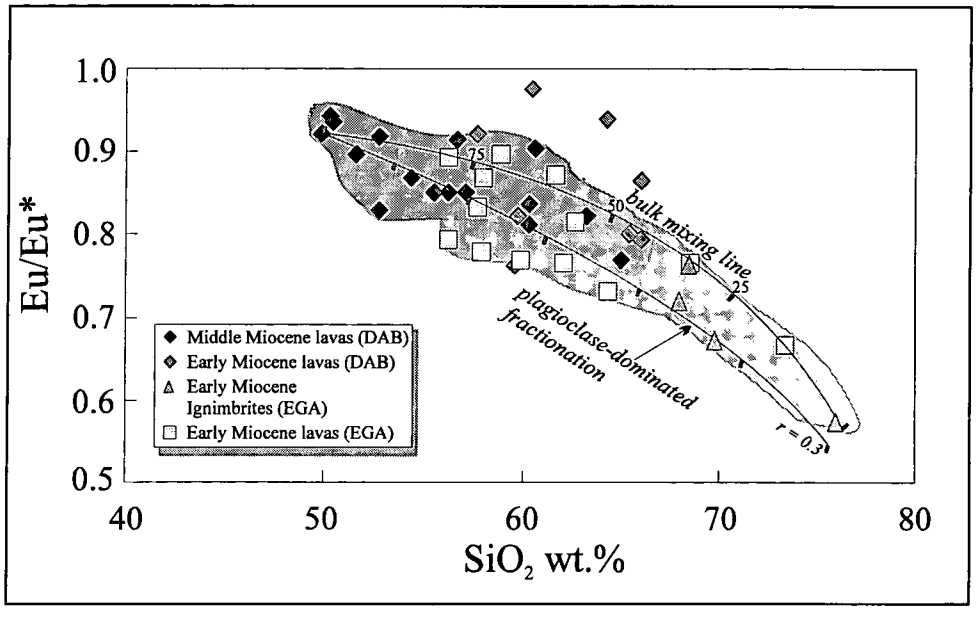

Figure 6.6. *Plot of Eu/Eu* (Eu anomalies) against silica showing the possible effects of plagioclase fractionation or contamination from plagioclase fractionated crustal material. The mixing line is for simple mixing between the most basic and the most acidic rocks. Numbers on the line are percentage of the most basic member in the modelled mixture. AFC line is representative for r = 0.3 and is drawn for a mineral assemblage of plg(60) + cpx(20) + amp(10) + opx(10).*

6.2.1.2 Assimilation combined with fractional crystallisation (AFC)

6.2.1.2.1 Evidence for assimilation and/or mixing: Overview

Petrographic and mineral chemical data provide the most compelling evidence that assimilation and/or mixing has taken place. In particular, the complex zoning patterns shown by the pyroxene and plagioclase phenocrysts in most rocks are difficult to reconcile with a simple, isobaric, fractional crystallisation. Furthermore, as mentioned in Section 6.1, the positive, curvilinear, correlation between Sr isotopic ratios and silica contents (Fig. 6.2) emphasises that crustal contamination was one of the most important processes in the magmatic evolution of the Western Anatolian volcanic rocks.

Crustal contamination can be modelled comparing observed trends or values of the data points and theoretical AFC curves on trace element and/or isotope ratio graphs. This type of modelling shows the amount of change that would take place when the end-members of known (or, in some cases, estimated) compositions are mixed during assimilation and fractional crystallisation.

Simultaneous assimilation and fractional crystallisation (AFC) has been modelled by numerous of workers (O'Hara, 1977; Allegre and Minster, 1978; Langmuir et al., 1978; DePaolo and Wasserburg, 1979; Taylor, 1980; DePaolo, 1981; Taylor and Sheppard, 1986; Aitcheson and Forrest, 1994; Roberts and Clemens, 1995). One of the most popular and widely employed equations is that of DePaolo (1981). His equations used here for AFC modelling are summarised below:

$$C_m/C_{mo} = F^{-z} + [r/(r-1)]\,[C_a/zC_{mo}]\,[1-F^{-z}] \quad \text{(not applicable for r = 1)}$$

$$C_m/C_{mo} = 1 + [r/(r-1)]\,[C_a/C_{mo}]\,lnF^{-z} \quad \text{(for the case of r+D = 1 and z = 0)}$$

$$[\varepsilon_m - \varepsilon_{mo}] / [\varepsilon_a - \varepsilon_{mo}] = 1 - (C_{mo} / C_m)F^{-z} \quad \text{(for the isotope ratios)}$$

where

$F = M_m/M_{mo}$ *(the ratio of magma mass to original magma mass)*
$r = M_a/M_c$ *(the ratio of the rate of assimilation to fractional crystallisation)*
$z = [r+D-1]/[r-1]$
M_m = *mass of magma*
M_{mo} = *initial mass of magma*
M_c = *crystallisation rate (mass/unit time)*
M_a = *assimilation rate (mass/unit time)*
C_a = *elemental concentration in wall-rock*
C_m = *elemental concentration in magma*
C_{mo} = *original elemental concentration in magma*
D = *bulk solid/liquid partition coefficient for the element.*
ε_m = *isotope ratio in the magma*
ε_{mo} = *initial isotope ratio in the magma*
ε_a = *isotope ratio in the wall-rock.*

6.2.1.2.2 Estimation of the end-member compositions and bulk partition coefficients

Estimation of the compositions of possible crustal contaminants and source components for the Western Anatolian volcanic rocks is difficult because of the lack of geochemical data on both the crustal and mantle rocks. The composition of the continental crust in the area has not yet been studied in detail, and therefore information about trace element compositions and isotopic ratios of the crustal rocks is very limited. Some workers (e.g. Gülen et al. 1987; Gülen, 1990) argue that the Miocene granitoids within the metamorphic Massifs of the Aegean domain (e.g. the Attic-Cycladic and the Menderes Massifs) are crustal derivatives, and hence represent the Aegean crust. Altherr et al. (1988) performed Sr and O (oxygen) isotope analyses on the metaluminous to peraluminous (I-type), Miocene granitoids (granodiorite, monzodiorite, qz-monzonite) of the Attic-Cycladic metamorphic Massif which is located to the south of the area studied. Their conclusion is that the granitoids in this area are mostly mantle-derived and have been affected by crustal contamination to some extent. However, no quantitative information is given to define the amount of contamination and possible source characteristics. Thus, it is difficult to estimate the crustal end-member composition using the granitoid data from the Aegean area.

The only published Nd-Sr isotope work on the metamorphic basement rocks in the Aegean area was carried out by Briqueu et al. (1986). They analysed a variety of metamorphic rocks (marble, schist, metavolcanics and glaucophane schist) from the basement of the Santorini and Milos islands of the Aegean. Although these islands are located some distance to the SW of the area studied, it has been shown by numerous authors that the basement lithologies in Western Anatolia (e.g. the Menderes Massif) show a great similarity to those of the Aegean islands (Attic-Cycladic Massif). In fact, some workers (e.g. Dürr et al. 1978) argue that the Menderes Massif is the eastern continuation of the Attic-Cycladic Massif. Thus, the isotope analyses reported by Briqueu et al. (1986) can be regarded as representative contaminant for the Western Anatolian volcanic rocks.

Similarly, the inference of the mantle source end-member composition is very difficult because there are no mantle xenoliths found in the volcanic rocks in Western Anatolia. Thus, the composition of the source material from which the magma was generated remains unknown. However, the composition of the most primitive (the least isotopically enriched and most basic) sample can be regarded as the source component,

as it is the least affected by crustal contamination. The most basic rock of Middle Miocene age is selected as the starting composition for all calc-alkaline and shoshonitic rocks for the following reasons.

(1) The basic rocks of Early Miocene age (with ~55 SiO_2 wt%) are unlikely to represent the source composition, because they have already been affected significantly by crustal contamination (evident from petrographic and chemical characteristics).

(2) It is evident from the isotope and trace element data that all calc-alkaline and shoshonitic rocks (from both the EGA and DAB area) were generated from similar sources.

(3) Compositionally, the Early-Middle Miocene rocks form a continuous trend and none of the samples indicates any evidence of source variations.

The bulk partition coefficients (D) used for AFC modelling were calculated using the same mineral/melt partition coefficient (Kd) (Keskin, 1994) values in the earlier fractional crystallisation modelling. AFC curves were calculated for two different cases. In the first case, the bulk partition coefficients for the selected elements are calculated for fractionating assemblage of $plg_{[45\%]}$ + $opx_{[25\%]}$ + $cpx_{[25\%]}$ + $olv_{[5\%]}$ (amphibole-free assemblage), which is the average phenocryst assemblage of the volcanic rocks from the EGA area. In the second case, the bulk distribution coefficients are calculated for a fractionating assemblage of $plg_{[35\%]}$ + $cpx_{[35\%]}$ + $amp_{[20\%]}$ + $olv_{[10\%]}$, which is the average phenocryst assemblage of the volcanic rocks from the DAB area.

6.2.1.2.3 AFC plots

Figure 6.7 displays the diagram of Th/U ratio plotted against Th for the calc-alkaline and shoshonitic volcanic rocks from Western Anatolia. Theoretical curves have been superimposed on these diagrams and show how the most primitive end-member would evolve by AFC for different values of r, the ratio of the rate of assimilation to fractional crystallisation and F, the ratio of the final mass of magma to the initial mass of magma. Values of F have been marked onto each curve at 5% intervals. Th/U ratio has been chosen for this plot because these elements are highly incompatible and are little affected by either the amphibole-bearing or amphibole-free fractionation assemblages observed in the rocks. It should be noted that the precise values of r are not very meaningful because of potential variations in end-member compositions and in bulk partition coefficient (D) of elements during the course of fractional crystallisation.

However, the values of r can still highlight the relative effects of AFC between the rocks with respect to each other and with respect to the most primitive composition.

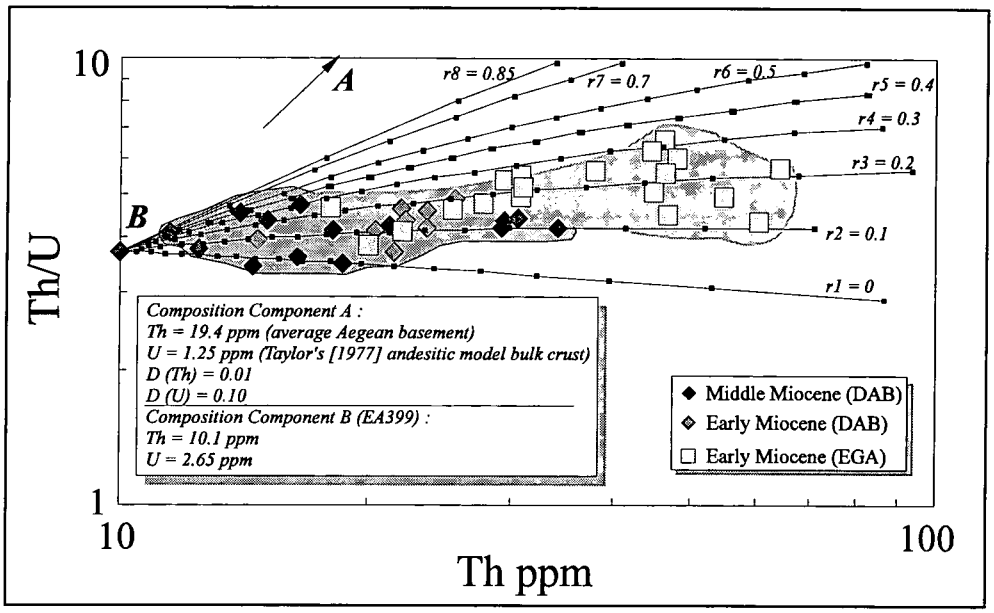

Figure 6.7. *Modeling of the AFC process based on the equations of DePaolo (1981) and using the assmmilation –sensitive ratio the Th/U for the calc-alkaline and shoshonitic rocks.*

The diagram shows that a number of samples from the Middle Miocene suite plot along the theoretical trend for r = 0, indicating no significant contamination from the crust. The constant Th/U ratio with increasing Th for these rocks can be explained by fractional crystallisation. The remaining samples from the same suite display a wide scatter and plot on AFC trends with values of r from 0.1 to 0.7, but mainly r <5. The samples from the Early Miocene DAB suite plot mostly in a restricted field with values of r from 0.2 to 0.3. The rocks from the EGA area, on the other hand, are generally characterised by slightly higher r values with respect to the rocks from the DAB area and plot mostly between r = 0.2 and r = 0.4, but they are mostly r <0.3.

A comparable model has been constructed using the Nd-Sr isotope ratios and the combination of trace elements (Th, U and Rb) and Nd-Sr isotope ratios (Fig. 6.8; 6.9). In the first two diagrams (Fig. 6.8a-b) ($^{143}Nd/^{144}Nd$ v $^{87}Sr/^{86}Sr$), the AFC trajectories are drawn for two different cases of bulk partition coefficients (D) calculated for different mineral assemblages as previously mentioned. It can be seen that variation in crystallisation phases has only a slight effect on the placements of the AFC trajectories. The reason is that the bulk distribution coefficients for Sr and Nd are only slightly affected by whether the crystallising assemblage is amphibole-bearing or

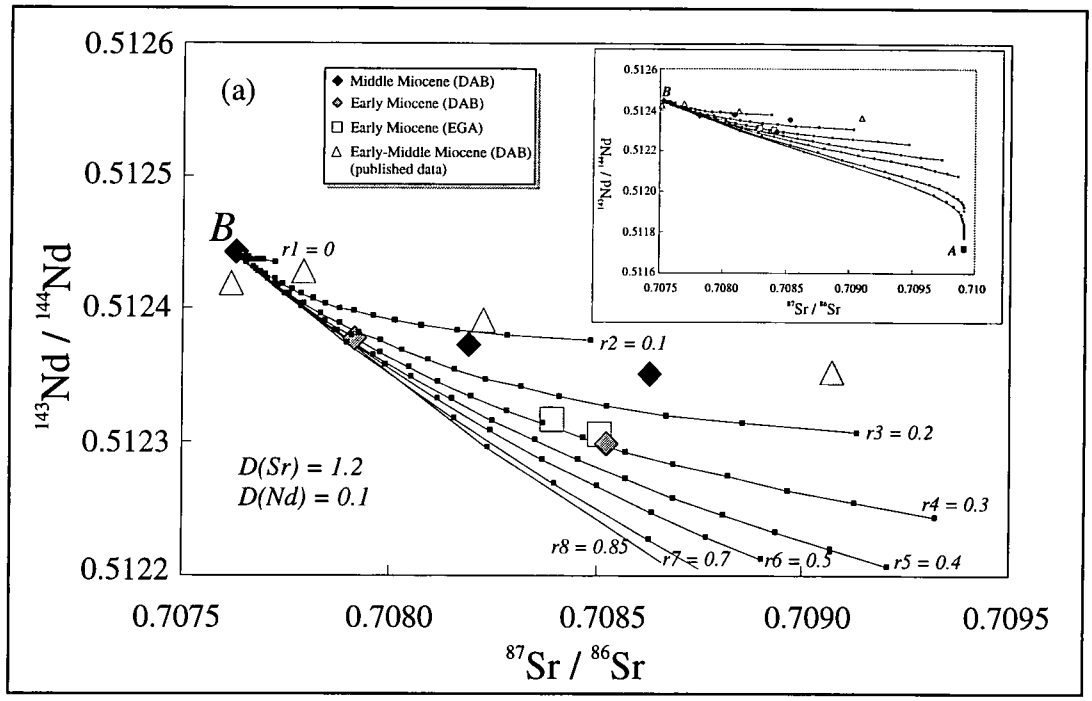

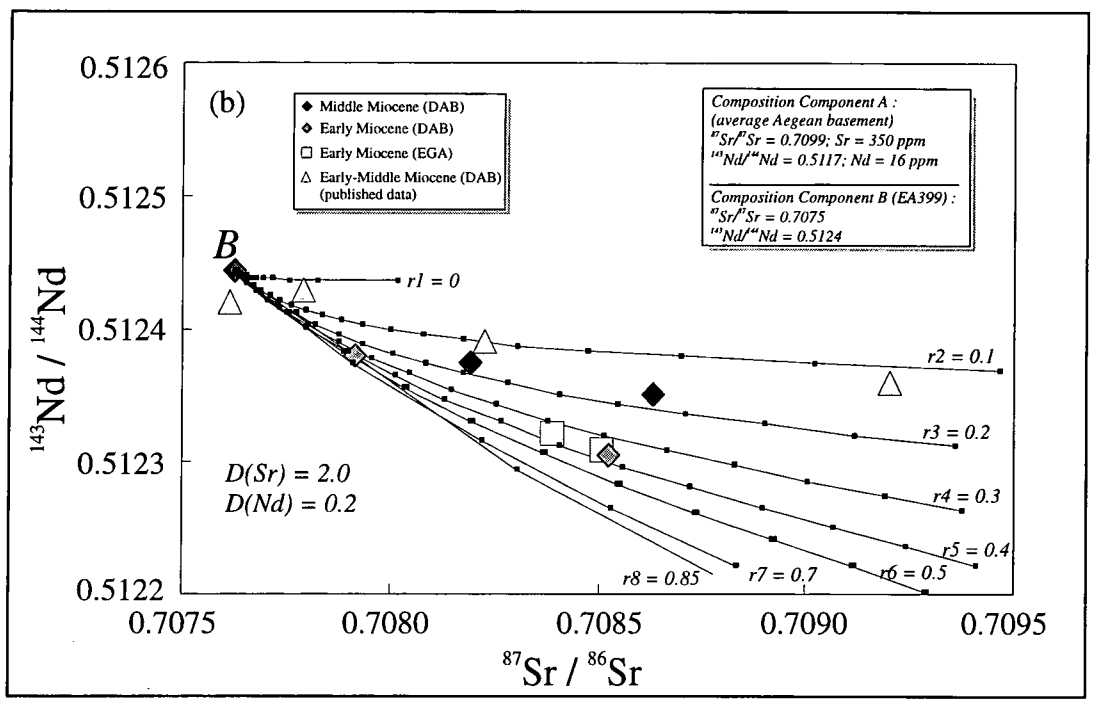

Figure 6.8. *Modelling of AFC processes using the Nd-Sr isotope ratios. AFC trajectories in Figure (a) and (b) were constructed for variable mineral assemblages (see text for details). Selected source and and contaminant end-member compositions represent the most primitive (the least isotopically enriched and most basic) sample and the Aegean basement (Briqueu et al., 1986) respectively (except for Nd which is taken from Goldstein et al., 1984).*

(a)

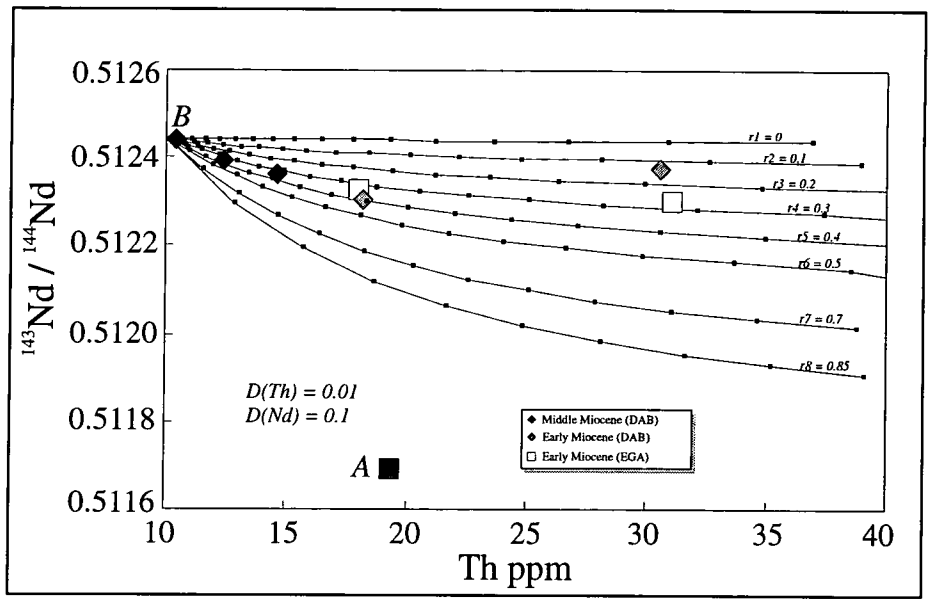

(b)

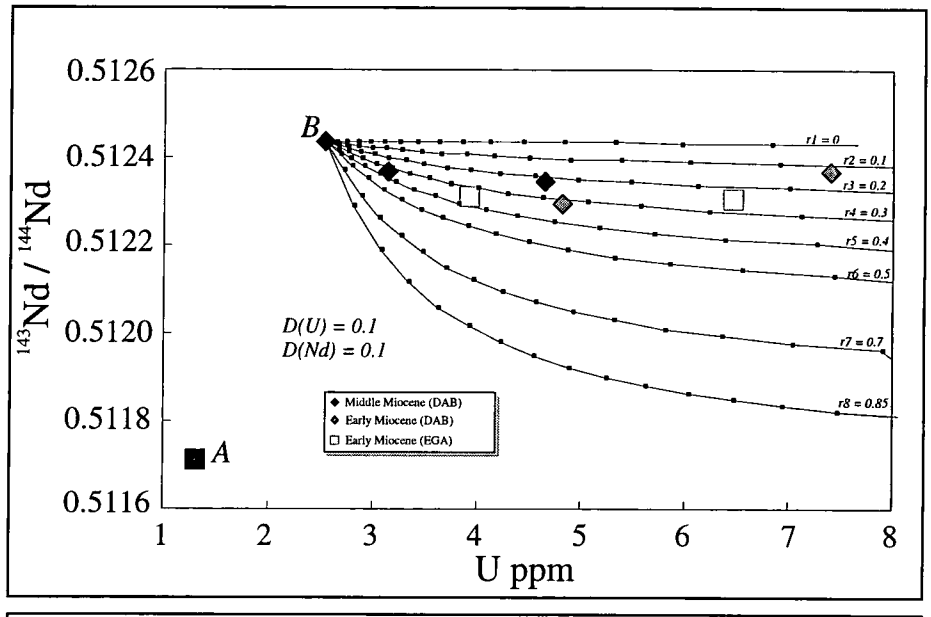

(c)

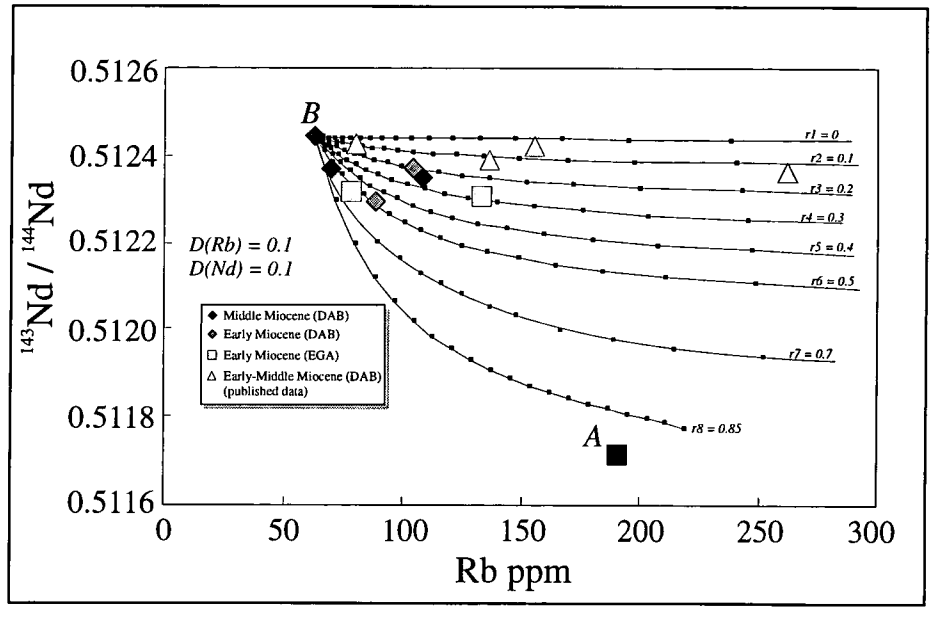

Figure 6.9. *AFC plots of Nd isotope ratios against (a) Th, (b) U and (c) Rb.*

amphibole-free (pyroxene-dominated). The diagrams mainly highlight the difference between the Early and Middle Miocene volcanic rocks in terms of the degree of crustal contamination. The Early Miocene rocks form both the EGA and DAB areas plot mostly along the AFC trajectory drawn for r = 0.3. The Middle Miocene rocks, together with the published data from the same area and age, on the other hand, generally lie between the trajectories drawn for r = 0.1 and r = 0.2. The plots of $^{143}Nd/^{144}Nd$ versus Th, U and Rb (Fig. 6.9a-c) are also consistent with the AFC modelling shown in Figure 6.8. Unlike the trace element plots of Th/U and Th/Rb ratios versus Th, isotope ratio plots do not show any difference in degree of contamination between the Early Miocene rocks from the EGA and DAB areas, although the isotope data are very limited.

Recently, Cavazzini (1996) has produced an equation to quantify the degree of contamination (amount of material contaminated) in magmas evolving by assimilation and fractional crystallisation (AFC). He realised that, if a trace element in the original magma is characterised by an isotope ratio that is different from the contaminant, then a linear correlation exists between the degree of contamination of the element and the isotope ratios. He, therefore, used this relationship to propose a method for calculation of the degree of contamination. His equations are:

$$C_i = 1 - (C_{mo} / C_m)F^{-z} \qquad \text{(for the trace element)}$$

$$\varepsilon_m = \varepsilon_{mo} + C_i(\varepsilon_a - \varepsilon_{mo}) \qquad \text{(for the isotope ratio)}$$

where

C_i is the degree of contamination; and the rest of the symbols are as listed previously (in Section 6.2.1.2.1).

A quantitative calculation of the degree of contamination has been attempted here using the available Nd isotope ratios and concentrations. Nd has been chosen because it is generally incompatible and because the $^{143}Nd/^{144}Nd$ ratios are generally not affected by alteration as Nd and Sm are generally immobile (Marsh, 1989). The results obtained from the calculations are listed in Table 6.4. It can be seen that the degree of contamination for the Western Anatolian volcanic rocks ranges between 9% and 20%. As in the previous AFC modelling, the volcanic rocks of the Middle Miocene age differ from those of the Early Miocene age with their lower degree of contamination (9% and 12%, compared to 17% and 20%). However, it should be noted that these estimates assume that the selected end-member represents the source composition.

Table 6.4. Estimated degree of crustal contamination for the calc-alkaline and shoshonitic rocks.

Sample	Locality and unit name	Rock Type	Age (Ma)	SiO_2 (wt %)	Sm (ppm)	Nd (ppm)	$^{143}Nd/^{144}Nd$	Degree of contamination (%)
EA348	Foca (Foca Dyke)	Basaltic And.	~15	54.40	5.35	28.84	0.512395 ± 5	*9.3*
EA314	Bergama (Egrigol And.)	Tra.Andesite	15.5	60.32	4.51	24.31	0.512372 ± 5	*12.0*
EA101	Dikili (Odaburnu Dyke)	Basaltic And.	~16	56.32	7.24	42.81	0.512398 ± 4	*9.4*
EA147	Ayvalik (Akcapinar Un.)	Dacite	19.0	65.08	6.19	35.96	0.512318 ± 4	*20.2*
EA418	Ayvacik (Kovacli Dyke)	Basaltic And.	20.1	56.24	7.06	43.49	0.512336 ± 4	*17.7*
EA37	Assos (Behram And.)	Tra.Andesite	20.3	61.67	6.48	42.10	0.512324 ± 5	*19.1*

6.2.1.3 Model for magma generation

The volcanological and petrographic characteristics of the rocks show that water plays an important role in the genesis of the Western Anatolian calc-alkaline and shoshonitic series. These include common explosive magmatic products, the development of highly vesicular products (pumice flows etc.; see Chapter 2 for details), eruption of phenocryst-rich magmas with dramatic zoning of phenocrysts, and frequent crystallisation and preservation of hydrous mineral phases (even in basaltic compositions; Chapters 4 and 5). Fractional crystallisation modelling further shows that crystallisation of amphibole in the genesis of the calc-alkaline and shoshonitic rocks may be of particular importance.

In recent years, a number of experimental studies have been carried out on basaltic and andesitic systems to define the possible role of amphibole crystallisation (with other mineral assemblages) on magma genesis in island arc and continental environments. The experimental studies of Gill (1981) and Green (1982) showed that amphibole is a liquid phase in basaltic to basaltic-andesitic magmas under near water-saturated conditions (>10% H_2O) under 8 to 25 kbar (between depths of 25 and 80 km). More recently, Foden and Green (1992) have conducted experiments in the high-Al basalt (with H_2O) system in the melting range at pressures between 1 atm and 10 kbar to define the amphibole stability field and the composition of the liquids which coexist with amphibole. As a result, they proposed a phase diagram for the high-Al basalt system with 5% H_2O illustrating the possible cooling paths and crystallisation products at different stages.

The phase diagram of Foden and Green (1992) is presented in Figure 6.10, together with the cartoon of the proposed petrological modelling which displays the general framework of the plumbing system in thickened continental crust beneath Western Anatolia. The approximate depth of proposed magma chambers have been

estimated using the crystallisation pressures (from the clinopyroxene and Al-in-hornblende barometers) previously calculated in Chapter 5 (see table 5.1) assuming the average density of crust to be approximately 2.7 $g.cm^{-3}$. The present total crustal thickness, as mentioned in Chapter 1, approximates to 30-35 km in the coastal section of the Western Anatolia. This thickness does, in fact, follow a considerable amount of extension and lithospheric thinning and hence does not represent the actual thickness of the Early-Middle Miocene period. However, the total crustal thickness can still be estimated using the average strain rate (given as $>2 \times 10^{-15}$ s^{-1} by Jackson, 1992) and the stretching factor (given as $\beta = 1.2 - 1.5$ by Paton, 1992) to have been around 45-52 km during the Early Miocene and 40-45km during the Middle Miocene. Note that these estimates assume that the regional extension in the area initiated in the latest Early Miocene or beginning of the Middle Miocene, which is evident from the field relationships of the volcanic rocks (e.g. the rocks of the Kalarga Andesite and the Egrigöl Andesite formed at the time of the graben formation; see Chapter 2 for details).

The crystallisation pressure calculations and petrographic characteristics showed that the volcanic rocks from the EGA area have a polybaric origin and are the composite products of more than one petrogenetic process. This is evident from the strong compositional variations in a single phenocryst, as well as the considerably variable crystallisation pressures. The rocks in this suite generally have large proportions of phenocrysts that crystallised at pressures between 3.0 and 7.0 kbar, corresponding to the crystallisation depth from 12 to 27 km. These are mainly plagioclase-, pyroxene- and magnetite-bearing assemblages. Amphibole xenocrysts in some of the rocks, on the other hand, yield higher pressures of between 6.4 and 9.1 kbar implying that the early crystallisation of the magma took place at depths of about 23 to 34 km.

The composition of amphiboles that Foden and Green (1992) synthesised in their experiments is mainly pargasitic hornblende. They showed that plagioclase is the anhydrous liquidus phase between 1 atm and 10 kbar, but that in the hydrous environments its role is taken by olivine at <7 kbar and then by clinopyroxene at more elevated pressures. Amphibole (pargasitic hornblende) may crystallise in magmatic systems if the body of magma as a whole remains motionless over a period of time and the magma undergoes extensive convection and mixing (closed-system equilibrium crystallisation), or if the wall-rocks with which the cooling, hydrous basaltic melts are in contact (in open magmatic systems) are composed of olivine and pyroxene as in the case

of upper mantle or lower crust (point C in Fig. 6.10).

The xenocrysts found in the rocks from the EGA area are pargasitic (or ferroan pargasitic) hornblende that yield high-pressure crystallisation conditions. This may imply that the primary magmas initially ponded in deep crustal reservoirs (~35 km) where they underwent combined fractional crystallisation and crustal assimilation, or mixing with crustal melts. Processes that affected the primary magma compositions in deep crustal reservoirs, may be similar to the MASH (melting, assimilation, storage and homogenisation) hypothesis proposed by Hildreth and Moorbath (1988). However, the effects of MASH are difficult to distinguish from those of AFC as the characteristics of the magmas have been widely modified by later contamination events and hence it is difficult to asses the geochemical characteristics of the deep magma chambers. The early fractionation in deep magma chambers is likely to have performed the function of re-establishing buoyant ascent of magma to form higher level magma chambers having variable depths, sizes and fractionation assemblages.

In the deep magma chambers, if the liquid tapped and extracted from the crystalline matrix, the crystallisation phases will move back into the field of olivine and clinopyroxene (with or without plagioclase) as the adiabatic temperature gradient of magma becomes significantly less than the gradient of the amphibole-out reaction (point D in Fig. 6.10; Foden and Green, 1992). As a consequence, the early-formed pargasitic amphiboles break down as a result of decompressive, incongruent melting, eventually forming corona-textured xenoliths or being completely resorbed. The resultant crystalline assemblages are either pyroxene- or olivine-dominated (with plagioclase). The estimated pressures for the rocks of the Kovacli Dyke Swarms range from 4.0 to 6.0 kbar at crystallisation temperatures of 900-1170 °C. This suggests that the pyroxenes (with plagioclase and minor olivine) crystallised at a depth of about 16-22km which corresponds to point D in Figure 6.10 (also shown as mid-crustal magma chambers). Petrographic observations indicate that the magmas in these chambers crystallised anhydrous phases such as plagioclase and pyroxene with minor olivine because amphibole was not equilibrium at these P-T conditions.

The cooling paths that produce amphibole-free crystallisation assemblages would be either F2 or F3 (Fig. 6.10). The former suggests a continuous adiabatic decompression, an ascending magma, which at depth had been in equilibrium with amphibole, may simply erupt with an anhydrous pyroxene-feldspar assemblage as the

ascending path will nor cross the amphibole-out curve, and the later indicates a possible late-stage heating. Resorption of plagioclase crystals, as previously discussed in Chapter 4, further indicates a late-stage heating which may be a consequence of either an entrainment of hotter mafic magmas by cooler felsic magmas during eruption of layered magma chamber, or the release of latent heat of crystallisation during enforced decompressive precipitation of plagioclase. In either case, the crystallising phases would be represented by pyroxene- and plagioclase-dominated and amphibole-free assemblages.

The crystallisation pressure estimates obtained from the highly porphyritic rocks (and ignimbrites) mostly yield values of 2.5 to 5.5 kbar, indicating that they were derived from magma chambers located between 10-15 km depth. These magma chambers are shown as high-level silicic magma chambers in Figure 6.10, because their products are dominantly acid-intermediate rocks. The crystallisation assemblages in the high level chambers are generally plagioclase-dominated with pyroxenes, K-feldspar and biotite. Foden and Green (1992) argued that the magmas become normative plagioclase-enriched after fractionation of clinopyroxene and olivine at point D (Fig. 6.10). Thus, the magma chambers near point D probably fed the high-level magma chambers as the magmas ascending to high-level silicic chambers should have crystallised clinopyroxene and olivine in the mid-crustal chambers.

In the high-level chambers, further assimilation of crustal material becomes very limited which is probably due to the fact that the magmas do not have enough energy to assimilate the crust significantly (DePaolo, 1992). As a result, the most important evolutionary process becomes fractional crystallisation, which produces large volumes of acidic magmas with isotopic characteristics similar to those of the basic/intermediate rocks of the Kovacli Dyke Swarms. Fractional crystallisation modelling of the acid-ignimbrites (discussed in Section 6.2.1.1) also provides a good evidence of more fractional crystallisation than crustal contamination in the high-level magma chambers.

In the DAB area, the effects of amphibole fractionation have already been demonstrated from petrographic observations (Chapter 4) and trace element characteristics (Section 6.2.1.1). The pressure estimates obtained from the Al-in hornblende geobarometer yield two different ranges of crystallisation pressures for the acid-intermediate Early Miocene rocks of the DAB area. These are: (1) pressures

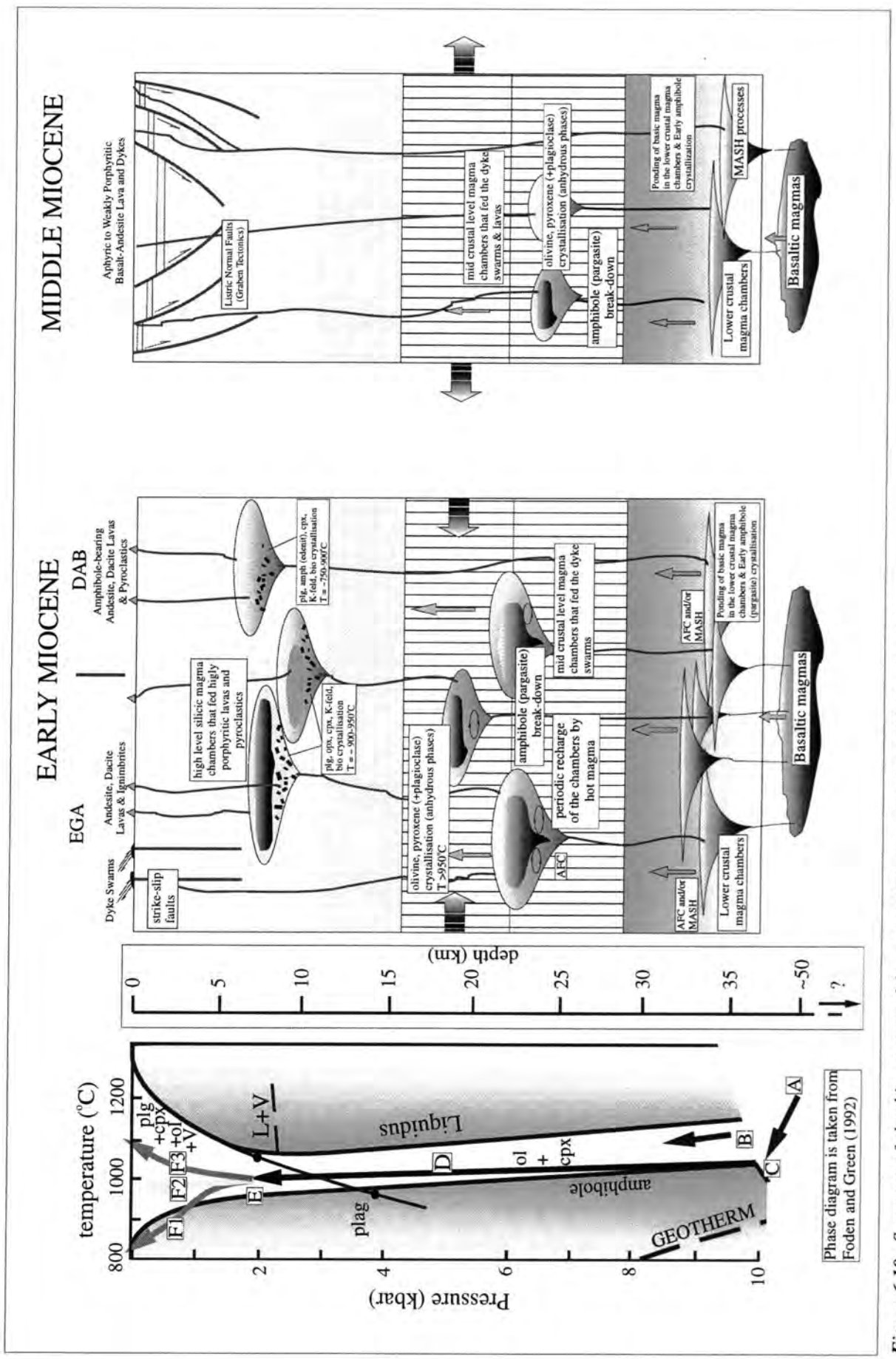

***Figure 6.10** . Summary of plumbing system of the post-collisional volcanics of Western Anatolia.*

of 7-7.5 kbar which correspond to crystallisation depths of 23-28 km; and (2) pressures of 2.0-3.5 kbar which indicate crystallisation depths of about 10-15 km. The amphibole xenoliths (mostly pargasitic) found in the porphyritic andesites and dacites of the DAB area are compositionally identical to those found in the rocks from the EGA area. This indicates that the early crystallisation histories of the magmas from both areas are similar to one another. However, the existence of edenitic hornblendes (the products of the high-level magma chambers) in the rocks from the DAB area suggests a later crystallisation which is different from the crystallisation history of the rocks from the EGA area. The experiments of Foden and Green (1992) suggested that the cooling paths of ascending magmas shallower than point E may change to produce smaller P/T slopes than those of the amphibole-out curve which they eventually re-cross (path F1 in Fig. 6.10). In this case, the commonly observed hornblende of siliceous andesite and dacite is crystallised. The temperature estimates (obtained from the hornblende-plagioclase thermometer) that range from 750-900 °C also indicate a low-temperature crystallisation for the acid-intermediate rocks from the DAB area which is consistent with the experimental result shown in Figure 6.10.

Amphibole xenocrysts with pargasitic composition have also been observed in some of the Middle Miocene intermediate rocks from the DAB area (e.g. the Egrigöl Andesite), indicating a similarly early fractionation history in the deep level magma chambers as the Early Miocene rocks. The pressure estimates, however, suggest that the Middle Miocene basic-intermediate rocks have not experienced high-level magma chamber fractionation as the crystallisation pressures for these rocks range between 5.3 and 10.2 kbar, but mostly >7 kbar. Trace element and isotopic characteristics also indicate less contamination by crustal material and less fractionation for the Middle Miocene rocks relative to those of the Early Miocene age. This can be attributed to the extensional tectonics and progressive crustal thinning which lead to the rapid movement of the magmas with primary compositions through the thinned and fractured crust. Rapid ascent of the magmas during the Middle Miocene period is also evident from the aphyric or weakly porphyritic nature of the Middle Miocene rocks.

6.2.1.4. Mantle melting in response to post-collisional tectonics

In Figure 6.11, the P-T diagram constructed by Pearce et al. (1990) for the Eastern Anatolian collision zone also shows the conditions and possible mechanisms of

melting across Western Anatolia, assuming that the proposed thermal and structural parameters (e.g. thickness and thermal gradients) are representative of the Western Anatolian collision zone. The thicknesses of rigid, mechanical boundary layer (MBL) and the thermal boundary layer (TBL) were both assumed to be 150 km. The MBL is assumed to have a linear geotherm of gradient 9°C km^{-1}, and the asthenosphere adiabatic gradient of 6°C km^{-1} with a potential temperature (T_p) of 1280°C (see Pearce et al., 1990 for details).

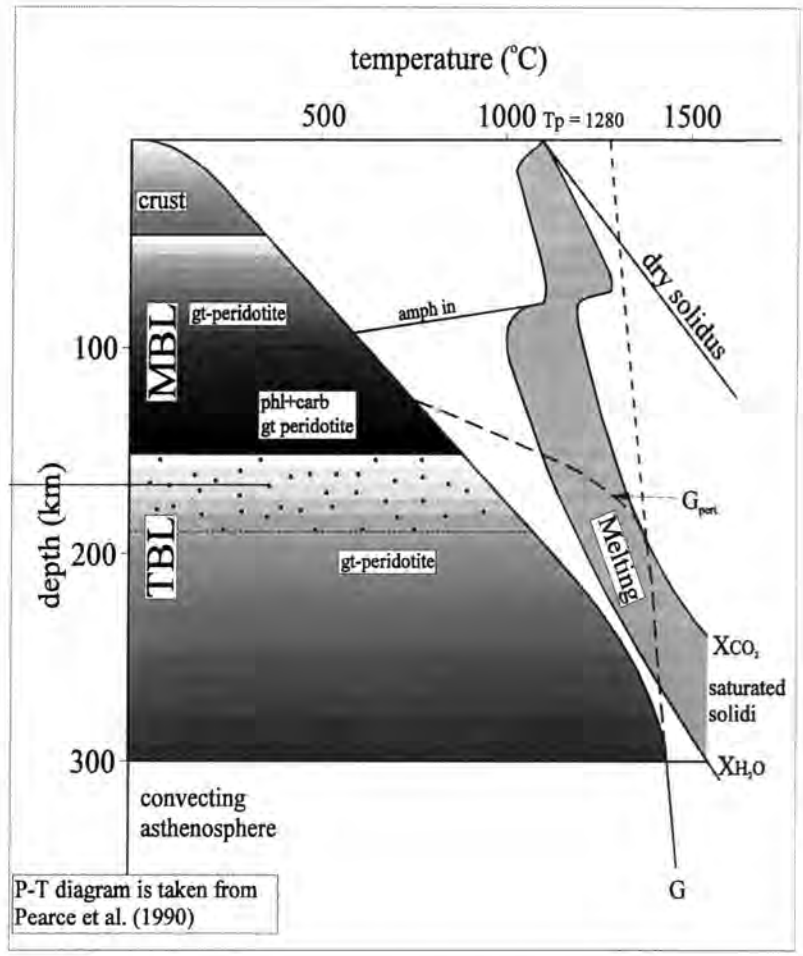

Figure 6.11. *P-T diagram showing conditions of melting in the thickened mantle lithosphere beneath Western Anatolia. MBL = Machanical Boundary Layer; TBL = Thermal Boundary Layer; G = continental geotherm; G_{pert} = perturbed geotherm; T_p = potential mantle temperature; Mantle compositions on the geotherm: gt = garnet; am = amphibole; phl = phologopite; carb = carbonate. Shaded region = field of initiation of melting of volatile-rich compositions ranging from pure water ($XH_2O = 1$) to pure carbondioxide ($XCO_2 = 1$).*

For the case of Western Anatolian Early-Middle Miocene volcanism, which has been shown to have generated from a subduction modified mantle source (Chapter 3 and Section 6.1.1), the possible mechanisms for magma generation are:

(1) Melting of mantle lithosphere by adiabatic decompression resulting from

lithospheric extension or uplift.

(2) Melting of mantle lithosphere by perturbation of the geotherm by heat from either a mantle plume or upwelling asthenospheric mantle.

The validity of the first option depends largely upon the amount and the age of initiation of extension in the area. Theoretically, mantle lithosphere with a peridotitic composition is unlikely to produce melt under dry conditions because the dry solidus curve will not cross the geotherm of the thickened lithosphere (Fig. 6.11) unless a considerable amount of extension takes place (conditions of the dry mantle melting are discussed in section 6.2.2.6). However, taking into account that the source region from which the Early-Middle Miocene magmatism was generated is a metasomatised mantle, it can be argued that depression of the metasomatic part of the mantle below the amphibole stability field may cause release of water (Pearce et al., 1990). This can then lower the melting temperature and initiate melting of the metasomatised mantle layer. Recent studies (e.g. Gallagher and Hawkesworth, 1992; Leeman and Harry, 1993, 1995) also showed that volatile enrichment (H_2O and CO_2) in the mantle can lower the solidus temperature for peridotite compositions by 300-500 ^{o}C at pressures of 2-5 GPa. Thus, volatile-saturated compositions of the mantle lithosphere may be near to their melting temperature prior to the extension and hence, may start to melt after small degrees of stretching. It can, therefore, be argued that the metasomatic nature of the mantle lithosphere beneath Western Anatolia is consistent with the theory of the initiation of melting by lithospheric extension.

Nevertheless, another important question is the timing of the onset of extension. As previously mentioned in Chapter 1, the oldest date for the onset of extension is that proposed by Seyitoglu and Scott (1992) and Seyitoglu et al. (1997). They argue that the N-S extension in Western Anatolia initiated in the Latest Oligocene-Early Miocene (24-20 Ma). Thus, they relate the initiation of the Miocene magmatism to the N-S extensional tectonics in the area. In this study, however, the oldest volcanic rocks formed in association with the extensional basins were found in the DAB area. These are the rocks of the Kalarga Andesite (dated as 17.6-17.3 Ma by Borsi et al., 1972) and the Egrigöl Andesite (dated as 15.5 Ma in this study). These dates are clearly much younger than the dates proposed by the above authors for the onset of the extension. Furthermore, the onset of the post-collision volcanism in Western Anatolia is much earlier than the Latest Oligocene-Early Miocene (see Chapter 1 for details). Thus, the

regional N-S extension, even if it starts in the Latest Oligocene-Early Miocene, cannot explain the initiation of melting in the source region.

In collision zones in general, localised stretching due to the lateral stress release associated with a transtensional tectonic regime can be considered as an alternative mechanism to create the thermal perturbation of the mantle lithosphere. In the area studied, there is no clear evidence to indicate the existence of strike-slip structures (e.g. fracture zones or pull-apart basins) formed during or before the Early Miocene. Furthermore, no evidence has been found to indicate a possible link between the possible strike-slip movements and the volcanism (e.g. linear alignment of the volcanic centres). However, taking into account the fact that it is very difficult to recognise the pre-Miocene structures because they are mostly covered by young volcanic and sedimentary rocks and/or are complicated by the Miocene-Recent structures, the possibility of the thermal perturbation by localised stretching cannot categorically be ruled out.

Melting of mantle lithosphere by perturbation of the geotherm by heat from a mantle plume is unlikely for Western Anatolia because there is no evidence for any elevated topography resulting from a domal uplift. Thus, a perturbation of the geotherm by heat from upwelling asthenospheric mantle would be the most likely mechanism for initiating melting in the mantle lithosphere. Although there is no geophysical data that can support the hypothesis, a possible analogy for this mechanism may be the model for the Eastern Anatolian collision zone proposed by Pearce et al. (1990). This model requires delamination of the thermal boundary layer (TBL) of the mantle lithosphere.

The concept of lithospheric delamination was first proposed and discussed by Bird (1978, 1979), Bird and Baumgardner (1981) and Housmann et al. (1981). Subsequently, several geophysical and geological research undertaken on collision zones showed that the delamination was potentially an important mechanism in these zones (England and McKenzie, 1982; Vilotte et al., 1986; Nelson, 1992). Delamination of the TBL is generally attributed to either convective removal (Platt and England, 1993) or to separation of a slab from beneath the mechanical boundary layer (MBL) following lithospheric thickening. Since the TBL is defined as a weak and convectively unstable temporary part of the lithosphere (Anderson, 1994), it can be delaminated following lithospheric thickening and internal cooling which in turn causes the TBL to be replaced by relatively less dense asthenospheric mantle material. Delamination of the

TBL may therefore cause the direct contact of hot asthenospheric mantle with the metasomatised part of the mantle lithosphere and initiate melting as the perturbation of the geotherm can bring a part of the metasomatised mantle lithosphere above its solidus (Fig. 6.11; 6.12).

It has been argued that one of the major consequences of lithospheric delamination is rapid uplift and extensional collapse which would result isostatically from replacing relatively dense (cold) mantle lithosphere by less dense (hot) asthenospheric mantle (Dewey, 1988; England and Houseman, 1988; Nelson, 1992; Platt and England, 1993). In the case of Western Anatolian collision zone, as discussed above, the lithospheric extension began no later than the latest Early Miocene (~17.6 Ma). Although, as discussed in Chapter 1, the extension may have been assisted by the westward movement and counterclockwise rotation of the Anatolian plate (which initiated about 13 Ma ago) and/or the subduction beneath the Aegean and the Anatolian plates along the Hellenic trench (which initiated about 12 Ma ago), the prime cause for the early beginning of extension should be gravitational collapse and spreading of the thickened and unstable lithosphere. This is because the first two processes initiated later than the onset of the extension. Theoretically, during collision, body forces arising from elevated topography and the corresponding lithospheric root are dynamically balanced by the plate boundary forces driving the collision. When the latter are removed, the belt will tend to collapse under its own weight. However, for this to occur following collision and uplift depends largely upon the thermal profile of the lithosphere at that time. If this thermal profile is hot enough the strength of the lithosphere would be too weak to resist collapse, and then geologically significant extension could occur on release of compression (Sonder and England, 1989; Sonder et al., 1987; Nelson, 1992). Conversely, if the thermal profile is not hot enough the lithosphere cannot flow rapidly and destruction of the belt may take several tens of million of years (Nelson, 1992). Therefore, if the delamination of the TBL is the cause of melting of the thickened lithosphere beneath Western Anatolia, it may be responsible, or perhaps the required, mechanism for the initiation of extension (Fig. 6.12).

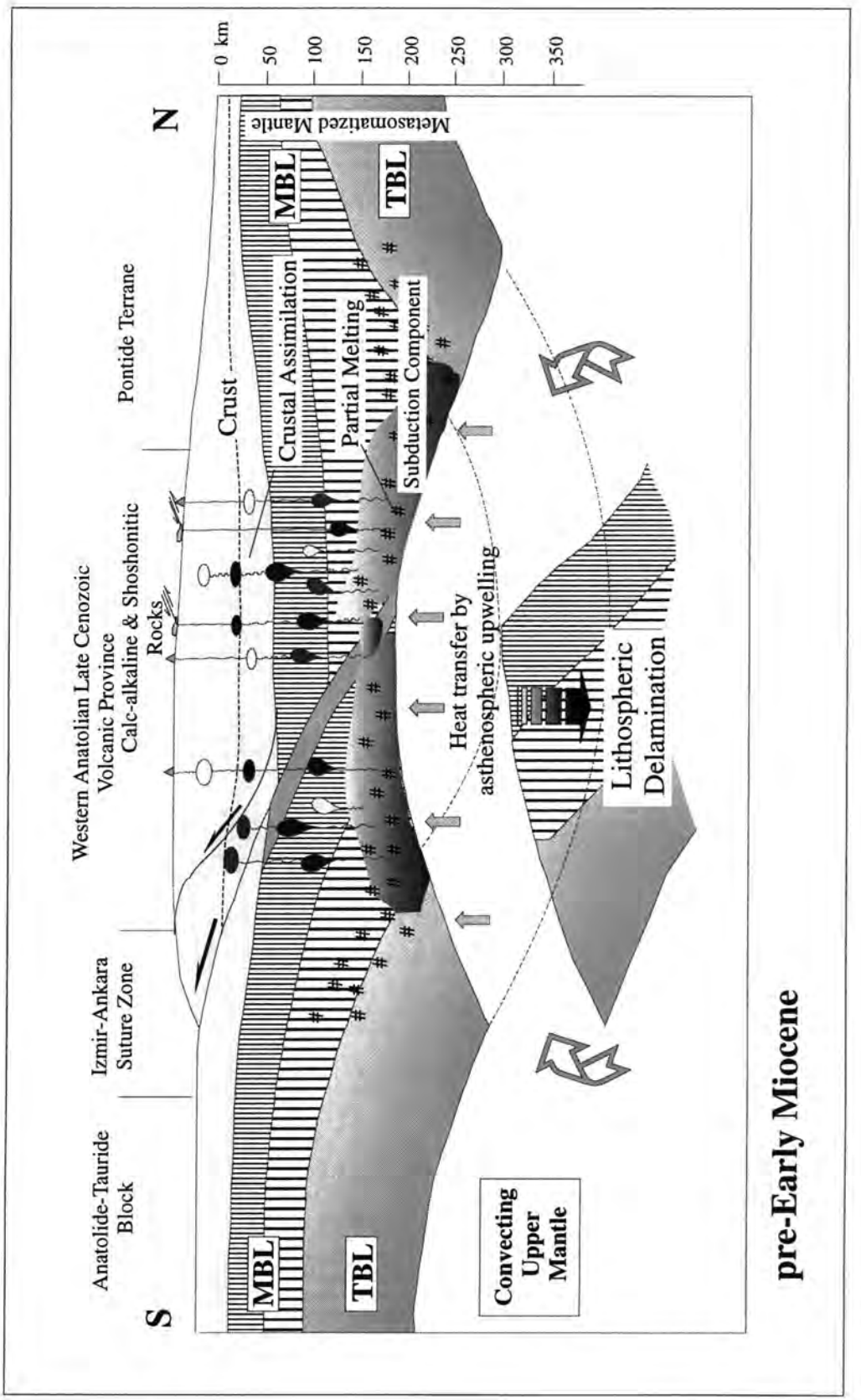

Figure 6.12. *Schematic section across the "Western Anatolian Volcanic Province" illustrating the magma genetic model deduced from petrological and geochemical data. MBL = Mechanical Boundary Layer; TBL = Thermal Boundary Layer.*

6.2.2 Petrogenesis of The Alkaline Volcanic Rocks (Late Miocene)

The following sections are aimed at addressing the melting and fractionation processes in order to (1) characterise the mineralogy and composition of the mantle source(s) of the alkaline basic volcanic rocks from Western Anatolia, and (2) define the degree of partial melting. The Western Anatolian alkaline rocks provide an excellent opportunity for using basalt data to define mantle source characteristics because the lavas erupted continuously during a short interval within a small geographic region. Moreover, most of the rocks in the alkaline suite fulfil several criteria for primary magmas (liquids generated by partial melting of a mantle source without any significant subsequent compositional modification), particularly the high Ni-Cr concentrations in the least basic members (~ 50 wt.% SiO_2). It is already established that the mantle source of the Western Anatolian alkaline rocks was isotopically homogenous and has not been affected by subduction processes. It has also been shown that crustal contamination processes have not affected the alkaline magma. Thus, this section will focus on the melting processes to evaluate the source compositions of the alkaline basic rocks. However, it is essential to evaluate the possible roles of fractional crystallisation and remove any such effects from the primary basalt compositions before considering any qualitative or quantitative melt modelling.

6.2.2.1 Fractional crystallisation

Petrographic observations have shown that olivine, clinopyroxene and Fe-Ti oxides (titano-magnetite and ilmenite) are the main crystallisation assemblages in all the alkaline rocks from the area studied. Although the effects of fractional crystallisation on primary magma compositions can be very difficult to distinguish from those of partial melting, the use of compatible-incompatible element plots may still be helpful. Fractionation of ferromagnesian minerals such as olivine and clinopyroxene would be expected to decrease the abundance of the compatible elements (e.g. Ni and Cr) and increase the abundance of the incompatible elements (e.g. Th, La and Nd) in the liquid.

The plots in Figure 6.13 indicate a time-related decrease in compatible and an increase in incompatible, element concentrations. This could be explained by fractional crystallisation. Nevertheless, Figure 6.13 also shows that decrease in compatible, and increase in incompatible, element concentrations are accompanied by a gradual decrease in SiO_2 content. This is the opposite of what would be expected during fractional

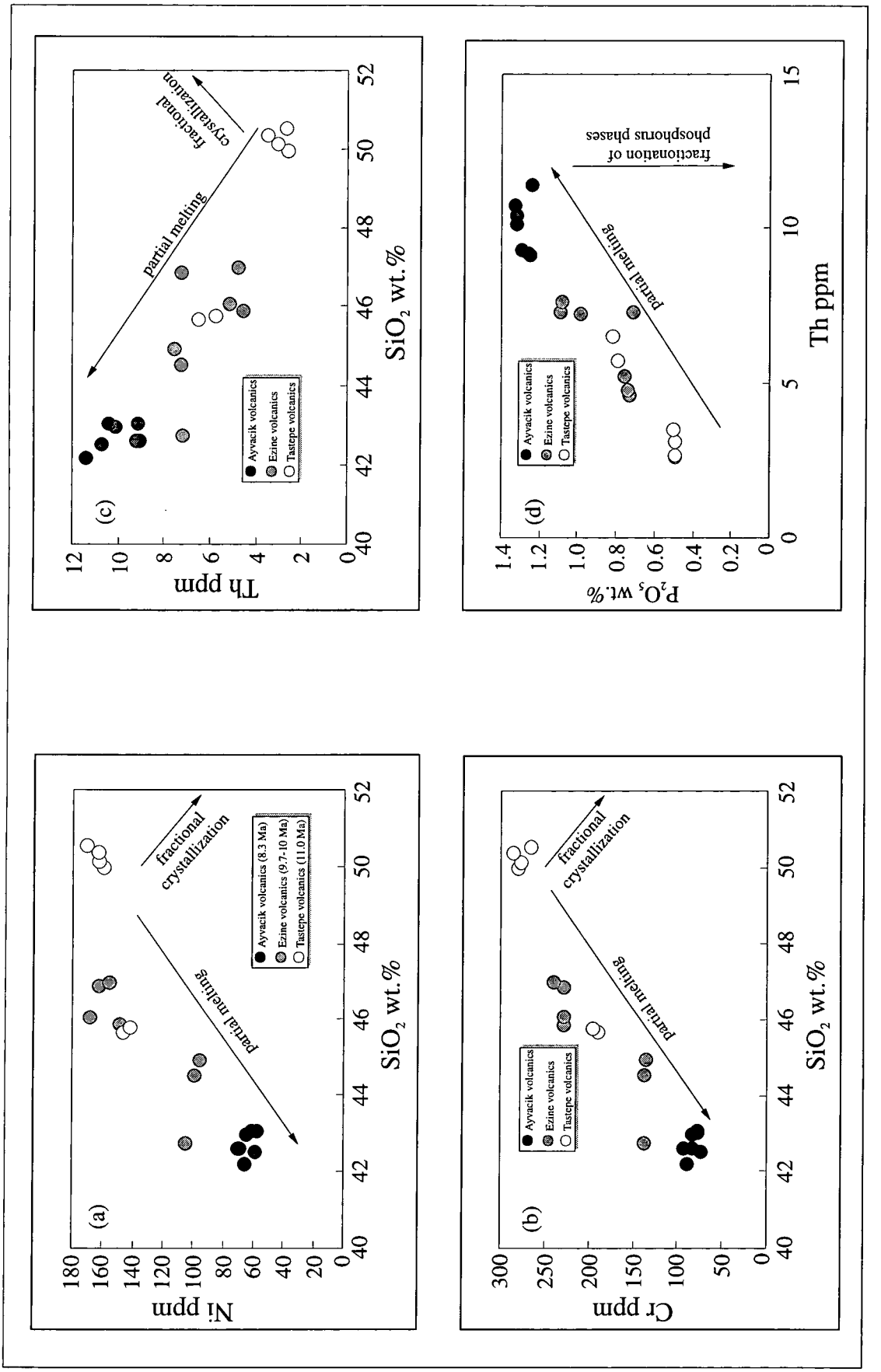

Figure 6.13. *Compatible (a-b) and highly-incompatible (c-d) element plots against SiO2 and Th showing the possible partial melting and fractional crystallisation trends for the alkaline rocks from Western Anatolia.*

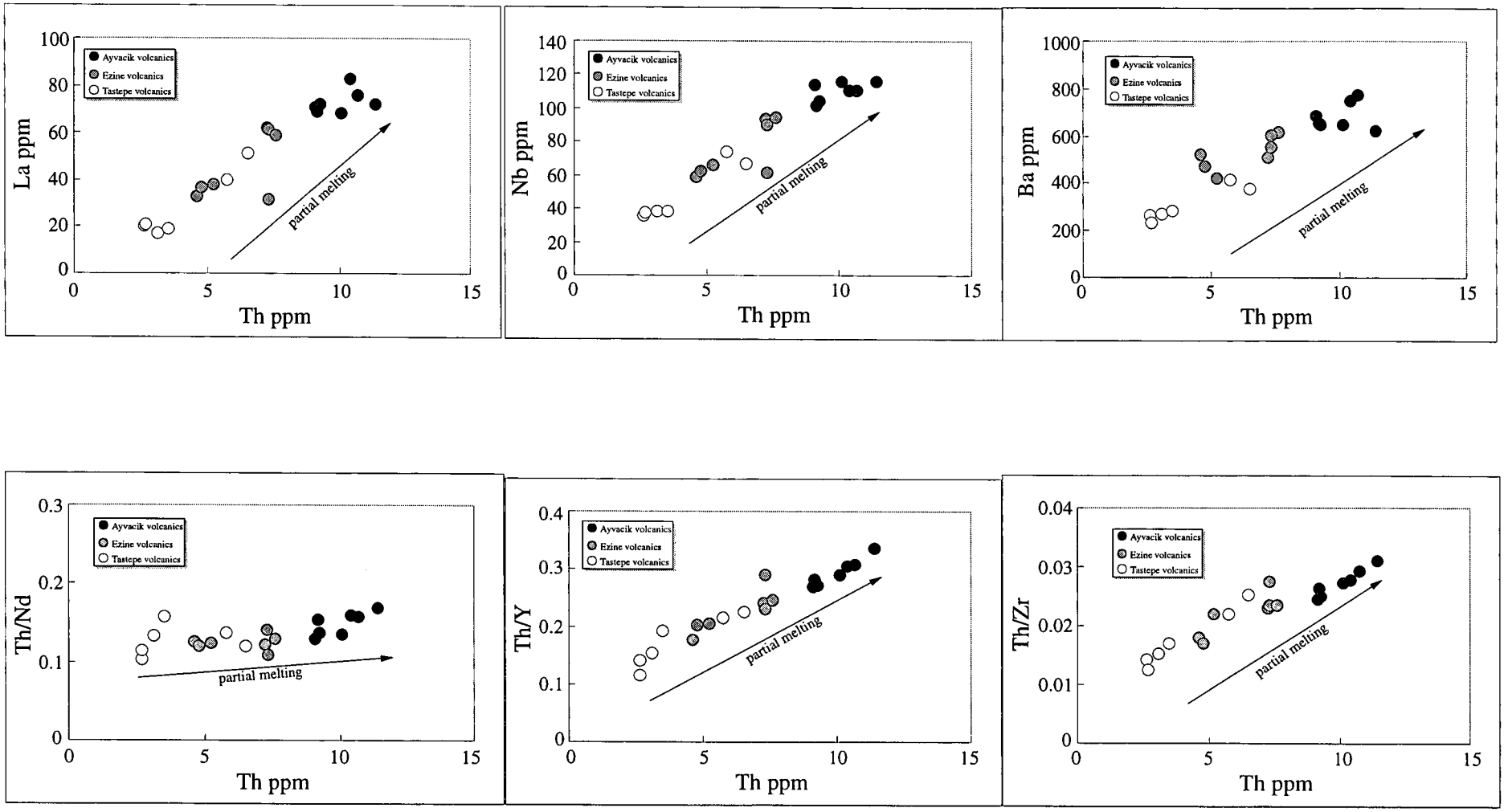

Figure 6.14. *Incompatible trace element abundance and ratio plots against Th showing the partial melting tr ends which are characterised by positive linear regressions.*

crystallisation. It could be argued that any possible mineral accumulation (e.g. olivine) might affect the silica concentration of the rocks and create patterns similar to those in Figure 6.13. However, the mostly aphyric or <10% phyric nature of the plotted alkaline samples makes it almost impossible to attribute the observed trends to this process. Thus, the observed trends can most likely be explained by variable degrees of partial melting of a mantle source.

Petrographic and mineral chemical characteristics of the alkaline rocks (e.g. equilibrium crystallisation of olivine and clinopyroxene) also support the idea that the alkaline magma has not been greatly affected by fractional crystallisation processes or mineral accumulation. Experimental studies (e.g. Takahashi and Kushiro, 1983) have shown that, under constant pressure conditions, a decrease in degree of melting is accompanied by a decrease in the SiO_2 content of the melt. The observed relationships in the alkaline rocks are consistent with a model in which low degrees of partial melting lead to less silicic primary melts (~42-44 SiO_2 wt.%) and higher abundances of incompatible elements. The plots of highly and moderately incompatible elements (Fig. 6.14) further suggest that the concentrations of most of these elements are mainly controlled by decreasing degrees of partial melting of a geochemically homogenous mantle source. More detailed modelling will be presented in the following sections of this Chapter to constrain the nature and the effects of the melting processes.

6.2.2.2 The source mineralogy

In Figure 6.15a-b, the Al_2O_3/CaO and Al_2O_3/TiO_2 ratios are plotted against Th abundance for the alkaline rocks. Th was chosen because it is the most incompatible element and its abundance should therefore increase systematically with decreasing degree of partial melting. The selected major element ratios are considered to be the best indicators to distinguish the effects of garnet from those of clinopyroxene in the source mantle. This is because garnet is the only mantle phase which retains Al_2O_3, at depth, whereas the CaO and TiO_2 contents of the liquid are mostly controlled by clinopyroxene (note that clinopyroxenes in the alkaline rocks, as shown in Chapter 5, are all high-Ti phases). The systematic decrease in the ratios of Al_2O_3/CaO and Al_2O_3/TiO_2 with decreasing degree of partial melting suggests a time-integrated increase of garnet/clinopyroxene ratio in the residue of the source.

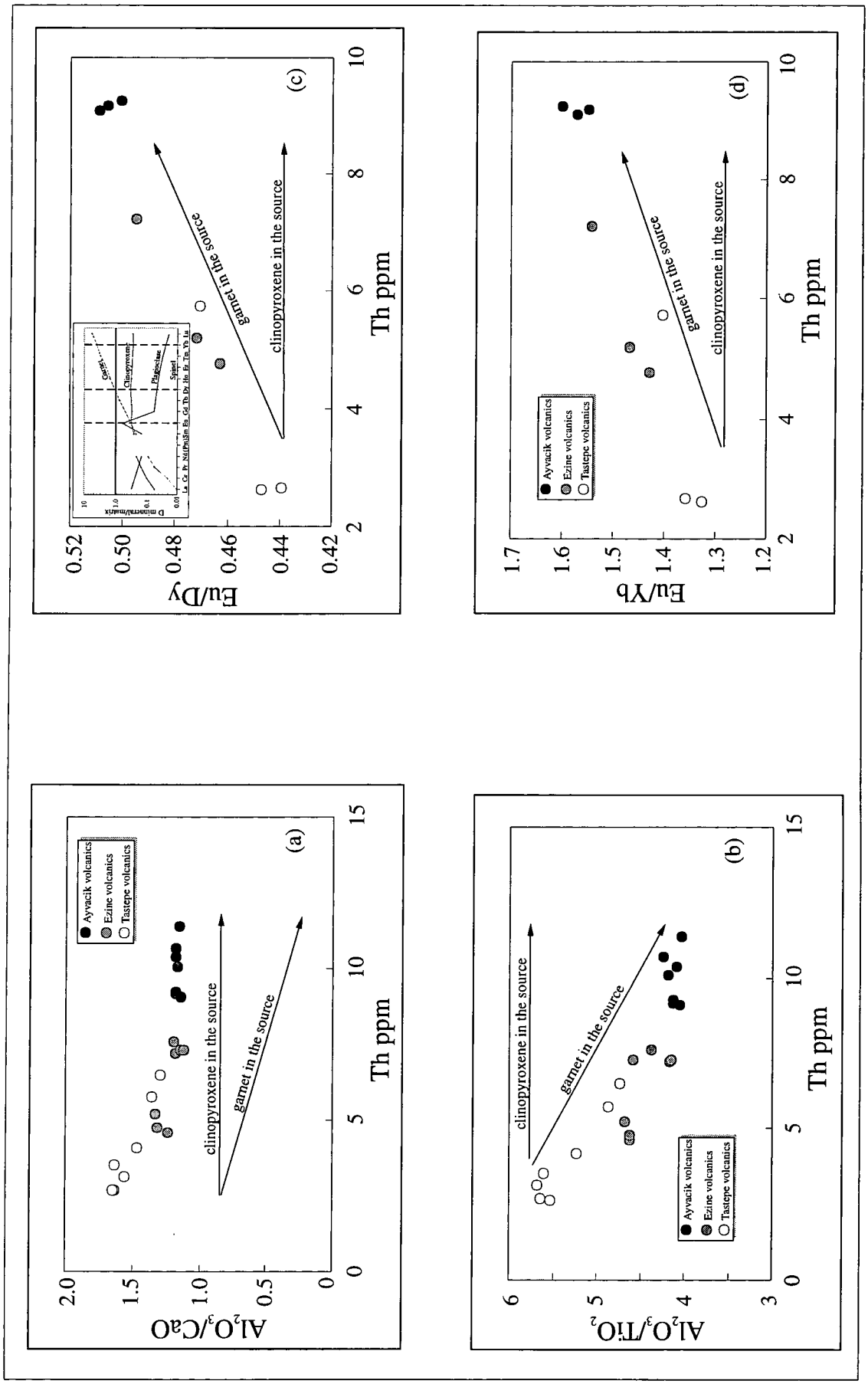

Figure 6.15. *(a-b) Major and (c-d) trace element ratio plots against Th showing the partial melting trends from a garnet- or clinopyroxene-bearing lherzolite source. The inset in (c) shows mineral/matrix partition coefficients for garnet, clinopyroxene, plagioclase and spinel. Partition coefficient values are from McKenzie and O'Nions (1991; 1995).*

The ratios, Eu/Dy and Eu/Yb, are plotted against Th as another means of evaluating the role of garnet in the genesis of the Western Anatolian alkaline rocks (Fig. 6.15c-d). These ratios are rather sensitive indices of garnet- versus clinopyroxene-dominated residual phases. As shown by the distribution coefficients of Eu, Dy and Yb in clinopyroxene, plagioclase, spinel and garnet (shown as inset diagram in Fig 6.15c), only garnet is able to fractionate these elements during the partial melting processes. It can be seen that both ratios increase significantly from alkaline basalt compositions (the Tastepe Volcanics) to basanites (the Ayvacik Volcanics). The decreasing degree of partial melting of a garnet-bearing lherzolite source (with residual garnet) should be marked by an increase of Eu/Dy and Eu/Yb ratios, due to the high distribution coefficients of Dy and Yb in garnet compared to Eu. Thus, garnet play an important role in the partial melting processes that generate the alkaline rocks from Western Anatolia.

6.2.2.3 Partial melting processes

6.2.2.3.1 Overview

There are mainly two types of melting and melt-extraction processes described in the geological literature: (1) equilibrium- or batch-melting; and (2) fractional- or Rayleigh-melting (Wilson, 1989; Rollinson, 1993). The first describes the partial melting process in which the melt continuously reacts and equilibrates with the solid residue while the bulk composition remains constant. The second describes the partial melting process in which the melt is instantaneously removed from the source.

The foundation of batch-melting was first laid down by Schilling and Winchester (1967). Several modifications were later introduced by Gast (1968), Shaw (1970) and Albarède (1983). Shaw (1970) postulated that a batch-melting equation could be written as:

$$C = C_0 / [D_0 + F(1 - P)]$$

where

C and C_0 are the concentrations of a trace element in the melt and the source, respectively, and F is the fraction of melt. D_0 the bulk distribution coefficient of the initial solid source and the P the total mineral/melt distribution coefficients weighted for their modal consumption into the melt.

It should be noted that this equation assumes that the distribution coefficients stay constant during the partial melting. The approximation of constant D_0 is valid providing the mineral proportions in the source are constant and the degree of partial

melting is significantly small so that none of the mineral phases are used up completely by the melt. P may be expected to remain approximately constant only for melting occurring under invariant (eutectic) melting conditions. For partial melting under variant (peritectic) conditions, P is expected to vary linearly with F (Albarède, 1995).

The fractional melting process produces distinctive magma series in which the first liquid (produced by a very small degree of melting) incorporates almost all the highly incompatible elements present in the source, and the successive liquids (generated from the residue) are strongly depleted in those elements relative to the previous melts. If there is no later mixing of the successive liquids, this process leads to characteristic concave downward patterns in normalised REE diagrams, even at small degrees of melting. In contrast, when the successive liquids are mixed, the resulting magma is almost identical to that produced by a single batch melting (Williams and Gill, 1989; Plank and Langmuir, 1992). The pooled result of fractional melting will therefore strongly resemble that of an equivalent amount of batch melting.

The melting equation outlined above have been widely criticised for being not realistic because the critical parameter is the ability of magma to separate from the solid matrix (e.g. the threshold value of the porosity of the source). Because of residual porosity after melting completion, some magma is expected to be left behind. Langmuir et al. (1977) called continuous melting (also known as dynamic melting) a fractional melting process with residual porosity. This model considers an upwelling of mantle material through a zone of melting with a continuous but incomplete removal of melt as melting proceeds. Dynamic melting can be considered as intermediate between batch- and fractional-melting because flow of melt through the system allows a substantial amount to interact with the residual solid. The process has been formulated by McKenzie (1985) and Williams and Gill (1989) as:

$$C = \frac{1}{X} \cdot \frac{C_0 G \cdot \left[1-(1-X)^{G(1-D)+1}\right]}{\left[G \cdot (1-D)+1\right]}$$

where

$$G = \frac{\left[\rho_f \cdot \phi + \rho_s (1-\phi)\right]}{\left[\rho_f \cdot \phi + \rho_s (1-\phi) D\right]}$$

C_0 is the initial concentration of the element in the source, X represents the mass

fraction of liquid extracted, D is the bulk distribution coefficient, ρ_f is the density of the melt, ρ_s is the density of the solid matrix and ϕ, expressed as a volume fraction, is the threshold value for melt separation or the porosity of the solid. Melt extraction begins when the melt fraction in the solid matrix is greater than f_0, threshold value for melt separation expressed as a mass fraction:

$$f_0 = \rho_f . \phi / [\rho_f . \phi + \rho_s(1 - \phi)]$$

As the melt porosity ϕ (and then f_0) approaches zero, the partial melting process approaches that of pure fractional melting (Williams and Gill, 1989).

6.2.2.3.2 Modelling mantle melting

An attempt has been made here to constrain, by semi-quantitative modelling, the source characteristics of the alkaline rocks from Western Anatolia in terms of trace element composition, mineralogy and the degree of melting. For the preliminary observations, the melt modelling was carried out using the non-modal batch melting equations of Shaw (1970). The modelling used the REE distribution coefficient compilation of McKenzie and O'Nions (1991; 1995) and the modal mineralogies and melting proportions of Kostopoulos and James (1992).

The purpose of the modelling was to discover whether the depleted MORB mantle (DMM) has the appropriate trace element composition to serve as the source region for Western Anatolian alkaline volcanic rocks. It should be noted that the DMM is assumed here to represent the convecting asthenospheric mantle with a composition of the hypothetical depleted MORB source proposed by McKenzie and O'Nions (1991; 1995). As the mantle source mineralogy is not precisely known, modelling was attempted with three different source compositions: (1) garnet lherzolite; (2) spinel lherzolite; and (3) mixing of garnet and spinel lherzolite (50% : 50%). The results of modelling are first looked at in terms of concentrations of highly incompatible (e.g. LRE) elements, as these are not affected significantly by variations in the source mineralogy. La and Ce were selected first in an effort to compare the concentrations of these elements in the alkaline rocks with what would be produced by variable degrees of melting of the DMM.

Figure 6.16 shows that most of the alkaline rocks from the Western Anatolian suite have La and Ce concentrations greater than that what could be generated by direct melting of a DMM, even when the degree of partial melting is very small (0.1 %). The

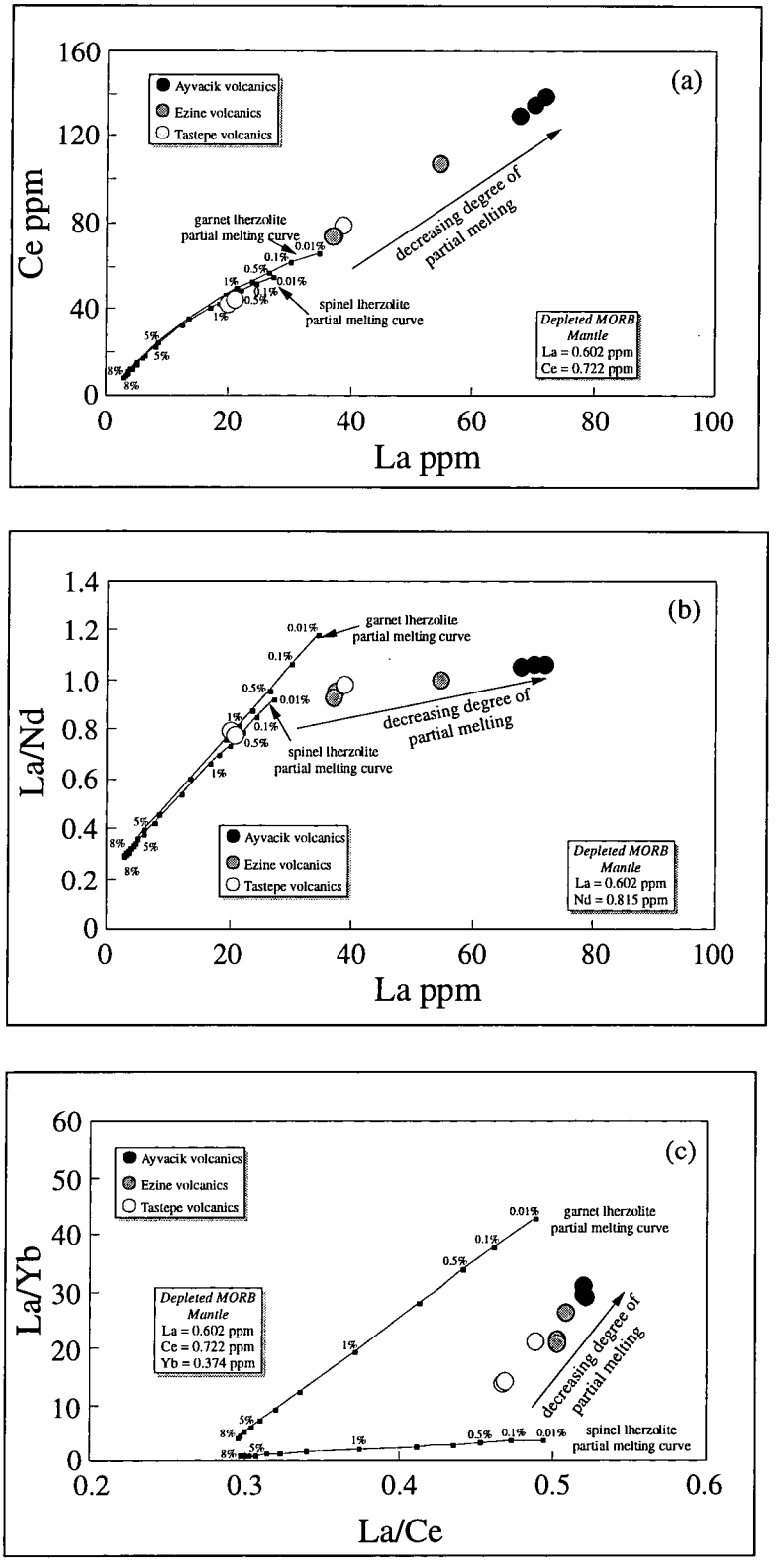

Figure 6.16. *Plots of (a) Ce and (b) La/Nd against La shows melting curves for Depleted MORB Mantle (DMM) and data from the Western Anatolian alkaline suite. The absolute abundances of plotted incompatible elements are unaffected by the mantle mineralogy, therefore the sole control is the bulk chemical composition of the source. (c) Variation of La/Yb vs La/Ce showing melting curves for a DMM-type source varying the source mineralogy. The points on the curves represent the degree of partial melting. The modal mineral proportions and distribution coefficients used in the modelling are from Table 6.6. DMM values are from McKenzie and O'Nions (1991).*

plots of La/Nd vs La and La/Yb vs La/Ce also show that the concentrations of these elements do not match those produced by direct melting of DMM-type mantle source.

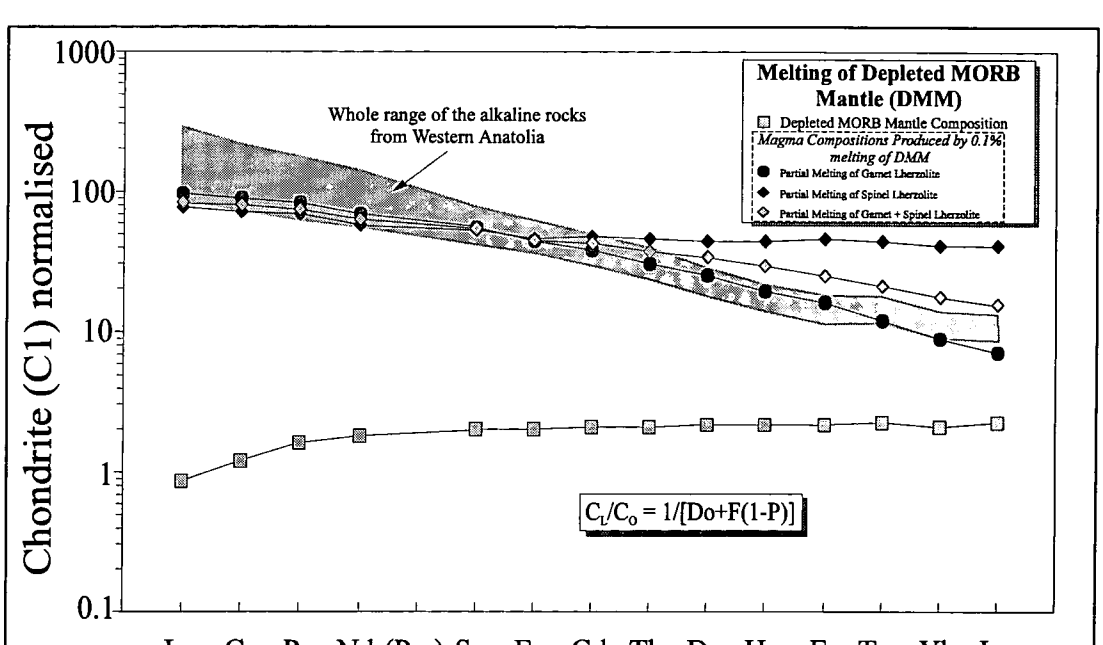

Figure 6.17. *Chondrite (C1) normalised REE patterns showing the compositions of modelled batch melts produced by 0.1% melting of a DMM-type source with mineral proportions of garnet-lherzolite, spinel-lherzolite and garnet (50%) + spinel (50%) lherzolite. The modal mineral proportions and distribution coefficients used in the modelling are from Table 6.6. Normalised values are from Boynton (1984) and the batch melting equation is from Shaw (1970). DMM values are from McKenzie and O'Nions (1991).*

When complete REE patterns are considered, the calculated concentrations of all LREE are lower than those of most alkaline rocks whereas concentrations of some MREE and all HREE vary significantly depending on the mantle mineralogy and, to lesser extent, melt proportion (Fig. 6.17). A small degree of partial melting of a spinel lherzolite source with element concentrations similar to the DMM, for example, cannot account for the M-HREE concentrations of the alkaline rocks. This indicates a residual garnet phase involvement in the source of the alkaline rocks as it creates a flat pattern in Figure 6.17.

Although using garnet or garnet + spinel lherzolite compositions may account for most M-HREE concentrations of the alkaline rocks, the model LREE abundances are still significantly lower than those of most alkaline rocks. Thus, it can be argued that the one-stage melting of DMM cannot produce magma with incompatible element concentrations similar to those of the alkaline rocks from Western Anatolia. Clearly, a mantle source that has been enriched in LREE with respect to DMM composition is

required to produce the composition of the alkaline rocks. The source compositions of the alkaline rocks will be discussed further in the following paragraphs after presenting a more rigorous trace element modelling.

6.2.2.4 Constraints on the degree of partial melting and the initial mantle composition

The characterisation of the source region from which the primitive magmas are generated is one of the major aims of the study of the mantle-derived basaltic magmatism. In recent years, as mentioned in Section 6.2.2.3.1, numerous quantitative approaches, based on geochemical data sets of increasing size and quality, have been performed to place constraints on the melting processes and parameters (e.g., nature of the melting processes, the degree of partial melting, the values for distribution coefficients between mantle minerals and magma and the chemical, isotopic and mineralogical composition of the mantle sources of the primitive basaltic magmas). Most of them rely on relatively simple models or hypothesis (e.g. the batch melting model of Shaw, 1970) and use a large number of assumptions (e.g. Hofmann and Feigenson, 1983; Ormerod et al., 1991; Feigenson and Carr, 1993), while others have developed sophisticated mathematical models (e.g., O'Hara, 1985; McKenzie and O'Nions, 1991; O'Hara, 1995) which are not always possible to test on natural systems. However, almost all of the proposed models on the mantle melting processes require making poorly-founded assumptions about melting parameters and processes. Estimation of the degree of partial melting using the conventional melting equations mentioned above, for example, requires assumptions about the element concentrations and mineral proportions (or the values for the bulk distribution coefficients) of the source mantle. However, an accurate estimation on the source concentrations is extremely difficult, especially for continental or OIB-type basalts because of possible source region metasomatism and/or interaction between magmas with different compositions. Thus, it would be useful if one could estimate the degree of partial melting without having to make assumptions about source concentrations.

There are two different methods reported for calculating the approximate degree of partial melting without making assumptions about source concentrations. One uses the concentration ratios in the source and is referred to as the source ratio (SR) method (Treuil and Joron, 1975; Minster and Allègre, 1978; Cebriá and López Ruiz, 1995). Use of the SR method is limited, as it can only be applicable to batch melting. The second is

called the concentration ratio (CR) method and uses the concentration ratios of two incompatible trace elements in at least two magmas presumed to derive from the same source. The CR method was first demonstrated by Maaløe (1994) with the equations deduced from the simple batch-melting model of Shaw (1970). Subsequently, Zou and Zindler (1996) argued that true batch-melting does not, in general, occur during basaltic magma extraction, and that dynamic melting would be a more realistic scenario. Thus, they formulated the CR method in the context of the dynamic partial melting (referred to as dynamic melting inversion or DMI method) to determine the approximate degree of melting and the source composition. The equations derived by Zou and Zindler (1996) are:

$$Q_a = \frac{C_{a1}}{C_{a2}} = \frac{X_2 \cdot \left[1-(1-X_1)^{G_a(1-D_a)+1}\right]}{X_1 \cdot \left[1-(1-X_2)^{G_a(1-D_a)+1}\right]}$$

$$Q_b = \frac{C_{b1}}{C_{b2}} = \frac{X_2 \cdot \left[1-(1-X_1)^{G_b(1-D_b)+1}\right]}{X_1 \cdot \left[1-(1-X_2)^{G_b(1-D_b)+1}\right]}$$

where

Q_a and Q_b are the enrichment ratios for two different incompatible elements between two different but cogenetic magmas (given as 1 and 2 respectively), and the rest of the parameters are given in the equation in Section 6.2.2.3.1.

After obtaining X_1 and X_2 by solving the equations (e.g. by Newton's method for a system of non-linear equations), the degree of partial melting can be calculated using the following equation;

$$f = X \cdot \left[\frac{\rho_s(1-\phi)}{(\rho_f \cdot \phi + \rho_s(1-\phi))}\right] + \left[\frac{(\rho_f \cdot \phi)}{(\rho_f \cdot \phi) + \rho_s(1-\phi)}\right]$$

(see the equation in Section 6.2.2.3 for the parameters).

The source concentrations can also be calculated from the relationship given by the equation in Section 6.2.2.3.1. It should be noted that the extent of partial melting and source composition are sensitive to variations in D_i and ϕ values, which have to be assumed. Since reported D_i values for the incompatible elements in mantle assemblages (e.g., olivine, clino- and orthopyroxenes) vary considerably (e.g., with a factor of 2 to 4 for the REEs: Frey et al., 1978; Minster and Allègre, 1978; Irvine, 1978; Leeman et al.,

1980; Chen et al., 1990; McKenzie and O'Nions, 1991) and ϕ value is not precisely known, the method should be used with caution. Zou and Zindler (1996) have tested these variations and shown that a 40% change in D_i (they used Nd as incompatible element) leads to a c.30% change in the degree of partial melting and the source composition and that a change in ϕ from 0.01 to 0.02 results in a c.20% change in these parameters.

The DMI method has been applied to the Late Miocene alkaline volcanic rocks from Western Anatolia. Several parameters should be considered in producing the above model numerically. The densities of the melt (ρ_f) and the solid matrix (ρ_s) are assumed to be 2.8 and 3.3 $g.cm^{-3}$ respectively and a value of 1% is selected as the porosity of the source (ϕ) which is considered as realistic by McKenzie (1985). For this modelling, aphyric or <10% phyric samples were selected to avoid any possible effect of mineral accumulation. The primary basalts used for the modelling range from alkaline basalts to basanites and cover the whole compositional range of the mafic alkaline suite of Western Anatolia. It is evident from the isotope data that they have been generated from the same source.

For the calculations, Th was selected as a highly incompatible element (D_{th} <0.001) to minimise the effect of the variations in the source mineralogy and the distribution coefficients on the calculations. One of the LREE (La is used here) was selected as the second (not-so-highly incompatible) component in order to achieve different enrichment ratios (Q_i) in magmas formed by different degrees of partial melting (Table 6.5). The bulk distribution coefficients for both the source mantle (D_i) and the extracted melt (P_i) were estimated using the same mineral proportions as those used in the previous melt modelling and are listed in Table 6.6. Using the enrichment ratios of (Q_{Th}) 3.88 and (Q_{La}) 3.51 between a basanite (EA270) and an alkaline basalt (EA249), degrees of partial melting of 2.9% and 10.1% have been obtained by solving the above equations (DMI method) (Table. 6.5).

For comparison, using the CR method for batch melting proposed by Maaløe (1994), degrees of partial melting have been calculated as 2.4% and 9.0% for the basanite and the alkaline basalt respectively. The difference between two methods is probably due to the ϕ value, which is not considered in the batch melt modelling. It should be noted that the estimated values of degree of melting are strongly dependent on the bulk distribution coefficients (D_i). In other words, uncertainties in the applied bulk

distribution coefficients may cause significant variations in the estimated values of degree of melting. Thus, an average estimate based on several incompatible elements would be comparable and more useful. To reduce the effect of the uncertainties in the bulk distribution coefficients, the calculations of the degree of melting have been attempted with 12 different incompatible elements using both the DMI and CR methods.

Table 6.5. *Estimation of partial melting degrees and mantle source composition for alkali basalt and basanite of the Western Anatolian suite.*

Element	D_i	P_i	Basanite (ppm)	Alkali Bas. (ppm)	Q_i	DMI		BM		Co (ppm)	$(Co)_N$
						f1 (%)	*f2 (%)*	*f1 (%)*	*f2 (%)*		
Th	0.00011	0.00021	10.20	2.63	3.88						
La	0.00559	0.03728	70.23	20.00	3.51	2.92	10.17	2.43	9.06	1.85	2.69
Ce	0.00916	0.06736	135.51	42.36	3.20	3.04	11.22	2.62	9.12	3.98	2.24
Nd	0.01942	0.05781	64.88	25.08	2.59	2.51	9.77	2.17	8.67	2.52	1.86
Ta	0.00722	0.0153	6.67	2.10	3.16	2.20	8.56	2.01	7.56	0.19	4.51
Nb	0.00782	0.01532	101.15	31.90	3.17	2.40	9.34	2.08	8.14	2.86	4.01
Average						2.61	9.81	2.26	8.51		

DMI = CR method for dynamic melting
BM = CR method for batch melting
Di = bulk distribution coefficient of the solid source; Pi = bulk distribution coefficient of the melt;
Qi = enrichment concentration ratio; *f*1 = partial melting degree for basanite; *f*2 = partial melting degree for alkali basalt;
Co = source concentration; $(Co)_N$ = C1 (chondrite) normalised Co concentrations
ϕ = 1%; *Pf* = 2.8 g/cm^3, *and Ps* = 3.3 g/cm^3

The results are given in Table 6.5 and 6.6, together with the calculated D_i and P_i values, the enrichment ratios (Q_i) and the estimated source compositions (C_0). It can be seen that the variations between the calculated degrees of melting are not significant for most of the incompatible elements. Exceptions are the HREE (Er, Tm, Yb and Lu) which behave as compatible elements in the presence of garnet in the source or in the melt mineralogy; thus, they are excluded from the estimates of the average degree of melting. The average estimates by the DMI method have been obtained as 2.8% (± 0.6) and 9.9% (± 1.5) for the basanite and the alkaline basalt samples respectively. The CR method, on the other hand, yields relatively low degrees of partial melting of 2.2% (± 0.3) and 9.2% (± 1.4) for the same samples.

The source concentrations for the Western Anatolian alkaline rocks were estimated for three different source mineral proportions. The results are plotted on a C1 (chondrite)-normalised REE diagram together with the representative compositional range of the alkaline rocks and the DMM and PM (primitive mantle) values (McKenzie

Table 6.6. Parameters used in melt modelling and estimations of degree of partial melting and source composition for the Western Anatolian alkaline rocks.

Modal proportions

Phase	Source melting mode		Solid source	
	gt-lherzolite	*sp-lherzolite*	*gt-lherzolite*	*sp-lherzolite*
oliv	0.10	0.10	0.598	0.578
opx	0.20	0.27	0.211	0.270
cpx	0.40	0.50	0.076	0.119
gt	0.30		0.115	
sp		0.13		0.033

Element	La	Ce	Pr	Nd	Sm	Eu	Gd	Tb	Dy	Ho	Er	Tm	Yb	Lu
D (crystal/matrix distribution coefficients for mantle phases in equilibrium with basaltic magma in the upper mantle)														
$D_{oliv/liq}$	0.0004	0.0005	0.0008	0.001	0.0013	0.0016	0.0015	0.0015	0.0017	0.0016	0.0015	0.0015	0.0015	0.0015
$D_{opx/liq}$	0.002	0.003	0.0048	0.0068	0.01	0.013	0.016	0.019	0.022	0.026	0.03	0.04	0.049	0.06
$D_{cpx/liq}$	0.054	0.098	0.15	0.21	0.26	0.31	0.3	0.31	0.33	0.31	0.3	0.29	0.28	0.28
$D_{gt/liq}$	0.01	0.021	0.054	0.087	0.217	0.32	0.498	0.75	1.06	1.53	2	3	4.03	5.5
$D_{sp/liq}$	0.01	0.01	0.01	0.01	0.01	0.01	0.01	0.01	0.01	0.01	0.01	0.01	0.01	0.01
D_i (Bulk distribution coefficient of the original solid)														
D_i *(gt-lherzolite)*	0.0056792	0.01029	0.0177832	0.0258668	0.0422404	0.0561408	0.071988	0.096076	0.1262656	0.1678488	0.210192	0.301592	0.395476	0.530152
D_i *(sp-lherzolite)*	0.0055936	0.009165	0.014026	0.0194288	0.0263852	0.0327594	0.036192	0.042565	0.0509188	0.0597024	0.069186	0.090596	0.112395	0.144116
P_i (Bulk distribution coefficient of minerals contributing to the melt)														
P_i *(gt-lherzolite)*	0.03728	0.067585	0.10392	0.14571	0.182835	0.21939	0.216585	0.228875	0.249155	0.24554	0.248725	0.263425	0.278575	0.309625
P_i *(sp-lherzolite)*	0.03728	0.067365	0.10304	0.14417	0.178695	0.21319	0.206825	0.214075	0.228155	0.21514	0.208925	0.203625	0.198175	0.199825
Compositional range of the primary basalt (from basanite to alkali basalt for Western Anatolian suite)														
EA270	70.23	135.14	15.89	64.88	12.33	3.73	10.17	1.47	7.33	1.27	2.94	0.45	2.37	0.34
EA249	20.00	42.86	5.57	25.08	5.93	1.94	5.85	0.85	4.35	0.77	1.78	0.28	1.47	0.21
EA260	54.65	107.47	12.97	53.75	10.51	3.20	8.89	1.30	6.46	1.12	2.62	0.40	2.07	0.29
EA254	38.68	79.27	9.34	39.59	8.29	2.57	7.39	1.09	5.46	0.97	2.23	0.34	1.83	0.26
EA82B	67.82	130.06	15.46	63.07	12.08	3.62	9.91	1.43	7.17	1.26	2.92	0.45	2.34	0.33
EA267	71.97	138.25	16.12	67.91	12.46	3.72	10.00	1.47	7.44	1.30	3.01	0.46	2.33	0.34
EA262	36.92	73.49	8.98	39.79	8.13	2.56	7.08	1.07	5.52	0.98	2.21	0.35	1.79	0.26
EA253	20.86	44.54	5.73	26.77	6.05	1.99	5.63	0.85	4.53	0.79	1.83	0.28	1.47	0.22
EA415	37.26	74.02	8.96	38.32	8.08	2.52	7.31	1.06	5.33	0.93	2.16	0.33	1.71	0.25

**D values are from McKenzie and O'Nions (1991)*

Table 6.6. (Continued)

Element	La	Ce	Pr	Nd	Sm	Eu	Gd	Tb	Dy	Ho	Er	Tm	Yb	Lu
Q_i (enrichment ratio)	3.5121	3.1530	2.8521	2.5871	2.0782	1.9171	1.7396	1.7282	1.6843	1.6632	1.6511	1.6241	1.6176	1.6115
Concentration Ratio (CR) Method for Batch Melting (Maaloe, 1994)														
f (degree of partial melting)														
gt-lherzolite														
f1	0.0192	0.0192	0.0229	0.0243	0.0147	0.0155	0.0113	0.0146	0.0175	0.0204				
f2	0.0827	0.0827	0.0956	0.1008	0.0669	0.0699	0.0552	0.0667	0.0769	0.0868				
sp-lherzolite														
f1	0.0183	0.0183	0.0218	0.0232	0.0140	0.0148	0.0108	0.0139	0.0167	0.0194				
f2	0.0788	0.0788	0.0910	0.0960	0.0637	0.0665	0.0525	0.0635	0.0733	0.0827				
Dynamic Melting Inversion (DMI) Method (Zou & Zindler, 1995)														
Φ (The threshold value of melt seperation /or the porosity of the residual solid)														
	0.01													
Ps (The density of the solid matrix [g/cm^3])														
	3.3													
Pf (The density of melt [g/cm^3])														
	2.8													
G (gt-lherzolite)	70.7781	53.4751	38.2705	29.2871	19.8495	15.5857	12.5197	9.6379	7.4800	5.7169	4.6103	3.2517	2.4962	1.8722
G (sp-lherzolite)	71.2058	56.8672	44.6338	36.0212	28.8528	24.4029	22.5316	19.7235	16.9538	14.7726	12.9709	10.1705	8.3377	6.6055
X (mass fraction of liquid extracted)														
X1	0.0189	0.0189	0.023	0.025	0.014	0.016	0.0089	0.015	0.021	0.026	0.033	0.043	0.05	0.07
X2	0.089	0.089	0.1	0.1	0.079	0.082	0.066	0.0817	0.095	0.11	0.12	0.16	0.19	0.25
f (degree of partial melting)														
f1 (for X1)	0.0272	0.0272	0.0313	0.0333	0.0224	0.0244	0.0173	0.0234	0.0293	0.0343				
f2 (for X2)	0.0967	0.0967	0.1076	0.1076	0.0868	0.0898	0.0739	0.0895	0.1027	0.1176				
Co (The source concentration; ppm)														
gt-lherzolite														
Co1 (for f1)	1.80	4.01	0.62	3.11	0.71	0.27	0.86	0.16	1.05	0.24	0.68	0.15	0.99	0.19
Co2 (for f2)	1.80	3.87	0.57	2.65	0.59	0.22	0.67	0.12	0.79	0.17	0.48	0.10	0.68	0.13
sp-lherzolite														
Co1 (for f1)	1.79	3.87	0.57	2.72	0.52	0.18	0.50	0.09	0.51	0.10	0.28	0.05	0.34	0.06
Co2 (for f2)	1.80	3.87	0.57	2.58	0.52	0.18	0.49	0.09	0.51	0.10	0.27	0.05	0.34	0.06

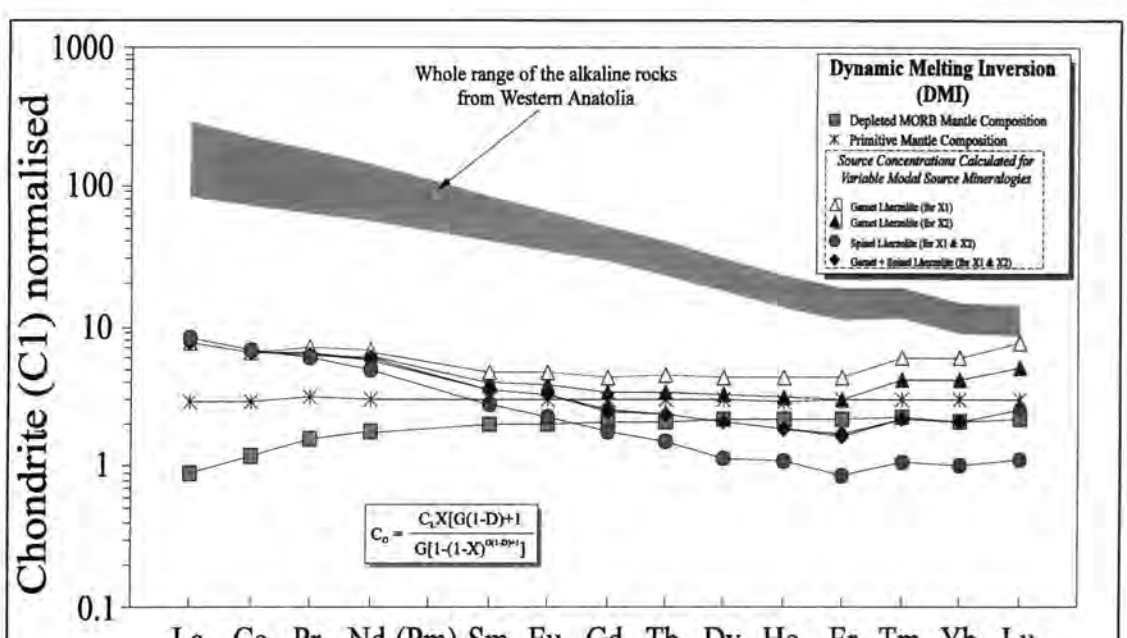

Figure 6.18. *Chondrite (C1) normalised REE patterns showing the source compositions calculated by the dynamic melting inversion (DMI) method (Zou and Zindler, 1996) using the data from the Western Anatolian alkaline basic rocks. See table 6.6 for the modal mineral proportions, the calculated source concentrations and distribution coefficients used in the modelling. Normalising values (C1) are from Boynton (1984) and DMM and PM values are from the compilation of McKenzie and O'Nions (1991).*

and O'Nions, 1991) (Fig. 6.18). It can be seen that the concentrations of the LREE are not affected by whether the source is garnet or spinel lherzolite, whereas the M-HREE are affected significantly by the source mineralogy. The estimated source concentrations range from 7.6 to 5.7 times C1 for the LREE, to 1.6 to 2.5 times C1 for the HREE when the source composition is taken as garnet + spinel lherzolite. It should be noted that two different calculations based on two different X (the mass fraction of liquid extracted) values yield similar source concentrations for all the REEs. On the other hand, using the garnet lherzolite composition yields two different ranges of source concentrations (for two different X values) for the HREE: 3.0 to 5.1 and 4.2 to 7.6 times C1 respectively. Notably, the greater the garnet involvement in the source region the greater the uncertainty of the estimated M-HREE concentrations.

An important point from the C1 normalised REE plots is that the estimated LREE concentrations of the source are always greater than those of the DMM as they range from 8.3 (La) to 3.3 (Nd) times DMM. The M-HREE, on the other hand, may be similar to those of the DMM depending on the modal mineralogy of the source.

Figure 6.19a-b show diagrams of Ce and La/Nd ratio against La for rocks representative of the whole compositional range of the Western Anatolian alkaline suite,

along with the theoretical melting curves calculated using the DMI equations. In both of these plots, the alkaline samples plot between 2% and 9% partial melting values, which decrease gradually from the Tastepe alkaline basalts towards the Ayvacik basanites.

A more useful approach to melt modelling is the use of plots of MREE/HREE against LREE abundance or LREE/HREE ratios, e.g. Eu/Yb vs La/Yb. These plots are particularly useful as they distinguish between melting of garnet- and spinel-lherzolite sources. Melting a spinel-lherzolite source produces little change in Eu/Yb ratios in melts compared with their mantle source and there is also little change in Eu/Yb with melt fraction as monitored by La/Yb ratios. Melting of a spinel lherzolite source will therefore create a horizontal trend. In contrast, melting of a garnet-lherzolite source produces large changes in Eu/Yb ratios with melt fraction, and then the melt faction is very different from the source ratio leading to a curvilinear trend on a Eu/Yb against La/Yb diagram.

Modelling of Eu/Yb and La/Yb ratios, coupled with plots of Yb against La and La/Yb against Zr/Nb is presented in Figure 6.20. It should be noted that the element concentration of the source mantle is taken as average of the DMI and CR methods. It can be seen that variable degrees of partial melting of a spinel lherzolite cannot generate the observed co-variation in Eu/Yb ratio with changing La/Yb ratio. Melting of a spinel lherzolite should produce a curvilinear trend on a diagram of Yb against La. This is clearly not the case for the observed trend of the alkaline rocks from Western Anatolia. Variable degrees of partial melting of a garnet lherzolite with mineral proportions given in Table 6.6 also cannot generate the observed trends on the Eu/Yb v La/Yb and Yb v La diagrams. First, melting of a garnet lherzolite with a given mantle composition produces melts with much higher Eu/Yb ratios than the Western Anatolian samples at a given degree of partial melting. Thus, the mantle source would require an unusually low Eu/Yb ratio if the samples were to be simply the product of garnet lherzolite melting. Second, melting of a garnet lherzolite should produce melts exhibiting a near-horizontal trend on the Yb v La diagram, as Yb is essentially retained or buffered by garnet in the source region.

The simplest model to account for the REE systematics of the Western Anatolian alkaline samples involves garnet + spinel mantle mineralogies. This is because the curved line calculated for variable degrees of melting of a source with mineral proportions accounted by 50% gt-lherzolite and 50% sp-lherzolite best fits the

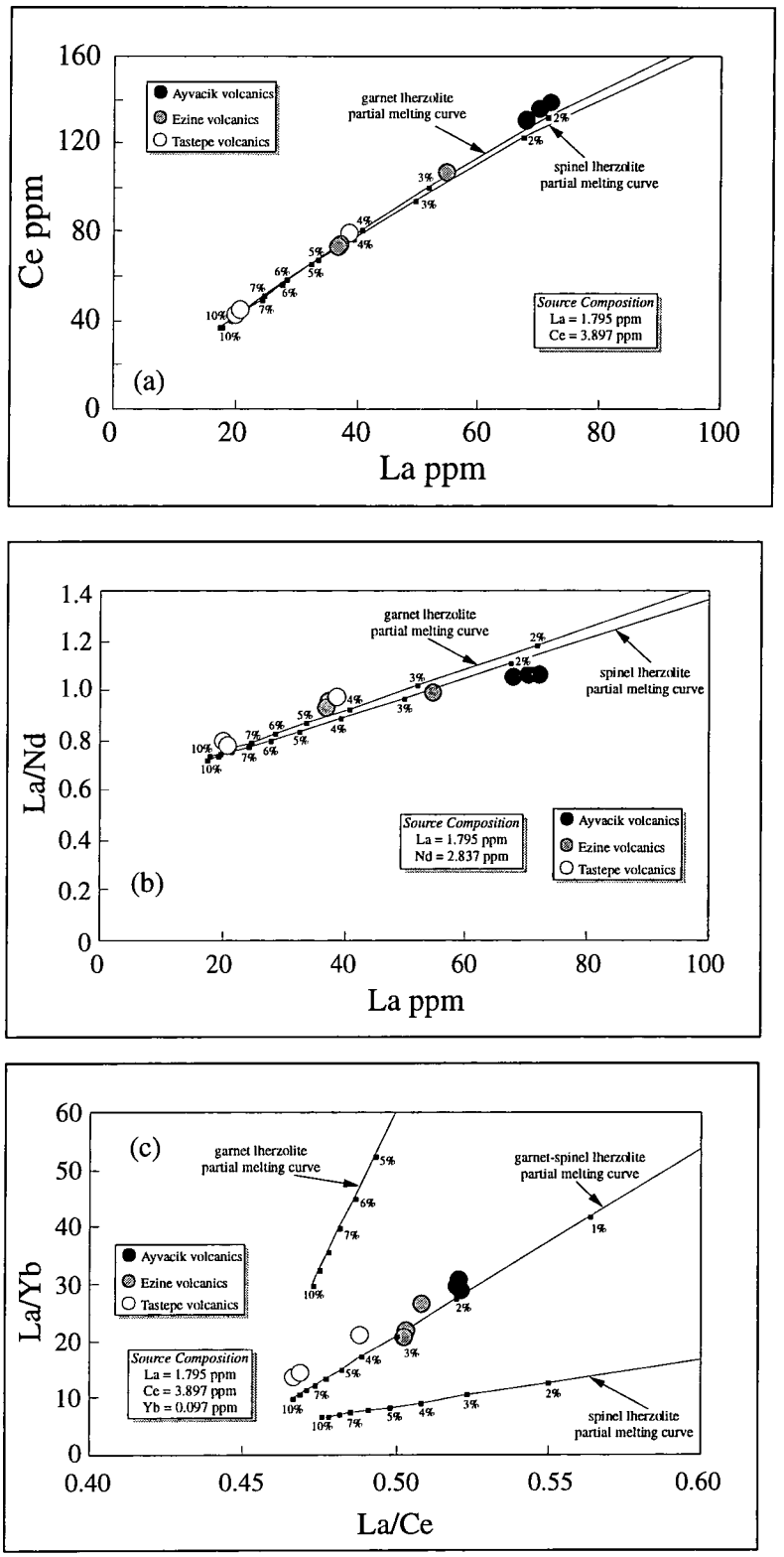

Figure 6.19. *Plots of (a) Ce and (b) La/Nd against La shows melting curves obtained using the Dynamic Melting Inversion (DMI) and data from the Western Anatolian alkaline suite. The absolute abundances of plotted incompatible elements are unaffected by the mantle mineralogy, therefore the sole control is the bulk chemical composition of the source. (c) Variation of La/Yb vs La/Ce showing melting curves obtained using DMI for varying proportions of source mineralogy. The points on the curves represent the degree of partial melting. See Table 6.6 for the modal mineral proportions and distribution coefficients used in the modelling.*

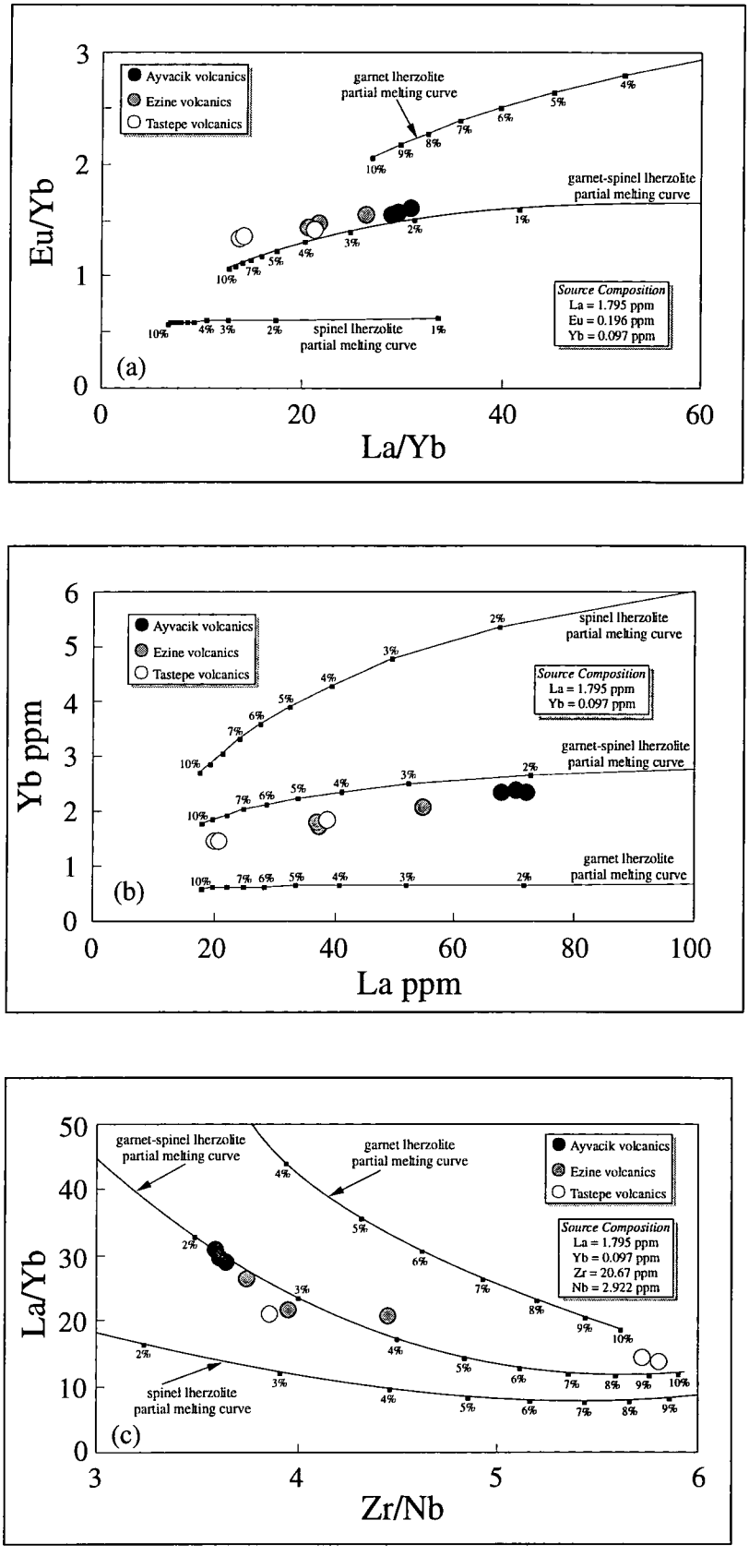

Figure 6.20. *Plots of (a) Eu/Yb vs La/Yb, (b) Yb vs La and (c) La/Yb vs Zr/Nb highlight the variation of trace element abundance and ratios with variable mineral proportions and the degree of partial melting. The parameters used in the modelling are the same as that in Figure 6.19.*

observed trends for the alkaline rocks on both the Eu/Yb v La/Yb and the Yb v La diagrams.

In summary, the compositions of the alkaline rocks of Western Anatolia represent melts from a source that is characterised by garnet involvement, although it is impossible to assess the precise composition of the source in terms of mineral abundances (e.g. garnet/clinopyroxene ratios). The average degree of partial melting apparently ranged from <2% to ~9%. The stratigraphic relationships of the alkaline rocks indicate that the degree of partial melting decreased gradually in time as the youngest rocks (the Ayvacik Volcanics) represent the smallest degrees of melting. The modelling of the bulk chemical compositions of the source indicates a source region that has been enriched in LREE relative to DMM, possibly a PM (primitive mantle)-like composition.

6.2.2.5 The Source Characteristics

The calculated REE concentrations for the mantle source of the alkaline volcanic rocks from Western Anatolia have shown that the model mantle source has considerably higher concentrations of moderately incompatible LREE with respect to the average DMM (depleted MORB mantle) source, although the concentrations of M-HREE may be similar to those of DMM. This indicates that the alkaline magma cannot be generated by a one-stage melting process from DMM even when the melt fraction is very small (<0.1%). In contrast, the Nd isotope ratios of the alkaline rocks are characterised by positive ε_{Nd} (+6.51 to +5.49) values indicating a source that was significantly depleted relative to Bulk Earth, though less depleted than most N-type MORB. It appears that this type of mantle source is the rule rather than the exception away from ridges, as many oceanic and continental alkalic primary suites have positive ε_{Nd} in association with strong LREE enrichments relative to DMM-derived rocks (N-MORB) (e.g. the Rhine graben of Western Europe and the Canary islands, the Calatrava province of Spain, the Kauai and Honolulu suites of Hawaii, the Basin and Range and the Great Basin provinces of the Western USA, SE Australia, the Tubuai suite of Austral islands: Wilson et al., 1995; Cebriá and López Ruiz, 1995; Maaløe et al., 1992; Fitton et al., 1991; Caroff et al., 1997; Hoernle et al., 1991).

The enriched nature of many oceanic and continental intraplate alkalic suites with respect to N-type MORB has been widely attributed to a lower mantle-derived

plume component in the source region. It is generally believed that the source regions from which plumes are generated are isolated from the convecting mantle, and thus have not been affected by depletion processes during MORB formation. Some scientists suggest that the most OIB components are derived from ancient recycled oceanic lithosphere, plus small amounts of sediments (also known as HIMU OIB source) (Hofmann and White, 1982; Zindler and Hart, 1986; Wilson, 1993). However, in the case of Western Anatolia, the alkaline magmatism cannot be explained by a mantle plume component because, as previously noted by McKenzie and O'Nions (1995), there is no evidence for a mantle plume beneath Western Anatolia. First, a mantle plume would be expected to produce a dynamic uplift and an elevated topography over an area about 1000-2000 km in diameter. This is clearly not the case for Western Anatolia. Second, the alkaline volcanic rocks in the area were formed in the localised extensional zones and show no symmetric expression.

An alternative view may be that the trace element concentrations are partly controlled by reactive melt transport during melting and ascent of magmas (e.g. chromatographic effects caused by percolation through partially molten mantle in the sense of Navon and Stolper, 1987, Vasseur et al., 1991 and Iwamori, 1993). It has been argued that the rate of interaction is faster in the incompatible elements than the compatible elements and, as a result, the abundance ratios of elements of different compatibilities can vary considerably with time. Thus, it could be argued that the alkali basic magma might have reacted with large volumes of solid mantle during melt migration and ascent, preferentially leaching incompatible elements from the surrounding mantle. The alkaline rocks from Western Anatolia, as mentioned in Section 6.2.2.1, show a temporal compositional trend of increasing incompatible elements with time. This is the opposite of what would be expected for reactive melt transport. As recently shown by Reiners (1998), the composition of the leading melt batch through a column of refractive mantle will be shifted towards the composition of an incipient partial melt of the mantle matrix. Successive melts migrating through and emerging from the columns will then show a temporal compositional trend that reflects the exhaustion of the reactive capacity of the mantle. Thus, these effects should be manifest as an enrichment of incompatible elements relative to the original input melt, and a temporal compositional trend of decreasing incompatible elements in erupted melt batches with time. Eventually, element concentrations should return to the original melt

concentrations in order of increasing compatibility (Reiners, 1998). Thus, enrichment in LREE concentrations cannot obviously be explained by reaction between melt and the source matrix.

Alternatively, as has often been pointed out, positive ε_{Nd} together with enrichment in LREE can be reconciled by proposing the long-term existence of a LREE-depleted source that has only recently become enriched and subsequently melted to produce the LREE-enriched magmas. These late enrichment processes are mostly considered to be due either to small volume melt fractions or to subduction.

McKenzie (1989) recognised that the bulk of continental basalt magmas probably come from metasomatised sub-continental lithospheric mantle (SCLM). He argued that a combination of small degree partial melt of asthenospheric mantle material beneath the continents and upward migration of such melts would lead to metasomatism of the base of the SCLM by melt strongly enriched in both incompatible elements (e.g. LREE) and volatiles. The enriched layer would melt at lower temperatures than normal dry mantle and, when involved in the magma genesis, would contribute to the enriched nature (in terms of LREE) of continental alkaline rocks relative to DMM-derived rocks. He also proposed that such small melts would have experienced strong fractionation of Rb from Sr, and Sm from Nd in their source region which can account for the depleted isotopic ratios observed in most continental basic alkaline rocks.

Andersen (1994) recently proposed that the convecting mantle (= asthenospheric mantle) initially has depleted trace element and isotopic characteristics (DMM-like) before upwelling and interacting with shallow and enriched (by subduction zone fluids and sediments and/or infiltration of melts from deeper mantle) mantle. He termed "perisphere", the enriched shallow mantle and suggested that it could be in the asthenosphere, or the lower part of the TBL. He further argued that the enriched part of the shallow mantle may provide the source region chemical characteristics (trace element and isotopes) similar to continental basaltic or OIB magmatism.

McKenzie and O'Nions (1995) argue that the enrichment of the SCLM and its subsequent remelting can account for the composition of all oceanic and continental basic volcanics that require an enriched (relative to DMM) source. Their model involves enrichment of the mechanical boundary layer (MBL) (in both continental and oceanic environments) by metasomatic small volume melts from the asthenosphere. They also argue that such a mechanism may account for the similarity between ocean-island and

small volume continental basalts. Their estimates of REE inversion modelling of the Kula alkaline volcanic rocks from Western Anatolia yield melt generation depths of between 55 and 70 km, a region that is 100°C or more below the solidus for anhydrous asthenospheric mantle. Their argument is that the anhydrous mantle at normal upper mantle temperatures only begins to melt when it is brought up to a depth of about 45 km, a statement based on the parameterisation by McKenzie and Bickle (1988). Thus, with no evidence for elevated mantle potential temperatures beneath Western Anatolia and, given the degree of lithospheric extension they argue that melting of anhydrous asthenospheric mantle is unlikely. Instead they propose a melt generation within a SCLM that had been previously enriched.

The proposed models (by McKenzie, 1989; McKenzie and O'Nions, 1995) outlined above require involvement of melts generated from the SCLM in order to provide the enriched compositions observed in most OIB and continental basalts. This involvement may be either by direct melting of metasomatised SCLM or by interaction of melts generated from depleted asthenospheric mantle (DMM-like) with enriched SCLM.

However, the difficulty with applying these models to Western Anatolia lies in the likely composition of the SCLM beneath Western Anatolia. It has already been shown that the SCLM beneath Western Anatolia carries a subduction component which is characterised by large negative Nb and Ta anomalies. It has also been shown that the alkaline rocks are unlikely to have generated from the same source as the earlier formed (Early-Middle Miocene), calc-alkaline and shoshonitic rocks which are the derivatives of the SCLM. Thus, the involvement of the SCLM in the genesis of the alkaline magmas is unlikely, as none of the alkaline rocks have negative Nb and Ta anomalies. The absence of hydrous mineral assemblages (unlike the Kula basalts which McKenzie and O'Nions (1995) examined) may further suggest that the involvement of the subduction modified SCLM in the genesis of the alkaline magmas is unlikely.

It could be argued that the earlier (Early-Middle Miocene) calc-alkaline and shoshonitic magmatism have removed the subduction component from the mantle that eventually provides OIB-type source (a model similar to that of Andersen, 1994). However, this requires almost total removal of incompatible trace elements from the enriched SCLM source in a geologically short period (~3Ma which is the time interval between the formation of the calc-alkaline and the alkaline magmatism), which is also

unlikely. Thus, on the basis of the assumption that the SCLM beneath Western Anatolia is not horizontally heterogeneous, the most likely site for the melt generation (for the alkaline magmas) is within asthenospheric mantle.

Since normal convecting asthenospheric mantle source with a DMM-like composition (or at least a single-stage melting of asthenospheric mantle) cannot account for the observed incompatible trace element and isotopic characteristics of the alkaline rocks, enrichment processes are required to explain the mantle source characteristics of the alkaline rocks (note that this statement is based on the assumption that the asthenospheric mantle is depleted). The Nd and Sr isotopic ratios for the alkaline samples clearly indicate time-integrated growth in reservoirs depleted in Rb/Sr and Nd/Sm relative to Bulk Earth. Thus the enrichment processes should have been recent. However, the isotopes lie between those of the MORB and HIMU-like compositions (see Fig. 6.1) and therefore do not provide strong constraints on whether the magmas are DMM derivatives. Unfortunately, there are no mantle xenoliths found either in the alkaline rocks in the area studied or elsewhere in Western Anatolia that would be useful to determine the composition of the source region. Thus, it is very difficult to assess the nature of the enrichment processes. However, in the light of the available data presented so far, several options are possible to explain the processes.

One possible explanation could be that the geochemical characteristics (in terms of trace elements and isotopes) of the asthenospheric mantle beneath Western Anatolia may be similar to that of HIMU-like component, in a manner similar to that proposed by Wilson et al. (1993) and Granet et al. (1995) for the European Asthenospheric Reservoir. From the recent work of Wilson et al. (1997) on the alkaline basaltic rocks from the north-west Central Anatolia (the Galatia province), it is apparent that the isotopic and trace element characteristics of these rocks are similar to the alkaline basalts of Western Anatolia (e.g. the Tastepe basalts). Wilson et al. (1997) proposed that the source component of the Galatia alkaline rocks (formed in a relation to the NAF) carries a HIMU-like component inferred to be present in the shallow asthenospheric mantle throughout Western and Central Europe. The difficulty with applying this model to Western Anatolia is that the isotopically-enriched nature of HIMU components relative to DMM is generally mantle plume related. Thus, enrichment processes in relation to a typical plume (e.g. as described by White and McKenzie, 1989) are unlikely for Western Anatolia for the reasons discussed above. On the other hand,

Granet et al. (1995) have recently proposed that the alkaline magmatism throughout Central and Western Europe is linked to the upwelling of a series of individual mantle diapirs which are of smaller diameter than the typical plumes (e.g. Hawaii and Iceland) and formed in association with continental break-up. A similar mechanism was invoked by Cebriá and López Ruiz (1995) to explain the genesis of the Calatrava alkaline volcanic province (Central Spain) in the absence of a typical mantle plume. Although a similar model could well explain the geochemical characteristics (in terms of trace element and isotopes) of the alkaline rocks from Western Anatolia, more data (e.g. geophysical and perhaps Hf isotopes) are needed to constrain this possibility.

An alternative explanation is that the enrichment event may be an integral part of the small degree partial melting processes of an asthenospheric mantle (DMM-like) source. In this context, it is possible that the enrichment documents an autometasomatic event, for example related to release of volatile-rich fluids in the subsolidus peridotite shortly before melting. This type of enrichment process was first discussed by Roden et al. (1984) to explain the source characteristics of the strongly LREE enriched (relative to N-MORB) and isotopically depleted OIB-type alkaline basalts from St. Paul's Island (0°56' N., 29°22' W; near the axis of the mid-Atlantic ridge). They argue that the metasomatic event is a result of the addition of either a silicate melt or a hydrous metasomatic fluid which was derived from the same mantle source as the alkaline basic rocks. Without knowing the nature of the mantle source from which the enriched material was derived, it is very difficult to assess whether it was a silicate melt or a hydrous metasomatic fluid. However, if this is the case for the enrichment process of the source region of the Western Anatolian alkaline rocks, enrichment by silica melts would be a more likely explanation rather than volatile-rich fluids, as there is no evidence for hydrous mineral assemblages in the genesis of the rocks. This then requires a multi-stage melting process in the source region.

A similar explanation has recently been proposed by Zou and Zindler (1996) for the enrichment processes in the source region of the Koloa and Honolulu volcanics of Hawaii. They argue that an integrated melting process, where the first stage affects a large volume of source material, produce, at or just prior to the true onset of melting, LREE enriched (relative to the original source material) and possibly CO_2-rich fluid or silicate melt. According to these authors, this early formed melt produced in the peripheral regions of a melting anomaly, will separate from its source and invade the

adjacent mantle to produce a second-stage source which will be affected by greater extents of melting.

If this is the mechanism that formed the melts and produced the alkaline lavas of the Western Anatolia, then, it could be argued that the model concentrations of the source that previously estimated using DMI and CR methods only characterise the second- or final-stage source that had already been modified by earlier stage of melting process(es). The original source composition prior to the metasomatism events may therefore be similar to that of DMM.

6.2.2.6 Mantle melting and magma generation in response to lithospheric extension

Adiabatic ascent is now the generally accepted mechanism for mantle melting in extensional systems. This mechanism is particularly well established at oceanic spreading centres where the system is in steady state and the physical parameters such as the potential mantle temperature, spreading rate and lithospheric thickness are reasonably well known. In continental settings, however, the mechanisms are more complicated as the mantle potential temperature, lithospheric thickness and the amount of extension have to be defined by poorly-constrained estimates. In an attempt to model magma generation processes in extensional systems, McKenzie and Bickle (1988) assumed that the melting behaviour of the mantle (both lithospheric and asthenospheric portions) could be constrained by the dry mantle peridotite solidus. The P-T diagram of Pearce et al., 1990 (used in Section 6.2.1.3) illustrates possible mechanisms that can contribute the melting and the magma production processes for the Western Anatolian alkaline magmatism (Fig. 6.21). Although there are no physical data to constrain the lithospheric structure beneath Western Anatolia, the average total lithospheric thickness has been estimated (using the average strain rate in the area) to have been not less than 70-80 km prior to the onset of the Late Miocene alkaline magmatism. The model assumes that the thermal parameters such as the mantle potential temperature (T_p), and the conductive and advective geotherm gradients are the same as that given in section 6.2.1.3.

Melting conditions of the mantle lithosphere will not be discussed here, as it is not relevant to the magma genesis of the alkaline lavas. The only possible mechanism for melt generation in asthenospheric mantle in the extensional system of Western Anatolia is melting of the normal mantle by adiabatic decompression. The validity of

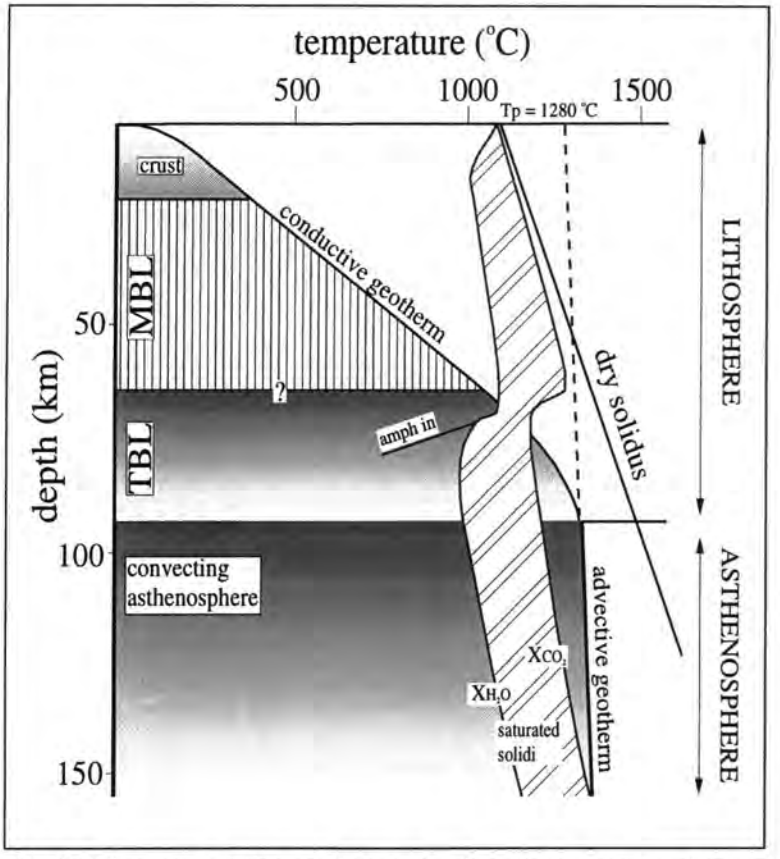

Figure 6.21. *P-T diagram showing conditions of melting in the asthenospheric mantle beneath Western Anatolia. MBL = Mechanical Boundary Layer; TBL = Thermal Boundary Layer; Tp = potential mantle temperature.*

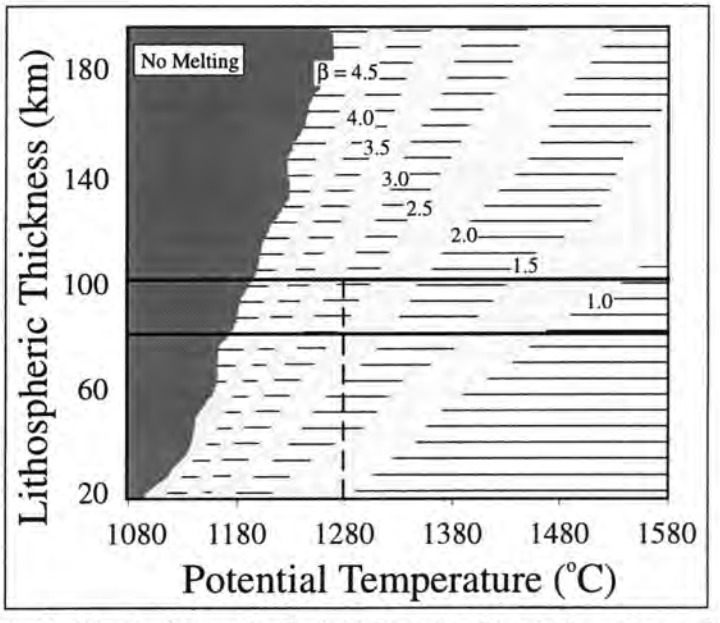

Figure 6.22. *Model calculations for the initiation of melting in the asthenospheric mantle. The contours are the stretching factor (β) required to initiate melting as a function of lithospheric thickness and the potential mantle temperature (from Bradshaw et al., 1993). The mantle viscosity is taken as 4 x 10^{15} (Bradshaw et al., 1993; Hawkesworth and Gallagher, 1993).*

this, however, depends upon the physical conditions of the asthenospheric mantle prior to melting (dry or volatile enriched) and the thickness of the overlying lithosphere which is a function of the stretching factor (β). Melting conditions in continental extensional systems have recently been discussed by Bradshaw et al. (1993) and Hawkesworth and Gallagher (1993). Figure 6.22 shows their model calculations for determining the value of β required to initiate melting (i.e. when the solidus temperature is intersected by the geotherm in Fig. 6.21) for given values of the initial lithospheric thickness (taken as MBL), mantle potential temperature and mantle viscosity. It can be seen that, for a MBL thickness of 80-100 km, melting of asthenospheric mantle under dry conditions requires β values higher than 2 – 2.5 if the mantle potential temperature is taken as 1280°C as assumed by McKenzie and Bickle (1988). The proposed β values (~1.5 Paton, 1992; McKenzie and O'Nions, 1995) for Western Anatolia are therefore not sufficient to initiate melting of the sublithospheric mantle beneath Western Anatolia. However, taking into account the fact that the alkaline volcanism in restricted to the area studied formed along the North Anatolian Fault (NAF; strike-slip), it could be argued that the melting processes are not related only to a simple or pure shear stretching, but also to lateral stretching. Consistency between the timing of the onset of the NAF and the alkaline magmatism in the area may also suggest a response to localised stretching due to the lateral stress release to initiate the melting and produce the alkaline magma.

6.3. Chapter 6 Summary

Consistent with the behaviour of the trace elements, described in Chapter 3, the isotopic characteristics also reveal two geochemically distinct sources for the Miocene volcanic rocks in Western Anatolia. These are: (1) a subduction modified, radiogenic mantle source characterised by high $^{87}Sr/^{86}Sr$ but low $^{143}Nd/^{144}Nd$ ratios (for the Early - Middle Miocene, calc-alkaline and shoshonitic volcanic rocks); and (2) an isotopically homogeneous and possibly OIB-type mantle source characterised by low $^{87}Sr/^{86}Sr$ but high $^{143}Nd/^{144}Nd$ ratios (for the Late Miocene alkaline volcanic rocks).

Fractional crystallisation modelling, combined with the estimates of the crystallisation pressures and temperatures (Chapter 5), showed that amphibole (pargasitic) crystallisation took place in deep (~28-35 km) magma chambers for almost all calc-alkaline and shoshonitic (Early-Middle Miocene) magma series from both the

EGA and DAB areas. Subsequent crystallisation histories in shallower magma chambers show some differences between the Early Miocene rocks from the EGA and DAB areas: (1) anhydrous (pyroxene + plagioclase-dominated) crystallisation assemblages in the EGA area; and (2) hydrous (edenitic hornblende + plagioclase + pyroxene) crystallisation in the DAB area. This difference is consistent with the crystallisation temperatures between the two areas (>900°C in the EGA area v <900°C in the DAB area). The Middle Miocene rocks show no indication of shallow magma chamber processes.

Fractional crystallisation modelling also showed that the ignimbrites are the products of feldspar- and biotite-dominated fractional crystallisation and their formation cannot be explained solely by crustal melting or crustal contamination.

AFC modelling showed that all Early-Middle Miocene calc-alkaline and shoshonitic rocks have been affected by assimilation combined with fractional crystallisation, but the effects of the assimilation decrease gradually from the Early Miocene into the Middle Miocene which can possibly be explained by extension and progressive crustal thinning in time.

With no evidence for elevated mantle temperatures beneath Western Anatolia (e.g. a mantle plume origin), initiation of magmatism has been inferred to have been caused by thermal perturbation of metasomatised (by subduction) sub-continental lithospheric mantle (SCLM). Because of the constraints in timing of the onset of the extension in the area and because of lack of evidence for localised extension (pre-Miocene), the likely mechanism is the delamination of the thermal boundary layer (TBL).

The alkaline magmas (the Late Miocene) have been shown to have been generated by variable degrees of partial melting of an isotopically homogenous source with garnet residue. REE inversion modelling indicates partial melting (with degrees of ~2% to ~10%) of a spinel + garnet lherzolite source with trace element compositions enriched in LREE with respect to a depleted MORB mantle (DMM) composition. On the basis of the consideration that the subduction modified SCLM beneath Western Anatolia cannot provide the observed trace element characteristics of the alkaline magmas, convecting asthenosphere is inferred to be the source for the alkaline rocks. Because of the assumption that convecting asthenospheric mantle is depleted, high levels of LREE contents (in association with depleted isotope characteristics) have been

attributed to a recent enrichment process which is either by small individual diapiric upwellings or by multiple-stage melting of convecting asthenospheric mantle.

CHAPTER SEVEN

CONCLUSIONS

Introduction

In this chapter, a general summary of results documented in previous chapters will be presented.

7.1. Volcano-stratigraphy

The evolution of the collision-related volcanism in Western Anatolia has been examined in two key areas: (1) the Ezine-Gulpinar-Ayvacik (EGA) area which is located in the southwest of the Biga Peninsula; and (2) the Dikili-Ayvalik-Bergama (DAB) area which is located further south, between the cities of Izmir and Edremit. The field observations, volcanological characteristics and radiometric data show that major volcanic activity took place both in the EGA and DAB areas during the Early Miocene. It produced a considerable volume of pyroclastics and lavas of intermediate-acid compositions. Radiometric data show that the Early Miocene volcanic activity in the area studied commenced about 21.3 ± 0.3 m.y. ago. This early stage activity in both areas was represented mainly by lava flows, domes and lava pyroclastic successions. The lavas are, in general, andesitic to rhyolitic in composition and are highly porphyritic. The pyroclastics generally form large ignimbrite deposits accompanied by minor debris (lahar) and ash flow deposits. They are mostly rhyolitic and dacitic. Clastic sedimentary deposits within the lava and pyroclastic successions indicate that the volcanic rocks formed by several eruptive phases. Abundant dyke swarms with prevalent orientations of NNW-SSE and NNE-SSW cut the volcanic successions.

Although the rock types and volcanological characteristics of the Early Miocene rocks from the two areas (EGA and DAB) are similar to one another, they show some differences in phenocryst assemblages. Amphibole is the main hydrous phase and orthopyroxene is rare or absent in the rocks from the DAB area. On the other hand, orthopyroxene is one of the most common phenocrysts and amphibole is absent in the rocks from the EGA area.

Radiometric data show that, in the EGA area, the youngest date for the Early Miocene activity is 19.7 ± 0.3 Ma. Middle Miocene activity is absent in this area. In the DAB area, the volcanic activity continued into the Middle Miocene with a gradual change in eruptive style and rock compositions. The Middle Miocene activity mostly produced lava flows and dyke swarms of basic-intermediate compositions. Pyroclastic eruptive products are absent in this period. The Middle Miocene volcanism lasted until 15.2 ± 0.4 Ma.

A new stage of volcanic activity in the EGA area began in the Late Miocene and produced locally developed small lava flows of basic and ultrabasic compositions. The Late Miocene activity continued from 11.0 ± 0.4 Ma to 8.32 ± 0.19 Ma.

7.2. Structural Evolution

In the area studied, the pre-Miocene structures cannot be recognised properly because they are mostly covered by young volcanic and sedimentary rocks and/or are complicated by the Miocene-Recent structures.

Two different structural patterns characterise the Miocene tectonics of Western Anatolia: (1) listric, normal faulting; and (2) strike-slip faulting. The former dominates the morphology, particularly in the DAB area, whereas the influence of the latter is best observed in the EGA area (along the North Anatolian Fault zone).

The major effect of the normal faulting in the area is the formation of the E-W and NE-SW trending graben (e.g. the Bergama and Edremit Graben). In most places (e.g. Edremit and Dikili), the normal faults cut the Early Miocene volcanic sequences confirming that they were formed later than the Early Miocene. The oldest volcanic rocks formed in association with the E-W trending extensional basins (graben) are the rocks of the Kalarga Andesite (17.6-17.3 Ma) and the Egrigol Andesite (15.5 Ma). These dates are much older than the Late Miocene (~12 Ma), which has been previously proposed by Sengör and Yilmaz (1981), Sengör et al. (1985), Yilmaz (1989; 1991) and Güleç (1991) for the onset of the N-S extension in Western Anatolia. The above dates are also younger than the Late Oligocene-Early Miocene (~ 24-20 Ma) which are the dates proposed by Seyitoglu and Scott (1992) and Seyitoglu et al. (1997) for the onset of the extension.

The strike-slip faults strongly control the morphology along the north side of Edremit Bay (the southern branch of the NAF) and along the Bayramic trough (the middle branch of the NAF). The distribution of the Late Miocene volcanic rocks along

the strike-slip faults implies a close relationship with the strike-slip movements in the area. The consistency between the timing of the onset of the strike-slip movement and the formation of the Late Miocene rocks also supports this hypothesis.

7.3. Magmatic evolution

The volcanic products of the Western Anatolian, Late Cenozoic Volcanic Province can be divided into two main groups on the basis of their major-trace element and isotopic characteristics. These are: (1) the Early-Middle Miocene calc-alkaline and shoshonitic rocks; and (2) the Late Miocene alkaline rocks.

The calc-alkaline and shoshonitic rocks have enrichments in LILE and LREE relative to the HFSE (characterised by negative Ta and Nb anomalies). This has been interpreted as evidence for enrichment of the magma source by a subduction component which is most probably inherited from pre-collision subduction event. The presence of this subduction component is well illustrated by multielement patterns and by the Th/Yb versus Ta/Yb ratio plot (Chapter 3). In the latter, the calc-alkaline and shoshonitic rocks display a consistent displacement from the mantle trend towards higher Th/Yb values. In keeping with the behaviour of the trace elements, the isotopic characteristics also reveal a subduction modified, radiogenic mantle source characterised by high $^{87}Sr/^{86}Sr$ but low $^{143}Nd/^{144}Nd$ ratios for the Early-Middle Miocene, calc-alkaline and shoshonitic volcanic rocks (Chapter 6).

The crystallisation pressure estimates (Chapter 5) and petrographic characteristics (Chapter 4) showed that the Early Miocene volcanic rocks from both the EGA and DAB areas have a polybaric origin and are the products of more than one petrogenetic processes. This is evident from the strong compositional variations in a single phenocryst, as well as from the highly variable crystallisation pressures.

Fractional crystallisation modelling, combined with the estimates of the crystallisation pressures and temperatures, showed that amphibole (pargasitic) crystallisation took place in deep (~28-35 km) magma chambers for almost all calc-alkaline and shoshonitic (Early-Middle Miocene) magma series from both the EGA and DAB areas. Subsequent crystallisation histories in shallower magma chambers show some differences between the Early Miocene rocks from the EGA and DAB areas: (1) anhydrous (pyroxene + plagioclase-dominated) crystallisation assemblages in the EGA area; and (2) hydrous (edenitic hornblende + plagioclase + pyroxene) crystallisation in the DAB area. This difference is consistent with the crystallisation temperatures

between the two areas (>900°C in the EGA area v <900°C in the DAB area). The Middle Miocene rocks show no indication of shallow magma chamber processes.

Fractional crystallisation modelling shows that the ignimbrites in the area are the products of feldspar- and biotite-dominated fractional crystallisation and that their formation cannot be explained solely by crustal melting or crustal contamination.

Modelling of the trace element and isotopic data (Chapter 6) shows that the Early-Middle Miocene calc-alkaline and shoshonitic rocks have been affected by assimilation combined with fractional crystallisation (AFC) processes, and that the effects of the assimilation decrease gradually from the Early Miocene into the Middle Miocene. This can most likely be explained by rapid ascent of the magmas through the continental crust as a consequence of progressive crustal thinning related to extensional tectonics from the latest Early Miocene onwards. Petrographic observations also reveal that the phenocryst contents of the rocks decrease from the Early Miocene into the Middle Miocene which can be attributed to a rapid movement of the magmas during their ascent through the crust.

Because of the weight of evidence against elevated mantle temperatures beneath Western Anatolia, and hence against a mantle plume origin, initiation of magmatism across the Western Anatolian collision zone has been inferred to have been caused by thermal perturbation of metasomatised (by subduction) sub-continental lithospheric mantle (SCLM). Because of the constraints in timing of the onset of the extension in the area (e.g. the magmatism started before the oldest date proposed for the onset of the extension) and because of lack of evidence for localised extension (pre-Miocene), the likely mechanism is the delamination of the thermal boundary layer (TBL) (Chapter 6). This delamination would have caused the direct contact of hot asthenospheric mantle with the metasomatised part of the SCLM beneath Western Anatolia and thus initiated the melting. Delamination of the MBL also have increased the thermal gradient, and hence weakened the lithosphere. This may then have assisted or initiated lithospheric extension (orogenic collapse) that followed collision and uplift.

The Late Miocene, alkaline rocks are mostly classified as basalts and basanites with their low silica contents ranging between 42 and 50 wt.% SiO_2. They are sodic alkaline ($[Na_2O-2]>K_2O$) and are characterised by high TiO_2 (2.5-3.1 wt.%) and low Al_2O_3 (12-15 wt. %) contents. In general, they show OIB-like trace element patterns characterised by enrichment in LILE, HFSE and L-MREE, and a slight depletion in HREE relative to the N-MORB composition. Unlike the Early-Middle Miocene

volcanic rocks, none of the alkali basalt or basanite samples of Late Miocene age have negative Ta or Nb anomalies. This indicates that: (1) the source region for the alkali basalts and basanites carry no subduction component; (2) the alkaline magmas have not been affected by crustal contamination processes; and (3) the Late Miocene alkaline rocks have not been derived from the same source as the earlier calc-alkaline and shoshonitic rocks. The isotopic characteristics also indicate an OIB-type mantle source characterised by low $^{87}Sr/^{86}Sr$ but high $^{143}Nd/^{144}Nd$ ratios for the Late Miocene, alkaline volcanic rocks.

The alkaline magmas have been shown, by semi-quantitative modelling, to have been generated by variable degrees of partial melting of an isotopically homogenous mantle source with a garnet residue. REE inversion modelling indicates partial melting (with degrees of ~2 to ~10) of a spinel + garnet lherzolite source with trace element compositions enriched in LREE with respect to a depleted MORB mantle (DMM) composition. Because subduction modified SCLM beneath Western Anatolia cannot produce the observed trace element characteristics of the alkaline magmas, convecting asthenosphere is inferred to have been the source for the alkaline rocks. Because of the general assumption that convecting asthenospheric mantle is depleted, high levels of LREE contents (in association with depleted isotope characteristics) have been attributed to a recent enrichment process, linked either to small individual mantle diapirs or to multiple-stage melting of convecting asthenospheric mantle. The likely mechanism for melting of the asthenospheric mantle in the area, where the stretching factor (β) is approximately 1.5, is decompression melting resulting from the movement of the North Anatolian Fault.

REFERENCES

ADAMIA, SH. A., CHKHOTUA, T., KEKELIA, M., LORDKIPANIDZE, M., SHAVISHILI, L. & ZAKARIADZE, G., 1981. Tectonics of the Caucasus and adjoining regions: implications for the evolution of the Tethys ocean. *Journal of Structural Geology*, **3**, 437-447.

AITCHENSON, S.J. & FORREST, A.H., 1994. Quantification of crustal contamination in open magmatic systems. *Journal of Petrology,* **35**, 461-488.

ALBARÉDE, F., 1995. Introduction to geochemical modelling. Cambridge University Press.

ALBARÉDE, F., 1983. Inversion of batch melting equations and the trace element pattern of the mantle. *Journal of Geophysical Research,* **88**, 10,573-10,583.

ALBARÉDE, F., 1992. How deep do common basalts form and differentiate? *Journal of Geophysical Research,* **97**, 10,997-11,009.

ALDANMAZ, E. & PEARCE, J.A., 1997. Geochemical characteristics of Late Cenozoic collision volcanism in Turkey. Terra abs., **9**, 52.

ALDANMAZ, E., PEARCE, J.A., THIRLWALL, M.F. & MITCHELL, J.G., (in prep.) Genesis of Late Cenozoic collision volcanism in Western Anatolia, Turkey.

ALLÉGRE, C.J. & MINSTER, J.F., 1978. Quantitative models of trace element behaviour in magmatic processes. *Earth and Planetary Science Letters,* **38**, 1.

ALTHERR, R., HENJES-KUNST, F., MATTHEWS, A., FRIEDRICHSEN, H. & HANSEN, B.T., 1988. O-Sr isotopic variations in Miocene granitoids from the Aegean: evidence for an origin by combined assimilation and fractional crystallisation. *Contributions to Mineralogy and Petrology,* **100**, 528-541.

ANDERSEN, D.J. & LINDSLEY, D.H., 1979. The olivine-ilmenite thermometer. Proceedings of the 10th Lunar and Planetary Science Conference, 493-508.

ANDERSEN, D.J. & LINDSLEY, D.H., 1981. A Valid Margules formulation for an asymmetric ternary solution: revision of the olivine-ilmenite thermometer. *Geochimica et Cosmochimica Acta,* **45**, 847-852.

ANDERSEN, D.J. & LINDSLEY, D.H., 1988. Internally consistent solution models for Fe-Mg-Mn-Ti oxides: Fe-Ti oxides. *American Mineralogist,* **73**, 714-726.

ANDERSON, D.L., 1994. The sublithospheric mantle as the source of continental flood basalts; the case against the continental lithosphere and plume had reservoirs. *Earth and Planetary Science Letters,* **123**, 269-280.

ANGELIER, J., DUMONT, J.F., KAHRAMANDERESI, H., POISSON, A., SIMSEK, S. & UYSAL, S., 1981. Analysis of fault mechanisms and expansion of southwestern Anatolia since the Late Miocene. *Tectonophysics,* **75**, 1-90.

ARNDT, N.T. & CHRISTENSEN, U.R., 1992. The role of lithospheric mantle in continental flood volcanism: thermal and geochemical constrains. *Journal of Geophysical Research,* **97**, 10,967-10,981.

ATAMAN, G., 1975. Plutonism calco-alkalin d'age Alpin and Anatolia du Nord-Quest. *Acad. Sci. Paris*, **280**, 2065-2068.

BACON, C.R. & HIRSCHMANN, M.M., 1988. Mg/Mn partitioning as a test for equilibrium between coexisting Fe-Ti oxides. *American Mineralogist,* **73**, 57-61.

BAILEY, D.K., 1987. Mantle metasomatism – perspective and prospect. *Geological Society, London, Special Publication,* **30**, 1-13.

BARKA, A.A. & KADINSKY-CADE, C., 1988. Strike-slip fault geometry in Turkey and its effort on earthquake activity. *Tectonics*, **7**, 663-684.

BARKA, A.A. & HANCOCK, P.L., 1984. Neotectonic deformation patterns in the convex-northwards arc of the North Anatolian Fault. In: J.E. Dixon and A.H.F. Robertson (Editors), The Geological Evolution of the Eastern Mediterranean. *Geological Society, London, Special Publication,* **17**, 763-773.

BENDA, L. & MEULENKAMP, J.E., 1979. Biostratigraphy correlations in the Eastern Mediterranean Neogene. 5. Calibration of sporomorph associations, marine microfossils and mammal zones and continental stages and the radiometric scale. *Ann. Geol. Pays Hell. (hors ser),* **1**, 61-70.

BERMAN, R.G., 1988. Internally-consistent themodynamic data for minerals in the system Na_2O-K_2O-CaO-MgO-FeO-Fe_2O_3-Al_2O_3-SiO_2-TiO_2-H_2O-CO_2. *Journal of Petrology*, **29**, 445-522.

BINGÖL, E., 1969. Geology of the central and southern sections of the Kazdag Massif. *Bulletin of Mineral Research and Exploration Inst. Turkey,* **72**, 102-123.

BINGÖL, E., 1971. Aplication of Rb-Sr and K-Ar geochronological measurements to the Kazdag Mountains, Turkey. *Bulletin of Geological Society of Turkey,* **14**, 1-6.

BINGÖL, E., 1977. Muratdagi jeolojisi ve ana kayac birimlerinin petrolojisi (Geology and petrology of Muratdagi region). *Bulletin of Geological Society of Turkey,* **20**, 13-67.

BINGÖL, E., DELALOYE, M. & ATAMAN, G., 1982. Granitic intrusions in western Anatolia: a contribution to the geodynamic study of this area. *Eclogae Geol. Helv.,* **75**, 437-446.

BIRD, P., 1978. Initiation intracontinental subduction in the Himalaya. *Journal of Geophysical Research,* **83**, 4,975-4,987.

BIRD, P., 1979. Continental delamination and the Colorado Plateau. *Journal of Geophysical Research,* **84**, 7,561-7,571.

BIRD, P. & BAUMGARDNER, J., 1981. Steady propogation of delamination events. *Journal of Geophysical Research,* **86**, 4,891-4,903.

BLUNDY, J.D. & HOLLAND, J.B., 1992. "Calcic amphibole equilibria and a new plagioclase-amphibole geothermometer": reply to the comments of Hammarstrom and Zen, and Rutherford and Johnson. *Contributions to Mineralogy and Petrology,* **111**, 269-272.

BLUNDY, J.D. & HOLLAND, J.B., 1992. "Calcic amphibole equilibria and a new plagioclase-amphibole geothermometer": reply to the comments of Poli and Schmidt. *Contributions to Mineralogy and Petrology,* **111**, 278-282.

BLUNDY, J.D. & HOLLAND, J.B., 1992. Calcic amphibole equilibria and a new plagioclase-amphibole geothermometer. *Contributions to Mineralogy and Petrology,* **104**, 208-224.

BOYD, F.R., 1973. A pyroxene geotherm. *Geochimica et Cosmochimica Acta,* **37**, 2,533-2,546.

BOYNTON, W.V., 1984. Geochemistry of the rare earth elements: meteorite studies, in P. Henderson editor (Editor), Rare Earth Element Geochemistry. Elsevier, pp. 63-114.

BORSI, S., FERRARA, G., INNOCENTI, F. & MAZUOLI, R., 1972. Geochronology and petrology of recent volcanics in the Eastern Aegean Sea. *Bulletin Volcanologique*, **36**, 473-96.

BOZKURT, E., WINCHESTER, J.A. & PARK, R.G., 1995. Geochemistry and tectonic significance of augen gneisses from southern Menderes Massif (West Turkey). *Geological Magazine,* **132**, 287-301.

BRADSHAW, T.K, HAWKESWORTH, C.J. & GALLAGHER, K., 1993. Basaltic volcanism in the southern basin and range: No role for a mantle plume. *Earth and Planetary Science Letters,* **116**, 45-57.

BRIQUEU, L., JAVOY, M., LANCELOT, J.R. & TATSUMOTO, M., 1986. Isotope geochemistry of recent magmatism in the Aegean arc: Sr, Nd, Hf and O isotopic ratios in the lavas of Milos and Santorini-geodynamic implications. *Earth and Planetary Science Letters,* **80**, 41-54.

BUDDINGTON, A.F. & LINDSLEY, D.H., 1964. Iron-titanium oxide minerals and synthetic equivalents. *Journal of Petrology,* **5**, 310-357.

BUDDINGTON, A.F., 1956. Thermometric and petrogenetic significance of titaniferous magnetite. *American Journal of Science*, **254**, 511-515.

CAMPBELL, I.H. & GRIFFITHS, R.W., 1990. Implications of mantle plume structure for the evolution of the flood-basalts. *Earth and Planetary Science Letters,* **99**, 79-93.

CAROFF, M., MAURY, R.C., GUILLE, G. & COTTEN, J., 1997. Partial melting below Tubuai (Austral Island, French Polynesia). *Contributions to Mineralogy and Petrology,* **127**, 369-382.

CAS, R.A.F. & WRIGHT, J.V., 1988. Volcanic Successions Modern and Ancient. Unwin Hyman, London, 485pp.

CAVAZZINI, G., 1996. Degrees of contamination in magmas evolving by assimilation-fractional crystallisation. *Geochimica et Cosmochimica Acta,* **60**, 2049-2052.

CEBRIÁ. J-M. & LÓPEZ-RUIZ. J., 1995. Alkali basalts and leucitites in an extensional intracontinental plate setting: the Late Cenozoic Calatrava Volcanic Province (central Spain). *Lithos*, **35**, 27-46.

CHEN, C.Y., FREY, F.A. & GARCIA, M.O., 1990. Evolution of alkali lavas at Haleakala volcano, east Maui, Hawaii. *Contributions to Mineralogy and Petrology,* **105**, 197-218. .

COX, K.G., BELL, J.D. & PANKHURST, R.J., 1989. The interpretation of igneous rocks, *sixth edition,* Unwin Hyman, London.

DAL NEGRO, A., MOLIN, G.M., SALVIULO, G., SECCO, L., CUNDARI, A. & PICCIRILLO, E.M., 1989a. Crystal chemistry of clinopyroxene and its petrogenetic significance: a new approach. In: A. Boriani, M. Bonafede, M. Piccardo and G.B Vali (Editors). The Lithosphere in Italy. Acc. Naz Lincei, Atti Convegni Lincei, **80**, 271-295.

DAL NEGRO, A., MANOLI, S., SECCO, L. & PICCIRILLO, E.M., 1989b. Megacrystic clinopyroxenes from Victoria (Australia): crystal chemical comparisons of pyroxenes from high and low-pressure regimes. *European Journal Mineralogy,* **1**, 105-121.

DEPAOLO, D.J., 1981. Trace element and isotopic effects of combined wall rock assimilation and fractional crystallisation. *Earth and Planetary Science Letters,* **53**, 189-202.

DEPAOLO, D.J. & WASSERBURG, G.J., 1979. Petrogenetic mixing models and Nd-Sr isotopic patterns. *Geochimica et Cosmochimica Acta,* **43**, 615-627.

DEWEY, J. F., 1988. Extensional collapse of orogens. *Tectonics*, **7**, 1123-1139.

DUNGAN , M.A. & RHODES, J.M., 1978. Residual glases and melt inclusions in basalts from DSDP Legs 45 and 46: Evidence for magma mixing. *Contributions to Mineralogy and Petrology,* **67**, 417-431.

DURR, S., ALTHERR, R., KELLER, J., OKRUSCH, M. & SEIDEL, E., 1978. The median Aegean crystalline belt: Stratigtaphy, structure, metamorphism, magmatism. In: H. Colos, Roeder, D. and K. Schmidth (Editors), Alps, Appenines, Hellenides. Schweizerbarth'sche Varlagsbuchhandlung, Stuttgart, pp. 455-477.

ELLAM, R.M., 1992. Lithospheric thickness as a control on basalt geochemistry. *Geology,* **20**, 153-156.

ELLAM, R.M. & COX, K.G., 1991. An interpretation of Karoo picrite basalts in terms of interaction between asthenospheric magmas and mantle lithosphere. *Earth and Planetary Science Letters,* **105**, 330-342.

ENGLAND, P.C. & HOUSEMAN, G.A., 1988. The mechanisms of the Tibetan Plateau. *Philosophical Transactions of Royal Society, London,* **A326**, 301-320.

ENGLAND, P.C. & THOMPSON, A., 1986. Some thermal and tectonic models for the crustal melting in continental collision zones. In: M.P. Coward and A.C. Ries (Editors) Collision Tectonics. *Geological Society Special Publication,* **19**, 83-94.

ERCAN, T., 1979. Bati Anadolu, Trakya ve Ege adalarindaki senozoyik volkanizmasi (The Cenozoic volcanism in West Anatolia, Trace and Aegean islands). *Bulletin of Geological Society of Turkey,* **9**, 23-46.

ERCAN, T., 1982. Kula yöresinin jeolojisi ve volkanitlerin petrolojisi (The geology of Kula area and petrology of volcanic rocks). *Bulletin of Geoscience, Istanbul,* **3**, 77-124.

ERCAN, T., SATIR, M., KREUZER, H., TÜRKECAN, A., GÜNAY, E., ÇEVIKBAŞ, A., ATEŞ, M. & CAN, B. 1984. Bati Anadolu Senozoyik volkanitlerine ait yeni kimyasal, izotopik ve radyometrik verilerin yorumu (Interpretation of new chemical. Isotopic and radiometric data on Cenozoic volcanics of western Anatolia). *Bulletin of Geological Society of Turkey,* **28**, 121-136.

ERCAN, T., SATIR, M., KREUZER, H., TÜRKECAN, A., AKYÜREK, B., ÇEVIKBAŞ, GÜNAY, E., A., ATEŞ, M. & CAN, B. 1986. Ayvalik cevresinin jeolojisi ve volkanik kayaclarin petrolojisi (The geology of Ayvalik area and petrology of volcanic rocks. *Geological Engineering,* **27**, 19-30.

ERCAN, T., TÜRKECAN, A., CAN, B. GÜNAY, E., ÇEVIKBAŞ, A. & ATEŞ, M. 1987. Bati Anadoluda Manisa-Balikesir arasindaki Tersiyer yasli yalanci basaltlarin ozellikleri (Characteristic features of the Tertiary aged Pseudobasalts of Manisa-Balikesir area). *Geological Engineering* , **30/31**, 31-42.

ERCAN, T., SATIR, M., STEINITZ, G., DORA, A., SARIFAKIOGLU, E., ADIS, C., WALTER, H.J. & YILDIRIM, T. 1995. Biga yarimadasi ile Gokceada, Bozcaada ve Tavsan adalarindaki (KB Anadolu) Tersiyer volcanismasinin ozellikleri (Characteristics of the Tertiary volcanism in the Biga Peninsula, Gokceada, Bozcaada and Tavsanadasi, western Anatolia). *Bulletin of Geological Society of Turkey,* **28**, 121-136. *Bulletin of Mineral Research and Exploration Inst. Turkey,* **117**, 55-86.

ERCAN, T., SATIR, M., 1994. Re-interpretation of radiometric dating of Tertiary volcanism of the Biga Peninsula (NW Anatolia, Turkey). International Volcanological Congress (IAVCEI) Ankara, Turkey. (Abstract).

ERTÜRK, O., DINCOZ, E. & ALAYGUT, D., 1990. Petrology of the Cenozoic volcanics in the Biga Peninsula, NW Turkey. *Proc. Int. Earth Sci. Congr. On Aegean Regions, Izmir,* 368-383.

EWART, A., HILDRETH, W. & CARMICHAEL, I.S.E., 1975. Quaternary acid magma in New Zelland. *Contributions to Mineralogy and Petrology,* **58**, 1-27.

EYIDOĞAN, H. & JACKSON, J., 1985. A seismological study of normal faulting in the Demirci, Alasehir and Gediz earthquakes of 1969-1970 in Western Turkey: implications for the nature and geometry of deformation in the continental crust. *Geophysical Journal of the Royal Astronomical Society,* **81**, 569-607.

FAURE, G., 1986. Principles of Isotope Geology. Wiley, New York, 589 pp.

FEIGENSON, M.D. & CARR, M.J., 1993. The source of central American lavas: inferences from geochemical inverse modelling. *Contributions to Mineralogy and Petrology,* **113**, 226-235.

FITTON, J.G. & JAMES, D., 1991. Basic magmatism associated with Late Cenozoic extension in the Western Untied States: compositional variations in space and time. *Journal of Geophysical Research,* **96 (B8)**, 13,693-13,711.

FITTON, J.G. & JAMES, D., KEMPTON, P.D., ORMEROD, D.S. & LEEMAN, W.P., 1988. The role of Lithospheric mantle in the generation of late Cenozoic basic magmas in the Western United States. *Journal of Petrology, Special Lithospheric issue,* pp. 331-349.

FLOYD, P.A., HELVACI, C. & MITTWEDE, S.K., 1998. Geochemical discrimination of volcanic rocks associated with borate deposits: an exploration tool. *Journal of Geochemical Exploration*, **60**, 185-205.

FODEN, J.D. & GREEN, D.H. , 1992. Possible role of amphibole in the origin of andesite: some experimental and natural evidence. *Contributions to Mineralogy and Petrology,* **109**, 479-493.

FREY, F.A., GREEN, D.F. & ROY, S.D., 1978. Integrated models of basalt petrogenesis: A study of quartz tholeiites to olivine melilitites from southeastern Australia utilising geochemical and experimental petrological data. *Journal of Petrology,* **19**, 463-513.

FYTIKAS, M., GUILANNI, O., INNOCENTI, F., MARIALLI, G. & MAZZUOLI, R., 1976. Geochronological data on recent magmatism of the Aegean Sea. *Tectonophysics,* **31**, 29-31.

FYTIKAS, M., INNOCENTI, F., MANETTI, P. & MAZZUOLI, R., PECCERILLO, A. & VILLARI, L., 1984. Tertiary to Quaternary evolution of volcanism in the Aegean region. In: J.E. Dixon and A.H.F. Robertson (Editors), The Geological Evolution of the Eastern Mediterranean. *Geological Society, London, Special Publication,* **17**, 106-129.

GALLAGHER, K. & HAWKESWORTH, C.J., (1992) Dehydration melting and the generation of continental flood basalts, *Nature*, **358**, 57-59.

GAMBLE, R.P. & TAYLOR, L.A., 1980. Crystal/liquid partitioning augite: affects of cooling rate. *Earth and Planetary Science Letters,* **47**, 21-33.

GARRY, M., MCAFEE, R. & WOLF, C.L., 1972. Glossary of geology. American Geological Institute, Washington DC.

GAST, P.W., 1968. Trace element fractionation and origin of tholeiitic and alkaline magma types. *Geochimica et Cosmochimica Acta,* **32**, 1057-1086.

GHIORSO, M.S. & CARMICHAEL, I.S.E., 1981. A FORTRAN IV computer program for evaluating temperatures and oxygen fugacities from the composition of coexisting iron-titanium oxides. *Comp. Geosc.*, **7**, 123-129.

GHIORSO, M.S. & SACK, R.O., 1991. Fe-Ti Oxide geothermometry: Thermodynamic formulation and the estimation of intensive variables in silicic magmas. *Contributions to Mineralogy and Petrology,* **108**, 485-510.

GIBSON, S.A., THOMPSON, R.N., LEAT, P.T., DICKIN, A.P., MORRISON, M.A., HENDRY, G.L. & MITCHELL, J.G., 1992. Asthenosphere-derived magmatism in the Rio-Grande rift, western USA: implications for continental break-up. In: B.C. Storey, T. Alabaster, R.J. Pankhurst (Editors), Magmatism and the causes of continental break-up: *Geological Society, London, Special Publication,* **68**, 61-89.

GILL, J.B., 1981. Orogenic Andesites and Plate Tectonics. Springer, Berlin, 390 pp.

GOLDSTEIN, S.L., O'NIONS, R.K. & HAMILTON, P.J., 1984. A Sm-Nd isotopic study of atmospheric dusts and particulates from major river systems. *Earth and Planetary Science Letters,* **70**, 221-236.

GÓMEZ, J.M.C., 1990. A program for pyroxene classification and calculation of end-members. *American Mineralogist*, **75**, 1426-1427.

GRAHAM, C.M. & POWELL, R., 1984. A garnet-hornblende geothermometer: calibration, testing and application to the Pelona Schist, southern California. *Earth and Planetary Science Letters,* **31**, 142-152.

GRANET, M., WILSON, M. & ACHAUER, U., 1995. Imaging a mantle plume beneath the French Massif Central. *Earth and Planetary Science Letters,* **136**, 281-296.

GREEN, T.H., 1982. Anatexis of mafic crust and high pressure crystallisation of andesite. In: R.S. Thorpe (Editor), Orogenic Andesites. Wiley, Chichester, U.K., pp. 465-487.

GREEN, T.H. & HIBBERSON, W., 1970. Experimental duplication of conditions of precipitation of high-pressure phenocrysts in a basaltic magma. *Phys. Earth Planet Inter.,* **3**, 247-254.

GROVE, T.L. & BENCE, A.E., 1977. Experimental study of pyroxene-liquid interaction in quartz-normative 15997. Eighteenth Lunar and Planetary Science Conference Proceedings, pp. 1549-1580.

GRUNDER, A.L. & MAHOOD, G.A., 1988. Physical and chemical models of zoned silicic magmas: the Loma Seca Tuff and Calabozos Caldera, South Andes. *Journal of Petrology,* **29**, 831-867.

GÜLEÇ, N., 1991. Crust-Mantle interaction in Western Turkey: implications from Sr and Nd isotope geochemistry of the Tertiary and Quaternary volcanics. *Geological Magazine,* **128**, 417-435.

GÜLEN, L., HART, S.R. & ERCAN, T., 1986. Metasomatised mantle below western Turkey: A Sr-Nd-Pb isotopic study of alkaline magmas and mantle xenoliths. *Terra Cognita,* **6**, 241.

GÜLEN, L., HART, S.R., SALTERS, V.J.M., WYERS, G.P. & BARTON, M., 1987. Sr, Nd, Pb isotopic constraints on the petrogenesis of the Aegean arc volcanics. *Terra Cognita,* **7**, 170-171.

GÜLEN, L., 1990. Isotopic characterisation of Aegean magmatism and geodynamic evolution of the Aegean subduction. *Proc. Int. Earth Sci. Congr. On Aegean Regions, Izmir,* 143-166.

HAMMARSTROM, J.M. & ZEN, E-AN, 1986. Aluminium in hornblende: an empirical igneous geobarometer. *American Mineralogist,* **71**, 1,297-1,313.

HAMMARSTROM, J.M. & ZEN, E-AN, 1992. Discussion on Blundy and Holland's (1990) "Calcic amphibole equilibria and a new amphibole-plagioclase geothermometer". *Contributions to Mineralogy and Petrology,* **111**, 264-266.

HARRIS, N.B.W., KELLEY, S. & OKAY, A.I., 1994. Post-collision magmatism and tectonics in northwest Anatolia. *Contributions to Mineralogy and Petrology,* **117**, 241-252.

HARRY, D.L. & LEEMAN, W.P., 1995. Partial melting of melt metasomatized subcontinental mantle and the magma source potential of the lower lithosphere. *Journal of Geophysical Research,* **100**, 10,255-10,269.

HART, S., HAURI, E.H., OSCHMANN, L.A. & WHITEHEAD, J.A., 1992. Mantle plumes and entrainment. *Science*, **256**, 517-520.

HARTMANN, G. & WEDEPOHL, K.H., 1990. Metasomatically altered peridotite xenoliths from the Hessinian depression (northwest Germany). *Geochimica et Cosmochimica Acta,* **54**, 71-86.

HAWKESWORTH, C.J. & GALLAGHER, K., 1993. Mantle hotspots, plumes and frgional tectonics as causes of intraplate magmatism. *Terra Nova,* **5**, 552-559.

HAWTHORNE, F.C., 1981. Crystal chemistry of amphiboles, In: D.R. Veblen (Editor), Amphiboles and Other Hydrous Pyroboles-Mineralogy. Chelsea, Michigan, USA, pp. 1-95.

HELVACI, C., 1990. Borate deposits: Field excursion A2, *Int. Earth Sci. Congr. On Aegean Regions, Izmir,* Publ. 4.

HETZEL, R., RING, U., AKAL, C & TROESCH, M., 1995. Miocene NNE directed extensional unroofing in the Menderes Massif, Southwestern Turkey. *Journal of Geological Society, London,* **152**, 639-654.

HEUBNER, J.S. & SATO, M., 1970. The oxygen fugacity-temperature relationshipsof manganese oxides and nickel oxide buffers. *American Mineralogist,* **55**, 934-952.

HIBBARD, M.J., 1981. The magma mixing origin of mantled feldspars. *Contributions to Mineralogy and Petrology,* **76**, 158-170.

HILDRETH, W. & MOORBART, S., 1988. Crustal contributions to arc magmatism in the Andes of Southern Chile. *Contributions to Mineralogy and Petrology,* **98**, 455-489.

HILDRETH, W., 1981. Gradients in silicic magma chambers: Implications for lithospheric magmatism. *Journal of Geophysical Research,* **86(B11),** 6115-6132.

HOERNLE, K., TILTON, G. & SCHMINCKE, H-U., 1991. Sr-Nd-Pb isotopic evolution of Gran Canaria: evidence for shallow enriched mantle beneath the Canary islands. *Earth and Planetary Science Letters,* **106**, 44-63.

HOFMANN, A.W. & FEIGENSON, M.D., 1983. Case studies on the origin of basalt. I. Theory and reassessment of Grenada basalt. *Contributions to Mineralogy and Petrology,* **84**, 382-389.

HOFMANN, A.W. & WHITE, W.M., 1982. Mantle plumes from ancient oceanic crust. *Earth and Planetary Science Letters,* **1982**, 421-436.

HOLLAND, T.J.B. & RICHARDSON, S.W., 1979. Amphibole zonation in metabasites as a guide to the evolution of the metamorphic conditions. *Contributions to Mineralogy and Petrology,* **70**, 143-148.

HOLLAND, T.J.B. & BLUNDY, J., 1994. Non-ideal interactions in calcic amphiboles and their bearing on amphibole-plagioclase thermometry. *Contributions to Mineralogy and Petrology,* **116**, 433-447.

HOLLISTER, L.S., GRISSOM, G.C., PETERS E.K., STOWELL, H.H. & SISSON, V.B., 1987. Confirmation of empirical corelation of Al-in-hornblende with pressure of solidification of calc-alkaline plutons. *American Mineralogist,* **72**, 231-239.

HOUSMAN, G.A. & ENGLAND, P.C., 1986. Finite strain calculations of continental deformation. 1, Method and general results for convergent zones. *Journal of Geophysical Research,* **86**, 6115-6132.

HUEBNER, J.S. & SATO, M., 1970. The oxygen fugacity relationship of manganese oxide and and nickel oxide buffers. *Ibid*, **55**, 934-952.

IDDINGS, J.P., 1895. Absarokite-shoshonite-banakite series. *Journal of Geology,* **3**, 935-959.

INNOCENTI, F. & MAZZUOLI, R., 1972. Petrology of the Izmir-Karaburun volcanic area (west Turkey). *Bulletin Volcanologique*, **36**, 83-104.

INNOCENTI, F., KOLIOS, N., MANETTI, P., RITA, F. & VILLARY, L., 1982. Acid and basic Late Neogene volcanism in central Aegean Sea: its nature and geotectonic significance. *Bulletin of Volcanology*, **45**, 87-97.

IRVINE, T.N. & BARAGER, W.R.A., 1971. A guide to the chemical classification of the common volcanic rocks. *Canadian Journal of Earth Science,* **8**, 523-448.

IRVING, A., 1978. Distribution of trace elements between garnet megacrysts and host volcanic liquids of kimberlitic to rhyolitic composition. *Geochimica et Cosmochimica Acta,* **42**, 771-787.

IWAMORI, H., 1993. A model for disequilibrium melting incorporating melt transport by porous and channel flows. *Nature*, **366**, 734-737.

JACKSON, J., 1992. Partitioning of strike-slip and convergent motion between Eurasia and Arabia in Eastern Turkey. *Journal of Geophysical Research,* **97**, 12,471-12,479.

JOHNSON, M.C. & RUTHERFORD, M.J., 1989. Experimental calibration of the aluminium-in-hornblende geobarometer with application to Long Valley caldera (California). *Geology,* **17**, 837-841.

KARACIK, Z. & YILMAZ, Y., 1995. Geology of the ignimbrite eruptions of Ezine-Ayvacik regin, NW Anatolia. *Proc. Int. Earth Sci. Congr. On Aegean Regions, Güllük,* 415-427.

KAYA, O., 1981. Miocene reference section for the coastal part of western Anatolia. *Newsletter Stratigraphy*, **10**, 164-191.

KAYA, O. & Mostler, H., 1992. Middle Triassic age for low-gradegreenschist facies metamorphic sequence in Bergama (Izmir), western Turkey: the first palaeontoligical age assigned and structural-stratigraphic implications. *Newsletter Stratigraphy*, **21(1)**, 1-17.

KELLER, J., 1983. Potassic volcanism in the Mediterranean area. *Journal of Volcanology and Geothermal Research,* **18**, 321-325.

KEMPTON, P.D., FITTON, J.G., HAWKESWORTH, C.J. & ORMEROD, D.S., 1991. Isotopic and trace element constrains on the composition and evolution of the lithosphere beneath the southwestern United States. *Journal of Geophysical Research,* **96(B8)**, 13,713-13,735.

KESKIN, M., 1994. Genesis of collision-related volcanism on the Erzurum-Kars Plateau, northeastern Turkey. Ph.D. Thesis, University of Durham.

KETIN, I., 1969. Relations between general tectonic features and the main earthquake regions of Turkey. *Bulletin Mineral Research and Exploration Inst. Turkey,* **71**, 63-74.

KNUTSON, J. & GREEN, D.H., 1975. Experimental duplication of a high-pressure megacryst cumulate assemblage in a near saturated hawaiite. *Contributions to Mineralogy and Petrology,* **52**, 121-132.

KONTAK, D.J., CLARK, A.H. & PEARCE, T.H., 1984. Recognition of simple and complex zoning in olivine and orthopyroxene phenocrysts using laser interference microscopy. *Mineralogical Magazine,* **48**, 547-550.

KOSTOPOULOS, D.K. & JAMES, S.D., 1992. Parameterisation of the melting regime of the shallow upper mantle and the effects of variable lithospheric stretching on mantle modal stratification and trace element concentrations in magmas. *Journal of Petrology*, **33**, 665-691.

KRETZ, R., 1982. Transfer and exchange equilibria in a portion of the pyroxene quadrilateral as deduced from natural and experimental data. *Geochimica et Cosmochimica Acta,* **46**, 411-422.

KRUSHENSKY, R.D., 1976. Neogene calc-alkaline extrusive and intrusive rocks of the Karalar-Yesiller area, Northwest Anatolia, Turkey. *Bulletin Volcanologique*, **40**, 336-360.

KUNO, H., 1936. Petrological notes on some pyroxene-andesites from Hakone volcano, with special reference to some types with piegonite phenocrysts. *Japan Journal of Geol. Geogr.,* **13**, 107-144.

LANGMUIR, C.H., VOCKE, R.D., HANSON, G.N. & HART, S.R., 1978. A general mixing equation with applications to Icelandic basalts. *Earth and Planetary Science Letters,* **37**, 380-392.

LANGMUIR, C.H., BENDER, J.F., BENCE, A.E., HANSON, G.N. & TAYLOR, S.R., 1977. Petrogenesis of basalts from the FAMOUS area: Mid-Atlantic Ridge. *Earth and Planetary Science Letters,* **36**, 133-156.

LATIN, D.M., DIXON, J.A. & FITTON, J.G., 1990. Rift-related magmatism in the North Sea basin. In: D.J. Blundell and A. Gibbs (Editors), Tectonic Evolution of the North Sea Rifts. Oxford Univ. Press.

LEAKE, B.E., 1978. Nomenclature of amphiboles. *Canadian Mineralogist,* **16**, 501-520.

LEAKE, B.E. & WINCHELL, H., 1979. Nomenclature of amphiboles. *American Mineralogist,* **63**, 1023-1052.

LE BAS, M.J., LE MAITRE, R.W., STRECKEISEN, A. & ZANETTIN, B., 1986. A chemical classification of volcanic rocks based on the total alkali-silica diagram. *Journal of Petrology,* **27**, 445-450.

LEE, J. & LISTER, G., 1992. Late Miocene ductile extension and detachment faulting, Mykonos, Greece. *Geology*, **20**, 907-910.

LEEMAN, W.P. & HARRY, D.L., 1993. A binary source model for extension related magmatism in the Great Basin, western North America. *Science*, **262**, 1550-1554.

LEEMAN, W.P. & FITTON, J.G., 1989. Magmatism associated with lithospheric extension: Introduction, *Journal of Geophysical Research,* **94,** 7682-7684.

LEEMAN, W.P., BUDAHN, R., GERLACH, D.C., SMITH, D.R. & POWELL, B.N., 1980. Origin of Hawaiian tholeiites: trace element constraints. *American Journal of Science*, **280A**, 794-819.

LE PICHON, X.N. & ANGELIER, J., 1979. The Hellenic arc and trench system: a key to the neotectonic evolution of the eastern Mediterranean area. *Tectonophysisc*, **60**, 1-42.

LE PICHON, X.N., LYBERIS, N. & ALVAREZ, F., 1984. Subsidence history of the North Aegean trough. In: J.E. Dixon and A.H.F. Robertson (Editors), The Geological Evolution of the Eastern Mediterranean. *Geological Society, London, Special Publication,* **17**, 727-741.

LE PENNEC, J.-L., BOURDIER, J.-L., FROGER, J.-L., TEMEL, A., CAMUS, G. & GOURGAUD, A., 1994. Neogene ignimbrites of the Nevsehir plateau (central Turkey): stratigraphy, distribution and source constraints. *Journal of Volcanology and Geothermal Research,* **63**, 59-87.

LINDSLEY, D.H., 1983. Pyroxene thermometry. *American Mineralogist,* **68**, 477-493.

LINDSLEY, D.H. & ANDERSEN, D.J., 1983. A two pyroxene thermometer: Proceedings of the Thirteenth Lunar and Planetary Science Conference, Part 2, *Journal of Geophysical research,* **88**, Supplement, pp, A887-A906.

LINDSLEY, D.H. & SPENCER, K.J., 1982. Fe-Ti oxide geothermometry: Reducing analyses of coexisting Ti-magnetite(Mt) and ilmenite (Ilm). *EOS*, **63**, 471.

LINDSLEY, D.H, FROST, B.R., ANDERSEN, D.J. & DAVIDSON, P.M., 1990. Fe-Ti oxide-silica equilibria: Assemblages with orthopyroxene. In: R.J. Spencer and I.-M. Chou (Editors). Fluid-mineral interactions: A tribute to H.P. Eugster, special publication 2, p. 103-119. The geochemical society, San Antonio, Texas.

LISTER, G.S., BANGA, G. & FEENSTRA, A.,1984. Metamorphic core complex of Cordilleran type in the Cyclades, Aegean Sea, Greece. *Geology*, **12**, 221-225.

LUHR, J.F. & CARMICHAEL, I.S.E., 1980. The colima volcanic complex, Mexico. I. Post-caldera andesites from Volcan Colima. *Mineralogy Petrology*, **71**, 343-372.

MAALØE. S., 1994. Estimation of the degree of partial melting using concentration ratios. *Geochimica et Cosmochimica Acta,* **58**, 2519-2525.

MAALØE. S., JAMES, D., SMEDLEY, P., PETERSEN, S. & GARMANN, L.B., 1992. The Koloa volcanic suiteof Kauai, Hawaii. *Journal of Petrology*, **33**, 761-784.

MAKRIS, J. & STOBBE, C., 1984A. Phsical properties and state of the crust and upper mantle of the Eastern Mediterranean Sea deduced from geophysical data. *Marine Geology,* **55**, *347-363.*

MAKRIS, J. & STOBBE, C., 1984B. Physical properties and state of the crust and upper mantle of the Eastern Mediterranean area. *Tectonophysisc*, **60**, 1-42.

MARSH, J., 1989. Geochemical constraints on coupled assimilation and fractional crystallisation involving upper crustal compositions and continental thoeliitic magma. *Earth and Planetary Science Letters,* **92**, 70-80.

MCKENZIE, D.P., 1985. ^{230}Th-^{238}Th disequilibrium and the melting processes beneath ridge axes. *Earth and Planetary Science Letters,* **72**, 149-157.

MCKENZIE, D.P., 1989. Some remarks on the movement of small volume melt fractions in the mantle. *Earth and Planetary Science Letters,* **95**, 53-72.

MCKENZIE, D.P. & BICKLE, M.J., 1988. The volume and composition of melt generated by extension of the lithosphere. *Journal of Petrology,* **29**, 627-679.

MCKENZIE, D.P. & O'NIONS, R.K., 1991. Partial melt distribution from inversion of rare earth element concentrations. *Journal of Petrology,* **32**, 1021-1991.

MCKENZIE, D.P. & O'NIONS, R.K., 1995. The source regions of Ocean Island Basalts. *Journal of Petrology,* **36**, 133-159.

MEISSNER, R., WEVER, T.H. & FLUH, E.R., 1987. The Moho in Europe: implications for crustal development. *Annales Geophsicae,* **5B**, 357-364.

MERCIER, J.C., 1976. Single pyroxene geothermometry and geobarometry. *American Mineralogist,* **61**, 603-615.

MEULANKAMP, J.E., WORTEL, W.J.R., VANWAMEL, W.A., SPAKMAN, W. & HOOGERDUYN STRATING, E., 1988. On the Hellenic subjection zone and geodynamic evolution of Crete since the late Middle Miocene. *Tectonophysisc,* **146**, 203-215.

MINDEVALLI, Y.Ö. & MITCHELL, J.B., 1989. Crustal structure and possible anisotropy in Turkey from seismic surface wave dispersion. *Geophysical Journal International,* **98**, 93-106.

MINSTER, J.F. & ALLEGRE, C.J., 1978. Systematic use of trace elements in igneous processes. *Contributions to Mineralogy and Petrology,* **68**, 37-52.

MORRISON, G.W., 1980. Characteristics and tectonic setting of the shoshonite rock association. *Lithos,* **13,** 97-108.

MYERS, J. & EUGSTER, H.P., 1983. The system Fe-Si-O: oxygen buffer calibrations to 1,500K. *Contributions to Mineralogy and Petrology,* **82**, 75-90.

NABELEK, C.R. & LINDSLEY, D.H., 1985. Tetrahedral Al in amphibole: A potential thermometer for some mafic rocks. *Geol. Soc. Am.*, Abstract with Prog., **17**, 673.

NAVON, O. & STOLPER, E., 1987. Geochemical consequences of melt percolation: the upper mantle as a chromatographic column. *Journal of Geology*, **95**, 285-307.

NELSON, K.D., 1992. Are crustal thickness variations in old mountain belts like the Appalachians a consequence of lithospheric delamination. *Geology*, **20**, 498-502.

NELSON, S.T. & MONTANA, A., 1992. Sieve-textured plagioclase in volcanic rocks produced by rapid decompression. *American Mineralogist*, **77**, 1242-1249.

NIMIS, P., 1995. A clinopyroxene geobarometer for basaltic systems based on crystal-structure modeling. *Contributions to Mineralogy and Petrology,* **121**, 115-125.

NIXON, G.T. & PEARCE, T.H., 1987. Laser-interferometry of oscillatory zoning in plagioclase: the record of magma mixing and phenocryst recycling in calc-alkaline magma chambers, Iztaccihuat Volcano, Mexico. *American Mineralogist*, **72**, 1144-1162.

NIXON, G.T., 1988. Petrology of the younger andesites and dacites at Iztaccihuat Volcano, Mexico: I. Disequilibrium phenocryst assemblages as indicators of magma chamber processes. *Journal of Petrology,* **29**, 213-264.

O'HARA, M.J., 1977. Geochemical evolution during fractional crystallisation of periodically refilled magma chamber. *Nature*, **266**, 503-507.

O'HARA, M.J., 1985. Importance of the 'shape' of the melting regime during partial melting of the mantle. *Nature*, **314**, 58-62.

O'HARA, M.J., 1995. Imperfect melt separation finite increment size and source region flow during fractional melting and the generation of reversed or subdued discrimination of incompatible trace elements. *Chemical Geology*, **121**, 27-50.

OKAY, A.I., SIYAKO, M. & BURKAN, K.A., 1991. Geology and tectonic evolution of the Biga Peninsula, NW Turkey. *Bulletin of the Technical University of Istanbul*, **44**, 191-256.

OKAY, A.I., SATIR, M., MALUSKI, H., SIYAKO, M., METZGER, R. & AKYUZ, S., 1996. palaeo- and neo-Tethyan events in northwest Turkey. In: A. Yin and M. Harrison (Editors), The Tectonic Evolution of Asia. Cambridge University Press.

ORMEROD, D.S., ROGERS, N.W. & HAWKESWORTH, C.J., 1991. Melting in the lithospheric mantle: inverse modelling of alkali-olivine basalts from the Big Pine Volcanic Field, California. *Contributions to Mineralogy and Petrology,* **108**, 305-317.

PATON, S.M., 1992a. The relationship between extension and volcanism in western Turkey, the Aegean Sea and central Greece. Ph.D. Thesis, Cambridge University.

PATON, S.M., 1992b. Active normal faulting, drainage patterns and sedimentation in southwestern Turkey. *Journal of the Geological Society,* **149**, 1031-1044.

PE-PIPER, G., 1980. Geochemistry of Miocene shoshonites, Lesbos, Greece. *Contributions to Mineralogy and Petrology,* **72**, 387-396.

PE-PIPER, G. & PIPER, D.J.W., 1989. Spatial and temporal variation in Late Cenozoic back-arc volcanic rocks, Aegean Sea region. *Tectonophysics*, **169**, 113-134.

PE-PIPER, G. & PIPER, D.J.W., 1992. Geochemical variation with time in the Cenozoic high-K volcanic rocks of the island of Lesbos, Greece: significance for shoshonite petrogenesis. *Journal of Volcanology and Geothermal Research,* **53**, 371-387.

PEARCE, J.A., 1982. Trace element characteristics of lavas from destructive plate margins. In: R.S. Thorpe (Editor), Andesites: Orogenic Andesites and Related Rocks. Wiley, New York, pp. 525-548.

PEARCE, J.A., 1983. Role of the sub-continental lithosphere in magma genesis at active continental margins. In: C.J. Hawkesworth and M.J. Norry (Editors), Continental Basalts and Mantle Xenoliths. Shiva, Cheshire, U.K., pp. 230-249.

PEARCE, J.A. & NORRY, M.J., 1979. Petrogenetic implications of Ti, Zr, Y and Nb variation in volcanic rocks. *Contributions to Mineralogy and Petrology,* **69**, 33-47.

PEARCE, J.A., BENDER, J.F., DELONG, S.E., KIDD, W.S.F., LOW, P.J, GÜNER, Y., SAROGLU, F., YILMAZ, Y., MOORBATH, S. & MITCHELL, J.G., 1990. Genesis of

collision volcanism in Eastern Anatolia, Turkey. *Journal of Volcanology and Geothermal Research,* **44**, 189-229.

PEARCE, J.A., SERRI, G. & INNOCENTI, F.,1994. Distribution, mechanisms and chemical characteristics of collision magmatism. International Volcanological Congress (IAVCEI) Ankara, Turkey. (Abstract).

PEARCE, J.A. & PEATE, D.W., 1995. Tectonic implications of the composition of the volcanic arc magmas. *Annual Reviews in Earth and Planetary Science,* **23**, 251-285.

PEARCE, J.A., BAKER, P.E., HARVEY, P.K. & LUFF, L.W., 1995. Geochemical evidence for subduction fluxes, mantle melting and fractional crystallisation beneath the South Sandwich Island Arc. *Journal of Petrology,* **36**, 1073-1109.

PECCERILLO, A. & TAYLOR, S.R., 1976. Geochemistry of Eocene calc-alkaline volcanic rocks from the Kastamonu area, Northern Turkey. *Contributions to Mineralogy and Petrology,* **58**, 63-91.

PICKETT, E.A. & ROBERTSON, A.H.F., 1996. Formation of the Late Palaeozoic-Early Mesozoic Karakaya complex and related ophiolites in NW Turkey by Palaeotethyan subjection-accretion. *Journal of the Geological Society,* **153**, 995-1009.

PICKETT, E.A., 1994. Tectonic evolution of the Palaeotethys Ocean in NW Turkey. Ph.D. Thesis, University of Edinburgh.

PLANK, T. & LANGMUIR, C.H., 1992. Effects of the melting regime on the composition of the oceanic crust. *Journal of Geophysical Research,* **97**, 19,749-19,770.

PLATT, J.P. & ENGLAND, P.C., 1993. Convective removal of lithosphere beneath mountain belts: thermal and mechanical consequences. *American Journal of Science*, **293**, 307-336.

PLYUSNINA, L.P., 1982. Geothermometry and geobarometry of plagioclase-hornblende bearing assemblages. *Contributions to Mineralogy and Petrology,* **80**, 140-146.

POLI, S. & SCHMIDT, M.W., 1992. A comment on "Calcic amphibole equilibria and a new amphibole-plagioclase geothermometer" by J.D. Blundy and T.J.B. Holland. (Contributions to Mineralogy and Petrology (1990), **104**, 208-224). *Contributions to Mineralogy and Petrology,* **111**, 273-282.

POWELL, R. & POWELL, M., 1977. Geothermometry and oxygen barometry using coexisting iron-titanium oxides: a reappraisal. *Mineralogical Magazine*, **41**, 257-263.

REILINGER, R.E., MCCLUSKY, S.C., ORAL, M.B., KING, R.W., TOKSÖZ, M.N., BARKA, A.A., KINIK, I., LENK, O. & SANLI, I., 1997. Global positioning system measurements of present-day crustal movements in the Arabian-Africa-Eurasia plate collision. . *Journal of Geophysical Research,* **102(B5)**, 9,983-9,999.

REINERS, P., 1998. Reactive melt transport in the mantle and geochemical signatures of Mantle-derived magmas. *Journal of Petrology*, **39**, 1039-1061.

RICHARDSON-BUNBURY, J.M., 1996. The Kula volcanic field, western Turkey: the development of a Holocene alkali basalt province and the adjacent normal-faulting graben. *Geological Magazine,* **133**, 275-283.

RICHARDSON-BUNBURY, J.M., 1992. The basalts of Kula. Ph.D. Thesis, Cambridge University.

ROBERT, U., FODEN, J. & VARNE, R., 1992. The Dodecanese Province, SE Aegean: A model for tectonic control on potassic magmatism. *Lithos,* **28**, 241-260.

ROBERTS, P.M. & CLEMENS, J.D., 1995. Feasibility of AFC models for the petrogenesis of calc-alkaline magma series. *Contributions to Mineralogy and Petrology,* **121**, 139-147.

ROBERTSON, A.H.F. & DIXON, J.E., 1984. Introduction: aspects of the geological evolution of the eastern Mediterranian. In: J.E. Dixon and A.H.F. Robertson (Editors), The Geological Evolution of the Eastern Mediterranean. *Geological Society, London, Special Publication,* **17**, 1-74.

RODEN, M.K., HART, S.R., FREY, F.A. & MELSON, W.G., 1984. Sr, Nd and Pb isotopes and REE geochemistry of St. Paul's rocks: The metamorphic and metasomatic development of an alkali basalt mantle source. *Contributions to Mineralogy and Petrology,* **85**, 376-390.

RODER, R.L. & EMSLIE, R.F., 1970. Olivine-liquid equilibrium. *Contributions to Mineralogy and Petrology,* **29**, 275-289.

ROGERS, N.W., 1992. Potassic magmatism as a key to trace element enrichment processes in the upper mantle. *Journal of Volcanology and Geothermal Research,* **50**, 85-99.

ROGERS, N.W., HAWKESWORTH, C.J., PARKER, R.J. & MARSH, J.S., 1985. The geochemistry of potassium lavas from Vulsini, Central Italy and Implications for mantle enrichment processes beneath the Roman region. *Contributions to Mineralogy and Petrology,* **90**, 244-257.

ROGERS, N.W., DE MULDER, M. & HAWKESWORTH, C.J., 1992. An enriched mantle source for potassic basanites: evidence from Karisimbi volcano, Virunga Province, Rwanda. *Contributions to Mineralogy and Petrology,* **111**, 543-556.

ROLLINSON, H., 1993. Using Geochemical Data: evaluation, presentation, interpretation. John Willey & Sons, New York.

ROSS, C.S. & SMITH, R.L., 1961. Ash-flow tuffs: their origin, geologic relations and identification. U.S. Geological Survey, Prof. Pap., **366**, 1-77.

SALVIULO, G., SECCO, L., ANTONINI, P. & PICCIRILLO, E.M., 1997. C2/c pyroxene from two alkaline sodic suites (Western Ross Embayment-Antarctica) crystal chemical characterisation and its petrologic significance. *Mineralogical Magazine*, **61**, 423-439.

SAVAŞÇIN, M.Y., 1990. Magmatic activities of Cenozoic compressional and extensional tectonic regimes in western Anatolia. *Proc. Int. Earth Sci. Congr. On Aegean Regions, Izmir,* 420-434.

SAVAŞÇIN, M.Y & GÜLEÇ, N., 1992. Neogene volcanism of Western Anatolia: Field excursion B3, *Int. Earth Sci. Congr. On Aegean Regions, Izmir, Turkey.*

SAVAŞÇIN, M.Y., 1977. Some alkaline rocks and hybrid magmas of the western Anatolia. Proceedings of the International Congress on Thermal Waters, *Geothermal Energy and Vulcanism of the Mediterranean Area*, 3, pp. 225-239.

SAXENA, S.K. & NEHRU, C.E., 1975. Enstatite-diopside solvus and geothermometry. *Contributions to Mineralogy and Petrology,* **49**, 259-267.

SCHILLING, J.G. & WINCHESTER, J.W., 1967. Rare-earth fractionation and magmatic processes. In: S.K. Runcorn (Editor). Mantles of Earth and Terrestrial Planets.

SCHLIESTTEDT, M., ALTHERR, R. & MATTHEWS, A., 1987. Evolution of the Cycladic crystalline complex: petrology, isotope geochemistry and geochronology. In: H.C. Helgeson (Editor), Chemical Transport in Metasomatic Processes. NATO-ASI series, Reidel, Dordrecht, pp. 389-428.

SCHMIDT, W.S., 1992. Amphibole composition in tonalite as a function of pressure: an experimental calibration of the Al-in hornblende barometer. *Contributions to Mineralogy and Petrology,* **110**, 304-310.

SCHUMACHER, R. & MUES-SCHUMACHER, U., 1997. The pre-ignimbrite (phreato) plinian and phreatomagmatic phases of the Akdag-Zelve ignimbrite eruption in Central Anatolia, Turkey. *Journal of Volcanology and Geothermal Research,* **78**, 139-153.

SENGÖR, A.M.C., 1979. The North Anatolian transform fault: its age, offset and tectonic significance. *Journal of Geological Society, London,* **136**, 269-282.

SENGÖR, A.M.C., YILMAZ, Y.. & KETIN, I., 1980. Remnants of a pre-Late Jurassic ocean in Northern Turkey: Fragments of Permian-Triassic Palaeo-Tethys? *Geological Society of America Bulletin,* **91**, 599-609.

SENGÖR, A.M.C., 1982. Ege'nin neotektonik evrimini yöneten etkenler. (Factors governing the neotectonic evolution of the Aegean.). In: O. Erol and V. Oygur (Editors), Batı Anadolunun genç tectoniği ve volkanizmasi paneli, 1982 Meet. Geological Society of Turkey.

SENGÖR, A.M.C. & YILMAZ, Y., 1981. Tethyan evolution of Turkey: A plate tectonic approach. *Tectonophysics,* **75**, 181-241.

SENGÖR, A.M.C., GÖRÜR, N. & ŞAROĞLU, F., 1985. Strike-slip deformation, basin formation and sedimentation: Strike-slip deformation and related basin formation in zones of tectonic escape: Turkey as a case study. *Soc. Econ. Paleonto. Mineral., spec. publ.* **37**, 227-264.

SENGÖR, A.M.C., SATIR, M. & AKKÖK, R., 1984. Timing of the tectonic events in the Menderes Massif, western Turkey: Implication for tectonic evolution and evidence for pan African basement in Turkey. *Tectonics,* **3**, 693-707.

SEYITOĞLU, G. & SCOTT, B.C., 1991. Late Cenozoic crustal extension and basin formation in west Turkey. *Geological Magazine,* **128**, 155-166.

SEYITOĞLU, G. & SCOTT, B.C., 1992a. The age of the Buyuk Menderes graben (west Turkey) and its tectonic implications. *Geological Magazine,* **129**, 239-242.

SEYITOĞLU, G. & SCOTT, B.C., 1992b. Late Cenozoic volcanic evolution of the NE Aegean region. *Journal of Volcanology and Geothermal Research,* **54**, 157-176.

SEYITOĞLU, G. & SCOTT, B.C., 1996. The cause of N-S extensional tectonics in western Turkey: Tectonic escape vs. back-arc spreading vs. orogenic collapse. *Journal of Geodynamic*, **22**, 145-153.

SEYITOĞLU, G., ANDERSON, D., NOWELL, G. & SCOTT, B.C., 1997. The evolution from Miocene potassic to Quaternary sodic magmatism in western Turkey: implications for enrichment processes in the lithospheric mantle. *Journal of Volcanology and Geothermal Research,* **76**, 127-147.

SHAW, D.M., 1970. Trace element fractionation during anatexis. *Geochimica et Cosmochimica Acta,* **34**, 237-243.

SHELLEY, D., 1993. Igneous and metamorphic rocks under the microscope. Chapman and Hall, London, 455 pp.

SONDER, L.J. & ENGLAND, P.C., 1989. Effects of a temperature-dependent rheology on large scale continental extension. *Journal of Geophysical Research,* **94**, 7,603-7619.

SONDER, L.J. , ENGLAND, P.C., WERNICKE, B.P. & CHRISTIANSEN, R.L., 1987. A phsical model for Cenozoic extension of western North America. In: M.P. Conward, J.F. Dewey and P.L. Hancock (Editors). Continental Extensional Tectonics. *Geological Society of London Special Publications*, **28**. 187-201.

STORMER, J.C., 1983. The effects of recalculation on estimates of temperature and oxygen fugacity from analyses of multi-component iron-titanium oxides. *American Mineralogist*, **68**, 585-594.

STORMER, J.C. & WHITNEY, J.A.,1985. Two feldspar and iron-titanium oxide equilibria in silicic magmas and the depth of origin of large volume ash-flow tuffs. *American Mineralogist*, **70**, 52-64.

SUN, S.S. & MCDONOUGH, W.F., 1989. Chemical and isotopic systematics of oceanic basalts: implications for mantle composition and processes. In: A.D. Saunders and M.J. Norry (Editors), Magmatism in the Ocean Basins. *Geological Society Special Publication,* **42**, 313-345.

TAYLOR, S.R. & MCLENNAN, S.M., 1985. The Continental Crust: Its Composition and Evolution. Geoscience Texts, Blackwell scientific publications, 312 pp.

TAYLOR, H.P., 1980. The effects of assimilation of country rocks by magmas on $^{18}O/^{16}O$ and $^{87}Sr.^{86}Sr$ systematics in igneous rocks. *Earth and Planetary Science Letters,* **47**, 243-254.

TAYLOR, H.P. & SHEPPARD, S.M.F., 1986. Igneous rocks: I. Processes of isotopic fractionation and isotope systematics. Stable isotopes in high temperature geological processes. *Rew. Mineral*, **16**, 227-271.

TAYMAZ, T., JACKSON, J. & MCKENZIE, D., 1991. Active tectonics of the north and central Aegean Sea. *Geophysical Journal International,* **106**, 433-490.

THOMAS, W.M. & ERNST, W.G., 1990. The aluminium content of hornblende in calc-alkaline granitic rocks: A mineralogic barometer calibrated experimentally to 12 kbars. In: R.J. Spencer and I-M. Chou (Editors). Fluid-mineral Interactions: *Geochemical Society Special Publication*, **2**, 59-63.

THOMPSON, R.N., LEAT, P.T., DICKIN, A.P., MORRISON, M.A., HENDRY, G.L. & GIBSON, S.A., 1989. Strongly potassic mafic magmas from lithospheric mantle sources during continental extension and heating: evidence from Miocene minettes of northwest Colorado, USA. *Earth and Planetary Science Letters,* **98**, 139-153.

TREUIL, M. & JORON, J.L., 1975. Utilisation des èlemènts hygromagmatophiles pour la simplification de la modelisation quantitative des processes magmatiques. Examples des L'Afar et de la Dorsale Mèdioatlantique. *Soc. Ital. Mineral. Petrol,* **31**, 125-174.

TSUCHIYAMA, A., 1985. Dissolution kinetics of plagioclase in the melt system diopside-albite-anorthite, and origin of dusty plagioclase in andesites. *Contributions to Mineralogy and Petrology,* **89**, 1-16.

VASSEUR, G. VERNIERES, J.& BODINIER, J.-L., 1991. Modelling of trace element transfer between mantle melt and heterogranular peridotite matrix. *Journal of petrology*, Special Lherzolites Issue 41-38.

VERGE, N.J., 1993. Oligo-Miocene orogenic collapse tectonics in Western Anatolia and the extensional axhumation of the Menderes Massif metamorphic core comples. In: M. Serrane and J. Malavielle (Editors), Late Orogenic Extension in Mountain Belts, Documents des Bureau de Recherches Geologique et Minieres (France), **219**, 202.

VILOTTE, J.P., MADARIAGA, R., DAINIERES, M. & ZIENKIEWICZ, O.C., 1986. Numerical study of continental collision: Influence of buoyancy forces and a stiff inclusion. *Royal Astronomical Society Geophysical Journal*, **84**, 279-310.

WASHINGTON, H.S., 1893. *The volcanoes of the Kula basin in Lydia.* Dissertation, Leipzig 1983, reprinted New York 1894.

WASHINGTON, H.S., 1900. The composition of Kulaite. *Journal of Geology,* **8**, 610-620.

WELLS, P.R.A., 1977. Pyroxene thermometry in simple and complex systems. *Contributions to Mineralogy and Petrology,* **62**, 129-139.

WESTAWAY, R., 1994. Evidence for dynamic coupling of surface processes with isostatic compensation in the lower crust during active extension of western Turkey. *Journal of Geophysical Research,* **99(B10)**, 20,203-20,223.

WHITNEY, D.L. & DILEK, Y., 1998. Metamorphism during Alpine crustal thickening and extension in Central Anatolia, Turkey: the Nigde metamorphic core complex. *Journal of Petrology,* **39**, 1385-1403.

WILLIAMS, R.W. & GILL, J.B., 1989. Effects of partial melting of the uranium decay series. *Geochimica et Cosmochimica Acta,* **53**, 1,607-1,619.

WILSON, M., ROSENBAUM, J.M. & DUNWORTH, E.A., 1995. Melilitites: partial melts of the thermal boundary layer. *Contributions to Mineralogy and Petrology,* **119**, 181-196.

WILSON, M., 1993. Geochemical characteristics of oceanic and continental basalts: a key to mantle dynamics? *Journal of the Geological Society, London,* **150**, 977-990.

WILSON, M. & DOWNES, H., 1992. Mafic alkaline magmatism associated with the European Cenozoic rift system. *Tectonophysics*, **208**, 173-182.

WILSON, M. & DOWNES, H., 1991. Tertiary-Quaternary extension-related alkaline magmatism in western and central Europe. *Journal of Petrology,* **32**, 811-849.

WILSON, M., TANKUT, A. & GÜLEÇ, N., 1997. Tertiary volcanism of the Galatia province, north-west Central Anatolia, Turkey. *Lithos*, **42**, 105-121.

WILSON, M., 1989. Igneous Petrogenesis. Chapman and Hall, London.

WYERS, G.P. & BARTON, M., 1987. Geochemistry of a transitional ne-trachybasalt – Q-trachyte lava series from Patmos (Dodecanese), Greece; further evidence for fractionation, mixing and assimilation. *Contributions to Mineralogy and Petrology,* **97**, 279-291.

YILMAZ, Y., 1989. An approach to the origin of young volcanic rocks of western Turkey. In A.M.C Sengor (Editor), Tectonic Evolution of the Tethyan region. Kluwer Academic Publishers, pp. 159-189.

YILMAZ, Y., 1990. Comparison of young volcanic associations of western and eastern Anatolia formed under a compressional regime: a review. *Journal of Volcanology and Geothermal Research,* **44**, 69-77.

ZANCHI, A. & ANGELIER, J., 1993. Seismotectonics of western Anatolia: regional stress orientation from geophysical and geological data. *Tectonophysics*, **222**, 259-274.

ZINDLER, A. & HART, S., 1986. Chemical geodynamics. *Annual Reviews in Earth and Planetary Science,* **14**, 493-571.

ZINDLER, A. & JAGOUTZ, E., 1987. Mantle cryptology. *Geochimica et Cosmochimica Acta,* **52**, 319-333.

ZOU, H. & ZINDLER, A., 1996. Constraints on the degree of dynamic partial melting and source composition using concentration ratios in magmas. *Geochimica et Cosmochimica Acta,* **60**, 711-717.

APPENDIX A

ANALYTICAL GEOCHEMISTRY

A1. PREPARATION OF THE SAMPLES FOR ANALYSES

A1.1 Powdered sample preparation

Bulk-rock samples collected in the field were between 0.5-1kg. Weathered surfaces were removed and samples were cut down to cubes about 4cm in diameter using a diamond-saw. The samples were then washed using water and a bristle brush to remove traces of dust and soil. The clean, dry rock pieces were crushed to a fine gravel in a 'Fritsch Pulverisette jaw crusher (type 01-704). To avoid contamination, the crushing equipment was thoroughly cleaned before use and between samples using wire brushes and absolute alcohol. Rock dust was kept to a minimum by using a vacuum cleaner.

A fraction of gravel sample was then put in a Fritsch agate ball mill for 15 to 20 minutes and ground down to a fine powder. The agate pots were carefully cleaned and dried between samples using water and absolute alcohol. Then powdered samples were bagged, labelled and stored in dry conditions.

A1.2 Preparation of the pressed powder pellets

Previously dried 6-7g of powdered sample was mixed thoroughly with 8 to 12 drops of Mowiol binding agent in glass baker by using a glass rod until an even consistency is obtained. The mixture was transferred to a stainless steel mould and compressed between a pair of polished steel discs using a hydraulic press at 10-15 bars. The pellet was then dried in an oven at 100°C prior to analysis.

A1.3 Determination of loss on ignition (L.O.I.)

3-4g of the sample powder from each sample was placed in 10ml glass vial and labelled. These powders were than dried at 100°C for >1hours to remove surface water. Loss on ignition values were then determined by heating an about 3g of powder of the sample in a porcelain crucible at >900°C for >2 hours.

A1.4 Preparation of fused discs

Previously ignited powder was mixed thoroughly with dried lithium tetraborate flux (Spectroflux 100B) in the proportion 1:5 (0.45g powdered sample: 2.25g flux) using an agate mortar and pestle. The mixture was then placed in platinum crucibles and heated to 1050°C for 20 minutes. The molten glass was then poured into graphite moulds standing on a hotplate and immediately flattened with a stainless steel plunger. Heated glass bakers were placed over the moulds to prevent quench shattering. After cooling, the discs were labelled and bagged, care being taken not to touch the analytical surface. The fusion discs were stored in a dessicator prior to analysis. The platinum crucibles were cleaned by boiling them in hot 50% HCl for >10 minutes between successive samples.

A2. ANALYTICAL PROCEDURES

A2.1 XRF analysis

X-Ray Fluorescence (XRF) analysis was carried out on a Philips PW 1500 spectrometer with a rhodium anode tube at the University of Durham. A total of 219 samples were analysed both on fused discs and pressed powder pellets for major (SiO_2, TiO_2, $Al2O_3$, Fe_2O_3, MnO, MgO, CaO, Na_2O, K_2O and P_2O_5) and trace (Rb, Sr, Ba, Zr, Y, Nb, Sc, Cr, V, Ni, Zn, Cu, Co, Ga, Ce, Nd, La, Th, Pb) elements respectively. A full range of international standards from across the compositional range were run as calibration standards. A number of internal standards were run over the full study period to monitor between run variations and machine drift. Estimates of analytical accuracy and precision were made by repeated analysis of international reference standards. Recommended values for standards were taken from Govindaraju (1989).

A2.2 ICP-MS analysis

A subset of 56 samples was analysed using Inductively Coupled Plasma Mass spectrometry (ICP-MS) for Cs, Hf, Ta, and Rare Earth Elements (REE) from La to Lu in addition to all the trace elements analysed by XRF. ICP-MS analysis was performed at the University of Durham.

Small amount of powdered samples were placed in glass containers in an oven at >100°C to dry. Savillex teflon vials were cleaned by rinsing with MQ water and then leaving them filled with 2ml Aristar concentrated HNO_3 on a hot-plate at >140°C for 2 hours. A powder aliquot of 0.1 ± 0.001g was weighed out from each sample and

transferred into the teflon vials. In addition to the samples, 6 international standards and 2 blanks were prepared. 1ml of Aristar HNO_3 and 4ml of HF were added into the teflon vials, their lids were closed tightly and the samples were left in the acid on a hot-plate at about 140°C for >2 days for complete digestion. The samples were then evaporated in order to eliminate HF acid from the system and to allow the formation of nitrate salts. 1ml of Aristar HNO_3 was added to the vials and evaporated again. This procedure was followed twice. Then 2.5ml of Aristar HNO_3 and about 20ml of MQ water were put into the vials, their lids were closed and boiled for >1 hour to dissolve salts. The solutions were allowed to cool, checked for any solid residue and then spiked with 1.25ml of 2 ppm Rh, Re and Bi internal standard spike solution. The solutions were then transferred into 50-ml polypropylene volumetric flasks and made up accurately to 50ml with MQ water. Finally, the solutions were transferred into polypropylene containers and kept in a cool place prior to analysis.

A2.3 Electron microprobe analysis

Polished thin-sections were prepared at the University of Durham and were carbon coated at the University of Edinburgh. Analyses were performed at Edinburgh on a Cameca CAMEBAX electron microprobe using natural minerals as standards. Operating procedures were ~20kV acceleration voltage, beam current ~2/nA, 30s. pk count, 15s. b/g count, 1mm^2 spot size and a 25mm^2 retard beam size.

A2.4 Radiogenic isotope analysis

Sr and Nd isotope analyses were determined using the VG354 5-collector mass spectrometer of the London University radiogenic isotope facility at Royal Holloway. Sr and Nd were extracted on the same dissolution from 200 ± 20mg of rock powder. The samples were leached in hot 6M HCl for >1 hr, and rinsed several times in ultra clean water in order to remove any alteration effects. The samples were then washed with MQ water and were dissolved using approximately 1ml of HNO_3 and 3-5ml of HF. After dissolution, the solution was evaporated to dryness. It was then converted to nitrate by the addition of 1ml of HNO_3, followed by evaporation and dryness. The residue was converted to chloride using 2.5M HCl.

The separation of Rb and Sr and the preliminary separation of Sm-Nd were performed on a cation exchange column eluted with 2.5M HCl. Before separation of the samples, the column resin was cleaned by passing sequential volumes of 50% acid and water. A small volume of the rock solution was loaded into the column, washed into the

resin bed carefully with eluent, and then washed through with more eluent until a fraction was collected when the desired element was released from the resin. This was evaporated to dryness, ready to load onto a single Ta filament for thermal ionisation in the mass spectrometer. Sm and Nd were separated on a cation exchange column eluted with dilute mineral acid and were run on a single Re filament with silica gel. Following the chemical separation, Sr and Nd were determined multidynamically with Nd determined as NdO (Thirlwall, 1991 a, b).

During the period of analyses, SRM987 gave $^{87}Sr/^{86}Sr$ of 0.710246 ± 21 (2s.d., N=58), while the Aldrich laboratory Nd standard gave $^{143}Nd/^{144}Nd$ of 0.511418 ± 8 (2s.d., N=28), equivalent to $^{143}Nd/^{144}Nd$ in the La Jolla standart of 0.511856. Blanks were around 1 ng and 200 pg for Sr and Nd respectively, and are insignificant. No age corrections were made on $^{87}Sr/^{86}Sr$, since the residues are likely to have Rb/Sr ratios too low to generate significant age corrections. Age corrections for $^{143}Nd/^{144}Nd$ were estimated from Sm and Nd concentrations determined by ICP-MS: uncertainty in this procedure would have no effect on the initial $^{143}Nd/^{144}Nd$ at ~20 Ma.

APPENDIX B

XRF, ICP-MS AND ELECTRON PROBE DATA SET

Symbols of Formations

Area	Symbols	Formation names
EGA	*Ayv. Vol.*	Ayvacik volcanics
	Ezn. Vol.	Ezine volcanics
	Tas. Vol.	Tastepe volcanics
	Kov. Dyke	Kovacli dyke swarms
	Bal. Ign.	Balabanli ignimbrite
	Berg. Ign	Bergas ignimbrite
	Koy. Ign.	Koyunevi ignimbrite
DAB	*Behr. And.*	Behram andesite
	Bak. Unit	Bakacak Unit
	Cice. And.	Ciceklik andesite
	Sur. And	Suruce andesite
	Bad. Unit.	Bademli Unit
	Bab. Unit	Babakale Unit
	Dad. Unit	Dededag Unit
	Ezn. Unit	Ezine Unit
	Kiz. Unit	Kiziltepe Unit
	Neb. Vol.	Nebiler volcanics
	Foc. Dyke	Foca dyke swarms
	Egr. And	Egrigol andesite
	Oda. Dyke	Odaburnu dyke swarms
	Klg. And	Kalarga andesite
	Krg. Unit	Karagol Unit
	Mt.Sey. U.	Mt. Seyret Unit
	Akc. Unit	Akcapinar Unit
	Kir. Unit	Kiratli Unit
	Ulb. Unit	Ulubey Unit
	Bal. Unit	Ballica Unit

XRF DATA SET

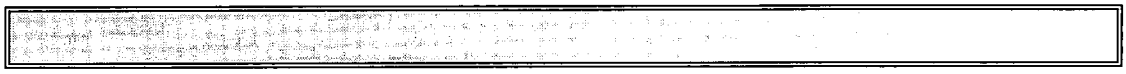

Area	EGA	EGA	EGA	EGA	EGA	EGA	EGA	EGA	EGA	EGA	EGA	EGA	EGA	EGA	EGA
Locality	**Ayvacik**	**Ayvacik**	**Ayvacik**	**Ayvacik**	**Ayvacik**	**Ayvacik**	**Ayvacik**	**Akkoy**	**Akkoy**	**Akkoy**	**Ezine**	**Ezine**	**Ezine**	**Ezine**	**Tastepe**
Sample no	**EA268**	**EA269**	**EA270**	**EA267**	**EA271**	**EA82B**	**EA272**	**EA260**	**EA258**	**EA259**	**EA261**	**EA415**	**EA264**	**EA262**	**EA252**
Unit	*Ayv. Vol.*	*Ayv. Vol.*	*Ayv. Vol.*	*Ayv. Vol.*	*Ayv. Vol.*	*Ayv. Vol.*	*Ayv. Vol.*	*Ezn. Vol.*	*Ezn. Vol.*	*Ezn. Vol.*	*Ezn. Vol.*	*Ezn. Vol.*	*Ezn. Vol.*	*Ezn. Vol.*	*Tas. Vol.*
Age	Late Mio.	Late Mio.	Late Mio.	Late Mio.	Late Mio.	Late Mio.	Late Mio.	Late Mio.	Late Mio.	Late Mio.	Late Mio.	Late Mio.	Late Mio.	Late Mio.	Late Mio.
Rock type	*Basanite*	*Basanite*	*Basanite*	*Basanite*	*Basanite*	*Basanite*	*Basanite*	*Basanite*	*Basanite*	*Basanite*	*Hawaiite*	*Basalt*	*Basalt*	*Hawaiite*	*Hawaiite*
wt %															
SiO_2	42.20	42.51	41.81	42.61	42.77	43.04	43.05	42.75	44.53	44.94	45.88	46.07	46.87	46.99	45.68
TiO_2	3.14	3.12	3.14	3.15	3.14	3.14	3.14	3.09	3.03	2.98	2.78	2.83	2.85	2.82	2.83
Al_2O_3	12.65	13.21	12.76	13.04	12.87	12.97	12.80	12.87	12.49	13.08	12.87	13.21	13.08	13.01	13.38
Fe_2O_3	14.39	14.11	14.38	14.24	14.01	14.11	14.15	14.30	13.92	13.62	12.43	12.04	12.28	12.22	12.19
MnO	0.23	0.22	0.22	0.22	0.23	0.22	0.22	0.21	0.19	0.20	0.20	0.16	0.15	0.18	0.17
MgO	7.94	6.67	7.74	7.98	7.55	8.05	7.89	8.19	8.33	7.52	8.43	9.25	7.72	8.38	9.48
CaO	10.96	11.13	11.03	11.06	11.12	10.97	10.94	10.91	10.84	10.92	11.79	10.91	11.64	10.76	10.35
Na_2O	4.33	5.64	5.33	4.62	4.85	4.74	4.58	4.33	4.29	4.42	3.47	3.14	3.19	3.49	3.78
K_2O	2.49	2.28	1.52	1.97	2.10	1.43	2.15	1.42	1.24	1.46	1.41	1.51	1.68	1.67	1.22
P_2O_5	1.24	1.33	1.25	1.29	1.32	1.26	1.32	0.99	1.09	1.08	0.73	0.76	0.71	0.74	0.82
L.O.I	1.83	3.36	1.27	2.44	3.48	2.72	2.36	1.57	1.83	1.30	2.94	2.83	2.66	1.86	2.08
Total (L.O.I. free)	99.57	100.21	99.19	100.18	99.96	99.94	100.25	99.07	99.95	100.22	99.99	99.88	100.17	100.25	99.89
ppm															
Sc	19.6	19.2	18.6	20.1	17.4	27.8	19.3	17.1	19.7	19.2	16.8	15.0	23.2	20.8	22.9
Cr	88.2	72.8	92.1	82.8	84.0	77.0	77.2	137.3	138.1	134.7	229.0	228.5	228.4	239.2	190.3
V	196.8	209.5	206.2	206.0	200.4	221.8	205.1	211.3	204.5	203.7	196.4	208.5	209.1	203.2	192.0
Ni	65.5	58.9	70.4	69.3	64.6	57.5	61.6	104.5	99.6	95.4	149.0	168.6	163.0	156.0	146.4
Co	45.3	43.2	47.2	46.3	45.2	39.2	44.7	50.9	49.0	48.1	41.9	47.7	48.3	46.8	50.1
Cu	41.3	43.2	44.8	48.6	37.1	41.8	51.2	43.3	40.6	43.1	47.7	43.5	54.3	52.7	52.2
Zn	131.8	126.3	123.8	125.6	131.4	129.5	128.8	120.7	127.9	128.6	105.2	99.2	105.0	108.4	100.8
Ga	20.7	24.6	24.0	24.5	23.2	24.4	23.0	23.2	19.6	21.1	20.1	21.3	18.6	21.4	24.1
Rb	48.2	24.0	22.5	26.1	41.6	28.9	49.6	18.5	10.9	12.3	21.6	25.4	26.6	22.2	18.4
Sr	1073.9	1215.2	1123.1	1147.2	1152.2	1103.9	1188.0	956.3	1010.2	998.3	1104.0	778.4	749.6	801.6	1169.3
Y	34.0	34.7	33.8	34.0	34.9	32.5	34.1	30.1	31.5	30.9	26.1	25.4	25.1	23.6	28.7
Zr	369.1	364.9	372.3	368.7	370.1	406.4	374.5	312.8	310.5	322.2	254.2	237.6	266.1	282.8	256.8
Nb	115.6	110.4	114.1	104.5	116.3	101.7	110.2	94.0	90.1	94.8	59.2	65.6	61.4	62.7	66.7
Ba	625.7	776.3	682.5	645.2	646.5	652.2	748.4	511.5	552.0	619.0	521.5	418.6	603.0	469.5	379.5
La	72.2	75.7	71.2	72.0	68.4	68.8	83.1	62.0	61.6	58.6	32.6	37.7	31.4	36.9	51.1
Ce	163.0	145.3	135.5	138.2	160.0	130.4	148.4	107.6	123.0	118.0	92.3	74.0	76.3	73.5	101.4
Nd	67.9	67.7	70.5	68.0	74.8	59.9	65.5	59.0	66.7	58.4	36.5	42.2	35.6	39.8	54.0
Pb	11.7	8.5	11.9	6.7	13.8	7.0	8.7	8.0	10.1	9.6	9.6	10.4	9.9	1.4	5.0
Th	11.4	10.7	9.1	9.3	10.1	9.2	10.4	7.2	7.3	7.6	4.6	5.2	7.3	4.8	6.5
U	2.6	0.3	6.0	1.5	4.5	2.7	0.9	2.7	4.5	2.4	3.6	2.7	1.8	1.7	1.6

Area	EGA	EGA	EGA	EGA	EGA	DAB	DAB	DAB	DAB	DAB	DAB	DAB	DAB	DAB	DAB
Locality	**Tastepe**	**Tastepe**	**Tastepe**	**Tastepe**	**Tastepe**	**Foca**	**Foca**	**Foca**	**Foca**	**Foca**	**Foca**	**Foca**	**Foca**	**Foca**	**Dikili**
Sample no	**EA254**	**EA249**	**EA251**	**EA256**	**EA253**	**EA409**	**EA410**	**EA348**	**EA402**	**EA400**	**EA411**	**EA404**	**EA407**	**95EA385**	**EA350**
Unit	*Tas. Vol.*	*Tas. Vol.*	*Tas. Vol.*	*Tas. Vol.*	*Tas. Vol.*	*Foc. Dyke*	*Foc. Dyke*	*Foc. Dyke*	*Foc. Dyke*	*Foc. Dyke*	*Foc. Dyke*	*Foc. Dyke*	*Foc. Dyke*	*Foc. Dyke*	*Neb. Vol.*
Age	Late Mio.	Late Mio.	Late Mio.	Late Mio.	Late Mio.	Mid. Mio.	Mid. Mio.	Mid. Mio.	Mid. Mio.	Mid. Mio.	Mid. Mio.	Mid. Mio.	Mid. Mio.	Mid. Mio.	Mid. Mio.
Rock type	*Basanite*	*Hawaiite*	*Hawaiite*	*Hawaiite*	*Hawaiite*	*TraBas*	*TraBas*	*BasAnd*	*TraBas*	*TraBas*	*TraBas*	*TraBas*	*BasTraAnd*	*TraBas*	*BaTraAnd*
wt %															
SiO_2	45.69	49.97	50.13	50.34	50.52	50.27	50.15	54.40	48.19	49.22	50.41	48.70	56.64	50.26	51.24
TiO_2	2.78	2.58	2.58	2.62	2.59	1.23	1.17	0.73	1.21	1.09	1.16	1.21	1.03	1.05	1.22
Al_2O_3	13.29	14.30	14.65	14.67	14.62	17.86	17.22	15.36	15.31	17.78	17.01	15.81	17.16	19.23	11.69
Fe_2O_3	12.13	10.69	10.66	10.78	10.63	8.58	8.49	7.36	8.68	8.74	8.13	8.65	7.43	8.09	7.51
MnO	0.17	0.14	0.14	0.12	0.13	0.16	0.16	0.12	0.15	0.17	0.15	0.15	0.08	0.15	0.12
MgO	9.62	6.90	6.54	6.59	6.89	6.09	5.94	9.06	8.70	4.95	5.23	8.80	2.04	4.83	12.62
CaO	9.96	8.74	9.43	8.98	8.90	8.86	9.37	8.25	11.85	9.84	10.44	11.77	8.83	9.52	7.58
Na_2O	4.25	3.51	3.65	3.68	3.57	4.09	3.84	2.78	3.10	3.14	3.26	2.57	3.37	3.06	1.70
K_2O	1.37	1.63	1.62	1.64	1.63	2.22	2.35	1.89	1.91	4.38	3.55	2.06	2.76	2.95	4.72
P_2O_5	0.79	0.49	0.49	0.50	0.49	0.43	0.46	0.24	0.36	0.50	0.46	0.38	0.32	0.47	0.67
L.O.I	1.27	1.46	1.65	1.79	1.62		2.57	1.27	2.50	2.29	4.22	2.13	1.14	2.38	2.54
Total (L.O.I. free)	100.05	98.95	99.89	99.92	99.97	99.79	99.16	100.19	99.46	99.81	99.80	100.09	99.66	99.61	99.06
ppm															
Sc	21.6	19.1	21.8	22.5	23.8	21.0	13.5	16.7	20.8	13.2	14.6	20.8	18.5	16.1	14.3
Cr	194.6	216.6	277.8	270.0	223.3	209.8	223.2	464.3	378.4	102.5	218.5	369.7	166.3	12.0	755.0
V	200.8	200.4	203.9	200.5	201.0	181.7	168.8	161.6	189.9	159.7	151.7	184.7	154.9	186.5	169.9
Ni	142.3	176.9	174.6	177.3	78.3	80.3	77.3	222.3	117.3	47.6	77.2	119.6	44.5	13.1	456.8
Co	47.9	35.4	36.8	38.2	38.0	27.9	29.3	34.4	30.5	24.4	24.6	32.1	15.6	33.2	31.9
Cu	47.6	13.3	33.5	35.1	23.9	39.8	37.5	16.0	48.1	41.0	31.2	49.0	33.6	16.2	42.3
Zn	107.0	95.5	96.8	101.5	97.3	70.3	68.5	59.3	61.2	74.7	67.4	57.2	55.7	70.9	55.7
Ga	22.7	20.6	16.0	17.9	21.9	13.8	17.8	13.1	12.7	17.2	11.4	15.4	18.7	17.1	17.0
Rb	17.0	19.4	18.6	20.1	18.2	62.8	63.6	64.2	109.4	151.4	102.8	106.9	99.0	105.3	168.7
Sr	1057.9	539.0	566.7	573.9	553.4	941.7	951.6	711.1	590.5	899.5	690.7	606.6	658.5	819.0	645.5
Y	26.6	22.8	20.2	18.2	18.9	27.2	25.9	21.0	25.9	30.8	26.1	27.2	24.4	27.9	22.3
Zr	259.8	184.9	204.6	206.3	212.5	181.1	157.0	122.1	162.0	220.5	153.0	163.7	189.5	199.2	381.6
Nb	74.2	35.7	38.7	38.4	37.6	16.4	15.3	7.4	13.7	22.0	15.2	13.9	18.1	13.0	28.4
Ba	415.8	265.2	272.2	283.7	230.0	849.5	836.1	1223.3	600.5	757.6	944.3	620.4	889.4	1462.3	927.1
La	39.7	20.2	17.1	18.9	20.9	61.1	63.3	28.6	53.2	74.4	58.1	51.2	47.7	36.9	49.1
Ce	77.8	42.4	46.8	47.7	44.5	141.3	119.2	58.4	76.6	130.9	102.2	81.1	87.3	89.0	113.7
Nd	41.9	25.4	23.3	22.1	23.4	66.1	47.7	21.9	42.6	45.2	46.2	39.5	33.8	45.8	55.2
Pb	8.9	8.7	4.6	4.3	1.2	21.7	21.4	25.9	18.0	6.6	21.1	19.8	24.1	36.6	22.8
Th	5.7	2.6	3.1	3.5	2.7	13.1	11.0	9.6	8.4	16.3	12.0	8.7	18.9	17.7	30.2
U	1.5	1.4	3.3	4.3	3.2	2.6	2.2	1.2	2.1	1.6	3.9	2.6	6.3	3.1	8.1

Area	DAB	DAB	DAB	DAB	DAB	DAB	DAB	DAB	DAB	DAB	DAB	DAB	DAB	DAB	DAB
Locality	**Dikili**	**Dikili**	**Dikili**	**Dikili**	**Dikili**	**Dikili**	**Dikili**	**Ayvalik**	**Ayvalik**	**Ayvalik**	**Ayvalik**	**Dikili**	**Ayvalik**	**Dikili**	**Dikili**
Sample no	**EA109**	**EA128**	**EA129**	**EA130**	**EA134**	**EA138**	**EA303**	**EA142**	**EA143**	**EA300**	**EA292**	**EA382**	**EA293**	**EA139**	**EA296**
Unit	*Neb. Vol.*	*Neb. Vol.*	*Neb. Vol.*	*Neb. Vol.*	*Neb. Vol.*	*Neb. Vol.*	*Neb. Vol.*	*Neb. Vol.*	*Neb. Vol.*	*Neb. Vol.*	*Neb. Vol.*	*Neb. Vol.*	*Neb. Vol.*	*Neb. Vol.*	*Neb. Vol.*
Age	Mid. Mio.	Mid. Mio.	Mid. Mio.	Mid. Mio.	Mid. Mio.	Mid. Mio.	Mid. Mio.	Mid. Mio.	Mid. Mio.	Mid. Mio.	Mid. Mio.	Mid. Mio.	Mid. Mio.	Mid. Mio.	Mid. Mio.
Rock type	*BaTraAnd*	*BasAnd*	*BaTraAnd*	*BaTraAnd*	*BaTraAnd*	*BasAnd*	*BaTraAnd*	*BaTraAnd*	*BasAnd*	*TraBas*	*BaTraAnd*	*TraBasalt*	*BaTraAnd*	*TracAnd*	*TracAnd*
wt %															
SiO_2	51.51	54.38	55.64	52.79	53.69	52.61	54.56	54.30	52.69	49.86	55.58	50.78	55.81	57.56	57.20
TiO_2	1.05	1.00	0.81	0.95	0.84	0.84	1.09	0.82	0.85	0.96	0.89	1.12	0.90	0.72	0.80
Al_2O_3	17.63	17.56	17.71	17.86	16.22	15.60	16.04	17.78	15.68	14.74	16.89	18.76	17.04	18.03	17.56
Fe_2O_3	8.20	8.46	6.97	8.30	7.14	7.50	7.69	7.37	7.44	8.18	6.58	8.85	6.64	5.67	6.02
MnO	0.15	0.13	0.12	0.23	0.11	0.13	0.13	0.10	0.13	0.14	0.12	0.15	0.11	0.12	0.06
MgO	5.32	4.98	4.02	4.89	5.83	7.62	5.29	3.49	7.53	9.30	4.64	5.16	5.08	2.93	4.16
CaO	8.36	6.52	6.15	6.08	9.62	9.81	7.88	8.67	10.01	9.94	7.61	9.12	7.38	5.38	7.13
Na_2O	3.23	2.59	3.00	3.57	2.79	2.68	3.26	3.18	2.58	2.67	3.17	3.13	3.33	3.34	3.47
K_2O	2.80	2.78	3.64	3.98	2.82	2.31	3.41	3.05	2.33	2.86	3.13	2.60	3.03	4.04	2.96
P_2O_5	0.49	0.32	0.29	0.37	0.29	0.28	0.50	0.31	0.26	0.96	0.39	0.41	0.41	0.33	0.30
L.O.I	1.78	1.31	2.69	2.55	2.61	1.64	2.01	2.52	1.82	1.57	1.54	1.15	1.40	1.81	0.94
Total (L.O.I. free)	98.74	98.72	98.34	99.02	99.34	99.37	99.84	99.06	99.50	99.60	99.00	100.07	99.72	98.12	99.66
ppm															
Sc	18.0	20.7	16.1	19.1	14.1	24.1	21.1	20.4	26.5	25.3	19.2	20.4	18.0	15.0	15.1
Cr	11.1	21.4	25.0	16.7	162.0	318.1	348.4	19.1	338.2	218.8	159.9	18.3	163.7	23.3	95.6
V	192.9	194.9	155.3	191.1	156.8	151.4	185.7	146.6	167.1	192.0	153.7	202.1	145.8	114.4	145.2
Ni	14.0	17.9	19.5	17.0	66.5	139.9	144.3	29.1	141.2	86.4	89.1	9.1	89.5	15.0	32.9
Co	30.1	24.6	17.6	17.9	21.2	36.4	29.8	12.6	34.4	35.1	21.9	30.4	23.1	11.0	13.8
Cu	19.7	7.9	50.9	52.9	53.5	36.0	42.5	11.1	32.9	49.2	42.0	27.3	31.7	10.1	20.2
Zn	73.4	81.9	102.4	190.0	75.3	63.6	79.5	63.7	65.5	65.0	64.6	71.3	58.9	62.0	61.8
Ga	17.9	17.2	15.6	23.3	18.4	13.5	18.7	15.4	16.7	16.8	22.7	16.1	17.1	19.2	21.4
Rb	96.8	90.0	107.5	100.0	86.3	71.0	126.9	83.1	68.7	64.2	98.1	82.8	90.3	117.7	117.3
Sr	744.9	835.0	732.2	737.0	635.5	632.0	853.9	867.9	630.6	645.1	841.5	699.0	820.8	771.8	639.3
Y	26.2	22.7	24.1	25.7	25.3	22.9	25.8	25.6	23.0	24.2	36.0	25.5	26.2	27.3	27.9
Zr	187.7	171.0	196.5	189.5	160.8	138.0	266.1	186.9	136.4	150.0	258.2	185.6	245.5	260.6	223.5
Nb	12.8	14.6	14.3	21.2	15.1	10.8	18.6	16.2	11.1	10.2	17.7	11.3	18.7	19.7	16.4
Ba	1347.6	1632.2	1676.1	1906.8	1374.9	1237.8	1514.7	1756.4	1261.6	1044.5	1509.2	1220.9	1591.8	1656.7	1182.8
La	34.1	43.7	52.6	49.6	48.6	38.4	42.5	53.9	27.6	27.0	52.0	40.1	51.2	52.2	45.4
Ce	80.8	77.8	76.5	80.5	68.4	53.8	93.6	81.5	43.3	58.6	98.8	83.4	93.3	90.6	74.9
Nd	37.6	34.9	31.1	38.0	23.6	25.8	44.1	38.3	20.5	27.9	44.5	37.2	35.8	43.6	31.4
Pb	30.5	35.8	64.1	97.6	25.6	20.2	21.8	28.5	18.5	26.6	32.3	22.4	36.2	33.4	29.5
Th	13.0	8.9	24.3	19.4	14.8	7.8	15.9	17.0	7.2	12.2	29.5	8.8	26.7	24.2	35.0
U	1.8						2.6		2.0	1.0	5.2	2.0	6.6		8.3

Area	DAB	DAB	DAB	DAB	DAB	DAB	DAB	DAB	DAB	DAB	DAB	DAB	DAB	DAB	DAB
Locality	**Dikili**	**Ayvalik**	**Dikili**	**Ayvalik**	**Ayvalik**	**Ayvalik**	**Ayvalik**	**Ayvalik**	**Ayvalik**	**Ayvalik**	**Bergama**	**Bergama**	**Bergama**	**Y.Sakran**	**Y.Sakran**
Sample no	**EA298**	**EA290**	**EA380**	**EA399**	**EA376**	**EA341**	**EA294**	**EA100**	**EA290**	**EA101**	**EA118**	**EA378**	**EA112**	**EA113**	**EA114**
Unit	*Neb. Vol.*	*Neb. Vol.*	*Neb. Vol.*	*Neb. Vol.*	*Oda. Dyke*	*Oda. Dyke*	*Oda. Dyke*	*Oda. Dyke*	*Oda. Dyke*	*Oda. Dyke*	*Egr. And*	*Egr. And*	*Egr. And*	*Egr. And*	*Egr. And*
Age	Mid. Mio.	Mid. Mio.	Mid. Mio.	Mid. Mio.	Mid. Mio.	Mid. Mio.	Mid. Mio.	Mid. Mio.	Mid. Mio.	Mid. Mio.	Mid. Mio.	Mid. Mio.	Mid. Mio.	Mid. Mio.	Mid. Mio.
Rock type	*TracAnd*	*TracAnd*	*Basalt*	*TraBas*	*BaTraAnd*	*BaTraAnd*	*BaTraAnd*	*BaTraAnd*	*TracAnd*	*BaTraAnd*	*Andesite*	*BasAnd*	*Andesite*	*Andesite*	*Andesite*
wt %															
SiO_2	57.07	58.33	50.35	49.82	52.90	56.39	56.29	55.74	58.33	56.32	62.34	55.21	59.92	60.62	58.93
TiO_2	0.80	0.85	0.93	1.19	0.98	0.76	0.72	0.91	0.85	0.90	0.73	0.91	0.72	0.72	0.80
Al_2O_3	17.66	16.09	15.37	17.30	17.40	16.21	15.74	17.33	16.09	17.26	16.52	17.51	16.19	16.41	16.01
Fe_2O_3	6.53	6.31	8.27	8.50	8.07	6.11	6.65	6.30	6.31	6.27	5.78	7.66	6.85	6.76	6.95
MnO	0.06	0.09	0.14	0.16	0.13	0.11	0.11	0.09	0.09	0.10	0.12	0.15	0.12	0.12	0.14
MgO	3.02	4.11	9.81	5.94	5.06	4.19	7.59	4.73	4.11	3.96	0.64	6.16	2.38	2.53	3.59
CaO	6.85	6.71	9.55	9.67	7.79	9.48	7.54	7.54	6.71	8.06	7.07	6.12	6.67	6.62	6.72
Na_2O	3.51	3.25	2.22	4.33	3.19	3.25	3.05	3.27	3.25	3.23	3.30	2.94	3.23	3.42	3.14
K_2O	3.09	3.20	2.18	1.85	3.05	2.69	2.14	3.01	3.20	3.16	2.33	1.63	2.33	2.47	2.22
P_2O_5	0.28	0.28	0.32	0.46	0.34	0.29	0.26	0.38	0.28	0.40	0.17	0.27	0.22	0.21	0.24
L.O.I	1.16	0.93	1.82	2.93	1.20	5.58	1.13	1.45	0.93	2.22	4.65	2.41	1.80	0.88	1.78
Total (L.O.I. free)	98.87	99.23	99.14	99.22	98.91	99.48	100.09	99.30	99.23	99.66	98.99	98.56	98.63	99.88	98.74
ppm															
Sc	16.4	11.9	27.3	18.0	17.0	17.8	19.4	20.2	11.9	21.2	18.0	13.0	23.6	20.7	21.9
Cr	107.9	60.9	400.5	217.8	51.5	281.2	328.7	149.0	60.9	137.4	6.2	20.9	16.9	17.8	11.7
V	117.9	143.5	225.7	156.4	188.1	146.2	159.1	152.3	143.5	158.6	160.8	196.6	188.0	160.7	162.2
Ni	43.9	29.2	163.9	76.9	33.9	149.8	146.6	86.0	29.2	73.4	9.3	14.1	12.3	9.4	7.5
Co	20.4	16.8	34.8	27.5	26.1	25.6	24.9	19.7	16.8	20.3	12.1	27.0	10.2	10.3	13.5
Cu	29.9	24.3	65.4	40.0	36.1	31.2	18.4	42.0	24.3	41.6	20.9	31.3	23.3	24.9	20.1
Zn	60.7	60.0	58.8	63.2	122.6	61.4	59.7	63.3	60.0	65.5	49.3	71.7	72.4	73.9	72.5
Ga	22.4	18.3	14.6	18.7	18.3	15.8	19.5	19.8	18.3	21.3	17.7	21.0	18.6	19.2	16.5
Rb	122.8	136.8	63.1	77.4	94.0	100.4	91.0	84.3	136.8	93.4	68.5	45.6	66.7	69.0	59.3
Sr	609.2	751.2	905.3	798.4	889.5	554.2	550.7	851.3	751.2	942.3	454.2	698.7	729.6	698.2	824.5
Y	22.8	28.0	21.0	27.7	25.7	22.9	20.0	26.0	28.0	23.9	19.5	22.7	25.8	28.1	28.7
Zr	217.0	244.1	112.6	160.1	160.7	152.6	155.7	248.3	244.1	254.8	126.9	166.5	144.8	143.4	152.5
Nb	17.0	17.4	8.6	15.4	10.4	11.2	11.0	23.3	17.4	20.7	9.0	12.6	8.8	8.3	9.6
Ba	1216.1	1452.1	1473.7	862.9	1858.4	932.3	947.6	1656.3	1452.1	1767.4	1093.4	1091.3	1376.6	1272.7	1277.5
La	45.8	57.7	41.6	61.4	53.9	28.5	24.7	49.6	57.7	48.0	30.9	45.6	32.4	38.6	49.5
Ce	87.9	108.4	83.1	122.4	103.3	52.2	49.2	81.2	108.4	78.9	54.9	96.4	54.9	65.8	76.4
Nd	33.2	39.1	26.9	46.5	41.3	23.9	26.2	36.5	39.1	41.6	26.7	33.3	28.4	33.9	35.1
Pb	32.8	39.2	29.4	22.1	62.7	22.0	35.1	32.3	39.2	38.1	23.1	38.8	26.6	21.5	25.2
Th	29.5	34.1	10.6	11.0	20.5	8.1	18.1	22.8	34.1	27.8	17.4	18.5	13.8	13.5	11.6
U	6.6	10.4	2.6	2.7	3.9	3.7	3.2		10.4			5.1			

Area	DAB	DAB	DAB	DAB	DAB	DAB	DAB	DAB	DAB	DAB	DAB	DAB	DAB	DAB	DAB
Locality	**Y.Sakran**	**Bergama**	**Bergama**	**Y.Sakran**	**Y.Sakran**	**Bergama**	**Bergama**	**Bergama**	**Bergama**	**Bergama**	**Bergama**	**Bergama**	**Ayvalik**	**Ayvalik**	**Ayvalik**
Sample no	**EA115**	**EA334**	**EA333**	**EA346**	**EA347**	**EA311**	**EA314**	**EA320**	**EA316**	**EA308**	**EA367**	**EA302**	**EA90**	**EA93**	**EA288**
Unit	*Egr. And*	*Egr. And*	*Egr. And*	*Egr. And*	*Egr. And*	*Egr. And*	*Egr. And*	*Klg. And*	*Klg. And*	*Klg. And*	*Klg. And*	*Klg. And*	*Bal. Unit*	*Bal. Unit*	*Bal. Unit*
Age	Mid. Mio.	Mid. Mio.	Mid. Mio.	Mid. Mio.	Mid. Mio.	Mid. Mio.	Mid. Mio.	Early Mio.	Early Mio.	Early Mio.	Early Mio.	Early Mio.	Early Mio.	Early Mio.	Early Mio.
Rock type	*Andesite*	*Andesite*	*Andesite*	*Andesite*	*Andesite*	*Andesite*	*TracAnd*	*Andesite*	*Dacite*	*TracAnd*	*Dacite*	*TracAnd*	*Dacite*	*TracAnd*	*TracAnd*
wt %															
SiO_2	60.83	59.64	59.95	60.41	60.97	60.01	60.32	61.47	62.33	62.55	64.07	59.60	67.19	62.91	59.39
TiO_2	0.70	0.57	0.58	0.64	0.64	0.60	0.59	0.56	0.56	0.60	0.44	0.92	0.50	0.54	0.71
Al_2O_3	17.27	15.95	17.39	15.88	16.04	17.09	17.17	15.93	15.05	17.47	17.33	16.24	15.98	16.64	18.58
Fe_2O_3	6.43	5.95	4.88	5.80	5.83	5.34	5.36	5.07	5.74	5.09	3.83	6.12	3.51	4.73	5.39
MnO	0.14	0.12	0.06	0.10	0.10	0.09	0.10	0.09	0.09	0.05	0.07	0.09	0.04	0.05	0.17
MgO	2.09	5.08	5.30	4.29	4.25	4.51	4.66	3.63	3.83	2.13	3.12	3.56	1.27	2.77	1.57
CaO	5.59	7.30	5.79	6.29	6.34	6.03	5.87	5.64	5.37	5.10	4.28	5.79	3.56	3.47	5.04
Na_2O	3.96	3.28	2.12	2.88	3.14	3.52	3.69	3.43	3.20	3.64	3.35	3.36	3.69	3.32	4.04
K_2O	2.34	2.51	2.24	2.57	2.47	2.60	2.67	3.11	2.80	2.93	3.23	3.04	3.69	4.39	4.36
P_2O_5	0.17	0.15	0.19	0.16	0.18	0.16	0.14	0.20	0.21	0.23	0.23	0.30	0.19	0.22	0.34
L.O.I	3.02	1.70	6.46	1.33	0.95	1.20	0.99	1.01	1.28	1.47	2.42	1.22	0.36	2.17	
Total (L.O.I. free)	99.52	100.56	98.50	99.02	99.96	99.95	100.57	99.12	99.19	99.79	99.96	99.02	99.62	99.04	99.60
ppm															
Sc	14.8	15.2	12.0	10.8	15.0	12.3	12.2	9.6	12.5	15.4	8.5	12.7	6.3	12.6	12.0
Cr	6.7	197.8	93.8	128.7	133.4	200.6	204.6	82.3	74.0	28.7	139.0	107.6	21.0	29.7	6.7
V	151.3	135.6	102.5	123.0	128.2	104.1	102.6	106.2	106.0	116.3	76.0	129.5	99.2	104.5	95.3
Ni	8.0	89.7	38.2	35.7	38.5	88.0	83.6	34.6	35.3	18.7	68.8	49.1	11.9	20.3	5.7
Co	15.8	22.9	17.8	15.2	19.0	17.4	17.1	17.5	10.2	12.3	9.3	18.0	8.0	14.7	13.8
Cu	9.9	35.6	12.9	21.7	26.9	22.2	24.0	27.0	23.8	16.8	8.7	25.1	15.7	28.6	7.9
Zn	104.0	60.2	62.5	61.9	53.8	56.5	53.5	54.1	55.3	53.8	51.4	82.1	45.2	53.8	68.3
Ga	20.6	14.3	15.3	16.8	14.0	17.7	14.6	16.8	19.0	17.7	17.9	22.1	19.8	19.2	18.4
Rb	57.9	80.3	75.0	81.8	74.3	104.9	106.2	108.6	109.7	102.6	122.4	117.8	118.5	161.5	159.8
Sr	806.9	582.0	335.2	573.6	591.6	415.3	410.4	605.8	615.7	661.1	799.4	468.9	605.6	670.7	789.3
Y	27.2	23.3	22.4	22.4	22.7	22.1	22.0	23.0	22.5	16.6	22.9	33.2	17.3	22.5	28.4
Zr	117.6	115.3	131.6	135.5	135.8	146.5	147.4	131.1	128.1	139.3	154.7	334.5	136.8	140.5	281.7
Nb	10.6	7.6	10.3	8.4	8.1	11.8	10.6	9.6	10.0	9.5	11.9	20.2	12.5	14.1	20.7
Ba	1300.5	1036.6	913.4	1188.1	1290.8	728.4	721.6	1235.1	1275.6	1499.1	1563.8	1071.5	1320.5	1685.7	1680.4
La	33.1	37.2	43.4	32.3	32.1	32.5	32.8	40.3	46.2	42.8	50.9	70.8	44.5	49.9	58.3
Ce	65.7	68.5	72.0	70.0	63.4	56.7	61.9	73.4	83.8	75.9	92.7	126.5	84.2	97.2	118.7
Nd	35.5	26.0	25.1	23.3	22.5	23.8	25.0	25.7	33.0	31.4	36.9	57.7	39.1	51.7	49.2
Pb	58.6	32.6	29.4	26.4	27.8	28.7	29.5	36.2	39.8	34.8	40.6	31.5	33.2	34.8	49.6
Th	15.4	9.2	17.2	6.5	7.2	12.9	11.7	17.2	19.9	15.3	20.3	11.9	21.7	21.6	30.7
U		3.0	3.4	0.5	1.8	3.8	3.8	3.3	5.0	4.7	4.3	3.7			4.4

Area	DAB	DAB	DAB	DAB	DAB	DAB	DAB	DAB	DAB	DAB	DAB	DAB	DAB	DAB	DAB
Locality	**Ayvalik**	**Ayvalik**	**Ayvalik**	**Ayvalik**	**Ayvalik**	**Y.Sakran**	**Ayvalik**	**Ayvalik**	**Ayvalik**	**Ayvalik**	**Ayvalik**	**Ayvalik**	**Ayvalik**	**Ayvalik**	**Ayvalik**
Sample no	**EA99**	**EA122**	**EA126**	**EA149**	**EA155**	**EA147**	**EA95**	**EA125**	**EA151**	**EA121**	**EA144a**	**EA153**	**EA154**	**EA103**	**EA106**
Unit	*Bal. Unit*	*Bal. Unit*	*Bal. Unit*	*Bal. Unit*	*Bal. Unit*	*Akc. Unit*	*Akc. Unit*	*Akc. Unit*	*Akc. Unit*	*Akc. Unit*	*Akc. Unit*	*Akc. Unit*	*Akc. Unit*	*Ulb. Unit*	*Ulb. Unit*
Age	Early Mio.	Early Mio.	Early Mio.	Early Mio.	Early Mio.	Mid. Mio.	Early Mio.	Early Mio.	Early Mio.	Early Mio.	Early Mio.	Early Mio.	Early Mio.	Early Mio.	Early Mio.
Rock type	*Dacite*	*Dacite*	*Andesite*	*Dacite*	*TracAnd*	*Dacite*	*TracAnd*	*TracAnd*	*Andesite*	*Dacite*	*Dacite*	*Dacite*	*Andesite*	*TracAnd*	*TraDacite*
wt %															
SiO_2	67.90	64.79	63.78	65.08	59.80	65.08	59.04	61.33	60.95	66.18	64.46	64.73	61.55	60.46	62.46
TiO_2	0.47	0.48	0.52	0.56	0.73	0.54	0.66	0.50	0.56	0.49	0.55	0.51	0.57	0.59	0.55
Al_2O_3	15.46	15.37	16.28	14.74	16.32	16.02	19.06	16.50	15.28	14.80	16.45	16.15	16.47	16.89	16.68
Fe_2O_3	3.64	4.36	4.56	4.09	7.08	4.53	5.38	4.27	4.51	3.80	3.63	4.45	4.43	5.04	4.95
MnO	0.04	0.07	0.07	0.04	0.16	0.06	0.09	0.08	0.08	0.10	0.07	0.05	0.08	0.15	0.12
MgO	1.48	1.37	2.71	2.75	2.57	2.38	1.77	3.33	3.70	1.74	2.07	2.03	3.36	2.63	1.79
CaO	3.47	4.54	4.51	4.24	5.66	5.45	5.06	5.64	6.14	4.87	4.89	3.91	5.27	5.26	4.94
Na_2O	3.38	3.52	3.37	3.01	3.14	3.32	3.98	3.11	2.84	2.87	3.37	3.45	3.15	3.63	3.94
K_2O	3.57	4.15	3.51	3.77	3.54	1.96	4.48	3.67	3.42	3.89	3.66	3.85	3.92	3.66	3.75
P_2O_5	0.21	0.21	0.22	0.23	0.25	0.22	0.34	0.21	0.25	0.28	0.23	0.21	0.23	0.25	0.23
L.O.I	0.51	1.36	3.64	0.92	2.82	1.48	1.88	1.88	2.90	1.74	2.35	0.54	2.58	1.99	3.47
Total (L.O.I. free)	99.62	98.86	99.53	98.51	99.24	99.56	99.86	98.63	97.73	99.01	99.38	99.34	99.02	98.56	99.41
ppm															
Sc	10.4	13.6	17.6	18.0	18.0	15.2	14.7	14.2	15.5	16.1	18.4	12.1	15.2	13.9	10.5
Cr	6.9	18.7	26.9	16.9	60.3	20.5	5.8	21.7	29.7	11.7	25.6	33.6	28.9	35.7	26.4
V	88.2	98.7	109.2	92.4	150.4	95.0	85.9	93.2	94.4	89.5	106.7	92.4	98.3	75.6	96.9
Ni	7.9	15.4	19.4	14.6	17.7	16.9	9.2	15.1	23.7	15.3	19.8	15.7	18.0	16.8	13.6
Co	7.6	9.3	11.3	9.2	23.8	9.2	9.4	7.4	15.7	3.8	8.4	8.8	9.2	13.1	10.0
Cu	14.2	17.6	24.2	19.0	30.1	17.3	9.5	17.8	23.5	18.3	14.5	31.3	26.4	15.8	11.9
Zn	45.7	47.8	49.1	48.3	79.4	59.4	62.0	56.8	54.3	41.1	66.7	53.1	49.1	58.8	63.6
Ga	17.4	19.2	17.1	22.3	16.8	17.3	17.3	17.2	16.1	16.5	16.3	17.6	18.6	17.8	19.5
Rb	112.5	159.6	107.3	130.7	110.7	84.0	153.5	124.4	111.4	112.4	116.9	142.6	119.6	133.5	127.6
Sr	636.3	708.0	670.1	594.9	762.7	884.1	821.7	598.5	770.4	684.9	705.8	844.2	610.2	592.1	605.6
Y	19.2	20.4	23.2	22.8	25.7	19.7	27.0	22.6	22.3	22.3	24.3	24.1	22.7	20.2	21.4
Zr	144.3	142.1	134.7	149.4	155.9	143.3	278.3	147.1	150.1	153.9	160.5	154.8	151.8	181.5	168.1
Nb	12.4	11.4	13.9	13.0	11.0	9.9	20.8	9.7	10.9	10.6	11.2	10.2	11.3	13.8	15.2
Ba	1323.4	1570.4	1830.5	1307.9	1672.1	1178.9	1688.7	1498.0	1598.9	1486.2	1474.1	1521.3	1755.9	2154.2	1529.2
La	37.0	48.0	41.9	40.2	49.7	49.2	62.6	49.7	49.6	45.7	45.7	57.8	47.6	46.9	46.7
Ce	59.1	80.9	70.1	76.7	85.2	73.9	97.5	76.3	77.7	73.3	73.8	97.7	75.6	85.5	78.8
Nd	23.8	35.1	33.4	37.5	41.4	36.3	44.2	35.6	42.6	37.2	38.9	45.4	34.2	35.7	35.1
Pb	30.4	32.8	27.4	31.7	32.7	29.3	33.3	31.2	33.3	28.4	36.3	38.7	34.3	35.6	36.9
Th	15.4	20.7	19.3	14.6	32.5	16.1	24.1	20.9	16.9	13.7	18.5	19.2	18.9	17.7	21.0
U															

Area	DAB	DAB	DAB	DAB	DAB	DAB	DAB	DAB	DAB	DAB	DAB	DAB	DAB	DAB	DAB
Locality	**Ayvalik**	**Ayvalik**	**Ayvalik**	**Ayvalik**	**Dikili**	**Dikili**	**Dikili**	**Dikili**	**Dikili**	**Dikili**	**Dikili**	**Dikili**	**Dikili**	**Dikili**	**Dikili**
Sample no	**EA144**	**EA144b**	**EA140**	**EA148**	**EA132**	**EA131**	**EA137**	**EA107**	**EA136**	**EA375**	**EA351**	**EA359**	**EA360**	**EA299**	**EA335**
Unit	*Ulb. Unit*	*Ulb. Unit*	*Ulb. Unit*	*Ulb. Unit*	*Mad. Dyke*	*Mad. Dyke*	*Mad. Dyke*	*Mad. Dyke*	*Mad. Dyke*	*Mt.Sey. U.*	*Mt.Sey. U.*	*Mt.Sey. U.*	*Mt.Sey. U.*	*Mt.Sey. U.*	*Mt.Sey. U.*
Age	Early Mio.	Early Mio.	Early Mio.	Early Mio.	Early Mio.	Early Mio.	Early Mio.	Early Mio.	Early Mio.	Early Mio.	Early Mio.	Early Mio.	Early Mio.	Early Mio.	Early Mio.
Rock type	*TracAnd*	*TracAnd*	*TracAnd.*	*TracAnd*	*TracAnd*	*TraDacite*	*TracAnd.*	*TraDacite*	*TracAnd*	*Andesite*	*TracAnd*	*TraDacite*	*Dacite*	*Dacite*	*Andesite*
wt %															
SiO_2	59.47	59.53	59.15	56.47	59.64	64.54	58.26	62.21	64.15	58.56	61.15	66.04	64.38	65.05	57.73
TiO_2	0.59	0.59	0.56	0.49	0.64	0.60	0.65	0.60	0.50	0.84	0.76	0.52	0.68	0.66	0.82
Al_2O_3	16.53	16.52	19.55	16.93	16.79	14.42	18.66	16.20	15.97	17.24	16.73	16.42	16.62	14.39	17.15
Fe_2O_3	5.35	5.46	4.17	4.95	5.80	3.48	5.36	5.04	4.13	6.47	5.12	3.30	4.46	5.06	6.69
MnO	0.14	0.14	0.13	0.26	0.11	0.09	0.10	0.07	0.09	0.08	0.09	0.08	0.07	0.11	0.14
MgO	2.27	2.31	1.25	4.74	3.31	2.35	2.44	1.75	2.83	2.53	2.24	1.86	2.10	1.59	3.05
CaO	6.64	6.71	8.60	8.12	6.31	4.43	4.28	4.83	4.36	7.33	5.52	3.84	4.06	4.73	7.80
Na_2O	3.46	3.48	0.57	2.21	3.27	3.07	4.17	3.39	2.92	2.99	3.74	3.05	2.98	2.86	2.95
K_2O	4.02	4.11	6.38	4.64	3.64	5.64	4.15	4.01	4.31	3.24	3.57	4.38	4.02	3.58	3.09
P_2O_5	0.23	0.23	0.18	0.19	0.21	0.40	0.30	0.26	0.23	0.32	0.32	0.26	0.39	0.33	0.40
L.O.I	2.02	2.02	2.21	3.02	0.71	3.60	2.40	0.86	1.54	0.93	0.69	2.28	3.32	1.18	3.18
Total (L.O.I. free)	98.70	99.09	100.53	99.01	99.71	99.02	98.36	98.36	99.49	99.60	99.23	99.75	99.77	98.36	99.82
ppm															
Sc	15.3	14.4	13.0	19.8	17.0	9.4	23.2	14.6	13.2	20.0	10.3	5.1	8.9	11.6	20.1
Cr	18.1	26.0	9.0	27.5	67.8	159.0	6.2	126.0	84.6	228.2	122.9	43.3	77.9	57.3	36.0
V	96.7	99.3	54.7	49.5	120.9	69.9	94.4	79.5	85.3	157.2	108.3	82.7	110.9	76.5	191.0
Ni	17.4	21.8	8.7	26.2	27.9	54.0	9.3	59.7	35.9	83.7	65.6	14.7	37.8	29.0	39.5
Co	6.7	9.7	6.2	3.1	11.8	9.1	11.0	12.7	11.8	21.2	12.6	8.6	25.4	15.2	25.7
Cu	34.4	17.0	7.1	13.7	22.0	18.9	17.3	16.5	22.7	34.1	26.1	2.4	21.4	29.8	55.2
Zn	100.7	66.5	48.0	75.3	61.8	40.1	62.7	56.0	48.4	68.6	50.1	55.1	49.5	38.2	74.9
Ga	19.0	21.2	15.1	14.3	20.5	15.7	21.7	19.5	13.8	13.8	15.9	13.7	17.1	13.2	18.9
Rb	108.7	117.4	188.7	111.9	134.0	237.5	140.3	165.3	165.9	182.8	155.2	158.5	161.8	146.2	84.4
Sr	657.0	702.6	147.1	603.2	785.0	444.6	705.5	530.4	458.2	821.8	533.5	514.2	576.1	624.3	807.0
Y	23.2	24.5	26.1	21.9	26.2	19.5	26.6	24.0	25.1	25.1	23.9	46.4	28.0	24.5	28.2
Zr	159.2	155.9	139.5	120.3	211.2	280.5	247.6	208.3	211.6	266.3	204.1	167.6	179.9	264.9	160.7
Nb	10.5	11.2	13.7	9.5	14.0	23.4	20.7	18.6	19.8	20.8	17.8	17.9	14.5	17.5	9.4
Ba	1355.8	1474.8	1436.1	1290.6	1583.6	1062.6	1540.6	1123.7	1107.1	1695.5	1034.7	1205.8	1805.2	3039.2	1535.5
La	45.4	43.3	41.6	34.4	53.4	46.1	49.9	43.2	46.6	47.6	39.5	45.8	36.3	51.9	55.6
Ce	75.4	72.1	72.0	56.6	80.7	78.3	94.3	69.3	75.4	109.1	69.3	83.3	71.7	89.9	85.3
Nd	36.5	38.8	32.9	33.1	38.9	30.8	48.1	26.9	33.6	40.2	35.0	41.6	32.0	37.2	38.9
Pb	32.0	34.2	27.4	26.6	42.1	34.2	31.2	33.7	30.7	47.9	27.8	30.3	27.4	37.2	31.7
Th	18.1	19.2	12.6	13.0	26.9	33.1	22.9	23.5	38.0	41.3	21.3	19.1	20.3	40.8	12.9
U										5.6	7.3	6.4	6.5	9.2	1.7

Area	DAB	DAB	DAB	DAB	DAB	DAB	DAB	DAB	DAB	DAB	DAB	DAB	DAB	DAB	DAB
Locality	**Dikili**	**Dikili**	**Dikili**	**Bergama**	**Bergama**	**Bergama**	**Bergama**	**Bergama**	**Dikili**	**Dikili**	**Dikili**	**Dikili**	**Dikili**	**Dikili**	**Dikili**
Sample no	**EA356**	**EA357**	**EA326**	**EA352**	**EA371**	**EA362**	**EA372**	**EA373**	**EA229**	**EA374**	**EA141**	**EA343**	**EA364**	**EA230**	**EA298**
Unit	*Mt.Sey. U.*	*Mt.Sey. U.*	*Mt.Sey. U.*	*Krg. Unit*	*Krg. Unit*	*Krg. Unit*	*Krg. Unit*	*Krg. Unit*	*Krg. Unit*	*Krg. Unit*	*Krg. Unit*	*Krg. Unit*	*Krg. Unit*	*Krg. Unit*	*Krg. Unit*
Age	Early Mio.	Early Mio.	Early Mio.	Early Mio.	Early Mio.	Early Mio.	Early Mio.	Early Mio.	Early Mio.	Early Mio.	Early Mio.	Early Mio.	Early Mio.	Early Mio.	Early Mio.
Rock type	*TracAnd*	*TracAnd*	*TraDacite*	*TracAnd*	*Dacite*	*TracAnd*	*Bas And*	*TraDacite*	*TracAnd*	*TraDacite*	*TracAnd*	*TraDacite*	*TraDacite*	*BaTraAnd*	*Rhyolite*
wt %															
SiO_2	60.33	59.03	65.46	64.77	68.28	57.80	54.73	63.86	58.26	63.08	58.26	62.28	65.25	54.70	69.29
TiO_2	0.80	0.80	0.53	0.73	0.50	0.97	0.99	0.82	1.00	0.90	0.72	0.68	0.59	1.17	0.53
Al_2O_3	16.76	16.56	14.16	16.16	14.77	14.92	14.60	15.01	16.47	15.43	16.80	16.02	15.89	18.18	14.58
Fe_2O_3	5.97	5.98	3.89	4.88	2.78	6.39	6.66	4.75	6.46	5.09	6.21	5.69	4.17	5.58	3.52
MnO	0.12	0.11	0.06	0.08	0.06	0.11	0.12	0.07	0.06	0.05	0.10	0.11	0.07	0.10	0.04
MgO	3.50	3.45	2.47	2.29	1.28	4.30	7.59	2.62	2.09	2.41	4.19	3.18	2.45	3.13	0.21
CaO	6.24	6.20	3.98	4.75	2.97	5.77	7.58	5.07	6.75	5.18	6.79	6.50	4.45	8.44	7.01
Na_2O	3.03	2.98	3.12	3.14	3.36	2.66	2.63	3.30	3.56	3.17	2.88	2.85	3.17	3.29	0.91
K_2O	3.12	3.02	3.79	3.64	4.00	4.44	3.99	4.30	4.17	4.10	3.60	2.50	3.64	3.96	3.63
P_2O_5	0.27	0.27	0.22	0.35	0.19	0.51	0.55	0.51	0.48	0.51	0.26	0.16	0.27	0.95	0.25
L.O.I	2.28	3.12	1.51	1.06	2.11	2.53	2.27	1.56	3.15	1.02	1.25	2.65	2.11	1.43	2.86
Total (L.O.I. free)	100.13	98.39	97.68	100.79	98.18	97.87	99.44	100.31	99.30	99.91	99.81	99.96	99.94	99.50	99.97
ppm															
Sc	14.6	17.1	9.8	12.6	6.9	14.2	17.0	12.2	20.8	14.9	19.9	14.8	9.9	20.5	5.1
Cr	136.4	139.5	34.2	45.8	10.7	368.0	633.4	139.3	22.9	221.6	150.3	121.0	14.8	34.3	5.2
V	133.9	137.7	89.3	101.2	57.5	146.0	175.0	105.8	175.4	119.6	134.0	134.7	110.3	266.6	56.6
Ni	51.3	50.2	16.3	19.1	7.0	191.8	205.3	35.2	15.9	52.3	56.6	38.8	10.4	16.1	5.4
Co	19.1	19.6	11.2	12.7	4.9	22.9	31.8	14.1	33.4	23.1	22.8	17.4	12.4	36.2	9.5
Cu	17.4	15.2	16.9	15.3	2.6	37.3	62.8	17.6	24.4	22.2	31.4	19.0	7.3	51.9	8.6
Zn	63.7	55.0	46.9	51.2	41.8	63.3	63.9	53.1	91.4	46.5	62.4	57.7	61.0	147.2	26.5
Ga	18.8	16.6	17.9	18.1	16.2	16.1	17.9	16.7	17.4	17.6	15.5	18.6	18.5	23.7	16.9
Rb	122.2	123.4	135.1	155.1	200.5	166.9	152.7	194.5	144.9	206.5	205.2	97.3	123.3	69.1	517.7
Sr	617.9	639.4	532.9	577.6	379.2	770.3	829.3	654.2	1240.7	679.0	662.1	609.6	714.1	1455.2	373.5
Y	21.9	21.2	20.1	20.3	15.8	25.6	23.9	23.2	28.5	23.1	28.2	22.1	21.5	37.5	14.5
Zr	179.6	182.6	132.9	181.4	162.6	311.3	276.8	257.8	255.4	295.4	274.5	145.6	168.2	289.9	210.5
Nb	14.2	14.1	11.3	14.9	18.6	18.7	15.9	19.1	12.6	19.7	18.9	9.4	12.5	12.5	16.7
Ba	1074.1	1088.7	1267.9	1248.9	863.5	1607.4	1226.5	1591.9	1944.2	1540.8	1520.4	1329.0	1397.4	2551.6	1317.4
La	38.3	33.7	42.5	30.5	41.1	46.2	49.4	41.1	62.8	44.9	49.9	26.7	45.1	80.7	47.5
Ce	69.1	71.1	84.6	58.6	64.1	103.5	118.0	77.0	120.8	93.9	86.5	69.3	93.8	139.9	84.7
Nd	32.3	25.8	34.3	29.2	23.2	51.9	55.0	35.3	57.9	43.4	38.2	25.4	38.9	65.1	35.3
Pb	24.5	23.9	38.2	26.7	33.4	25.8	22.3	30.8	53.2	30.3	42.9	32.8	33.4	52.4	1.9
Th	17.6	15.9	21.3	18.8	32.2	23.4	23.3	26.5	23.5	25.9	49.2	11.6	20.2	25.9	1.1
U	4.3	3.9	4.1	3.8	8.2	3.5	4.5	5.5	2.5	7.1		2.1	3.6	4.1	0.9

Area	DAB	DAB	DAB	DAB	DAB	DAB	DAB	DAB	EGA	EGA	EGA	EGA	EGA	EGA	EGA
Locality	**Dikili**	**Dikili**	**Dikili**	**Dikili**	**Dikili**	**Dikili**	**Dikili**	**Dikili**	**Babakale**	**Babakale**	**Babakale**	**Assos**	**Assos**	**Assos**	**Assos**
Sample no	**EA331**	**EA305**	**EA306**	**EA336**	**EA323**	**EA332**	**EA329**	**EA302**	**EA43**	**EA44**	**EA45**	**EA413**	**EA412**	**EA418**	**EA274**
Unit	*Kab. Dac.*	*Kab. Dac.*	*Kab. Dac.*	*Kir. Unit*	*Kir. Unit*	*Kir. Unit*	*Kir. Unit*	*Kir. Unit*	*Kov. Dyke*	*Kov. Dyke*	*Kov. Dyke*	*Kov. Dyke*	*Kov. Dyke*	*Kov. Dyke*	*Kov. Dyke*
Age	Early Mio.	Early Mio.	Early Mio.	Early Mio.	Early Mio.	Early Mio.	Early Mio.	Early Mio.	Early Mio.	Early Mio.	Early Mio.	Early Mio.	Early Mio.	Early Mio.	Early Mio.
Rock type	*TraDacite*	*TraDacite*	*TraDacite*	*TraDacite*	*TraDacite*	*TracAnd*	*Rhyolite*	*TracAnd*	*TracAnd.*	*TracAnd.*	*TracAnd*	*TracAnd*	*TracAnd*	*BaTraAnd*	*Andesite*
wt %															
SiO_2	62.83	64.33	63.20	58.07	64.29	59.39	67.51	59.60	58.66	58.61	57.73	56.29	58.01	56.24	62.68
TiO_2	0.59	0.75	0.65	0.63	0.59	0.71	0.57	0.92	0.75	0.75	0.73	1.07	0.87	0.87	0.84
Al_2O_3	15.73	16.69	15.84	18.52	15.69	15.73	15.41	16.24	16.51	16.52	16.71	19.30	15.45	18.45	16.98
Fe_2O_3	4.53	5.00	4.90	5.03	4.30	5.72	4.02	6.12	6.04	6.11	5.74	6.20	6.99	6.40	4.85
MnO	0.13	0.08	0.08	0.10	0.07	0.12	0.06	0.09	0.10	0.11	0.09	0.08	0.08	0.09	0.04
MgO	3.13	1.59	2.35	5.71	2.97	4.08	1.47	3.56	3.65	4.12	3.75	2.06	5.86	3.83	1.20
CaO	5.72	5.23	5.69	5.73	4.54	7.49	3.64	5.79	6.58	6.64	6.78	6.53	7.27	7.90	5.02
Na_2O	3.07	3.40	3.06	2.10	2.94	2.95	3.30	3.36	3.49	3.48	3.43	3.96	3.20	3.87	3.93
K_2O	3.56	2.82	2.56	3.66	3.74	3.82	3.77	3.04	3.09	2.98	3.07	3.18	2.48	1.84	3.75
P_2O_5	0.23	0.20	0.16	0.21	0.23	0.20	0.22	0.30	0.25	0.27	0.25	0.37	0.25	0.29	0.22
L.O.I	1.78	2.09	2.16	1.26	1.64	1.61	2.18	1.22	1.85	1.56	1.58	1.02	0.96	1.26	1.10
Total (L.O.I. free)	99.52	100.09	98.49	99.76	99.36	100.22	99.97	99.02	99.12	99.59	98.28	99.04	100.46	99.78	99.50
ppm															
Sc	11.8	13.6	13.5	14.0	9.0	19.0	10.7	12.7	21.7	19.6	20.6	13.6	18.0	19.7	9.1
Cr	42.6	30.1	81.1	48.1	37.9	94.2	37.1	107.6	76.9	85.2	76.8	8.0	212.3	38.6	4.3
V	95.4	120.8	111.1	140.4	117.3	111.0	84.5	129.5	146.5	151.6	139.1	152.5	149.3	169.2	108.5
Ni	16.7	14.6	30.4	18.5	17.6	38.5	13.1	49.1	35.6	40.4	37.7	22.3	78.7	37.7	10.1
Co	9.1	13.0	12.2	12.7	10.9	15.5	7.9	18.0	15.7	15.0	17.8	18.6	26.4	24.7	10.6
Cu	11.4	9.6	17.3	18.3	15.1	39.2	8.6	25.1	55.4	54.5	51.9	59.9	37.2	67.4	7.9
Zn	57.3	59.2	58.5	65.3	55.4	54.0	33.0	82.1	62.6	64.6	57.4	58.2	64.1	63.4	64.5
Ga	16.4	18.9	17.2	17.8	16.8	12.8	13.6	22.1	23.0	20.7	17.8	22.4	18.2	19.9	18.6
Rb	124.7	95.3	94.0	105.8	137.9	139.5	142.6	117.8	108.8	110.8	102.3	119.4	107.7	66.7	161.8
Sr	546.6	447.8	380.7	546.3	624.6	618.2	560.2	468.9	838.5	827.5	873.0	968.3	962.6	942.0	733.6
Y	21.7	27.7	24.4	21.0	21.3	22.3	16.3	33.2	23.3	22.6	21.9	29.0	23.1	22.3	20.6
Zr	146.5	196.7	182.3	130.0	153.7	136.6	147.9	334.5	210.1	209.2	204.1	299.3	224.7	171.7	224.8
Nb	11.4	12.0	10.8	10.3	12.2	10.0	12.0	20.2	13.8	14.0	11.8	16.2	11.5	9.0	12.4
Ba	1572.6	1295.4	974.3	1581.5	1351.6	1366.4	1384.9	1071.5	1428.2	1417.0	1428.8	1458.7	1238.5	1368.6	1630.8
La	39.7	46.5	30.7	39.4	48.5	31.5	44.1	70.8	65.8	58.8	60.8	70.3	45.8	53.6	48.2
Ce	84.9	77.5	62.5	78.1	84.3	58.7	79.8	126.5	108.3	111.0	98.6	148.5	105.2	104.3	87.4
Nd	30.9	36.5	23.9	30.8	37.0	25.9	29.9	57.7	42.8	54.0	48.0	50.1	35.8	39.7	39.7
Pb	40.7	29.2	24.6	33.2	40.6	39.1	40.2	31.5	36.9	42.5	31.7	56.7	57.3	34.6	38.4
Th	24.4	15.5	13.2	20.2	21.5	19.1	24.3	11.9	21.8	22.5	26.4	35.9	24.9	10.3	18.8
U	3.9	2.8	2.8	3.2	4.7	3.4	3.6	3.7				7.3	4.8	1.2	2.9

Area	EGA	EGA	EGA	EGA	DAB	EGA	EGA	EGA	EGA	EGA	EGA	EGA	EGA	EGA	EGA
Locality	**Assos**	**Assos**	**Babakale**	**Babakale**	**Babakale**	**Babakale**	**Babakale**	**Babakale**	**Babakale**	**Gulpinar**	**Gulpinar**	**Gulpinar**	**Tamis**	**Tamis**	**Tamis**
Sample no	**EA85**	**EA88**	**EA89**	**EA51**	**EA76**	**EA53**	**EA228**	**EA209**	**EA55**	**EA27**	**EA33A**	**EA77**	**EA390**	**EA420**	**EA388**
Unit	*Kov. Dyke*	*Kov. Dyke*	*Kov. Dyke*	*Kov. Dyke*	*Kov. Dyke*	*Kov. Dyke*	*Kov. Dyke*	*Kov. Dyke*	*Kov. Dyke*	*Bal. Ign.*	*Bal. Ign.*	*Bal. Ign.*	*Bal. Ign.*	*Bal. Ign.*	*Bal. Ign.*
Age	Early Mio.	Early Mio.	Early Mio.	Early Mio.	Early Mio.	Early Mio.	Early Mio.	Early Mio.	Early Mio.	Early Mio.	Early Mio.	Early Mio.	Early Mio.	Early Mio.	Early Mio.
Rock type	*Andesite*	*TracAnd.*	*Andesite*	*TracAnd.*	*BaTraAnd*	*TracAnd*	*TracAnd*	*TracAnd*	*TracAnd.*	*TracDacite*	*Rhyolite*	*Rhyolite*	*Rhyolite*	*Rhyolite*	*Rhyolite*
wt %															
SiO_2	61.81	58.27	58.97	58.46	54.90	58.95	60.04	56.99	58.09	67.41	69.80	73.43	75.50	74.52	75.62
TiO_2	0.67	0.68	0.74	0.83	1.08	0.83	1.04	1.17	0.83	0.51	0.46	0.38	0.11	0.09	0.22
Al_2O_3	17.03	16.26	16.64	19.25	17.27	19.75	19.21	18.42	19.25	16.46	15.40	14.06	14.19	13.17	12.92
Fe_2O_3	4.95	5.33	5.81	4.89	6.00	4.74	4.75	6.20	5.05	3.13	2.82	1.62	0.99	0.85	1.56
MnO	0.08	0.09	0.10	0.07	0.09	0.07	0.04	0.05	0.08	0.06	0.05	0.02	0.05	0.06	0.03
MgO	3.09	3.53	3.96	1.62	3.42	1.15	1.38	1.18	1.19	0.59	0.37	0.15	0.27	0.22	0.03
CaO	5.37	6.04	6.54	6.23	8.36	6.31	4.73	5.45	6.96	1.51	1.32	0.83	1.00	0.81	0.77
Na_2O	3.53	3.56	3.38	4.07	3.18	3.98	3.85	4.13	4.04	3.22	4.18	4.09	2.14	2.94	3.22
K_2O	2.79	4.20	3.02	3.36	4.18	3.42	4.02	4.15	3.31	5.48	5.09	5.04	5.08	3.99	5.00
P_2O_5	0.22	0.36	0.27	0.33	0.83	0.35	0.41	0.40	0.33	0.11	0.11	0.08	0.00	0.01	0.03
L.O.I	1.07	0.80	1.73	0.76	1.09	1.49	2.33	2.18	2.64	1.47	0.63	0.70	2.18	3.86	0.57
Total (L.O.I. free)	99.54	98.33	99.42	99.10	99.31	99.55	99.47	98.13	99.13	98.48	99.60	99.70	99.32	96.66	99.40
ppm															
Sc	13.5	14.3	20.0	12.0	22.8	15.9	16.9	13.5	16.6	6.2	4.2	3.6	2.0	1.7	3.5
Cr	47.8	25.5	72.1	8.4	31.9	4.5	50.8	3.6	13.6	4.8	1.6	0.8	0.0	0.0	0.0
V	92.7	126.5	137.4	141.6	280.5	131.3	258.6	167.5	146.7	30.4	39.9	30.6	2.8	3.1	9.5
Ni	33.2	18.5	31.0	12.9	21.9	18.6	17.1	14.1	12.3	6.1	4.2	3.4	13.9	2.0	1.6
Co	13.8	11.4	14.8	10.1	17.9	6.1	21.8	14.0	10.5	2.9	3.6	2.5	0.8	0.0	1.2
Cu	9.0	36.5	54.3	58.7	115.0	89.7	28.3	16.7	86.8	22.3	22.8	14.4	11.1	0.0	0.0
Zn	72.5	62.4	61.5	53.3	88.6	54.3	72.7	55.6	60.3	56.7	51.5	27.3	41.9	24.3	23.9
Ga	18.3	17.7	20.0	23.8	19.4	20.4	19.2	17.8	21.1	22.6	17.2	20.3	14.6	12.9	15.7
Rb	104.8	180.0	154.1	116.4	77.5	113.4	173.7	188.0	113.9	208.1	201.6	177.4	168.6	157.5	151.1
Sr	1147.1	918.7	855.2	1062.8	1295.8	1089.1	1165.5	915.4	1064.5	340.7	299.2	215.4	126.5	65.2	92.2
Y	28.1	26.2	24.3	20.5	28.7	21.8	33.3	27.7	23.0	33.4	29.1	34.5	7.3	6.0	13.8
Zr	193.2	225.3	211.8	241.8	246.7	242.4	298.5	333.4	231.5	407.9	398.7	394.7	102.8	93.7	139.1
Nb	10.7	14.9	11.8	14.3	19.1	12.9	16.8	17.9	14.7	19.3	17.8	18.3	21.0	20.3	28.6
Ba	1634.4	1429.8	1463.4	1689.4	2446.2	1808.1	1716.1	1387.1	1664.8	2060.4	1926.2	1898.7	520.0	323.2	284.2
La	55.1	76.1	66.5	73.7	77.9	69.0	88.9	72.1	72.6	89.3	96.4	91.2	31.4	29.9	37.3
Ce	90.5	137.5	101.4	121.4	130.0	119.6	167.7	149.5	118.3	170.1	182.9	160.2	52.1	45.9	61.6
Nd	44.7	59.1	56.0	48.6	56.4	57.0	74.4	61.1	45.5	65.0	71.6	65.4	14.1	13.6	16.8
Pb	62.3	55.2	38.2	37.7	37.7	36.8	54.0	47.1	67.5	63.5	55.2	48.7	42.1	38.1	50.5
Th	11.8	31.8	23.7	28.7	18.7	24.8	32.1	29.1	25.6	43.7	44.6	40.7	40.7	39.0	48.0
U							6.3	2.9				6.0	10.2	10.0	9.4

Area	EGA	EGA	EGA	EGA	EGA	DAB	EGA	EGA	EGA	EGA	EGA	EGA	EGA	EGA	DAB
Locality	**Babakale**	**Babakale**	**Babakale**	**Assos**	**Assos**	**Assos**	**Assos**	**Babakale**	**Babakale**	**Babakale**	**Babakale**	**Babakale**	**Babakale**	**Babakale**	**Babakale**
Sample no	**EA394**	**EA111**	**EA219**	**EA206**	**EA218**	**EA215**	**EA225**	**EA220**	**EA232**	**EA202**	**EA280**	**EA281**	**EA224**	**EA283**	**EA307**
Unit	*Bal. Ign.*	*Bal. Ign.*	*Bal. Ign.*	*Berg. Ign*	*Berg. Ign*	*Berg. Ign*	*Berg. Ign*	*Berg. Ign*	*Berg. Ign*	*Berg. Ign*	*Berg. Ign*	*Koy. Ign.*	*Koy. Ign.*	*Koy. Ign.*	*Koy. Ign.*
Age	Early Mio.	Early Mio.	Early Mio.	Early Mio.	Early Mio.	Early Mio.	Early Mio.	Early Mio.	Early Mio.	Early Mio.	Early Mio.	Early Mio.	Early Mio.	Early Mio.	Early Mio.
Rock type	*Rhyolite*	*Rhyolite*	*Rhyolite*	*TracDacite*	*Rhyolite*	*TracDacite*	*TracDacite*	*Rhyolite*	*Rhyolite*	*Rhyolite*	*Rhyolite*	*Rhyolite*	*Dacite*	*TracDacite*	*Rhyolite*
wt %															
SiO_2	74.99	72.53	77.94	68.49	79.28	70.46	68.38	72.36	74.36	69.49	70.09	68.50	66.32	69.15	76.12
TiO_2	0.25	0.29	0.35	0.53	0.27	0.51	0.34	0.38	0.38	0.45	0.31	0.33	0.53	0.32	0.14
Al_2O_3	13.60	14.60	11.43	16.27	11.03	15.77	15.26	13.97	13.28	15.10	15.56	15.74	15.63	16.01	14.23
Fe_2O_3	1.73	2.24	1.43	2.98	1.60	0.78	2.35	1.65	1.65	2.56	2.39	2.60	4.24	2.47	0.77
MnO	0.04	0.07	0.03	0.06	0.01	0.01	0.05	0.03	0.03	0.04	0.03	0.09	0.03	0.05	0.06
MgO	0.12	0.32	0.12	0.80	0.10	0.52	0.34	0.18	0.17	0.36	0.21	0.40	2.04	0.22	0.13
CaO	1.34	1.20	0.70	1.55	1.30	2.10	1.23	1.84	0.75	1.91	1.07	1.34	4.01	1.21	0.81
Na_2O	3.01	3.48	3.57	2.79	3.04	3.66	4.88	3.96	4.20	4.41	4.12	4.12	2.86	4.72	2.51
K_2O	4.88	5.16	3.84	5.16	3.74	4.55	5.37	4.34	4.48	4.58	5.60	5.81	3.08	5.69	4.65
P_2O_5	0.07	0.07	0.07	0.11	0.11	0.22	0.03	0.08	0.07	0.08	0.04	0.08	0.22	0.04	0.03
L.O.I	1.09	0.76	0.80	0.96	1.27	0.84	0.54	0.48	0.55	0.74	0.78	0.77	0.77	0.61	0.58
Total (L.O.I. free)	100.03	99.96	99.48	98.74	100.48	98.57	98.23	98.78	99.38	98.98	99.42	99.01	98.97	99.88	99.45
ppm															
Sc	2.9	6.8	1.9	7.9	5.8	3.8	6.7	4.8	5.8	4.1	5.4	4.3	4.1	2.8	3.4
Cr	0.6	4.2	0.0	4.7	0.0	0.0	0.7	0.0	0.0	0.0	2.4	0.0	0.0	0.0	0.7
V	25.0	27.4	24.9	21.7	21.0	44.4	15.7	21.8	28.1	37.1	27.6	36.5	6.4	23.7	0.8
Ni	5.7	7.4	5.8	1.6	1.3	11.5	0.6	3.4	4.6	6.7	5.9	7.1	2.9	6.3	0.4
Co	2.7	2.8	0.0	1.4	0.4	1.8	3.0	0.0	2.2	2.9	2.9	4.7	1.3	2.6	-0.4
Cu	1.4	11.4	0.0	8.8	0.9	7.1	0.0	0.0	1.3	9.2	3.9	8.5	1.3	1.8	-1.2
Zn	29.9	33.5	19.9	55.9	19.6	22.6	33.4	20.6	20.0	47.4	35.4	36.7	16.7	31.6	36.2
Ga	17.0	15.1	14.1	17.9	10.4	18.0	13.9	17.6	15.8	15.7	15.9	16.8	14.1	20.7	14.4
Rb	134.5	182.6	138.4	241.7	123.3	147.5	255.9	187.0	155.9	202.1	205.7	214.6	222.7	203.7	138.2
Sr	115.3	324.9	191.4	319.2	298.9	801.4	372.5	223.2	202.2	280.1	321.4	347.0	270.1	340.5	112.8
Y	19.6	23.0	24.5	37.4	19.4	21.9	28.0	30.7	31.6	24.4	22.5	27.6	19.6	23.9	14.4
Zr	146.9	386.8	352.5	407.6	300.3	221.7	413.2	399.3	401.9	418.5	402.0	400.2	371.1	415.4	79.6
Nb	28.3	19.2	20.2	24.9	19.6	17.2	23.4	22.8	23.4	20.7	24.3	24.1	21.0	24.3	12.8
Ba	334.0	1414.3	1401.1	2083.6	1147.1	2531.4	1397.4	1732.4	1576.6	2345.4	1328.4	1404.6	1303.6	1371.4	1575.5
La	39.6	72.1	76.8	118.4	56.0	61.6	64.1	91.9	95.1	95.1	80.1	78.6	84.0	78.2	32.6
Ce	67.4	123.6	132.3	218.1	93.2	111.4	111.7	154.1	156.1	154.1	148.0	136.9	136.3	132.6	55.0
Nd	19.5	48.1	50.5	85.8	38.5	38.5	39.0	65.0	71.1	68.0	60.6	55.1	44.9	51.9	21.9
Pb	43.9	42.5	45.2	64.3	33.4	50.1	47.0	41.4	38.1	55.1	52.1	48.7	42.6	44.8	35.9
Th	43.1	37.9	39.1	46.3	33.0	36.2	45.8	42.5	43.8	46.0	44.2	46.4	46.7	45.4	22.2
U	8.4		5.9	5.4	5.6	6.3	6.5	6.4	6.2	8.4	7.2	8.1	4.9	8.0	4.4

Area	EGA	EGA	EGA	EGA	EGA	EGA	EGA	EGA	EGA	EGA	EGA	EGA	EGA	EGA	EGA
Locality	**Babakale**	**Babakale**	**Ezine**	**Ezine**	**Ezine**	**Ezine**	**Ezine**	**Ezine**	**Ezine**	**Ezine**	**Ezine**	**Ayvacik**	**Ayvacik**	**Ayvacik**	**Ayvacik**
Sample no	**EA286**	**EA117**	**EA6**	**EA9**	**EA11**	**EA35**	**EA36**	**EA66**	**EA67**	**EA33**	**EA70**	**EA245**	**EA231**	**EA20**	**EAR1**
Unit	*Koy. Ign.*	*Koy. Ign.*	*Kiz. Unit*	*Kiz. Unit*	*Kiz. Unit*	*Kiz. Unit*	*Ezn. Unit*	*Ezn. Unit*	*Bak. Unit*	*Ezn. Unit*	*Ezn. Unit*	*Ded. Unit*	*Bad. Unit*	*Ded. Unit*	*Ded. Unit*
Age	Early Mio.	Early Mio.	Early Mio.	Early Mio.	Early Mio.	Early Mio.	Early Mio.	Early Mio.	Early Mio.	Early Mio.	Early Mio.	Early Mio.	Early Mio.	Early Mio.	Early Mio.
Rock type	*Rhyolite*	*Rhyolite*	*TracDacite*	*TracDacite*	*TracDacite*	*TracDacite*	*TracDacite*	*TracDacite*	*TracAnd*	*TracDacite*	*TracDacite*	*TracDacite*	*TracAnd*	*TracDacite*	*TracDacite*
wt %															
SiO_2	79.93	70.27	62.13	62.45	62.68	62.97	63.00	64.56	59.96	61.47	65.16	61.39	58.24	61.45	63.73
TiO_2	0.24	0.32	0.57	0.60	0.44	0.58	0.63	0.60	0.75	0.64	0.63	0.73	0.93	0.67	0.57
Al_2O_3	9.86	16.38	15.69	16.20	16.25	15.67	15.82	15.45	16.38	16.37	15.65	15.22	17.45	17.09	16.44
Fe_2O_3	1.78	1.91	4.44	4.55	3.81	4.73	4.73	3.68	5.89	5.16	4.74	5.41	5.74	5.51	3.72
MnO	0.01	0.02	0.09	0.08	0.10	0.08	0.06	0.07	0.06	0.07	0.05	0.09	0.07	0.09	0.07
MgO	0.57	0.61	2.51	2.59	2.41	1.77	2.40	1.79	2.33	1.56	0.77	2.30	2.01	1.33	1.93
CaO	0.98	2.46	3.72	4.42	4.27	4.08	4.15	3.25	5.42	3.87	3.36	6.13	5.92	3.41	3.78
Na_2O	2.24	2.53	3.73	3.60	3.95	3.44	3.68	3.92	3.22	3.80	3.54	3.62	3.97	3.57	3.40
K_2O	3.81	4.97	5.45	4.38	4.72	4.92	4.83	5.03	4.77	4.88	4.53	4.64	4.63	5.05	4.94
P_2O_5	0.06	0.11	0.33	0.30	0.23	0.32	0.36	0.29	0.40	0.37	0.36	0.38	0.42	0.40	0.28
L.O.I	1.35	2.66	2.19	1.95	2.08	0.31	0.56	2.36	1.43	0.59	1.01	1.56	0.93	0.74	2.04
Total (L.O.I. free)	99.48	99.59	98.66	99.17	98.86	98.56	99.66	98.64	99.19	98.18	98.80	99.91	99.38	98.57	98.85
ppm															
Sc	3.7	4.4	12.1	11.5	9.1	8.6	12.6	7.6	18.8	12.4	9.8	14.5	16.6	10.9	9.7
Cr	0.0	7.0	55.2	40.8	9.9	10.3	13.9	14.4	47.6	14.7	14.3	36.6	47.3	12.8	15.1
V	23.6	44.8	95.0	95.5	80.2	88.1	103.6	87.7	190.9	109.0	86.5	150.0	172.2	74.6	93.6
Ni	4.5	11.2	21.5	23.4	8.6	11.6	13.7	14.6	21.9	11.6	8.1	21.1	15.3	13.2	16.4
Co	1.2	4.2	15.0	13.9	6.5	9.6	12.8	9.3	13.5	7.2	6.7	18.1	20.3	17.0	8.0
Cu	4.6	8.3	28.1	27.5	15.0	9.1	11.7	21.3	34.3	12.2	8.1	34.7	39.3	26.4	12.8
Zn	12.9	70.5	59.7	59.5	47.9	41.8	57.1	50.5	63.6	49.1	40.1	59.7	109.3	50.2	54.1
Ga	9.1	16.3	19.3	20.3	17.8	18.8	23.0	18.8	19.9	17.5	18.8	17.4	20.3	19.3	20.3
Rb	122.1	175.7	209.3	195.4	181.1	226.6	198.1	204.0	192.7	197.7	165.1	206.4	152.9	235.3	222.8
Sr	257.7	470.9	620.8	761.5	875.1	917.8	1086.4	757.7	1010.8	1069.9	969.9	1059.5	1161.8	951.0	798.1
Y	17.2	25.2	30.0	33.2	37.4	33.3	37.2	31.3	28.8	33.4	33.9	32.2	26.0	32.4	27.9
Zr	261.4	184.3	237.9	202.0	223.7	246.1	251.6	211.9	248.4	266.6	310.3	264.9	293.4	262.5	204.3
Nb	15.5	17.6	14.5	11.6	12.8	14.7	15.3	13.2	15.0	16.1	16.3	17.5	15.4	15.2	12.6
Ba	1348.9	1267.4	1382.7	1264.7	1247.7	1305.4	1609.8	1241.1	1594.1	1630.5	1380.1	1583.1	1677.9	1528.2	1288.8
La	51.5	51.6	87.2	76.0	75.4	95.2	120.2	76.7	91.3	119.9	91.8	73.3	83.7	94.1	74.5
Ce	87.9	82.8	150.9	112.6	108.1	151.2	187.3	132.6	142.3	189.5	153.9	160.8	158.5	188.0	123.5
Nd	37.2	30.0	66.3	50.7	52.2	67.3	86.0	59.9	68.0	81.6	72.5	64.6	73.1	74.4	55.6
Pb	33.6	29.6	46.6	58.9	65.5	67.0	62.2	73.0	59.0	63.5	43.3	66.8	68.5	65.3	73.5
Th	26.2	32.5	50.6	32.8	64.2	64.6	63.7	45.0	49.5	64.4	32.8	53.3	34.0	64.1	43.4
U	6.6											10.7	2.3		

Area	EGA	EGA	EGA	EGA	EGA	EGA	EGA	EGA	EGA	EGA	DAB	DAB	EGA	EGA	EGA
Locality	**Assos**	**Assos**	**Assos**	**Babakale**	**Babakale**	**Babakale**	**Babakale**	**Assos**	**Assos**	**Assos**	**Assos**	**Assos**	**Assos**	**Assos**	**Assos**
Sample no	**EA273**	**EA238**	**EA235**	**EA86**	**EA87**	**EA224**	**EA210**	**EA28**	**95EA211**	**EA241**	**95EA213**	**EA73**	**EA365**	**EA81**	**EA246**
Unit	*Bad. Unit*	*Bad. Unit*	*Bad. Unit*	*Bab. Unit*	*Bab. Unit*	*Bab. Unit*	*Bab. Unit*	*Bak. Unit*	*Bak. Unit*	*Bak. Unit*	*Bak. Unit*	*Cice. And.*	*Bak. Unit*	*Behr. And.*	*Behr. And.*
Age	Early Mio.	Early Mio.	Early Mio.	Early Mio.	Early Mio.	Early Mio.	Early Mio.	Early Mio.	Early Mio.	Early Mio.	Early Mio.	Early Mio.	Early Mio.	Early Mio.	Early Mio.
Rock type	*TracAnd*	*TracAnd*	*TracAnd*	*TracAnd*	*Dacite*	*Dacite*	*TracDacite*	*TracDacite*	*TracDacite*	*Rhyolite*	*Rhyolite*	*TracAnd*	*Dacite*	*TracAnd*	*TracAnd*
wt %															
SiO_2	60.38	60.88	61.39	60.31	67.01	67.20	65.77	62.21	61.88	70.24	69.15	54.45	65.77	62.36	62.47
TiO_2	0.73	0.96	0.90	0.68	0.59	0.48	0.45	0.81	0.70	0.51	0.56	0.80	0.45	0.59	0.69
Al_2O_3	17.57	18.58	15.50	15.10	15.25	15.42	15.86	16.79	17.30	16.25	17.72	17.37	15.63	17.11	16.09
Fe_2O_3	5.51	5.35	6.24	5.14	4.46	4.35	3.23	5.72	4.97	1.21	2.31	7.68	4.08	4.68	4.48
MnO	0.07	0.03	0.04	0.15	0.02	0.04	0.06	0.07	0.09	0.01	0.02	0.15	0.08	0.08	0.08
MgO	2.08	0.83	1.79	1.65	0.60	1.34	1.05	1.24	2.19	0.47	0.46	2.31	2.48	2.32	2.56
CaO	6.07	4.99	4.66	8.46	3.22	3.58	3.77	4.22	6.40	1.78	1.77	6.67	4.27	4.71	4.79
Na_2O	3.69	4.10	3.77	3.18	3.17	3.40	3.90	3.79	3.47	3.27	3.40	3.84	3.55	3.40	3.49
K_2O	4.05	3.73	4.45	4.18	4.25	3.68	4.54	4.50	3.11	4.50	4.20	4.66	2.71	3.72	3.38
P_2O_5	0.23	0.34	0.45	0.30	0.30	0.19	0.15	0.34	0.24	0.23	0.25	0.64	0.24	0.21	0.24
L.O.I	1.44	1.37	1.85	5.47	2.77	0.77	1.79	0.69	0.56	1.24	1.93	1.02	3.25	2.23	1.45
Total (L.O.I. free)	100.38	99.78	99.19	99.15	98.87	99.67	98.79	99.69	100.35	98.47	99.83	98.58	99.26	99.18	98.26
ppm															
Sc	10.1	10.4	15.7	18.9	14.5	13.0	6.1	9.6	14.7	3.4	5.4	17.2	9.3	13.6	11.2
Cr	16.9	2.4	49.2	30.6	21.1	33.3	7.0	31.5	11.1	0.0	12.6	2.8	140.7	9.4	11.4
V	106.7	99.5	168.6	146.9	97.1	161.1	46.8	115.5	117.0	73.9	71.6	181.4	52.9	92.8	112.8
Ni	12.8	7.9	19.1	12.8	20.6	18.9	3.5	22.7	12.2	6.4	-1.5	13.8	73.9	12.9	11.7
Co	18.2	9.1	16.3	10.1	10.1	19.4	3.8	20.2	12.6	2.1	3.9	15.7	11.4	9.1	13.4
Cu	13.9	32.0	33.9	20.7	42.4	28.2	6.0	30.0	22.1	7.8	6.5	12.9	15.1	31.6	36.2
Zn	62.5	58.0	58.7	35.7	27.5	72.3	46.0	62.1	55.2	11.1	26.4	92.1	53.4	52.3	46.1
Ga	18.5	17.5	15.5	17.8	16.2	18.6	16.2	21.1	14.5	15.5	14.9	20.1	21.5	15.7	14.8
Rb	167.9	180.2	183.7	145.4	163.0	222.3	225.7	197.6	120.4	197.8	194.2	145.1	134.5	130.5	136.5
Sr	757.8	953.4	1204.4	792.1	726.3	1204.1	555.3	894.2	891.3	676.8	704.3	1522.1	845.9	783.0	772.3
Y	23.8	28.1	31.9	19.9	29.7	35.0	35.1	31.8	26.6	32.3	34.3	17.0	31.5	25.9	20.5
Zr	201.1	328.3	308.9	169.5	194.9	392.1	372.8	242.2	193.1	251.1	261.9	348.6	148.7	178.6	192.3
Nb	11.3	17.2	17.2	12.4	12.1	21.9	22.1	15.1	11.2	20.2	17.4	17.1	12.4	10.2	12.5
Ba	1278.8	1492.5	1769.6	1560.4	1250.1	1871.0	1471.8	1393.7	1768.8	1466.5	3515.7	1644.7	1493.9	1466.1	1567.6
La	43.5	75.3	84.6	56.9	63.2	96.5	70.2	90.9	55.4	66.5	79.3	109.8	46.2	56.8	54.8
Ce	94.9	140.3	186.7	99.1	110.4	197.9	133.9	149.1	104.4	128.3	132.4	179.9	93.0	87.7	112.5
Nd	28.4	56.5	79.5	43.0	44.7	84.9	51.1	66.5	38.5	49.2	60.5	94.7	33.0	35.8	41.1
Pb	40.1	56.3	58.3	57.5	46.4	63.4	50.7	64.3	52.0	49.9	54.5	55.5	41.7	46.8	48.5
Th	16.1	35.6	40.8	29.4	30.1	62.8	37.4	49.0	25.0	38.2	45.2	29.7	20.7	27.0	28.0
U	4.5	4.7	8.2			11.3	5.3		4.4	6.7	4.9		6.1		4.2

Area	EGA	EGA	EGA	DAB	DAB	EGA	EGA	EGA	EGA	EGA	EGA	EGA	EGA	EGA	EGA
Locality	Assos	Assos	Assos	Assos	Assos	Assos	Assos	Assos	Suruce	Suruce	Suruce	Suruce	Suruce	Suruce	Suruce
Sample no	EA37	EA30	EA52	EA275	EA278	EA57	EA59	EA68	EA79	EA217	EA243	EA248	EA207	EA212	EA236
Unit	*Behr. And.*	*Behr. And.*	*Behr. And.*	*Behr. And.*	*Behr. And.*	*Behr. And.*	*Behr. And.*	*Behr. And.*	*Cice. And.*	*Cice. And.*	*Cice. And.*	*Cice. And.*	*Sur. And*	*Sur. And*	*Sur. And*
Age	Early Mio.	Early Mio.	Early Mio.	Early Mio.	Early Mio.	Early Mio.	Early Mio.	Early Mio.	Early Mio.	Early Mio.	Early Mio.	Early Mio.	Early Mio.	Early Mio.	Early Mio.
Rock type	*TracAnd*	*TracAnd*	*Dacite*	*TracAnd*	*TracAnd*	*TracAnd.*	*TracAnd.*	*TracAnd*	*TracAnd*	*Andesite*	*TraDacite*	*TracAnd*	*TracAnd*	*TracAnd*	*TracAnd*
wt %															
SiO_2	61.67	58.20	62.93	57.86	59.40	61.10	59.75	56.48	59.88	59.11	63.04	57.19	56.90	61.70	59.53
TiO_2	0.58	1.05	0.69	0.76	0.70	0.72	0.72	0.82	0.93	0.64	0.79	1.14	1.04	0.95	0.91
Al_2O_3	16.68	17.28	17.61	16.98	17.10	16.17	15.96	15.95	18.22	16.98	18.01	19.71	19.43	19.51	19.67
Fe_2O_3	4.74	6.26	4.03	6.90	6.90	5.68	6.09	5.22	5.84	5.93	3.58	6.09	7.02	2.24	5.17
MnO	0.08	0.08	0.06	0.16	0.15	0.10	0.11	0.09	0.02	0.09	0.05	0.04	0.06	0.01	0.02
MgO	2.39	2.43	1.98	3.00	2.87	2.32	3.21	2.82	1.43	2.95	0.45	0.88	1.34	1.61	0.63
CaO	4.74	6.86	4.63	6.88	6.33	5.28	5.60	8.62	4.84	6.41	4.07	5.34	6.03	5.26	5.05
Na_2O	3.44	3.56	3.39	3.33	3.11	3.47	3.50	3.42	3.84	3.16	4.24	4.30	4.26	3.64	4.36
K_2O	3.53	3.10	3.49	3.01	3.27	4.75	4.40	5.27	3.82	2.79	5.17	3.79	3.41	3.31	3.88
P_2O_5	0.21	0.31	0.23	0.25	0.22	0.37	0.35	0.50	0.34	0.35	0.23	0.36	0.39	0.43	0.36
L.O.I	1.34	1.15	2.31	1.33	1.49	0.84	0.58	2.98	1.20	1.27	0.54	0.86	1.45	1.89	0.97
Total (L.O.I. free)	98.06	99.12	99.03	99.13	100.05	99.96	99.69	99.19	99.15	98.41	99.63	98.84	99.87	98.65	99.59
ppm															
Sc	12.3	18.8	10.8	12.0	10.6	14.2	12.9	20.9	12.6	15.0	7.7	10.1	16.5	7.3	8.2
Cr	9.5	116.0	25.6	13.4	14.0	30.9	28.5	91.2	22.8	53.8	0.0	0.0	79.7	1.9	0.0
V	100.1	157.7	80.6	158.2	138.9	152.5	99.7	134.6	126.8	114.3	69.0	130.8	197.8	155.7	113.3
Ni	14.0	51.5	14.7	4.9	4.3	21.5	19.8	77.8	19.7	27.8	10.0	11.9	56.9	13.1	12.4
Co	9.6	17.1	9.1	18.2	16.3	12.8	12.9	17.9	8.5	16.4	6.2	11.7	15.4	7.5	10.1
Cu	29.4	48.0	11.4	23.1	23.2	45.6	35.9	100.0	35.1	34.1	26.5	29.1	35.3	49.4	26.5
Zn	57.2	73.8	86.0	83.9	77.1	63.5	67.6	78.2	61.7	62.0	37.6	59.2	55.8	66.7	51.8
Ga	18.5	22.7	18.9	17.9	16.9	19.9	20.7	15.9	19.7	17.2	20.5	18.7	21.5	20.9	19.0
Rb	128.0	137.7	198.7	130.9	123.2	189.7	159.9	206.8	163.6	118.7	194.5	178.6	157.2	134.0	184.9
Sr	770.4	794.9	751.5	598.9	567.4	992.2	980.9	812.4	1034.9	675.8	606.4	890.2	934.2	1099.7	968.3
Y	27.3	23.7	23.3	23.4	28.7	31.3	29.3	23.0	21.1	23.2	30.4	28.7	21.7	26.3	26.9
Zr	187.4	336.8	237.1	200.8	196.8	247.9	243.6	345.4	256.9	214.0	375.4	310.3	285.7	225.6	306.3
Nb	9.7	16.8	12.0	13.5	13.7	17.4	16.5	18.7	13.9	10.5	20.9	17.9	15.1	15.7	17.5
Ba	1437.5	1315.7	1408.1	860.7	839.5	1643.8	1702.0	1551.7	1620.9	1557.4	2063.4	1481.8	1289.3	1731.1	1602.6
La	60.7	73.4	55.0	43.3	42.1	88.7	85.2	89.6	51.7	49.2	94.1	72.8	62.5	69.8	70.3
Ce	95.6	119.0	92.3	80.9	79.7	155.9	150.1	161.6	102.2	82.9	168.9	132.3	130.5	124.9	143.8
Nd	44.4	44.5	42.1	36.5	36.1	66.4	65.2	78.5	44.3	36.4	64.3	47.3	46.2	55.2	54.2
Pb	45.4	52.3	49.3	24.1	25.5	71.2	59.2	48.8	53.0	25.4	57.4	55.8	55.6	47.8	58.6
Th	27.3	31.3	16.8	13.4	19.5	48.4	47.2	51.7	24.2	11.4	43.5	32.9	33.1	26.1	34.1
U				5.6	5.7					6.3	5.7	5.5	2.5	5.8	7.7

ICP-MS DATA SET

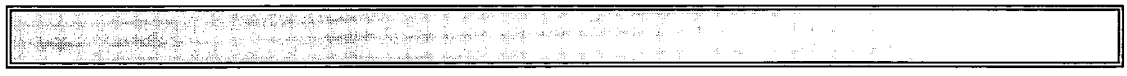

Area	EGA	EGA	EGA	EGA	EGA	EGA	EGA	EGA	EGA	DAB	DAB	DAB	DAB	DAB	DAB	DAB
Locality	**Ayvacik**	**Ayvacik**	**Ayvacik**	**Akkoy**	**Ezine**	**Ezine**	**Tastepe**	**Tastepe**	**Tastepe**	**Foca**	**Foca**	**Foca**	**Dikili**	**Dikili**	**Ayvalik**	**Dikili**
Sample no	**EA270**	**EA267**	**EA82B**	**EA260**	**EA415**	**EA262**	**EA254**	**EA249**	**EA253**	**EA348**	**EA407**	**95EA385**	**EA350**	**EA380**	**EA300**	**94EA109**
Unit	*Ayv. Vol.*	*Ayv. Vol.*	*Ayv. Vol.*	*Ezn. Vol.*	*Ezn. Vol.*	*Ezn. Vol.*	*Tas. Vol.*	*Tas. Vol.*	*Tas. Vol.*	*Foc. Dyke*	*Foc. Dyke*	*Foc. Dyke*	*Neb. Vol.*	*Neb. Vol.*	*Neb. Vol.*	*Neb. Vol.*
Age	Late Mio.	Late Mio.	Late Mio.	Late Mio.	Late Mio.	Late Mio.	Late Mio.	Late Mio.	Late Mio.	Mid. Mio.	Mid. Mio.	Mid. Mio.	Mid. Mio.	Mid. Mio.	Mid. Mio.	Mid. Mio.
Rock type	*Basanite*	*Basanite*	*Basanite*	*Basanite*	*Basalt*	*Hawaiite*	*Basanite*	*Hawaiite*	*Hawaiite*	*BasAnd*	*BasTraAnd*	*TraBas*	*BaTraAnd*	*Basalt*	*TraBas*	*BaTraAnd*
wt %																
SiO_2	41.81	42.61	43.04	42.75	46.07	46.99	45.69	49.97	50.52	54.40	56.64	50.26	51.24	50.35	49.86	51.51
TiO_2	3.14	3.15	3.14	3.09	2.83	2.82	2.78	2.58	2.59	0.73	1.03	1.05	1.22	0.93	0.96	1.05
Al_2O_3	12.76	13.04	12.97	12.87	13.21	13.01	13.29	14.30	14.62	15.36	17.16	19.23	11.69	15.37	14.74	17.63
Fe_2O_3	14.38	14.24	14.11	14.30	12.04	12.22	12.13	10.69	10.63	7.36	7.43	8.09	7.51	8.27	8.18	8.20
MnO	0.22	0.22	0.22	0.21	0.16	0.18	0.17	0.14	0.13	0.12	0.08	0.15	0.12	0.14	0.14	0.15
MgO	7.74	7.98	8.05	8.19	9.25	8.38	9.62	6.90	6.89	9.06	2.04	4.83	12.62	9.81	9.30	5.32
CaO	11.03	11.06	10.97	10.91	10.91	10.76	9.96	8.74	8.90	8.25	8.83	9.52	7.58	9.55	9.94	8.36
Na_2O	5.33	4.62	4.74	4.33	3.14	3.49	4.25	3.51	3.57	2.78	3.37	3.06	1.70	2.22	2.67	3.23
K_2O	1.52	1.97	1.43	1.42	1.51	1.67	1.37	1.63	1.63	1.89	2.76	2.95	4.72	2.18	2.86	2.80
P_2O_5	1.25	1.29	1.26	0.99	0.76	0.74	0.79	0.49	0.49	0.24	0.32	0.47	0.67	0.32	0.96	0.49
L.O.I	1.27	2.44	2.72	1.57	2.83	1.86	1.27	1.46	1.62	1.27	1.14	2.38	2.54	1.82	1.57	1.78
Total (L.O.I. free)	99.19	100.18	99.94	99.07	99.88	100.25	100.05	98.95	99.97	100.19	99.66	99.61	99.06	99.14	99.60	98.74
ppm																
Rb	21.3	23.2	33.5	17.3	24.1	21.7	16.5	17.9	18.2	63.3	98.6	155.7	173.8	63.1	62.4	95.5
Sr	1077.4	1131.1	1073.1	908.3	728.6	788.6	1015.2	505.9	487.3	714.6	637.8	526.0	713.4	1006.5	639.4	734.2
Y	35.4	37.0	35.1	31.5	25.8	27.3	27.7	21.3	22.2	21.5	23.8	19.7	21.7	22.0	23.5	27.7
Zr	364.8	376.8	364.7	314.1	246.5	264.9	267.4	185.3	193.6	127.3	191.5	199.2	408.5	119.4	142.6	186.0
Nb	101.2	104.8	100.3	83.9	62.5	59.6	69.2	31.9	33.8	7.5	17.3	14.1	30.0	11.1	10.1	12.8
Cs	0.8	0.7	0.9	0.5	1.2	0.3	3.6	1.7	2.7	1.8	4.7	6.7	6.2	4.0	4.0	7.1
Ba	682.5	645.2	652.2	511.5	418.6	469.5	415.8	245.0	230.0	1164.1	919.8	1179.9	917.9	1436.7	1012.0	1303.2
La	70.23	71.97	67.82	54.65	37.26	36.92	38.68	20.00	20.86	31.92	46.44	41.23	43.75	42.28	31.05	39.52
Ce	135.14	138.25	130.06	107.47	74.02	73.49	79.27	42.86	44.54	62.67	84.08	77.13	107.20	81.30	61.01	78.13
Pr	15.58	16.12	15.16	12.72	8.79	8.98	9.34	5.57	5.73	7.09	9.11	7.64	13.99	9.32	6.91	8.77
Nd	65.62	67.91	64.36	54.85	39.10	39.79	39.59	25.36	26.77	28.84	35.31	28.67	60.45	37.73	28.52	36.04
Sm	12.40	12.46	12.08	10.51	8.08	8.13	8.29	6.01	6.05	5.35	5.76	4.64	9.57	6.49	5.26	6.66
Eu	3.73	3.72	3.62	3.20	2.52	2.56	2.57	1.94	1.99	1.39	1.54	1.20	1.97	1.76	1.45	1.81
Gd	10.17	10.00	9.91	8.89	7.31	7.08	7.39	5.85	5.63	4.44	4.56	3.64	6.04	4.98	4.35	5.67
Tb	1.47	1.47	1.43	1.30	1.06	1.07	1.09	0.85	0.85	0.67	0.70	0.58	0.83	0.74	0.69	0.85
Dy	7.33	7.44	7.17	6.46	5.33	5.52	5.46	4.35	4.53	3.69	3.90	3.20	4.07	3.96	3.99	4.55
Ho	1.27	1.30	1.26	1.12	0.93	0.98	0.97	0.77	0.79	0.74	0.79	0.64	0.73	0.74	0.78	0.91
Er	2.94	3.01	2.92	2.62	2.16	2.21	2.23	1.78	1.83	1.98	2.17	1.69	1.77	1.91	2.03	2.43
Tm	0.45	0.46	0.45	0.40	0.33	0.35	0.34	0.28	0.28	0.35	0.39	0.30	0.30	0.32	0.36	0.40
Yb	2.37	2.33	2.34	2.07	1.71	1.79	1.83	1.47	1.47	1.97	2.26	1.74	1.65	1.76	1.99	2.38
Lu	0.34	0.34	0.33	0.29	0.25	0.26	0.26	0.21	0.22	0.31	0.36	0.27	0.26	0.28	0.32	0.37
Hf	7.91	7.79	7.73	6.99	5.52	5.57	5.88	4.34	4.40	3.22	4.73	2.17	10.62	3.02	3.42	4.60
Ta	6.68	6.56	6.57	5.65	4.04	3.79	4.46	2.11	2.16	0.53	1.29	1.28	1.87	0.65	0.66	0.81
Th	9.10	9.26	9.17	7.22	5.21	4.77	5.74	2.63	2.66	12.16	18.57	21.57	29.30	14.71	12.17	15.10
U	2.91	3.35	2.96	2.32	1.13	1.61	1.90	0.70	0.55	2.69	5.35	6.10	7.01	2.73	2.51	3.47

Area	DAB	DAB	DAB	DAB	DAB	DAB	DAB	DAB	DAB	DAB	DAB	DAB	DAB	DAB	DAB	DAB
Locality	**Dikili**	**Ayvalik**	**Dikili**	**Ayvalik**	**Ayvalik**	**Ayvalik**	**Y.Sakran**	**Y.Sakran**	**Bergama**	**Bergama**	**Bergama**	**Bergama**	**Y.Sakran**	**Ayvalik**	**Ayvalik**	**Dikili**
Sample no	**EA296**	**EA143**	**EA130**	**EA292**	**EA399**	**EA101**	**EA113**	**EA346**	**EA314**	**EA334**	**EA316**	**EA367**	**EA147**	**EA103**	**EA155**	**EA335**
Unit	*Neb. Vol.*	*Neb. Vol.*	*Neb. Vol.*	*Neb. Vol.*	*Neb. Vol.*	*Oda. Dyke*	*Egr. And*	*Egr. And*	*Egr. And*	*Egr. And*	*Klg. And*	*Klg. And*	*Akc. Unit*	*Ulb. Unit*	*Bal. Unit*	*Mt.Sey. U.*
Age	Mid. Mio.	Mid. Mio.	Mid. Mio.	Mid. Mio.	Mid. Mio.	Mid. Mio.	Mid. Mio.	Mid. Mio.	Mid. Mio.	Mid. Mio.	Early Mio.	Early Mio.	Mid. Mio.	Early Mio.	Early Mio.	Early Mio.
Rock type	*TracAnd*	*BasAnd*	*BaTraAnd*	*BaTraAnd*	*TraBas*	*BaTraAnd*	*Andesite*	*Andesite*	*TracAnd*	*Andesite*	*Dacite*	*Dacite*	*Dacite*	*TracAnd*	*TracAnd*	*Andesite*
wt %																
SiO_2	57.20	52.69	52.79	55.58	49.82	56.32	60.62	60.41	60.32	59.64	62.33	64.07	65.08	60.46	59.80	57.73
TiO_2	0.80	0.85	0.95	0.89	1.19	0.90	0.72	0.64	0.59	0.57	0.56	0.44	0.54	0.59	0.73	0.82
Al_2O_3	17.56	15.68	17.86	16.89	17.30	17.26	16.41	15.88	17.17	15.95	15.05	17.33	16.02	16.89	16.32	17.15
Fe_2O_3	6.02	7.44	8.30	6.58	8.50	6.27	6.76	5.80	5.36	5.95	5.74	3.83	4.53	5.04	7.08	6.69
MnO	0.06	0.13	0.23	0.12	0.16	0.10	0.12	0.10	0.10	0.12	0.09	0.07	0.06	0.15	0.16	0.14
MgO	4.16	7.53	4.89	4.64	5.94	3.96	2.53	4.29	4.66	5.08	3.83	3.12	2.38	2.63	2.57	3.05
CaO	7.13	10.01	6.08	7.61	9.67	8.06	6.62	6.29	5.87	7.30	5.37	4.28	5.45	5.26	5.66	7.80
Na_2O	3.47	2.58	3.57	3.17	4.33	3.23	3.42	2.88	3.69	3.28	3.20	3.35	3.32	3.63	3.14	2.95
K_2O	2.96	2.33	3.98	3.13	1.85	3.16	2.47	2.57	2.67	2.51	2.80	3.23	1.96	3.66	3.54	3.09
P_2O_5	0.30	0.26	0.37	0.39	0.46	0.40	0.21	0.16	0.14	0.15	0.21	0.23	0.22	0.25	0.25	0.40
L.O.I	0.94	1.82	2.55	1.54	2.93	2.22	0.88	1.33	0.99	1.70	1.28	2.42	1.48	1.99	2.82	3.18
Total (L.O.I. free)	99.66	99.50	99.02	99.00	99.22	99.66	99.88	99.02	100.57	100.56	99.19	99.96	99.56	98.56	99.24	99.82
ppm																
Rb	117.0	81.5	105.3	93.9	62.8	103.9	74.4	83.6	108.4	84.1	109.8	123.6	88.6	138.9	125.4	79.4
Sr	632.6	627.8	725.1	823.1	797.0	907.8	675.9	576.5	441.1	611.8	610.4	790.4	849.8	579.6	773.3	693.5
Y	24.3	23.6	23.6	25.1	27.4	25.1	28.7	22.5	21.3	22.4	22.0	21.7	20.6	20.5	21.0	22.9
Zr	227.3	139.8	189.5	249.3	167.4	252.3	143.4	140.8	148.2	115.3	128.1	154.7	143.3	181.5	155.9	115.3
Nb	19.4	9.4	15.7	20.1	15.8	20.7	6.7	8.1	9.7	7.7	9.5	10.9	8.7	12.4	8.8	10.2
Cs	4.0	5.3	5.9	6.2	6.1	5.8	6.3	2.8	4.5	1.7	4.4	4.2	5.1	4.8	4.4	3.0
Ba	1208.1	1095.7	1830.5	1534.0	844.5	1571.3	1193.1	1195.0	748.3	1045.6	1245.2	1507.0	1044.1	2022.7	1483.1	2192.9
La	44.31	34.75	50.73	50.19	59.89	53.04	37.54	31.02	29.33	34.05	45.60	53.73	42.74	45.30	44.69	45.34
Ce	81.07	68.03	93.76	95.28	118.77	101.62	74.01	59.47	57.14	64.62	83.81	103.57	85.23	83.80	88.25	88.13
Pr	8.93	7.55	10.05	10.49	13.16	11.10	8.05	6.43	6.28	6.90	8.84	11.09	9.36	8.54	9.61	9.36
Nd	34.59	30.63	39.02	41.08	52.40	42.81	31.36	25.30	24.31	27.02	33.33	40.98	35.96	31.29	35.65	34.26
Sm	5.83	5.79	6.74	6.95	9.43	7.24	5.98	4.75	4.51	4.96	5.62	6.70	6.19	5.13	6.14	6.03
Eu	1.47	1.45	1.86	1.70	2.54	1.76	1.67	1.22	1.08	1.15	1.35	1.51	1.36	1.46	1.45	1.61
Gd	4.69	4.86	5.65	5.27	7.11	5.52	5.33	4.15	3.70	4.27	4.44	4.85	4.65	4.05	4.59	4.64
Tb	0.72	0.71	0.79	0.81	1.01	0.81	0.81	0.65	0.62	0.65	0.67	0.72	0.67	0.60	0.66	0.71
Dy	3.93	3.87	4.14	4.32	5.06	4.37	4.59	3.65	3.53	3.63	3.65	3.71	3.57	3.37	3.53	3.88
Ho	0.79	0.79	0.80	0.84	0.93	0.85	0.94	0.74	0.72	0.73	0.72	0.72	0.69	0.67	0.68	0.76
Er	2.11	2.10	2.09	2.22	2.31	2.25	2.53	2.01	1.96	2.00	1.94	1.85	1.77	1.83	1.76	2.03
Tm	0.36	0.35	0.36	0.39	0.38	0.39	0.44	0.34	0.35	0.34	0.34	0.31	0.30	0.32	0.30	0.36
Yb	2.17	2.11	2.04	2.20	2.13	2.23	2.63	2.08	2.05	2.06	2.01	1.82	1.74	1.93	1.77	2.09
Lu	0.35	0.33	0.32	0.34	0.33	0.36	0.42	0.32	0.33	0.32	0.32	0.29	0.27	0.32	0.28	0.33
Hf	5.58	3.48	1.25	6.25	3.50	6.27	2.93	3.64	4.00	2.90	2.44	3.80	2.65	3.70	2.57	2.95
Ta	1.41	0.64	1.10	1.37	0.98	1.37	0.57	0.59	0.89	0.69	0.92	0.89	0.76	1.00	0.78	0.90
Th	34.27	14.02	16.58	29.38	10.10	30.56	16.01	11.48	14.47	14.64	21.31	23.61	18.16	23.68	21.92	20.42
U	8.15	2.98	3.11	6.75	2.68	6.97	5.05	2.82	4.20	3.72	5.00	5.61	4.39	5.19	4.76	4.94

Area	DAB	DAB	DAB	EGA	EGA	EGA	EGA	EGA	EGA	EGA	DAB	EGA	EGA	EGA	DAB	EGA
Locality	**Dikili**	**Dikili**	**Dikili**	**Assos**	**Babakale**	**Babakale**	**Babakale**	**Assos**	**Babakale**	**Babakale**	**Babakale**	**Gulpinar**	**Gulpinar**	**Babakale**	**Assos**	**Ezine**
Sample no	**EA359**	**EA360**	**EA326**	**EA413**	**EA53**	**EA45**	**EA55**	**EA418**	**EA286**	**EA281**	**95EA307**	**EA77**	**EA33A**	**EA202**	**EA215**	**EA6**
Unit	*Mt.Sey. U.*	*Mt.Sey. U.*	*Mt.Sey. U.*	*Kov. Dyke*	*Kov. Dyke*	*Kov. Dyke*	*Kov. Dyke*	*Kov. Dyke*	*Koy. Ign.*	*Koy. Ign.*	*Koy. Ign.*	*Bal. Ign.*	*Bal. Ign.*	*Berg. Ign*	*Berg. Ign*	*Kiz. Unit*
Age	Early Mio.	Early Mio.	Early Mio.	Early Mio.	Early Mio.	Early Mio.	Early Mio.	Early Mio.	Early Mio.	Early Mio.	Early Mio.	Early Mio.	Early Mio.	Early Mio.	Early Mio.	Early Mio.
Rock type	*TraDacite*	*Dacite*	*TraDacite*	*TracAnd*	*TracAnd*	*TracAnd*	*TracAnd.*	*BaTraAnd*	*Rhyolite*	*Rhyolite*	*Rhyolite*	*Rhyolite*	*Rhyolite*	*Rhyolite*	*TracDacite*	*TracDacite*
wt %																
SiO_2	66.04	64.38	65.46	56.29	58.95	57.73	58.09	56.24	79.93	68.50	76.12	73.43	69.80	69.49	70.46	62.13
TiO_2	0.52	0.68	0.53	1.07	0.83	0.73	0.83	0.87	0.24	0.33	0.14	0.38	0.46	0.45	0.51	0.57
Al_2O_3	16.42	16.62	14.16	19.30	19.75	16.71	19.25	18.45	9.86	15.74	14.23	14.06	15.40	15.10	15.77	15.69
Fe_2O_3	3.30	4.46	3.89	6.20	4.74	5.74	5.05	6.40	1.78	2.60	0.77	1.62	2.82	2.56	0.78	4.44
MnO	0.08	0.07	0.06	0.08	0.07	0.09	0.08	0.09	0.01	0.09	0.06	0.02	0.05	0.04	0.01	0.09
MgO	1.86	2.10	2.47	2.06	1.15	3.75	1.19	3.83	0.57	0.40	0.13	0.15	0.37	0.36	0.52	2.51
CaO	3.84	4.06	3.98	6.53	6.31	6.78	6.96	7.90	0.98	1.34	0.81	0.83	1.32	1.91	2.10	3.72
Na_2O	3.05	2.98	3.12	3.96	3.98	3.43	4.04	3.87	2.24	4.12	2.51	4.09	4.18	4.41	3.66	3.73
K_2O	4.38	4.02	3.79	3.18	3.42	3.07	3.31	1.84	3.81	5.81	4.65	5.04	5.09	4.58	4.55	5.45
P_2O_5	0.26	0.39	0.22	0.37	0.35	0.25	0.33	0.29	0.06	0.08	0.03	0.08	0.11	0.08	0.22	0.33
L.O.I	2.28	3.32	1.51	1.02	1.49	1.58	2.64	1.26	1.35	0.77	0.58	0.70	0.63	0.74	0.84	2.19
Total (L.O.I. free)	99.75	99.77	97.68	99.04	99.55	98.28	99.13	99.78	99.48	99.01	99.45	99.70	99.60	98.98	98.57	98.66
ppm																
Rb	125.5	162.6	138.7	120.3	122.9	107.5	119.3	68.3	123.4	214.7	138.5	200.8	193.0	202.1	205.3	209.7
Sr	458.5	574.1	537.4	1002.2	1037.2	826.6	1018.2	944.8	226.2	341.4	112.0	199.0	309.2	246.7	790.0	644.7
Y	42.3	27.2	22.4	26.8	20.9	21.5	21.1	22.0	17.0	26.5	20.5	27.6	28.2	24.9	18.7	27.1
Zr	69.9	179.9	66.0	311.5	248.0	204.1	240.6	184.7	261.4	400.2	79.6	394.7	398.7	418.5	221.7	134.4
Nb	14.0	13.6	11.3	15.0	11.9	10.3	11.1	8.5	12.7	19.8	11.3	17.8	17.3	18.7	15.6	16.6
Cs	6.8	5.8	6.3	5.8	3.7	3.7	7.0	6.4	5.5	5.4	4.1	4.8	5.5	6.7	6.6	3.3
Ba	1195.9	1848.6	1308.5	1416.2	1595.5	1309.4	1553.5	1358.2	1342.1	1405.9	1581.2	1848.7	1868.6	2507.4	2616.3	1336.3
La	45.21	39.55	50.29	70.61	66.85	60.14	68.36	52.15	49.19	69.17	36.02	87.11	94.60	86.92	71.12	84.92
Ce	77.37	71.19	90.32	134.86	127.17	113.74	127.43	100.19	93.14	134.73	71.57	166.25	173.69	143.65	127.72	159.31
Pr	9.44	7.43	9.69	14.76	13.84	12.26	13.83	11.14	9.99	14.26	7.35	17.40	18.55	17.20	13.47	17.70
Nd	39.61	28.21	36.05	55.84	52.80	46.85	52.75	43.49	35.29	50.20	25.12	59.78	66.90	59.16	49.88	66.74
Sm	7.22	4.72	5.83	8.53	7.89	7.36	7.90	7.06	5.36	7.62	4.30	8.74	9.75	8.68	7.90	10.67
Eu	1.75	1.35	1.33	1.91	1.94	1.69	1.88	1.77	1.18	1.61	1.00	1.57	1.74	1.89	2.16	2.25
Gd	6.48	4.08	4.26	6.09	5.24	5.00	5.22	5.11	3.50	5.18	3.25	5.54	5.99	5.55	5.27	7.24
Tb	1.06	0.65	0.67	0.88	0.72	0.72	0.72	0.73	0.52	0.79	0.56	0.84	0.93	0.82	0.71	1.00
Dy	6.10	3.73	3.75	4.68	3.69	3.77	3.66	3.86	2.76	4.19	3.22	4.56	4.89	4.26	3.48	4.83
Ho	1.25	0.81	0.72	0.91	0.69	0.74	0.70	0.75	0.54	0.82	0.65	0.88	0.94	0.83	0.61	0.84
Er	3.25	2.26	1.88	2.37	1.79	1.94	1.80	1.95	1.46	2.23	1.79	2.33	2.54	2.18	1.48	2.07
Tm	0.55	0.40	0.34	0.40	0.30	0.34	0.31	0.33	0.27	0.39	0.32	0.40	0.46	0.38	0.24	0.34
Yb	3.08	2.25	1.93	2.23	1.78	1.96	1.77	1.91	1.63	2.36	1.94	2.33	2.63	2.30	1.37	1.94
Lu	0.49	0.36	0.31	0.36	0.27	0.31	0.27	0.30	0.27	0.38	0.31	0.36	0.42	0.36	0.21	0.30
Hf	2.18	3.01	2.24	7.65	6.22	5.41	6.01	4.75	5.81	8.38	2.79	5.81	8.50	6.56	5.55	4.27
Ta	1.27	1.16	1.04	0.97	0.76	0.72	0.73	0.56	0.92	1.38	0.90	1.18	1.19	1.23	1.32	1.43
Th	22.28	21.48	25.59	38.14	29.32	26.22	28.20	17.95	30.70	44.80	21.89	46.37	46.29	48.00	44.73	54.66
U	5.10	5.83	5.26	6.79	5.49	5.17	5.42	3.48	6.22	8.86	4.89	6.61	8.30	7.98	6.81	11.11

Area	EGA	EGA	EGA	DAB	EGA	EGA	EGA	EGA
Locality	Ezine	Assos	Assos	Assos	Ezine	Suruce	Assos	Bergas
Sample no	EA11	EA68	EA37	EA278	EA67	EA212	SAS1	SAS2
Unit	*Kiz. Unit*	*Behr. And.*	*Behr. And.*	*Behr. And.*	*Bak. Unit*	*Sur. And*	*Met. Base.*	*Met. Base.*
Age	Early Mio.	Early Mio.	Early Mio.	Early Mio.	Early Mio.	Early Mio.		
Rock type	*TracDacite*	*TracAnd*	*TracAnd*	*TracAnd*	*TracAnd*	*TracAnd*	*Met. Sed.*	*Met. Sed.*
wt %								
SiO_2	62.68	56.48	61.67	59.40	59.96	61.70		
TiO_2	0.44	0.82	0.58	0.70	0.75	0.95		
Al_2O_3	16.25	15.95	16.68	17.10	16.38	19.51		
Fe_2O_3	3.81	5.22	4.74	6.90	5.89	2.24		
MnO	0.10	0.09	0.08	0.15	0.06	0.01		
MgO	2.41	2.82	2.39	2.87	2.33	1.61		
CaO	4.27	8.62	4.74	6.33	5.42	5.26		
Na_2O	3.95	3.42	3.44	3.11	3.22	3.64		
K_2O	4.72	5.27	3.53	3.27	4.77	3.31		
P_2O_5	0.23	0.50	0.21	0.22	0.40	0.43		
L.O.I	2.08	2.98	1.34	1.49	1.43	1.89		
Total (L.O.I. free)	98.86	99.19	98.06	100.05	99.19	98.65		
ppm								
Rb	177.4	234.5	132.9	123.0	189.7	117.3	93.7	109.1
Sr	819.3	812.2	760.9	574.0	960.4	997.0	341.4	112.0
Y	37.7	26.6	20.4	28.8	29.6	21.7	28.5	20.4
Zr	223.7	354.3	187.4	196.8	248.4	264.2	398.2	79.3
Nb	16.9	21.0	10.5	11.7	15.9	12.8	17.7	11.4
Cs	3.5	6.3	7.5	6.6	6.3	5.2	4.87	6.73
Ba	1236.6	1391.1	1346.8	844.0	1515.7	1665.4	863.27	592.35
La	87.24	81.05	59.18	39.69	92.79	70.47	49.61	62.7
Ce	152.98	158.24	112.31	79.08	178.85	139.97	68.39	110.17
Pr	16.24	19.19	11.65	8.89	20.00	14.74	3.17	4.1
Nd	60.28	78.36	42.10	35.29	77.73	55.78	7.63	11.27
Sm	9.77	13.11	6.48	6.44	12.93	8.52	2.3	3.68
Eu	2.21	2.73	1.52	1.50	2.76	2.02	0.63	0.96
Gd	6.72	8.75	4.38	5.28	8.84	5.53	1.67	2.54
Tb	0.98	1.10	0.64	0.84	1.17	0.77	0.21	0.38
Dy	4.83	5.09	3.44	4.68	5.48	3.92	1.87	2.11
Ho	0.88	0.88	0.67	0.95	0.97	0.72	0.35	0.68
Er	2.28	2.09	1.79	2.64	2.33	1.82	1.07	1.38
Tm	0.40	0.34	0.31	0.47	0.38	0.29	0.21	0.24
Yb	2.33	1.91	1.85	2.78	2.12	1.64	0.33	0.72
Lu	0.36	0.30	0.29	0.45	0.33	0.25	0.17	0.29
Hf	3.56	9.32	3.44	4.61	5.89	6.65	2.1	4.61
Ta	1.23	1.89	0.78	0.89	1.39	0.81	0.96	1.26
Th	64.07	56.45	31.06	20.55	52.12	30.71	17.5	21.4
U	11.22	17.58	6.02	6.18	13.46	5.63	3.48	4.65

ELECTRON PROBE DATA SET

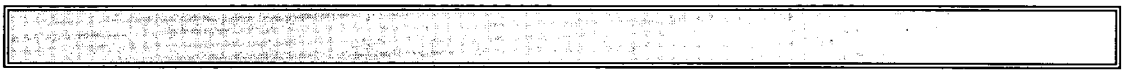

OLIVINES

Sample no	EA270	EA270	EA82b	EA82b	EA255	EA255	EA252	EA252	EA252	EA252	EA415	EA415	EA350	EA350	EA350	EA350	EA134
Unit	*Ayv. Vol.*	*Ayv. Vol.*	*Ayv. Vol.*	*Ayv. Vol.*	*Tas. Vol.*	*Tas. Vol.*	*Tas. Vol.*	*Tas. Vol.*	*Tas. Vol.*	*Tas. Vol.*	*Ezn. Vol.*	*Ezn. Vol.*	*Neb. Vol.*	*Neb. Vol.*	*Neb. Vol.*	*Neb. Vol.*	*Neb. Vol.*
Phenocryst no	*1*	*1*	*2*	*2*	*3*	*3*	*4*	*4*	*5*	*5*	*6*	*6*	*7*	*7*	*8*	*8*	*9*
(c)ore/(r)im	c	r	c	r	c	r	c	r	c	r	c	r	c	r	c	r	c
SiO_2	38.61	38.27	38.28	37.98	38.59	38.32	38.88	38.36	39.17	38.77	38.71	38.42	38.96	39.94	39.61	39.83	39.24
Fe_2O_3	18.85	20.20	17.81	17.74	18.56	17.87	15.37	17.33	14.40	14.99	15.35	15.92	13.29	8.93	10.15	9.94	14.24
MnO	0.39	0.54	0.33	0.33	0.35	0.33	0.24	0.27	0.21	0.24	0.23	0.23	0.23	0.15	0.18	0.16	0.32
MgO	41.10	39.97	41.88	42.38	41.61	41.33	45.12	43.15	45.52	45.50	44.85	44.60	46.48	50.21	48.73	49.03	44.71
CaO	0.32	0.33	0.29	0.38	0.26	0.26	0.30	0.31	0.26	0.26	0.25	0.26	0.17	0.20	0.22	0.14	0.20
Total	99.28	99.31	98.58	98.81	99.37	98.11	99.91	99.42	99.56	99.76	99.39	99.43	99.13	99.43	98.89	99.10	98.70
Si	1.00	0.99	0.99	0.98	0.99	1.00	0.98	0.98	0.98	0.97	0.98	0.97	0.97	0.98	0.98	0.98	1.00
Fe	0.41	0.44	0.39	0.38	0.40	0.39	0.32	0.36	0.30	0.31	0.32	0.33	0.27	0.18	0.21	0.20	0.30
Mn	0.01	0.01	0.01	0.01	0.01	0.01	0.01	0.01	0.00	0.01	0.01	0.01	0.01	0.00	0.00	0.00	0.01
Mg	1.58	1.55	1.61	1.63	1.60	1.60	1.69	1.64	1.70	1.70	1.69	1.68	1.73	1.83	1.80	1.80	1.69
Ca	0.01	0.01	0.01	0.01	0.01	0.01	0.01	0.01	0.01	0.01	0.01	0.01	0.01	0.01	0.01	0.00	0.01
Total	3.00	3.00	3.00	3.01	3.00	3.00	3.00	3.00	3.00	3.00	3.00	3.00	3.00	3.00	3.00	3.00	3.00
Fo	79.53	77.91	80.73	80.98	79.98	80.48	84.14	81.86	85.09	84.66	84.08	83.54	86.43	91.21	89.68	89.97	84.84
Fa	20.47	22.09	19.27	19.02	20.02	19.52	15.86	18.14	14.91	15.34	15.92	16.46	13.57	8.79	10.32	10.03	15.16

Sample no	EA134	EA134	EA134	EA348	EA348	EA348	EA348	EA409	EA409	EA309	EA309	EA309	EA309	EA313	EA313	EA101	EA101
Unit	*Neb. Vol.*	*Neb. Vol.*	*Neb. Vol.*	*Foc. Dyke*	*Foc. Dyke*	*Foc. Dyke*	*Foc. Dyke*	*Foc. Dyke*	*Foc. Dyke*	*Foc. Dyke*	*Foc. Dyke*	*Foc. Dyke*	*Foc. Dyke*	*Egr. And*	*Egr. And*	*Oda. Dyke*	*Oda. Dyke*
Phenocryst no	*9*	*10*	*10*	*11*	*11*	*12*	*12*	*13*	*13*	*14*	*14*	*15*	*15*	*16*	*16*	*17*	*17*
(c)ore/(r)im	r	c	r	c	r	c	r	c	r	c	r	c	r	c	r	c	r
SiO_2	38.72	38.48	38.37	38.51	37.52	36.98	36.92	36.78	38.00	39.83	39.14	39.90	39.81	38.10	37.77	36.14	36.17
Fe_2O_3	15.74	17.23	18.12	15.37	20.28	24.16	24.40	23.52	21.30	10.42	14.40	11.00	11.41	21.86	23.72	28.00	28.63
MnO	0.35	0.32	0.36	0.25	0.39	0.52	0.50	0.49	0.37	0.20	0.26	0.21	0.21	0.44	0.48	0.63	0.63
MgO	44.32	43.21	42.78	44.66	40.75	37.47	37.06	36.44	38.81	48.72	45.16	48.30	48.10	39.44	37.77	34.03	33.47
CaO	0.19	0.12	0.13	0.13	0.17	0.17	0.12	0.26	0.30	0.32	0.35	0.33	0.33	0.12	0.13	0.35	0.37
Total	99.31	99.36	99.76	98.92	99.11	99.30	99.00	97.50	98.78	99.49	99.31	99.74	99.86	99.95	99.86	99.15	99.27
Si	0.98	0.98	0.98	0.98	0.97	0.98	0.98	0.99	1.00	0.98	0.99	0.98	0.98	0.99	0.99	0.98	0.98
Fe	0.33	0.36	0.38	0.32	0.43	0.53	0.54	0.53	0.47	0.21	0.30	0.22	0.23	0.47	0.52	0.63	0.64
Mn	0.01	0.01	0.01	0.01	0.01	0.01	0.01	0.01	0.01	0.00	0.01	0.01	0.00	0.01	0.01	0.01	0.02
Mg	1.68	1.64	1.62	1.69	1.57	1.47	1.47	1.46	1.52	1.79	1.70	1.77	1.77	1.53	1.48	1.37	1.35
Ca	0.01	0.00	0.00	0.00	0.01	0.01	0.00	0.01	0.01	0.01	0.01	0.01	0.01	0.00	0.00	0.01	0.01
Total	3.02	3.00	3.00	3.00	3.00	3.00	3.00	3.01	3.00	3.00	3.00	3.00	3.00	3.01	3.01	3.00	3.00
Fo	83.39	81.92	81.03	84.04	78.39	73.63	73.21	73.42	76.46	89.49	84.96	88.79	88.44	76.28	73.94	68.61	67.75
Fa	16.61	18.08	18.97	15.96	21.61	26.37	26.79	26.58	23.54	10.51	15.04	11.21	11.56	23.72	26.06	31.39	32.25

CLINOPYROXENES

Sample no	EA270	EA270	EA270	EA270	EA270	EA270	EA82b	EA82b	EA256	EA256	EA256	EA256	EA256	EA256	EA252
Unit	*Ayv. Vol.*	*Ayv. Vol.*	*Ayv. Vol.*	*Ayv. Vol.*	*Ayv. Vol.*	*Ayv. Vol.*	*Ayv. Vol.*	*Ayv. Vol.*	*Tas. Vol.*	*Tas. Vol.*	*Tas. Vol.*	*Tas. Vol.*	*Tas. Vol.*	*Tas. Vol.*	*Tas. Vol.*
Phenocryst no	1	1	2	2	3	3	4	4	5	5	6	6	7	7	8
(c)ore/(r)im	c	r	c	r	c	r	c	r	c	r	c	r	c	r	c
SiO_2	49.01	48.00	48.65	47.82	47.95	49.03	48.88	51.05	50.35	44.19	47.18	47.13	47.59	47.21	49.40
TiO_2	1.95	2.40	2.08	2.46	2.40	2.11	1.87	1.13	1.83	3.68	2.96	2.35	2.21	2.33	1.79
Al_2O_3	3.90	4.74	4.63	4.67	4.92	3.83	3.78	2.53	2.85	7.69	5.95	5.46	5.35	5.65	3.07
Fe_2O_3	6.92	7.28	6.83	7.49	6.54	6.52	6.64	5.25	5.43	7.50	6.18	6.15	6.25	6.63	6.53
MnO	0.14	0.19	0.14	0.16	0.10	0.14	0.11	0.12	0.11	0.12	0.19	0.07	0.10	0.10	0.14
MgO	13.48	12.87	13.41	12.91	13.27	13.86	14.71	15.72	15.01	12.82	13.19	13.41	13.21	13.78	14.86
CaO	23.23	23.23	23.03	22.96	23.41	23.23	23.17	22.92	23.05	22.59	22.90	22.83	22.89	22.87	22.82
Na_2O	0.50	0.65	0.57	0.59	0.61	0.48	0.49	0.39	0.40	0.55	0.50	0.52	0.48	0.48	0.41
Total	**99.13**	**99.36**	**99.33**	**99.04**	**99.18**	**99.21**	**99.65**	**99.11**	**99.02**	**99.13**	**99.04**	**97.91**	**98.07**	**99.06**	**99.02**
O = 6															
Si	1.85	1.81	1.83	1.81	1.81	1.84	1.83	1.90	1.88	1.68	1.78	1.79	1.81	1.78	1.86
Ti	0.06	0.07	0.06	0.07	0.07	0.06	0.05	0.03	0.05	0.11	0.08	0.07	0.06	0.07	0.05
Al	0.17	0.21	0.21	0.21	0.22	0.17	0.17	0.11	0.13	0.34	0.26	0.24	0.24	0.25	0.14
Fe	0.22	0.23	0.21	0.24	0.21	0.20	0.21	0.16	0.17	0.24	0.19	0.20	0.20	0.21	0.21
Mn	0.00	0.01	0.00	0.01	0.00	0.00	0.00	0.00	0.00	0.00	0.01	0.00	0.00	0.00	0.00
Mg	0.76	0.72	0.75	0.73	0.75	0.78	0.82	0.87	0.84	0.73	0.74	0.76	0.75	0.78	0.83
Ca	0.94	0.94	0.93	0.93	0.95	0.94	0.93	0.91	0.92	0.92	0.92	0.93	0.93	0.92	0.92
Na	0.04	0.05	0.04	0.04	0.04	0.04	0.04	0.03	0.03	0.04	0.04	0.04	0.03	0.04	0.03
Total	**4.03**	**4.04**	**4.03**	**4.04**	**4.04**	**4.03**	**4.05**	**4.03**	**4.02**	**4.06**	**4.03**	**4.04**	**4.03**	**4.05**	**4.04**
En	**39.73**	**36.99**	**39.59**	**38.42**	**39.23**	**40.40**	**46.73**	**46.58**	**43.27**	**36.54**	**39.73**	**40.25**	**39.76**	**40.05**	**43.91**
Fs	**11.03**	**12.66**	**11.54**	**12.45**	**11.01**	**10.90**	**7.31**	**8.73**	**8.97**	**13.23**	**10.66**	**10.48**	**10.73**	**10.36**	**10.33**
Wo	**49.24**	**50.35**	**48.87**	**49.13**	**49.76**	**48.70**	**45.96**	**44.69**	**47.77**	**50.23**	**49.61**	**49.27**	**49.52**	**49.59**	**45.76**

Sample no	EA252	EA252	EA252	EA252	EA252	EA415	EA415	EA415	EA415	EA409	EA409	EA409	EA409	EA309	EA309
Unit	*Tas. Vol.*	*Tas. Vol.*	*Tas. Vol.*	*Tas. Vol.*	*Tas. Vol.*	*Ezn. Vol.*	*Ezn. Vol.*	*Ezn. Vol.*	*Ezn. Vol.*	*Foc. Dyke*	*Foc. Dyke*	*Foc. Dyke*	*Foc. Dyke*	*Foc. Dyke*	*Foc. Dyke*
Phenocryst no	8	9	9	10	10	11	11	12	12	13	13	14	14	15	15
(c)ore/(r)im	r	c	r	c	r	c	r	c	r	c	r	c	r	c	r
SiO_2	49.40	49.21	48.28	49.67	49.31	48.24	49.93	49.20	47.87	49.33	51.01	47.88	48.86	48.16	49.12
TiO_2	1.85	1.64	2.06	1.96	1.88	1.81	1.50	1.68	2.14	1.19	0.60	1.54	1.12	1.44	1.02
Al_2O_3	2.97	3.31	3.76	3.09	3.26	4.66	2.84	3.69	5.10	4.81	3.43	7.15	4.26	5.38	5.25
Fe_2O_3	6.16	6.53	7.41	6.00	6.56	6.80	6.03	7.02	6.05	6.76	4.28	6.27	8.36	5.98	5.78
MnO	0.12	0.13	0.12	0.11	0.14	0.12	0.14	0.15	0.11	0.14	0.10	0.14	0.25	0.14	0.12
MgO	14.80	14.95	14.06	14.96	14.55	14.23	15.30	14.43	14.76	14.02	15.74	13.06	14.11	14.20	14.56
CaO	22.66	23.01	22.86	23.08	22.97	22.75	22.37	22.28	22.84	22.60	22.98	22.97	21.94	23.35	23.19
Na_2O	0.41	0.42	0.45	0.37	0.39	0.51	0.35	0.47	0.51	0.27	0.27	0.32	0.39	0.29	0.29
Total	**98.37**	**99.20**	**99.00**	**99.24**	**99.06**	**99.12**	**98.46**	**98.92**	**99.38**	**99.12**	**98.41**	**99.33**	**99.28**	**98.94**	**99.33**
O = 6															
Si	1.87	1.85	1.83	1.86	1.85	1.82	1.88	1.85	1.79	1.85	1.90	1.79	1.84	1.81	1.83
Ti	0.05	0.05	0.06	0.06	0.05	0.05	0.04	0.05	0.06	0.03	0.02	0.04	0.03	0.04	0.03
Al	0.13	0.15	0.17	0.14	0.14	0.21	0.13	0.16	0.23	0.21	0.15	0.31	0.19	0.24	0.23
Fe	0.19	0.21	0.23	0.19	0.21	0.21	0.19	0.22	0.19	0.21	0.13	0.20	0.26	0.19	0.18
Mn	0.00	0.00	0.00	0.00	0.00	0.00	0.00	0.00	0.00	0.00	0.00	0.00	0.01	0.00	0.00
Mg	0.83	0.84	0.79	0.84	0.82	0.80	0.86	0.81	0.82	0.78	0.87	0.73	0.79	0.80	0.81
Ca	0.92	0.93	0.93	0.93	0.93	0.92	0.90	0.90	0.92	0.91	0.92	0.92	0.89	0.94	0.93
Na	0.03	0.03	0.03	0.03	0.03	0.04	0.03	0.03	0.04	0.02	0.02	0.02	0.03	0.02	0.02
Total	**4.03**	**4.05**	**4.05**	**4.03**	**4.03**	**4.05**	**4.03**	**4.03**	**4.05**	**4.02**	**4.02**	**4.02**	**4.04**	**4.04**	**4.03**
En	**44.21**	**43.11**	**41.47**	**44.04**	**43.01**	**45.12**	**45.66**	**43.25**	**44.31**	**41.07**	**45.34**	**39.37**	**39.88**	**43.16**	**43.97**
Fs	**10.32**	**10.78**	**12.26**	**9.91**	**10.88**	**10.32**	**10.10**	**11.81**	**10.70**	**11.33**	**7.08**	**10.84**	**14.34**	**10.03**	**9.79**
Wo	**45.47**	**46.11**	**46.27**	**46.05**	**46.11**	**44.56**	**44.24**	**44.95**	**44.99**	**47.60**	**47.58**	**49.79**	**46.79**	**46.82**	**46.23**

Sample no	EA309	EA309	EA309	EA309	EA350	EA350	EA350	EA350	EA348	EA348	EA348	EA348	EA348	EA348	EA134
Unit	*Foc. Dyke*	*Foc. Dyke*	*Foc. Dyke*	*Foc. Dyke*	*Neb. Vol.*	*Neb. Vol.*	*Neb. Vol.*	*Neb. Vol.*	*Foc. Dyke*	*Foc. Dyke*	*Foc. Dyke*	*Foc. Dyke*	*Foc. Dyke*	*Foc. Dyke*	*Neb. Vol.*
Phenocryst no	16	16	17	17	18	18	19	19	20	20	21	21	22	22	23
(c)ore/(r)im	c	r	c	r	c	r	c	r	c	r	c	r	c	r	c
SiO_2	48.65	48.00	48.56	47.80	52.73	52.62	52.84	52.29	51.49	51.98	51.58	50.38	51.77	51.00	52.29
TiO_2	1.18	1.25	0.91	1.44	0.53	0.72	0.51	0.61	0.44	0.79	0.63	0.97	0.45	0.67	0.33
Al_2O_3	5.79	6.13	3.95	5.76	1.15	1.18	1.11	1.19	2.43	2.05	2.19	3.16	2.27	3.98	2.18
Fe_2O_3	7.40	6.48	11.67	8.60	4.41	4.74	4.15	4.62	5.49	5.66	6.99	9.11	5.53	5.69	4.28
MnO	0.18	0.14	0.48	0.21	0.12	0.13	0.13	0.14	0.17	0.18	0.20	0.27	0.17	0.16	0.11
MgO	13.71	13.90	11.35	12.74	17.09	17.34	17.27	17.41	16.82	17.26	16.90	15.45	16.73	15.64	16.62
CaO	22.62	23.09	21.74	22.50	22.78	22.23	23.09	22.42	21.97	21.26	21.18	19.85	21.86	22.04	23.13
Na_2O	0.36	0.35	0.51	0.40	0.15	0.15	0.18	0.16	0.22	0.21	0.17	0.33	0.20	0.26	0.20
Total	**99.89**	**99.34**	**99.17**	**99.45**	**98.96**	**99.11**	**99.28**	**98.84**	**99.03**	**99.39**	**99.84**	**99.52**	**98.98**	**99.44**	**99.15**
O = 6															
Si	1.82	1.80	1.86	1.81	1.95	1.95	1.95	1.94	1.91	1.92	1.91	1.89	1.92	1.89	1.93
Ti	0.03	0.04	0.03	0.04	0.01	0.02	0.01	0.02	0.01	0.02	0.02	0.03	0.01	0.02	0.01
Al	0.25	0.27	0.18	0.26	0.05	0.05	0.05	0.05	0.11	0.09	0.10	0.14	0.10	0.17	0.10
Fe	0.23	0.20	0.37	0.27	0.14	0.15	0.13	0.14	0.17	0.17	0.22	0.29	0.17	0.18	0.13
Mn	0.01	0.00	0.02	0.01	0.00	0.00	0.00	0.00	0.01	0.01	0.01	0.01	0.01	0.01	0.00
Mg	0.76	0.78	0.65	0.72	0.94	0.96	0.95	0.96	0.93	0.95	0.93	0.86	0.93	0.86	0.92
Ca	0.91	0.93	0.89	0.91	0.90	0.88	0.91	0.89	0.87	0.84	0.84	0.80	0.87	0.87	0.92
Na	0.03	0.03	0.04	0.03	0.01	0.01	0.01	0.01	0.02	0.02	0.01	0.02	0.01	0.02	0.01
Total	**4.04**	**4.04**	**4.04**	**4.04**	**4.01**	**4.01**	**4.02**	**4.02**	**4.03**	**4.02**	**4.03**	**4.03**	**4.02**	**4.02**	**4.02**
En	**41.54**	**42.36**	**34.94**	**39.07**	**48.30**	**49.37**	**48.66**	**48.64**	**47.70**	**49.09**	**48.17**	**44.82**	**47.90**	**47.07**	**47.28**
Fs	**12.58**	**11.08**	**20.16**	**14.80**	**6.99**	**6.93**	**6.56**	**7.24**	**8.84**	**9.03**	**9.58**	**14.83**	**8.88**	**9.61**	**5.42**
Wo	**45.88**	**46.56**	**44.91**	**46.13**	**44.71**	**43.70**	**44.78**	**44.12**	**43.46**	**41.88**	**42.25**	**40.36**	**43.22**	**43.32**	**47.31**

Sample no	EA134	EA134	EA134	EA134	EA134	EA109	EA109	EA109	EA109	EA143	EA143	EA143	EA143	EA143	EA143
Unit	*Neb. Vol.*	*Neb. Vol.*	*Neb. Vol.*	*Neb. Vol.*	*Neb. Vol.*	*Neb. Vol.*	*Neb. Vol.*	*Neb. Vol.*	*Neb. Vol.*	*Neb. Vol.*	*Neb. Vol.*	*Neb. Vol.*	*Neb. Vol.*	*Neb. Vol.*	*Neb. Vol.*
Phenocryst no	23	24	24	25	25	26	26	27	27	28	28	29	29	30	30
(c)ore/(r)im	r	c	r	c	r	c	r	c	r	c	r	c	r	c	r
SiO_2	52.54	52.41	51.21	51.52	50.41	47.03	49.50	50.50	49.87	52.14	50.72	52.41	51.82	51.08	50.70
TiO_2	0.44	0.36	0.58	0.62	0.66	1.48	1.14	0.74	0.88	0.39	0.85	0.30	0.61	0.90	0.86
Al_2O_3	2.91	2.34	3.74	3.12	4.21	6.10	2.89	3.46	3.91	2.76	3.41	2.86	2.31	2.85	3.15
Fe_2O_3	4.05	3.57	4.33	5.25	4.75	8.63	9.13	7.17	7.84	5.16	7.00	3.92	6.95	6.77	6.74
MnO	0.11	0.10	0.10	0.14	0.11	0.21	0.24	0.21	0.22	0.13	0.19	0.12	0.19	0.19	0.22
MgO	16.12	16.49	15.57	16.07	15.41	12.24	13.40	13.94	13.40	15.73	14.66	16.16	15.78	15.34	15.60
CaO	22.94	23.04	23.14	22.70	23.03	21.91	21.70	21.88	22.01	22.08	20.50	22.20	20.61	20.97	21.13
Na_2O	0.20	0.21	0.24	0.19	0.25	0.34	0.37	0.30	0.34	0.33	0.36	0.31	0.31	0.32	0.33
Total	**99.31**	**98.52**	**98.91**	**99.61**	**98.81**	**97.93**	**98.38**	**98.20**	**98.48**	**98.72**	**97.68**	**98.29**	**98.58**	**98.43**	**98.73**
O = 6															
Si	1.93	1.94	1.90	1.90	1.88	1.80	1.89	1.91	1.89	1.94	1.91	1.94	1.94	1.92	1.90
Ti	0.01	0.01	0.02	0.02	0.02	0.04	0.03	0.02	0.03	0.01	0.02	0.01	0.02	0.03	0.02
Al	0.13	0.10	0.16	0.14	0.18	0.28	0.13	0.15	0.17	0.12	0.15	0.13	0.10	0.13	0.14
Fe	0.12	0.11	0.13	0.16	0.15	0.28	0.29	0.23	0.25	0.16	0.22	0.12	0.22	0.21	0.21
Mn	0.00	0.00	0.00	0.00	0.00	0.01	0.01	0.01	0.01	0.00	0.01	0.00	0.01	0.01	0.01
Mg	0.88	0.91	0.86	0.89	0.86	0.70	0.76	0.78	0.76	0.87	0.82	0.89	0.88	0.86	0.87
Ca	0.90	0.91	0.92	0.90	0.92	0.90	0.89	0.89	0.89	0.88	0.83	0.88	0.83	0.84	0.85
Na	0.01	0.02	0.02	0.01	0.02	0.03	0.03	0.02	0.02	0.02	0.03	0.02	0.02	0.02	0.02
Total	**4.00**	**4.01**	**4.01**	**4.02**	**4.02**	**4.03**	**4.03**	**4.01**	**4.01**	**4.00**	**4.00**	**4.00**	**4.01**	**4.01**	**4.02**
En	**46.12**	**46.50**	**44.41**	**44.92**	**43.96**	**38.82**	**39.78**	**42.72**	**41.16**	**49.00**	**47.38**	**50.79**	**48.13**	**47.87**	**50.81**
Fs	**6.69**	**5.86**	**7.17**	**8.55**	**7.86**	**15.50**	**15.35**	**12.45**	**13.64**	**8.27**	**12.82**	**6.98**	**10.94**	**10.53**	**8.72**
Wo	**47.20**	**47.64**	**48.42**	**46.53**	**48.18**	**45.68**	**44.87**	**44.84**	**45.21**	**42.74**	**39.81**	**42.23**	**40.92**	**41.60**	**40.47**

Sample no	EA101	EA101	EA313	EA313	EA112	EA112	EA112	EA112	EA316	EA316	EA45	EA45	EA418	EA418	EA418
Unit	*Oda. Dyke*	*Oda. Dyke*	*Egr. And*	*Egr. And*	*Egr. And*	*Egr. And*	*Egr. And*	*Egr. And*	*Klg. And*	*Klg. And*	*Kov. Dyke*	*Kov. Dyke*	*Kov. Dyke*	*Kov. Dyke*	*Kov. Dyke*
Phenocryst no	31	31	32	32	34	34	35	35	33	33	36	36	37	37	38
(c)ore/(r)im	c	r	c	r	c	r	c	r	c	r	c	r	c	r	c
SiO_2	51.06	49.49	53.42	51.50	51.06	50.86	51.12	51.53	52.57	49.44	50.83	51.48	51.23	50.46	51.07
TiO_2	0.72	0.73	0.26	0.52	0.40	0.46	0.65	0.55	0.37	0.94	0.78	0.48	0.77	0.75	0.77
Al_2O_3	2.00	4.07	1.43	3.58	2.21	2.30	2.19	1.80	2.18	5.18	2.08	1.44	1.94	2.29	2.17
Fe_2O_3	7.71	6.27	5.95	4.97	9.48	9.08	9.79	9.45	6.41	7.09	9.69	9.36	9.96	9.51	8.36
MnO	0.26	0.15	0.23	0.15	0.51	0.50	0.43	0.39	0.22	0.18	0.30	0.33	0.30	0.27	0.24
MgO	15.91	14.86	18.34	16.20	13.79	13.22	13.98	14.04	17.00	14.41	14.87	14.82	13.85	14.73	14.38
CaO	20.44	21.80	19.44	22.13	20.88	21.60	20.31	20.45	20.70	21.79	19.94	20.75	19.40	19.36	20.41
Na_2O	0.27	0.34	0.20	0.34	0.47	0.49	0.39	0.39	0.27	0.27	0.39	0.41	0.34	0.37	0.31
Total	**98.36**	**97.71**	**99.26**	**99.39**	**98.81**	**98.51**	**98.86**	**98.59**	**99.72**	**99.30**	**98.87**	**99.07**	**97.78**	**97.74**	**97.71**
O = 6															
Si	1.92	1.87	1.96	1.90	1.93	1.93	1.93	1.95	1.94	1.85	1.92	1.94	1.95	1.92	1.94
Ti	0.02	0.02	0.01	0.01	0.01	0.01	0.02	0.02	0.01	0.03	0.02	0.01	0.02	0.02	0.02
Al	0.09	0.18	0.06	0.16	0.10	0.10	0.10	0.08	0.09	0.23	0.09	0.06	0.09	0.10	0.10
Fe	0.24	0.20	0.18	0.15	0.30	0.29	0.31	0.30	0.20	0.22	0.31	0.30	0.32	0.30	0.27
Mn	0.01	0.00	0.01	0.00	0.02	0.02	0.01	0.01	0.01	0.01	0.01	0.01	0.01	0.01	0.01
Mg	0.89	0.84	1.00	0.89	0.78	0.75	0.79	0.79	0.93	0.80	0.84	0.83	0.79	0.84	0.81
Ca	0.82	0.88	0.77	0.87	0.85	0.88	0.82	0.83	0.82	0.87	0.81	0.84	0.79	0.79	0.83
Na	0.02	0.02	0.01	0.02	0.03	0.04	0.03	0.03	0.02	0.02	0.03	0.03	0.03	0.03	0.02
Total	**4.02**	**4.03**	**4.01**	**4.02**	**4.02**	**4.02**	**4.01**	**4.01**	**4.02**	**4.02**	**4.03**	**4.03**	**3.99**	**4.02**	**4.00**
En	**49.95**	**52.19**	**50.80**	**45.86**	**44.93**	**43.34**	**43.95**	**43.13**	**47.29**	**41.76**	**47.39**	**45.74**	**42.63**	**43.95**	**43.67**
Fs	**10.01**	**7.23**	**9.71**	**8.21**	**13.54**	**13.25**	**15.08**	**14.99**	**10.46**	**11.95**	**13.11**	**12.55**	**17.37**	**16.09**	**14.39**
Wo	**40.04**	**40.59**	**39.49**	**45.93**	**41.53**	**43.41**	**40.97**	**41.89**	**42.25**	**46.30**	**39.50**	**41.71**	**40.01**	**39.97**	**41.95**

Sample no	EA418	EA418	EA418	EA412	EA412	EA412	EA412	EA76	EA76	EAR1	EAR1	EA37	EA37	EA275	EA275
Unit	*Kov. Dyke*	*Kov. Dyke*	*Kov. Dyke*	*Kov. Dyke*	*Kov. Dyke*	*Kov. Dyke*	*Kov. Dyke*	*Kov. Dyke*	*Kov. Dyke*	*Ded. Unit*	*Ded. Unit*	*Behr. And.*	*Behr. And.*	*Behr. And.*	*Behr. And.*
Phenocryst no	38	39	39	40	40	41	41	42	42	43	43	44	44	45	45
(c)ore/(r)im	r	c	r	c	r	c	r	c	r			c	r	c	r
SiO_2	51.03	50.29	50.88	50.81	50.46	51.22	51.59	48.59	50.10	52.03	52.03	51.72	49.93	51.98	52.58
TiO_2	0.75	0.83	0.84	0.96	0.98	0.93	0.93	1.14	0.78	0.21	0.21	0.45	0.25	0.45	0.25
Al_2O_3	1.87	2.58	2.20	3.09	3.21	3.02	2.71	5.35	3.71	1.29	1.29	1.71	1.19	1.78	0.98
Fe_2O_3	9.74	10.11	9.95	10.60	10.32	10.06	9.66	8.63	8.94	8.57	8.57	8.62	8.48	9.53	9.62
MnO	0.31	0.28	0.29	0.26	0.28	0.28	0.26	0.23	0.30	0.52	0.52	0.37	0.41	0.56	0.65
MgO	14.28	14.94	15.34	15.08	15.21	15.30	15.88	13.47	14.21	13.44	13.44	14.60	13.76	14.43	14.43
CaO	19.43	19.67	19.47	18.47	18.19	18.37	18.64	22.09	21.09	22.37	22.37	21.34	21.59	20.96	21.25
Na_2O	0.40	0.40	0.35	0.53	0.54	0.55	0.43	0.40	0.45	0.51	0.51	0.32	0.33	0.39	0.29
Total	**97.80**	**99.10**	**99.32**	**99.79**	**99.18**	**99.73**	**100.09**	**99.89**	**99.58**	**98.93**	**98.93**	**99.14**	**95.94**	**100.07**	**100.06**
O = 6															
Si	1.95	1.90	1.91	1.90	1.90	1.91	1.91	1.82	1.88	1.97	1.97	1.94	1.95	1.94	1.97
Ti	0.02	0.02	0.02	0.03	0.03	0.03	0.03	0.03	0.02	0.01	0.01	0.01	0.01	0.01	0.01
Al	0.08	0.11	0.10	0.14	0.14	0.13	0.12	0.24	0.16	0.06	0.06	0.08	0.05	0.08	0.04
Fe	0.31	0.32	0.31	0.33	0.32	0.31	0.30	0.27	0.28	0.27	0.27	0.27	0.28	0.30	0.30
Mn	0.01	0.01	0.01	0.01	0.01	0.01	0.01	0.01	0.01	0.02	0.02	0.01	0.01	0.02	0.02
Mg	0.81	0.84	0.86	0.84	0.85	0.85	0.88	0.75	0.80	0.76	0.76	0.82	0.80	0.80	0.80
Ca	0.79	0.80	0.78	0.74	0.73	0.73	0.74	0.89	0.85	0.91	0.91	0.86	0.90	0.84	0.85
Na	0.03	0.03	0.03	0.04	0.04	0.04	0.03	0.03	0.03	0.04	0.04	0.02	0.02	0.03	0.02
Total	**4.01**	**4.03**	**4.03**	**4.02**	**4.02**	**4.02**	**4.02**	**4.04**	**4.03**	**4.02**	**4.02**	**4.02**	**4.03**	**4.02**	**4.02**
En	**43.26**	**43.32**	**44.13**	**43.36**	**44.01**	**44.18**	**45.15**	**38.83**	**40.71**	**42.08**	**42.08**	**45.37**	**43.81**	**40.62**	**40.25**
Fs	**16.71**	**16.61**	**16.22**	**17.70**	**17.39**	**16.92**	**15.98**	**14.48**	**15.01**	**12.12**	**12.12**	**12.27**	**11.66**	**16.11**	**16.27**
Wo	**40.03**	**40.08**	**39.66**	**38.95**	**38.60**	**38.90**	**38.87**	**46.70**	**44.29**	**45.80**	**45.80**	**42.37**	**44.53**	**43.27**	**43.48**

Sample no	EA275	EA275	EA62	EA62	EA273	EA273	EA231	EA231	EA231	EA231	EA231	EA231	EA73	EA73	EA73
Unit	*Behr. And.*	*Behr. And.*	*Bak. Unit*	*Bak. Unit*	*Bad. Unit*	*Bad. Unit*	*Bad. Unit*	*Bad. Unit*	*Bad. Unit*	*Bad. Unit*	*Bad. Unit*	*Bad. Unit*	*Cice. And.*	*Cice. And.*	*Cice. And.*
Phenocryst no	46	46	47	47	48	48	49	49	50	50	51	51	52	52	53
(c)ore/(r)im	c	r	c	r	c	r	c	r	c	r	c	r	c	r	c
SiO_2	52.89	52.75	52.66	52.59	50.98	50.29	50.36	50.42	49.93	50.21	51.47	50.41	48.44	49.48	50.19
TiO_2	0.16	0.23	0.24	0.23	0.47	0.67	0.59	0.55	0.65	0.70	0.44	0.53	0.87	0.60	0.55
Al_2O_3	0.73	1.19	1.22	1.09	2.04	2.85	3.05	2.95	3.59	3.10	2.02	3.09	4.97	3.95	4.15
Fe_2O_3	9.51	8.61	8.40	8.45	10.22	9.06	9.03	8.72	8.47	8.67	8.26	8.76	10.54	9.95	7.30
MnO	0.69	0.61	0.58	0.54	0.34	0.26	0.41	0.39	0.32	0.36	0.44	0.32	0.44	0.47	0.17
MgO	14.45	14.96	13.78	13.66	13.60	13.53	14.25	14.39	14.37	14.44	15.10	14.26	12.01	12.71	14.41
CaO	21.39	21.30	22.55	22.80	19.93	20.73	21.24	21.25	21.85	21.88	21.62	21.93	21.99	22.28	22.98
Na_2O	0.30	0.35	0.40	0.44	0.46	0.39	0.53	0.47	0.43	0.40	0.38	0.38	0.73	0.63	0.40
Total	**100.11**	**100.01**	**99.82**	**99.80**	**98.05**	**97.77**	**99.46**	**99.13**	**99.62**	**99.76**	**99.73**	**99.67**	**99.99**	**100.07**	**100.15**
O = 6															
Si	1.98	1.96	1.97	1.97	1.95	1.92	1.90	1.90	1.87	1.88	1.92	1.89	1.84	1.87	1.87
Ti	0.00	0.01	0.01	0.01	0.01	0.02	0.02	0.02	0.02	0.02	0.01	0.01	0.02	0.02	0.02
Al	0.03	0.05	0.05	0.05	0.09	0.13	0.14	0.13	0.16	0.14	0.09	0.14	0.22	0.18	0.18
Fe	0.30	0.27	0.26	0.26	0.33	0.29	0.28	0.27	0.27	0.27	0.26	0.27	0.33	0.31	0.23
Mn	0.02	0.02	0.02	0.02	0.01	0.01	0.01	0.01	0.01	0.01	0.01	0.01	0.01	0.02	0.01
Mg	0.81	0.83	0.77	0.76	0.77	0.77	0.80	0.81	0.80	0.81	0.84	0.80	0.68	0.72	0.80
Ca	0.86	0.85	0.90	0.92	0.82	0.85	0.86	0.86	0.88	0.88	0.87	0.88	0.89	0.90	0.92
Na	0.02	0.03	0.03	0.03	0.03	0.03	0.04	0.03	0.03	0.03	0.03	0.03	0.05	0.05	0.03
Total	**4.01**	**4.02**	**4.01**	**4.02**	**4.01**	**4.01**	**4.04**	**4.04**	**4.04**	**4.04**	**4.03**	**4.04**	**4.06**	**4.05**	**4.04**
En	**40.23**	**41.77**	**38.91**	**38.50**	**41.23**	**41.35**	**41.75**	**42.06**	**41.56**	**41.34**	**42.91**	**41.04**	**36.52**	**37.64**	**41.64**
Fs	**16.11**	**14.61**	**14.39**	**14.38**	**17.56**	**15.70**	**14.99**	**14.43**	**13.89**	**14.06**	**13.31**	**14.28**	**18.18**	**16.69**	**11.96**
Wo	**43.66**	**43.62**	**46.71**	**47.12**	**41.21**	**42.95**	**43.26**	**43.51**	**44.56**	**44.60**	**43.79**	**44.68**	**45.30**	**45.67**	**46.40**

ORTHOPYROXENES

Sample no	EA45	EA45	EA45	EA45	EA45	EA45	EA45	EA45	EA412	EA412	EA412	EA412	EA418	EA418	EA37
Unit	*Kov. Dyke*	*Kov. Dyke*	*Kov. Dyke*	*Kov. Dyke*	*Kov. Dyke*	*Kov. Dyke*	*Kov. Dyke*	*Kov. Dyke*	*Kov. Dyke*	*Kov. Dyke*	*Kov. Dyke*	*Kov. Dyke*	*Kov. Dyke*	*Kov. Dyke*	*Behr. And.*
Phenocryst no	1	1	2	2	3	3	4	4	5	5	6	6	7	7	8
(c)ore/(r)im	r	c	r	c	r	c	r	c	c	r	c	r	r	c	c
SiO_2	53.69	53.59	52.93	53.46	53.81	52.88	53.40	53.34	53.07	53.40	52.64	52.72	52.78	52.56	51.94
TiO_2	0.30	0.34	0.36	0.26	0.24	0.37	0.33	0.35	0.52	0.49	0.44	0.50	0.40	0.41	0.15
Al_2O_3	1.03	0.97	1.04	0.92	0.82	0.95	1.29	0.90	1.97	1.92	1.85	1.75	1.14	1.43	0.85
Fe_2O_3	15.53	15.36	18.03	16.49	15.22	17.50	15.39	17.07	17.18	17.06	18.22	18.02	17.39	17.71	20.11
MnO	0.40	0.46	0.56	0.46	0.42	0.50	0.39	0.50	0.39	0.38	0.37	0.40	0.42	0.44	0.95
MgO	26.82	26.86	24.55	25.40	27.07	24.96	26.85	25.46	24.86	24.25	24.22	24.19	23.98	24.61	23.85
CaO	1.46	1.58	1.63	1.53	1.54	1.57	1.46	1.62	1.94	1.95	1.82	2.00	1.85	1.94	0.96
Total	**99.23**	**99.16**	**99.10**	**98.52**	**99.12**	**98.72**	**99.11**	**99.24**	**99.94**	**99.46**	**99.55**	**99.57**	**97.96**	**99.10**	**98.79**
O = 6															
Si	1.96	1.96	1.96	1.97	1.96	1.96	1.95	1.96	1.94	1.96	1.94	1.94	1.97	1.94	1.95
Ti	0.01	0.01	0.01	0.01	0.01	0.01	0.01	0.01	0.01	0.01	0.01	0.01	0.01	0.01	0.00
Al	0.04	0.04	0.05	0.04	0.04	0.04	0.06	0.04	0.08	0.08	0.08	0.08	0.05	0.06	0.04
Fe	0.47	0.47	0.56	0.51	0.46	0.54	0.47	0.52	0.52	0.52	0.56	0.55	0.54	0.55	0.63
Mn	0.01	0.01	0.02	0.01	0.01	0.02	0.01	0.02	0.01	0.01	0.01	0.01	0.01	0.01	0.03
Mg	1.46	1.46	1.35	1.40	1.47	1.38	1.46	1.39	1.35	1.32	1.33	1.33	1.33	1.36	1.33
Ca	0.06	0.06	0.06	0.06	0.06	0.06	0.06	0.06	0.08	0.08	0.07	0.08	0.07	0.08	0.04
Total	**4.01**	**4.01**	**4.01**	**4.00**	**4.01**	**4.01**	**4.01**	**4.01**	**4.00**	**3.99**	**4.01**	**4.00**	**3.99**	**4.01**	**4.03**
En	74.20	74.07	69.24	71.25	74.45	70.08	74.73	70.87	68.62	68.81	67.14	67.03	64.50	68.24	67.43
Fs	22.78	22.68	27.32	25.57	22.40	26.63	22.20	25.77	27.50	27.28	29.20	28.95	27.66	27.83	30.53
Wo	3.02	3.25	3.45	3.18	3.15	3.29	3.07	3.36	3.88	3.90	3.66	4.02	7.84	3.93	2.03

ORTHOPYROXENES

Sample no	**EA37**	**EA37**	**EA37**	**EA73**	**EA73**	**EA62**	**EA63**	**EA273**	**EA313**	**EA313**	**EA313**	**EA313**
Unit	*Behr. And.*	*Behr. And.*	*Behr. And.*	*Cice. And.*	*Cice. And.*	*Bak. Unit*	*Bak. Unit*	*Bad. Unit*	*Egr. And*	*Egr. And*	*Egr. And*	*Egr. And*
Phenocryst no	8	9	9	10	10	11	11	12	13	13	14	14
(c)ore/(r)im	**r**	**c**	**r**	**r**	**c**	**r**	**c**	**c**	**c**	**r**	**c**	**r**
SiO_2	52.30	52.50	52.70	53.21	53.12	53.72	52.68	53.04	55.46	54.86	55.67	54.43
TiO_2	0.14	0.12	0.11	0.17	0.15	0.18	0.25	0.30	0.13	0.12	0.12	0.11
Al_2O_3	0.63	0.60	0.73	0.60	0.88	0.91	1.31	1.39	2.38	2.40	2.23	2.39
Fe_2O_3	20.65	20.22	20.46	20.40	20.93	18.09	20.09	17.32	8.31	8.50	8.45	8.27
MnO	0.95	1.24	1.32	1.26	1.17	0.80	0.80	0.51	0.19	0.13	0.15	0.21
MgO	23.53	22.93	22.98	22.56	22.02	24.10	22.52	24.21	31.98	32.10	31.20	31.64
CaO	0.94	0.94	0.85	1.21	1.23	1.38	1.56	1.63	1.04	1.12	1.16	1.10
Total	**99.14**	**98.54**	**99.15**	**99.40**	**99.50**	**99.19**	**99.21**	**98.39**	**99.49**	**99.23**	**98.98**	**98.15**
O = 6												
Si	1.96	1.98	1.97	1.98	1.98	1.98	1.97	1.97	1.94	1.93	1.96	1.94
Ti	0.00	0.00	0.01	0.00	0.00	0.00	0.01	0.00	0.00	0.00	0.00	0.00
Al	0.03	0.03	0.06	0.03	0.04	0.04	0.06	0.05	0.10	0.10	0.09	0.10
Fe	0.65	0.64	0.63	0.64	0.65	0.56	0.63	0.62	0.24	0.25	0.25	0.25
Mn	0.03	0.04	0.03	0.04	0.04	0.03	0.03	0.04	0.01	0.00	0.00	0.01
Mg	1.31	1.29	1.25	1.25	1.23	1.33	1.25	1.25	1.67	1.68	1.64	1.68
Ca	0.04	0.04	0.06	0.05	0.05	0.05	0.06	0.05	0.04	0.04	0.04	0.04
Total	**4.02**	**4.01**	**4.00**	**4.00**	**3.99**	**3.99**	**4.00**	**3.99**	**4.00**	**4.02**	**3.99**	**4.01**
En	65.95	66.07	66.07	62.54	63.35	68.33	64.71	68.75	85.15	85.15	85.15	85.15
Fs	32.01	31.92	31.92	35.03	34.19	28.94	32.18	27.82	12.84	12.84	12.84	12.84
Wo	2.04	2.01	2.01	2.43	2.45	2.73	3.11	3.38	2.02	2.02	2.02	2.02

PLAGIOCLASES

Sample no	EA409	EA409	EA409	EA409	EA409	EA409	EA309	EA309	EA348	EA348	EA109	EA109	EA143	EA143	EA143
Unit	*Foc. Dyke*	*Foc. Dyke*	*Foc. Dyke*	*Foc. Dyke*	*Foc. Dyke*	*Foc. Dyke*	*Foc. Dyke*	*Foc. Dyke*	*Foc. Dyke*	*Foc. Dyke*	*Neb. Vol.*	*Neb. Vol.*	*Neb. Vol.*	*Neb. Vol.*	*Neb. Vol.*
Phenocryst no	1	1	2	2	3	3	4	4	5	5	6	6	7	7	8
(c)ore/(r)im/ (g)roundmass	c	r	c	r	c	r	c	r	c	r	c	r	c	r	c
SiO_2	45.67	46.83	45.06	50.43	46.37	46.87	44.66	47.28	48.56	52.83	52.39	58.89	50.17	53.01	51.63
TiO_2	0.05	0.05	0.04	0.05	0.03	0.05	0.08	0.01	0.00	0.09	0.10	0.09	0.05	0.11	0.08
Al_2O_3	33.58	32.80	33.76	30.89	33.44	32.88	33.91	32.03	30.96	27.97	29.01	23.86	29.90	28.03	28.67
Fe_2O_3	0.61	0.58	0.61	0.47	0.48	0.54	0.58	0.60	0.84	1.07	0.42	1.17	0.51	0.58	0.52
CaO	17.57	16.71	17.86	13.90	17.15	16.62	18.19	16.04	15.11	11.71	12.05	5.60	13.74	11.39	12.47
Na_2O	1.50	1.99	1.27	3.52	1.68	2.07	1.13	2.40	2.85	4.66	4.34	6.08	3.45	4.59	4.18
K_2O	0.06	0.10	0.08	0.20	0.08	0.10	0.10	0.17	0.22	0.31	0.31	1.68	0.45	0.72	0.52
Total	**99.02**	**99.07**	**98.67**	**99.44**	**99.23**	**99.13**	**98.65**	**98.53**	**98.54**	**98.64**	**98.62**	**97.37**	**98.26**	**98.43**	**98.06**
O = 8															
Si	2.12	2.16	2.10	2.30	2.14	2.16	2.09	2.20	2.26	2.43	2.41	2.69	2.33	2.44	2.40
Ti	0.00	0.00	0.00	0.00	0.00	0.00	0.00	0.00	0.00	0.00	0.00	0.00	0.00	0.00	0.00
Al	1.83	1.79	1.85	1.66	1.82	1.79	1.87	1.76	1.70	1.52	1.57	1.29	1.64	1.52	1.57
Fe	0.05	0.04	0.05	0.04	0.04	0.04	0.02	0.02	0.03	0.04	0.02	0.05	0.02	0.02	0.02
Ca	0.87	0.83	0.89	0.68	0.85	0.82	0.91	0.80	0.75	0.58	0.59	0.28	0.68	0.56	0.62
Na	0.13	0.18	0.11	0.31	0.15	0.19	0.10	0.22	0.26	0.42	0.39	0.54	0.31	0.41	0.38
K	0.00	0.01	0.00	0.01	0.00	0.01	0.01	0.01	0.01	0.02	0.02	0.10	0.03	0.04	0.03
Total	**5.01**	**5.01**	**5.01**	**5.00**	**5.00**	**5.01**	**5.01**	**5.01**	**5.00**	**5.00**	**5.00**	**4.94**	**5.01**	**5.01**	**5.01**
An	86.36	81.77	88.19	67.81	84.56	81.14	89.33	77.92	73.58	57.07	59.42	30.15	67.03	55.42	60.37
Ab	13.32	17.65	11.35	31.05	14.99	18.31	10.08	21.11	25.15	41.15	38.78	59.10	30.42	40.43	36.61
Or	0.33	0.58	0.46	1.14	0.45	0.55	0.59	0.97	1.27	1.78	1.80	10.75	2.55	4.14	3.02

Sample no	EA143	EA143	EA143	EA101	EA101	EA101	EA101	EA313	EA313	EA313	EA313	EA313	EA313	EA313	EA313
Unit	*Neb. Vol.*	*Neb. Vol.*	*Neb. Vol.*	*Oda. Dyke*	*Oda. Dyke*	*Oda. Dyke*	*Oda. Dyke*	*Egr. And*	*Egr. And*	*Egr. And*	*Egr. And*	*Egr. And*	*Egr. And*	*Egr. And*	*Egr. And*
Phenocryst no	8	9	9	10	10	11	11	12	12	13	13	14	14	15	15
(c)ore/(r)im/ (g)roundmass	r	c	r	c	r	c	r	c	r	c	r	c	r	c	r
SiO_2	51.15	52.12	52.91	48.63	50.96	45.91	50.10	50.85	51.79	51.10	48.66	48.20	51.66	50.70	51.71
TiO_2	0.09	0.10	0.09	0.04	0.10	0.03	0.04	0.06	0.06	0.04	0.03	0.02	0.04	0.03	0.05
Al_2O_3	29.40	29.12	28.35	31.02	29.22	32.87	30.02	30.08	29.44	30.03	31.90	32.19	29.81	29.83	29.51
Fe_2O_3	0.52	0.47	0.61	0.51	0.62	0.50	0.51	0.67	0.73	0.67	0.49	0.49	0.59	0.75	0.60
CaO	13.01	12.29	11.80	14.88	13.04	16.87	13.66	13.57	12.97	13.48	15.31	15.84	13.10	13.39	12.93
Na_2O	3.75	3.68	4.18	2.83	3.63	1.72	3.38	3.63	3.99	3.66	2.66	2.41	3.93	3.61	3.90
K_2O	0.52	0.65	0.59	0.31	0.52	0.16	0.40	0.29	0.40	0.28	0.16	0.13	0.33	0.31	0.31
Total	**98.43**	**98.42**	**98.55**	**98.21**	**98.07**	**98.06**	**98.09**	**99.14**	**99.37**	**99.25**	**99.22**	**99.27**	**99.46**	**98.62**	**99.00**
O = 8															
Si	2.37	2.40	2.43	2.27	2.37	2.16	2.33	2.32	2.36	2.33	2.23	2.21	2.35	2.33	2.36
Ti	0.00	0.00	0.00	0.00	0.00	0.00	0.00	0.00	0.00	0.00	0.00	0.00	0.00	0.00	0.00
Al	1.60	1.58	1.54	1.70	1.60	1.82	1.64	1.62	1.58	1.61	1.73	1.74	1.60	1.61	1.59
Fe	0.02	0.02	0.02	0.02	0.02	0.02	0.02	0.05	0.06	0.05	0.04	0.04	0.05	0.06	0.05
Ca	0.64	0.61	0.58	0.74	0.65	0.85	0.68	0.66	0.63	0.66	0.75	0.78	0.64	0.66	0.63
Na	0.34	0.33	0.37	0.26	0.33	0.16	0.30	0.32	0.35	0.32	0.24	0.21	0.35	0.32	0.35
K	0.03	0.04	0.04	0.02	0.03	0.01	0.02	0.02	0.02	0.02	0.01	0.01	0.02	0.02	0.02
Total	**5.00**	**4.98**	**4.99**	**5.01**	**5.00**	**5.01**	**5.00**	**5.00**	**5.00**	**5.00**	**5.00**	**5.00**	**5.00**	**5.00**	**4.99**
An	63.70	62.32	58.79	73.13	64.51	83.65	67.46	66.26	62.77	65.96	75.35	77.80	63.57	66.01	63.55
Ab	33.23	33.78	37.68	25.10	32.41	15.37	30.16	32.07	34.95	32.41	23.69	21.44	34.54	32.19	34.66
Or	3.07	3.90	3.54	1.77	3.08	0.99	2.38	1.67	2.28	1.63	0.96	0.75	1.89	1.81	1.78

Sample no	EA112	EA112	EA316	EA316	EA316	EA316	EA316	EA316	EA316	EA316	EA326	EA326	EA326	EA326	EA326
Unit	*Egr. And*	*Egr. And*	*Klg. And*	*Klg. And*	*Klg. And*	*Klg. And*	*Klg. And*	*Klg. And*	*Klg. And*	*Klg. And*	*Mt.Sey. U.*	*Mt.Sey. U.*	*Mt.Sey. U.*	*Mt.Sey. U.*	*Mt.Sey. U.*
Phenocryst no	16	16	17	17	18	18	19	19	20	20	21	21	22	22	23
(c)ore/(r)im/ (g)roundmass	c	r	c	r	c	r	c	r	c	r	c	r	c	r	c
SiO_2	48.22	55.89	59.03	58.42	58.46	57.84	59.80	53.98	57.37	52.62	58.97	57.07	57.61	58.46	57.77
TiO_2	0.05	0.05	0.03	0.02	0.03	0.02	0.02	0.03	0.01	0.05	0.02	0.02	0.02	0.01	0.03
Al_2O_3	31.29	26.48	25.23	25.58	25.40	25.90	24.91	28.39	26.24	28.42	25.29	25.95	25.86	25.47	25.71
Fe_2O_3	0.45	0.45	0.23	0.30	0.25	0.29	0.26	0.25	0.23	1.27	0.24	0.27	0.25	0.26	0.28
CaO	15.26	9.22	7.45	7.80	7.72	8.25	6.97	11.19	8.59	12.26	7.50	8.42	8.19	7.67	8.04
Na_2O	2.72	5.49	6.85	6.39	6.34	6.18	6.67	5.00	6.29	4.05	6.88	6.30	6.41	6.60	6.42
K_2O	0.22	0.85	0.76	0.69	0.72	0.64	0.85	0.31	0.55	0.32	0.75	0.61	0.63	0.72	0.64
Total	**98.21**	**98.43**	**99.57**	**99.22**	**98.93**	**99.12**	**99.47**	**99.15**	**99.28**	**98.99**	**99.65**	**98.63**	**98.97**	**99.19**	**98.89**
O = 8															
Si	2.25	2.56	2.65	2.63	2.64	2.61	2.67	2.45	2.59	2.37	2.64	2.59	2.60	2.63	2.61
Ti	0.00	0.00	0.00	0.00	0.00	0.00	0.00	0.00	0.00	0.00	0.00	0.00	0.00	0.00	0.00
Al	1.72	1.43	1.33	1.36	1.35	1.38	1.31	1.52	1.39	1.51	1.34	1.39	1.38	1.35	1.37
Fe	0.02	0.02	0.02	0.02	0.02	0.02	0.02	0.02	0.02	0.10	0.02	0.02	0.02	0.02	0.02
Ca	0.76	0.45	0.36	0.38	0.37	0.40	0.33	0.55	0.41	0.59	0.36	0.41	0.40	0.37	0.39
Na	0.25	0.49	0.60	0.56	0.55	0.54	0.58	0.44	0.55	0.35	0.60	0.55	0.56	0.58	0.56
K	0.01	0.05	0.04	0.04	0.04	0.04	0.05	0.02	0.03	0.02	0.04	0.04	0.04	0.04	0.04
Total	**5.01**	**4.99**	**4.99**	**4.98**	**4.97**	**4.98**	**4.97**	**5.00**	**5.00**	**4.94**	**5.00**	**5.00**	**4.99**	**4.99**	**4.99**
An	74.66	45.70	35.90	38.64	38.51	40.86	34.77	54.31	41.63	61.40	35.98	40.98	39.87	37.47	39.35
Ab	24.07	49.24	59.74	57.28	57.22	55.38	60.21	43.88	55.19	36.69	59.76	55.49	56.47	58.37	56.90
Or	1.27	5.06	4.35	4.09	4.27	3.76	5.02	1.81	3.18	1.91	4.27	3.53	3.66	4.16	3.75

Sample no	EA326	EA99	EA99	EA364	EA364	EA364	EA364	94EA147	94EA147	94EA147	94EA147	94EA147	94EA147	94EA147	94EA147
Unit	*Mt.Sey. U.*	*Bal. Unit*	*Bal. Unit*	*Krg. Unit*	*Krg. Unit*	*Krg. Unit*	*Krg. Unit*	*Akc. Unit*	*Akc. Unit*	*Akc. Unit*	*Akc. Unit*	*Akc. Unit*	*Akc. Unit*	*Akc. Unit*	*Akc. Unit*
Phenocryst no	23	24	24	25	25	26	26	27	27	28	28	29	29	30	30
(c)ore/(r)im/ (g)groundmass	r	c	r	c	r	c	r	c	r	c	r	c	r	c	r
SiO_2	57.71	54.39	52.68	57.33	59.23	57.16	57.51	55.91	57.29	57.84	56.81	58.15	58.81	55.18	59.13
TiO_2	0.01	0.03	0.04	0.03	0.00	0.01	0.02	0.02	0.03	0.03	0.03	0.03	0.03	0.02	0.04
Al_2O_3	26.05	27.79	28.60	25.84	24.80	26.03	25.85	26.63	25.62	25.53	26.03	25.42	24.71	27.19	24.74
Fe_2O_3	0.34	0.42	0.52	0.24	0.28	0.31	0.31	0.26	0.30	0.26	0.26	0.26	0.24	0.26	0.27
CaO	8.35	10.68	11.79	8.21	6.99	8.57	8.24	9.14	7.94	7.89	8.49	7.83	7.03	9.62	6.94
Na_2O	6.38	5.32	4.65	6.57	7.14	6.30	6.52	5.94	6.63	6.62	6.14	6.73	7.02	5.78	7.02
K_2O	0.60	0.31	0.24	0.51	0.68	0.55	0.61	0.48	0.61	0.66	0.69	0.68	0.78	0.47	0.81
Total	**99.44**	**98.94**	**98.52**	**98.73**	**99.12**	**98.93**	**99.06**	**98.38**	**98.42**	**98.82**	**98.46**	**99.09**	**98.62**	**98.51**	**98.96**
O = 8															
Si	2.59	2.48	2.42	2.60	2.67	2.59	2.60	2.56	2.61	2.62	2.59	2.63	2.67	2.52	2.67
Ti	0.00	0.00	0.00	0.00	0.00	0.00	0.00	0.00	0.00	0.00	0.00	0.00	0.00	0.00	0.00
Al	1.38	1.50	1.55	1.38	1.32	1.39	1.38	1.43	1.38	1.36	1.40	1.36	1.32	1.47	1.32
Fe	0.03	0.01	0.02	0.01	0.01	0.01	0.01	0.01	0.01	0.01	0.01	0.01	0.01	0.01	0.01
Ca	0.40	0.52	0.58	0.40	0.34	0.42	0.40	0.45	0.39	0.38	0.42	0.38	0.34	0.47	0.34
Na	0.56	0.47	0.41	0.58	0.62	0.55	0.57	0.53	0.59	0.58	0.54	0.59	0.62	0.51	0.62
K	0.03	0.02	0.01	0.03	0.04	0.03	0.04	0.03	0.04	0.04	0.04	0.04	0.05	0.03	0.05
Total	**4.99**	**5.00**	**5.00**	**5.00**	**5.00**	**5.00**	**5.00**	**5.00**	**5.01**	**5.00**	**5.00**	**5.00**	**5.00**	**5.01**	**5.00**
An	40.51	51.63	57.58	39.64	33.70	41.52	39.72	44.66	38.35	38.19	41.58	37.60	34.00	46.63	33.67
Ab	56.01	46.59	41.03	57.38	62.40	55.29	56.80	52.55	58.08	58.03	54.41	58.53	61.52	50.69	61.62
Or	3.48	1.78	1.39	2.97	3.90	3.19	3.48	2.80	3.57	3.79	4.01	3.87	4.49	2.67	4.71

Sample no	94EA147	94EA147	94EA147	94EA147	EA45	EA45	EA45	EA45	EA45	EA45	EA412	EA412	EA412	EA412	EA412
Unit	*Akc. Unit*	*Akc. Unit*	*Akc. Unit*	*Akc. Unit*	*Kov. Dyke*	*Kov. Dyke*	*Kov. Dyke*	*Kov. Dyke*	*Kov. Dyke*	*Kov. Dyke*	*Kov. Dyke*	*Kov. Dyke*	*Kov. Dyke*	*Kov. Dyke*	*Kov. Dyke*
Phenocryst no	31	31	32	32	33	33	34	34	35	35	36	36	37	37	38
(c)ore/(r)im/ (g)roundmass	c	r	c	r	c	r	c	r	c	r	c	r	c	r	c
SiO_2	54.77	57.25	54.53	58.41	54.70	54.04	53.11	51.41	53.74	54.28	50.32	51.91	52.13	52.36	52.07
TiO_2	0.04	0.03	0.04	0.02	0.09	0.07	0.06	0.07	0.06	0.04	0.05	0.07	0.10	0.07	0.07
Al_2O_3	26.90	26.09	27.66	25.08	27.11	27.50	27.87	28.95	27.65	27.24	29.82	29.09	29.30	27.56	29.22
Fe_2O_3	0.58	0.30	0.41	0.24	0.64	0.64	0.65	0.66	0.57	0.52	0.61	0.67	0.63	0.81	0.59
CaO	10.17	8.57	10.58	7.45	10.31	10.91	11.53	12.71	11.01	10.57	13.57	12.62	12.70	11.40	12.90
Na_2O	4.27	6.31	5.36	6.91	4.99	4.68	4.37	3.88	4.73	4.90	3.56	4.10	3.98	4.52	3.97
K_2O	1.29	0.57	0.38	0.74	0.70	0.62	0.50	0.41	0.62	0.69	0.33	0.44	0.44	0.53	0.41
Total	**98.01**	**99.12**	**98.97**	**98.86**	**98.54**	**98.45**	**98.08**	**98.08**	**98.38**	**98.24**	**98.25**	**98.89**	**99.27**	**97.26**	**99.23**
O = 8															
Si	2.52	2.59	2.49	2.65	2.51	2.48	2.45	2.39	2.47	2.50	2.32	2.37	2.37	2.42	2.37
Ti	0.00	0.00	0.00	0.00	0.00	0.00	0.00	0.00	0.00	0.00	0.00	0.00	0.00	0.00	0.00
Al	1.46	1.39	1.49	1.34	1.47	1.49	1.52	1.58	1.50	1.48	1.62	1.57	1.57	1.50	1.57
Fe	0.02	0.01	0.02	0.01	0.02	0.03	0.03	0.03	0.02	0.02	0.05	0.05	0.05	0.06	0.05
Ca	0.50	0.42	0.52	0.36	0.51	0.54	0.57	0.63	0.54	0.52	0.67	0.62	0.62	0.56	0.63
Na	0.38	0.55	0.48	0.61	0.44	0.42	0.39	0.35	0.42	0.44	0.32	0.36	0.35	0.41	0.35
K	0.08	0.03	0.02	0.04	0.04	0.04	0.03	0.02	0.04	0.04	0.02	0.03	0.03	0.03	0.02
Total	**4.97**	**5.00**	**5.01**	**5.01**	**4.99**	**4.99**	**4.99**	**5.00**	**5.00**	**5.00**	**5.00**	**5.00**	**4.99**	**4.99**	**4.99**
An	52.29	41.48	51.03	35.77	51.11	54.24	57.62	62.89	54.25	52.15	66.49	61.34	62.20	56.40	62.71
Ab	39.79	55.23	46.80	59.98	44.76	42.12	39.46	34.73	42.16	43.74	31.56	36.10	35.26	40.47	34.95
Or	7.92	3.29	2.17	4.25	4.13	3.64	2.93	2.39	3.60	4.10	1.95	2.56	2.54	3.13	2.34

Sample no	EA412	EA76	EA76	EA73	EA73	EAR1	EAR1	EA37	EA37	EA275	EA275	EA275	EA275	EA62	EA62
Unit	*Kov. Dyke*	*Kov. Dyke*	*Kov. Dyke*	*Cice. And.*	*Cice. And.*	*Ded. Unit*	*Ded. Unit*	*Behr. And.*	*Behr. And.*	*Behr. And.*	*Behr. And.*	*Behr. And.*	*Behr. And.*	*Bak. Unit*	*Bak. Unit*
Phenocryst no	38	39	39	40	40	41	41	42	42	43	43	44	44	45	45
(c)ore/(r)im/ (g)roundmass	r	c	r	c	r	c	*r*	c	r	c	r	c	c	c	r
SiO_2	55.19	52.06	54.25	54.56	53.04	58.52	58.23	57.85	59.01	53.98	58.36	54.74	57.87	59.65	58.71
TiO_2	0.08	0.06	0.08	0.03	0.02	0.03	0.02	0.02	0.03	0.03	0.05	0.03	0.04	0.03	0.04
Al_2O_3	27.32	29.17	27.11	27.12	28.24	24.95	25.11	25.30	24.75	28.26	25.10	27.75	26.04	25.22	25.33
Fe_2O_3	0.51	0.57	0.68	0.60	0.57	0.32	0.35	0.35	0.33	0.44	0.47	0.42	0.17	0.32	0.32
CaO	10.12	12.31	10.00	10.06	11.19	7.34	7.43	7.73	6.92	11.16	7.74	10.72	7.92	7.20	7.25
Na_2O	5.01	3.97	4.52	5.22	4.76	6.57	6.58	6.15	6.66	4.68	6.19	4.97	6.32	6.73	6.19
K_2O	0.94	0.63	1.59	0.83	0.66	0.91	0.81	0.81	0.97	0.53	1.29	0.62	0.75	0.91	0.91
Total	**99.17**	**98.77**	**98.23**	**98.42**	**98.48**	**98.63**	**98.53**	**98.22**	**98.67**	**99.07**	**99.19**	**99.25**	**99.10**	**100.05**	**98.75**
O = 8															
Si	2.50	2.38	2.49	2.50	2.44	2.66	2.65	2.64	2.67	2.45	2.63	2.48	2.61	2.66	2.65
Ti	0.00	0.00	0.00	0.00	0.00	0.00	0.00	0.00	0.00	0.00	0.00	0.00	0.00	0.00	0.00
Al	1.46	1.57	1.46	1.47	1.53	1.33	1.34	1.36	1.32	1.51	1.33	1.48	1.38	1.32	1.35
Fe	0.04	0.04	0.05	0.02	0.02	0.01	0.01	0.01	0.01	0.03	0.04	0.03	0.01	0.02	0.02
Ca	0.49	0.60	0.49	0.50	0.55	0.36	0.36	0.38	0.34	0.54	0.37	0.52	0.38	0.34	0.35
Na	0.44	0.35	0.40	0.47	0.43	0.58	0.58	0.54	0.59	0.41	0.54	0.44	0.55	0.58	0.54
K	0.05	0.04	0.09	0.05	0.04	0.05	0.05	0.05	0.06	0.03	0.07	0.04	0.04	0.05	0.05
Total	**4.99**	**4.99**	**4.99**	**5.00**	**5.01**	**4.99**	**4.99**	**4.98**	**4.98**	**4.99**	**4.99**	**4.99**	**4.99**	**4.98**	**4.96**
An	49.85	60.80	49.82	49.06	54.33	36.13	36.60	38.95	34.39	55.11	37.82	52.39	39.11	35.19	37.11
Ab	44.66	35.51	40.74	46.09	41.83	58.50	58.65	56.20	59.88	41.80	54.69	43.99	56.48	59.53	57.34
Or	5.49	3.69	9.44	4.86	3.84	5.36	4.75	4.86	5.73	3.09	7.49	3.61	4.41	5.28	5.55

Sample no	EA273	EA273	EA231	EA231	EA256	EA256	EA256	EA256	EA256	EA256	EA415	EA415	EA409	EA409	94EA143
Unit	*Bad. Unit*	*Bad. Unit*	*Bad. Unit*	*Bad. Unit*	*Tas. Vol.*	*Tas. Vol.*	*Tas. Vol.*	*Tas. Vol.*	*Tas. Vol.*	*Tas. Vol.*	*Ezn. Vol.*	*Ezn. Vol.*	*Foc. Dyke*	*Foc. Dyke*	*Neb. Vol.*
Phenocryst no	46	46	47	47	48	49	50	51	52	53	54	55	56	57	58
(c)ore/(r)im/ (g)roundmass	c	r	c	r	g	g	g	g	g	g	g	g	g	g	g
SiO_2	53.51	52.41	53.08	53.20	53.99	56.77	53.53	52.41	51.81	54.31	53.70	51.40	49.60	49.52	51.10
TiO_2	0.04	0.06	0.03	0.05	0.19	0.15	0.19	0.15	0.18	0.19	0.34	0.06	0.05	0.06	0.08
Al_2O_3	27.50	28.27	27.99	28.08	28.22	26.74	28.20	28.74	28.94	27.81	27.79	29.21	30.30	30.35	29.55
Fe_2O_3	0.55	0.61	0.58	0.64	0.59	0.48	0.80	0.72	0.85	0.67	0.86	0.86	1.20	1.02	0.56
CaO	10.69	11.75	11.20	11.24	10.79	8.64	11.09	11.90	12.26	10.51	9.94	12.70	14.19	14.26	13.28
Na_2O	4.98	4.33	4.60	4.63	5.18	6.27	5.11	4.67	4.39	4.95	4.50	4.18	3.27	3.32	3.73
K_2O	0.74	0.61	0.70	0.68	0.21	0.38	0.33	0.24	0.27	0.35	1.14	0.22	0.18	0.18	0.49
Total	**98.01**	**98.04**	**98.18**	**98.52**	**99.17**	**99.44**	**99.25**	**98.83**	**98.70**	**98.79**	**98.27**	**98.63**	**98.79**	**98.71**	**98.77**
O = 8															
Si	2.47	2.42	2.45	2.45	2.45	2.55	2.44	2.41	2.39	2.48	2.45	2.37	2.30	2.30	2.36
Ti	0.00	0.00	0.00	0.00	0.01	0.01	0.01	0.01	0.01	0.01	0.01	0.00	0.00	0.00	0.00
Al	1.50	1.54	1.52	1.52	1.51	1.42	1.52	1.56	1.57	1.50	1.50	1.59	1.65	1.66	1.61
Fe	0.02	0.02	0.02	0.02	0.04	0.04	0.03	0.03	0.03	0.03	0.07	0.03	0.04	0.04	0.02
Ca	0.53	0.58	0.55	0.55	0.52	0.42	0.54	0.59	0.61	0.51	0.49	0.63	0.70	0.71	0.66
Na	0.45	0.39	0.41	0.41	0.46	0.55	0.45	0.42	0.39	0.44	0.40	0.37	0.29	0.30	0.33
K	0.04	0.04	0.04	0.04	0.01	0.02	0.02	0.01	0.02	0.02	0.07	0.01	0.01	0.01	0.03
Total	**5.01**	**5.00**	**5.00**	**5.00**	**5.00**	**5.00**	**5.00**	**5.01**	**5.00**	**4.98**	**4.98**	**5.01**	**5.00**	**5.01**	**5.01**
An	51.91	57.89	55.01	55.07	52.84	42.27	53.50	57.64	59.72	52.88	51.11	61.87	69.84	69.62	64.44
Ab	43.77	38.53	40.91	40.95	45.92	55.50	44.62	40.99	38.70	45.06	41.89	36.85	29.07	29.30	32.71
Or	4.32	3.57	4.07	3.98	1.24	2.23	1.88	1.38	1.58	2.06	7.00	1.28	1.09	1.08	2.85

Sample no	94EA143	EA134	EA134	EA134	EA134	EA101	EA313	EA313	EA364	EA418	EA418	EA45	EA412	EA412	EA326
Unit	*Neb. Vol.*	*Neb. Vol.*	*Neb. Vol.*	*Neb. Vol.*	*Neb. Vol.*	*Oda. Dyke*	*Egr. And*	*Egr. And*	*Krg. Unit*	*Kov. Dyke*	*Kov. Dyke*	*Kov. Dyke*	*Kov. Dyke*	*Kov. Dyke*	*Mt.Sey. U.*
Phenocryst no	59	60	61	62	63	64	65	66	67	68	69	70	71	72	73
(c)ore/(r)im/ (g)roundmass	g	g	g	g	g	g	g	g	g	g	g	g	g	g	g
SiO_2	51.93	48.47	49.13	48.78	48.25	52.89	50.70	50.57	54.77	50.71	50.76	52.68	52.15	52.56	57.65
TiO_2	0.09	0.07	0.07	0.06	0.05	0.10	0.03	0.05	0.04	0.06	0.03	0.05	0.07	0.10	0.01
Al_2O_3	28.97	31.08	30.87	31.14	31.39	27.55	29.83	29.64	27.64	29.50	29.55	28.02	29.46	28.67	26.06
Fe_2O_3	0.51	1.12	1.15	1.10	1.02	0.89	0.75	0.79	0.45	0.71	0.83	0.79	0.58	0.71	0.24
CaO	12.47	15.01	14.75	14.89	15.25	11.34	13.39	13.41	10.34	13.16	13.25	11.59	12.71	12.00	8.36
Na_2O	4.00	2.67	2.97	2.80	2.68	4.33	3.61	3.79	5.45	3.49	3.71	4.46	3.94	4.21	6.51
K_2O	0.60	0.22	0.21	0.22	0.19	0.76	0.31	0.23	0.40	0.39	0.37	0.52	0.45	0.50	0.58
Total	**98.56**	**98.64**	**99.15**	**98.98**	**98.83**	**97.86**	**98.62**	**98.48**	**99.09**	**98.02**	**98.50**	**98.11**	**99.36**	**98.75**	**99.41**
O = 8															
Si	2.39	2.23	2.25	2.24	2.22	2.45	2.33	2.34	2.49	2.36	2.35	2.44	2.37	2.40	2.59
Ti	0.00	0.00	0.00	0.00	0.00	0.00	0.00	0.00	0.00	0.00	0.00	0.00	0.00	0.00	0.00
Al	1.57	1.68	1.67	1.68	1.70	1.51	1.61	1.62	1.48	1.62	1.61	1.53	1.58	1.54	1.38
Fe	0.02	0.09	0.09	0.08	0.08	0.03	0.06	0.03	0.02	0.03	0.03	0.03	0.04	0.05	0.02
Ca	0.62	0.74	0.72	0.73	0.75	0.56	0.66	0.67	0.51	0.66	0.66	0.58	0.62	0.59	0.40
Na	0.36	0.24	0.26	0.25	0.24	0.39	0.32	0.34	0.48	0.32	0.33	0.40	0.35	0.37	0.57
K	0.04	0.01	0.01	0.01	0.01	0.05	0.02	0.01	0.02	0.02	0.02	0.03	0.03	0.03	0.03
Total	**5.00**	**4.99**	**5.00**	**5.00**	**5.01**	**5.00**	**5.00**	**5.01**	**5.00**	**4.99**	**5.00**	**5.01**	**4.99**	**4.99**	**5.00**
An	61.11	74.69	72.40	73.63	75.01	56.46	66.01	65.32	50.05	65.96	64.95	57.16	62.36	59.37	40.11
Ab	35.42	24.02	26.40	25.08	23.87	39.04	32.19	33.40	47.67	31.72	32.87	39.76	34.99	37.70	56.56
Or	3.47	1.29	1.20	1.29	1.12	4.50	1.81	1.28	2.28	2.32	2.18	3.08	2.65	2.94	3.33

Sample no	EA275	EA275	EA275	EA275	EA275
Unit	*Behr. And.*	*Behr. And.*	*Behr. And.*	*Behr. And.*	*Behr. And.*
Phenocryst no	74	75	76	77	78
(c)ore/(r)im/ (g)roundmass	g	g	g	g	g
SiO_2	55.08	55.44	52.68	53.78	55.69
TiO_2	0.04	0.04	0.06	0.06	0.05
Al_2O_3	27.60	27.47	29.31	28.65	27.00
Fe_2O_3	0.44	0.43	0.57	0.61	0.40
CaO	10.38	10.23	12.41	11.61	9.91
Na_2O	5.17	5.21	4.22	4.69	5.28
K_2O	0.67	0.69	0.42	0.49	0.69
Total	**99.38**	**99.50**	**99.66**	**99.89**	**99.02**
O = 8					
Si	2.49	2.50	2.39	2.43	2.52
Ti	0.00	0.00	0.00	0.00	0.00
Al	1.47	1.46	1.57	1.52	1.44
Fe	0.03	0.03	0.04	0.05	0.03
Ca	0.50	0.50	0.60	0.56	0.48
Na	0.45	0.46	0.37	0.41	0.46
K	0.04	0.04	0.02	0.03	0.04
Total	**4.99**	**4.99**	**5.00**	**5.00**	**4.99**
An	50.57	49.99	60.41	56.14	48.86
Ab	45.54	46.03	37.16	41.03	47.11
Or	3.89	3.98	2.43	2.83	4.03

AMPHIBOLES

Sample no	EA147	EA147	EA147	EA147	EA99	EA99	EA99	EA99	EA364	EA364	EA364	EA364	EA316	EA316	EA316	EA316
Unit	*Akc. Unit*	*Akc. Unit*	*Akc. Unit*	*Akc. Unit*	*Bal. Unit*	*Bal. Unit*	*Bal. Unit*	*Bal. Unit*	*Krg. Unit*	*Krg. Unit*	*Krg. Unit*	*Krg. Unit*	*Klg. And*	*Klg. And*	*Klg. And*	*Klg. And*
Phenocryst no	1	2	3	4	5	6	7	8	9	10	11	12	13	14	15	16
SiO_2	45.52	45.36	45.58	44.68	45.47	44.39	44.45	45.47	38.42	47.23	42.50	41.49	45.16	45.28	46.38	41.80
TiO_2	1.50	1.57	1.52	1.61	1.36	1.16	1.35	1.27	2.64	1.07	2.32	2.49	1.49	1.51	1.40	1.93
Al_2O_3	7.46	7.57	7.64	7.86	7.49	8.19	8.31	7.44	13.52	6.13	10.85	11.47	7.84	7.76	7.26	12.14
Fe_2O_3	13.14	13.20	13.36	13.51	14.01	15.55	15.61	15.48	13.46	13.47	10.98	11.11	14.24	14.37	13.55	11.96
MnO	0.38	0.41	0.37	0.33	0.40	0.41	0.44	0.41	0.19	0.43	0.17	0.17	0.43	0.44	0.43	0.17
MgO	13.79	13.90	13.83	13.18	13.66	12.64	12.53	12.73	11.86	14.31	14.64	14.26	13.32	13.14	13.90	13.90
CaO	11.43	11.46	11.36	11.40	11.60	11.68	11.75	11.68	11.94	11.74	11.49	11.57	11.54	11.46	11.59	11.28
Na_2O	1.48	1.55	1.54	1.49	1.35	1.40	1.52	1.39	1.96	1.13	2.02	2.02	1.47	1.44	1.37	2.26
K_2O	0.68	0.72	0.74	0.82	0.75	1.00	0.96	0.81	2.01	0.60	1.06	1.11	0.83	0.80	0.68	0.78
Total	**95.41**	**95.77**	**95.95**	**94.89**	**96.12**	**96.45**	**96.95**	**96.77**	**96.05**	**96.15**	**96.09**	**95.76**	**96.32**	**96.19**	**96.61**	**96.23**
Si	6.87	6.83	6.84	6.80	6.84	6.73	6.71	6.85	5.90	7.05	6.35	6.24	6.79	6.82	6.91	6.26
Ti	0.17	0.18	0.17	0.18	0.15	0.13	0.15	0.14	0.30	0.12	0.26	0.28	0.17	0.17	0.16	0.22
Al	1.33	1.34	1.35	1.41	1.33	1.46	1.48	1.32	2.45	1.08	1.91	2.03	1.39	1.38	1.28	2.14
Fe	1.66	1.66	1.68	1.72	1.76	1.97	1.97	1.95	1.73	1.68	1.37	1.40	1.79	1.81	1.69	1.50
Mn	0.05	0.05	0.05	0.04	0.05	0.05	0.06	0.05	0.02	0.05	0.02	0.02	0.05	0.06	0.05	0.02
Mg	3.10	3.12	3.09	2.99	3.06	2.86	2.82	2.86	2.71	3.19	3.26	3.20	2.99	2.95	3.09	3.10
Ca	1.85	1.85	1.83	1.86	1.87	1.90	1.90	1.89	1.96	1.88	1.84	1.86	1.86	1.85	1.85	1.81
Na	0.43	0.45	0.45	0.44	0.39	0.41	0.44	0.41	0.58	0.33	0.59	0.59	0.43	0.42	0.40	0.66
K	0.13	0.14	0.14	0.16	0.14	0.19	0.18	0.16	0.39	0.12	0.20	0.21	0.16	0.15	0.13	0.15
Total	**15.58**	**15.62**	**15.60**	**15.61**	**15.61**	**15.71**	**15.71**	**15.63**	**16.06**	**15.50**	**15.82**	**15.85**	**15.64**	**15.61**	**15.56**	**15.86**

Sample no	EA326	EA326	EA326	EA326	EA326	EA112	EA112	EA113	EA113	EA113	EA231	EA231	EA273	EA273
Unit	*Mt.Sey. U.*	*Mt.Sey. U.*	*Mt.Sey. U.*	*Mt.Sey. U.*	*Mt.Sey. U.*	*Egr. And*	*Egr. And*	*Egr. And*	*Egr. And*	*Egr. And*	*Bad. Unit*	*Bad. Unit*	*Bad. Unit*	*Bad. Unit*
Phenocryst no	17	18	19	20	21	22	23	24	25	26	27	28	29	30
SiO_2	45.72	44.99	45.65	45.44	46.04	39.83	39.99	40.44	41.01	41.06	40.69	48.30	38.50	38.07
TiO_2	1.46	1.66	1.54	1.41	1.42	2.85	2.38	2.23	2.33	2.11	2.88	0.89	2.37	2.46
Al_2O_3	7.61	8.04	7.62	7.53	7.26	12.83	12.64	12.83	12.34	12.06	11.85	5.26	13.66	13.97
Fe_2O_3	13.39	13.99	13.66	13.64	12.93	11.25	12.11	11.63	10.20	10.55	11.24	12.01	13.31	13.81
MnO	0.39	0.39	0.42	0.44	0.39	0.15	0.21	0.16	0.14	0.16	0.14	0.52	0.19	0.23
MgO	13.97	13.44	13.92	13.81	14.24	13.14	12.94	14.11	15.04	15.08	13.45	15.39	12.30	11.54
CaO	11.53	11.52	11.44	11.55	11.59	11.66	11.76	11.05	11.61	11.42	11.55	11.86	11.90	11.92
Na_2O	1.46	1.51	1.43	1.37	1.38	2.16	2.22	2.43	2.42	2.53	2.19	1.36	1.95	1.90
K_2O	0.77	0.82	0.78	0.79	0.68	1.25	1.34	0.86	0.81	0.77	1.07	0.58	2.12	2.02
Total	**96.33**	**96.38**	**96.45**	**95.98**	**95.96**	**95.16**	**95.60**	**95.79**	**96.03**	**95.80**	**95.17**	**96.19**	**96.31**	**95.96**
Si	6.84	6.76	6.83	6.84	6.89	6.06	6.09	6.10	6.13	6.16	6.18	7.16	5.89	5.86
Ti	0.16	0.19	0.17	0.16	0.16	0.33	0.27	0.25	0.26	0.24	0.33	0.10	0.27	0.29
Al	1.34	1.42	1.34	1.33	1.28	2.30	2.27	2.28	2.17	2.13	2.12	0.92	2.46	2.53
Fe	1.68	1.76	1.71	1.72	1.62	1.43	1.54	1.47	1.28	1.32	1.43	1.49	1.70	1.78
Mn	0.05	0.05	0.05	0.06	0.05	0.02	0.03	0.02	0.02	0.02	0.02	0.07	0.03	0.03
Mg	3.12	3.01	3.11	3.10	3.18	2.98	2.94	3.17	3.35	3.37	3.04	3.40	2.80	2.65
Ca	1.85	1.85	1.83	1.86	1.86	1.90	1.92	1.79	1.86	1.84	1.88	1.89	1.95	1.97
Na	0.42	0.44	0.41	0.40	0.40	0.64	0.66	0.71	0.70	0.74	0.64	0.39	0.58	0.57
K	0.15	0.16	0.15	0.15	0.13	0.24	0.26	0.17	0.16	0.15	0.21	0.11	0.41	0.40
Total	**15.61**	**15.64**	**15.61**	**15.61**	**15.57**	**15.90**	**15.96**	**15.95**	**15.94**	**15.97**	**15.86**	**15.53**	**16.10**	**16.06**

BIOTITE / PHLOGOPITE

Sample no	EA109	EA109	EA109	EA109	EA109	EA109	EA350	EA350	EA350	EA350	EA134	EA134	EA134	EA316	EA147	EA147	EAR1
Unit	*Neb. Vol.*	*Neb. Vol.*	*Neb. Vol.*	*Neb. Vol.*	*Neb. Vol.*	*Neb. Vol.*	*Neb. Vol.*	*Neb. Vol.*	*Neb. Vol.*	*Neb. Vol.*	*Neb. Vol.*	*Neb. Vol.*	*Neb. Vol.*	*Klg. And*	*Akc. Unit*	*Akc. Unit*	*Ded. Unit*
Phenocryst no	1	2	3	4	5	6	7	8	9	10	11	12	13	14	15	16	17
SiO_2	38.11	38.24	37.82	37.46	38.64	38.59	38.95	39.66	37.72	37.04	37.79	38.98	39.75	36.18	36.23	35.95	36.30
TiO_2	5.92	5.04	5.64	6.06	5.45	5.01	7.12	6.87	7.51	7.18	6.02	6.40	5.51	4.55	5.17	4.56	4.74
Al_2O_3	12.22	11.84	12.08	12.15	12.92	11.75	12.89	12.71	12.43	12.39	11.86	12.12	12.11	13.45	13.30	13.40	13.72
Fe_2O_3	9.68	9.32	10.22	10.64	9.37	8.32	7.91	7.96	9.02	9.24	7.54	7.28	6.63	15.90	14.13	16.10	15.82
MnO	0.11	0.09	0.09	0.14	0.13	0.11	0.06	0.07	0.09	0.08	0.14	0.09	0.08	0.23	0.14	0.24	0.24
MgO	16.46	17.45	16.62	16.39	16.61	17.80	19.11	19.21	17.32	17.74	19.52	19.18	20.12	14.13	15.20	13.65	14.05
Na_2O	0.58	1.05	0.64	0.72	0.69	0.62	0.47	0.55	0.45	0.54	0.80	0.78	0.76	0.50	0.59	0.52	0.51
K_2O	9.23	9.28	9.35	9.12	8.86	9.03	9.41	9.45	9.55	8.99	8.29	8.73	8.80	8.29	8.59	8.70	8.43
Total	**92.37**	**92.40**	**92.57**	**92.75**	**93.02**	**91.30**	**96.20**	**96.67**	**94.26**	**93.43**	**91.95**	**93.55**	**93.77**	**93.23**	**93.35**	**93.11**	**93.79**
Si	5.74	5.76	5.71	5.66	5.75	5.83	5.59	5.66	5.57	5.52	5.87	5.97	6.05	5.80	5.77	5.80	5.79
Ti	0.67	0.57	0.64	0.69	0.61	0.57	0.77	0.74	0.83	0.80	0.70	0.74	0.63	0.55	0.62	0.55	0.57
Al	2.17	2.10	2.15	2.16	2.27	2.09	2.18	2.14	2.17	2.18	2.17	2.19	2.17	2.54	2.50	2.55	2.58
Fe	1.22	1.18	1.29	1.35	1.17	1.05	0.95	0.95	1.12	1.15	0.98	0.93	0.84	2.13	1.88	2.17	2.11
Mn	0.01	0.01	0.01	0.02	0.02	0.01	0.01	0.01	0.01	0.01	0.02	0.01	0.01	0.03	0.02	0.03	0.03
Mg	3.70	3.92	3.74	3.69	3.69	4.01	4.09	4.08	3.82	3.94	4.52	4.38	4.56	3.38	3.61	3.28	3.34
Na	0.17	0.31	0.19	0.21	0.20	0.18	0.13	0.15	0.13	0.16	0.24	0.23	0.23	0.15	0.18	0.16	0.16
K	1.77	1.78	1.80	1.76	1.68	1.74	1.72	1.72	1.80	1.71	1.64	1.71	1.71	1.70	1.75	1.79	1.71
Total	**15.46**	**15.65**	**15.55**	**15.55**	**15.44**	**15.50**	**15.47**	**15.47**	**15.47**	**15.51**	**16.28**	**16.17**	**16.21**	**16.30**	**16.33**	**16.35**	**16.29**

Sample no	EA37	EA231	EA231	EA73
Unit	*Behr. And.*	*Bad. Unit*	*Bad. Unit*	*Cice. And.*
Phenocryst no	18	19	20	21
SiO_2	36.20	34.97	34.96	35.21
TiO_2	5.19	5.48	4.96	4.68
Al_2O_3	13.63	14.60	13.84	14.42
Fe_2O_3	14.19	14.54	16.13	14.80
MnO	0.14	0.15	0.22	0.24
MgO	15.13	14.36	13.79	14.69
Na_2O	0.63	0.61	0.60	0.67
K_2O	8.73	8.71	8.66	8.56
Total	**93.84**	**93.52**	**93.27**	**93.36**
Si	5.74	5.33	5.39	5.38
Ti	0.62	0.63	0.57	0.54
Al	2.55	2.62	2.51	2.60
Fe	1.88	1.85	2.08	1.89
Mn	0.02	0.02	0.03	0.03
Mg	3.58	3.26	3.17	3.34
Na	0.19	0.18	0.18	0.20
K	1.77	1.69	1.70	1.67
Total	**16.35**	**15.60**	**15.65**	**15.65**

MAGNETITE / Ti-MAGNETITE

Sample no	EA270	EA270	EA270	EA270	EA256	EA256	EA256	EA252	EA252	EA252	EA415	EA415	EA309	EA309	EA309	EA350	EA350	EA350
Unit	*Ayv. Vol.*	*Ayv. Vol.*	*Ayv. Vol.*	*Ayv. Vol.*	*Tas. Vol.*	*Tas. Vol.*	*Tas. Vol.*	*Tas. Vol.*	*Tas. Vol.*	*Tas. Vol.*	*Ezn. Vol.*	*Ezn. Vol.*	*Foc. Dyke*	*Foc. Dyke*	*Foc. Dyke*	*Neb. Vol.*	*Neb. Vol.*	*Neb. Vol.*
Phenocryst no	1	2	3	4	6	7	8	9	11	12	13	14	15	16	17	18	19	20
SiO_2	0.08	0.09	0.07	0.08	0.08	0.11	0.17	0.09	0.27	0.17	0.15	0.55	0.08	0.10	0.08	0.06	0.06	0.10
TiO_2	17.53	17.82	18.17	18.41	11.16	20.65	19.53	30.08	24.41	9.63	25.45	26.85	22.45	23.90	19.92	12.20	13.79	12.04
Al_2O_3	1.16	0.74	2.17	0.85	2.60	1.99	2.22	0.30	1.31	2.31	0.99	0.24	2.64	2.15	3.48	2.84	3.15	2.78
Cr_2O_3	0.12	0.11	0.00	0.00	0.46	0.00	0.00	0.06	0.03	0.11	0.17	0.10	0.18	0.06	0.11	0.63	3.08	1.10
FeO	40.52	40.76	51.12	51.51	39.19	47.44	46.64	45.66	48.65	34.30	50.58	50.61	49.82	49.02	46.97	39.58	36.57	34.61
Fe_2O_3	34.59	34.42	23.97	24.89	42.62	25.18	26.67	19.69	21.43	50.87	19.07	16.68	21.96	21.34	26.43	40.30	37.76	41.87
MnO	0.94	0.92	0.91	0.99	0.55	0.70	0.75	0.71	0.81	0.37	1.53	1.13	0.81	0.90	0.70	0.62	0.60	0.59
MgO	3.55	3.36	4.26	3.59	1.85	3.31	1.98	2.61	2.48	2.00	1.03	1.39	1.99	1.74	2.18	3.17	4.07	3.43
CaO	0.14	0.25	0.14	0.08	0.14	0.14	0.18	0.64	0.46	0.17	0.17	0.45	0.04	0.17	0.10	0.12	0.07	2.49
Total	**98.63**	**98.47**	**100.80**	**100.39**	**98.65**	**99.52**	**98.14**	**99.84**	**99.85**	**99.93**	**99.14**	**98.00**	**99.97**	**99.38**	**99.97**	**99.52**	**99.15**	**99.01**

	EA348	EA348	EA348	EA109	EA109	EA109	EA109	EA134	EA134	EA316	EA326	EA326	EA412	EA418	EA231	EA231	EA275	EA275
Unit	*Neb. Vol.*	*Neb. Vol.*	*Neb. Vol.*	*Neb. Vol.*	*Neb. Vol.*	*Neb. Vol.*	*Neb. Vol.*	*Neb. Vol.*	*Neb. Vol.*	*Klg. And*	*Mt.Sey. U.*	*Mt.Sey. U.*	*Kov. Dyke*	*Kov. Dyke*	*Bad. Unit*	*Bad. Unit*	*Behr. And.*	*Behr. And.*
Phenocryst no	21	22	24	25	26	27	28	29	30	31	32	33	34	35	36	37	38	39
SiO_2	0.28	0.12	0.04	0.09	0.05	0.08	0.05	0.18	0.15	0.08	0.09	0.88	0.15	0.19	0.50	0.18	1.50	0.67
TiO_2	6.29	5.10	8.99	21.48	16.98	19.88	20.18	13.23	10.72	4.63	3.28	4.47	11.35	12.35	9.56	14.02	11.16	10.60
Al_2O_3	2.37	0.95	2.04	2.31	2.78	1.98	2.36	2.19	2.58	1.48	1.72	1.07	0.83	2.22	3.35	2.21	2.62	1.93
Cr_2O_3	0.14	0.32	8.68	0.03	1.43	0.06	0.05	0.00	0.00	0.00	0.00	0.00	0.00	0.22	0.13	0.08	0.00	0.00
FeO	33.51	35.27	35.57	34.57	42.07	47.60	45.41	51.92	53.67	63.27	61.73	61.04	55.91	37.49	35.57	41.54	52.80	55.34
Fe_2O_3	54.03	55.33	40.48	37.11	31.97	26.64	28.16	29.15	29.23	28.82	29.79	29.61	29.20	43.11	42.50	37.27	28.04	28.21
MnO	0.27	0.14	0.41	0.87	0.85	0.80	0.77	1.19	0.90	0.37	0.48	0.89	0.51	0.52	0.72	0.80	0.64	1.19
MgO	1.30	0.67	2.17	1.65	2.25	1.38	1.87	0.11	0.07	1.23	0.59	0.04	0.49	2.12	1.77	1.30	1.48	1.46
CaO	0.10	0.12	0.00	0.05	0.14	0.15	0.05	0.17	0.27	0.09	0.05	0.13	0.06	0.22	0.11	0.11	0.06	0.31
Total	**98.29**	**98.02**	**98.38**	**98.15**	**98.52**	**98.57**	**98.90**	**98.12**	**97.58**	**99.97**	**97.73**	**98.12**	**98.51**	**98.44**	**94.21**	**97.51**	**98.30**	**99.71**

ILMENITE

Sample no	EA270	EA270	EA256	EA256	EA256	EA256	EA256	EA256	EA252	EA252	EA252	EA252	EA252	EA350	EA350	EA350	EA348
Unit	*Ayv. Vol.*	*Ayv. Vol.*	*Tas. Vol.*	*Tas. Vol.*	*Tas. Vol.*	*Tas. Vol.*	*Tas. Vol.*	*Tas. Vol.*	*Tas. Vol.*	*Tas. Vol.*	*Tas. Vol.*	*Tas. Vol.*	*Tas. Vol.*	*Neb. Vol.*	*Neb. Vol.*	*Neb. Vol.*	*Foc.Dyke*
Phenocryst no	1	2	3	4	5	6	7	8	9	10	11	12	13	14	15	16	17
SiO_2	0.09	0.08	0.06	0.07	0.04	0.40	0.10	0.19	1.31	0.31	0.22	0.23	0.08	0.13	0.09	0.14	0.11
TiO_2	51.32	51.09	50.61	50.82	47.70	48.86	36.03	53.71	45.77	45.04	43.09	42.00	43.11	48.00	47.22	40.41	44.50
Al_2O_3	0.11	0.15	0.06	0.12	0.09	0.41	0.85	0.08	1.58	0.82	0.68	0.76	0.32	0.19	0.14	1.13	0.18
Cr_2O_3	0.00	0.00	0.00	0.00	0.17	0.05	0.21	0.03	0.04	0.06	0.05	0.05	0.08	0.08	0.15	0.17	0.13
FeO	20.71	20.53	20.62	20.85	33.05	24.06	10.05	25.58	38.17	34.03	32.27	37.96	33.97	31.23	31.03	24.81	32.00
Fe_2O_3	21.85	22.84	23.03	22.62	12.07	13.19	39.96	4.75	9.10	16.97	18.25	15.95	19.83	12.55	12.96	25.44	17.15
MnO	0.87	0.88	1.03	0.87	1.05	1.91	1.04	2.19	0.25	0.29	0.78	0.94	0.19	0.71	0.57	0.69	0.51
MgO	5.38	4.75	4.46	4.76	4.73	9.83	11.66	13.50	1.73	1.02	2.88	1.32	0.78	5.86	5.66	5.68	3.88
CaO	0.06	0.07	0.03	0.22	0.15	0.30	0.33	0.33	0.42	0.46	0.36	0.48	0.26	0.36	0.27	0.20	0.27
Total	100.39	100.39	99.90	100.34	99.05	99.01	100.23	100.36	98.37	99.00	98.58	99.69	98.62	99.11	98.09	98.67	98.73

Sample no	EA348	EA348	EA231	EA231
Unit	*Foc.Dyke*	*Foc.Dyke*	*Bad. Unit*	*Bad. Unit*
Phenocryst no	18	19	20	21
SiO_2	0.08	0.11	0.22	0.48
TiO_2	43.86	42.05	42.87	34.20
Al_2O_3	0.07	0.11	0.11	0.48
Cr_2O_3	0.18	0.17	0.03	0.05
FeO	34.37	32.98	34.35	28.37
Fe_2O_3	16.59	19.20	15.98	32.95
MnO	0.61	0.39	1.78	1.41
MgO	2.19	2.12	1.86	1.57
CaO	0.17	0.28	0.52	0.25
Total	98.12	97.41	97.72	99.76

Appendix C

XRF and ICP-MS ERROR CALCULATIONS

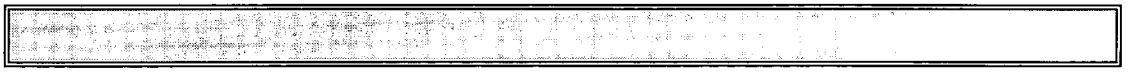

International standards run as unknowns outside the calibration (XRF-Major elements)

	AGV-1			BHVO-1			G-2		
	Recomm.	Aver. (n=5)	2 s.d.	Recomm.	Aver. (n=3)	2 s.d.	Recomm.	Aver. (n=4)	2 s.d.
SiO_2	*59.79*	60.13	*1.27*	*49.94*	49.86	*0.18*	*69.08*	68.86	*1.37*
TiO_2	*1.05*	1.06	*0.03*	*2.7*	2.73	*0.04*	*0.48*	0.49	*0.05*
Al_2O_3	*17.14*	17.71	*0.61*	*13.8*	13.66	*0.24*	*15.38*	15.46	*0.41*
Fe_2O_3	*6.726*	6.90	*0.19*	*10.4*	11.27	*0.93*	*2.68*	2.64	*0.09*
MnO	*0.092*	0.10	*0.01*	*0.168*	0.17	*0.01*	*0.03*	0.03	*0.01*
MgO	*1.53*	1.65	*0.12*	*7.23*	7.39	*0.09*	*0.75*	0.81	*0.03*
CaO	*4.94*	4.98	*0.06*	*11.4*	11.42	*0.05*	*1.96*	1.93	*0.04*
Na_2O	*4.26*	4.40	*0.16*	*2.26*	2.37	*0.1*	*4.08*	4.33	*0.11*
K_2O	*2.91*	2.97	*0.08*	*0.52*	0.52	*0.03*	*4.08*	4.47	*0.08*
P_2O_5	*0.49*	0.50	*0.04*	*0.273*	0.29	*0.01*	*0.14*	0.13	*0.02*
Total	*98.928*	100.398		*98.691*	99.686		*98.66*	99.37	

	QLO-1			W-2			BOB-1		
	Recomm.	Aver. (n=4)	2 s.d.	Recomm.	Aver. (n=3)	2 s.d.	Recomm.	Aver. (n=3)	2 s.d.
SiO_2	*65.55*	66.23	*0.63*	*52.44*	52.13	*0.21*	*50.2*	50.81	*0.63*
TiO_2	*0.62*	0.61	*0.02*	*1.06*	1.06	*0.02*	*1.29*	1.27	*0.17*
Al_2O_3	*16.18*	16.64	*0.47*	*15.35*	15.38	*0.27*	*16.5*	16.79	*0.31*
Fe_2O_3	*3.98*	4.13	*0.1*	*10.661*	10.88	*0.11*	*8.61*	8.54	*0.09*
MnO	*0.09*	0.09	*0.01*	*0.163*	0.17	*0.01*	*0.14*	0.15	*0.02*
MgO	*1*	1.13	*0.11*	*6.37*	6.52	*0.16*	*7.57*	7.86	*0.08*
CaO	*3.17*	3.19	*0.04*	*10.87*	10.94	*0.09*	*11.21*	11.22	*0.04*
Na_2O	*4.2*	4.23	*0.09*	*2.14*	2.19	*0.03*	*3.15*	3.31	*0.11*
K_2O	*3.6*	3.61	*0.04*	*0.627*	0.63	*0.02*	*0.35*	0.39	*0.06*
P_2O_5	*0.25*	0.25	*0.01*	*0.131*	0.13	*0.01*	*0.17*	0.15	*0.02*
Total	*99.37*	100.11		*99.81*	100.02		*99.19*	100.49	

International standards run as unknowns outside the calibration (XRF-Trace elements)

	BHVO1			GS-N			BE-N		
	Recomm.	Aver. (n=4)	2 s.d.	Recomm.	Aver. (n=3)	2 s.d.	Recomm.	Aver. (n=3)	2 s.d.
Sc	31.8	34.1	*0.17*	7.3	6.5	*0.19*	22	32.7	*2.17*
Cr	289	275.6	*0.22*	55	59.1	*0.20*	360	359.1	*0.67*
V	317	319.1	*4.62*	65	66.2	*5.08*	235	236.1	*3.54*
Ni	121	131.3	*9.37*	34	35.6	*5.17*	267	268.9	*1.29*
Ga	21	17.9	*1.63*	22	18.2	*1.47*	17	16.3	*2.04*
Rb	11	10.7	*0.91*	185	185.4	*1.00*	47	48.7	*0.78*
Sr	403	411.6	*1.29*	570	577.9	*1.16*	1370	1387.6	*3.83*
Y	27.6	29.1	*0.86*	19	19.4	*0.95*	30	32.1	*0.57*
Zr	179	173.9	*2.13*	235	226.7	*1.92*	265	264.5	*2.59*
Nb	19	17.8	*0.61*	21	20.7	*0.55*	100	98.7	*1.02*
Ba	139	135.7	*1.38*	1400	1390.9	*1.52*	1025	1039.4	*3.92*
La	15.8	16.3	*1.58*	75	72.9	*1.42*	82	78.6	*2.38*
Ce	39	37.1	*0.96*	135	132.4	*1.13*	152	148.3	*1.91*
Nd	25.2	26.4	*1.15*	50	51	*1.04*	70	70.3	*0.85*

	AGV-1			DR-N			QLO-1		
	Recomm.	Aver. (n=4)	2 s.d.	Recomm.	Aver. (n=3)	2 s.d.	Recomm.	Aver. (n=3)	2 s.d.
Sc	12.1	14.2	0.204	28	30.8	0.22	8.9	9.6	2.604
Cr	12	13.9	0.176	42	45.2	0.16	3.2	3.5	0.804
V	123	125	3.696	220	217.5	4.07	54	57	2.832
Ni	17	19.4	11.244	15	14.6	4.14	5.8	6.1	1.548
Ga	20	19.5	1.304	22	19.9	1.76	17	15.9	1.632
Rb	67	66.3	1.092	73	76.3	1.30	74	79.1	0.624
Sr	662	668.2	1.032	400	411.2	1.51	336	341.5	4.596
Y	21	19.9	0.688	28	26.9	1.23	24	22.8	0.456
Zr	225	223.8	2.556	125	131.4	2.49	185	191.4	2.072
Nb	15	14.1	0.488	8	7.6	0.71	10.3	11.7	1.224
Ba	1221	1226.2	1.104	385	391.3	1.21	1370	1377.6	3.136
La	38	36.5	1.896	21	24.5	1.14	27	29.1	1.904
Ce	66	63.8	1.152	46	42.7	0.90	54	52.9	2.292
Nd	34	35.1	1.38	23	22.1	0.83	26	28.6	1.02

ICP-MS error calculations

	AGV-1	BE-N	BHVO-1	DR-N	QLO-1	GS-N	*Std. error (±)*
Cs *recommended*	***1.26***	***0.80***	***0.13***	***6.00***	***1.75***	***5.70***	***0.12***
1st. run	1.29	0.75	0.08	6.31	1.71	5.69	
2nd. run	1.26	0.73	0.08	6.37	1.66	5.57	
3rd. run	1.24	0.77	0.10	6.17	1.66	5.62	
4th. run	1.25	0.72	0.09			5.66	
5th. run	1.26					5.66	
6th. run	1.28						
standart dev.	0.02	0.02	0.01	0.10	0.03	0.05	
La *recommended*	***38.00***	***82.00***	***15.80***	***21.00***	***27.00***	***75.00***	***1.02***
1st. run	38.64	81.75	15.56	21.32	26.55	71.57	
2nd. run	38.63	82.55	16.20	21.19	26.92	73.28	
3rd. run	39.31	81.88	15.41	21.58	27.24	73.55	
4th. run	39.47	83.21	15.62			74.18	
5th. run	39.28	83.64				73.53	
6th. run	38.42						
standart dev.	0.44	0.82	0.35	0.20	0.35	0.98	
Ce *recommended*	***66.00***	***152.00***	***39.00***	***46.00***	***54.00***	***135.00***	***1.63***
1st. run	69.69	150.55	38.39	48.17	55.96	135.76	
2nd. run	69.81	153.25	39.67	47.09	53.91	135.63	
3rd. run	70.14	152.13	41.76	45.93	51.30	135.95	
4th. run	71.15	151.72	37.77			137.31	
5th. run	70.75	153.76				136.19	
6th. run	67.58						
standart dev.	1.24	1.27	1.76	1.12	2.34	0.67	
Pr *recommended*	***6.50***	***16.90***	***5.70***	***5.70***	***6.01***	***14.00***	***0.97***
1st. run	8.39	17.01	5.36	5.62	5.90	14.23	
2nd. run	8.46	17.56	5.52	5.61	5.71	14.00	
3rd. run	8.51	17.04	5.28	5.45	5.76	14.10	
4th. run	8.56	16.69	5.14			14.16	
5th. run	8.59	17.06				14.08	
6th. run	8.32						
standart dev.	0.10	0.31	0.16	0.10	0.10	0.09	
Nd *recommended*	***34.00***	***70.00***	***25.20***	***23.00***	***26.00***	***50.00***	***1.17***
1st. run	33.89	69.71	26.17	24.53	24.52	51.38	
2nd. run	33.61	71.59	26.73	24.70	23.91	51.74	
3rd. run	34.28	69.87	25.95	24.14	25.88	52.42	
4th. run	34.53	69.52	25.64			52.49	
5th. run	34.45	70.94				50.13	
6th. run	33.72						
standart dev.	0.39	0.90	0.46	0.29	1.01	0.96	

	AGV-1	BE-N	BHVO-1	DR-N	QLO-1	GS-N	*Std. error (±)*
Sm *recommended*	***5.90***	***12.00***	***6.20***	***5.30***	***4.88***	***7.70***	***0.11***
1st. run	5.69	12.13	6.14	5.19	4.70	7.34	
2nd. run	5.90	12.30	6.17	5.30	4.66	7.57	
3rd. run	5.97	12.14	6.12	5.21	4.69	7.61	
4th. run	5.97	12.25	6.23			7.50	
5th. run	5.90	12.73				7.54	
6th. run	5.71						
standart dev.	0.13	0.25	0.05	0.06	0.02	0.10	
Eu *recommended*	***1.66***	***3.60***	***2.06***	***1.45***	***1.43***	***1.70***	***0.04***
1st. run	1.66	3.63	2.01	1.43	1.34	1.62	
2nd. run	1.65	3.68	2.07	1.46	1.31	1.61	
3rd. run	1.68	3.61	2.04	1.44	1.35	1.65	
4th. run	1.67	3.71	2.07			1.65	
5th. run	1.66	3.79				1.63	
6th. run	1.66						
standart dev.	0.01	0.07	0.03	0.01	0.02	0.02	
Gd *recommended*	***5.20***	***9.00***	***6.40***	***4.70***	***4.70***	***5.20***	***0.59***
1st. run	4.64	9.72	5.85	5.01	4.20	4.47	
2nd. run	4.49	9.80	5.98	5.13	4.13	5.75	
3rd. run	4.60	9.62	6.04	4.65	4.20	5.83	
4th. run	4.44	10.00	5.35			6.01	
5th. run	4.55	10.36				5.94	
6th. run	4.57						
standart dev.	0.07	0.29	0.31	0.25	0.04	0.64	
Tb *recommended*	***0.71***	***1.30***	***0.96***	***0.80***	***0.71***	***0.60***	***0.03***
1st. run	0.68	1.32	0.95	0.81	0.68	0.63	
2nd. run	0.67	1.35	0.98	0.82	0.67	0.63	
3rd. run	0.68	1.32	0.96	0.81	0.69	0.64	
4th. run	0.68	1.31	0.97			0.64	
5th. run	0.68	1.36				0.65	
6th. run	0.67						
standart dev.	0.01	0.02	0.01	0.00	0.01	0.01	
Dy *recommended*	***3.80***	***6.29***	***5.20***	***4.35***	***3.80***	***3.00***	***0.19***
1st. run	3.66	6.34	5.25	4.78	4.00	3.16	
2nd. run	3.61	6.59	5.36	4.74	3.78	3.06	
3rd. run	3.64	6.32	5.33	4.65	3.88	3.11	
4th. run	3.66	6.23	5.22			3.06	
5th. run	3.68	6.33				3.10	
6th. run	3.58						
standart dev.	0.04	0.14	0.06	0.06	0.11	0.04	

ICP-MS error calculations

	AGV-1	BE-N	BHVO-1	DR-N	QLO-1	GS-N	*Std. error (±)*
Ho *recommended*	***0.73***	***1.03***	***0.99***	***0.91***	***0.86***	***0.50***	***0.06***
1st. run	0.68	1.07	0.98	0.96	0.82	0.58	
2nd. run	0.68	1.09	0.99	0.98	0.81	0.57	
3rd. run	0.69	1.07	0.99	0.95	0.82	0.58	
4th. run	0.68	1.07	0.97			0.57	
5th. run	0.69	1.09				0.58	
6th. run	0.68						
standart dev.	0.01	0.01	0.01	0.01	0.01	0.00	
Er *recommended*	***1.61***	***2.48***	***2.40***	***2.46***	***2.30***	***1.70***	***0.13***
1st. run	1.76	2.41	2.37	2.57	2.28	1.46	
2nd. run	1.69	2.45	2.40	2.57	2.30	1.50	
3rd. run	1.76	2.43	2.37	2.57	2.30	1.48	
4th. run	1.70	2.39	2.43			1.50	
5th. run	1.77	2.51				1.51	
6th. run	1.73						
standart dev.	0.03	0.04	0.03	0.00	0.01	0.02	
Tm *recommended*	***0.32***	***0.37***	***0.33***		***0.37***		***0.04***
1st. run	0.30	0.35	0.37	0.44	0.40	0.25	
2nd. run	0.29	0.36	0.37	0.45	0.40	0.25	
3rd. run	0.29	0.36	0.37	0.43	0.40	0.25	
4th. run	0.29	0.35	0.36			0.25	
5th. run	0.29	0.35				0.25	
6th. run	0.29						
standart dev.	0.00	0.00	0.00	0.01	0.00	0.00	
Yb *recommended*	***1.67***	***1.80***	***2.02***	***2.70***	***2.32***	***1.50***	***0.11***
1st. run	1.68	1.84	1.97	2.55	2.44	1.45	
2nd. run	1.61	1.80	2.00	2.54	2.48	1.45	
3rd. run	1.58	1.82	2.02	2.54	2.48	1.46	
4th. run	1.69	1.86	2.01			1.49	
5th. run	1.63	1.84				1.45	
6th. run	1.65						
standart dev.	0.04	0.02	0.02	0.00	0.02	0.02	
Lu *recommended*	***0.28***	***0.24***	***0.29***	***0.40***	***0.37***	***0.22***	***0.02***
1st. run	0.26	0.26	0.29	0.39	0.40	0.22	
2nd. run	0.26	0.26	0.29	0.39	0.39	0.22	
3rd. run	0.26	0.26	0.29	0.38	0.40	0.23	
4th. run	0.26	0.26	0.29			0.22	
5th. run	0.26	0.26				0.22	
6th. run	0.26						
standart dev.	0.00	0.00	0.00	0.00	0.01	0.00	

	AGV-1	BE-N	BHVO-1	DR-N	QLO-1	GS-N	*Std. error (±)*
Hf *recommended*	***5.10***	***5.40***	***4.38***	***3.20***	***4.60***	***6.20***	***0.63***
1st. run	5.08	5.49	4.29	2.55	4.47	4.27	
2nd. run	5.05	5.54	4.27	3.55	4.47	5.73	
3rd. run	5.03	5.61	4.32	1.28	4.55	6.82	
4th. run	5.00	5.68	4.36			3.80	
5th. run	4.99	5.68				3.74	
6th. run	4.93						
standart dev.	0.05	0.08	0.04	1.14	0.05	1.35	
Ta *recommended*	***0.92***	***5.50***	***1.23***	***0.60***	***0.82***	***2.60***	***0.08***
1st. run	0.94	5.53	1.15	0.59	0.79	2.51	
2nd. run	0.85	5.61	1.15	0.58	0.80	2.38	
3rd. run	0.84	5.54	1.13	0.57	0.81	2.40	
4th. run	0.94	5.64	1.20			2.40	
5th. run	0.84	5.64				2.51	
6th. run	0.93						
standart dev.	0.05	0.05	0.03	0.01	0.01	0.07	
Th *recommended*	***6.50***	***11.00***	***1.08***	***5.00***	***4.50***	***42.00***	***0.26***
1st. run	6.65	10.90	1.27	4.87	4.81	41.81	
2nd. run	6.59	10.82	1.26	4.91	4.86	42.06	
3rd. run	6.58	11.03	1.26	4.22	4.97	41.26	
4th. run	6.55	10.93	1.27			41.63	
5th. run	6.59	11.17				42.60	
6th. run	6.44						
standart dev.	0.07	0.14	0.01	0.39	0.08	0.50	
U *recommended*	***1.89***	***2.40***	***0.42***	***1.50***	***1.94***	***8.00***	***0.06***
1st. run	1.90	2.39	0.41	1.51	1.78	7.40	
2nd. run	1.89	2.36	0.40	1.52	1.95	7.95	
3rd. run	1.88	2.44	0.42	1.34	1.98	7.84	
4th. run	1.90	2.56	0.44			7.93	
5th. run	1.88	2.63				8.01	
6th. run	1.83						
standart dev.	0.02	0.12	0.02	0.10	0.11	0.25	